

GEOCHEMICAL INDICATORS OF SUBSURFACE TEMPERATURE—
PART 2, ESTIMATION OF TEMPERATURE AND FRACTION OF
HOT WATER MIXED WITH COLD WATER

By R. O. FOURNIER and A. H. TRUESDELL, Menlo Park, Calif.

Abstract.—The water in many warm springs with large rates of flow consists of mixtures of hot water that has come from depth and of shallow cold water. Under favorable conditions the original temperature of the hot water and the fraction of the cold water in the mixture can be estimated by using the measured temperature and silica content of the warm spring water and the temperature and silica content of non-thermal water in the region. The method has been applied with apparent success at Yellowstone National Park.

Warm (<80°C) springs with large rates of discharge occur in many places throughout the world. Some of these warm springs originate through deep circulation of meteoric water that is heated mainly by conductive heat transfer from the rock to the water. Other warm springs originate through mixing of high-temperature (>100°C) water with cold meteoric water.

As discussed in part 1 by Fournier, White, and Truesdell (companion article on p. 259 of this issue), water discharged from springs with rates of flow greater than about 100–200 l/min can be assumed to have lost little heat to the wallrock per unit mass of water during the upward movement. For nonboiling springs, if mixing has not occurred, the temperature of the spring is close to the highest temperature attained by that water. If mixing has occurred, however, water of very high temperature may be present at comparatively shallow depth. These possible differences in subsurface conditions may be differentiated in many places on chemical grounds. Specifically, the chemical composition of a water heated only to its eventual discharge temperature is likely to reflect water-rock equilibration at about that temperature, whereas the composition of a mixed water is likely to indicate marked nonequilibrium between the water and rock at the spring temperature.

If the composition suggests that the warm spring water is produced by the mixing of cold meteoric water with high-temperature water, it is possible under certain conditions to calculate the temperature and fraction of the hot-water component.

TEST FOR A MIXED WATER

If several springs are present, variations in the temperature or in content of chloride, boron, or other relatively nonreactive

constituents may indicate mixed water. Such water is particularly indicated where there is a regular variation in water temperature and chlorinity.

Another approach is to test whether or not the composition of a large flowing spring indicates chemical equilibration at a temperature within about ±25°C of the spring water. Marked nonequilibrium suggests a mixed water.

The Na-K-Ca geothermometer (Fournier and Truesdell, 1973) appears to work well for testing chemical equilibration. Water composition, in molality, is related to temperature by the empirically derived equation

$$\log(\text{Na/K}) + \beta \log(\sqrt{\text{Ca/Na}}) = \frac{1647}{273 + t_c} - 2.24 \quad (1)$$

in which $\beta=1/3$ for water equilibrated above 100°C, and $\beta=4/3$ for water equilibrated below 100°C. First, test to see if $\beta=4/3$ yields a temperature below 100°C; if it does not, use $\beta=1/3$ to estimate the equilibration temperature.

A more sophisticated approach is to perform a complete chemical analysis of the water and then use a computer and appropriate program (Kharaka and Barnes, 1974; Truesdell and Jones, 1973) to test various possible equilibria at the temperature of the spring and selected higher temperatures.

The silica geothermometer (Fournier and Rowe, 1966) has been the most reliable single chemical indicator of reservoir temperature in spring systems that are high in silica and are characterized by sinter deposits and boiling waters. There is an ambiguity, however, in using the silica content of a warm spring to test for water-rock equilibration at the spring temperature: a high silica content in the spring water may be due to either solution of quartz at a much higher temperature (with or without subsequent mixing of hot and cold waters) or solution of cristobalite or amorphous silica at the spring temperature. Therefore, the silica geothermometer (Fournier and Rowe, 1966) should be used with great caution to test for water-rock equilibration at the spring temperature. Although supersaturated silica solutions may occur in nature over a wide range in temperatures, they are not likely to persist for long

periods of time above about 150°C (Fournier, 1973). This is critical for the models that we present in this paper.

MIXING MODELS

Two mixing models that allow calculation of the temperature and fraction of the hot water component are shown schematically in figure 1. In model 1, figure 1A, hot water ascends from depth along a permeable channel, possibly a fault or joint. Depending on the initial temperature, the water may boil (cool adiabatically) as it rises. In this event, the water and newly forming steam rise together. At some point, M in figure 1A, the hot water encounters cold water from a permeable stratum. At the depth of mixing the weight of a column of cold water extending up to the surface is greater than the weight of the warm mixed water. Thus, the pressure relations are such that cold water enters the hot-water channel and the mixture flows to the surface and is discharged as a warm spring. Depending on the proportion of hot to cold water and the initial enthalpies of each, the spring may have a temperature ranging from very low to boiling.

In model 2, figure 1B we assume that boiling occurs in the rising hot water and that some or all of the resulting steam escapes from that water (point S) before the hot water mixes

with cold water. We show a fumarole where the steam emerges and a warm spring where the hot water mixed with cold water emerges. Alternatively, the separated steam might possibly condense and combine with shallow ground water and give rise to other warm springs that are not amenable to the methods suggested in this report.

If the channel above S is filled with steam, boiling at S will be at atmospheric pressure, provided there are few constrictions in the channel or impediments to the escape of steam (no throttling occurs). If throttling of the steam occurs, or if the channel is partly or completely filled with water, boiling and escape of steam at S will be at greater than atmospheric pressure.

In both models of figure 1 the calculations depend upon ones knowing the temperatures and silica content of the cold water before mixing¹ and those of the warm spring water after mixing. In addition, it must be assumed that the initial silica content of the deep hot water is controlled by the solubility of quartz and that no further solution or deposition of silica occurs before or after mixing. Numerous observations have shown that natural water deep in hot-spring systems generally is just saturated with quartz (Mahon, 1966; Fournier and Truesdell, 1970; Ellis, 1970; Fournier, 1973). Furthermore,

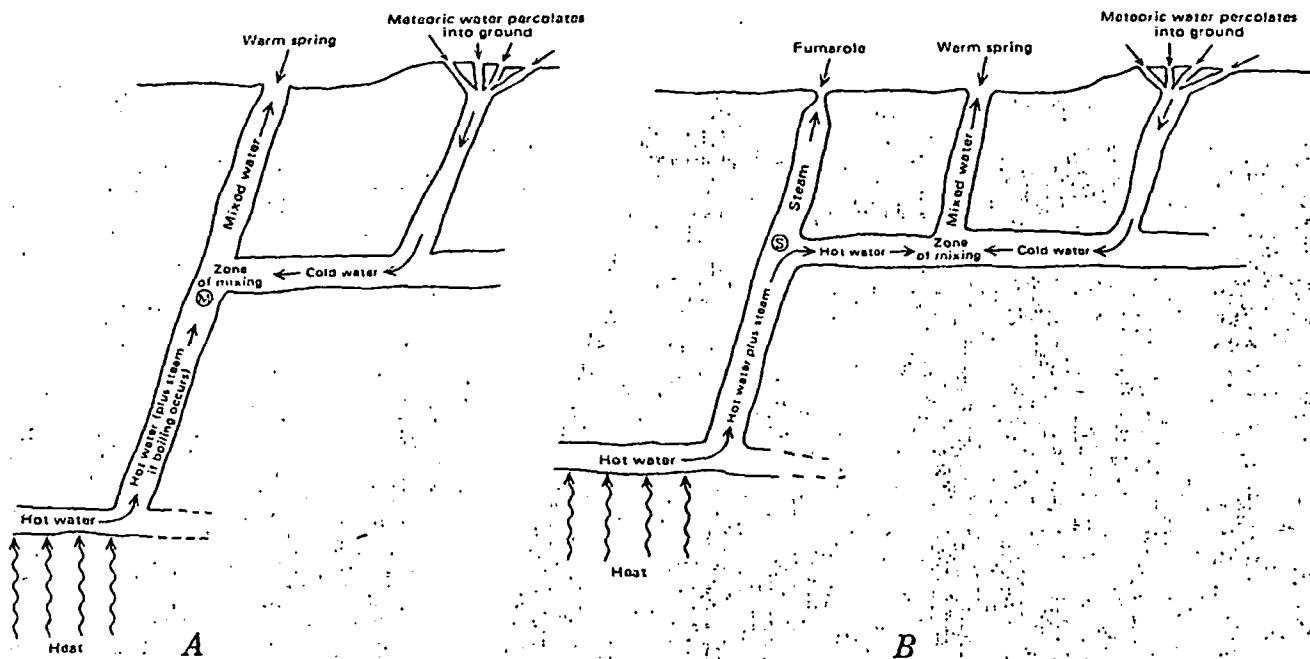


Figure 1.—Schematic model (A) for obtaining a mixed-water warm spring in which both the enthalpy and silica content of the hot-water content are the same as in the original deep water (model 1) and schematic model (B) in which the hot-water component has lost steam before mixing with cold water (model 2). (See text for discussion.)

¹ If the average temperature and silica content of nonthermal ground water in the region are not known, we suggest estimating the mean annual temperature and using 25 mg/l of silica as a first approximation.

our observations in Yellowstone National Park (Fournier and Truesdell, 1970) and elsewhere (White, 1974) suggest that ascending boiling water generally does not dissolve or precipitate silica if the rate of upflow is fast.

In the calculations that follow, model 1 gives a probable maximum subsurface temperature attained by the hot-water component, and model 2, a probable minimum subsurface temperature. On the basis of the total chemical and physical character of the warm spring, its relation to other hot springs and fumaroles, and its geologic environment, it may be possible to choose the temperature that is more likely to be correct. Even where this is not possible, information on the range of possible subsurface temperatures will be of great interest.

CALCULATIONS

Model 1

In this model the enthalpy of the hot water plus steam that heats the cold water is the same as the initial enthalpy of the deep hot water. Two equations can be written to solve for the two unknowns—the temperature of the hot water and the proportions of the hot and cold water—because the silica content and temperature of the warm spring are different functions of the original temperature of the hot-water component. The first equation relates the heat contents or enthalpies of the hot water, H_{hot} ; cold water, H_{cold} ; and spring water, H_{spg} ; and the fractions of cold water, X , and of hot water, $1-X$, as follows:

$$(H_{cold})(X) + (H_{hot})(1-X) = H_{spg} \quad (2)$$

Below 100°C the enthalpy of liquid water coexisting with steam (saturated water) in calories per gram is essentially equivalent in magnitude to the temperature of the water in degrees Celsius. Above 100°C the relation of temperature and enthalpy of saturated water can be found in steam tables (Keenan and Keyes, 1936; Keenan and others, 1969). Selected values are given in table 1.

Table 1.—Enthalpies of liquid water and quartz solubilities at selected temperatures and pressures appropriate for coexistent steam and liquid water
[Enthalpies from Keenan and others (1969). Quartz solubilities at and below 225°C from Morey and others (1962); above 225°C from unpublished data of R. O. Fournier]

Temperature (°C)	Enthalpy (cal/g)	Silica (mg/l)	Temperature (°C)	Enthalpy (cal/g)	Silica (mg/l)
50	50.0	13.5	200	203.6	265
75	75.0	26.6	225	230.9	365
100	100.1	48	250	259.2	486
125	125.4	80	275	289.0	614
150	151.0	125	300	321.0	692
175	177.0	185			

In a similar manner the second equation relates the silica contents of hot water, Si_{hot} ; cold water, Si_{cold} ; and spring water, Si_{spg} :

$$(Si_{cold})(X) + (Si_{hot})(1-X) = Si_{spg} \quad (3)$$

The relation of dissolved silica to the temperature of the aquifer supplying the hot-water component is given by the solubility of quartz at the vapor pressure of the solution (Morey and others, 1962; Fournier, unpub. data, 1974). Selected values are given in table 1.

We use a computer program (Truesdell and others, 1973) to solve equations 2 and 3 and obtain the temperature of the hot water and the fraction of cold water in the mixture, using measurements of the spring temperature and silica content, measurements or estimates of the lowest temperature and average silica content of cold springs in the area, and tabular values of heat content of liquid water and quartz solubilities. Alternatively, a graphical solution can be obtained as follows:

1. Assume a series of values of enthalpy of hot water for the temperatures listed in table 1 and calculate X_t for each, as follows:

$$X_t = \frac{(T_w = H_w) - (T_c = H_c)}{(T_w = H_w) - (T_c = H_c)}$$

2. Plot the calculated values of X_t in relation to the temperatures from which the assumed hot-water enthalpy values were derived (see fig. 2, curve A).

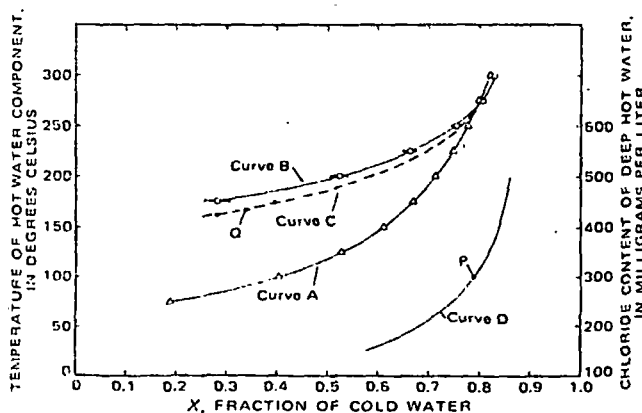


Figure 2.—Fraction of cold water relative to temperature and chloride content of hot-water component in Terrace Spring. Triangles, X_t values listed in table 2; circles, X_{Si} values. The horizontal bars show the possible error due to uncertainty in the silica analysis of the spring water. Points P and Q discussed in text. Curve A, Fraction of cold water based on model 1 enthalpy considerations. Curve B, Fraction of cold water based on model 1 silica considerations. Curve C, Fraction of cold water based on model 2 silica considerations. Curve D, Required chloride contents of deep water.

3. Assume a series of silica contents of hot water appropriate for the temperature listed in table 1 and evaluate X_{Si} for each silica content, as follows:

$$X_{Si} = \frac{(\text{Silica in hot water}) - (\text{Silica in warm spring})}{(\text{Silica in hot water}) - (\text{Silica in cold spring})}$$

4. On the graph previously used, plot the calculated values of X_{Si} in relation to the temperatures for which the silica contents were obtained (see fig. 2, curve B).
5. The point of intersection gives the estimated temperature of the hot-water component and the fraction of cold water.

The two curves possibly may not intersect (fig. 3) or they may intersect at an unreasonably high temperature. These situations would arise if the ascending hot water lost steam or heat before mixing with the cold water (model 2) or if the mixed water dissolved additional silica owing to contact with amorphous silica or rock containing glass. Therefore, we recommend that the mixing model described above be used with extreme caution for warm spring water that has silica contents about equal to the solubility of amorphous silica at the temperature of the spring. For temperatures below 200°C, the approximate solubility of amorphous silica can be calculated from the equation

$$-\log C = \frac{731}{T} - 4.52 \quad (6)$$

where C is silica solubility in milligrams per liter and T is absolute temperature.

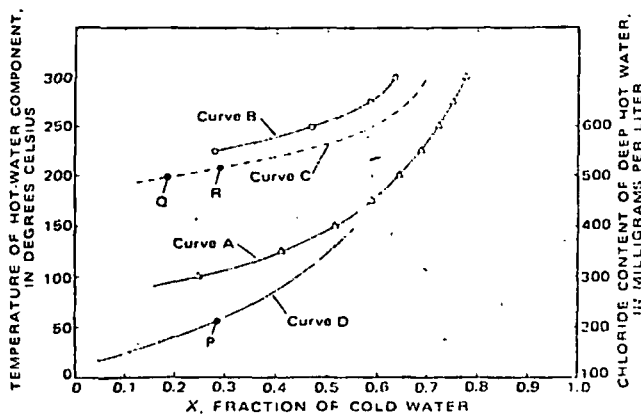


Figure 3.—Fraction of cold water relative to temperature and chloride content of hot-water component in Interchange Spring. Points P, Q, and R discussed in text. See figure 2 for explanation of symbols and curves.

The actual temperature and silica content of the "cold" component at the point of mixing can seldom if ever be known with certainty. If either the temperature or silica content of the cold water were higher than the assumed value, the resulting estimated temperature of the hot-water component would be too high.

Model 2

The enthalpy of the hot water in the zone of mixing is less than the enthalpy of the hot water at depth owing to escape of steam during ascent. The silica content of the hot-water component, however, is fixed by quartz solubility at depth and subsequent enrichment in the liquid water fraction as steam separates. At the point where steam escapes from the ascending hot water and steam mixture, S in figure 1B, the residual silica concentration in the hot water increases and is given by the equation

$$\text{Residual silica} = \frac{\text{Original silica}}{1-y} < 1 \quad (7)$$

where y is the fraction of steam formed during movement of water from depth to S.

If one assumes a temperature, t_s , at which steam escapes, it is possible to calculate the residual silica for that condition and, using that information, estimate the original hot-water temperature before steam separates. In general, we set t_s equal to the boiling temperature imposed by local atmospheric conditions. This requires that escape of steam at point S of figure 1B occurs at atmospheric pressure, and our calculation yields a minimum probable temperature for the hot-water aquifer. The calculation is carried out as follows:

1. Use the atmospheric boiling temperature for the value of H_{hot} in equation 2 and calculate the corresponding value of X .
2. Use that value of X in equation 3 to estimate the residual silica content of the hot water at t_s .
3. Use the calculated residual silica content and curve A of Fournier and Rowe (1966, fig. 5) to estimate the original subsurface temperature before separation of steam. Curve A of Fournier and Rowe is roughly approximated by the equation

$$-\log C = \frac{1522}{t_{\circ C} + 273} - 5.75 \quad (8)$$

If superheated steam emerges from nearby fumaroles or if there are other reasons for believing that steam escapes at greater than atmospheric pressure, an alternate procedure should be used:

1. Assume a value of t_s appropriate for the pressure at which steam is thought to escape at point S of figure 1B.
2. Use steam tables (or table 1) to determine the heat content of liquid water in calories per gram at t_s and substitute

that value in equation 2 to estimate a corresponding value of X .

- Use that value of X in equation 3 to estimate the residual silica content of the hot water at t_s .
- Estimate the silica content, C , that would have been present in the hot-water component if steam had escaped at atmospheric pressure using the relation

$$C = \frac{\text{Residual silica}}{1 - \frac{x}{1-y}} \quad (9)$$

where X is the fraction of steam that would be formed in going from t_s to the boiling temperature at atmospheric pressure (see fig. 4) and y is the fraction of steam formed in going from the original temperature to t_s . Both y and C are unknown in equation 8. However, the value of y will generally range from 0 to about 0.3, and as a first approximation it can be set equal to 0.1.

- Use the value of C and Curve A of Fournier and Rowe (1966, fig. 5) or equation 8 to estimate the original subsurface temperature before separation of steam.

A more precise estimate is possible if an iterative process is used in which the value of y is adjusted to reflect successive estimates of the original temperature. In general, we do not believe that the overall accuracy of the method warrants this additional effort.

EXAMPLES OF APPLICATION

These mixing models proposed have been applied to a few large-flowing warm springs in Yellowstone National Park. The results are geologically reasonable but have been substantiated by shallow drilling in the proximity of only one (Interchange Spring) of the springs in question.

The average silica content of the nonthermal ground water in the park was found to be 25 ± 2 mg/l and the temperature of the coldest spring was 5°C , in good agreement with the mean annual temperature of 4°C .

Terrace Spring near Madison Junction flows at about 5,500 l/min, the water temperature is 62°C , and silica content is 140 mg/l (Allen and Day, 1935, p. 353-354). The sodium, potassium, and calcium contents of the water yield an estimated aquifer temperature of 200°C , using the method of Fournier and Truesdell (1973). As this temperature is far greater than the spring temperature of 62°C , the spring is assumed to be a mixed-water type.

Calculated fractions of cold water, assuming various temperatures of hot water and using model 1 and equations 4 and 5, are listed in table 2, column 1, and are plotted in figure 2, curves A and B. The curves intersect at 265°C and a cold water fraction of 0.79. This is a very high estimated aquifer temperature and can be thought of as the maximum probable temperature of the hot-water component.

Although there are no nearby fumaroles, boiling pools, or other physical evidence that points to model 2 as a reasonable possibility, we have applied that model to Terrace Spring in order to establish a lower limit to the probable maximum subsurface temperature at that locality.

Curve C of figure 2 was generated by assuming various values of t_s and using equations 7 and 9 and other relations as discussed in the section on calculations. If steam escaped at atmospheric pressure from an ascending boiling water, the hot-water component would have been at about 92°C at the time of mixing with cold water, and the original temperature of that hot water would have been 165°C (point Q, fig. 2). This is the minimum probable temperature of the aquifer supplying the hot-water component. If higher pressures are assumed for escape of steam, larger fractions of cold water are required and higher estimated aquifer temperatures result, as shown by curve C, figure 2. Again, the probable upper temperature limit is about 265°C where curves A, B, and C intersect at a common point.

For Terrace Spring the aquifer supplying the hot water is probably closer to 265° than 165°C . The spring is located between Lower Geyser Basin (9 km to the south) and Norris Geyser Basin (14.5 km to the northeast) at a relatively low topographic position along the bounding fault of a large caldera (Keefer, 1971; Christiansen and Blank, 1972). Recent drilling by the U.S. Geological Survey has shown that subsurface temperatures beneath parts of Lower Geyser Basin exceed 205°C ; those beneath Norris Geyser Basin exceed 240°C (White and others, 1968). Silica and Na-K-Ca geo-

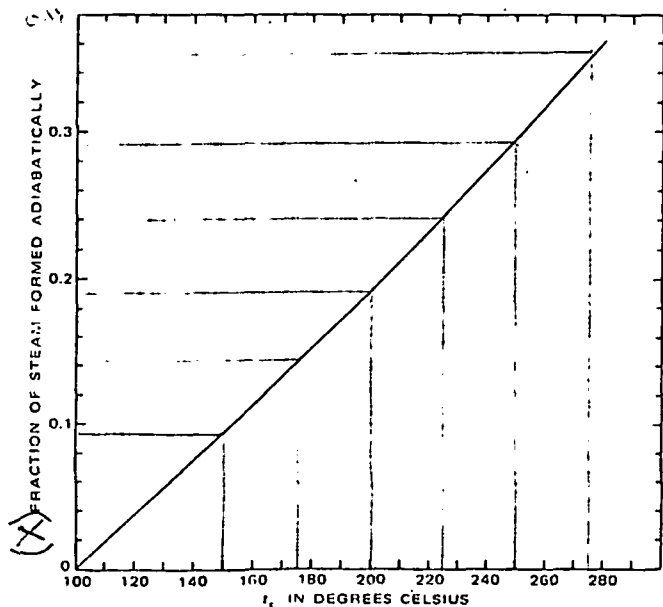


Figure 4.—Fraction of steam that would form by adiabatic cooling from t_s to 100°C .

Table 2.—Values of X_1 and X_{Si} at different assumed temperatures of the hot-water component for warm springs in Yellowstone National Park [See text for details]

Temperature (assumed) of hot water (°C)	1		2		3		4	
	X_1 ($t=62^\circ\text{C}$)	X_{Si} ($\text{SiO}_2=140\text{ mg/l}$)	X_1 ($t=49^\circ\text{C}$)	X_{Si} ($\text{SiO}_2=100\text{ mg/l}$)	X_1 ($t=61^\circ\text{C}$)	X_{Si} ($\text{SiO}_2=122\text{ mg/l}$)	X_1 ($t=76^\circ\text{C}$)	X_{Si} ($\text{SiO}_2=270\text{ mg/l}$)
50	0.022
75	0.186371	0.200
100	.401537410	0.253
125	.527635534410
150	.610699	0.250	.616	0.030	.514
175	.669	0.280	.744	.531	.674	.394	.587
200	.713	.521	.778	.688	.718	.596	.642
225	.748	.662	.805	.779	.792	.715	.686	0.279
250	.776	.751	.827	.837	.780	.790	.721	.469
275	.799	.805	.845	.873	.803	.835	.750	.584
300	.820	.828	.861	.888	.823	.855	.775	.633

1. Terrace Spring near Madison Junction. Flow approximately 5,550 l/min. Data from Allen and Day (1935).

2. Spring 1.4 km N. of Biscuite Basin, about 8 m E. of road. Flow about 190 l/min.

3. Spring 2.25 km N. of Biscuite Basin, about 60 m E. of road. Flow about 100 l/min.

4. Interchange Spring, Black Sand Basin. Flow about 2,300 l/min.

thermometers applied to boiling hot-spring water at Norris suggest subsurface temperatures of 250° to 270°C .

The chloride content of Terrace Spring, 64 mg/l is consistent with the higher aquifer temperature and correspondingly large calculated fraction of cold water. Given the chloride concentration in the spring and the average chloride in nonthermal water in the region ($<1\text{ mg/l}$), the chloride content of the deep hot water can be calculated, assuming any given proportion of hot and cold water. Curve D, figure 2, shows the results of that calculation. For a cold-water fraction of 0.79, the chloride content of the hot-water fraction would be about 300 mg/l (point P, fig. 2). This is close to the chloride content of thermal water (before steam loss) found at Lower Geysir Basin.

The second example is one in which mixing model 1 fails, but model 2 gives excellent results. Interchange Spring in Black Sand Basin came into being as a result of an excavation for a highway interchange for diverting traffic around the Old Faithful area. The spring had a temperature of 76°C , a silica content of 270 mg/l, and a flow rate of about 2,000 l/min. The Na-K-Ca content suggests a temperature of 205°C . The calculated fractions of cold water at given temperatures of the hot-water component are listed in table 2, column 4, and plotted in figure 3.

The most notable feature of figure 3 is that curve A, based on enthalpy considerations, and curve B, based on model 1 silica considerations, do not intersect. Evidently either steam escaped from the hot-water component before mixing or the warm spring water dissolved extra silica after mixing occurred. The warm water may be picking up extra silica, for it emerges from sands and gravels composed mostly of fresh obsidian. The obsidian glass could dissolve and raise aqueous silica to saturation with respect to amorphous silica. At 76°C the solubility of amorphous silica is 266 mg/l, which is within the

analytical error of the 270 mg/l silica found in the spring water.

We favor the first alternative because the large rate of flow makes equilibration with amorphous silica unlikely and because model 2 gives results in close agreement with what is known about subsurface temperatures near Interchange Spring.

The variation of original hot water temperature relative to the fraction of cold water in the warm spring, curve C, figure 3, is based on model 2 silica considerations. If steam escaped at atmospheric pressure before mixing of hot and cold water, the remaining hot water would have been at 92°C (boiling temperature at the altitude of the spring) and its original temperature would have been about 200°C (point Q, fig. 3).

About the same temperature is estimated from chloride considerations. The chloride content of Interchange Spring is 224 mg/l, the calculated chloride contents of the hot-water component, assuming various fractions of mixed cold water, are shown by curve D, figure 3. The highest concentration of chloride found in discharging boiling springs and geysers in Black Sand Basin was 315 mg/l. Presumably this is the residual chloride concentration attained after maximum separation of steam owing to adiabatic cooling of the ascending water. Therefore, the maximum chloride content of the hot-water component in Interchange Spring is likely to have been 315 mg/l; the corresponding maximum fraction of cold water, 0.285 (point P, fig. 3). This requires that the hot-water component have a temperature of 110°C or less at the time of mixing. For a cold water fraction of 0.285, curve C of figure 3 shows an original hot-water temperature of about 208°C (point R).

The silica contents of boiling springs and geysers in the vicinity of Interchange Spring indicate an aquifer temperature of 190° to 205°C . In addition, two shallow holes drilled near-

by indicate subsurface temperatures exceeding 170° to 180°C. Both holes were terminated before a maximum or leveling-off temperature was attained. One hole is about 900 m to the southeast and had a bottom-hole temperature of 180°C (Fenner, 1936). The other is about 600 m to the west and had a bottom-hole temperature of 170°C (White and others, 1968; Honda and Muffler, 1970).

Apparently the hydrologic system supplying water to Interchange Spring is very similar to model 2. We suggest that the hot-water fraction of the mixed water in Interchange Spring comes from an aquifer at 200° to 208°C. That water cools adiabatically, forming steam as it rises toward the surface. At a shallow level, but before mixing with cold water occurs, the high-enthalpy steam fraction escapes from the remaining lower enthalpy liquid water. This low-enthalpy water at 92° to 110°C then encounters cold ground water and a mixed water at 76°C results. The separated steam fraction probably emerges 350 m northwest of Interchange Spring at the Pine Springs group, where violently boiling springs occur with little or no discharge.

Ideally, large-flow warm springs in a given locality with different temperatures and different compositions should give the same estimated hot-water temperature. Such is found for two large-flow unnamed springs located between Biscuit Basin and Midway Geyer Basin in Yellowstone National Park. The springs have temperatures of 49° and 61°C and silica contents of 100 and 122 mg/l respectively, (table 2, cols. 2 and 3). Applying model 1, the intersection of curves A and B, figure 5, indicates a cold-water fraction of 0.82 for the 49°C spring and 243°C as the maximum probable temperature of the hot-water component. The intersection of curves C and D, figure 5, gives exactly the same temperature, 243°C; for the high-temperature component of the 61°C water. As expected, the fraction of cold water, 0.77, is less in the 61°C water than in the 49°C water. Applying model 2, and assuming $t_s = 100^\circ\text{C}$, a minimum probable temperature of 166°C is obtained for the original temperature of the hot-water component in each spring, which indicates clearly that two waters are mixing in different proportions. Unfortunately, additional data is insufficient to indicate whether the higher or lower estimated temperature of hot-water component is more nearly correct.

CONCLUSIONS

The water in both boiling and nonboiling springs may be a mixture of hot water coming from depth and of cold, near-surface meteoric water. Under favorable conditions nonboiling thermal springs with large rates of flow may yield information about the temperature or range in probable temperatures of the hot-water component and the fraction of cold water in the mixture.

The assumptions necessary for using the mixing models described in this paper probably will not be met in most places. However, even a 10-percent success rate would make

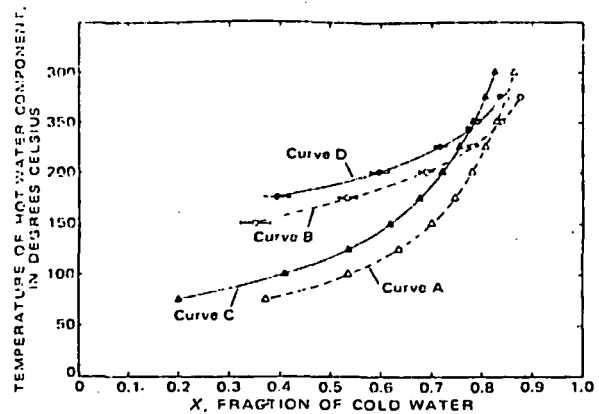


Figure 5.—Fraction of cold water relative to temperature of hot-water component in two springs located between Biscuit and Midway Basins. See figure 2 for explanation of curves and symbols: open symbols refer to the 49°C water and solid symbols to the 61°C water.

them valuable adjuncts of other methods for evaluating the geothermal potential of an area.

REFERENCES CITED

- Allen, E. T., and Day, A. L., 1935, Hot springs of the Yellowstone National Park: Carnegie Inst. Washington Pub. 466, 525 p.
- Christiansen, R. L., and Blank, H. R., Jr., 1972, Volcanic stratigraphy of the Quaternary rhyolite plateau in Yellowstone National Park: U.S. Geol. Survey Prof. Paper 729-B, 18 p.
- Ellis, A. J., 1970, Quantitative interpretation of chemical characteristics of hydrothermal systems, in United Nations Symposium on the Development and Utilization of Geothermal Resources, Pisa 1970, v. 2, pt. 1: Geothermics, Spec. Issue 2, p. 516–528.
- Fenner, C. N., 1936, Bore-hole investigations in Yellowstone Park: Jour. Geology, v. 44, p. 225–315.
- Fournier, R. O., 1973, Silica in thermal waters: Laboratory and field investigations, in Proceedings of International Symposium on Hydrogeochemistry and Biogeochemistry, Japan 1970, Volume 1, Hydrochemistry: Washington, D.C., J. W. Clark, p. 122–139.
- Fournier, R. O., and Rowe, J. J., 1966, Estimation of underground temperatures from the silica content of water from hot springs and wet-steam wells: Am. Jour. Sci., v. 264, p. 685–697.
- Fournier, R. O., and Truesdell, A. H., 1970, Chemical indicators of subsurface temperature applied to hot spring waters of Yellowstone National Park, Wyoming U.S.A., in United Nations Symposium on Development and Utilization of Geothermal Resources, Pisa 1970, Proc., v. 2, pt. 1: Geothermics, Spec. Issue 2, p. 529–535.
- Fournier, R. O., and Truesdell, A. H., 1973, An empirical Na-K-Ca geothermometer for natural waters: Geochim. et Cosmochim. Acta, v. 37, p. 1255–1275.
- Fournier, R. O., White, D. E., and Truesdell, A. H., 1974, Geochemical indicators of subsurface temperature—Part 1, Basic assumptions: U.S. Geol. Survey Jour. Research, v. 2, no. 3, p. 259–262.
- Honda, S., and Muffler, L. J. P., 1970, Hydrothermal alteration in core from research drill hole Y-1, Upper Geyser Basin, Yellowstone National Park, Wyoming: Am. Mineralogist, v. 55, p. 1714–1737.
- Keefer, W. R., 1971, The geologic story of Yellowstone National Park: U.S. Geol. Survey Bull. 1347, 92 p., 1 plate.
- Keenan, J. H., and Keyes, F. G., 1936, Thermodynamic properties of steam: New York, John Wiley, 89 p.

Keenan, J. H., Keyes, F. G., and Moore, J. G., 1969, Steam tables. Thermodynamic properties of water, including vapour, liquid, and solid phases: New York, John Wiley, 162 p.

Kharaka, Y. K., and Barnes, Ivan, 1974, SOLMNEQ: Solution mineral equilibrium computations: U.S. Dept. Commerce, Natl. Tech. Inf. Service, PB-215 899, 82 p.

Mahon, W. A. J., 1966, Silica in hot water discharged from drillholes at Wairakei, New Zealand: New Zealand Jour. Sci, v. 9, p. 135-144.

Morey, C. W., Fournier, R. O., and Rowe, J. J., 1962, The solubility of quartz in water in the temperature interval from 29° to 300°C: *Geochim. et Cosmochim. Acta*, v. 26, p. 1029-1043.

Truesdell, A. H., Fournier, R. O., and Thompson, J. M., 1973, Mixture, a computer program for the calculation of hot water temperature

and mixing fractions of large volume warm springs of mixed water origin: U.S. Dept. Commerce, Natl. Tech. Inf. Service, PB-220 732, 12 p.

Truesdell, A. H., and Jones, B. F., 1973, WATEQ, a computer program for calculating chemical equilibria in natural waters: U.S. Dept. Commerce, Natl. Tech. Inf. Service, PB-220 464, 77 p.

White, D. E., Muffler, L. J. P., Truesdell, A. H., and Fournier, R. O., 1968, Preliminary results of research drilling in Yellowstone thermal areas [abs.]: *Am. Geophys. Union Trans.*, v. 49, p. 358.

White, D. E., 1974, Geochemistry applied to the discovery, evaluation, and exploitation of geothermal energy resources, in *United Nations Symposium on Development and Utilization of Geothermal Resources*, Pisa 1970, v. 1, pt. 2: *Geothermics*, Spec. Issue 2 (In press.)

SUBJ
GCHM
GRF

UNIVERSITY OF UTAH
RESEARCH INSTITUTE
EARTH SCIENCE LAB.

CHAPTER 7—GENETIC AND RADIOACTIVITY FEATURES OF SELECTED LAMPROPHYRES

By R. C. EMMONS, C. D. REYNOLDS, AND D. F. SAUNDERS

INTRODUCTION AND CONCLUSIONS

In Chapters 5 and 6 we have called attention to the mobile late alkaline solutions formed on the cooling of feldspar. In Chapter 6 we suggested their role in the formation of nepheline syenite, a leucocratic rock type, and here we outline their apparent influence in the formation of lamprophyre, a melanocratic rock type. Our conclusion is that lamprophyre dikes are derived from the immediate walls of their host rocks, as an accumulation of deuteric-type material composed prominently of these alkaline solutions, modified by selectively resorbed mafic material encountered enroute to centers of accumulation. The source areas of mafic material may be recognized. Whereas the syenites were described as forming at temperatures of normal granite crystallization, whatever that temperature may be, lamprophyres, we believe, form at the lower temperature of the deuteric solutions of granite, again an unknown value.

We have studied the mafic-mineral content of some Wisconsin granites after observing that most of the granite quarries of the area have one or more lamprophyre dikes and that those which do not have, such as the Athelstane quarry, are higher in mafic minerals. The study revealed a quantitative relationship.

We have learned, too, that some radioactive materials are closely associated with lamprophyric accumulations. Lamprophyric materials, in contrast to radioactive materials, are highly pigmented and therefore readily recognized in the field. We suggest the value of lamprophyric accumulations to indicate potential radioactive concentrations.

CURRENT OPINIONS

Several writers have recognized unique features in the analyses of lamprophyres, such as the high content of iron and magnesium together with the high content of the alkalis. Harker (1935, p. 150) says "Chemically they are characterized by containing with a medium or low silica percentage, a considerable relative quantity of alkalis (especially potash) while the oxides of the diatomic elements are also abundantly represented". Bowen (1928, p. 259) in discussing the alnoites says "The general character of the group is a richness in ferromagnesian constituents combined with a richness in alkalis, which combination of characters is indeed rather distinctive of lamprophyres in general."

Lamprophyres, in their high iron and magnesium content, resemble the early products of crystal fractionation, but in their high alkali content resemble the late products of crystal fractionation. The problem is to reconcile these two apparently incompatible aspects. Also, the highly varied composition of lamprophyres, reflected in their extensive classification, is quite as demanding of an explanation, though it is less commonly cited as a problem. Bowen (1928, p. 258) says, "Perhaps lamprophyres are too broad and ill-defined a group to enable one to make a general state-

Handwritten marks or scribbles in the top right corner.

A single small black dot or mark in the center of the page.

ment concerning them, to which no exception might be taken." If we regard lamprophyres as diaschistic dikes, their compositional range, mineralogically and chemically, stands in baffling contrast to that of their leucocratic equivalents.

To explain lamprophyres Bowen (1928, p. 259) pertinently developed a theory of reaction between an alkali liquid and augite and olivine with the production of new minerals. He speaks (p. 270) of the sinking of hornblende into a region of somewhat hotter liquid, not to be redissolved as such, and (p. 271) of the sinking of biotite either alone or with hornblende, and its reactive solution in "hot" liquid. He defines "hot" liquid as "not superheated liquid but merely liquid not yet saturated with hornblende." Of the resulting complex liquid with its crystal burden he says "The separation of liquid from crystals, say by a squeezing out process, would appear to be the most promising method of developing liquids that are strongly alkaline and at the same time rich in ferromagnesian constituents. . . ." Smith (1936, p. 378) proposed a reaction between magma and xenolithic material to produce lamprophyric liquid. Reynolds (1938) called on transfusion phenomena to explain the varieties of lamprophyric rocks in the Newbery district.

THE PRESENT PROPOSAL

Our studies of selected Wisconsin lamprophyres suggest that lamprophyre dikes and similar mafic-mineral segregations are (1) the products of very late reactions in the cooling history of an igneous rock, (2) derived from the walls of a fracture under the influence of differential pressures created dilatantly, (3) commonly gathered from small tributary fractures into larger fractures, providing a gradation from small dark "deuteric veinlets" through dikelets to sizeable dikes. The lamprophyres of one group of four closely spaced quarries (NE $\frac{1}{4}$ SW $\frac{1}{4}$ Sec. 36, T. 30 N., R. 8 E.) indicate possible movement of lamprophyric material a quarter of a mile. Probably the movement is usually less than that except in large dikes.

The inception of lamprophyric material appears to be attributable to a reaction between very late alkaline liquid and already crystallized mafic minerals such as hornblende, biotite, and even chlorite, to bring about the selective resolution of their constituent oxides. Bowen has developed the chemistry of such reaction in his discussion of the sinking of ferromagnesian minerals in alkaline liquid. The alkaline liquid referred to in this discussion is the interstitial liquid formed on the cooling of feldspar. It is therefore dispersed throughout the rock and is in intimate contact with the crystallized mafic minerals from which it gathers its iron and magnesium. From this interstitial position it apparently migrates under differential pressures, created by the fracturing of the rock, to those fractures where it appears as deuteric veinlets. Here it may remain or with continued fracturing it may gather further to form dikes (Pl. 11, figs. 3, 4, 5, 6, 8). Near the source of the lamprophyric liquids the wall rocks are measurably robbed of mafic constituents, which is interpreted as the result of the migration of solutions, with their newly acquired mafic content, to fractures and to dikes.

One occurrence showed a reversal of the pressure in a dike of accumulated lamprophyric material. The footwall of this nearly horizontal dike is dark but the hanging wall is not abnormally colored. Penetration of the wall must have been by gravity

in a manner s
dark at the di
maximum at

We sample
widths of the

Quarry
See figure
Footage from dike
Mafic mineral pe
Biotite per cent.
Chlorite per cent
N, of biotite

Lake Wausau
50, 15, 6, 1 from
Mt. Thom quar
1 from the dike.
per cent at 10 feet
Mundt quarry
at footages 50, 25
side, and .050-.09

mined by Rosi
was measured t
of mafic constit
dikes were mac
made on sampl
These studies
the dikes. Also
indicating a loss
a bleached zone
In one occurren
fingers out into
bleached. The p
Several illustr
able bleaching,
apparent stream
that all the lam
lection of mafic
follow support th
24, 25, 26, 27.

* Rosiwal counts, hea
and radioactivity dete

in a manner similar to ground water percolation. The footwall color grades from very dark at the dike wall to that of the granite 3 feet away. Saunders found a radioactive maximum at the contact (see below).

SELECTED OCCURRENCES

We sampled three quarries across the strikes of their lamprophyres for the full widths of the quarry exposures. The mafic mineral content of the samples was deter-

TABLE 10.—*Mafic mineral content of granite adjacent to lamprophyre*

Quarry.....	Lake Wausau		Mt. Thom		Mundt	
See figure.....	24		25		26, 27	
Footage from dike.....	80	1	100	1	50	1
Mafic mineral per cent.....	3.5	0.5	7.7	3.5	10-11	6-7
Biotite per cent.....	2.3	0.0	6.7	2.0	9-10	2-5.5
Chlorite per cent.....	1.2	0.5	1.0	1.3	0.8-2.2	3.8
N _z of biotite.....	1.666	1.660	1.663	1.658	1.645-1.653	1.640-1.645

Lake Wausau quarry—NE¼ SW¼ Sec. 36, R. 8 E., T. 30 N. 5 samples taken at footages 80, 50, 15, 6, 1 from the dike.

Mt. Thom quarry—NE¼ NE¼ Sec. 30, R. 30 E., T. 33 N. 3 samples taken at footages 100, 10, 1 from the dike. Not included in the table is amphibole—0.4 per cent at 1 and 100 feet and 0.1 per cent at 10 feet; also fluorite—1.5 per cent at 100 feet and 0 per cent at 1 foot.

Mundt quarry—SE¼ NE¼ Sec. 7, R. 21 E., T. 35 N. 6 samples taken, 3 on each side of the dike at footages 50, 25, 1 from the dike. Biotite birefringence at 50 feet ranges from .060-.100 on one side, and .050-.090 on the other. At 1 foot it is .010.

mined by Rosiwal count in thin section and the birefringence of the mafic minerals was measured to learn changes in relationship to the dikes. Heavy liquid separations of mafic constituents were made in the laboratory; geiger-counter studies across the dikes were made in the field; and thermoluminescence and radiation studies were made on samples in the chemistry department radiation laboratory.⁶

These studies show that the mafic mineral content in each quarry decreases toward the dikes. Also the refractive index (N_z) of the biotite decreases toward the dikes indicating a loss of iron. Many of the smaller lamprophyres studied in the field show a bleached zone on both sides of the dikelets, striking enough to be photographed. In one occurrence (Pl. 12, fig. 6) a well formed half-inch wide lamprophyre dikelet fingers out into a group of deuteritic veinlets around which the rock is distinctly bleached. The photograph is of a quarry block.

Several illustrations of this general effect (Pl. 11; Pl. 12, figs. 1, 4, 6) show noticeable bleaching, resulting from the depletion of mafic minerals, and also show an apparent streaming effect of the mafic minerals toward the lamprophyre. We believe that all the lamprophyric materials studied can be attributed confidently to the collection of mafic material from the walls of the dikes. The radioactivity studies to follow support this explanation. Detailed data are given in Table 10 and Figures 24, 25, 26, 27.

⁶ Rosiwal counts, heavy-liquid separations, and optical determinations were done by Reynolds. Thermoluminescence and radioactivity determinations were done by Saunders.

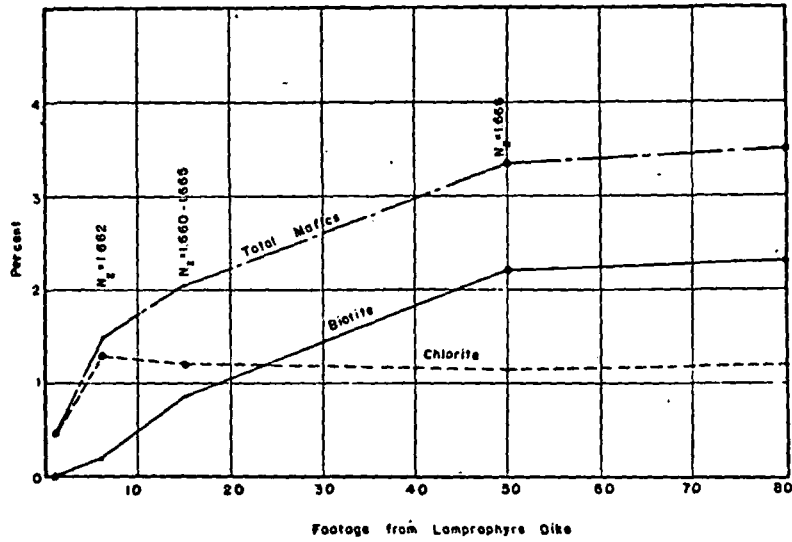


FIGURE 24.—Quantitative distribution of mafic minerals in the granite of the Lake Wausau quarry with respect to distance from the lamprophyre dike

Refractive indices for the biotite are given. Figures 24 to 27 are offered in support of the thesis that lamprophyric concentrations are derived from the rocks adjacent to them, through the selective resorption by deuteric solutions of the constituents of mafic minerals.

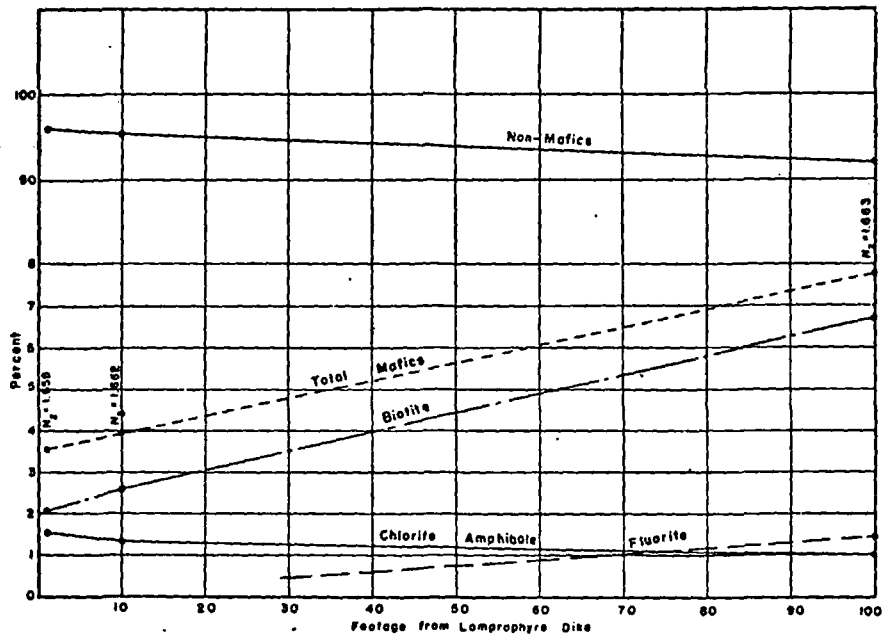


FIGURE 25.—Quantitative distribution of mafic minerals in the granite of the Mt. Thom quarry with respect to distance from the lamprophyre dike
Refractive indices for the biotite are given.

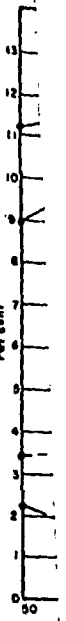


FIGURE 26.

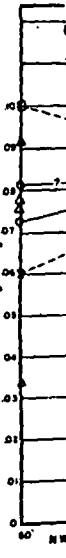


FIGURE 27.

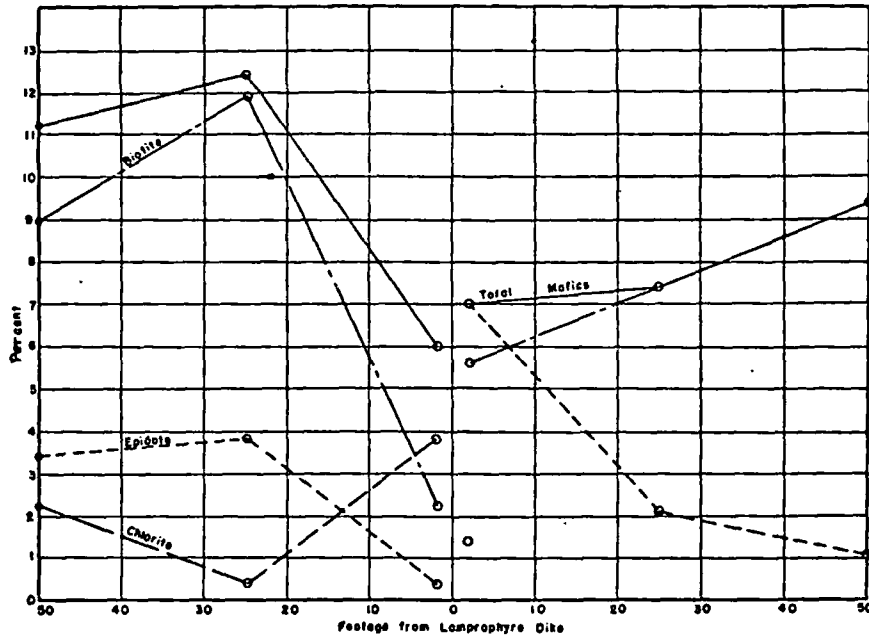


FIGURE 26.—Quantitative distribution of mafic minerals in the granite of the Mundt quarry, with respect to distance from the lamprophyre dike

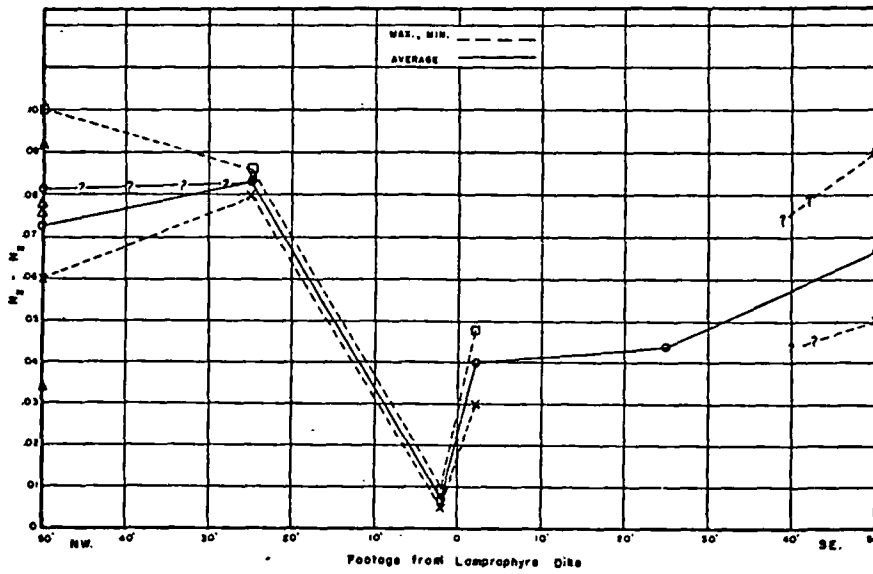


FIGURE 27.—Birefringence of biotite in granite of the Mundt quarry, with respect to distance from the lamprophyre

Fluorite is a prominent constituent of the wall rocks of some of the dikes but is usually limited to the areas somewhat remote from the dikes themselves or in them and their feeders. Fluorite and similar low-temperature constituents seem to behave as does the iron which colors the granite—it moves under pressure differentials to the area of lamprophyric accumulation. Fluorite is a prominent accessory in the large thin sections shown in the photomicrographs (Pl. 11, figs. 4, 8). It occurs only in association with the mafic minerals.

ASSOCIATION OF LAMPROPHYRES WITH PITCHBLENDE

On a highway traverse from Port Arthur to Kirkland Lake and the Soo, in company with Farrington Daniels of the Department of Chemistry of the University of Wisconsin, we visited several pitchblende localities including the Camray Mine on Theano Point at the east end of Lake Superior. The consistent association of pitchblende with lamprophyric materials was noticed but was recognized as outstandingly critical at the Camray Mine. Theano Point is areally transected by many reticulating lamprophyre dikes. All the pitchblende uncovered at that time was in the immediate walls of the dikes, in fractures in the granite. In Plate 12, figure 3 the main working is shown, located in a topographic depression attributable to a weathered-out lamprophyre.

Quantitative radioactivity measurements. Impelled by these observations we revisited several Wisconsin lamprophyres to study the distribution of radioactive material. This study included laboratory determinations of thermoluminescence and of radioactivity by new techniques developed by Daniels, and Geiger-counter measurements made in the field.

The amount of radioactivity was determined by counting the alpha tracks made on Eastman nuclear track plates, exposed for a month on smooth rock sections of granite cut by lamprophyric materials. The counting was done on a microscope equipped with a mechanical stage to make several traverses across each plate. The tracks within every fifth millimeter were counted, starting at the lamprophyre contact and measuring outward from it.

In every rock section studied, a maximum in the radioactivity distribution was found at the lamprophyre, and a concentration was found within some of the lamprophyric veinlets (Fig. 28). Figure 29, representing one section of a veinlet with accompanying bleached zones (Pl. 11, fig. 1), shows low radioactivity within the bleached zones and a higher concentration in the vein and beyond the bleached zones. Another section (Fig. 30) shows two concentrations at 15 mm from the dikelet (Pl. 9, fig. 7) in addition to that of the lamprophyre, possibly due to a second dilatant action which caused the central concentration. The height of the curve at the central concentration depends on the part of the vein which the section represents. It may be pitchblende as in Plate 11 figures 2, 4, 6 and 8.

Thermoluminescence studies were also made on these lamprophyric materials by special techniques to be described elsewhere. The method yields photos of luminescent minerals in heated sections and curves of luminescence on heating, recorded photoelectrically. We have termed these curves glow curves. Plate 10 figure 5 shows a heated section cut from the specimen shown in Plate 11 figure 3. The "hot spot"

is pitchbl
shows a c
From th
tances fro

28. Lo
T.
fig
Pla

29. Loc
T 3
figu

30. Loca
T 29
figure

FIGURES 28-30.

intense luminescence
in this veinlet
ably activated
thermoluminescence
granite, similar
their activation

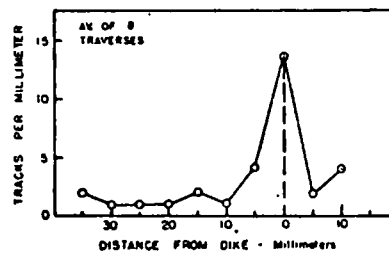
In the field,
meter equipped
represent the average
granite host at
a background c

The lamprophyre
and reveals only

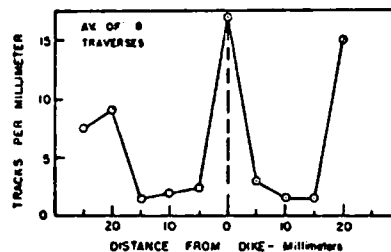
is pitchblende. A radioautograph of this section on Eastman nuclear track plates shows a corresponding concentration of radioactivity.

From this same specimen, sections parallel to the veinlet were cut at various distances from it for thermoluminescence study. There is a marked concentration of

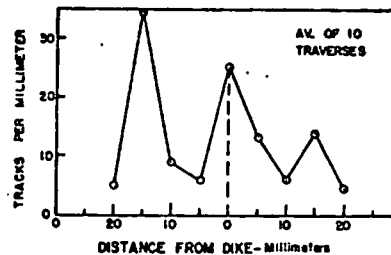
28. Location SW $\frac{1}{4}$ SW $\frac{1}{4}$ Sec. 14, R 7 E, T 30 N. Specimen shown in Plate 11, figure 3, and a polished section in Plate 11, figure 6.



29. Location NE $\frac{1}{4}$ SW $\frac{1}{4}$ Sec. 26, R 19 E, T 38 N. Specimen shown in Plate 11, figure 1 and in Plate 12, figure 4.



30. Location NW $\frac{1}{4}$ NW $\frac{1}{4}$ Sec. 28, R 7 E, T 29 N. Specimen shown in Plate 9, figure 7.



FIGURES 28-30. Distribution of radioactive material with respect to proximity to lamprophyric dikelets (deuteric veinlets)

intense luminescence at the veinlet (Fig. 31). Since pitchblende has been recognized in this veinlet the intense spots of thermoluminescence in this specimen were probably activated by the alpha particles from pitchblende. The distribution of intense thermoluminescence shows the distribution of radioactivity. In other specimens of granite, similar intense spots correspond to the locations of inclusions of zircon, their activations presumably accomplished by thorium.

In the field, analogous measurements were made with a Geiger-type field survey meter equipped with earphones. All the recorded values for gamma intensity represent the averages of several counts of 1-minute duration. The count taken over the granite host at the greatest possible distance from the lamprophyre was considered a background count.

The lamprophyre of the Lake Wausau Quarry is at the bottom of the workings and reveals only one contact. Counts (Table 11a) were made on freshly quarried

granite blocks containing a lamprophyre contact, on an adjacent zone of granite rich in mafic minerals, and on the host granite where it is relatively free of mafic minerals. There are two radioactivity maxima, one at the contact and one near the border of the mafic-rich granite.

Table 11b gives the record of gamma counts on a 6-foot wide lamprophyre in granite of the Red Granite Quarry at Red Granite, Wisconsin. Again the concentra-

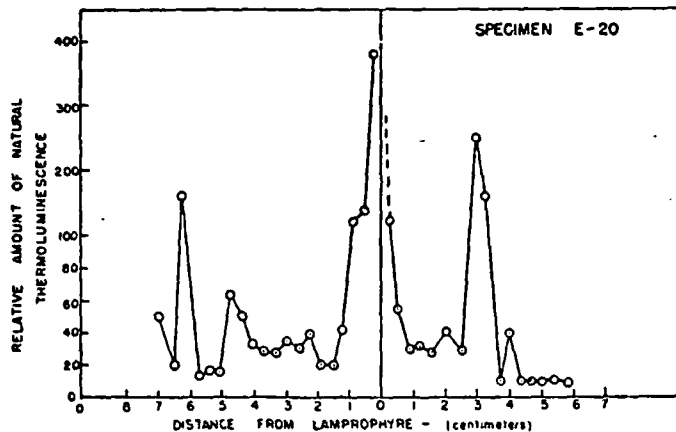


FIGURE 31.—Natural thermoluminescence near a lamprophyre dikelet
Specimen shown in Plate 11, figure 3.

tion of radioactivity is at the lamprophyre contact and is low both within and outside the dike. The pattern holds too for an associated 1-inch dike.

Pegmatitic material was studied in two contiguous gray syenite quarries (SW $\frac{1}{4}$ SE $\frac{1}{4}$ Sec. 14 and NE $\frac{1}{4}$ NW $\frac{1}{4}$ Sec. 23, R. 6 E., T. 29 N.) characterized especially by anorthoclase and arfvedsonite. Four quarried blocks were selected (Table 11c). Minor maxima occur in the pegmatites but are related to the amount of associated arfvedsonite. Major maxima occur in arfvedsonite concentrations.

In general the radioactivity has been concentrated at the lamprophyre-granite contacts and in deuteric veinlets—probably feeders. The highest concentration found was in the syenite pegmatites and especially in the lamprophyrelike lenses of arfvedsonite in and associated with pegmatites. A low background count was found in the syenite wall rocks of the syenite pegmatites.

INTERPRETATION OF THE GEOCHEMISTRY OF URANIUM

In the light of these findings we propose an outline of a part of the geologic behavior of uranium.⁷ It is most mobile as a halide and is a gas at slightly elevated temperatures as a fluoride (UF₆). On contact with water the hexafluoride is probably converted to the more stable tetrafluoride (UF₄) which is soluble, and therefore also mobile. Uranium halides which at most are a trace constituent of granite gather with the unmixed feldspathic, alkaline liquid discussed by Gates and drain deuteri-

⁷ We are indebted to Professor Farrington Daniels of the Chemistry Department, University of Wisconsin and to Dr. Josef Katz of the Argonne National Laboratory for helpful suggestions on the chemistry of uranium.

TABLE 11.—Radioactive measurements

Description	Count Range (c/m)	Determinations	Average Count (c/m)
a) Lake Wausau Quarry:			
Background.....	17-22	8	20
Lamprophyre-granite contact.....	32-46	7	36
Center of mafic-rich granite (6" from contact).....	18-20	3	19
Border of mafic-rich granite (1' from contact).....	28-32	3	29
Mafic-free granite (2' from contact).....	20-24	3	22
b) Red Granite Quarry:			
Background.....		3	20
Center of lamprophyre.....		2	18
Lamprophyre-granite contact.....		2	28
One foot from lamprophyre.....		2	19
Six feet from lamprophyre.....		2	20
One inch thick lamprophyre (100 feet from large dike).....		2	30
c) Gray Syenite Quarries:			
Block I			
Background (two feet from pegmatite wall).....		3	11
Center of pegmatite (with large crystals of arfvedsonite).....		3	19
Six inch wall zone concentration of medium-sized crystals of arfvedsonite..		3	23
Block II			
Background (two feet from pegmatite wall).....		2	13
Center of pegmatite (with large crystals of arfvedsonite).....		3	28
Four inch wall zone concentration of medium sized crystals of arfvedsonite.....		2	33
Block III			
Syenite, background (one foot from pegmatite wall).....		2	19
Syenite, six inches from pegmatite wall.		2	17
Arfvedsonite-free pegmatite.....		2	19
Arfvedsonite lens.....		3	55
Block IV			
Syenite, background (one foot from arfvedsonite lens).....		2	15
Arfvedsonite lens.....		3	34

cally into fractures along with accumulating lamprophyric materials. This liquid now consisting of alkaline materials derived from felspar, mafic materials derived from fractionally resorbed mafic minerals, and halides of such elements as iron and uranium is of very local origin but is fed into larger fractures. With increasing size of fracture it is less local in origin (Pl. 12, figs. 3 and 6). The amount of lampro-

SE
zone of granite
ely free of mafic
and one near the

lamprophyre in
n the concentra-

det

within and out-

quarries (SW 1/4
rized especially
ed (Table 11c).
nt of associated

rophyre-granite
entration found
e lenses of arf-
at was found in

UM

ologic behavior
vated tempera-
; probably con-
l therefore also
granite gather
l drain deuteri-

of Wisconsin and to
uranium.

phyre on Theano Point is so great it could scarcely be derived from the immediate walls. Some of the dikes are more than 20 feet wide, and they are numerous. On crystallization of the lamprophyre liquid the halides become a prominent constituent of its rest magma and are exuded at temperatures which for fluorite may be very low (Twenhofel, 1947). Observations indicate that the uranium halides may be precipitated at the immediate walls of the dikes as the oxide pitchblende, presumably

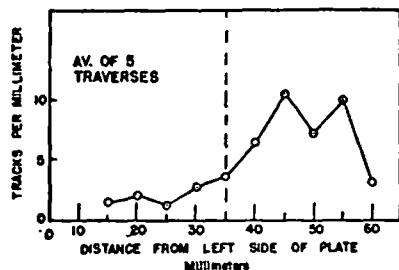


FIGURE 32.—Distribution of radioactive material with respect to proximity to a mafic (lamprophyric) segregation

Location NW $\frac{1}{4}$ SE $\frac{1}{4}$ Sec. 33, R 8 E T 30 N. Specimen shown in Plate 11, figure 7.

on contact with oxygen-bearing water, but may also move along shears and fault channels for some distance from the source. Iron halides behave similarly but are less sharply precipitated. They are carried farther to be dispersed as an oxide dust along the fractures of the granite or other host. This "iron stain" is a recognized uranium prospector's criterion.

We view pitchblende as a very low-temperature mineral of hydrothermal origin equivalent in temperature to fluorite. In this it is contrasted with uraninite. The concentration of uranium in commercial quantities is contingent on the agency of halogens which may or may not play a part in the formation of lamprophyres. Hence some lamprophyres are potential agents for the deposition of uranium and some are not.⁸

Some deuteric veinlet feeders to lamprophyres fail to convey their uranium content to its economic destination but carry "hot spots" of pitchblende in the veinlets (Pl. 10, fig. 5; Pl. 11, figs. 2, 3, 4, 6, 8). Such paper-thin veinlets may give an entire outcrop of granite the capacity to register on a Geiger counter above background. An interesting large-scale example of this type of occurrence is found on the property being developed at the west end of Jean Lake, north of Goldfields, Saskatchewan.

Thin sections were cut from specimens collected on the Camray property by Messrs. Kilgour and Heale at various places along the lamprophyre dikes, selected for proximity to or remoteness from spots of pitchblende concentration. Near such concentrations, the lamprophyre in section is paler and has mafic minerals of lower birefringence and less pleochroism. We believe that the iron has been partly carried out along with the uranium through halogen influence, and has been dispersed in the granite host. Mr. Kilgour called our attention to the color contrast in the thin

⁸ Since this was written the following incomplete experiment was made: Pitchblende in the presence of gently moving chlorine gas below 200°C transferred to a cooler part of the containing chamber and deposited a translucent gelatinous and botryoidal encrustation on feldspar surfaces. The deposit is probably uranyl chloride. By introducing a very small amount of air the gelatinous encrustation was converted to a black hard botryoidal material which appears to be pitchblende.

section
helpful

During
so com
or horn
common
which t
SE $\frac{1}{4}$ S
a radio
supports
sions—ti

Lamp
body. In
be fed b
of the hi
of the al
tive reso
position
sorption

section seen merely by holding it to the light. This general observation may be a helpful prospecting guide.

CONCLUDING REMARKS

During the years of this study we have viewed the segregations of mafic materials so common in granite, usually explained as dispersed xenolithic material of chloritic or hornblendic character (Pl. 12, fig. 5). This explanation militates against the very common observation of true xenoliths in all stages of ghost disappearance during which they retain their outlines undisturbed. One specimen (Pl. 11, fig. 7) (NW $\frac{1}{4}$ SE $\frac{1}{4}$ Sec. 33, R. 8 E., T. 30 N.) studied with Eastman nuclear track plates showed a radioactivity distribution analogous to that of lamprophyres (Fig. 32). This strongly supports the view that such mafic segregations are truly segregated and not dispersions—they are lamprophyric.

Lamprophyric material ranges widely in degree of concentration and in size of body. In veinlets it is readily recognized as deuteritic, but in dikes which appear to be fed by these veinlets its deuteritic character is less apparent. A simple explanation of the highly varied composition of lamprophyres is the possible range in composition of the alkaline feldspathic liquid, which demands much further study, and the selective resorption of mafic materials by this liquid. Not only is there a range in the composition possible in the original liquid but there is also a range in the fractional resorption by such a liquid.

USE

in the immediate
re numerous. On
inent constituent
ite may be very
ides may be pre-
ende, presumably

of radioactive
proximity to a
segregation

Sec. 33, R 8 E
in Plate 11,

shears and fault
similarly but are
as an oxide dust
" is a recognized

hydrothermal origin
th uraninite. The
on the agency of
prophyres. Hence
ium and some are

their uranium con-
de in the veinlets
lets may give an
enter above back-
ce is found on the
f Goldfields, Sas-

ray property by
re dikes, selected
ration. Near such
minerals of lower
een partly carried
been dispersed in
ntrast in the thin

presence of gently moving
a translucent gelatinous
introducing a very small
material which appears to

*From draft of
GeoTh Index in the, #2*

TABLE OF CONTENTS

	Page
Geochemical Thermometers	35
Summary of Geochemical Thermometers Available	35
Silica Geochemical Thermometers	36
The Sodium-Potassium and Sodium-Potassium- Calcium Geochemical Thermometers	37
Dilution Effects, the Use of the Geochemical Thermometers and Mixing Models	38

TABLES

Table	Page
1. Enthalpies of liquid water and quartz solubilities	39
2. X_t and X_{Si} values at specified temperatures and silica concentrations for thermal waters of the Camas-Prairie area	42

ILLUSTRATIONS

Figure	Page
1. Silica concentration in geothermal water vs. estimated temperature	36
2. Silica in thermal waters	37
3. Fraction of cold water relative to temperature for well 1S-17E-23aabl	41

*3. X_t and X_{Si} values at specified
 temperatures and silica concentrations
 for thermal waters of the
 Camas-Prairie area*

*4. X_t and X_{Si} values at specified
 temperatures and silica concentrations
 for thermal waters of the
 Camas-Prairie area*

*5. X_t and X_{Si} values at specified
 temperatures and silica concentrations
 for thermal waters of the
 Camas-Prairie area*

GEOCHEMICAL THERMOMETERS

Young and Mitchell (1973) gave a brief review of the then available geochemical thermometers. Their summary is as follows:

"Summary of Geochemical Thermometers Available

In recent years the concentrations of certain chemical constituents dissolved in thermal waters have been used to estimate water temperatures in the thermal aquifer. However, these geochemical thermometers are useful only if the geothermal system is of the more common hot-water type rather than of the vapor-dominated or steam type, none of which is known to occur in Idaho.

Geochemical thermometers that are useful in describing and evaluating geothermal systems (excluding the sodium-potassium-calcium thermometer) have been summarized by White (1970). Part of his summary is as follows:

'Chemical indicators of subsurface temperatures in hot-water systems.

Indicator	Comments
1) SiO ₂ content	Best of indicators; assumes quartz equilibrium at high temperature, with no dilution or precipitation after cooling.
2) Na/K	Generally significant for ratios between 20/1 to 8/1 and for some systems outside these limits; see text.
3) Ca and HCO ₃ contents	Qualitatively useful for near-neutral waters; solubility of CaCO ₃ inversely related to subsurface temperatures; see text and ELLIS (1970).
4) Mg; Mg/Ca	Low values indicate high subsurface temperature, and vice versa.
5)
6) Na/Ca	High ratios may indicate high temperatures (MAHON, 1970) but not for high Ca brines; less direct than 3?
7) Cl/HCO ₃ + CO ₃	Highest ratios in related waters indicate highest subsurface temperatures (FOURNIER, TRUESDELL 1970) and vice versa.
8) Cl/F	High ratios may indicate high temperature (MAHON, 1970) but Ca content (as controlled by pH and CO ₃ ²⁻ contents) prevents quantitative application.

9) ...

10) Sinter deposits

Reliable indicator of subsurface temperatures (now or formerly) 180°C.

11) Travertine deposits

Strong indicator of low subsurface temperatures unless bicarbonate waters have contacted limestone after cooling.

The general principles and assumptions on which the use of geochemical thermometers (White, 1970) is based are: (1) the chemical reactions controlling the amount of a chemical constituent taken into solution by hot water are temperature dependent; (2) an adequate supply of these chemical constituents is present in the aquifer; (3) chemical equilibrium has been established between the hot water and the specific aquifer minerals which supply the chemical constituents; (4) hot water from the aquifer flows rapidly to the surface; and (5) the chemical composition of the hot water does not change as it ascends from the aquifer to the surface.

The fact that these principles and assumptions more often than not cannot readily be verified in a field situation requires that the concept of geochemical thermometers be applied with caution and in full recognition of the uncertainties involved. With that understanding, geochemical thermometers provide a useful point of departure for reconnaissance screening and provisional evaluation of thermal areas.

Silica Geochemical Thermometer

The silica method of estimating aquifer temperatures (Fournier and Rowe, 1966) appears to be the most accurate and useful proposed to date. Experimental evidence has established that the solubility of silica in water is most commonly a function of temperature and the silica species being dissolved, (fig. 1).

Practical use of the silica geochemical thermometer assumes that there is

equilibration of dissolved silica with quartz minerals in high-temperature aquifers and that the equilibrium composition is largely preserved in the silica-bearing thermal waters during their ascent to the surface. White (1970) stated that while equilibrium is generally attained at high aquifer temperatures, silica may precipitate rapidly as waters cool to about 180°C and, therefore, the silica method commonly fails to predict actual aquifer temperatures much above 180°C. The rate of precipitation of silica decreases rapidly as the temperature cools below 180°C.

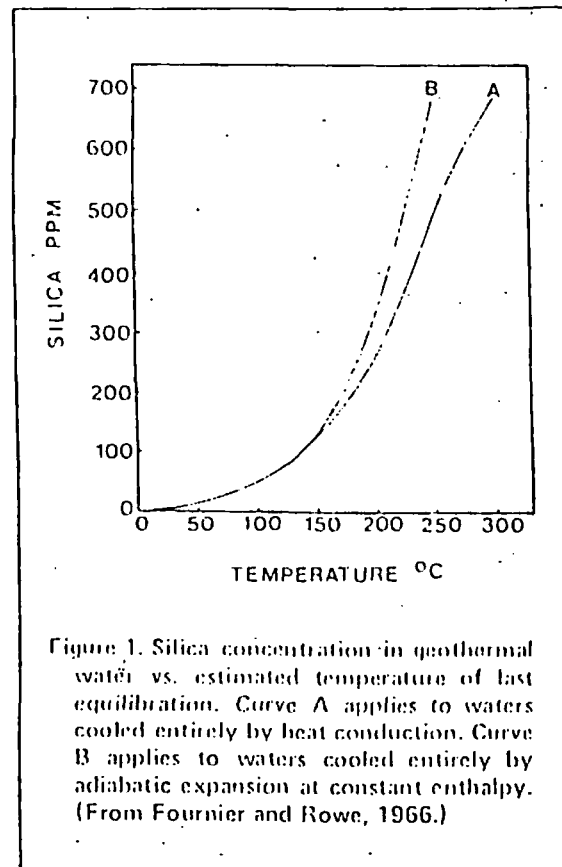


Figure 1. Silica concentration in geothermal water vs. estimated temperature of last equilibration. Curve A applies to waters cooled entirely by heat conduction. Curve B applies to waters cooled entirely by adiabatic expansion at constant enthalpy. (From Fournier and Rowe, 1966.)

White (1970) also cautioned against using the silica geochemical thermometer in acid waters which have a low chloride concentration, because at temperatures near or below 100°C these waters are actively decomposing silicate minerals and thereby releasing highly soluble amorphous SiO₂. In this case, the basic assumption of equilibration with quartz would be rendered invalid."

The amorphous silica curve (fig. 2) would give more accurate aquifer temperature predictions in acid waters.

Arnórsson (1970, p. 537, 1975, p. 763) found that chalcedony generally controls silica concentration in Iceland's thermal waters when aquifer temperatures are below 100-110°C. The chalcedony curve

(fig. 2) probably should be given consideration when the silica method using the quartz curve indicates temperatures about 10-20°C above Arnórsson's 110°C upper limit.

"The Sodium-Potassium and Sodium-Potassium-Calcium Geochemical Thermometers

The sodium-potassium (Na/K) geochemical thermometer plots the log of the atomic ratios of Na/K against the reciprocal of the absolute temperature. White (1970) stated that ratios are of general significance only in the ratio range between 8/1 and 20/1. He also reported that Na/K temperatures are not significant for most

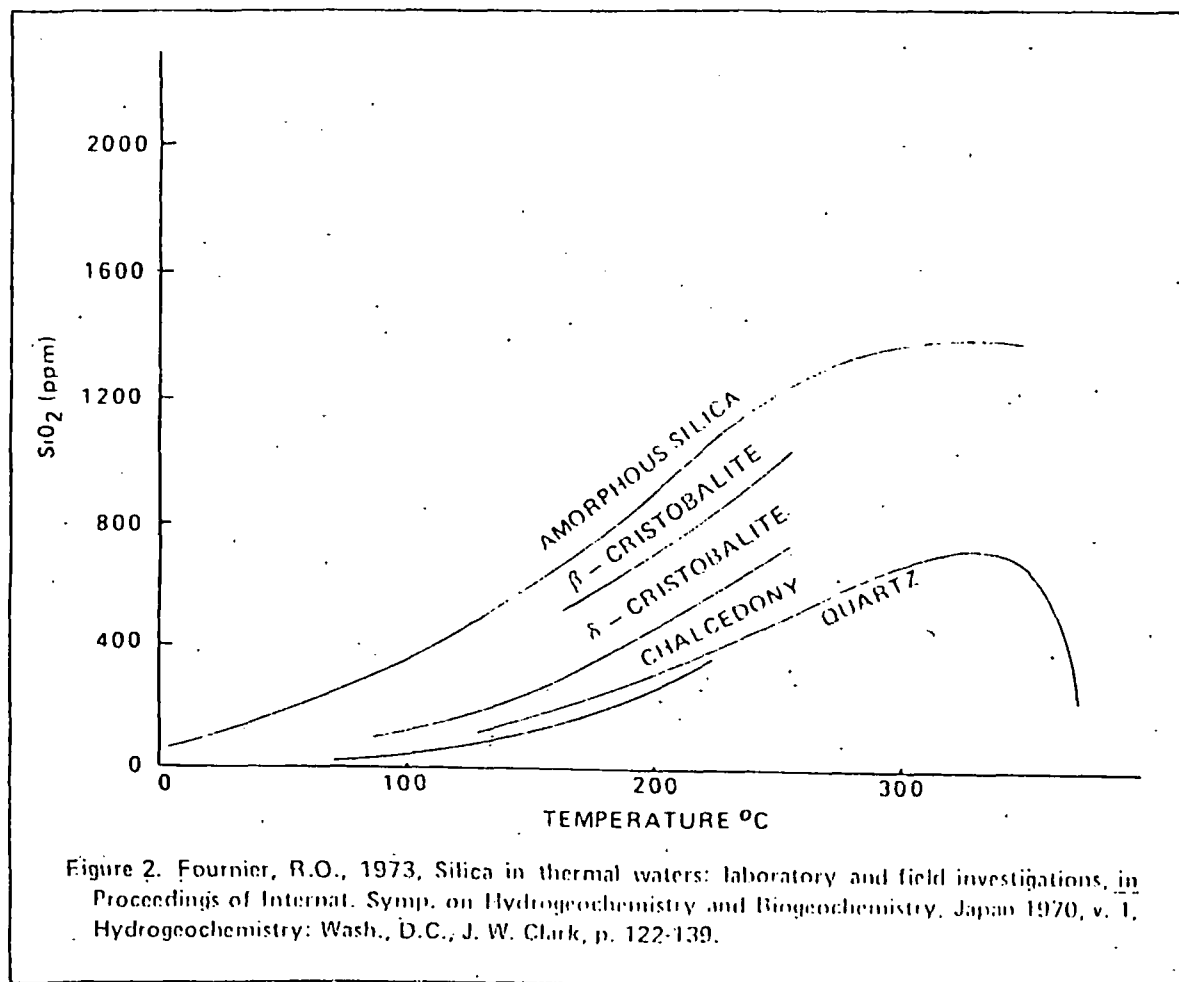


Figure 2. Fournier, R.O., 1973, Silica in thermal waters: laboratory and field investigations, in Proceedings of Internat. Symp. on Hydrogeochemistry and Biogeochemistry, Japan 1970, v. 1, Hydrogeochemistry: Wash., D.C., J. W. Clark, p. 122-139.

Brook and others, 1978, recommend that alkaline geothermal waters issuing from granitic terrans that do not evolve CO₂ gas probably should be corrected for the discreation of silicic acid (H₄SiO₄) by hydroxide (OH) to H₃SiO₃ and H₂SiO₂. Mariner (personal communication) recommended care in applying this correction to the silica geochemical thermometers as the pH involved in the correction is assumed to be reservoir or aquifer pH, and this may change as water ascends to the surface. The method may, therefore, lack quantitative application.

acid waters, although a few acid-sulfate chloride waters yield reasonable temperatures. Fournier and Truesdell (1973) point out that Ca enters into silicate reactions in competition with Na and K and the amount of Ca in solution is greatly dependent upon carbonate equilibria. Calcium concentration from carbonates decreases as temperature increases, and may increase or decrease as the partial pressure of carbon dioxide increases, depending on pH considerations. Therefore, the Na/K ratio should not be used for purposes of geochemical thermometry when partial pressures of carbon dioxide are large, as higher carbon dioxide partial pressures may permit more Ca to remain in solution and consequently a smaller Na/K ratio. Fournier and Truesdell (1973) suggest that this ratio should not be used when the $\sqrt{M_{Ca}}/M_{Na}$ (square root of molar concentration of calcium/molar concentration of sodium) is greater than 1.

The sodium-potassium-calcium (Na-K-Ca) geochemical thermometer devised by Fournier and Truesdell (1973) is a method of estimating aquifer temperatures based on the molar concentrations of Na, K, and Ca in natural

thermal waters. Accumulated evidence suggests that thermal, calcium-rich waters do not give reasonable temperature estimates using Na/K atomic ratios alone, and that the Ca concentration must be given consideration.

Fournier and Truesdell (1973) showed that molar concentrations of Na-K-Ca for most geothermal waters cluster near a straight line when plotted as the function $\log K^* = \log (Na/K) + \beta \log (\sqrt{Ca}/Na)$ versus the reciprocal of the absolute temperature, where β is either 1/3 or 4/3, depending upon whether the waters equilibrated above or below about 100°C and where K^* is an equilibrium constant. For most waters they tested, the Na-K-Ca method gave better results than the Na/K method. It is generally believed that the Na-K-Ca geochemical thermometer will give better results for calcium-rich environments provided calcium carbonate has not been deposited after the water has left the aquifer. Where calcium carbonate has been deposited, the Na-K-Ca geochemical thermometer may give anomalously high aquifer temperatures. Fournier and Truesdell (1973) caution against using the Na-K-Ca geochemical thermometer in acid waters that are low in chloride."

Dilution Effects, the Use of the Geochemical Thermometers and Mixing Models

Dilution effects caused by mixing of thermal with nonthermal waters can be a cause of erroneous temperature estimates. Cool groundwaters containing low silica concentrations that mix with thermal waters rich in silica would effectively lower the silica concentration of the thermal water, and a lower aquifer temperature would be indicated. Generally, the possible effect of both dilution and enrichment of thermal waters on the temperature calculated using any geochemical thermometer must be considered.

Fournier and others (1974) suggested several starting assumptions to apply to the interpretation of chemical data for hot springs and wells where little information on hydrologic conditions is available. They emphasized that these assumptions are not hard, fast rules applicable to every situation. Their recommended procedures are based on: (1) the discharge of the spring or well, and (2) the recorded surface temperature, as outlined below.

APPENDIX II

Many apparently low-temperature, magnesium rich thermal waters give Na-K-Ca estimated temperatures above 150°C and cast doubt on the usefulness of this geochemical thermometer. Fournier and Potter (1978) have devised a correction to be applied to the Na-K-Ca geochemical thermometers when Na-K-Ca estimated temperatures are above 70°C and when R values [R = Mg/(mg + Ca + K) x 100] are between 5 and 50. If R (in equivalents) is above 50 it is best to assume either rock-water equilibration at about measured surface temperature (irrespective of much higher calculated Na-K-Ca temperature) or that non-equilibrium conditions exist. Their correction, in equation form, is

$$\Delta T_{mg} = a_1 - b_1 R + c_1 (\log R)^2 - d_1 (\log R)^2 / T^2 - e_1 (\log R)^2 / T^2 + f_1 (\log R)^3 / T^3 \quad (1)$$

Where: ΔT_{mg} is the temperature in °C to be subtracted from the Na-K-Ca temperature in degrees Kelvin, $a_1 = 10.66$, $b_1 = 4.7415$, $c_1 = 325.867$, $d_1 = 1.0321 \times 10^5$, $e_1 = 1.9683 \times 10^7$, and $f_1 = 1.6053 \times 10^7$.

For R values less than 5, Fournier and Potter recommended the following equation be used.

$$\Delta T_{mg} = -a_2 + b_2 \log R + c_2 (\log R)^2 - d_2 (\log R)^2 / T - e_2 \log R / T^2, \quad (2)$$

Where: $a_2 = 1.02995$, $b_2 = 59.97116$, $c_2 = 145.049$, $d_2 = 36711.6$, and $e_2 = 1.67516 \times 10^7$. For solving for ΔT_{mg} graphically, Fournier and Potter recommended using Figure ___ and ___.

Paces (1978, p 34) thought that inaccuracies in Na-K-Ca geothermometer for temperatures below 75°C in felsic rocks were the result of a chemical steady-state between water and felsic rocks rather than chemical equilibrium if partial pressure of CO₂ in the aquifer were above 10⁻⁴ atm. The steady state is brought about by (1) fast percolation of water and (2) a flux of an acidifying agent such as CO₂. If these are fast enough, the steady state may be realized in which case the chemical composition of the water

deviates from the equilibrium state expressed by $\log K$. Paces recommended subtracting a term ($I = -1.36 - 0.253 \log PCO_2$) from the right side of the $\log K$ equation.

$$\log K = \log \frac{Na}{K} + \frac{4}{3} \frac{\gamma Ca}{Na} - I.$$

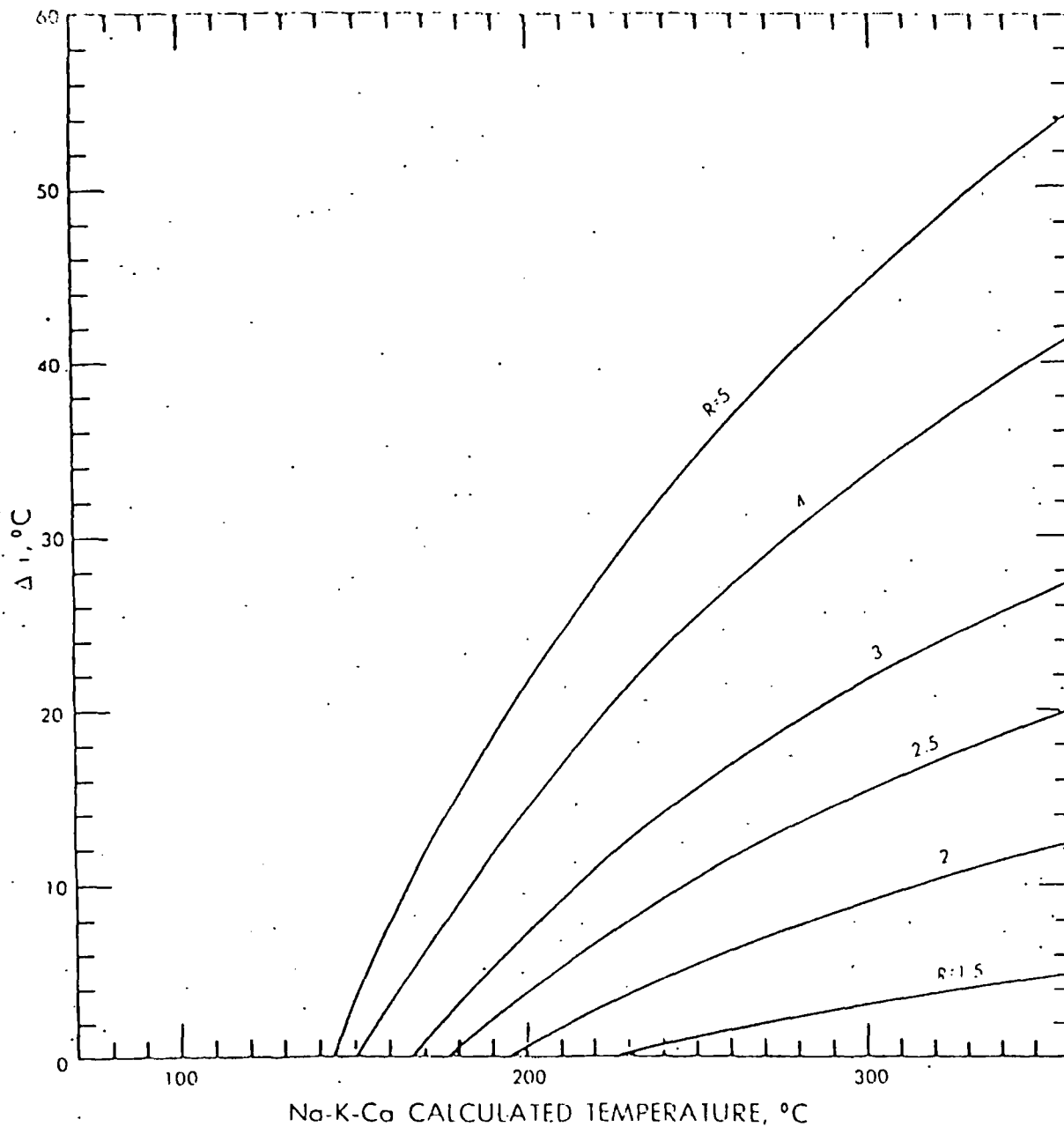


Figure 7.-- Graph for estimating the magnesium temperature correction, Δt , using Na-K-Ca calculated temperatures and R values ranging from 1.5 to 5. The curves were drawn using equation (2). Move directly up from the calculated Na-K-Ca temperature to the intersection (or interpolated value) of the line having the calculated R value. Move horizontally from the R value intersection and read the Δt_{mg} value on the ordinate.

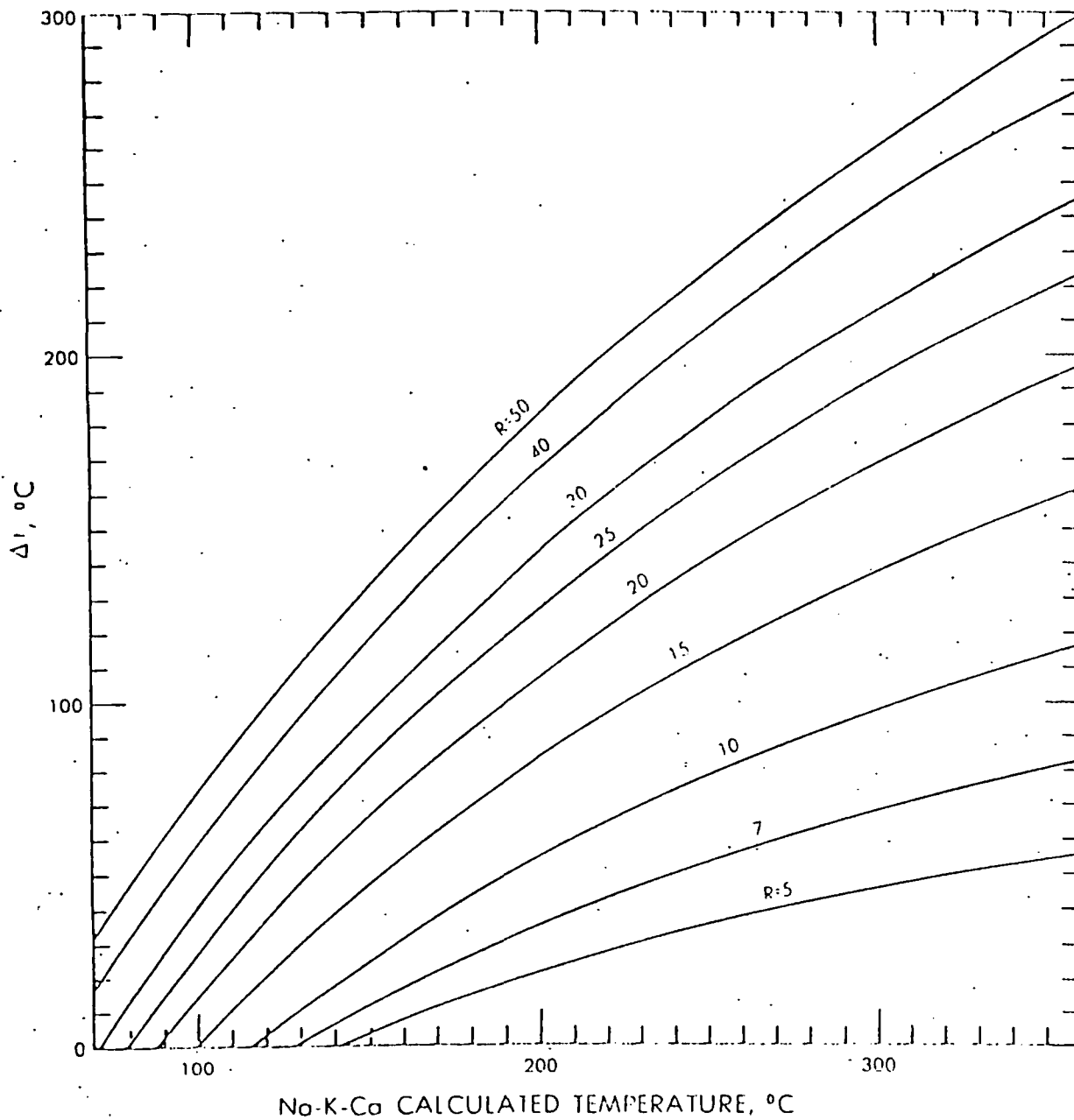


Figure 6.-- Graph for estimating the magnesium temperature correction, Δt , using Na-K-Ca calculated temperatures and R values ranging from 5 to 50. The curves were drawn using equation (1). Move directly up from the calculated Na-K-Ca temperature to the intersection (or interpolated value) of the line having the calculated R value. Move horizontally from the R value intersection and read the Δt_{mg} value on the ordinate.

	Small Discharge	Large Discharge
Boiling Springs	Assume mostly conductive cooling. Apply chemical indicators assuming little or no steam loss (adiabatic cooling).	Assume steam loss (adiabatic cooling). Assume maximum steam loss, apply geochemical thermometers accordingly.
Springs below boiling	Probably no clearcut interpretation. May be (1) water that has never been very hot, (2) mixed water from different sources at different temperatures, (3) hot water cooled by conduction. Indicated temperatures most likely, minimum.	Assume no conductive cooling. Geochemical thermometers, particularly Na-K-Ca, if within $\pm 25^\circ\text{C}$ of measured surface temperature may be suggestive of equilibrium conditions. Higher indicated temperatures suggests a mixed water.

Small discharge was defined to be less than 200 l/min for single isolated spring, and 20 l/min for single spring vents of larger groups.

Fournier and Truesdell (1974) have developed a method of testing thermal waters to determine if mixing may be taking place. They maintain that mixing should be suspect where: (1) regular variations in surface temperatures with chloride, boron, or other nonreactive chemical constituents from several springs of an area are observed, (2) the Na-K-Ca geochemical thermometer indicates nonequilibrium conditions (Na-K-Ca indicated temperatures varies from the observed surface temperature by more than 20°C).

Under ideal conditions, Fournier and Truesdell's mixing models allow prediction of the temperature of the hot water before mixing. The models assume that enthalpy (heat content - H_c) of the cold water multiplied by the fraction of cold water (X) plus the enthalpy of the hot water (H_h) multiplied by the fraction of the hot water (1-X) is equal to the enthalpy of the emerging spring-water (H_{spg}). Stated mathematically:

$$(H_c)(X) + (H_h)(1-X) = H_{spg} \quad (1)$$

Similarly;

$$(Si_c)(X) + (Si_h)(1-X) = Si_{spg} \quad (2)$$

Where Si_c is the silica content of cold spring, Si_{spg} is the silica content of the hot spring water and Si_h is the enthalpy value for silica in hot water (table 1 - equation 5). Equations 1 and 2 are each solved for the unknown X by simple algebraic rearrangement to give equations 3 and 4.

Fournier and Truesdell's suggested graphical method of solution for mixing model 1, in which the enthalpy of the hot water plus separated steam which heats cold water is the same as the initial enthalpy of hot water before steam separates (no steam loss by system, hence, no evaporative concentration), is as follows:

- "1. Assume a series of values of temperature of hot water and using this corresponding enthalpy values listed in table 1 calculate X_t for each one, using equation 3.5

$$X_t = \frac{(\text{Enthalpy of hot water}) - (\text{temp of warm spg})}{(\text{Enthalpy of hot water}) - (\text{temp of cold spg})} \quad (3)$$

2. Plot the calculated values of X_t vs. the assumed temperatures from which the hot water enthalpy values were derived. (See fig. 5, curve A for sample plot.)

3. Using a series of silica contents of hot water appropriate for the temperatures listed in table 1 evaluate X_{Si} for each silica content using equation 4.6

$$X_{Si} = \frac{(\text{Silica in hot water}) - (\text{Silica in warm spg})}{(\text{Silica in hot water}) - (\text{Silica in cold spg})} \quad (4)$$

4. On the same graph previously used, plot the calculated values of X_{Si} vs. the temperatures for which the silica contents were obtained (see fig. 5 curve B)."

Table 1¹

Enthalpies of liquid water and quartz solubilities at selected temperatures and at pressures appropriate for steam and liquid water to coexist. Enthalpies from Keenan et al. (1969). Quartz solubilities at and below 225°C from Morey et al. (1962); above 225°C from unpublished data of R. O. Fournier.

Temperature °C	Enthalpy cal/gm	Silica ppm
50	50.0	13.5
75	75.0	26.6
100	100.1	48
125	125.4	80
150	151.0	125
175	177.0	185
200	203.6	265
225	230.9	365
250	259.2	486
275	289.0	614
300	321	692

¹Table from Fournier and Truesdell, 1974.

Table 2 gives the calculated X_t and X_{Si} values at selected temperatures and silica concentrations for this mixing model from sampled springs and wells in the northern Cache Valley area.

The intersection of the two curves represent the percent of cold water mixing with the hot (read directly below intersection point on the horizontal axis of the graph) and the temperature of the hot water component before mixing (read on the vertical axis of the graph directly to the left of the intersection point).

Their solution for mixing model 2, in which the enthalpy of hot water in the zone of mixing is less than the enthalpy of the hot water at depth, due to escape of steam during ascent is as follows:

1. Use the atmospheric boiling temperature for the value of H_h in equation 2 and calculate the corresponding value of X_s
2. Use that value of X in equation 3 to estimate the residual silica content of hot water at t_s .
3. Use the calculated residual silica content and curve A of Fournier and Rowe (1966, fig. 5) to estimate the original subsurface temperature before separation of steam. Curve A of Fournier and Rowe is roughly approximated by the equation

$$\log C = \frac{1522}{t_{°C} - 273} - 5.75 \quad (5)$$

where C is the silica concentration, and t is temperature in degrees Celsius."

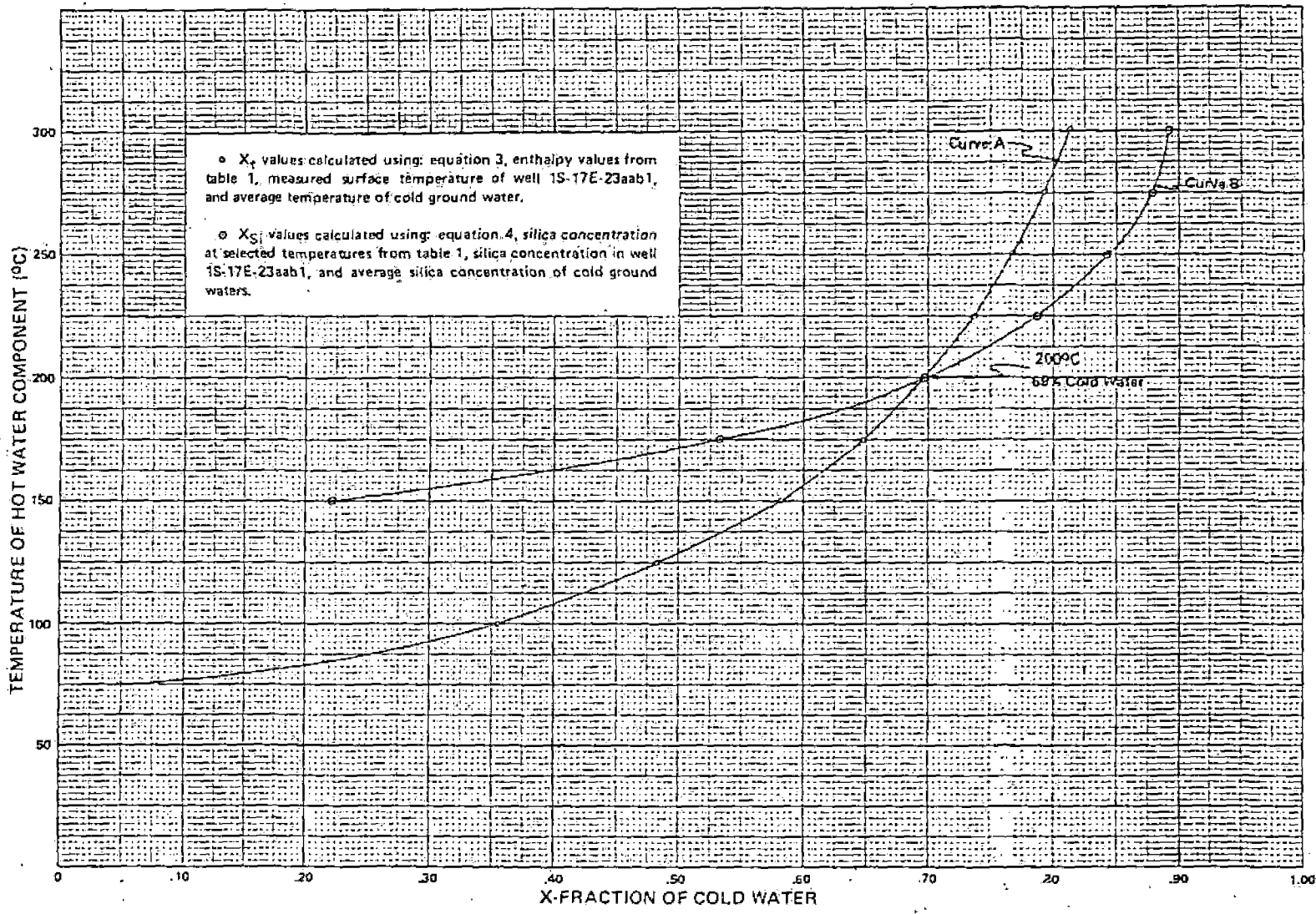


FIGURE 3. Fraction of cold water relative to temperature for well 1S-17E-23aab1.

Table 2. X_t and X_{Si} Values at Specified Temperatures and Silica Concentrations for Thermal Waters of the Camas Prairie Area
(Temperature °C) (Continued)

Spring No. 1S-13E-34bcc1S			Well No. 1S-17E-23aab1		
Surface temperature = 73°			Surface temperature = 72°		
Silica = 84 mg/l			Silica = 105 mg/l		
Background silica = 35 mg/l			Background silica = 35 mg/l		
Background temperature = 15°			Background temperature = 15°		
Boiling temperature = 95°			Boiling temperature = 95°		
T	X_t	X_{Si}	T	X_t	X_{Si}
75	0.033	.	75	0.050	.
100	.318	.	100	.320	.
125	.475	.	125	.484	.
150	.574	0.456	150	.581	0.222
175	.642	.673	175	.648	.533
200	.692	.787	200	.698	.696
225	.731	.852	225	.736	.788
250	.762	.890	250	.767	.843
275	.788	.915	275	.792	.879
300	.810	.925	300	.814	.893
Temperature of unmixed hot water = 169°			Temperature of unmixed hot water = 200°		
Percent of cold water = 62.			Percent of cold water = 69.		

1976 in: ^{U. N.} Second United Nations Symposium on the
Development and Use of Geothermal Resources,
Proceedings; Lawrence Berkeley Laboratory,
28 p.

Ward

UNIVERSITY OF UTAH
RESEARCH INSTITUTE
EARTH SCIENCE LAB.

SUBJ
GCHM
GTE

Summary of Section III Geochemical Techniques in Exploration

ALFRED H. TRUESDELL

U.S. Geological Survey, Menlo Park, California 94025, USA

INTRODUCTION

Considerable advances have been made in the knowledge of the chemistry of geothermal fluids in the five years between the first and second United Nations Geothermal Symposia held in Pisa (1970) and San Francisco (1975). At the Pisa Symposium, Donald E. White reviewed the entire field of geothermal geochemistry. He emphasized the distinction between hot-water and vapor-dominated geothermal systems and carefully reviewed the application of quantitative and qualitative geothermometers to each type of system. Geothermal chemistry was also recently reviewed by Sigvaldason (1973), Ellis (1973, 1975), and Mahon (1973). In reporting on fluid chemistry papers from the San Francisco Symposium, I shall build on these earlier reports and include Symposium papers and abstracts with geochemical data, as well as some recent papers not submitted to the Symposium. The literature in this field is expanding so rapidly that some worthy papers were probably missed.

Geothermal fluid chemistry finds its widest application in exploration, and it is this aspect that will be stressed in this report. Recent exploration activities have resulted in new chemical data on thermal fluids from springs and wells in Afars and Issas, Canada, Chile, Columbia, Czechoslovakia, El Salvador, Ethiopia, France, Greece, Guadeloupe, Hungary, Iceland, India, Indonesia, Israel, Italy, Japan, Kenya, Mexico, New Britain, New Zealand, the Philippines, Poland, the Red Sea, Rhodesia, Swaziland, Switzerland, Taiwan, Turkey, the United States, the USSR, and Yugoslavia. New methods for estimating subsurface temperatures have been proposed based on chemical and isotopic analyses of surface and well discharges. Chemical indices based on trace constituents of spring fluids and deposits, altered rocks, soils, and soil gases have been proposed as aids to geothermal exploration. Chemical models of interaction of geothermal fluids with reservoir rocks have been constructed. Studies of alteration in geothermal systems have aided exploration and exploitation. Finally, studies of geothermal rare gases suggest that although most are atmospheric in origin, excess ^3He in some systems may come from the Earth's mantle.

Although not covered in this report, chemical studies also assist in the exploitation of geothermal resources. Analyses of produced fluids indicate subsurface temperatures and production zones. Problems of scale deposition, corrosion of piping, and disposition of environmentally harmful chemical substances in geothermal fluids have been studied and

solved in some applications. Plans continue for the recovery of valuable chemicals from geothermal fluids.

CHEMICAL COMPOSITION OF FLUIDS

Summaries of analytical data on selected thermal spring and well discharges, indicated geothermometer temperatures, and references to data sources are presented in Table 1. Most data are from papers submitted to this Symposium. The classification of geothermal system type in Table 1 is based on the assumed genesis of their anomalous heat and follows, in a general way, classifications proposed by Mahon (p. 755), Arnórsson (1974), Ivanov (1967), Kononov and Polak (p. 767), and White (1970). Volcanic systems (where the heat sources are inferred to be recent igneous intrusions) dominated by hot water or steam are distinguished from nonvolcanic systems in which the heat source is normal or elevated regional heat flow and the waters are heated by deep circulation along faults or by their position in broad downwarped sedimentary basins. There are many chemical studies of volcanic geothermal systems because these are most easily exploited with current technology; fault-related and sedimentary systems are poorly understood chemically, although these may yield large quantities of heat for non-electrical uses. Additional data on nonvolcanic geothermal systems may be found in the Proceedings of the Symposium on ~~Water-Rock~~ Interactions held in Prague in 1974 (Čadež, 1976). Because of their distinctive and relatively uniform chemistry, I have treated seawater systems separately and discussed them in a special section.

Mahon's Classification

Mahon (p. 775) characterizes geothermal fluids as originating from volcanic and subvolcanic geothermal systems, which may be either water or steam systems, and from nonvolcanic geothermal systems. Volcanic water systems are usually characterized at depth by waters of the neutral sodium chloride type which may be altered during passage to the surface by addition of acid sulfate, calcium, or bicarbonate components. The concentration of chloride may range from tens to tens of thousands of ppm. The origin of the water itself is dominantly meteoric, and the concentrations of readily soluble components such as Cl, B, Br, Li, Cs, and As are related to their concentrations in the rock, to the subsurface temperature, and possibly to

contributions from deep fluids related to the volcanic heat source. Other less soluble constituents such as SiO_2 , Ca, Mg, Rb, K, Na, SO_4 , HCO_3 , and CO_3 are controlled by subsurface temperature, mineral solubility, mineral equilibria, and pH. Gases in these systems normally include CO_2 , H_2S , H_2 , CH_4 , N_2 , and inert gases, with CO_2 predominant, and constitute 0 to 5% by weight of the deep fluid.

The near-surface fluids of volcanic steam (vapor-dominated) systems are low in chloride (except for fundamentally unrelated high-temperature volcanic fumaroles with HCl). They contain only elements soluble in some form in low-pressure steam (SO_4 as H_2S , HCO_3 as CO_2 , B as HBO_2 , Hg, NH_3). The gases are similar to those in volcanic water systems. Because of their relative rarity and because vapor rather than liquid is produced (although liquid may predominate at depth), the geochemistry of these systems is not well understood.

Nonvolcanic geothermal systems have a wide range of water compositions and concentrations, from dilute meteoric waters to connate waters, metamorphic waters, and oil field brines. The controls on their compositions are less well known than those of volcanic waters.

Arnórsson's Classification

Arnórsson (1974) classifies Icelandic thermal fluids as related to (1) temperature, (2) rock type, and (3) influx of seawater. Low-temperature waters ($<150^\circ\text{C}$) are the result of deep circulation in regions dominated by conductive heat flow (up to 4 to 5 hfu, which is above average for most of the world) and are characterized by low dissolved solids contents (200 to 400 ppm) and gases dominated by nitrogen. Higher temperature waters ($>200^\circ\text{C}$) result from intrusions of igneous rocks and are characterized by higher dissolved solids contents (700 to 1400 ppm) and by gases with large amounts of CO_2 , H_2S , and H_2 . Fluids in silicic rocks tend to be higher in Cl and other dissolved solids than fluids of the same temperature in basaltic rocks if seawater is not involved.

Classifications of Ivanov and Kononov and Polak

Ivanov (1967) proposed a classification of thermal fluids based on gas contents, which has been expanded by Kononov and Polak (p. 767). Fluids directly related to volcanic processes are characterized either by H_2S - CO_2 gases and acid sulfate or acid sulfate-chloride waters in the oxidizing zone, or by N_2 - CO_2 gases and alkaline sodium chloride waters in the reducing zone. Fluids related to thermometamorphic processes have high CO_2 gases and carbonated waters, which may in part be connate. Fluids of deep circulation but outside of volcanic and thermometamorphic zones have N_2 gases and dilute sodium chloride-sulfate waters. Kononov and Polak further divide volcanic fluids into "geyseric" with H_2 - CO_2 gases and "riftogenic" with H_2 gases, which occur in spreading centers and characterize the highest temperature ($>300^\circ\text{C}$) geothermal systems. It is only in "riftogenic" fluids that anomalous contents of ^3He and H_2S with $\delta^{34}\text{S}$ near zero are expected. Parts of this classification are applied in detail to Icelandic thermal fluids by Arnórsson, Kononov, and Polak (1974).

Although this classification may need modification based on the chemistry of fluids in drilled systems, it has the advantage of focusing attention on geothermal gases, which

deserve more study. The occurrence of excess ^3He in the hydrothermal fluids of Kamchatka (Gutsalo, p. 745), Lassen, and Hawaii (Craig, 1976) and of Yellowstone $\delta^{34}\text{S}$ values near zero (Schoen and Rye, 1970) suggests these fluids are "riftogenic" when, in fact, they are far from present spreading centers.

Classifications of White

Reviews by D. E. White of mineral and thermal water chemistry (1957a, b, 1968, 1970, 1974) have greatly influenced most workers in this field. Space does not allow adequate description of his water classification schemes, which have evolved as more chemical and isotopic data became available. In brief, *meteoric* waters dominate shallow crustal circulation and mix with more saline deep waters of all types. Meteoric waters may also circulate deeply under the influence of magmatic heat and receive additions of NaCl, CO_2 , H_2S , and other substances from rock leaching, thermal metamorphism, and possibly magmatic fluids. These moderately saline sodium chloride deep waters of *volcanic* association undergo near-surface rock reactions and atmospheric oxidation to form the range of observed surface volcanic waters. *Oceanic* water is incorporated in marine sediments and, by extended low-temperature reactions, becomes *evolved-connate* water. Deep burial and higher-temperature reactions cause expulsion of highly altered *metamorphic* waters from rocks undergoing regional metamorphism. *Magmatic* water has been dissolved in magma but may have various ultimate origins. The existence of *juvenile* water new to the hydrologic cycle is certain, but its recognition is doubtful. Recent work by White and his coworkers has elaborated the chemical distinctions between hot-water and vapor-dominated systems (White, Truesdell, and Muffler, 1971; Truesdell and White, 1973) and demonstrated the existence of thermal water of nonmeteoric origin in the California Coast Ranges (White, Barnes, and O'Neil, 1973).

VOLCANIC HOT-WATER SYSTEMS

Deep Fluids

Hot-water geothermal systems with volcanic heat sources have been very thoroughly studied. The deep fluids of these systems are, in general, waters of dominantly meteoric origin with chloride contents of 50 to 3000 ppm, unless seawater, connate water, or evaporites are involved. Components of these fluids, such as Na, K, Ca, Mg, and SiO_2 , that are present in major amounts in most volcanic reservoir rocks almost certainly originate from rock-water reactions. Other fluid components, such as Cl, F, B, CO_2 , and H_2S , are present in these rocks only in trace quantities and have been explained as magmatic contributions (Allen and Day, 1935; White, 1957a). Experimental rock-leaching studies (Ellis and Mahon, 1964, 1967) have shown, however, that these soluble components may be extracted from most rocks at moderate temperatures (200 to 300°C), and isotope studies (see below) have failed to detect magmatic water in geothermal systems. Rock leaching as a sole source of chloride has been criticized by White (1970) because it appears to require unreasonable rock volumes or unreasonable original rock chloride contents to maintain the chloride flux of old geothermal systems, such as Steamboat Springs, Nevada (age 1 to 3 m.y.; Silberman and White, 1975), or Wairakei.

New Zealand (age 500 000 years; Banwell, 1963; Healy, p. 415, suggests half this figure).

Recent isotope studies of fresh and altered Wairakei rocks suggest that the apparent water:rock mass ratio of drilled parts of this system is at least 4.3:1 (Clayton and Steiner, 1975). Since the Cl contents of possible rocks at depth in this system are less than 1000 ppm (Ellis and Mahon, 1964), a mechanism other than simple leaching would appear necessary to produce the 1400-ppm-Cl Wairakei deep water. More probably, however, the rock leached of chloride was at much deeper levels as in the deep reservoir hypothesized by Hochstein (Abstract I-16) and at those levels the water:rock ratio was much lower. However, a lower water:rock ratio requires a larger volume of rock which, if the predrilling flux of chloride (2.5×10^{10} g/year; Ellis and Wilson, 1955) has been maintained over the life of the system, requires more than 5×10^3 km³ of leached rock; this is more than ten times the possible volume of the system estimated by Hochstein (Abstract I-16). To resolve this problem, Wilson (1966) and Ellis (1966) suggested that flow in geothermal systems is intermittent and that present activity is much greater than that of the past. Ellis (1970) suggests this cycle might have a period of 10^5 years with the active part of the cycle complete in 10^3 years. Experimental and model studies of nonuniformly heated fluid in porous media by Horne and O'Sullivan (1974) produced intermittent flow, which may support this suggestion. However, the numerous dormant geothermal systems (99% of the total) required by this model would be easily recognizable by fossil sinter deposits and have not been found.

The efficacy of rock leaching as a source of dissolved constituents in geothermal waters must depend on the availability of fresh rock surfaces. Heat transfer and leaching from established fractures should be rapid, and solute concentrations and temperatures would be expected to decrease rapidly. This may not occur because the growth of thermal stress fractures (Harlow and Pracht, 1972; Smith et al., 1973; Lister, Abstract II-27) would provide fresh rock surfaces and heat transfer at the same rate so that the chemical and thermal properties of convecting fluids would be uniform in time. Studies of fluid inclusions from Broadlands, New Zealand, suggest that changes of fluid concentration and temperature may have been small over the 10^5 -year life of this system (Browne, Roedder, and Wodzicki, 1976). Careful chemical and physical modeling is needed to further test the rock-leaching hypothesis.

The opposite hypothesis, that small quantities of magmatic fluids of high salinity supply a significant part of geothermal solutes, has been defended by White (1957a, 1970). Recent fluid inclusion and isotopic studies (reviewed by White, 1974; see also later issues of *Economic Geology*) indicate that two fluids were involved in the generation of many ore deposits. Initial fluids of porphyry copper, epithermal base metal, and other ore deposits were probably magmatic in origin, and later fluids were local meteoric waters. However, magmatic waters have not yet been positively identified in epithermal gold-silver deposits, which are most closely related to active geothermal systems. The presence of mantle-derived ³He in geothermal fluids (Kononov and Polak, p. 767; Gutsalo, p. 745; and Craig, 1976) may not indicate direct contribution of other juvenile or even magmatic components because of the possibility that helium may migrate independently of other fluids or may be contained in some volcanic rocks (Lupton and Craig, 1975)

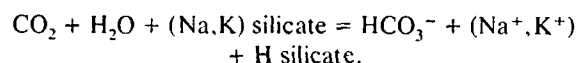
and enter geothermal fluids from rock leaching.

Perhaps the most persuasive evidence for the participation of at least small amounts of magmatic components in geothermal fluids is the close temporal and spatial relation and analogous geochemical behavior of certain volcanic and geothermal systems. The volcanic zone in Taupo, New Zealand, with numerous geothermal systems, has the active volcanoes of White Island at its north end and Ruapehu and Ngauruhoe at its south end. Chemical studies of White Island have shown that fumarole discharges alternate between typical high-temperature (to 800°C) volcanic emanations with high sulfur:carbon ratios when flows of volcanic gases are not impeded, and nearly typical geothermal steam at temperatures below 300°C with low sulfur:carbon ratios when the gases are forced to pass through surface waters (Giggenbach, 1976). Some fluids of geothermal systems associated with near-active volcanoes of the Tatun Shan, Taiwan (Chen and Chern, written commun., 1975) and of Tamagawa (Iwasaki et al., 1963) and Hakone (Noguchi et al., 1970), Japan, may be similar to the drowned volcanic emanations of White Island. Hydrolysis of sulfur or near-surface oxidation of H₂S cannot produce the HCl acidity proven at Hakone and Tamagawa and indicated at Tatun (analysis Ta 1, Table 1, from New Zealand Dept. Sci. Ind. Res., quoted by Chen and Chern) which must originate from high-temperature, probably magmatic, processes (White and Truesdell, 1972; R. O. Fournier and J. M. Thompson, unpub. data). Magmatic fluid contributions to these geothermal systems appear probable, but proof is lacking. More work is needed on this problem, possibly through more extensive isotopic studies of elements dissolved in geothermal waters. However, fractionation during crystallization and re-solution of trace constituents is expected to be small, so leached material may be indistinguishable from direct magmatic contributions.

Near-surface Alteration of Hot Waters

Near-surface processes producing the varied compositions of geothermal waters of volcanic systems include steam separation during adiabatic cooling, mixture with cold shallow meteoric waters, and chemical reactions involving rock minerals, dissolved gases, dissolved constituents of diluting waters, and atmospheric gases. Many indicators of subsurface flow (see below) depend on the effects of these processes on ascending geothermal fluids. Fluid component ratios that are not affected by these processes, such as Cl:B, are useful in indicating the homogeneity of subsurface fluids and thus the continuity and size of geothermal systems (Stefánsson and Arnórsson, p. 1207; Cusicanqui, Mahon, and Ellis, p. 703).

Subsurface reactions with dissolved gases and rock minerals control the contents in the water of most components present in excess in the rock or in the dissolved gas. Most of the bicarbonate and part of the sodium and potassium are produced by reaction of dissolved CO₂ with the rocks to produce mica or clay minerals and bicarbonate and alkali ions (Fournier and Truesdell, 1970).

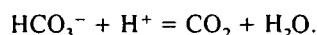


The coupled increase in HCO₃:Cl and decrease in CO₂:other gases during lateral flow through a near-surface aquifer has

been demonstrated for Shoshone Geyser Basin, Yellowstone (analysis US30), where near-surface rocks are glacial sediments composed of rhyolitic glass (Truesdell, 1976a). Crystallized rhyolite and ash flow tuff are not as reactive as glassy rocks, so CO_2 is converted to HCO_3^- less rapidly, as at Norris Geyser Basin, Yellowstone, where waters flowing in devitrified ash flow tuff are low in HCO_3^- (analysis US34).

Mixture of deep hot water with cold meteoric waters produces variations in the concentrations (but not the ratios) of Cl, B, and other components not involved in lower-temperature rock reactions. The resulting temperatures in subsurface aquifers where mixture takes place (Truesdell and Fournier, p. 837) affect all temperature-sensitive equilibria such as quartz solution and exchange of dissolved cations with aluminosilicate minerals. With sufficient dilution, subsurface boiling may be prevented and a high partial pressure of CO_2 retained in waters at temperatures well below 200°C. Under these conditions, the solubility of calcite is relatively high (Holland, 1967) and calcium can be leached from volcanic rocks. When these dilute high P_{CO_2} -high Ca solutions emerge at the surface, they lose CO_2 and deposit travertine as well as silica.

Steam separation produces changes in water chemistry because most salts are nearly insoluble in low-pressure steam (Krauskopf, 1964) and remain entirely in the liquid phase, while gases partition strongly into the vapor (Ellis and Golding, 1963; Kozintseva, 1964). The result of these processes is an increase in nonvolatile salts and a decrease in dissolved gases (principally CO_2 and H_2S) in the liquid phase. The loss of gas produces an increase in pH from about 6 at depth to near 9 at the surface (Ellis, 1967; Truesdell and Singers, 1971) through the reaction



The effect of CO_2 loss is greatest in waters with large contents of bicarbonate such as those from Shoshone Geyser Basin, Yellowstone (analysis US30) or Orakeikorako, New Zealand (analysis NZ7), so these waters become very alkaline whereas waters with little bicarbonate (for example Norris waters, analysis US34) remain near neutral.

Sulfate can originate from oxidation of H_2S by atmospheric oxygen dissolved in meteoric water of deep or shallow circulation. The amount of sulfate ion that can be formed in this manner is 22 ppm from rain water percolating underground after equilibrating with air at 0°C (Truesdell, 1976). This is close to the observed sulfate contents in water not affected by near-surface oxidation of H_2S in volcanic rocks with low sulfate contents, such as those in the Yellowstone caldera (analyses US29-34) and the Taupo volcanic zone (analyses NZ1-10). Higher contents of sulfate in volcanic hot water probably originate from leaching of sulfate contained in some volcanic rocks. Sulfate in low-temperature waters in basalts probably has this source (analyses 1c 1-3). In high-temperature areas the self oxidation of SO_2 to H_2S and SO_4 must also be considered. The sulfate contents of thermal waters in sedimentary aquifers are usually much higher as a result of solution of sedimentary sulfate from the rock (for example Kızıldere, Turkey, analyses T1-2).

Acid waters with very high sulfate contents are produced by direct superficial atmospheric oxidation of H_2S to sulfuric acid in areas of drowned fumaroles or steaming ground

(White, 1957b). The acid-sulfate-chloride waters at Waimangu, New Zealand, and Norris, Yellowstone, probably result from percolation of this acid sulfate water into near-surface reservoirs where it mixes with chloride water from below. The change from deep, slightly acid chloride waters, to neutral $\text{Cl-HCO}_3\text{-SO}_4$ waters, to acid sulfate waters with decreasing depth in the Onikobe caldera has been described by Yamada (p. 665).

Roots of Volcanic Hot Water Systems

Knowledge of the deepest parts of geothermal systems must come chiefly from refined geophysical studies and from fossil geothermal systems exposed by erosion; but experimental studies of the thermodynamic chemistry of water and rock minerals provide important constraints for modeling.

From chemical and isotopic compositions of surface fluids and the phase chemistry of water and silica, Truesdell et al. (Abstract III-87) have proposed that a 3- to 6-km-deep reservoir of dilute (1000 ppm NaCl) water at 340 to 370°C underlies much of Yellowstone. This reservoir may correspond to the deep (also 3 to 6 km) reservoir proposed by Hochstein (Abstract I-16) on geophysical evidence to underlie the Taupo volcanic zone, New Zealand. Fournier, White, and Truesdell (p. 731) proposed that the solubility maximum of quartz (at 340°C for dilute steam-saturated water; increasing with salinity and, to a lesser extent, pressure) acts as a thermostatic mechanism for deep waters because circulation to higher temperatures would cause rapid quartz deposition and permeability decrease. Circulation of fluids through the zone of quartz solubility maximum should produce additional porosity by solution.

STEAM (VAPOR-DOMINATED) SYSTEMS

Certain geothermal systems (Larderello and Monte Amiata, Italy; The Geysers, California; Matsukawa, Japan; Mud Volcano, Yellowstone; and others) are characterized by production of saturated or slightly superheated steam without liquid water. Despite intensive search, few examples of this type of system have been found. Two new discoveries, the Kawah Kamojang and Salak fields of Indonesia, have been reported to this Symposium and another likely candidate has been identified in Mt. Lassen National Park, California (Renner, White, and Williams, 1975).

Although known systems have been intensively drilled, the character of the reservoir fluid, the mechanism of steam production, and the origin of these systems have been highly controversial and at least seven major models have been proposed. The latest of these models (White, Muffler, and Truesdell, 1971) has utilized the chemistry of superficial fluids and deep pressure and temperature measurements to conclude that both steam and water are present in these reservoirs. The model was elaborated and the mechanism of superheated steam production explained in a later paper (Truesdell and White, 1973).

New data on the Kawah Kamojang, Indonesia, field (Hochstein, p. 1049; Kartokusumo, Mahon, and Seal, p. 757) indicate that it is vapor dominated. Drillholes to 600 m showed the reservoir temperature below 550 m (390 m below the water table) to be 238°C, close to that of steam of maximum enthalpy (236°C), as predicted for these systems (James, 1968). Production initially was a steam-water mixture

that changed to saturated steam and finally superheated steam. Surface drainage and borehole fluids are nearly chloride-free (<2 ppm in hot waters; 3 to 6 ppm in drainage waters), as expected in a system with only steam flow from depth. The resistivity to 500-m depth is 2 to 5 ohm·meters, indicating a near-surface water-saturated zone above the reservoir. Deeper resistivity is >10 ohm·meters, probably indicating the presence of steam. This resistivity structure is similar to that found in the vapor-dominated Mud Volcano, Yellowstone, geothermal system (Zohdy, Anderson, and Muffler, 1973). Deeper drilling is needed at Kawah Kamojang to confirm the presence of the predicted low "vapostatic" pressure gradient. The Salak, Indonesia, field is also considered to be vapor dominated, as indicated by surface fluid chemistry (Kartokusumo and Seal, Abstract III-49).

Isotope chemistry of Larderello, Italy, steam has shown that increased production has drawn fluids from recent inflow at the sides of the reservoir and from deeper levels in the center (Celati et al., 1973; Panichi et al., 1974). Marginal inflow was also indicated by a hydrologic balance (Petracco and Squarci, p. 521). Steam from the central area has been shown to carry up to 60 ppm chloride associated with ammonia and boron (F. D'Amore, oral commun., 1975), which may indicate boiling from a high-chloride brine water table. Reassessment of original pressures of this system has indicated that, in general, they conform to the vapor-dominated model (Celati et al., p. 1583).

NONVOLCANIC HOT-WATER SYSTEMS

Earth temperatures increase generally with depth, and although most normal thermal gradients average 25°C/km, there are broad regions where thermal gradients are 40 to 75°C/km or higher (White, 1973). In these regions, hot water may be exploited by drilling in sedimentary basins or along fault zones where deep circulation occurs. Chemical data on these waters are sparse, but thermal water in sedimentary basins appears similar to nonthermal waters in similar geologic situations. The fault-controlled waters are similar to, but more dilute than, volcanic waters. The recent review of the chemistry of subsurface water by Barnes and Hem (1973) may be useful.

Examples of thermal systems that are considered nonvolcanic in Czechoslovakia, France, Iceland, India, Israel, Japan, Switzerland, Turkey, the United States, and Yugoslavia are given in Table 1. The waters of the Pannonian and related sedimentary basins of Czechoslovakia, Hungary, and Yugoslavia appear to be crudely zoned, with bicarbonate predominating near the top of the aquifer and chloride at greater depths (for example analysis Cz1; Franko and Mucha, p. 979; Boldizsár and Korim, p. 297; Petrović, p. 531). Waters in carbonate aquifers (analysis H1, Y2?) have relatively high contents of bicarbonate, calcium, and magnesium as might be expected, and gases appear to contain more CO₂ than in sandstone aquifers, which have more nitrogen. Methane is also present. Sedimentary basins in Russia are reported to yield water at 40 to 105°C with 1 to 10 g/l salinity at depths of 2500 to 3000 m without further chemical data (Mavritsky and Khelkvist, p. 179). More studies are needed on thermal waters of sedimentary basins.

Waters heated by deep circulation along faults may be very dilute with only atmospheric dissolved gases if their temperatures are low (analysis US4) and become much more concentrated with more CO₂ and H₂S as their subsurface

temperatures approach those of volcanic systems (analysis US26 for example). The water source is meteoric and salts are probably leached from rock, although evaporites may be associated with some fault-heated waters. Wollenberg (p. 1283) suggests that uranium may accumulate at depth in some of these systems owing to reducing conditions.

SEAWATER GEOTHERMAL SYSTEMS

Many geothermal systems in coastal areas have remarkably similar thermal fluids which are mixtures of local meteoric waters and thermally altered seawater. The effect on seawater of high temperature reaction with rock is marked increase in calcium and smaller increase in potassium and occasionally chloride, with marked decreases in magnesium, sulfate, and bicarbonate, and often a smaller decrease in sodium. These changes are apparently due to formation of montmorillonite, chlorite, and albite from calcic feldspars, which releases calcium and causes consequent precipitation of anhydrite and calcite (Mizutani and Hamasuna, 1972; Bischoff and Dickson, 1975). The salinity is affected by dilution and subsurface boiling. Chemical and isotopic studies have shown the presence of altered seawater in coastal thermal areas of Fiji (Healy, 1960), Greece (analyses G1-7; Dominco and Papastamatoki, p. 109; Stahl, Aust, and Dounas, 1974), Guadeloupe (analysis Gu1; Demians d'Archimbaud and Munier-Jolain, p. 101), Iceland (analyses Ic7-10; Björnsson, Arnórsson, and Tómasson, 1972; Arnórsson, 1974; Arnórsson et al., p. 853), Israel (analysis Is1; Eckstein, p. 713), Italy (analyses It1-2; Baldi, Ferrara, and Panichi, p. 687), Japan (analyses J1-2; Mizutani and Hamasuna, 1972; Matsubaya et al., 1973; Sakai and Matsubaya, 1974), New Britain (analysis NB1; Ferguson and Lambert, 1972), New Zealand (Crafer, 1974; Skinner, 1974), and Turkey (analyses T3 and T6; Kurtman and Şamilgil, p. 447). The composition of normal seawater is given in Table 1 for comparison (analysis SW1).

The application of chemical and isotopic geothermometers to seawater thermal fluids has some unusual features. Silica geothermometers apparently behave normally, but may reequilibrate more rapidly upon cooling because of the high salinity, thus indicating lower temperatures (Fournier, 1973). Cold seawater and partly altered seawater in low-to-moderate-temperature thermal systems indicate anomalously high temperatures, near 100°C from Na:K and 170°C from Na:Ca. The sulfate-water isotope geothermometer also indicates temperatures near 180°C for cold and partially altered seawater. These high-temperature indications may be relics of partial equilibration in submarine geothermal convection systems located along spreading centers (Lister, p. 459; Williams, Abstract I-40), with the seawaters resisting reequilibration in moderate-temperature coastal geothermal systems because of insufficient rock alteration to affect their high ion contents. Seawater-rock interaction experiments now in progress (Hajash, 1974; Mottl, Corr, and Holland, 1974; Bischoff and Dickson, 1975) will provide more data on this problem and may suggest new geothermometers for these systems. Where thermal seawaters have higher chlorinities than local seawaters and there is no evidence of evaporite contribution, I have calculated the subsurface temperatures required to produce the observed concentrations by boiling (analyses G7, Ic7, NB1, and T6). The indicated subsurface temperature of the Reykjanes, Iceland, seawater geothermal system agrees with that ob-

served. Chloride leached from rocks and conductive heating would tend to increase apparent temperatures and mixing with dilute waters would tend to lower them.

GEOOTHERMOMETERS

Where fluids from geothermal convection systems reach the surface in springs or wells, the chemical and isotopic compositions of these fluids may indicate the subsurface temperature and flow patterns, as well as the recharge source, type of reservoir rock, and other important parameters of the system. Component concentrations or ratios that can be related to subsurface temperatures are called geothermometers. Chemical geothermometers may be quantitative, so that specific subsurface temperatures may be calculated, or qualitative, so that only relative temperatures may be inferred. Important advances in the application of quantitative and qualitative geothermometers have been made since the first UN Geothermal Symposium in Pisa in 1970.

Quantitative Chemical Geothermometers

The theory of quantitative chemical geothermometers has been discussed by Fournier, White, and Truesdell (1974). These thermometers depend on the existence of temperature-dependent equilibria at depth which are quenched or frozen during passage to the surface.

At the time of the Pisa Symposium (1970), the quartz-saturation geothermometer (Mahon, 1966; Fournier and Rowe, 1966), which depends on the near-universal equilibrium with quartz in geothermal fluids above 100 to 150°C, and on the relative reluctance of quartz to precipitate from supersaturated solutions, was widely used in exploration and in monitoring well discharges. Temperatures above 200 to 230°C are seldom indicated by this geothermometer from spring analyses because reequilibration above 200°C is relatively rapid and solutions initially saturated with quartz at higher temperatures can precipitate amorphous silica during passage to the surface (Fournier, 1973; Truesdell and Fournier, p. 837). Lower-temperature waters may be saturated with chalcedony rather than quartz (Fournier and Truesdell, 1970), with some Icelandic waters suggesting chalcedony saturation at temperatures as high as 180°C and others suggesting quartz saturation as low as 110°C (Arnórsson, 1970, 1974, 1975). Examples of many thermal waters with probable quartz or chalcedony saturation are given in Table 1, and equations (data from Fournier, 1973, 1976) for quartz saturation with conductive and adiabatic (maximum steam loss) cooling and for chalcedony saturation are given in Table 2. Adiabatic cooling is probably most common in high-temperature geothermal systems (M. Nathenson, unpub. calculations), but loss of silica from reequilibration during upward flow may make conductive quartz temperatures appear to indicate reservoir temperatures more accurately (White, 1970). Systems with both adiabatic and conductive cooling have been discussed by Fournier, White, and Truesdell (p. 731).

The other geothermometer widely used 5 years ago was the Na:K ratio. The empirical calibration of this geothermometer does not agree with experimental studies of feldspar and mica equilibria, and in 1970 there was wide divergence between calibration scales. Syntheses of available data (mostly from the Pisa Symposium) by White and Ellis (quoted in White, 1970) and by Fournier and Truesdell (1973) have

produced two slightly different scales, which are approximated by equations given in Table 2. Since the White-Ellis curve is more widely used, it has been adopted for calculations in Table 1.

Because the Na:K geothermometer fails at temperatures below 100 to 120°C and yields improbably high temperatures for solutions with high calcium contents, an empirical Na:KCa geothermometer was proposed by Fournier and Truesdell (1973). NaKCa temperatures have been found to be closer to quartz-saturation temperatures for thermal springs of Nevada by Hebert and Bowman (p. 751), but Na:K temperatures appear to be equally accurate for 200 to 300°C low-calcium well discharges (Table 1), and may correctly indicate fluid temperatures and movement in drilled systems (Mercado, p. 487).

The cation (Na:K and NaKCa) geothermometers are useful in initial evaluations of the geothermal potential of large regions because they are less affected by reequilibration and near-surface dilution than are the silica geothermometers. Cation geothermometers have been used in regional evaluations in Canada (Souther, p. 259), Iceland (Stefánsson and Arnórsson, p. 1207), India (Krishnaswamy, p. 143; Gupta, Narain, and Gaur, p. 387), Israel (Eckstein, p. 713), Italy (Fancelli and Nuti, 1974), the Philippines (Glover, 1974a, b, 1975), and the United States (Young and Mitchell, 1973; Swanberg, 1974, 1975; Mariner et al., 1974a, b; Renner, White, and Williams, 1975; Reed, 1975).

Cation geothermometers, although empirical, apparently depend on equilibria between thermal waters and aluminosilicate minerals original to the host rock or produced by alteration. If equilibrium is not achieved, or if the mineral suite is unusual, misleading temperatures may be indicated. Thus, cation geothermometers must be used with caution in geothermal systems involving seawater, because in many of these, equilibrium with rocks probably is not reached because of the resistance to chemical change of the concentrated solution; and apparent temperatures are close to those indicated by cold seawater (analysis SW 1— $t_{\text{Na:K}}$, 100°C and t_{NaKCa} , 170°C). However, in some high-temperature geothermal systems, seawater does appear to have nearly equilibrated with rock and indicated temperatures are close to those observed in drillholes (analyses Ic7-9; analyses J1-2). Acid sulfate springs in which silica and cations are leached from surface rocks are not suitable for chemical geothermometry, although acid sulfate chloride waters of deep origin give reasonable indicated temperatures (analyses J12, Ta1-2). Cation (and silica) geothermometers may also give misleading results when applied to waters in highly reactive volcanic rocks (Fournier and Truesdell, 1970; Baldi et al., 1973; Arnórsson, 1975), especially those rocks with high contents of potassium (Calamai et al., p. 305), or to warm waters that emerge in peat-containing soils (Stefánsson and Arnórsson, p. 1207). Paces (1975) has suggested a correction factor for the NaKCa geothermometer when applied to high-CO₂ waters.

Although many other high-temperature chemical equilibria exist, most of these equilibria are affected by subsurface conditions other than temperature, reequilibrate rapidly, or are affected by other reactions during ascent to the surface. These equilibria can, however, be used as qualitative geothermometers (see below) and, in specialized circumstances, as quantitative geothermometers.

The content of magnesium in thermal waters varies inversely with temperature, but it is also affected by CO₂

pressure. Experimental calibration by Ellis (1971) allows magnesium contents to be used as a quantitative geothermometer if CO₂ pressures can be otherwise calculated.

Waters with high calcium and sulfate and low bicarbonate contents, such as thermally altered seawater (see discussion above), may be saturated with anhydrite at depth and become undersaturated during ascent because of the inverse temperature dependence of anhydrite solubility (analyses J1-2; Sakai and Matsubaya, 1974). The contents of calcium and fluoride in geothermal waters are in part controlled by equilibrium with fluorite (Nordstrom and Jenne, Abstract III-70), but reequilibration apparently is rapid.

The reaction $\text{CO}_2 + 4\text{H}_2 = \text{CH}_4 + 2\text{H}_2\text{O}$ may occur in geothermal reservoirs (Craig, 1953; Hulston, 1964; but see Gunter and Musgrave, 1966, 1971), and the amounts of these gases in surface discharges may indicate subsurface temperatures. Temperatures calculated from Wairakei borehole gases (analysis NZ1; Hulston and McCabe, 1962a; Lyon, 1974) are reasonable, but Arnórsson et al. (p. 853) have applied this method to fumarole discharges with somewhat ambiguous results.

Mixing Models

Although mixing of thermal waters with cold near-surface waters limits the direct application of chemical geothermometers, the dilution and cooling resulting from mixing may prevent reequilibration or loss of steam and allow the calculation of deep temperatures and chemical conditions. The chloride contents and surface temperatures of springs were used to calculate minimum subsurface temperatures in early New Zealand geothermal surveys (Mahon, 1970). More recently, models have been proposed based on surface temperature and silica contents of cold and warm springs (the warm spring mixing models in: Truesdell, 1971; Fournier and Truesdell, 1974; Truesdell and Fournier, 1976), and on the temperature, chloride, and silica concentrations of mixed boiling springs and the chloride concentrations and temperatures of cold springs and nonmixed boiling springs (the boiling spring mixing model in: Truesdell and Fournier, p. 837; Fournier, White and Truesdell, p. 731). A mixing model using chloride-enthalpy relations of cold, warm, and boiling springs was proposed by Glover (1974a) for Tongonan, Philippines, geothermal waters (analysis Ph1). Related diagrams of chloride and enthalpy (or temperature) have been used to analyze subsurface processes in drilled systems (Giggenbach, 1971; Mahon and Finlayson, 1972; Cusicanqui, Mahon, and Ellis, p. 703).

The warm spring mixing model depends on the assumption of conservation of enthalpy and silica and on the nonlinear temperature dependence of quartz solubility. The boiling spring mixing model depends on assumed conservation of chloride and enthalpy and reequilibration with quartz after mixing. Proper application of these mixing models depends therefore on the fulfillment of a number of assumptions, the validity of which should be considered in each case. Mixing model temperatures have been calculated for appropriate spring and well analyses in Table 1. The accuracy of mixing model calculations depends to a great degree on measurement or accurate estimation of the chemistry and temperature of local cold subsurface water. For these calculations, as well as for isotope hydrology (see below), collection and analysis of cold waters should be an important part of a geochemical exploration program. The warm spring

mixing model was applied by Gupta, Saxena, and Sukhija (p. 741) to the Manikaran, India, geothermal system and by Young and Whitehead (1975a,b) to Idaho thermal waters.

Components other than silica and chloride may be used in mixing models. The temperature and salinity of a hypothetical concentrated high-temperature component have been calculated by Mazor, Kaufman, and Carmi (1973) from ¹⁴C contents and by Mizutani and Hamasuna (1972) from sulfate and water isotopes (analyses Is3 and J1).

Qualitative Geothermometers

Qualitative geothermometers were reviewed at the first UN Geothermal Symposium by Mahon (1970), Tonani (1970), and White (1970). These geothermometers may be applied to spring waters and gases, fumarole gases, altered rock, soils, and soil gases. Ratios and contents of dissolved hot-spring constituents and gases resulting from high-temperature reactions, but not susceptible to quantitative temperature calculation, are useful for indicating subsurface flow paths when siting wells (Mahon, p. 775).

Substances carried in steam are important in the study of systems without hot springs and may indicate subsurface flow paths more effectively than liquid water discharges, which are more subject to lateral flow (Healy, p. 415; Healy and Hochstein, 1973). Gas discharges were used by Glover (1972) to indicate upflow zones in Kenya geothermal systems, where hot water discharges were lacking or grossly contaminated with surface waters. Gas ratios were also useful at El Tatio, Chile (Cusicanqui, Mahon, and Ellis, p. 703), where extensive lateral flow of hot water occurs (see discussion below). Ammonia and boron have been used as indicators in thermal seawaters which are otherwise unresponsive to subsurface temperature (Domingo and Papastamatoki, p. 109).

New studies using sensitive analytical methods have shown that soil gases in geothermal areas have anomalous concentrations of mercury (Koga and Noda, p. 761) and helium (Roberts et al., 1975), and contain CO₂ with anomalously high ¹³C:¹²C ratios (Rightmire and Truesdell, 1974). Volatile substances dispersed from geothermal fluids may accumulate in soils and altered rocks, and patterns of soil mercury (Matlick and Buseck, p. 785) and of mercury, arsenic, and boron in altered rocks (Koga and Noda, p. 761) may indicate subsurface fluid flow, as may alteration patterns (Sumi and Takashima, p. 625).

The most important application of qualitative geothermometers is in preliminary exploration over large areas. "Blind" convection systems may exist or surface fluid flows may be inconspicuous or difficult to distinguish from non-thermal sources. In these cases, it may be possible to analyze surface fluids for distinctive "geothermal" components. Lithium in surface waters of central Italy has been tested as a geothermal indicator by Brondi, Dall'Aglio, and Vitroni (1973); and, in a study of the same area, criteria for distinguishing river sulfate of geothermal origin (from H₂S oxidation) from sulfate resulting from solution of evaporites or from oxidation of sulfide minerals have been developed by Dall'Aglio and Tonani (1973). Much anomalous boron in surface waters (other than those in closed basins) is probably of geothermal origin (Morgan, 1976), and Larderello steam has been shown to contribute large quantities of boron to surficial waters (Celati, Ferrara, and Panichi, Abstract III-11). Anomalous arsenic from natural and exploited geo-

thermal systems has been found in the Waikato River, New Zealand (Rothbaum and Anderton, p. 1417), and in the Madison River, Montana (Stauffer and Jenne, Abstract IV-14). Fish in the Waikato River appear to accumulate mercury of geothermal origin (Weissberg and Zobel, 1973), but Yellowstone fish do not (L. K. Luoma and E. A. Jenne, oral commun., 1976).

Geothermal waters of meteoric origin may exchange oxygen isotopes with rock during deep circulation, and this "oxygen shift" has been used as a positive or negative qualitative geothermometer (Fancelli, Nuti, and Noto, Abstract III-23; Fouillac et al., p. 721).

Although sampling is difficult, gases and solids can also be used in regional exploration. In a reconnaissance study of much of central and southern Italy, Panichi and Tongiorgi (p. 815) found carbon isotopes in CO_2 , and travertine associated with known and prospective geothermal areas, to be distinctly heavy compared with those from other sources. The use of other isotopes in regional exploration (^{34}S in air gases for instance) should be investigated. Mercury vapor has been found in the atmosphere of the Beppu, Japan, geothermal system (Koga and Noda, p. 761) and might be detectable in a regional survey.

ISOTOPE HYDROLOGY AND THERMOMETRY

Isotope compositions and rare gas contents of geothermal fluids have been used to indicate sources of recharge, time of circulation, fluid mixing, and subsurface temperatures. Geothermal isotope and nuclear studies have been the subject of symposia at Spoleto, Italy (Tongiorgi, 1963), Dallas, Texas (Hall, 1974), and Pisa, Italy (Gonfiantini and Tongiorgi, 1976), and were extensively reviewed by White (1970, 1974). Many papers on nuclear hydrology with application to geothermal studies were recently presented at Vienna (International Atomic Energy Agency, 1974).

Hydrology

A major discovery resulting from early measurements of the oxygen-18, deuterium, and tritium contents of thermal fluids was that local meteoric water overwhelmingly dominates recharge of most geothermal systems (Craig, Boato, and White, 1956; Craig, 1963; Begemann, 1963). More recent studies (reviewed by White, 1970) agree with the early data with a few exceptions. New ^{18}O , deuterium and tritium measurements of cold and thermal fluids of Larderello, Italy, demonstrate local meteoric recharge with both long and short circulation times (Celati et al., 1973; Panichi et al., 1974). Meteoric water dominance has also been demonstrated for thermal fluids of El Tatio, Chile (Cusicanqui, Mahon, and Ellis, p. 703), Kawah Kamojang, Indonesia (Kartokusumo, Mahon, and Seal, p. 757), the Massif Central, France (Fouillac et al., p. 721), Iceland (Arnason, 1976; Tómasson, Fridleifsson, and Stefánsson, p. 643), Lake Assal, Afars and Issas (Bosch et al., 1976), Broadlands, New Zealand (Giggenbach, 1971), Yellowstone, Wyoming (Truesdell et al., Abstract III-87), Long Valley, California (Mariner and Willey, 1976), and southwestern Idaho (Rightmire, Young, and Whitehead, 1976). In most of these systems (El Tatio, Yellowstone, Iceland, Idaho, and Long Valley), hot-spring waters are a mixture of a local cold meteoric component and a hot thermal water component, also of meteoric origin but from higher elevation and somewhat distant from the hot-spring area.

Mixing of local cold water with hot seawater has been demonstrated by ^{18}O and deuterium studies of coastal geothermal systems of Greece (Stahl, Aust, and Dounas, 1974), Italy (Baldi, Ferrara, and Panichi, p. 687), and Japan (Mizutani and Hamasuna, 1972; Matsubaya et al., 1973; Sakai and Matsubaya, 1974). Thermal connate and metamorphic waters were shown to mix with meteoric water in the California Coast Ranges by White, Barnes, and O'Neil (1973). Meteoric thermal waters are interpreted to mix with cold saline lake waters at Lake Assal, Afars and Issas, by Bosch et al. (1976), although the high salinity of borehole waters from this area (Gringarten and Stieltjes, 1976) suggests a more complicated system.

Tritium measurements have been used to demonstrate mixing with young near-surface waters. Gupta, Saxena, and Sukhija (p. 741), using this approach, calculate hot-water fractions for spring waters of Manikaran, India, that agree with those calculated from the warm-spring mixing model.

In general, radioactive isotopes have not been successful in indicating the circulation times of geothermal systems. This results from the generally long circulation times involved (except for some Larderello steam discussed above), which are usually beyond the range of tritium dating: from the large quantities of metamorphically produced old CO_2 , which prevent use of ^{14}C measurements; and from the common admixture of young near-surface waters with old deep waters in surface thermal discharges. Recent improvements in low-level tritium analysis may improve the situation. The radioactive ^{39}Ar isotope has a half-life of 269 years, which allows a dating range of 50 to 1000 years, and has been used successfully to estimate a <70-year age for water in a Swiss thermal spring (Oeschger et al., 1974). This analysis, although difficult, should also be possible for drilled high-temperature geothermal systems.

Geothermometry

Certain isotope geothermometers equilibrate more slowly than chemical geothermometers and are capable of indicating temperatures in the deeper parts of geothermal systems. By considering a number of chemical and isotopic geothermometers with various rates of equilibration, it may be possible to calculate the temperature history of a thermal water. This calculation would depend on the existence of considerably more rate data than are now available.

At the time of the first UN Geothermal Symposium, only the distribution of carbon isotopes between CO_2 and CH_4 , ($\Delta^{13}\text{C}[\text{CO}_2, \text{CH}_4]$), had been tested as a geothermometer. Analyses of well discharges of Larderello (analysis It8; Ferrara, Ferrara, and Gonfiantini, 1963) and Wairakei (analysis NZ1; Hulston and McCabe, 1962b) indicated temperatures in good agreement with measured reservoir temperatures. These indicated temperatures were based on fractionation factors calculated by Craig (1953) which have been shown to be somewhat in error by Bottinga (1969). Using the corrected fractionation factors, indicated temperatures are increased by 50 to 75°C and the new temperatures are higher than those found in the reservoir. Experimental work is needed on this geothermometer to confirm the new fractionation factors, but the indicated temperatures may be real and exist in these systems below drilled depths. CO_2 - CH_4 temperatures at Broadlands, New Zealand (analysis NZ3), range from 385 to 425°C (Lyon, 1974) considerably above the reservoir temperatures (~270°C), although tem-

peratures in a deep Broadlands drillhole reached 307°C. New measurements at Larderello (C. Panichi, oral commun., 1975) indicate subsurface temperatures that vary with, but are higher than, observed reservoir temperatures. Temperatures for $\Delta^{13}\text{C}(\text{CO}_2, \text{CH}_4)$ have also been calculated for geothermal fluids from Indonesia (analysis Ids 1), Kenya (analyses K1-3), and the United States (analyses US5 and US36).

Hydrogen isotope geothermometers, $\Delta\text{D}(\text{H}_2, \text{CH}_4)$ and $\Delta\text{D}(\text{H}_2, \text{H}_2\text{O})$, have been tested in a few systems in Kenya; New Zealand; the Imperial Valley, California; and Yellowstone; but appear to reequilibrate rapidly and in most cases, indicate temperatures that approximate those of collection (analyses K2, NZ3, US5 and US36). Recently, Horibe and Craig (*in* Craig, 1976) have experimentally calibrated the $\text{H}_2\text{-CH}_4$ geothermometer, which should encourage more isotopic analyses of these gases.

Although gas isotope geothermometers are the only ones available for vapor-dominated systems, they leave much to be desired as practical exploration tools for hot-water systems. Equilibrium may be achieved only below drillable depths ($\text{CO}_2\text{-CH}_4$) or continue up to the sampling point ($\text{H}_2\text{-CH}_4$, $\text{H}_2\text{-H}_2\text{O}$), and most geothermal gases (especially from hot springs) are so low in methane that collection and separation are difficult.

For hot-water systems the most useful proven isotope geothermometer may be the fractionation of oxygen isotopes between water and its dissolved sulfate, which appears to equilibrate in geothermal reservoirs at temperatures as low as 95°C, and to reequilibrate so slowly during fluid ascent to the surface that evidence of temperatures above 300°C is preserved in some hot-spring waters. Experimental equilibrium and kinetic data have been measured by Lloyd (1968), Mizutani and Rafter (1969), and Mizutani (1972). Equilibrium has been demonstrated between dissolved sulfate and borehole water from Wairakei (analysis NZ1; Mizutani and Rafter, 1969; Kusakabe, 1974), Otake, Japan (analysis J6; Mizutani, 1972), Larderello (analysis It8; Cortecchi, 1974), and Raft River and Bruneau-Grandview, Idaho (analyses US15 and US17; Truesdell et al., unpub. data, 1975). The application of this geothermometer to boiling springs of Yellowstone, correcting for the effect of steam loss on ^{18}O content of the water, was made by McKenzie and Truesdell (Abstract III-65), and unpublished measurements have been made on several other United States spring systems (analyses US7, US10, US18, US24, US26-27). Estimates of subsurface temperatures in Japanese geothermal systems without deep drillholes and uncorrected for steam loss appear reasonable (analyses J1-5; Mizutani and Hamasuna, 1972; Sakai and Matsubaya, 1974).

Two other geothermometers need more testing. The first, $\Delta^{34}\text{S}(\text{SO}_4, \text{H}_2\text{S})$, which has recently been calibrated experimentally by Robinson (1973), indicated unreasonably high temperatures for Wairakei bore fluids (analysis NZ2, Kusakabe, 1974) and for Mammoth, Yellowstone, water (analysis US35; Schoen and Rye, 1970). The second, $\Delta^{13}\text{C}(\text{CO}_2, \text{HCO}_3)$ may indicate the temperature of bicarbonate formation at Steamboat Springs, Nevada, and Yellowstone (analyses US24, US30, and US32), but experimental data in this system need reevaluation (O'Neil et al., Abstract III-71).

In the rather special circumstances where water and steam phases may be separately analyzed, or steam analyzed and water isotopes estimated from other samples, the liquid-vapor fractionation of deuterium or ^{18}O may be used to estimate temperatures of phase separation. This has been

done at Wairakei (Giggenbach, 1971), Campi Flegrei, Italy (Baldi, Ferrara, and Panichi, p. 687), Kawah Kamojang, Indonesia (Kartokusumo, Mahon, and Seal, p. 757), and White Island, New Zealand (Stewart and Hulston, 1976).

Rare Gas Studies

Rare gases (He, Ne, Ar, Kr, and Xe) have been analyzed in geothermal fluids and shown to indicate the source of water recharge and, less certainly, the mechanism of steam loss (Mazor, p. 793). Ne, ^{36}Ar , Kr, and Xe are not produced in rocks and do not undergo chemical reactions. However, they are affected by phase changes and their distribution between liquid and vapor is temperature dependent. For this reason, their contents in geothermal waters that have not boiled indicate that recharge waters are meteoric and allow calculation of temperatures of last equilibration with the atmosphere. In systems with subsurface boiling, the water phase is depleted in gases and their concentration patterns may indicate dilution and boiling mechanisms.

Other rare gases (^4He and ^{40}Ar) are produced from radioactive decay of rock materials and their concentrations may indicate rate of water movement through the system (Mazor, Verhagen, and Negreanv, 1974). High-temperature thermal waters in young volcanic rocks of Yellowstone and New Zealand apparently do not contain anomalous ^{40}Ar (Mazor and Fournier, 1973; Hulston and McCabe, 1962b), although young volcanic rocks that have not lost volatile elements have high ^{40}Ar contents (for example, Dalrymple and Moore, 1968). The origin and fate of ^{40}Ar in geothermal systems needs much closer study.

Several recent studies have been made of excess ^3He in ocean water (Craig, Clarke, and Beg, 1975), volcanic rocks (Lupton and Craig, 1975), and geothermal fluids of Iceland (Kononov and Polak, p. 767), Kamchatka (Gutsalo, p. 745), and Imperial Valley, Lassen, and Kilauea in the United States (Craig, unpub. data, 1975). ^3He has been depleted from the atmosphere and crust because it is lost into space at a greater rate than ^4He , and its enrichment in waters and rocks associated with spreading centers indicates contributions from the mantle. As noted earlier, mantle contribution of this isotope does not necessarily indicate that other mantle-derived components are present in geothermal fluids.

CHEMICAL MODELING AND METHODOLOGY

Modeling

Geothermal systems are chemically very active. Deep minerals are altered in response to the prevailing pressure, temperature, and chemical conditions, and ascending fluids change their physical and chemical properties rapidly over relatively short distances and effect profound mineralogical changes in rocks traversed. Mineralogical changes in these processes were reported by Bird and Elders (p. 285) and Reed (p. 539). It would appear both challenging and rewarding to model these changes, but disappointingly few attempts have been made.

Pampura, Karpov, and Kazmin (p. 809) report a chemical model for the changing compositions of ascending fluids of the Puzhetsk geothermal system. Many of the changes described earlier as occurring during the near-surface alteration of volcanic waters are successfully modeled, but the

absence of potassium in the fluids and of aluminosilicate minerals is a severe limitation. A relatively simple model for computing the downhole character of geothermal fluids (Truesdell and Singers, 1971) has been used to calculate deep pH values.

Using established models for solution and mineral equilibria, mineral alteration has been related to deep fluid chemistry for Broadlands, New Zealand, by Browne and Ellis (1970) and for Cerro Prieto, Mexico, by Reed (p. 539). In both these systems, deep waters are in near equilibrium with rock minerals and produced their observed metamorphism. Mass transfers in the Dunes, Imperial Valley, geothermal system were deduced from mineralogical changes by Bird and Elders (p. 285).

Methodology and Data

The geochemical investigations described in this report depend both on the accurate chemical and isotopic analysis of natural fluids and on laboratory measurements of the properties of chemical substances over a range of temperature and pressure. Because analyses of many samples from a geothermal system allow a more complete reconstruction of chemical processes and deep conditions, analytical methods that are rapid and inexpensive or that can be automated are useful. Bowman et al. (p. 699) and Hebert and Bowman (p. 751) describe automated instrumental methods of water analysis that appear to be rapid and accurate and can provide analyses for trace constituents not normally measured. Some of these traces may provide geothermometers when their behavior is better understood.

Geothermometer components are necessarily not in equilibrium under surface conditions, and special care must be taken to preserve them for analysis by dilution (SiO_2) or filtration and acidification (Ca). Thompson (1975) and Presser and Barnes (1974) report methods for collection and preservation or field analysis of geothermal waters. Akeno (1973) describes methods for preservation and analysis of geothermal gases. Downhole samplers for geothermal wells have been described by Fournier and Morganstern (1971) and Klyen (1973). Collection of geothermal fluids was the subject of a recent workshop (Gilmore, 1976).

Potter (p. 827) and Potter, Shaw, and Haas (1975) have compiled and assessed the status of studies on the density and other volumetric properties of geothermal brine components, and, using critically evaluated data, Haas (1971) has calculated boiling point-to-depth curves for sodium chloride solutions. Compilations of geochemical data are also being made by the Lawrence Berkeley Laboratory (Henderson, Phillips, and Trippe, Abstract I-15).

It is impossible to review here the many experimental studies of solution chemistry at high temperatures and pressures that are directly applicable to geothermal systems. These studies have been recently reviewed by Ellis (1967, 1970), Franck (1973), Helgeson (1969), Helgeson and Kirkham (1974), and Marshall (1968, 1972). When sophisticated chemical models are constructed for geothermal systems in their natural and disturbed states, these experimental studies will provide vital data.

AN EXAMPLE OF EXPLORATION GEOCHEMISTRY

The role of chemistry in geothermal exploration is well illustrated by investigations at El Tatio, Chile, reported by

Cusicanqui, Mahon, and Ellis (p. 703), Lahsen and Trujillo (p. 157), and Armbrust et al. (1974), that were made in conjunction with geological and geophysical studies (Healy and Hochstein, 1973; Hochstein, Abstract III-39; Healy, p. 415) by New Zealand and Chilean scientists with United Nations support. El Tatio lies at an altitude of 4250 m in the high Andes. There are over 200 hot springs, most of which boil (at 85.5°C at this altitude) and deposit sinter and halite. Many of these springs were analyzed for major and minor components and some, along with cold springs and snow samples, were analyzed for ^{18}O and deuterium. Fumaroles were analyzed for gases.

The analyzed spring waters showed narrow ranges of Cl:B and Na:Li ratios, indicating homogeneous thermal water at depth. Waters of the northernmost spring group were rather uniform in composition, with 8000 ± 200 ppm chloride, SiO_2 contents of $260 \pm$ ppm, and Na:K weight ratios near 8.2. To the south and west, spring waters have lower SiO_2 contents, higher Na:K ratios, and Cl contents of about 4000 to 6000 ppm, indicating mixing with near-surface waters.

Direct application of chemical geothermometers to high-chloride spring waters indicated minimum subsurface temperatures averaging 160°C from quartz saturation, 167°C from Na:K ratios, and 205°C from NaKCa relations. Maximum indicated temperatures were 189°C (quartz saturation), 210°C (Na:K), and 231°C (NaKCa). The boiling-spring mixing model of Truesdell and Fournier (p. 837), not yet developed at the time of the original investigations, can be applied to these spring waters assuming that those to the north were not diluted and that those to the south and west were mixtures with cold dilute water ($t = 4^\circ\text{C}$, $\text{Cl} = 2$ ppm). Average calculated subsurface temperatures are 208°C, but the maximum indicated temperature of 274°C is considered to be a better indication of the maximum aquifer temperature. Some of the high-chloride El Tatio springs issue at temperatures below boiling, and warm-spring mixing calculations, assuming cold waters of 4°C and 25 ppm SiO_2 , indicate an average subsurface temperature of 269°C (standard deviation 13°C).

The patterns of Cl contents, SiO_2 contents, Na:K ratios, and Na:Ca ratios were interpreted to indicate that cold near-surface drainage from the east was entering a shallow aquifer in the western and southern areas, and diluting high-chloride water rising from greater depths.

Deuterium analyses of the thermal waters agreed with the general picture of near-surface mixing, but suggested that the deep recharge was from higher elevation precipitation with lower deuterium values. Cold-water samples from the higher mountains to the east also tended to have lower deuterium values than local precipitation and were considered possible recharge waters.

Fumarole gas analyses also suggested movement from east to west, but at shallower depths. Eastern fumaroles had much higher contents of CO_2 and H_2S than other gases, and higher ratios of $\text{H}_2\text{S}:\text{CO}_2$. Quantitative interpretation of gas concentrations is difficult because of the effects of rock reaction and fractional separation into steam. In general, gases tend to decrease in CO_2 and H_2S content and in $\text{H}_2\text{S}:\text{CO}_2$ ratio with lateral flow (Mahon, 1970; Truesdell, 1976a). In retrospect, more weight should have been given to the fumarole chemistry in siting exploratory wells.

On the basis of resistivity surveys and spring chemistry, six slim holes were drilled to about 600-m depth. In the west and northwest, holes 1, 2, and 4 encountered maximum

temperatures of 212 to 230°C, with temperature inversions toward the bottoms of the wells. In wells 3 and 6, in the southwest, temperature inversions were not found and 254°C was measured in well 3. Seven production wells were located near No. 3, and the best of these (No. 7) tapped fluids of 263°C. A shallow (about 170-m) aquifer at 160°C was encountered in the Trucle dacite, which is probably where mixing with near-surface water occurs to produce the lower chloride waters of the western and southern springs. Deeper aquifers in the Puripicar ignimbrite (500 to 600 m) and the Penaliri (Salado) tuffs and breccias (700 to 900 m) were at about 230 and 200 to 260°C, respectively.

Comparison of drillhole and spring analyses indicates that the most concentrated spring waters are undiluted samples of the deep thermal fluids. The quartz saturation, Na:K, and Na:KCa geothermometer temperatures are low, indicating considerable subsurface reequilibration. The mixing calculation temperatures are, however, surprisingly accurate.

Lateral subsurface flow from east to west, indicated by water isotopes and fumarole gases, was confirmed by drillhole measurements. Tritium contents of drillhole fluids suggested that the subsurface transit time was 15 years (unusually short for geothermal waters), but small additions of young near-surface water would also explain the results. The early resistivity survey did not indicate lateral flow, and a resurvey was made after the exploratory holes were

drilled. This showed a much larger anomaly that could be interpreted as due to deep lateral flow.

Two chloride inventories were made to estimate the total heat flow from the heat:chloride ratio of the thermal waters, which was established from drillhole fluid temperatures and chloride contents. These were not very accurate because of salt accumulation at the surface, but indicated a heat flow of 30 to 50 × 10⁶ cal/sec.

EI Tatio is very favorable for the application of geochemical methods because there are a large number of springs with rapid flow from the thermal aquifer, and the surface chemistry indicated subsurface conditions with reasonable accuracy. Gas and isotope analyses correctly suggested subsurface flow patterns, and chemical geothermometers and mixing models predicted temperatures at increasing depths in the system.

ACKNOWLEDGMENTS

I wish to thank Carolyn Kriet, Nancy Nehring, and Lane Tanner for help in the preparation of this paper, and Robert Fournier, Donald White, Patrick Muffler, Everett Jenne, Manuel Nathenson, and Stefan Arnórsson for reviews and continuing useful discussions. I also wish to thank those colleagues whose unpublished data or calculations have been used in this paper.

Table 1. Chemical summaries and geothermometer temperatures for selected thermal fluids. (See end of table for explanatory notes.)

Area	System Type	Sample Type	Sampling Temp °C	Analyses	Water Type	TDS	Gases	t _{SiO₂ adia} °C	t _{SiO₂ cond} °C	t _{Na/K} °C	t _{NaKCa} °C	Other Geothermometers °C	Observed Temp °C (depth)	References	
Afars and Issas															
Af1	Lake Assal, Spr 6	VW	s	83	w, i	Na>Ca>>K>>Mg Cl>>SO ₄ >>HCO ₃	66000	156	166	174	202	~165 Na-Ca-SiO ₂ 272 WSMM	253 (1050 m) TDS = 190000	Bosch et al. (1976); Gringarten and Stieltjes (1976)	
Canada															
British Columbia															
Ca1	Tawah Creek (#40)	VW	s	43	w	Na>Mg>K>Ca HCO ₃ >>Cl>>SO ₄	2400	162	177	210	227			Souther (p. 259); Nevin and Stauder (p. 1161)	
Ca2	Meager Creek (#52)	VW	s	55	w	Na>K>Ca>Mg Cl>HCO ₃ >SO ₄	2000	171	187	197	211		69 (347 m)		
Ca3	Hot Springs Isl. (#57)	VW	s	76	pw	Na>Ca>>K		138	145	161	190	205 WSMM			
Chile															
El Tatio															
Ch1	Spr 181	VW	s	84.5	w, tr, i	Na>>K>Ca>>>Mg Cl>>>HCO ₃ >>SO ₄	7060	142	149	195	211	229 BSMM		Cusicanqui, Mahon and Ellis (p. 703); Lahsen and Trujillo (p. 157); Armbrust et al. (1974)	
Ch2	Spr 226		s	83	w	Na>K>Ca Cl>>SO ₄ >HCO ₃	14000	184	199	210	230				
Ch3	Well 7		w	85.5	w, g	Na>>K>>Ca>>>Mg Cl>>>HCO ₃ >SO ₄	15600	CO ₂ >>>H ₂ S	257	261	261	262 BSMM	263 (800 m)		
Ch4	Average of 26 springs with standard deviation (σ) and maximum		s	52-85.5				160 ave 15 σ 189 max		205 ave 20 σ 231 max	208 ave 27 σ 274 max	209 ave 13 σ 283 max	229 BSMM, 269 ave WSMM	140-170, 190-235, 236-263	Truesdell and Fournier (p. 837)
Columbia															
Co1	Ruiz, Spr A1	VW	s	90	pw, i	Na>>K>>Ca>>Mg Cl>>HCO ₃ >SO ₄	1570	CO ₂ , H ₂ S		255	234			Arango et al. (1970)	
Czechoslovakia															
Cz1	Danube lowland	NVS	w			inc depth HCO ₃ -Na HCO ₃ -Cl-Na Cl-HCO ₃ -Na	<1000 ≤5000 ≤10000	N ₂ , CH ₄ , ±CO ₂					38 1000 m gradient	Franko and Mucha (p. 979)	
Cz2	Stranka	NVF	w		pw					36	115	20 Na-K-Ca-CO ₂ 73 Chal	40 (1005 m)	Pačes and Čermák (p. 803)	
Cz3	Karlovy Vary	NVF	w	72	pw					154	188	44 Na-K-Ca-CO ₂ 91 Chal	72 (6 m)		
Cz4	Jachymov	NVF	w		pw					137	92	21 Na-K-Ca-CO ₂ 66 Chal	30 (493 m)		
Central depression (Danube lowland)															
Cz5	Chorvotský Grob	NVS	w	46		Cl-HCO ₃ -Na	1800						46 (970-1210m)	Franko and Račický (p. 131)	
Cz6	Topolníky	NVS	w	90		HCO ₃ -Cl-Na	3900						90(2040-2490m)		
Cz7	Levice block, Podhájska	NVS	w	80		Cl-Na	19600						80(1160-1900m)		
Cz8	Liptov depression, Besenova	NVS	w	34		SO ₄ -HCO ₃ -Ca-Mg	3200						34 (420m)		
El Salvador															
Ahuachapán															
ES1	Salitre	VW	s	63	w, tr, g, i	Na>>Ca>K>>>Mg Cl>>>SO ₄	1330	CO ₂ >>>N ₂ >>>CH ₄	162	175	230	207		Sigvaldason and Cuéllar (1970); Glover and Cuéllar (1970); Cataldi et al. (II-43)	
ES2	Ah-1		w	~96	w	Na>>K>Ca>>>Mg Cl>>>SO ₄	19300		249	259	256		231		

Area	System Type	Sample Type	Sampling Temp °C	Analyses	Water Type	TDS	Gases	t _{SiO₂ adid} °C	t _{SiO₂ cond} °C	t _{Na/K} °C	t _{Na/KCa} °C	Other Geothermometers °C	Observed Temp °C (depth)	References
Ethiopia														
E1	East of Awasa (Spr 6-4)	VW	s	87	w, tr	Na>>K>>Ca>Mg HCO ₃ >>SO ₄ >>Cl	1640	151	158	196	207	225 WSMH		UNDP (1971); Demissie and Kahai (I-10); Gonfiantini, Borsa, Ferrara and Panichi, 1973, Earth and Planetary Sci. Letters, v. 18, p. 13-21.
E2	Aluto Spr 10	VW	s	96.5	w, tr	Na>>K>>Ca>Mg HCO ₃ >Cl>SO ₄	2510	159	168	158	211			
E3	Tendaho Spr 15	VW	s	100	w, tr	Na>>K>Ca>>>Mg Cl>>SO ₄ >>HCO ₃	1950	206	224	193	204			
E4	Lake Afrera Spr 31	VW	s	57.5	w, tr	Na>Ca>>K>>Mg Cl>>>SO ₄ >>>HCO ₃	19100	124	130	150	179	208 WSMH		
France														
Massif Central														
F1	Chateauneuf, bain tempéré	NVF	s	37	pw	Na>>Ca>K		143	155	154	178	~50 Na-K-Ca-CO ₂ 130 Chalc		Fouillac et al. (p. 721)
F2	Chatelguon, Alice	NVF	s	35.5	pw, i	Na>Ca>>K		139	150	198	183	~50 Na-K-Ca-CO ₂ 124 Chalc		
F3	Ste. Marguerite, Rive d'Allier	NVF	s	29	pw	Na>>Ca>K		137	148	215	203	~50 Na-K-Ca-CO ₂ 122 Chalc		
F4	Royat, Eugénie	NVF	s	33	pw	Na>>Ca>K		126	136	215	195	~50 Na-K-Ca-CO ₂ 108 Chalc		
Greece														
G1	Kamena Vorla, Gamma 9	VSw	w	47.9	w	Na>>Ca>Mg>K Cl>>SO ₄ >HCO ₃	18900	96	99	121	169	67 Chalc		Dominco and Papastamatoki (p. 109); Stahl, Aust and Dounas (1974)
G2	Thermopylae, Psaroniria	VSw	s	32.5	w, i	Na>>Ca>Mg>K Cl>>SO ₄ >>HCO ₃	27800	45	45	119	173	11 Chalc		
G3	Edipsos, Damaris	VSw	s	78.5	w	Na>>Ca>>K>Mg Cl>>>SO ₄ >HCO ₃	33400	110	112	120	174	81 Chalc		
G4	Lesbos, Arginos	VSw	s	81	w	Na>>Ca>K>Mg Cl>>SO ₄ >>HCO ₃	11800	135	141	171	191	113 Chalc 198 WSMH		
G5	Nisiros, Demotika Loutra	VSw	s	48.5	w	Na>>Ca>Mg>K Cl>>>SO ₄ >>HCO ₃	32000	160	174	114	167			
G6	Milos, Mavros Gremos	VSw	w	45	s	Na>>Ca>K>>Mg Cl>>>SO ₄ >>HCO ₃	33800	172	185	232	205		138 (70 m)	
G7	Sousaki, borehole	VSw	w	73	pw	Na>>K>Ca>Mg Cl>>>SO ₄	45100			249	265	>120 boiling calc.	73 (145 m)	
Guadeloupe														
Gu1	Bouillante 2	VSw	w	~99	pw, tr, g	Na>>Ca>K>>>Mg	>24600			242	232		242 (338 m)	Demians d'Archimbaud and Munier-Jolain (p. 101); Cormy, Demians d'Archimbaud and Surcin (1970)
Gu2	Spr G52.4	s	s	59	w	Na>Ca>>K>>Mg Cl>>>SO ₄ >HCO ₃	3020	152	164	199	189	200 WSMH2		
Hungary														
Pannonian Basin														
H1	Triassic dolomite	NVS	w	100?	w	Na>>Ca>>Mg>K HCO ₃ >SO ₄ >Cl	1410		103	181	75		150? (950±m)	Boldizsár and Korim (p. 297)
H2	U-Plio. sandstone	NVS	w	99?	w	Na>>>K>>Ca HCO ₃ >>>SO ₄ =Cl	1560		107	119	164		100-150 (2250±m)	

Table 1. Chemical summaries and geothermometer temperatures for selected thermal fluids (continued).

Area	System Type	Sample Type	Sampling Temp °C	Analyses	Water Type	TDS	Gasos	t _{SiO₂ adia} °C	t _{SiO₂ cond} °C	t _{Na/K} °C	t _{Na/KCa} °C	Other Geothermometers °C	Observed Temp °C (depth)	References	
Iceland															
Ic1	Selfoss	NVP	s	79	w,i	Na>>Ca>>K>>>Mg Cl>>SO ₄ >CO ₂	667 N ₂ >>CO ₂	122	126	87	120	96 Chal	91	Arnórsson (1974); Arnason (1976); Tómasson, Fridleifsson and Stefánsson (p. 643); Björnsson, Arnórsson and Tómasson (1972); Arnórsson et al. (p. 853)	
Ic2	Deildartunga	NVP	s	99	w,i	Na>>Ca>>K>>>Mg SO ₄ >Cl>CO ₂		145	150	86	123	124 Chal			
Ic3	Seltjarnarnes	NVP	s	83	w,i	Na>>Ca>>K>>>Mg Cl>>SO ₄ >>>CO ₂		1110	137	143	109	115 Chal	119		
Ic4	Lýsuhóll	NVP	s	40	w,i	Na>>Ca>>K>>Mg CO ₂ >>>Cl>>SO ₄	1670 CO ₂ >>>H ₂	160	176	162	174	153 Chal			
Ic5	Torfajokull, Eyrarhver	VW	s	95	w,i	Na>>>K>>>Ca>>>Mg Cl>>SO ₄ >>CO ₂		1350	194	209	148	199	193 Chal		
Ic6	Geysir	VW	s	84	w,i	Na>>>K>>>Ca>>>Mg CO ₂ >>Cl>>SO ₄		1130	227	256	200	220			
Ic7	Reykjanes	VSw	s	99	w, tr, g	Na>>Ca>>K>>>Mg Cl>>>SO ₄ >>>CO ₂	48300 CO ₂ >>>N ₂ >H ₂ S >O ₂ >>CH ₄	234	262	210	231	262 boiling calc.			
Ic8	Reykjanes Well 8	VSw	w	270	w,i	Na>>Ca>>K>>>Mg Cl>>>CO ₂ >>>SO ₄		33650		270	234	240	270		
Ic9	Svartsengi Well 3	VSw	w	236	w,i	Na>>>K>>>Ca>>>Mg Cl>>>CO ₂ >>>SO ₄		22460		241	251	245	236		
Ic10	Krisuvik Well 6	VSw?	w	258	w	Na>>>K>>Ca>>>Mg Cl>>>HCO ₃ >>SO ₄		2600		257	260	234	215-240 K(CO ₂ =CH ₄)		258 (500 m)
Ic11	Námafjall Well 4	VW	w	258	w, g, i	Na>>>K>>>Ca>>>Mg CO ₂ >>SO ₄ >Cl	956 H ₂ >CO ₂ >H ₂ S >N ₂ >>CH ₄		261	262	237		258		
Ic12	Hveragerdi Well 4	VW	w	198	w, g, i	Na>>>K>>>Ca>>>Mg CO ₂ >>Cl>SO ₄	681 CO ₂ >>>H ₂ = H ₂ S>>CH ₄		200	169	187	182 Chal	198		
India															
Puga, Ladakh (NW Himalaya subprov. I)															
Ida1	Spr 101	VW	s	83	w	Na>>>K>>>Ca=Mg HCO ₃ >Cl>>SO ₄		2850	149	157	258	247	221 WSMM		Shanker et al. (p. 245); Chaturvedi and Raymahashay (p. 329); Gupta, Saxena and Sukhija (p. 741); Jangi et al. (p. 1085); Krishnaswamy (p. 143); Gupta, Narain and Gaur (p. 387)
Ida2	Well GW5	VW	w	100	w	Na>>>K>>>Ca>>>Mg HCO ₃ >Cl>>SO ₄		2420	163	171	248	234	231 WSMM	100 (51 m) max 135 (42 m)	
Chumathang, Ladakh (NW Himalaya I)															
Ida3	Spr 40	VW	s	49	w	Na>>>K>>Ca>>>Mg HCO ₃ >SO ₄ >>>Cl		1250	153	166	148	170			
Ida4	Well CGW1	VW	w	85	w	Na>>>K>>Ca>>>Mg HCO ₃ >SO ₄ >Cl		1480	161	171	151	171	102 (20 m) max 109 (30 m)		
Manikaran, Himachal Pd. (NW Him. II)															
Ida5	Spr 4	VW	s	81	w, T	Na>>Ca>>K>>Mg HCO ₃ >Cl>>SO ₄		595	141	148	288	204	209 WSMM		
Ida6	Spr 11	VW	s	82	w	Ca>Na>Mg>K HCO ₃ >>>Cl>>SO ₄		550	127	131	268	194	170 WSMM		
Ida7	Kasol (NW Him. II)	VW	s	42	w	Ca>Na>Mg>K HCO ₃ >>>SO ₄ =Cl		531	105	111	322	195	224 WSMM		
Ida8	Tatwani (NW Him. III)	VW	s	57	w	Na>>>Ca>>K>>Mg Cl>HCO ₃ >>>SO ₄		611	90	93	117	146	113 WSMM		
Ida9	Kopili, Naga-Lushai	VW?	s	57	w	Na>>>Ca>>>K>>Mg HCO ₃ =SO ₄ >Cl		449	116	122	108	129			
Ida10	Tural Ratnigiri, West Coast	VW?	s	61	w	Na>Ca>>K>>>Mg Cl>>SO ₄ >HCO ₃		922	119	125	279	207	203 WSMM		
Ida11	Tuwa, Cambay	NVS	s	63	w	Ca>>>Na>>K>>>Mg Cl>>>SO ₄		3527	119	124			110-151 (2700m) 170(>3400m)		
Ida12	Bakreshwar, W. Bengal (E.I. province)	VW?	s	81	w	Na>>>K>>Ca=Mg Cl=HCO ₃ >SO ₄		468	120	124	50	114			
Ida13	Dug well, Sohna	NVS?	s	42	w	Na>Ca>>Mg>K HCO ₃ >Cl>>SO ₄		701	94	97	192	161	165 WSMM		

Area	System Type	Sample Type	Sampling Temp °C	Analyses	Water Type	TDS	Gases	$t_{SiO_2}^{adia}$ °C	$t_{SiO_2}^{cond}$ °C	$t_{Na/K}$ °C	$t_{Na/KCa}$ °C	Other Geothermometers °C	Observed Temp °C (depth)	References	
Indonesia															
Ids1	Kawah Komojang, Well 6	VS	w	238	w,pl,pg	Na>>K>>>Ca SO ₄ >>>Cl	730	CO ₂ >>H ₂ S		240	232	217	220-230 "Isotope" 260 $\Delta^{13}C$ (CO ₂ ,CH ₄)	238 (620 m)	Kartokusumo, Mahon and Seal (p. 757); Ellis (pers. commun., 1975)
Ids2	Dieng, Pulosari Spr	VW	s	55	w	Na ₂ Ca>K ₂ Mg Cl>SO ₄ =HCO ₃	1340		143	153	436	250	203 WSM2	173 (139 m)	Truesdell (1971); Radja (p. 233) quoted from Danilchik (1973)
Israel															
Is1	Hamam El Farun	NVS?	s	72	pw	Na>>Ca>>K	>12900				93	143			Eckstein (p. 713)
Is2	Rift Valley Spr	NVF?	s		pg										Mazor (p. 793)
Is3	Hammat Gader	NVP	s	52±	pw,i,g, 14C	Na>Ca>>Mg>K Cl>HCO ₃ >SO ₄	1490	N ₂ >O ₂ >CH ₄ , rare gases			175	90	68 ¹⁴ C mixing		Mazor, Kaufman and Carmi (1973)
Italy															
Campi Flegrei															
It1	Spr 6D	VSw	s	34	w, tr, i	Na>>Ca ₂ K>>Mg Cl>>>SO ₄ >HCO ₃	3600		116	123	252	217	271 WSM	>300 (1800 m)	Baldi, Ferrara and Panichi (p. 687); Cameli et al. (p. 315)
It2	Spr 5	VSw	s	88	w, tr, i	Na>>>Ca ₂ K Cl>>>SO ₄ >HCO ₃	25500		161	171	97	167	130-190 $\Delta^{18}O$ -D (steam-water)		
It3	Stufe d'Nerone		s										>300		Meidav and Tonani (p. 1143)
It4	Tuscany, Romana, Spr 50 (group C)	VW	s	56	w, tr, g	Ca>>Mg>>K=Na SO ₄ >HCO ₃ >>>Cl	2390	CO ₂ >>>N ₂ >>>O ₂	108	113	760	260	82 ChalC 163 WSM		Baldi et al. (1973)
It5	Cesano Well 1	VW	w		w, tr	Na>K>>>Ca>>Mg SO ₄ >>Cl>>HCO ₃	356000		148	153	548	521		210 (1400 m)	Calamai et al. (p. 305)
It6	Tuscany Spr 12836	VW	s	38	w	Ca ₂ Na>Mg>>K HCO ₃ >>SO ₄ >Cl	6400		74	77	190	78			Brondi, Dall'Aglio and Vittrani (1973)
It7	Acqua Borra Larderello	VW	s	37	pw, i	Na>>>Ca>K	>10600				169	198			Fancelli and Nuti (1974)
It8	Wells	VS	w		i, T								220-390 $\Delta^{13}C$ (CO ₂ ,CH ₄) 152-329 $\Delta^{18}O$ (SO ₄ ,H ₂ O)	~240	Panichi et al. (1974); Ferrara, Ferrara and Gonfiantini (1963); Cortecchi (1974)
It9	B.S. Michele	VS	s	47	pw, i	Na ₂ Mg>Ca>>K Cl>HCO ₃ >SO ₄	357				312	84			
Japan															
Coastal Waters															
J1	Shimogamo 20	VSw	w	100	pw, i, i(SO ₄)	Ca ₂ Na>>>K>>>Mg Cl>>>SO ₄ >HCO ₃	~18000				154	174	200 $\Delta^{18}O$ (SO ₄ -H ₂ O) 150 CaSO ₄ sat. 221-335 isotope mixing	n.a. (179 m)	Mizutani and Hamasuna (1972); Sakai and Matsubaya (1974)
J2	Ibusuki 4	VSw	s	97	pw, i, i(SO ₄)	Na>>Ca>K>>Mg Cl>>>SO ₄	~19000				167	200	200 $\Delta^{18}O$ (SO ₄ -H ₂ O) ~200 CaSO ₄ sat.		Sakai and Matsubaya (1974); Matsubaya et al. (1973)
Arima Type															
J3	Yashio	NVS?	s	1	pw, i, i(SO ₄)	Ne>>K ₂ Ca>>Mg Cl>HCO ₃ >SO ₄	~34000				183	231	170 $\Delta^{18}O$ (SO ₄ -H ₂ O)		
Greentuff Type															
J4	Tottori	NVS?	s	48	pw, i, i(SO ₄)	Na>>Ca>>>K>Mg SO ₄ >Cl>HCO ₃	~4700				76	130	102 $\Delta^{18}O$ (SO ₄ -H ₂ O)		
Volcanic Type															
J5	Beppu	VW	s	100	pw, i, i(SO ₄)	Na>>K>Ca>Mg Cl>>SO ₄ >>>HCO ₃	~3800				232	239	193 $\Delta^{18}O$ (SO ₄ -H ₂ O)		
J6	Otaki 8	VW	w		w, tr, i, i(SO ₄)	Na>>K>>>Ca>>>Mg Cl>>SO ₄ >HCO ₃	3190		227	222	229	220 $\Delta^{18}O$ (SO ₄ -H ₂ O)	195 (500 m)	Mizutani (1972); Koga (1970)	
J7	Otaki Spr		s	97	w	Na>>K>>Ca ₂ Mg Cl>>>SO ₄ >HCO ₃	3680		236		210	223			Nakamura (1969)
Matsukawa															
J8	Well MR3	VS	w	~99	w	Na>K>Ca>>>Mg SO ₄ >>>HCO ₃ >Cl	2760				429	273			Sumi and Maeda (1973)

Table 1. Chemical summaries and geothermometer temperatures for selected thermal fluids (continued).

Area	System Type	Sample Type	Sampling Temp °C	Analyses	Water Type	TDS	Gases	$t_{SiO_2}^{adia}$ °C	$t_{SiO_2}^{cond}$ °C	$t_{Na/K}$ °C	$t_{Na/KCa}$ °C	Other Geothermometers °C	Observed Temp °C (depth)	References		
Japan (continued)																
Volcanic Type																
Matsukawa																
J9	Akagawa	s	42	w	Na>>K>Ca>>Mg SO ₄ >>>Cl	800		239		358	232		250 (1100 m)	Fujii and Akeno (1970); Baba et al. (1970)		
J10	Matsukawa	w		c	NH ₄ >>HBO ₂ >F>>Hg>>As	20								Koga and Noda (p. 761)		
Onikobe																
J11	Mitaki	VW	54.5	pw	Na>>Ca>K>>>Mg Cl>>HCO ₃ >>SO ₄	1540				252	208			Yamada (p. 665); Hitosugi and Yonetani (1972)		
J12	Katayama GO-10	VW	w	pw	Na>Ca>K>>Mg Cl>>>SO ₄ >>>HCO ₃	10800				361	270		295 (1300 m)			
Kenya																
K1	Olkaria #2	VW	w		Cl>HCO ₃			240		250		360 Δ ¹³ C(CO ₂ , CH ₄) >300 K(CO ₂ -CH ₄)	286 (1300 m)	Noble and Ojiambo (p. 189); recal. from Lyon, Cox and Hulston (1973 a,b); Glover (1972, 1973)		
K2	Eburru	VW?	f									490 Δ ¹³ C(CO ₂ , CH ₄) ~130 ΔD(H ₂ , CH ₄)				
K3	Hannington	VW?	s			6000-14500		170		47-68		240-500 Δ ¹³ C(CO ₂ , CH ₄)				
Mexico																
Cerro Prieto																
M1	Well M5	VW	w	99	w, pg	Na>>K>Ca>>>Li>>>Mg Cl>>>HCO ₃ >>>SO ₄	27600	CO ₂ >>H ₂ S	278	319	292	288 BSMM	289 (1300 m)	Reed (p. 539); Mercado (p. 487)		
M2	Well M9	VW	w	99	w, pg	Na>>K>Ca>>>Li>>Mg Cl>>>HCO ₃ >>SO ₄	17500	CO ₂ >>H ₂ S	228	249	250	292 BSMM	228 (1400 m)			
New Britain																
NB1	Matupi-Rabalankaia	VSw	s	85	pw, pg	Na>>Mg>Ca>K Cl>>SO ₄	34200	CO ₂ >>>H ₂ S		143	189	>150 boiling calc.		Ferguson and Lambert (1972)		
New Zealand																
Wairakoi																
NZ1	Well 44	VW	w	~99	w, i, g	Na>>K>>>Ca>>>Mg Cl>>>SO ₄ >>HCO ₃	4600	CO ₂ >>>N ₂ >H ₂ >>O ₂ >CH ₄ >Ar	248	255	259	360 Δ ¹³ C(CO ₂ , CH ₄) 200 K(CO ₂ -CH ₄) 40Ar/36Ar=290	248	Mahon (1973); Lyon and Hulston (1970); Lyon (1974)		
NZ2	Well 28		w	~99	i							305 Δ ¹⁸ O(SO ₄ , H ₂ O) 400 Δ ³⁴ S(SO ₄ , H ₂ S)		Kusakabe (1974)		
Broadlands																
NZ3	Well 8	VW	w	~99	w, i, g, tr	Na>>K>>>Ca>>>Mg Cl>>>HCO ₃ >>>SO ₄	4120	CO ₂ >>>CH ₄ >N ₂ >>H ₂ >>>Ar>O ₂	278	311	302	385 Δ ¹³ C(CO ₂ , CH ₄) 275 ΔD(CH ₄ , H ₂) 265 ΔD(H ₂ , H ₂ O) 325 K(CO ₂ -CH ₄) 40Ar/36Ar=270	273 (771 m) 307 (2160 m)	Mahon and Finlayson (1972); Giggenbach (1971); Soward (1974); Ritchie (1973); recal. from Lyon (1974); Macdonald (p. 1113)		
NZ4	Springs		s					179 ave 11 σ 202 max				183 ave 17 σ 218 max	270 ave 23 σ 306 max	BSMM	260, 265, 272	Truesdell and Fournier (p. 837); Mahon (1973, 1972)
Kawerau																
NZ5	Well 8	VW	w	~99	w, g	Na>>K>>>Ca>Mg Cl>>HCO ₃ >>SO ₄	3070	CO ₂ >>>H ₂ S 2HC>N ₂ >H ₂	263	265	283		260			
NZ6	Springs		s					188 ave 7 σ 199 max				227 ave 8 σ 239 max	225 ave 24 σ 267 max	BSMM	185, 218, 235 260, 265, 281	

Area	System Type	Sample Type	Sampling Temp °C	Analyses	Water Type	TDS	Gases	tSiO ₂ adia °C	tSiO ₂ cond °C	tNa/K °C	tNaKCa °C	Other Geothermometers °C	Observed Temp °C (depth)	References	
New Zealand (continued)															
Orakeikorako															
NZ7	Well 3	VW	w	~99	w	Na>>K>>>Ca>Mg Cl>>>HCO ₃ >SO ₄		234		250	249		237±		
NZ8	Spr 179 (Area 2)	s	98.5	w	Na>>K>>>Ca HCO ₃ =Cl>>>SO ₄	1230		192		220	245	252 BSMM			
NZ9	Springs (Area 2)	s						188 ave 6 σ 197 max		232 ave 7 σ 245 max	246 ave 7 σ 252 max	BSMM	232-241		
Waiotapu															
NZ10	Well 6	VW	w	~99	w, g	Na>>K>>>Ca>>>Mg Cl>>>HCO ₃ >SO ₄	3370	CO ₂ >>H ₂ S>>> H ₂ >N ₂ >HC	257	269	260		260		
NZ11	Springs	s						187 ave 22 σ 210 max		185 ave 46 σ 236 max	293 BSMM		210, 260, 295		
NZ12	Ngawha Well 1	VW	w	~99	w	Na>>>K>Ca Cl>B>HCO ₃ >>>SO ₄	4700		220	157	193		220-225		
Philippines															
Ph1	Tongonan 222	VW	s	85.6	w, i	Na>>K>Ca>>>Hg Cl>>>HCO ₃ >>>SO ₄	3170		154	163	224	216	243 BSMM 246 Cl-E	196 (305 m) well TGE 4	Glover (1974a,b; 1975)
Ph2	Okoy R. PA6	VW	s	94	w, i	Na>>K>Ca>>>Mg Cl>>>HCO ₃ >SO ₄	5400		171	182	190	207	198 BSMM		
Poland															
West Carpathians and Sudeties															
P1	Koszuty	NVS	w	40.5	w	Na>>>Ca>>Mg>K Cl>>SO ₄ >>HCO ₃	9540			57	18	98	75 WSMM	40.5 (1020 m)	Dowgiatko (p. 123)
P2	Zakopane	NVS	w	36	pw, i		328						37-47 Δ ¹⁸ O(SO ₄ , H ₂ O)	36 (1560 m)	Cortecchi and Dowgiatko (1975)
Red Sea Brine															
RS1	Atlantis II deep	VSw		56	w, tr, i	Na>>>Ca>K>Mg Cl>>>SO ₄	257000		108	62	159	210 heat balance 211 WSMM 261 Δ ¹⁸ O(SO ₄ , H ₂ O)		Schoell (p. 583); Brewer and Spencer (1969); Longinelli and Craig (1967)	
Rhodesia															
RI	Binga Spr			100	pg								>boiling rare gas	Mazor (p. 793)	
SW1	Sea Water			4-30+	w	Na>>Mg>>Ca=K Cl>>>SO ₄ >>>HCO ₃	34500		<25	101	173	180± Δ ¹⁸ O(SO ₄ , H ₂ O)		Hood (1972); Longinelli and Craig (1967)	
Swaziland															
SW1	Mkoba Sprs	s		51.5	pw, pg, i	Na>>>Ca>>K HCO ₃ >>>Cl>>>SO ₄	190	rare gases		53	54			Mazor, Verhagen and Negreanv (1974)	
Switzerland															
SW1	Lavey les Bains	NVP?	w	63										rare gases	Mazor (p. 793)
Taiwan															
Tatun Shan															
Ta1	Hsinpeitou	VW	s	98	w	Na>K>Ca>>Mg Cl>SO ₄	8180		168	177	405	278	263 WSMM		White and Truesdell (1972); Chen and Chern (written commun., 1975)
Ta2	Matsao E205		w	~99	w, g	Na>>K>Ca=Mg Cl>>>SO ₄	15000	CO ₂ >H ₂ S	251	264	246		240 (293 in E208)		
Ta3	Ilan Tuchung IT-1	VW?	w	98	w, g, i	Na>>>K HCO ₃ >>>SO ₄ >Cl	3640	CO ₂ >>H ₂ S	178	189	45	~160	187 Δ ¹⁸ O(SO ₄ , H ₂ O)	164 max 173 (240 m)	Fournier, Nehring and MRSO (unpub. data, 1976)

Area	System Type	Sample Type	Sampling Temp °C	Analyses	Water Type	TDS	Gases	$t_{SiO_2}^{adia}$ °C	$t_{SiO_2}^{cond}$ °C	$t_{H_2/K}$ °C	$t_{Na/KCa}$ °C	Other Geothermometers °C	Observed Temp °C (depth)	References
United States (continued)														
Idaho														
Raft River														
US16	Crank Well	NVP	w	90	w,i,g	Na>>Ca>>K>>>Mg Cl>>>SO ₄ >HCO ₃	3360 N ₂ >>CO ₂ >>O ₂ >>R	131	136	90	139	142 $\Delta^{18}O(SO_4, H_2O)$	RRCEL 147 (1526 m)	Young and Mitchell (1973); Young and Whitehead (1975a,b); Williams et al. (p. 1273); Rightmire, Young and Whitehead (1976); Truesdell, Nehring and Thompson (unpub. data, 1975)
US18	Well 11S25E-11		w	60	w	Na>>>Ca>K>>Mg HCO ₃ >SO ₄ >Cl		107	111	98	131	145 WSM		
US17	Bruneau-Grandview, Well 5S3E-28	NVS?	w	65	w,g,i	Na>>>K>Ca HCO ₃ >>Cl>SO ₄	324 N ₂ >>O ₂ >CH ₄	129	136	40	105	115 $\Delta^{18}O(SO_4, H_2O)$ 108 Chal		
US18	Weiser, Well 11N6W-10	NVP?	s	76	w,i	Na>>>K>Ca SO ₄ >HCO ₃ >Cl		149	157	95	141	228 WSM 234 $\Delta^{18}O(SO_4, H_2O)$		
Montana														
US19	Marysville	NVP?	w	98		Na>>>K>Ca>>>Mg HCO ₃ >SO ₄ >>Cl		690	125	128	124	158 98 Chal	98 (1000 m)	Blackwell and Morgan (p. 895); Morgan (written commun., 1976)
US20	Big Creek	?	s	93	w	Na>>>K>Ca>>>Mg HCO ₃ >>>SO ₄ >Cl		975	154	161	143	173 223 WSM		Robertson, Fournier and Strong (p. 553)
Nevada														
US21	Beowane	NVP?	s	98	w	Na>>>K>>>Ca>>>Mg HCO ₃ >SO ₄ >Cl	1140	198	214	151	194		212 (400 m)	Mariner et al. (1974a); Bowman et al. (p. 699); Wollenberg (p. 1283); White (1968); Truesdell and Nehring (unpub. data, 1975)
US22	Buffalo Valley	NVP?	s	49	w, tr	Na>>Ca>K>Mg HCO ₃ >>SO ₄ >>Cl	1370	118	125	223	197	215 WSM		
US23	Kyle	NVP?	s	77	w, tr	Na>>Ca>K>Mg Cl>HCO ₃ >>>SO ₄	2270	152	161	234	211	257 WSM		
US24	Steamboat	VW?	s	94	w	Na>>>K>>Ca>>>Mg Cl>HCO ₃ >>>SO ₄	2370	188	201	184	207	220± $\Delta^{18}O(SO_4, H_2O)$ 190± $\Delta^{18}C(CO_2, HCO_3)$	186 (222 m)	
New Mexico														
US25	Jemez Mtn., Jemez Spr	VW	s	75	w	Na>>Ca>K>>>Mg Cl>HCO ₃ >>>SO ₄	3500	122	125	215	202	165 WSM		Trainer (1974)
Oregon														
US26	Alvord	NVP?	s	76	w	Na>>>K>>Ca>>Mg HCO ₃ >Cl>>>SO ₄	3400	140	148		198	217 WSM 209 $\Delta^{18}O(SO_4, H_2O)$		Mariner et al. (1974b); Lund, Culver and Svanevik (p. 2147); Truesdell, Sammel, Mariner and Nehring (unpub. data, 1975)
US27	Klamath Falls, Olene Gap	NVP?	s	74	w	Na>>Ca>>K>>>Mg SO ₄ >>>Cl>HCO ₃	850	130	136	102	130	192 WSM 196 $\Delta^{18}O(SO_4, H_2O)$		
Utah														
US28	Roosevelt Hot Spr	VW?	s	85	w	Na>>K>>>Ca Cl>>>HCO ₃ >SO ₄	7850	196	202	273	284		260+	Mundorff (1970); Swanberg (1974); Beaver County News (1976)
Wyoming														
Yellowstone Park														
Shoshone Basin														
US29	Area I Sprs	VW	s					190 ave 10 σ 203 max				175 ave 16 σ 223 max	267 ave BSM 5 σ 272 max	Truesdell and Fournier (p. 837, σ = std. dev.); McKenzie and Truesdell (III-65); Thompson et al. (1975); White et al. (1975); Truesdell and Fournier (1976b); Truesdell (unpub. data, 1975)
US30	Spr 35		s	93	w	Na>>>K>>>Ca>Mg HCO ₃ >Cl>>>SO ₄	1250 CO ₂ >>>R>>>H ₂ S	185	199	110	171	272 BSM 260 $\Delta^{18}O(SO_4, H_2O)$ 190± $\Delta^{13}C(CO_2, HCO_3)$		
Upper Basin														
US31	Springs	VW	s					195 ave 11 σ 210 max				186 ave 20 σ 221 max	230 ave BSM 18 σ 280 max	181 (152 m)
US32	Ear Spr		s	95	w	Na>>>K>>>Ca>>>Mg Cl>>>HCO ₃ >>>SO ₄	1370	206	224	122	186	314 $\Delta^{18}O(SO_4, H_2O)$ 201 $\Delta^{13}C(CO_2, HCO_3)$		
Norris Basin														
US33	Springs	VW	s					210 ave 22 σ 255 max				251 ave 32 σ 294 max	276 ave BSM 32 σ 374 max	237.5 (332 m)
US34	Porcelain Terrace		s			Na>>>K>>>Ca>>>Mg Cl>>>HCO ₃ >SO ₄	2000	250	291	289	272	309 $\Delta^{18}O(SO_4, H_2O)$		

Table 1. Chemical summaries and geothermometer temperatures for selected thermal fluids (continued).

Area	System Type	Sample Type	Sampling Temp °C	Analyses	Water Type	TDS	Gases	$t_{SiO_2}^{adia}$ °C	$t_{SiO_2}^{cond}$ °C	$t_{Na/K}$ °C	t_{NaKCa} °C	Other Geothermometers °C	Observed Temp °C (depth)	References	
United States (continued)															
Wyoming															
Yellowstone Park															
Mammoth															
US35	New Highland	VW	s	73.5	w, i, g	Ca>Na>K>Mg HCO ₃ >SO ₄ >>Cl	2270	CO ₂ >>>H ₂ S>>R	103	105	421	96	300 $\Delta^3H_S(SO_4, H_2S)$ 74 Chalc	73 (15-113 m)	Schoen and Rye (1970); Robinson (1973)
US36	Washburn Spr	VS	f	82	w, trg, i								380 $\Delta^1^3C(CO_2, CH_4)$ 115 $\Delta D(H_2, H_2O)$ 70 $\Delta D(CH_4, H_2)$		Recalc. from Gunter and Musgrave (1966, 1971)
US37	Research Wells	VW	w				rare gases						>boiling rare gases		Mazor (p. 793)
USSR															
Kamchatka															
Panzhotka															
UR1	Well 4	VW	w	?	w	Na>>>K>Ca>>>Mg Cl>>>SO ₄ >HCO ₃	3180		193?	209	194	209		219	Vakin et al. (1970); Manukhin (II-29)
UR2	Paryaschy		s	99	w	Na>>>K>Ca>>Mg Cl>>>SO ₄ >HCO ₃	3110		160	168	156	186			
Bolshe Banny															
UR3	Well 35	VW	w	?	w	Na>>>K>Ca SO ₄ >>Cl>HCO ₃	1330		177?	188	161	177		171	
UR4	Spr 4		s	99	w	Na>>>K>Ca SO ₄ >>Cl>HCO ₃	1200		160	168	167	183			
Yugoslavia															
Y1	Pannonian Basin	NVS		80-90		HCO ₃ -Na, Cl-HCO ₃ -Na, Cl-Na	<35000	N ₂ , CH ₄							Petrović (p. 531)
Y2	Middle Serbia	NVS				HCO ₃ -Na-Ca-Mg		CO ₂							
Y3	Crystalline and young tectonic areas	NVF?				HCO ₃ -SO ₄ -Na-Ca-Mg	<1000	N ₂ , O ₂ , ±Rn							

Note: The following abbreviations are used in Table 1.

System Type

VW volcanic hot water system
 VS volcanic steam (vapor-dominated) system
 VS_w volcanic system involving seawater
 NVS_w nonvolcanic system involving seawater
 NVS nonvolcanic sedimentary basin with thermal water
 NVF nonvolcanic system with heat from deep circulation along faults

Sample Type

s spring
 f fumarole
 w well

Sampling Temperature is the surface temperature for a spring or a nonboiling well discharge, the temperature of steam separation for well discharges above boiling, or the downhole temperature if a downhole sampler was used or if the analysis was recalculated to downhole conditions.

Analyses

w water analysis with all major ions and SiO₂
 pw partial water analysis
 pg partial gas analysis

$t_{SiO_2}^{adia}$ is the quartz saturation temperature (°C) assuming maximum steam loss during cooling (adiabatic cooling) calculated by the computer program GEOTHERM (Truesdell, p. 831), along with $t_{SiO_2}^{cond}$, $t_{Na/K}$, WSMM, and BSMM, which are defined below. No allowance has been made for dissociation of dissolved silica. Some spring systems have data indicated as ave. (average), max. (maximum), and σ (standard deviation).

$t_{SiO_2}^{cond}$ is the quartz saturation temperature assuming no steam loss during cooling (conductive cooling).

$t_{Na/K}$ is the temperature calculated from the ratio of Na to K using the White-Ellis curve of Table 2.

t_{NaKCa} is the NaKCa temperature calculated using the equation of Table 2.

Other Geothermometers

Na-K-Ca-CO₂: The NaKCa geothermometer with correction applied for high CO₂ contents (Paces, 1975).

Chalc: The chalcedony saturation geothermometer with conductive cooling (Table 2).

CaSO₄ sat.: Temperature calculated for saturation of anhydrite (see text).

WSMM: The warm spring mixing model described in the text with no steam loss before mixing. Where no other data were available, the cold water component temperature was estimated as equal to the mean annual temperature and the SiO₂ content was assumed to be 25 ppm.

WSMM2: The warm spring mixing model, assuming steam separation at 100°C before mixing. Same assumed cold water component as above.

BSMM: The boiling spring mixing model described in the text. The cold spring temperature was estimated as above and the Cl contents estimated (in the absence of data) as 2 to 15 ppm according to the distance from the ocean.

tr trace water analysis
 trg trace gas analysis
 g gas analysis
 i water (¹⁸O,D) or other isotopes
 T,¹⁴C tritium, carbon-14

Water Type is calculated on a *weight* basis. The symbols mean:

A = B A approximately equals B in concentration
 A ≈ B A is 1 to 1.2 times the concentration of B
 A > B A is 1.2 to 3 times the concentration of B
 A >> B A is 3 to 10 times the concentration of B
 A >>> B A is more than 10 times the concentration of B

TDS is the sum of the reported constituents of the analysis in ppm (mg/kg).

Gases are in order of molar or volume abundance with the same symbols as for water type.

$\Delta^{13}\text{C}(\text{CO}_2, \text{CH}_4)$: Temperatures indicated by the fractionation of ¹³C between CO₂ and CH₄. The notation for this and other isotope geothermometers is self-evident (see text).

K(CO₂ → CH₄): Temperature calculated from chemical equilibrium constants for the reaction CO₂ + 4H₂ = CH₄ + 2H₂O.

Boiling calculation: Temperature calculated from the apparent increase in concentration of seawater due to boiling.

Na-Ca-SiO₂, isotope mixing, ¹⁴C mixing, "isotope", heat balance, Cl-E: Special methods explained in the original references.

Observed Temperature is *aquifer* temperature rather than maximum temperature where aquifers are identified; otherwise, maximum recorded temperature.

References in many cases are grouped where data for a well, spring, or geothermal system are from more than one source. "recalc. from" means that temperatures were calculated from a calibration curve other than that used by the author.

Table 2. Equations for geothermometers.

<i>Silica Geothermometers</i> (SiO ₂ in ppm)*	
Quartz, adiabatic cooling (± 2°C from 125–275°C)	$t^\circ\text{C} = \frac{1533.5}{5.768 - \log \text{SiO}_2} - 273.15$
Quartz, conductive cooling (± 0.5°C from 125–250°C)	$t^\circ\text{C} = \frac{1315}{5.205 - \log \text{SiO}_2} - 273.15$
Chalcedony, conductive cooling	$t^\circ\text{C} = \frac{1015.1}{4.655 - \log \text{SiO}_2} - 273.15$
<i>Na/K Geothermometers</i> (Na, K in ppm)	
White and Ellis (see text) (± 2°C from 100–275°C)	$t^\circ\text{C} = \frac{855.6}{\log(\text{Na}/\text{K}) + 0.8573} - 273.15$
Fournier and Truesdell (1973)	$t^\circ\text{C} = \frac{777}{\log(\text{Na}/\text{K}) + 0.70} - 273.15$
<i>NaKCa Geothermometer</i> (Na, K, Ca in moles/liter)	
Fournier and Truesdell (1973, 1974)	$t^\circ\text{C} = \frac{1647}{\log(\text{Na}/\text{K}) + \beta \log(\sqrt{\text{Ca}}/\text{Na}) + 2.24} - 273.15$
$\beta = 4/3$ for $\sqrt{\text{Ca}}/\text{Na} > 1$ and $t < 100^\circ\text{C}$	
$\beta = 1/3$ for $\sqrt{\text{Ca}}/\text{Na} < 1$ or $t_{4/3} > 100^\circ\text{C}$	

*Data from Fournier (written commun., 1973)

REFERENCES CITED

- Akeno, T., 1973. Rapid chemical analysis of volcanic gases in geothermal fields: Jour. Japan Geothermal Energy Assoc., v. 10, no. 1, p. 13-21.
- Allen, E. T., and Day, A. L., 1935. Hot springs of the Yellowstone National Park: Carnegie Inst. Wash. Pub. 466. 525 p.
- Arango, E., Buitrago A., J., Cataldi, R., Ferrara, G. C., Panichi, C., and Villegas V., J., 1970. Preliminary study on the Ruiz Geothermal Project (Columbia): UN Symposium on the Development and Utilization of Geothermal Resources, Pisa, Proceedings (Geothermics, Spec. Iss. 2), v. 2, pt. 1, p. 43-56.
- Arnbrust, G. A., Arias, J., Lahsen, A., and Trujillo, P., 1974. Geochemistry of the hydrothermal alteration at the El Tatio Geothermal Field, Chile: IAVCEI-Symposium Internacional de Volcanologia, Santiago, Chile, September 9-14. Proceedings.
- Arnason, B., 1976. The hydrogen and water isotope thermometer applied to geothermal areas in Iceland: International Atomic Energy Agency Advisory Group Meeting on the Application of Nuclear Techniques to Geothermal Studies, Pisa, Italy, September 8-12, 1975, Proceedings.
- Arnórsson, S., 1970. Underground temperatures in hydrothermal areas in Iceland as deduced from the silica content of the thermal water: UN Symposium on the Development and Utilization of Geothermal Resources, Pisa, Proceedings, (Geothermics, Special Issue 2), v. 2, pt. 1, p. 536-541.
- . 1974. The composition of thermal fluids in Iceland and geological features related to the thermal activity, in Kristjansson, ed., Geodynamics of Iceland and the North Atlantic area: Dordrecht, D. Reidel, p. 307-323.
- . 1975. Application of the silica geothermometer in low temperature hydrothermal areas in Iceland: Am. Jour. Sci., v. 275, no. 7, p. 763-784.
- Arnórsson, S., Kononov, V. I., and Polyak, B. G., 1974. The geochemical features of Iceland hydrotherms: Geochim. Internat., v. 11, p. 1224-1240.
- Baba, K., Tahaki, S., Matsuo, G., and Katagiri, K., 1970. A study of the reservoir at the Matsukawa Geothermal Field: UN Symposium on the Development and Utilization of Geothermal Resources, Pisa, Proceedings (Geothermics Spec. Iss. 2), v. 2, pt. 2, p. 1440-1447.
- Baldi, P., Ferrara, G. C., Masselli, L., and Pieretti, G., 1973. Hydrogeochemistry of the region between Monte Amiata and Rome: Geothermics, v. 2, nos. 3-4, p. 124-141.
- Banwell, C. J., 1963. Oxygen and hydrogen isotopes in New Zealand thermal areas, in Tongiorgi, E., ed., Nuclear geology on geothermal areas, Spoleto, 1963: Pisa, Consiglio Nazionale delle Ricerche Laboratorio di Geologia Nucleare, p. 95-138.
- Barnes, I., and Hem, J. D., 1973. Chemistry of subsurface waters. in Donath, F. A., ed., Annual review of earth and planetary sciences, v. 1: Palo Alto, Annual Reviews Inc., p. 157-182.
- Barnes, I., Hinkle, M. E., Rapp, J. B., Heropoulos, C., and Vaughn, W. W., 1973. Chemical composition of naturally occurring fluids in relation to mercury deposits in part of north-central California: U.S. Geol. Survey Bull. 1382-A. p. A1-A19.
- Barnes, I., O'Neil, J. R., Rapp, J. B., and White, D. E., 1973. Silica-carbonate alteration of serpentine: Wall rock alteration in mercury deposits of the California Coast Ranges: Econ. Geology, v. 68, no. 3, p. 388-390.
- Beaver County News, 1976. Phillips to flow for five day test: Milford, Utah, v. 76, no. 7, p. 1.
- Bedinger, M. S., Pearson, F. J., Jr., Reed, J. E., Sniegocki, R. T., and Stone, C. G., 1974. The waters of Hot Springs National Park, Arkansas—their origin, nature, and management: U.S. Geol. Survey open-file report, 122 p.
- Begemann, F., 1963. The tritium content of hot springs in some geothermal areas, in Tongiorgi, E., ed., Nuclear geology on geothermal areas, Spoleto, 1963: Pisa, Consiglio Nazionale delle Ricerche Laboratorio di Geologia Nucleare, p. 55-70.
- Berkstresser, C. F., Jr., 1968. Data for springs in the Northern Coast Ranges and Klamath Mountains of California: U.S. Geol. Survey open-file report, 16 p.
- Bischoff, J. L., and Dickson, F. W., 1975. Seawater basalt interaction at 200°C and 500 bars: Implications for origin of sea floor heavy metal deposits and regulation of seawater chemistry: Earth and Planetary Sci. Letters, v. 25, p. 385-397.
- Björnsson, S., Arnórsson, S., and Tómasson, J., 1972. Economic evaluation of Reykjanes thermal brine area, Iceland: American Assoc. Petroleum Geologists Bull., v. 56, no. 12, p. 2380-2391.
- Bosch, B., Deschamps, J., Leleu, M., Lopoukhine, M., Marce, A., and Vilbert, C., 1976. The geothermal zone of Lake Assal (F.T.A.I.): Geochemical and experimental studies: International Symposium on Water-Rock Interactions, Prague, Czechoslovakia, 1974, Proceedings.
- Bottinga, Y., 1969. Calculated fractionation factors for carbon and hydrogen isotope exchange in the system calcite-carbon dioxide-graphite-methane-hydrogen-water vapor: Geochim. et Cosmochim. Acta, v. 33, p. 49-64.
- Brewer, P. G., and Spencer, D. W., 1969. A note on the chemical composition of the Red Sea brines, in Degens, E. T., and Ross, D. A., eds., Hot brines and recent heavy metal deposits in the Red Sea: New York, Springer-Verlag, p. 174-179.
- Brondi, M., Dall'Aglio, M., and Vitrani, F., 1973. Lithium as a pathfinder element in the large scale hydrogeochemical exploration for hydrothermal systems: Geothermics, v. 2, nos. 3-4, p. 142-153.
- Browne, P. R. L., and Ellis, A. J., 1970. Ohaki-Broadlands hydrothermal area, New Zealand: mineralogy and related geochemistry: Am. Jour. Sci., v. 269, no. 2, p. 97-131.
- Browne, P. R. L., Roedder, E., and Wodzicki, A., 1976. Comparison of past and present geothermal waters from a study of fluid inclusions: Proceedings, International Symposium on Water-Rock Interactions, Prague, Czechoslovakia, 1974, Proceedings.
- Cadek, J., ed., 1976. Proceedings: International Symposium on Water-Rock Interactions, Prague, Czechoslovakia, 1974.
- Celati, R., Noto, P., Panichi, C., Squarci, P., and Taffi, L., 1973. Interactions between the steam reservoir and surrounding aquifers in the Larderello geothermal field: Geothermics, v. 2, nos. 3-4, p. 174-185.
- Clayton, R. N., and Steiner, A., 1975. Oxygen isotope studies of the geothermal system at Wairakei, New Zealand: Geochim. et Cosmochim. Acta, v. 39, p. 1179-1186.
- Cormy, G., Demians d'Archimbaud, J., and Surcin, J., 1970. Prospection géothermique aux Antilles françaises, Guadeloupe et Martinique: UN Symposium on the Development and Utilization of Geothermal Resources, Pisa, Proceedings (Geothermics, Spec. Iss. 2), v. 2, pt. 1, p. 57-72.
- Cortecci, G., 1974. Oxygen isotopic ratios of sulfate ions—water pairs as a possible geothermometer: Geothermics, v. 3, no. 2, p. 60-64.
- Cortecci, G., and Dowgiallo, J., 1975. Oxygen and sulfur isotopic composition of the sulfate ions from mineral

- and thermal groundwaters of Poland: *Jour. Hydrology*, v. 24, p. 271-282.
- Crafar, W. M.**, 1974, Hauraki geothermal region, Tauranga geothermal field, minerals of New Zealand. Part D—Geothermal resources: *New Zealand Geol. Survey Rept.* 38, 5 p.
- Craig, H.**, 1953, The geochemistry of the stable carbon isotopes: *Geochim. et Cosmochim. Acta*, v. 3, p. 53-92.
- , 1963, The isotopic geochemistry of water and carbon in geothermal areas, in Tongiorgi, E., ed., *Nuclear geology on geothermal areas*, Spoleto, 1963: Pisa, Consiglio Nazionale delle Ricerche Laboratorio di Geologia Nucleare, p. 17-54.
- , 1976, Isotopic temperatures in geothermal systems: International Atomic Energy Agency Advisory Group Meeting on the Application of Nuclear Techniques to Geothermal Studies, Pisa, Italy, September 8-12, 1975, *Proceedings*.
- Craig, H., Boato, G., and White, D. E.**, 1956, Isotopic geochemistry of thermal waters: *Natl. Acad. Sci.-Nat. Research Council Pub. No.* 400, p. 29-38.
- Craig, H., Clarke, W. B., and Beg, M. A.**, 1975, Excess He^3 in deep water on the East Pacific Rise: *Earth and Planetary Sci. Letters*, v. 26, no. 2, p. 125-132.
- Dall'Aglio, M., and Tonani, F.**, 1973, Hydrogeochemical exploration for sulfide deposits. Correlation between sulfate and other constituents, in Jones, M. J., ed., *Geochemical exploration*, Proceedings of International Geochemical Exploration Symposium 1972: London, Inst. Mining and Metallurgy, p. 305-314.
- Datrymple, G. B., and Moore, J. G.**, 1968, Argon-40: Excess in submarine pillow basalts from Kilauea Volcano, Hawaii: *Science*, v. 161, p. 1132-1135.
- Danilchik, W.**, 1973, Dieng Geothermal Exploration Drilling Project, Indonesia, during 1972—interim report: U.S. Geol. Survey Project Report (IR) IND-28, 53 p.
- Dominco, E., and Şamilgil, E.**, The geochemistry of the Kızıdere geothermal field, in the framework of the Sarayköy-Denizli geothermal area: UN Symposium on the Development and Utilization of Geothermal Resources, Pisa, *Proceedings (Geothermics Spec. Iss. 2)*, v. 2, pt. 1, p. 553-560.
- Ellis, A. J.**, 1966, Volcanic hydrothermal areas and the interpretation of thermal water compositions: *Bull. Volcanol.*, v. 29, p. 575-584.
- , 1967, The chemistry of some explored geothermal systems, in Barnes, H. L., ed., *Geochemistry of hydrothermal ore deposits*: New York, Holt, Rinehart and Winston, p. 465-514.
- , 1970, Quantitative interpretation of chemical characteristics of hydrothermal systems: UN Symposium on the Development and Utilization of Geothermal Resources, Pisa, *Proceedings (Geothermics, Spec. Iss. 2)*, v. 2, pt. 1, p. 516-528.
- , 1971, Magnesium ion concentrations in the presence of magnesium chlorite, calcite, carbon dioxide, quartz: *Am. Jour. Sci.*, v. 271, p. 481-489.
- , 1973, Chemical processes in hydrothermal systems—a review, in *Proceedings, International Symposium on Hydrogeochemistry and Biogeochemistry*, Japan, 1970, v. 1, Hydrogeochemistry: Washington, D.C., J. W. Clark, p. 1-26.
- , 1975, Geothermal systems and power development: *Am. Scientist*, v. 63, no. 5, p. 510-521.
- Ellis, A. J., and Golding, R. M.**, 1963, The solubility of carbon dioxide above 100°C in water and in sodium chloride solutions: *Am. Jour. Sci.*, v. 261, p. 47-60.
- Ellis, A. J., and Mahon, W. A. J.**, 1964, Natural hydrothermal systems and experimental hot-water/rock interactions: *Geochim. et Cosmochim. Acta*, v. 28, p. 1323-1357.
- , 1967, Natural hydrothermal systems and experimental hot-water/rock interactions (pt. II): *Geochim. et Cosmochim. Acta*, v. 31, p. 519-538.
- Ellis, A. J., and Wilson, S. H.**, 1955, The heat from the Wairakei-Taupo thermal region calculated from the chloride output: *New Zealand Jour. Sci. and Technology*, v. 36B, p. 622-631.
- Fancelli, R., and Nuti, S.**, 1974, Locating interesting geothermal areas in the Tuscany region (Italy) by geochemical and isotopic methods: *Geothermics*, v. 3, no. 4, p. 146-152.
- Ferguson, J., and Lambert, I. B.**, 1972, Volcanic exhalations and metal enrichments at Matupi Harbor, New Britain, T.P.N.G.: *Econ. Geology*, v. 67, p. 25-37.
- Ferrara, G. C., Ferrara, G., and Gouffanti, R.**, 1963, Carbon isotopic composition of carbon dioxide and methane from steam jets of Tuscany, in Tongiorgi, E., ed., *Nuclear geology on geothermal areas*, Spoleto, 1963: Pisa, Consiglio Nazionale delle Ricerche Laboratorio di Geologia Nucleare, p. 277-284.
- Fournier, R. O.**, 1973, Silica in thermal waters: laboratory and field investigations, in *Proceedings, International Symposium on Hydrogeochemistry and Biogeochemistry*, Japan, 1970, v. 1, Hydrogeochemistry: Washington, D.C., J. W. Clark, p. 122-139.
- , 1976, Geochemical thermometers and mixing models for geothermal systems: International Atomic Energy Agency Advisory Group Meeting on the Application of Nuclear Techniques to Geothermal Studies, Pisa, Italy, September 8-12, 1975, *Proceedings*.
- Fournier, R. O., and Morganstern, J. C.**, 1971, A device for collecting down-hole water and gas samples in geothermal wells: U.S. Geol. Survey Prof. Paper 750-C, p. C151-C155.
- Fournier, R. O., and Rowe, J. J.**, 1966, Estimation of underground temperatures from the silica content of water from hot springs and wet-steam wells: *Am. Jour. Sci.*, v. 264, no. 9, p. 685-697.
- Fournier, R. O., and Truesdell, A. H.**, 1970, Chemical indicators of subsurface temperature applied to hot spring waters of Yellowstone National Park, Wyoming, USA: UN Symposium on the Development and Utilization of Geothermal Resources, Pisa, *Proceedings (Geothermics Spec. Iss. 2)*, v. 2, pt. 1, p. 529-535.
- , 1973, An empirical Na-K-Ca geothermometer for natural waters: *Geochim. et Cosmochim. Acta*, v. 37, p. 1255-1275.
- , 1974, Geochemical indicators of subsurface temperature—Part 2. Estimation of temperature and fraction of hot water mixed with cold water: *U.S. Geol. Survey Jour. Research*, v. 2, no. 3, p. 263-269.
- Fournier, R. O., White, D. E., and Truesdell, A. H.**, 1974, Geochemical indicators of subsurface temperature—Part 1. Basic assumptions: *U.S. Geol. Survey Jour. Research*, v. 2, no. 3, p. 259-262.
- Franck, E. V.**, 1973, Concentrated electrolyte solutions at high temperatures and pressures: *Jour. Solution Chemistry*, v. 2, nos. 2/3, p. 339-356.
- Fujii, Y., and Akeno, T.**, 1970, Chemical prospecting of steam and hot water in the Matsukawa geothermal area: UN Symposium on the Development and Utilization of Geothermal Resources, Pisa, *Proceedings (Geothermics, Spec. Iss. 2)* v. 2, pt. 1, p. 1416-1421.
- Giggenbach, W. F.**, 1971, Isotopic composition of waters of the Broadlands geothermal field: *New Zealand Jour. Sci.* v. 14, no. 4, p. 959-970.
- , 1976, Variations in the carbon, sulfur and chlorine contents of volcanic gas discharges from White Island, New Zealand: *Bull. Volcanol.*
- Gilmore, D. B.**, ed., 1976, *Proceedings, Workshop on Sam-*

- pling Geothermal Effluents, Las Vegas, Nevada, October 1975: Environmental Protection Agency Report.
- Glover, R. B.**, 1972, Chemical characteristics of water and steam discharges in the Rift Valley of Kenya: United Nations-Kenya Government Geothermal Exploration Project Report, August, 106 p.
- , 1973, Geothermal investigations in Kenya: New Zealand Geochem. Group Newsletter, v. 4, no. 32, p. 84.
- , 1974a, Report on visit to Philippines May 1974—Part 4: New Zealand Dept. Sci. and Indus. Research Report, August, 27 p.
- , 1974b, Report on visit to Philippines May 1974—Part 5 (Interpretation of oxygen-deuterium analyses): New Zealand Dept. Sci. and Indus. Research Report, December, 6 p.
- , 1975, Chemical analyses of waters from Negros Oriental, Philippines and their geothermal significance: New Zealand Dept. Sci. and Indus. Research Report, October, 28 p.
- Glover, R. B., and Cuéllar, G.**, 1970, Geochemical investigations of the Ahuachapán geothermal field: Report for United Nations Development Programme, Special Fund Project, Survey of Geothermal Resources in El Salvador, 54 p.
- Gonfiantini, R., and Tongiorgi, E.**, eds., 1976, Proceedings, International Atomic Energy Agency Advisory Group Meeting on the Application of Nuclear Techniques to Geothermal Studies, Pisa, Italy, September 8-12, 1975.
- Gringarten, A. C., and Stieltjes, L.**, 1976, Study of a geothermal field in the Assal active volcanic rift zone (French Territory of Afars and Issas, East Africa): Stanford, California, Workshop on Geothermal Reservoir Engineering, Stanford University, December 15-17, 1975.
- Gunter, B. D., and Musgrave, B. C.**, 1966, Gas chromatographic measurements of hydrothermal emanations at Yellowstone National Park: *Geochim. et Cosmochim. Acta*, v. 30, p. 1175-1189.
- , 1971, New evidence on the origin of methane in hydrothermal gases: *Geochim. et Cosmochim. Acta*, v. 35, p. 113-118.
- Haas, J. L., Jr.**, 1971, The effect of salinity on the maximum thermal gradient of a hydrothermal system at hydrostatic pressure: *Econ. Geology*, v. 66, p. 940-946.
- Hajash, A.**, 1974, An experimental investigation of high temperature seawater-basalt interactions [abs]: *Geol. Soc. America Abs. with Programs*, v. 6, no. 7, p. 771.
- Hall, W. E.**, ed., 1974, Proceedings, Symposium on Stable Isotopes as Applied to Problems of Ore Deposits, Dallas, Texas, November 11-12, 1973: *Econ. Geology*, v. 69, p. 755-1006.
- Harlow, F. H., and Pracht, W. E.**, 1972, A theoretical study of geothermal energy extraction: *Jour. Geophys. Research*, v. 77, no. 35, p. 7038-7048.
- Healy, J.**, 1960, The hot springs and geothermal resources of Fiji: New Zealand Dept. Sci. and Indus. Research Bull. 136, 77 p.
- Healy, J., and Hochstein, M. P.**, 1973, Horizontal flow in hydrothermal systems: *Jour. Hydrology (New Zealand)*, v. 12, no. 2, p. 71-82.
- Helgeson, H. C.**, 1969, Thermodynamics of hydrothermal systems at elevated temperatures and pressures: *Am. Jour. Sci.*, v. 267, p. 729-804.
- Helgeson, H. C., and Kirkham, K. H.**, 1974, Theoretical prediction of the thermodynamic behavior of aqueous electrolytes at high pressures and temperatures. I. Summary of the thermodynamic/electrostatic properties of the solvent; II. Debye-Hückel parameters for activity coefficients and relative partial molal properties: *Am. Jour. Sci.*, v. 274, no. 10, p. 1089-1261.
- Hitosugi, T., and Yonetani, M.**, 1972, On the drillings of the shallow wells in Onikobe: *Jour. Japan Geothermal Energy Assoc.*, v. 9, no. 1, p. 15-29.
- Holland, H. D.**, 1967, Gangue minerals in hydrothermal deposits, in Barnes, H. L., ed., *Geochemistry of hydrothermal ore deposits*: New York, Holt, Rinehart and Winston, p. 382-436.
- Hood, D. W.**, 1972, Seawater chemistry, in Fairbridge, R. W., ed., *The encyclopedia of geochemistry and environmental sciences*: New York, Van Nostrand Reinhold, p. 1062-1070.
- Horne, R. N., and O'Sullivan, M. J.**, 1974, Oscillatory convection in a porous medium heated from below: *Jour. Fluid Mechanics*, v. 66, pt. 2, p. 339-352.
- Hulston, J. R.**, 1964, Isotope geology in the hydrothermal areas of New Zealand, in Proceedings, United Nations Conference on New Sources of Energy, Rome, 1961, v. 2, *Geothermal Energy: 1*: New York, United Nations, p. 259-263.
- Hulston, J. R., and McCabe, W. J.**, 1962a, Mass spectrometer measurements in the thermal areas of New Zealand. Part 1. Carbon dioxide and residual gas analyses: *Geochim. et Cosmochim. Acta*, v. 26, p. 383-397.
- , 1962b, Mass spectrometer measurements in the thermal areas of New Zealand. Part 2. Carbon isotopic ratios: *Geochim. et Cosmochim. Acta*, v. 26, p. 399-410.
- International Atomic Energy Agency**, 1974, Isotope techniques in groundwater hydrology (Proceedings, Symposium on Isotope Techniques in Groundwater Hydrology, Vienna, March 11-15, 1974): Vienna, International Atomic Energy Agency, IAEA-SM-182/35, 2 v.
- Ivanov, V. V.**, 1967, Principal geochemical environments and processes of the formation of hydrothermal waters in regions of recent volcanic activity, in Vinogradov, A. P., ed., *Chemistry of the Earth's crust*, v. 2: Jerusalem, Israel Prog. Scientific Translation Ltd., p. 260-281.
- Iwasaki, I., Katsura, T., Tarutani, T., Ozawa, T., Toshida, M., Iwasaki, B., Hirayama, M., and Kamada, M.**, 1963, Geochemical studies on Tamagawa hot springs, in Minami, E., ed., *Geochemistry of the Tamagawa hot springs*: Tokyo, p. 7-72.
- James, R.**, 1968, Wairakei and Larderello: geothermal power systems compared: *New Zealand Jour. Sci. and Tech.*, v. 11, p. 706-719.
- Klyen, L. E.**, 1973, A vessel for collecting subsurface water samples from geothermal drillholes: *Geothermics*, v. 2, no. 2, p. 57-60.
- Koga, A.**, 1970, Geochemistry of the waters discharged from drillholes in the Otake and Hatchobaru areas: UN Symposium on the Development and Utilization of Geothermal Resources, Pisa, Proceedings (Geothermics, Spec. Iss. 2), v. 2, pt. 2, p. 1422-1425.
- Kozintseva, T. N.**, 1964, Solubility of hydrogen sulfide in water at elevated temperatures: *Geochem. Internat.*, p. 750-756.
- Krauskopf, K. B.**, 1964, The possible role of volatile metal compounds in ore genesis: *Econ. Geology*, v. 59, no. 1, p. 22-45.
- Kusakabe, M.**, 1974, Sulphur isotopic variations in nature. 10. Oxygen and sulphur isotope study of Wairakei geothermal well discharges: *New Zealand Jour. Sci.*, v. 17, p. 183-191.
- Lloyd, R. M.**, 1968, Oxygen isotope behavior in the sulfate-water system: *Jour. Geophys. Research*, v. 73, no. 18, p. 6099-6110.
- Longinelli, A., and Craig, H.**, 1967, Oxygen-18 variations in sulfate ions in sea water and saline lakes: *Science*, v. 156, no. 3771, p. 56-59.
- Lupton, J. E., and Craig, H.**, 1975, Excess He-3 in oceanic

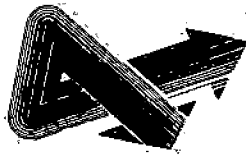
- basalts. Evidence for terrestrial primordial helium: *Earth and Planetary Sci. Letters*, v. 26, no. 2, p. 133-139.
- Lyon, G. L.**, 1974, Geothermal gases, in Kaplan, I. R., ed., *Natural gases in marine sediments*: New York, Plenum Press, p. 141-150.
- Lyon, G. L., and Hulston, J. R.**, 1970, Recent carbon isotope and residual gas measurements in relation to geothermal temperatures: *New Zealand Inst. Nuclear Sci. Contribution No. 407*, 11 p.
- Lyon, G. L., Cox, M. A., and Hulston, J. R.**, 1973a, Geothermometry in geothermal areas: *New Zealand Dept. Sci. and Indus. Research, Inst. of Nuclear Sciences Progress Rept. 19*, p. 51-52.
- , 1973b, Gas geothermometry: *New Zealand Dept. Sci. and Indus. Research, Institute of Nuclear Sciences Progress Report 20*, p. 41.
- Mahon, W. A. J.**, 1966, Silica in hot water discharged from drillholes at Wairakei, New Zealand: *New Zealand Jour. Sci.*, v. 9, p. 135-144.
- , 1970, Chemistry in the exploration and exploitation of hydrothermal systems: *UN Symposium on the Development and Utilization of Geothermal Resources, Pisa, Proceedings (Geothermics, Spec. Iss. 2)*, v. 2, pt. 2, p. 1310-1322.
- , 1972, The chemistry of the Orakeikorako hot spring waters, in Lloyd, E. F., ed., *Geology and hot springs of Orakeikorako*: *New Zealand Geol. Survey Bull. 85*, p. 104-112.
- , 1973, The chemical composition of natural thermal waters, in *Proceedings, International Symposium on Hydrogeochemistry and Biogeochemistry, Japan, 1970*, v. 1, *Hydrogeochemistry: Washington, D.C., J. W. Clark*, p. 196-210.
- Mahon, W. A. J., and Finlayson, J. B.**, 1972, The chemistry of the Broadlands geothermal area, New Zealand: *Am. Jour. Sci.*, v. 272, p. 48-68.
- Mariner, R. H., Rapp, J. B., Willey, L. M., and Presser, T. S.**, 1974a, The chemical composition and estimated minimum thermal reservoir temperatures of the principal hot springs of northern and central Nevada: *U.S. Geol. Survey open-file report*, 32 p.
- , 1974b, The chemical composition and estimated minimum thermal reservoir temperatures of selected hot springs in Oregon: *U.S. Geol. Survey open-file report*, 27 p.
- Mariner, R. H., and Willey, L. M.**, 1976, Geochemistry of thermal waters in Long Valley, California: *Jour. Geophys. Research*, v. 81, p. 792-800.
- Marshall, W. L.**, 1968, Conductances and equilibria of aqueous electrolytes over extreme ranges of temperature and pressure: *Rev. Pure and Applied Chemistry*, v. 18, p. 167-186.
- , 1972, Predictions of the geochemical behavior of aqueous electrolytes at high temperatures and pressures: *Chem. Geology*, v. 10, no. 1, p. 59-68.
- Matsubaya, O., Sakai, H., Kusachi, I., and Satake, H.**, 1973, Hydrogen and oxygen isotopic ratios and major element chemistry of Japanese thermal water systems: *Geochem. Jour.*, v. 7, p. 123-151.
- Mazor, E., and Fournier, R. O.**, 1973, More on noble gases in Yellowstone National Park hot waters: *Geochim. et Cosmochim. Acta*, v. 37, p. 515-525.
- Mazor, E., Kaufman, A., and Carmi, I.**, 1973, Hammat Gader (Israel): Geochemistry of a mixed thermal spring complex. *Jour. Hydrology*, v. 18, p. 289-303.
- Mazor, E., Verhagen, B. T., and Negreanv, E.**, 1974, Hot springs of the igneous terrain of Swaziland: Their noble gases, hydrogen, oxygen, and carbon isotopes and dissolved ions, in *Isotope techniques in groundwater hydrology*, v. 2: Vienna, International Atomic Energy Agency, IAEA-SM-182/28, p. 29-47.
- Miller, T. P.**, 1973, Distribution and chemical analyses of thermal springs in Alaska: *U.S. Geol. Survey open-file map*.
- Miller, T. P., Barnes, I., and Patton, W. W., Jr.**, 1975, Geologic setting and chemical characteristics of hot springs in west-central Alaska: *U.S. Geol. Survey Jour. Research*, v. 3, no. 2, p. 149-162.
- Mizutani, Y.**, 1972, Isotopic composition and underground temperature of the Otake geothermal water, Kyushu, Japan: *Geochem. Jour.*, v. 6, p. 67-73.
- Mizutani, Y., and Hamasuna, T.**, 1972, Origin of the Shimogamo geothermal brine, Izu: *Bull. Volcanol. Soc. Japan*, v. 17, p. 123-134.
- Mizutani, Y., and Rafter, T. A.**, 1969, Oxygen isotopic composition of sulphates—Part 3. Oxygen isotopic fractionation in the bisulphate ion-water system: *New Zealand Jour. Sci.* v. 12, no. 1, p. 54-59.
- Morgan, V.**, 1976, Boron geochemistry, in Thompson, R., ed., *Mellor's comprehensive treatise of inorganic chemistry—boron volume (supplement)*, v. 1: London, Longmans-Green.
- Mottl, M. J., Corr, R. F., and Holland, H. D.**, 1974, Chemical exchange between sea water and mid-ocean ridge basalt during hydrothermal alteration: an experimental study [abs]: *Geol. Soc. America Abs. with Programs*, v. 6, no. 7, p. 879-880.
- Mundorff, J. C.**, 1970, Major thermal springs of Utah: *Utah Geol. and Mineral Survey, Water Resources Bull. 13*, 60 p.
- Nakamura, H.**, 1969, Mineral and thermal waters of Japan: 23rd International Geology Congress, Prague, Czechoslovakia, v. 19, p. 45-62.
- Noguchi, K., Goto, T., Ueno, S., and Imahasi, M.**, 1970, A geochemical investigation of the strong acid water from the bored wells in Hakone, Japan: *UN Symposium on the Development and Utilization of Geothermal Resources, Pisa, Proceedings (Geothermics, Spec. Iss. 2)*, v. 2, pt. 1, p. 561-563.
- Oeschger, H., Gugelmann, A., Loosli, H., Schotterer, U., Siegenthaler, U., and Wiest, W.**, 1974, ^{39}Ar dating of groundwater, in *Isotope techniques in groundwater hydrology*, v. 2: Vienna, International Atomic Energy Agency, IAEA-SM-182/37, p. 179-190.
- Paces, T.**, 1975, A systematic deviation from Na-K-Ca geothermometer below 75°C and above 10^{-4} atm P_{CO_2} : *Geochim. et Cosmochim. Acta*, v. 39, p. 541-544.
- Panichi, C., Celati, R., Noto, P., Squarci, P., Taffi, L., and Tongiorgi, E.**, 1974, Oxygen and hydrogen isotope studies of the Larderello (Italy) geothermal system, in *Isotope techniques in groundwater hydrology*, v. 2: Vienna, International Atomic Energy Agency, IAEA-SM-182/35, p. 3-28.
- Potter, R. W., II, Shaw, D. R., and Haas, J. L., Jr.**, 1975, Annotated bibliography of studies on the density and other volumetric properties for major components in geothermal waters 1928-74: *U.S. Geol. Survey Bull. 1417*, 78 p.
- Presser, T. S., and Barnes, I.**, 1974, Special techniques for determining chemical properties of geothermal water: *U.S. Geol. Survey Water Resources Invest. 22-74*, 15 p.
- Reed, M. J.**, 1975, Chemistry of thermal water in selected geothermal areas of California: *California State Div. Oil and Gas Rept. No. TR15*, 31 p.
- Renner, J. L., White, D. E., and Williams, D. L.**, 1975, Hydrothermal convection systems, in White, D. E., and Williams, D. L., eds., *Assessment of geothermal resources of the United States—1975*: *U.S. Geol. Survey Circ. 726*, p. 5-57.

- Rightmire, C. T., and Truesdell, A. H.**, 1974. Carbon isotope composition of soil gases as an indicator of geothermal areas [abs]: *Geol. Soc. America Abs. with Programs*, v. 6, no. 7, p. 927.
- Rightmire, C. T., Young, H. W., and Whitehead, R. L.**, 1976. Geothermal investigations in Idaho. Part IV. Isotopic and geochemical analyses of water from the Bruneau-Grandview and Weiser areas, southwest Idaho: Idaho Department of Water Resources, *Water Information Bulletin*.
- Ritchie, J. A.**, 1973. A determination of some base metals in Broadlands geothermal waters: New Zealand Dept. Sci. and Industrial Research Rept. No. C.D. 2164, 24 p.
- Roberts, A. A., Friedman, I., Donovan, J. J., and Denton, E. H.**, 1975. Helium survey, a possible technique for locating geothermal reservoirs: *Geophys. Research Letters*, v. 2, p. 209-210.
- Robinson, B. W.**, 1973. Sulphur isotope equilibrium during sulphur hydrolysis at high temperatures: *Earth and Planetary Sci. Letters*, v. 18, p. 443-450.
- Sakai, H., and Matsubaya, O.**, 1974. Isotopic geochemistry of the thermal waters of Japan and its bearing on the Kuroko ore solutions: *Econ. Geology*, v. 69, p. 974-991.
- Schoen, R., and Rye, R. O.**, 1970. Sulfur isotope distribution in solfataras, Yellowstone National Park: *Science*, v. 170, p. 1082-1084.
- Seward, T. M.**, 1974. Equilibrium and oxidation potential in geothermal waters at Broadlands. New Zealand: *Am. Jour. Sci.*, v. 274, p. 190-192.
- Sigvaldason, G. E.**, 1973. Geochemical methods in geothermal exploration, in *Armstead, H.C.H., ed., Geothermal energy: review of research and development (Earth Sciences, 12): Paris. UNESCO*, p. 49-59.
- Sigvaldason, G. E., and Cuéllar, G.**, 1970. Geochemistry of the Ahuachapán thermal area, El Salvador. Central America: UN Symposium on the Development and Utilization of Geothermal Resources, Pisa, *Proceedings (Geothermics Spec. Iss. 2)*, v. 2, pt. 2, p. 1392-1399.
- Silberman, M. L., and White, D. E.**, 1975. Limits on the duration of hydrothermal activity at Steamboat Springs, Nevada, by K-Ar ages of spatially associated altered and unaltered volcanic rocks [abs]: *Geol. Soc. America Abs. with Programs*, v. 7, no. 7, p. 1272-1273.
- Skinner, D. N. B.**, 1974. Hauraki geothermal region. Hot Water Beach geothermal field, in *Minerals of New Zealand. Part D: geothermal resources: New Zealand Geol. Survey Rept.* 38, 4 p.
- Smith, M., Potter, R., Brown, D., and Aamodt, R. L.**, 1973. Induction and growth of fractures in hot rock, in *Kruger, P., and Otte, C., eds., Geothermal energy: resources, production, stimulation: Stanford, California, Stanford University Press*, p. 251-268.
- Sorey, M. L., and Lewis, R.**, 1976. Discharge of hot spring systems in the Long Valley caldera: *Jour. Geophys. Research*, v. 81, p. 785-791.
- Stahl, W., Aust, H., and Dounas, A.**, 1974. Origin of artesian and thermal waters determined by oxygen, hydrogen and carbon isotope analyses of water samples from the Sperkios Valley, Greece, in *Isotope techniques in groundwater hydrology*, v. 2: Vienna, International Atomic Energy Agency, IAEA-SM-182/15, p. 317-339.
- Stewart, M. K., and Hulston, J. R.**, 1976. Stable isotope ratios of volcanic steam from White Island, New Zealand: *Bull. Volcanol.*
- Sumi, K., and Maeda, K.**, 1973. Hydrothermal alteration of main productive formation of the steam for power at Matsukawa, Japan, in *Proceedings, International Symposium on Hydrogeochemistry and Biogeochemistry, Japan, 1970*, v. 1, Hydrogeochemistry: Washington, D.C., J. W. Clark, p. 211-228.
- Swanberg, C. A.**, 1974. The application of the Na-K-Ca geothermometer to thermal areas of Utah and the Imperial Valley, California: *Geothermics*, v. 3, no. 2, p. 53-59.
- , 1975. Detection of geothermal components in groundwaters of Dona Ana County, southern Rio Grande rift, New Mexico: *New Mexico Geol. Soc. Guidebook, 26th Field Conference, Las Cruces County*, p. 175-180.
- Thompson, J. M.**, 1975. Selecting and collecting thermal springs for chemical analysis: A method for field personnel: U.S. Geol. Survey open-file report 75-68, 11 p.
- Thompson, J. M., Presser, T. S., Barnes, R. B., and Bird, D. B.**, 1975. Chemical analysis of the waters of Yellowstone National Park, Wyoming from 1965 to 1973: U.S. Geol. Survey open-file report 75-25, 59 p.
- Tonani, F.**, 1970. Geochemical methods of exploration for geothermal energy: UN Symposium on the Development and Utilization of Geothermal Resources, Pisa, *Proceedings (Geothermics, Spec. Iss. 2)*, v. 2, pt. 1, p. 492-515.
- Tongiorgi, E., ed.**, 1963. Nuclear geology on geothermal areas, Spoleto, 1963: Pisa, Consiglio Nazionale delle Ricerche Laboratorio di Geologia Nucleare, 284 p.
- Trainer, F. W.**, 1974. Ground water in the southwestern part of the Jemez Mountains volcanic region, New Mexico: *New Mexico Geol. Soc. Guidebook, 25th Field Conference, Ghost Ranch*, p. 337-345.
- Truesdell, A. H.**, 1971. Geochemical evaluation of the Dieng Mountains, central Java, for the production of geothermal energy: U.S. Geol. Survey open-file report (IR) IND-8, 29 p.
- , 1976. Chemical evidence for subsurface structure and fluid flow in a geothermal system: International Symposium on Water-Rock Interactions, Prague, Czechoslovakia, 1974 Proceedings.
- Truesdell, A. H., and Fournier, R. O.**, 1976a. Procedure for estimating the temperature of a hot water component in a mixed water using a plot of dissolved silica vs. enthalpy: U.S. Geol. Survey Research Jour.
- , 1976b. Deep conditions in the geothermal system of Yellowstone Park, Wyoming from chemical, isotopic, and geophysical data: U.S. Geol. Survey open-file report.
- Truesdell, A. H., and Singers, W.**, 1971. Computer calculation of down-hole chemistry in geothermal areas: New Zealand Dept. Sci. and Indus. Research Report No. CD 2136, 145 p. (See also *Journal of Research of the U.S. Geol. Survey*, v. 2, no. 3, p. 271-278).
- Truesdell, A. H., and White, D. E.**, 1973. Production of superheated steam from vapor-dominated geothermal reservoirs: *Geothermics*, v. 2, nos. 3-4, p. 154-173.
- United Nations Development Programme**, 1971. Report on the geology, geochemistry and hydrology of the hot springs of the East African rift system in Ethiopia: Investigation of geothermal resources for power development (ETH-26): New York, United Nations, 433 p.
- Vakin, E. A., Polak, B. G., Sugrobov, V. M., Erlikh, E. N., Belousov, V. I., and Pilipenko, G. F.**, 1970. Recent hydrothermal systems of Kamchatka: UN Symposium on the Development and Utilization of Geothermal Resources, Pisa, *Proceedings (Geothermics, Spec. Iss. 2)*, v. 2, pt. 2, p. 1116-1133.
- Weissberg, B. G., and Zobel, M. G. R.**, 1973. Geothermal mercury pollution in New Zealand: *Bull. Environmental Contamination and Toxicology*, no. 9, p. 148-155.
- White, D. E.**, 1957a. Magmatic, connate, and metamorphic waters: *Geol. Soc. America Bull.*, v. 68, p. 1659-1682.
- , 1957b. Thermal waters of volcanic origin: *Geol. Soc.*

- America Bull., v. 68, p. 1637-1658.
- , 1968, Environments of generation of some base-metal ore deposits: *Econ. Geology*, v. 63, p. 301-335.
- , 1970, Geochemistry applied to the discovery, evaluation, and exploitation of geothermal energy resources: rapporteur's report: UN Symposium on the Development and Utilization of Geothermal Resources, Pisa, Proceedings, (Geothermics, Spec. Iss. 2), v. 1, p. 58-80.
- , 1973, Characteristics of geothermal resources, in Kruger, P., and Otté, C., eds., *Geothermal energy: resources, production, stimulation*: Stanford, California, Stanford University Press, p. 69-94.
- , 1974, Diverse origins of hydrothermal ore fluids: *Econ. Geology*, v. 69, p. 954-973.
- White, D. E., Barnes, I., and O'Neil, J. R.**, 1973, Thermal and mineral waters of nonmeteoric origin, California Coast Ranges: *Geol. Soc. America Bull.*, v. 84, p. 547-560.
- White, D. E., Fournier, R. O., Muffler, L. J. P., and Truesdell, A. H.**, 1975, Physical results of research drilling in thermal areas of Yellowstone National Park, Wyoming: U.S. Geol. Survey Prof. Paper 892, 70 p.
- White, D. E., Hem, J. D., and Waring, G. A.**, 1963, Chemical composition of subsurface waters, in Fleischer, M., ed., *Data of geochemistry*: U.S. Geol. Survey Prof. Paper 440-F, p. F1-F67.
- White, D. E., Muffler, L. J. P., and Truesdell, A. H.**, 1971, Vapor-dominated hydrothermal systems, compared with hot-water systems: *Econ. Geology*, v. 66, no. 1, p. 75-97.
- White, D. E., and Truesdell, A. H.**, 1972, The geothermal resources of Taiwan: Mining Research and Service Organization (Taiwan) Report No. 105, p. 51-81.
- Wilson, S. H.**, 1966, Sulphur isotope ratios in relation to volcanological and geothermal problems: *Bull. Volcanol.*, v. 29, p. 671-690.
- Young, H. W., and Mitchell, J. C.**, 1973, Geothermal investigations in Idaho. Part 1. Geochemistry and geologic setting of selected thermal waters: Idaho Dept. Water Admin., Water Inf. Bull. No. 30, 43 p.
- Young, H. W., and Whitehead, R. L.**, 1975a, Geothermal investigations in Idaho. Part 2. An evaluation of thermal water in the Bruneau-Grandview area, southwest Idaho: Idaho Dept. Water Resources, Water Inf. Bull. No. 30, 125 p.
- , 1975b, Geothermal investigations in Idaho. Part 3. An evaluation of thermal water in the Weiser area, Idaho: Idaho Dept. Water Resources, Water Inf. Bull. No. 30, 35 p.
- Zohdy, A. A. R., Anderson, L. A., and Muffler, L. J. P.**, 1973, Resistivity self-potential, and induced-polarization surveys of a vapor-dominated geothermal system: *Geophysics*, v. 38, no. 6, p. 1130-1144.

Western Systems, Inc.

SCIENTIFIC SERVICES DIVISION
P.O. Box 2133/Evergreen, CO 80439/U.S.A.
Telephone: (303) 674-9811



HELIUM

A GUIDE TO GEOTHERMAL ENERGY RESOURCES

David E. Kahler

ABSTRACT

Radioactive decay of uranium in basement rocks generates helium, which enters the geothermal system. Helium released during pressure and temperature reduction of this system can be measured near the surface in water, soil and soil-gas samples. These samples can be analyzed for helium concentrations to better than 10 ppb and the resulting anomalies can then be used in conjunction with other exploration methods to define drilling target areas for geothermal reservoir confirmation. Sampling equipment and precision helium analyses are available from Western Systems, Inc.

INTRODUCTION

Radioactive decay of uranium in basement rocks is accepted as an ultimate source for geothermal systems. During this radioactive decay alpha particles are emitted from uranium-238 and its daughter products, which combine with electrons to form helium atoms. This helium (due to its relative insolubility, in high temperature and pressure conditions of this geothermal system, helium will be scavenged from the enclosing rocks and carried along with gases and Helium will be lost from the system as temperatures and pressures drop helium will "seek daylight" through minute faults, fractures and pore space movement continues upward to the surface and into the atmosphere, where it is eventually lost to space.

The ability of helium to migrate away from its ultimate source of radiation and to accompany geothermal systems provides a convenient geochemical In fact it appears that helium might even be considered a direct tracer of geothermal reservoirs since elevated levels of helium are observed at many sites.

EXPLORATION TECHNIQUES

Helium surveys have been developed and perfected as a time and cost-effective geothermal exploration method. The ability of helium to migrate through the entire geologic column creates large-halo, helium anomalies that can be defined by water, soil and soil-gas sampling.

UNIVERSITY OF UTAH
RESEARCH INSTITUTE
EARTH SCIENCE LAB.

SUBC
GCHM
HGGE

In addition to helium many other techniques are relied upon for outlining geothermal resource areas. The most common and direct approach has been with the use of surface heat flow mapping (not too reliable for deep reservoirs) and borehole temperature probing (expensive). These temperature methods aren't generally used in an initial exploration phase, but rather as follow ups to discoveries of hot springs, volcanic areas and subsurface (drill hole) temperature anomalies. Other techniques have evolved in the past several years to augment temperature gradient surveys in order to precisely define the ultimate heat source or fracture system. These include the usual literature search, photogeology and imagery, as well as isotope ratioing, chemical thermometry, surface/subsurface alteration studies, microearthquake monitoring and various other geophysical and geochemical methods. However, when the heat source is deeply buried, as perhaps in the case of broad sedimentary basins with insulating rock layers, then many of these exploration methods can be costly and prohibitively time consuming.

HELIUM SURVEYS

Helium surveys provide a rapid sampling technique that can be used with minimum effort and at a very low cost. Samples can be collected as water, soil or soil gas and then analyzed for helium concentrations to better than 10 parts per billion in the gaseous sample. It is this precise analytic capability that only recently has permitted helium to be utilized as an effective trace element.

Due to helium's ability to escape from the geothermal system at depth, anomalies will be noted above fractures connected to the geothermal reservoir. This may be the only identifiable tracer, since precipitated calcite and silica may have effectively sealed the reservoir and prevented heavier elements from reaching the surface. Similarly, although there may be an active reservoir at depth, temperature anomalies may be slight or even non-existent.

The event that temperature anomalies are positive, they will usually coincide with helium anomalies, although there may be some offset. This is a very significant correlation and gives the geothermal explorationist an additional method with which to define optimum drill sites for reservoir confirmation.

Helium surveys generally require a sample density of one to five samples per square mile. Detailed exploration is usually conducted with a 0.1 mile grid which can be followed up with sample spacing of 50 to 100 feet in the anomalous zones. If an elongate reservoir is expected (such as a rift or parallel fracture zone), then the grid can be modified as necessary.

SYSTEMS INCORPORATED

Western Systems has been providing precise helium measurements for the exploration industry since 1978. As a leader in helium geochemical analysis, Western Systems has been active in domestic and international projects in mineral and energy evaluation. Western Systems is available to discuss your particular geothermal exploration project and to set up a sampling program to fit your require-

HELIUM EXPLORATION FOR GEOTHERMAL RESOURCES
SELECTED REFERENCES

- Ball, L. et al, 1979, The National Geothermal Exploration Technology Program: Geophysics, v. 44, no. 10, pp. 1721-1737.
- Bergquist, L. E., 1979, Helium, an Exploration Tool for Geothermal Sites: Transactions, Geothermal Resources Council, v. 3, pp. 59-60.
- Bergquist, L. E., 1980, Helium Emanometry, an Energy Exploration Guide: Fiftieth Annual International Meeting and Exposition, Society of Exploration Geophysicists, Houston, Technical Papers, v. 5, pp. 2567-2578.
- Craig, H. et al, 1978, Helium Isotope Ratios in Yellowstone and Lassen Park Volcanic Gases: Geophysical Research Letters, v. 5, no. 11, pp. 897-900.
- Denton, E. H., 1976, Helium Sniffer Field Test, Newcastle, Utah, 10-26 March, 1976: U. S. Geological Survey, Open-File Report 76-421, 4p.
- Denton, E. H., 1977, Helium Sniffer Field Test, Roosevelt Hot Springs, Utah: U. S. Geological Survey, Open-File Report 77-606, 6p.
- Gutsalo, L. K., 1976, On the Sources and Distribution of Helium and Argon Isotopes in the Thermal Waters of the Kurile Islands and Kamchatka: Geochemistry International, v. 13, no. 3, pp. 167-175.
- Hinkle, M. E., 1978, Helium, Mercury, Sulfur Compounds, and Carbon Dioxide in Soil Gases of the Puhimau Thermal Area, Hawaii: U. S. Geological Survey, Open-File Report 78-246, 14p.
- Hinkle, M. E. et al, 1978, Helium in Soil Gases of the Roosevelt Hot Springs Known Geothermal Resource Area, Beaver County, Utah: Journal Research, U. S. Geological Survey, v. 6, no. 5, pp. 563-570.
- Mazor, E., 1972, Paleotemperatures and Other Hydrological Parameters Deduced from Noble Gases Dissolved in Groundwaters; Jordan Rift Valley, Israel: Geochimica et Cosmochimica Acta, v. 36, pp. 1321-1336.
- Mazor, E. and Fournier, R. O., 1973, More on Noble Gases in Yellowstone National Park Hot Waters: Geochimica et Cosmochimica Acta, v. 37, pp. 515-525.
- Mazor, E., 1975, Atmospheric and Radiogenic Noble Gases in Thermal Waters; Their Potential Application to Prospecting and Steam Production Studies: Proceedings, Second United Nations Symposium on the Development and Use of Geothermal Resources, pp. 793-802.

continued

HELIUM EXPLORATION FOR GEOTHERMAL RESOURCES
SELECTED REFERENCES (continued)

- Mazor, E. and Verhagen, B., 1976, Hot Springs of Rhodesia, Their Noble Gases, Isotopic and Chemical Composition: *Journal of Hydrology*, v. 28, pp. 29-43.
- Mazor, E., 1977, Geothermal Tracing with Atmospheric and Radiogenic Noble Gases: *Geothermics*, v. 5, pp. 21-36.
- Naughton, J. J. et al, 1973, Helium Flux from the Earth's Mantle as Estimated from Hawaiian Fumerolic Degassing: *Science*, v. 180, pp. 55-57.
- Pray, H. A. et al, 1952, Solubility of Hydrogen, Oxygen, Nitrogen and Helium in Water at Elevated Temperatures: *Industrial and Engineering Chemistry*, v. 44, no. 5, pp. 1146-1151.
- Roberts, A. A. et al, 1975, Helium Survey, A Possible Technique for Locating Geothermal Reservoirs: *Geophysical Research Letters*, v. 2, no. 6, pp. 209-210.
- Roberts, A. A., 1975, Helium Surveys Over Known Geothermal Resource Areas in the Imperial Valley, California: U. S. Geological Survey, Open-File Report 75-427, 6p.
- Thomas, D. M. and Naughton, J. J., 1979, Helium/Carbon Dioxide Ratios as Premonitors of Volcanic Activity: *Science*, v. 204, pp. 1195-1196.
- Welhan, J. A. et al, 1977, Gas Chemistry and Helium Isotopes at Cerro Prieto, Scripps Institution of Oceanography, La Jolla, California.
- Wescott, E. and Turner, D. (Editors), 1981, Geological and Geophysical Study of the Chena Hot Springs Geothermal Area, Alaska: A geothermal resource investigation by the Geophysical Institute, University of Alaska for the U. S. Department of Energy, Division of Geothermal Energy, 65p., plus plates.

HELIUM: AN EXPLORATION TOOL FOR GEOTHERMAL SITES

Lyle E. Berquist

Western Systems, Inc.
Evergreen, Colorado

ABSTRACT

Helium anomalies near geothermal sites are an effective guide in determining the extent of the geothermal reserves. Advanced sampling and analytical techniques for measuring helium concentrations in water, soils, and soil gases permit the exploration team to quickly collect the samples, store them in leak-free containers, and send them to the laboratory for analysis. Precise analytical methods in the laboratory measure the helium in a gaseous sample to 10 ppb. With these accurate results the explorer can determine potential locations for drilling and use.

INTRODUCTION

Helium anomalies have been detected near geothermal sites throughout the world. The exact reason for the helium anomaly is unknown, but theories have been expressed. First, most geothermal waters are believed to come from deep sources below the earth's mantle where the mixing with atmospheric air is nearly impossible. Secondly, there may be uranium-thorium decaying in the vicinity of the geothermal source, which produces helium from the alpha particles in the process of uranium decay.

Pressurized hot water will entrap large amounts of helium and release the helium as it cools, and since helium is highly mobile it will find faults and minute fractures and paths to rise to the surface. Some helium may be entrapped in the rocks and sands, but because its atomic structure is nearly spherical, the entrapment is difficult.

Thus, in soils and waters near geothermal sites one finds helium anomalies that are greater than 5.24 ppm which is the nominal amount found in the atmosphere.

During the past few years several researchers have published papers on helium anomalies near geothermal sites. Mazor (1972) published his findings at sites in Israel. He reports that large anomalies of H_2 , N_2 , and A_r exist in these waters. Craig et al. (1978) reported similar results from research in Yellowstone Park. Naughton et al. (1973) reported finding high helium concentrations in the

geothermal sites around the Kilauea Volcano in Hawaii. Welhan et al. (1979) reports high helium concentrations in Cerro Prieto geothermal field in Mexico. Roberts et al. (1975) reported helium anomalies at Indian Springs near Idaho Springs, Colorado. Hinkle et al. (1978) found large anomalies at Roosevelt Hot Springs in Utah.

The sampling and analytical techniques of helium detection are now well enough developed that the helium exploration program is useful to geothermal explorers.

TECHNICAL APPROACH

Helium detection instrumentation has improved during the past few years so that precise and meaningful results can be provided. Also, sampling devices are now available so that samples can be collected in the field, sealed and sent back to the laboratory without sample dilution. Samples of spring or well water and soils or gases are used for a typical survey. Sampling devices and methods vary but the techniques related in this report have been found to be effective even under adverse conditions.

Water samples give the largest anomalies and frequently will have many times the level of helium found in the atmosphere. Quantities as great as 1000 times larger are not unusual. In India water samples are taken to see if helium is present and, if so, in large enough quantities so that helium can be removed and used for commercial applications.

Helium in soils and soil gases around geothermal sites provides anomalies that aid in exploration. Soils need to be undisturbed and, if sandy, the sample must be taken below the sand. If one cannot go below this level, then in regions where sand is present the anomaly will be much less. The exploration team needs to keep records of soil conditions, so when the data are plotted the change in helium concentration levels from sandy sites will be considered.

SAMPLING TECHNIQUES

The three types of samples; water, soil and soil gases are collected in different manners. Water is collected directly from the source

either from a well, spring, geothermal artesian well, or from a closed system which has not aerated. Helium in water exposed to air will leave almost immediately, making that sample meaningless.

The approach we use in collecting water samples is to fill a 500 ml plastic bottle to a predetermined level, which leaves an air space of 30 ml. The bottle cap is immediately screwed on tightly. The cap has a septum on it so a gas sample can be removed. The bottle is shaken for about one minute, then let stand for one minute so the gas can come to equilibrium. A hypodermic syringe is used to remove at least 20 ml of gas from the bottle. This gas is immediately transferred into an evacuated 10 ml cylinder through a septum in the opening end. The end is then sealed with a metal cap which contains a lead seal. The leak rate through the lead is less than 10^{-15} atmospheric ml/sec and the enclosed sample will last indefinitely without atmospheric dilution. The cylinder is then marked and sent to the laboratory for analysis.

To collect a soil gas sample a probe is driven 30 inches into the ground. The probe which is a tube has an inside diameter of .065 inches. On the top of the probe a septum is held tightly by a tube fitting to isolate the atmospheric air. A hypodermic syringe is used to collect the sample. The first sample collected is expelled into the atmosphere to empty the tube of atmospheric air. The second sample is then taken and stored in a metal cylinder in the same manner as the gas from the water sample.

In soil sampling a hole is dug in the ground, with an auger, to a depth of at least 30 inches. The soil in the bottom of the hole is then removed and placed in a 500 ml metal container and sealed immediately. The metal container has an inner surface of thin plastic film to prevent leakage and minimizes atmospheric dilution to less than 1% in 60 days. After sealing, the container is labeled and ready to be sent to the laboratory for analysis.

ANALYTICAL TECHNIQUE

The analysis is made on a Dupont Helium Mass Spectrometer. This mass spectrometer when received from the manufacturer has a basic sensitivity for detecting 1 part of helium in 10 million parts of the atmosphere. In our instrument we have added a precise pressure-measuring system for the inlet gases. The active gases are removed and only the noble gases remain. This allows one to use a sample that is 100 times larger than normal, thus enhancing the helium concentration by 100. In our system the fluctuation normally caused by instability on a diffusion pump has been eliminated.

The output of the mass spectrometer is measured by a digital electrometer, and the signal usually reads 1.945 for a known calibrated air sample which contains 5.24 parts per million

of helium. The gas sample was calibrated by the U.S. Bureau of Mines. The gas in the inlet system is inserted into a 3 ml manifold through a septum. A hypodermic syringe is used to remove the gas sample from the sample cylinder and insert it into the previously evacuated manifold. The pressure in the manifold is measured to a precision of better than .05%. The temperature of the manifold is held to within .1°C between sample and reference gases. A metered portion of this gas is then admitted into the active gas filter and later into the analyzer for measurement.

A known sample is analyzed, then an unknown, then another known sample. The repeatability of the known samples is within ± 1 digit on the digital electrometer. With this system we are able to measure the concentration in a known sample to a precision better than 10 parts per billion, which is necessary to provide precise data.

In the analysis the inlet pressure is always recorded and also the output from the electrometer. Using these data, the unknown sample results are always compared with the known sample just previously run and the one following the unknown. The measurement is given in parts per million of helium in the sample.

CONCLUSION

The sampling and helium analysis of water, soils, and soil gases provide an excellent guide for locating the potential of geothermal sites. Advanced instrumentation and sampling techniques are now developed so precise results are available to the geothermal explorer.

REFERENCES

- Craig, H., Lupton, J.E., Welhan, J.A. and Poreda, R., 1978, Helium isotope ratios in Yellowstone and Lassen Park volcanic gases: Geophysical Research Letters, v. 5, p. 897-899.
- Hinkle, M.E., Denton, E.H., Bigelow, R.C. and Turner, R.L., 1978, Helium in soil gases of the Roosevelt Hot Springs known geothermal resource area, Beaver County, Utah: Jour. Research U.S. Geol. Survey, v.6, p.563-570.
- Mazor, E., 1972, Paleotemperatures and other hydrological parameters deduced from noble gases dissolved in groundwaters; Jordan Rift Valley, Israel: Geochemica et Cosmochimica Acta, v. 36, p. 1321-1336.
- Naughton, J.J., Lee, J.H. and Keeling, D., 1973, Helium flux from the earth's mantle as estimated from Hawaiian fumarolic degassing: Science, v. 180, p. 55-56.
- Roberts, A.A., Friedman, I., Donovan, T.J. and Denton, E.H., 1975, Helium survey, a possible technique for locating geothermal reservoirs: Geophysical Research Letters, v. 2, p. 209-210.
- Welhan, J.A., Poreda, R., Lupton, J.E. and Craig, H., 1979, Gas chemistry and helium isotopes at Cerro Prieto: Scripps Institution of Oceanography, La Jolla, Calif. (to be published).

HELIUM SURVEY, A POSSIBLE TECHNIQUE FOR LOCATING GEOTHERMAL RESERVOIRS

Alan A. Roberts, Irving Friedman, Terrence J. Donovan, and Edward H. Denton

U.S. Geological Survey, Denver, Colorado 80225

Abstract. Measurements were made of the helium concentration in the soil gases surrounding the Indian Hot Springs, Idaho Springs, Colorado. The helium concentration was shown to vary in a regular manner from the background level of 5.2 ppm to a high of more than 100 ppm near a warm (26°C) water seep, and more than 1,000 ppm near a hot (40°C) water seep. Such an association of helium in the soil gas with these hot waters near the earth's surface suggests the possible utility of helium surveys in locating hidden geothermal reservoirs.

It is becoming increasingly apparent that geothermal energy may one day be a significant contributor to our energy supply. (See for example Anderson and Axtell, 1972; Armstead, 1973; Hickel, 1972.) However, exploration capability is in the infant stage. To quote Walter Hickel, (1972, p. 22) "At the present time, the most reliable exploration technique for new geothermal reservoirs is to find areas containing hot springs, a situation similar to that in the petroleum industry in the early 1900's when petroleum exploration consisted of finding areas of surface oil seeps."

Preliminary work by Margaret Hinkle and co-workers at the U.S. Geological Survey (oral communication, 1975) has shown a high concentration of helium (>100 ppm) in the gases dissolved in the water from seven widely scattered hot springs in the western United States. These investigators also found anomalously high helium levels in the soil gases near a hot spring in Yellowstone National Park.

We attempted therefore to apply a portable helium detector that we have been developing for oil and gas exploration to the problem of locating geothermal resource areas. We present here our work on the concentration of helium in the soil gases around the Indian Hot Springs Resort, Idaho Springs, Clear Creek County, Colorado (Long. 105° 30'; Lat. 39° 45').

Sample Collection and Analysis

Measurements of helium in soil gases were made with a commercial helium leak detector mounted in a small truck. This instrument consists of a small (1 cm radius) mass spectrometer set to collect helium (mass 4) ions. These ions are distinguishable from triply-charged carbon, the only ions at nominal mass 4 that we might expect to interfere. The electron accelerating voltage can be adjusted to ionize helium without producing triply-charged carbon ions. The power to the leak detector was supplied by a propane-fueled generator which was

electronically stabilized in voltage, frequency and wave form. High source pressure and high filament temperature maximized sensitivity of the mass spectrometer to helium.

The sample probes (steel tubing) were driven into the soil to a depth of about 0.5 m. Gas was slowly pumped out of the probe. A small amount of this gas was allowed to leak into the mass spectrometer source. Periodically the mass spectrometer was switched to a sample of helium in compressed air standardized chromatographically by the U.S. Bureau of Mines, Helium Division at 5.26 ± 0.05 ppm as well as to a sample containing 7.60 ± 0.05 ppm helium for calibration of sensitivity. With this comparison technique our instrumentation detects changes in helium abundance in the gas

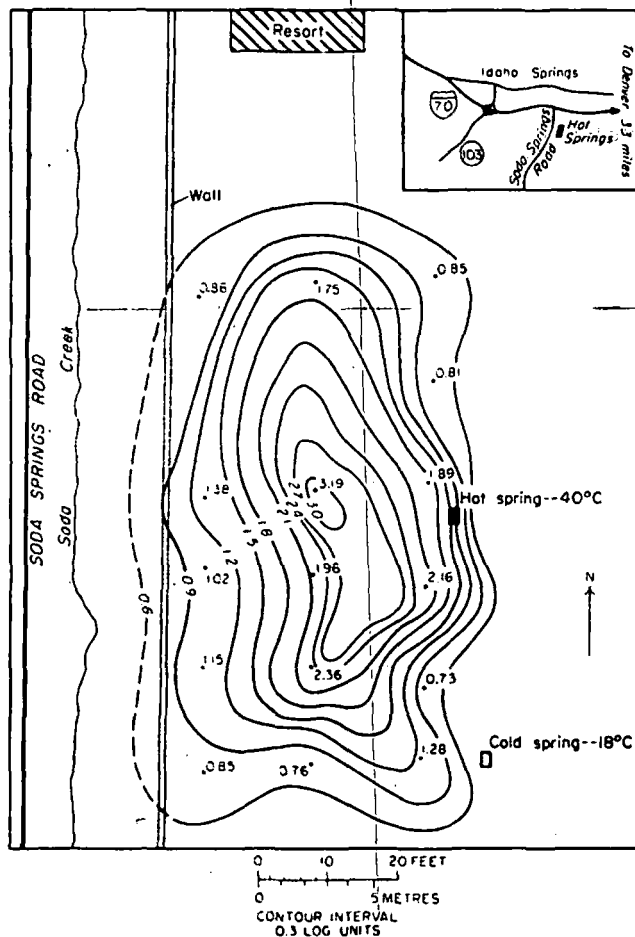


Figure 1. Map showing isopleths of the logarithm of the helium concentrations (ppm) in soil gases around a hot spring south of the Indian Hot Springs Resort, Idaho Springs, Colorado.

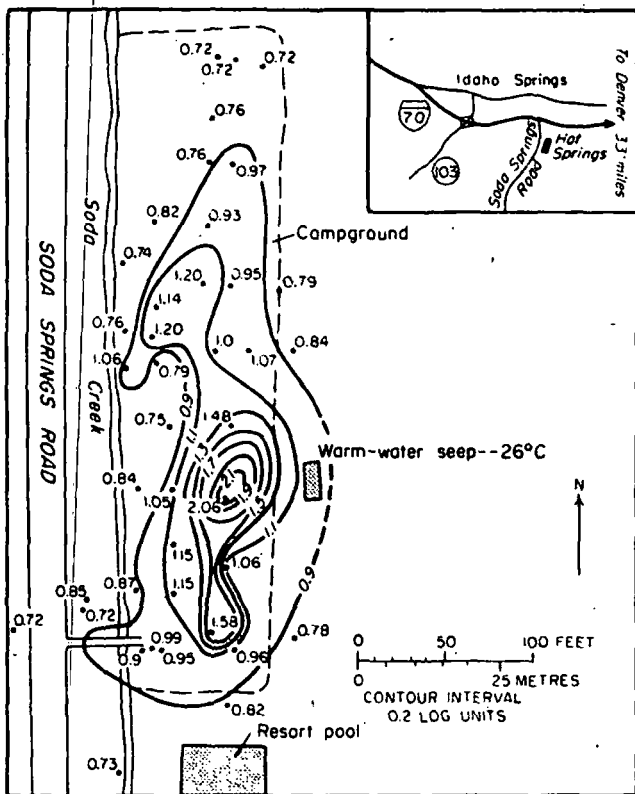


Figure 2. Map showing isopleths of the logarithm of the helium concentrations (ppm) in soil gases around a hot spring north of the Indian Hot Springs Resort, Idaho Springs, Colorado.

stream of about 0.05 ppm (50 parts per billion). A single measurement takes about 3 to 4 minutes, including the time to insert and extract the probe.

Results

The results of the helium survey involving 63 stations taken near the Indian Hot Springs Resort are shown in Figures 1 and 2. Figure 1 shows that the concentration of helium in the soil gases varies in a regular manner from a low of 5.4 ppm (0.73 log units) in front of the cold (18°C) water seep to a high of more than 1,000 ppm (3.19 log units) in front of the hot (40°C) water seep. In contrast, numerous readings taken in the surrounding few square kilometres of countryside showed only the 5.2 ppm concentration of helium that is typical of the atmosphere.

Figure 2 illustrates a similar increase in helium concentration to a peak greater than 100 ppm (2.1 log units) located near a warm (26°C) water seep about 100 metres north of the hot seep. Subsequent replicate readings taken under different weather conditions showed that temperature, wind velocity, and barometric pressure have no observable effect on the concentration of helium in soil gas at Indian Hot Springs Resort.

Discussion

The above results demonstrated dramatically a definite association of helium in soil gases with near-surface hot waters. Preliminary work done in several other hot-spring areas by us and at Yellowstone National Park by Margaret Hinkle (oral communication, 1975) suggests that this association is a common occurrence.

The solubility of helium in water is unusual in that it does not continually decrease with increasing temperature. It decreases up to 30°C and increases above that (Mazor, 1972). We believe that hot water under pressure can act as an excellent scavenger of the helium being produced from the radioactive decay of uranium and thorium in rocks and soil. As this water nears the surface it will be both cooler and under less pressure, thereby allowing the helium to escape from solution and diffuse up through the soil to the surface where it can be measured.

Acknowledgments. The authors thank William D. Long and Mary Dalziel for their friendly assistance in sample collection and analysis.

References

- Anderson, David N. and L. H. Axtell, eds., Compendium of First-Day Papers presented at the First Conference of the Geothermal Resources Council: El Centro, California, Geothermal Resources Council, pp. 1-77, 1972.
- Armstead, C. H., ed., Geothermal Energy, Review of Research and Development: Paris, UNESCO, pp. 1-186, 1973.
- Hickel, W. J., Geothermal Energy--A National Proposal for Geothermal Resources Research: University of Alaska, p. 22, 1972.
- Mazor, E., Paleotemperatures and other Hydrological Parameters Deduced from Noble Gases Dissolved in Groundwaters, Jordan Rift Valley, Israel: *Geochimica et Cosmochimica Acta*, v. 36, p. 1321-1336, 1972.

(Received March 24, 1975

Accepted April 9, 1975)

Western Systems, Inc.

SCIENTIFIC SERVICES DIVISION
P.O. Box 2133/Evergreen, CO 80439/U.S.A.
Telephone: (303) 674-9811

SUBJ
GCHM
HGGG

UNIVERSITY OF UTAH
RESEARCH INSTITUTE
EARTH SCIENCE LAB.



HELIUM...

A GASEOUS GEOCHEMICAL GUIDE TO ORE DEPOSITS

David E. Kahler

ABSTRACT

The ability of explorationists to locate hidden fracture zones provides a significant step towards identifying favorable ore deposit targets. One convenient method used to define these fracture zones is the gaseous geochemical survey. Helium, due to its ability to migrate from great depths along faults and minute fractures, is an excellent trace element to use in such surveys. Western Systems Incorporated provides sampling equipment and precision analyses for helium surveys.

INTRODUCTION

Well conceived, integrated, geological/geochemical/geophysical programs are essential for successful exploration projects. The use of noble gases as trace elements for the discovery of deeply-buried mineral deposits is increasing and should be considered for early stage reconnaissance geochemical investigations. The application of helium surveys is a time and cost effective method for locating fracture zones through which gases easily migrate and thus, indirectly, mineral deposits can be located.

HELIUM SURVEYS AND ORE DEPOSIT FORECASTING

It is reasonable to say that the discovery of ore deposits is becoming increasingly difficult. The modern explorationist must now commonly use methods that only a few years ago were considered esoteric at best. Geochemical investigations are standard for regional evaluations and geochemists are working closely with geologists and geophysicists to devise techniques that will rapidly highlight potential ore bearing areas. The expense of drilling for ore deposits almost demands that such research efforts be utilized to the fullest extent possible.

The use of gaseous geochemical surveys (including helium) has been increasing and is now routinely applied in the search for highly-permeable fissured zones. These fractured areas are associated with not only intrusives that create arching, but also with major tectonic features inherent with subsidence structures and thrusting. Helium bearing anomalies will be associated with these fractures, since helium migrates through the most permeable route to the surface. Obviously the geologist who can easily define deeply-buried fracture zones will have a significant advantage over the competition.

Continued



HELIUM: ITS SOURCE AND MIGRATION CHARACTERISTICS

Helium is formed in the Earth's crust, mantle and core by alpha decay of uranium and thorium. The quantity of helium produced is approximately 5,000 tons annually of which perhaps only 10% escapes to the atmosphere. Since helium is light, stable and inert, it is quite mobile and migrates readily from its source rock and into natural gas and ground water. Helium loss from great depths occurs along faults and the greatest loss is from deep horizons in extensively jointed and faulted rock units. Such rock units are also customarily mineralized and are more porous than the enclosing rocks. If in addition there is associated radioactive mineralization, then there will be a significant increase in helium flow from the faults.

It appears that maximum helium concentrations occur below sediments near the basement crystalline rocks. Therefore, gas surveying (i.e., helium and others) can provide a guide to large intrusive masses and indirectly assist the geologist in locating ore deposits.

HELIUM IN ORE DEPOSITS

From the foregoing it is apparent that helium produced at great depths will migrate preferentially within the geothermal/hydrothermal system. Although it hardly seems possible to define specific mineral assemblages based on helium anomalies, a regionally high level of helium in the subsurface soil and/or water can point to common feeder channels. Such discoveries will provide geologists with favorable exploration targets and additional geochemical and geophysical data should refine these targets.

Helium anomalies are known to occur with carbonatites, lead-zinc, iron, gold, mercury, kimberlite pipes, etc. In fact there are gold, copper and polymetallic mines in South Africa, Russia and Sweden that produce so much gas (including helium) that mining is difficult. However, such extreme cases are uncommon, but nevertheless demonstrate the significance of gaseous geochemistry for exploration.

In general then it can be stated that abnormal helium flow is to be expected in zones of tectonic weakness. Since ore deposition is similarly expected in such zones, the appearance of anomalous helium in the subsurface will signal favorable exploration sites.

HELIUM SURVEYS

Regional surveys can be carried out by means of soil, soil-gas or water sampling or by any combination of these methods. Each method is simple and provides a rapid and inexpensive, preliminary reconnaissance technique in untested areas. One to five samples are usually collected per square mile for regional surveys, with detailed and follow-up sampling conducted on a 0.1 mile grid. As with any geochemical method, orientation surveys are desirable and should be used to modify grids to fit known trends defined by geological or geophysical surveying. The samples can be analyzed in the laboratory for helium concentrations to better than 10 ppb in the gaseous sample, with reference to normal atmospheric helium concentration of 5240 ppb.

WESTERN SYSTEMS INCORPORATED

Western Systems Incorporated has been providing precise helium measurements for the exploration industry since 1978. As a leader in helium geochemical analysis, Western Systems has been active in domestic and international projects in mineral and energy resource evaluation. Western Systems is available to discuss your particular exploration project and to set-up a sampling program to fit your requirements.

HELIUM EXPLORATION FOR FAULTS, FRACTURES AND ORE DEPOSITS SELECTED REFERENCES

(Some of these articles appear also in the publication Chemical Abstracts [CA] and are so noted with volume and item number)

- Berzina, A. P. et al, 1977, The Composition of Gases in Mineral Forming Solutions of Copper-Molybdenum Deposits: AGI Doklady, v. 228, pp. 203-205. (CA 85-127192.)
- Bhimasankaram, V. L. S. et al, 1979, Helium Survey for Structural Mapping – A Case Study: Current Science, v. 48, no. 6, pp. 238-240. (CA 90-20770.)
- Bowie, S. H. U., 1958, Helium in Natural Gasses in the Witwatersrand: Nature, v. 182, p. 1082.
- Bulashevich, Y. P. and Bashorin, V. N., 1971, Helium in Ground Water Along a Deep Seismic Sounding Profile East of the Urals: AGI Doklady, v. 193, pp. 6-7. (CA 73-90172.)
- Bulashevich, Y. P. and Bashorin, V. N., 1972, Confinement of High Helium Concentrations in Ground Water to Intersections of Faults: AGI Doklady, v. 201, pp. 36-37. (CA 76-48469.)
- Bulashevich, Y. P. and Bashorin, V. N., 1973, On the Detection of Faults Along the Sverdlovsk DSS Profile from High Concentrations of Helium in Underground Water: Physics of the Solid Earth, no. 3, pp. 185-189. (CA 79-33635.)
- Bulashevich, Y. P. and Bashorin, V. N., 1974, Arrangement of Permeable Faults in the Crust in Northwestern Kazakhstan, from the Distribution of Helium in Underground Waters: Geotectonics, no. 3, pp. 159-161. (CA 81-124455.)
- Bulashevich, Y. P. et al, 1974, Helium in Ground Water Along the Sverdlovsk Deep Seismic Sounding Traverse: AGI Doklady, v. 208, pp. 15-18. (CA 79-128209.)
- Bulashevich, Y. P. and Kartashov, N. P., 1978, Application of the Helium Method to Structural Studies in Mineralized Areas: AGI Doklady, v. 229, pp. 137-139. (CA 86-19655 and 92-166633.)
- Dikun, A. V. et al, 1975, Some Indications of Existence of Transcrustal Gas Flow: Geochemistry International, v. 12, no. 6, pp. 73-78. (CA 84-108925.)
- Dikun, A. V. et al, 1976, Some Features of Development of Helium Surveying: International Geology Review, v. 18, no. 1, pp. 98-100, (CA 83-82722.)
- Eremeev, A. N. et al, 1972, Application of Helium Surveying to Structural Mapping and Ore Deposit Forecasting: in Geochemical Exploration 1972, Proceedings of the Fourth International Geochemical Exploration Symposium, IMM, London, pp. 183-192.
- Ewers, G. R. and Keays, R. R., 1977, Volatile and Precious Metal Zoning in the Broadlands Geothermal Field, New Zealand: Economic Geology, v. 72, pp. 1337-1354.
- Fridman, A. I. and Petrov, V. A., 1976, Principal Results of Gas Surveying in Ore Deposits Under Permafrost Conditions (Noril'sk Region): International Geology Review, v. 18, no. 5, pp. 545-550. (CA 83-100876.)
- Fridman, A. I. et al, 1981, Natural Gases in Mercury Deposits of Donbass and Northwestern Caucasus: International Geology Review, v. 23, no. 2, pp. 199-204. (CA 90-207618.)
- Gavrilenko, B. V. and Fugzan, M. M., 1975, Helium in Sulfide Minerals of Metamorphic Rocks of the Kolmozero-Voron'ya Zone, Kola Peninsula: AGI Doklady, v. 214, pp. 212-213. (CA 81-52323.)
- Henley, R. W. and Thornley, P., 1979, Some Geothermal Aspects of Polymetallic Massive Sulfide Formation: Economic Geology, v. 74, no. 7, pp. 1600-1612.
- Hinkle, M. E., 1978, Helium, Mercury, Sulfur Compounds and Carbon Dioxide in Soil Gases of the Puhimau Thermal Area, Hawaii Volcanoes National Park, Hawaii: U. S. Geological Survey, Open File Report 78-246, 7p. plus 7 plates.
- Hugo, P. J., 1963, Helium in the Orange Free State Gold-Field: Department of Mines, Geological Survey, Republic of South Africa, Bulletin 39, 26p. Plus 2 maps.
- Kravtsov, A. I. and Fridman, A. I., 1966, Natural Gases of Ore Deposits: AGI Doklady, v. 165, pp. 192-193. (CA 64-7882.)
- Kravtsov, A. I. et al, 1977, Gases and Bitumens in Rocks of the Udachnaya Pipe: AGI Doklady, v. 228, pp. 231-234. (CA 86-92756.)

- Ovchinnikov, L. N. et al, 1977, Integrated Gaseous Geochemical Methods in Structural Mapping and Prospecting for Ore Deposits: in Geochemical Exploration 1972, Proceedings of the Fourth International Geochemical Exploration Symposium, IMM, London, pp. 177-182.
- Pereira, E. B. and Adams, J. A. S., 1979, Surface Anomalies and Migration of Helium-4 and Radon-222: Abstract in EOS, American Geophysical Union Transactions, v. 60, no. 46, S73, p. 883.
- Petersil'ye, I. A. et al, 1975, Hydrocarbon Gases and Organic Carbon in Proterozoic Rocks of the Kola Peninsula: AGI Doklady, v. 215, pp. 201-204. (CA 81-124231.)
- Petersil'ye, I. A. and Pripachkin, V. A., 1979, Hydrogen, Carbon, Nitrogen and Helium in Gases from Igneous Rocks: Geochemistry International, v. 16, no. 4, pp. 50-55. See also (CA 91-143641 and 91-178502.)
- Petersilje, I. A. and Pripachkin, W. A., 1979, Hydrogen, Carbon, Nitrogen and Helium in Gases of Igneous Rocks: in Origin and Distribution of the Elements, Proceedings of the Second Symposium, Paris, May, 1977, Pergamon Press, Oxford, Published as v. 11 of Physics and Chemistry of the Earth, pp. 541-545.
- Rosler, H. J. et al, 1977, Integrated Geochemical Exploration for Deep-Seated Solid and Gaseous Mineral Resources: Journal of Geochemical Exploration, v. 8, no. 1/2, pp. 415-429.
- Rozen, O. M. and Yanitskiy, 1975, Main Structures of the Precambrian Kokchetav Block and Subsurface Helium Flow: AGI Doklady, v. 216, pp. 53-56. (CA 81-173111.)
- Voitov, G. I. et al, 1976, Natural Gases of the Yuzhno-Belozerskoye Iron Ore Deposit (Ukrainian Crystalline Shield): AGI Doklady, v. 220, pp. 204-206. (CA 83-30916.)
- Zhirov, K. K. et al, 1972, Endogenetic Gas Atmosphere During Sulfide Mineralization (Primary Helium, Argon and Nitrogen in Sulfide Ore Deposits): in Geology of Ore Deposits, Academy of Sciences of the USSR, v. 14, no. 2, pp. 23-39, Russian text; Abstract in Economic Geology, v. 70, no. 5, p. 1001 (1975.)

ADDENDUM TO SELECTED REFERENCES

The following articles, which relate to helium applications in the search for faults, fractures and ore deposits, have been abstracted in English and appear in the publication Chemical Abstracts as noted:

Volume-Number	Title
80-39377	Helium-Bearing Capacity of Betpak-Dala Structures (W, Mo, Cu and other ores.)
81-52499	Geochemical Methods for the Exploration and Prospecting of Sulfide Ore Deposits.
81-108692	Possible Use of Gas Surveys for Nickel Prospecting in the Kola Peninsula.
81-156119	Distribution of Helium and Argon Across the Trend of a Quartz-Molybdenite Vein.
88-156293	Mapping the Zones of Deep-Seated Tectonic Faults by Water-Helium Surveying.
89-27819	Anomalies of Helium Distribution During the Study of Ore Field Structure.
89-46477	Possibility of a Helium Survey for Predicting Endogenic Mineralization (Fe, Au, Cu, pyrite-polymetallic-rare elements and graphite.)
92-166632	Gas Mapping in Chalcopyrite Deposits of the Molodezhnoe Ore Region.

SCIENTIFIC SERVICES DIVISION
P.O. Box 2133/Evergreen, CO 80439/U.S.A.
Telephone: (303) 674-9811



A GEOCHEMICAL GUIDE TO PETROLEUM RESERVOIRS

ABSTRACT

David E. Kahler

Helium is produced during alpha decay of radioisotopes of uranium and thorium in sedimentary reservoir formations and from radioactive elements in basement rocks. Due to its relative insolubility, light weight, extremely small molecular size and chemical inertness, helium can easily migrate from its source to the surface. Since helium is often a component of oil and gas deposits, the delineation of near surface helium anomalies will provide a significant guide to petroleum reservoirs. Helium geochemical surveys can be carried out rapidly and inexpensively in all types of terrain with water, soil and soil-gas sampling. Western Systems Incorporated provides complete sampling equipment and precision analyses for these surveys.

INTRODUCTION

Hydrocarbon geochemistry is a direct, remote sensing exploration technique, which is based upon vertical seepage of hydrocarbon components from petroleum reservoirs. The interpretation of these geochemical survey results may be complicated by hydrocarbons generated by near surface decaying organic matter. Helium, however, is never biogenically produced and thus helium geochemical anomalies will normally be associated with deeper sources. Helium movement through the geologic column is a highly complex combination of fluid transport and gaseous diffusion. With regard to migration from petroleum reservoirs, helium's extremely small molecular size (half the size of a methane molecule) and spherical shape permit it to easily migrate through microfractures in the caprock. The helium will continue to move upwards where it eventually reaches the surface, escapes to the atmosphere and is finally lost to outer space. This long distance migration capability provides a unique basis for helium geochemistry applications in oil and gas exploration.

This paper examines characteristics and sources of helium, migration theories and reservoir occurrences, helium geochemical survey techniques, and sample density and analysis. In addition a number of case histories are referenced in a comprehensive bibliography of helium exploration for petroleum reservoirs.

CHARACTERISTICS AND SOURCES OF HELIUM

Helium is the second lightest known element with a specific gravity of 0.1381 (hydrogen is 0.0695 and air is 1). It has a molecular and atomic weight of 4 and is a colorless, odorless, inert, elemental gas with no known chemical compounds. Helium's low solubility in water, monatomic molecular structure, low cross-section capture coefficient, extremely light weight, chemical inertness and high diffusivity make it a valuable commodity for scientific and commercial applications. These same properties give helium a unique advantage over other geochemical trace elements in that helium will always migrate from its source to the surface of the earth.

Helium is steadily generated by radioactive elements in rocks and minerals. This occurs when alpha particles (released by decay in the uranium and thorium isotope series) ultimately capture two electrons to form atoms of inert helium. Other sources of helium on earth, such as those due to primordial accumulations, cosmic radiation, meteorites, radioactive tritium decay, etc., do not contribute significantly to the total annual production.

According to Yakutseni et al (1969), helium yield differs considerably with respect to rocks, regions and geospheres due to variable, radioactive element content. They report that helium production from alpha decay in the earth's core, mantle and crust is 5,200 tons or $2.94 \times 10^{13} \text{cm}^3$ per year. Helium loss to the atmosphere is only one tenth of its rate of production and sedimentation occurs more rapidly than helium is lost.

MIGRATION THEORIES AND RESERVOIR OCCURRENCES

Newton and Round (1960) suggest that helium can migrate in three ways: as bubbles, in solution and by molecular diffusion. They state that helium, which is in constant motion, will transfer from regions of high concentration to regions of low concentration. Both bubble and solution transfer mechanisms are rejected for various reasons, and through complex mathematical equations they develop plausible theories for relationships between sedimentation rates and helium diffusion rates. Golubev et al (1970) on the other hand develop an equally logical case for migration of helium on the basis of a fluid transport model. They conclude that the distance helium moves by diffusion is several orders of magnitude smaller than the distance moved in equal time by fluid transport.

A statistical approach to helium occurrences was used by Tongish (1980) in a detailed study of 10,086 gas samples in 6,455 reservoirs in 35 states (U.S.A.). While he makes no direct statements concerning helium migration per se, the interrelationships of helium with geographic location, geologic age and reservoir depth are thoroughly examined. The results of his study suggest that helium migrates throughout the geologic system and is concentrated in reservoirs of all ages and depths. There is considerable evidence that richer helium occurs in reservoirs at depths less than 9,000 feet and that the most favorable depths for high helium concentrations appear to be less than 5,000 feet. These conclusions relate strictly to samples from U.S.A. reservoirs and may not have worldwide validity.

Based upon the concept of helium generation from alpha decay of radioactive minerals in basement rocks, significant quantities of helium should be found at the sedimentary/basement contacts. This then would lead to migration of large volumes of helium into traps in geologic systems closest to basement rocks. There is some evidence for this according to Pierce (1960), who noted an increase of helium content with increasing geologic age of the reservoir rocks. Tongish (1980) confirmed this when speaking of erathems (i.e. Cenozoic, Mesozoic and Paleozoic), but noted several discrepancies when considering individual geologic systems.

Another approach to the problem of helium migration, and thus the effective use of helium as a guide to petroleum exploration, is covered by Tiratsoo (1967). He observed that in Canada helium in natural gases occurs in greater concentrations in regions of structural tension and fracturing, such as the Sweetgrass Arch, Peace River Arch and Alberta basin hinge belt. Tiratsoo reasoned that such fracturing would accelerate the release of occluded helium. This conclusion is consistent with more recent reports concerning helium loss from: deep crustal faults (Bulashevich and Bashorin, 1970; Rösler et al, 1977); volcanoes (Naughton et al, 1973; Thomas and Naughton, 1979); and geothermal systems (Gutsalo, 1976; Mazor, 1977; and Roberts, 1975).

In an early treatise on helium use as a geochemical index for petroleum prospecting, Gutsalo (1966) considers hydrochemical zoning and concludes that helium accumulates in the strata waters of older water-containing rocks. He also observed that helium concentration is a function of the degree of mineralization in these waters. From this he concluded that helium content in groundwater is governed mainly by the concentration of soluble radium salts in the groundwater.

Thus it appears that migration through the geologic system by helium is definitely a complex matter. Nevertheless, it can be reasonably stated that helium is a component of most oil and gas reservoir systems, and helium's migration characteristics can generally be correlated with those of the associated hydrocarbons. It follows then that measurements of helium concentrations near the earth's surface and in water adjacent to petroleum deposits will provide a significant guide to the discovery of these reservoirs.

HELIUM GEOCHEMICAL SURVEY TECHNIQUES

Water: Water sampling from various depths and formations may provide a near-source, helium anomaly to identify petroleum reservoirs adjacent to "dry holes". Gutsalo (1966) concluded that there are positive helium anomalies in groundwaters around petroleum and gas deposits; and also that a helium determination should be included among the gas and hydrochemical tests used in searching for petroleum and gas deposits. Since helium readily degasses from water, only those samples that have not aerated can be considered. Thus surface lake samples and stream samples are of little value, but wells, springs, lakes below the thermocline and water near the ocean floor can be used. Because helium will migrate through the water system from formation-to-formation, helium in groundwater sampling is an excellent tool. Of course this type of sampling is subject to the availability of sampling points.

Soil gas: This is a direct sampling technique whereby a near-surface gas sample is collected through a hollow probe driven into the ground to a depth of approximately 75 cm. The steel probe has a small opening at the tip and a rubber septum on top. By evacuating the probe with a syringe, a small gas sample will be collected from an area near the tip and will represent soil-gas

conditions at that point. The gas sample thus obtained is then transferred to a steel tube which has a rubber septum and is sealed with a lead lined cap. Soil-gas sampling is rapid, environmentally non-destructive and inexpensive. One or two persons can collect 50 to 100 samples per day with light-weight, hand carried equipment.

Soil: Soil surveys are essentially time-integrated, soil-gas samples where helium has accumulated in moisture and in soil micropores. An auger is used to collect a small sample, which is then canned and sealed, and allowed to equilibrate with air in the container. After the soil is degassed, a gaseous sample is withdrawn for analysis. Soil surveys generally provide somewhat higher anomalies than the soil-gas method, but do take longer to carry out. When running helium surveys in frozen or extremely wet soil, the soil survey must be used since collecting a gas sample with a probe is often impossible under such conditions.

SAMPLE DENSITY AND ANALYSIS

Water, soil or soil-gas samples can be collected at spacings ranging from one sample per 100 square miles (kms.) to 100 or more samples per square mile (km.). A customary spacing of one to five samples per square mile (km.) will give sufficient data to reduce a regional area of interest for more detailed surveys. As with any exploration technique, sample density must be determined on the basis of geological, geochemical and geophysical knowledge of the area.

The gaseous samples are analyzed with a modified, helium leak detector mass spectrometer in the laboratory. The modifications result in the removal of active gases from the measurement samples, thus permitting a 100 times larger sample to be injected into the mass spectrometer. In addition highly sensitive pressure and temperature indicators, thermal insulation and other changes provide instrument accuracy in the range of ± 10 ppb with reference to atmospheric helium concentration of 5,240 ppb.

WESTERN SYSTEMS INCORPORATED

Western Systems has been providing precise helium measurements for the exploration industry since 1978. As a leader in helium geochemical analysis, Western Systems has been active in domestic and international projects in mineral and energy resources evaluation. Western Systems is available to discuss your particular exploration projects and to set up a sampling program to fit your requirements.

REFERENCES

- Bulashevich, Y. P. and Bashorin, V. N., 1973, On the Detection of Faults Along the Sverdlovsk DDS Profile from High Concentrations of Helium in Underground Water: *Physics of the Solid Earth*, no. 1, January, 1973, pp. 185-189.
- Golubev, V. S. et al, 1970, Some Characteristics of Migration of Helium in the Permeable Systems of the Upper Part of the Earth's Crust: Translated from *Geokhimiya*, in *Geochemistry International*, 1970, pp. 943-950.
- Gutsalo, L. K., 1966, Importance of Groundwater Helium Saturation in Oil and Gas Prospecting: Translated (1970) from *Izvestiya AN SSSR, Ser. Geologicheskaya*, 31 (9) 111-116 (1966), through University of California, UCRL-Trans-10483.
- Gutsalo, L. K., 1976, On the Sources and Distribution of Helium and Argon Isotopes in the Thermal Waters of the Kurile Islands and Kamchatka: Translated from *Geokhimiya*, no. 6, in *Geochemistry International*, v. 13, no. 3, pp. 167-175.
- Mazor, E., 1977, Geothermal Tracing with Atmospheric and Radiogenic Noble Gases: *Geothermics*, v. 5, pp. 21-36.
- Naughton, J. J. et al, 1973, Helium Flux from the Earth's Mantle as Estimated from Hawaiian Fumerolic Degassing: *Science*, v. 180, pp. 55-57.
- Newton, R. and Round, G. F., 1961, The Diffusion of Helium through Sedimentary Rocks: *Geochimica et Cosmochimica Acta*, v. 22, pp. 106-132.
- Pierce, A. P., 1960, Studies of Helium and Associated Natural Gases: U. S. Geological Survey Professional Paper 400-B, pp. B77-B79.
- Roberts, A. A. et al, 1975, Helium Survey, a Possible Technique for Locating Geothermal Reservoirs: *Geophysical Research Letters*, v. 2, no. 6, pp. 209-210.
- Rösler, H. J. et al, 1977, Integrated Geochemical Exploration for Deep-Seated Solid and Gaseous Mineral Resources: *Journal of Geochemical Exploration*, v. 8, no. 1 & 2, pp. 415-429.
- Thomas, D. M. and Naughton, J. J., 1979, Helium/Carbon Dioxide Ratios as Premonitors of Volcanic Activity: *Science*, v. 204, pp. 1195-1196.
- Tiratsoo, E. N., 1967, *Natural Gas, a Study*: Scientific Press, London, pp. 32-36.

Tongish, C. A., 1980, Helium - Its Relationship to Geologic Systems and Its Occurrence with the Natural Gases, Nitrogen, Carbon Dioxide, and Argon: U. S. Department of the Interior, Bureau of Mines, Report of Investigations 8444, 176 p.

Yakutseni et al, 1969, Distribution of Helium in the Sedimentary Mantle and the Conditions of Formation of Economic Helium Deposits: *Geokhimiya*, no. 2, pp. 76-90.

ADDITIONAL READING

Bagirov, V. I. et al, 1976, Developing Geochemical Methods for Marine Exploration of Oil and Gas: *International Geology Review*, v. 18, no. 5, pp. 560-562.

Ball, N. L. and Snowdon, L. R., 1973, A Preliminary Evaluation of the Applicability of the Helium Survey Technique to Prospecting for Petroleum: *Geological Survey of Canada*, paper 73-1B, pp. 199-202.

Bergquist, L. E. et al, 1980, Helium Emanometry, an Energy Exploration Guide: Fiftieth Annual International Meeting and Exposition, Society of Exploration Geophysicists, Houston, Technical Papers, v. 5, pp. 2567-2578.

Cook, E., 1979, The Helium Question: *Science*, v. 206, no. 4423, pp. 1141-1147.

Dyck, W., 1976, The Use of Helium in Mineral Exploration: *Journal of Geochemical Exploration*, v. 5, no. 1, pp. 3-20.

Holland, P. W. and Emerson, D. E., 1979, Helium in Ground Water and Soil Gas in the Vicinity of Bush Dome Reservoir, Cliffside Field, Potter County, Texas: U. S. Department of the Interior, Bureau of Mines Information Circular IC 8807, 22p. (*A Case History*).

Hunt, J. M., 1979, *Petroleum Geochemistry and Geology*, Published by W. H. Freeman and Company, San Francisco, Calif., 617 p.

Levinson, A. A., 1974, *Introduction to Exploration Geochemistry*, Published by Applied Pub. Co., Wilmette, Ill., 924 p.

Mast, R. F., 1978, U. S. Geological Survey Oil and Gas Resource Investigations Program, U. S. Geological Survey, Open-File Report 78-303, 81 p.

Moore, C. A. and Esfandiari, B., 1971, Geochemistry and Geology of Helium: in *Advances in Geophysics*, v. 15, pp. 1-57.

Nikonov, V. F., 1972, Formation of Helium - Bearing Gases and Trends in Prospecting for Them: Translated in *International Geology Review* (1973), v. 15, pp. 534-541.

Palacas, J. P. and Roberts, A. A., 1980, Helium Anomaly in Surficial Deposits of South Florida, Possible Indicator of Deep Subsurface Petroleum or Shallow Uranium-Associated Phosphate Deposits: U. S. Geological Survey, Open-File Report 80-91, 14 p. (*A Case History*).

Panchenko, A. S., 1974, Positive and Negative Gas Hydrochemical Halos and Their Significance for Oil and Gas Prospecting: Translated from *Izvestiya AN SSSR*, in *International Geology Review*, v. 16, no. 3, pp. 259-262.

Pierce, A. P., 1955, Radon and Helium Studies: Geologic Investigations of Radioactive Deposits, Semi-Annual Progress Report, U. S. Department of the Interior, TEI-540, pp. 233-237.

Pierce, A. P. et al, 1964, Uranium and Helium in the Panhandle Gas Field, Texas and Adjacent Areas: U. S. Geological Survey, Professional Paper 454-C, 56p.

Pirson, S. J., 1969, Geological, Geophysical and Chemical Modifications of Sediments in the Environment of Oil Fields: in *Unconventional Methods in Exploration for Petroleum and Natural Gas*, Published by Southern Methodist University Press, Dallas, Texas, pp. 159-186.

Pray, H. A. et al, 1952, Solubility of Hydrogen, Oxygen, Nitrogen and Helium in Water at Elevated Temperatures: *Industrial and Engineering Chemistry*, v. 44, no. 5, pp. 1146-1151.

Reimer, G. M. et al, 1980, Helium Soil Gas Concentrations in the Torrington, Newcastle, Gillette (Wyoming) and Ekalaka (Montana) 1° x 2° Quadrangles; Data from a Reconnaissance Survey: U. S. Geological Survey, Open-File Report 80-452, 14p. plus 4 plates. (*A Case History*).

Riley, G. H., 1979, Helium Isotopes in Energy Exploration: *Bulletin, Australia Society of Exploration Geophysicists*, v. 10, no. 3, pp. 234-236.

Roberts, A. A. and Dalziel, M., 1976, A Possible Petroleum Related Helium Anomaly in Soil Gas, Boulder and Counties, Colorado: U. S. Geological Survey, Open-File Report 76-544, 7p. plus 3 plates. (*A Case History*).

Roberts, A. A., 1979, Helium Emanometry for Hydrocarbons, II: To be published in *Unconventional Techniques in Exploration for Petroleum and Natural Gas*, Southern Methodist University Press, Dallas, Texas. (*A Case History*).

Tissot, B. P. and Welte, D. H., 1978, *Petroleum Formation and Occurrence, a New Approach to Oil and Gas Exploration*, Published by Springer-Verlag, Berlin, 538p.

Weiss, R. F., 1971, Solubility of Helium and Neon in Water and Seawater: *Journal of Chemical and Engineering Data*, v. 16, no. 2, pp. 235-241.

Zarella, W. M., 1969, Applications of Geochemistry to Petroleum Exploration: in *Unconventional Methods in Exploration for Petroleum and Natural Gas*, Pub. by Southern Methodist Univ. Press, Dallas, Texas, pp. 29-41.

SCIENTIFIC SERVICES DIVISION
P.O. Box 2133/Evergreen, CO 80439/U.S.A.
Telephone: (303) 674-9811



A PREMONITOR OF SEISMIC (EARTHQUAKE) ACTIVITY

By David E. Kahler

ABSTRACT

Helium, which is produced in basement crystalline rocks during alpha decay of uranium-238 and other radioactive nuclides, migrates readily to the surface along deep-seated faults and fractures. Considerable research has indicated that gradual or abrupt changes in the helium flux from faults may signal pending seismic (earthquake) activity. Western Systems provides sampling equipment and precision analyses for helium measurements to identify these flux variations.

INTRODUCTION

The use of helium geochemical surveys in the search for petroleum, uranium and geothermal sources, and for fracture mapping as a guide to ore deposits is well known. The basis for such surveys is the constant generation of helium from radioactive decay of uranium, thorium and their daughter products. During these transformations a number of alpha particles are emitted, which readily pick up free electrons to form helium atoms. Helium is stable, inert, lightweight and will migrate through the geologic column to the atmosphere where it is eventually lost to outer space. The detection of anomalous helium values near the earth's surface provides a geochemical tracer for energy resources and ore deposits.

Many factors influence the movement of helium, but most importantly helium tends to migrate along faults as pathways of least resistance. With regard to earthquake prediction, helium can be used as a premonitor, since its rate of movement along fault systems is governed by pressure and temperature changes. These changes are characteristics of pre-seismic events and thus variations in helium flux will occur in conjunction with earthquakes. With adequate monitoring of helium levels along fault zones, any significant increases or decreases in the helium flux can be viewed as precursors to earthquakes.

EARTHQUAKE FORECASTING METHODS

Much of course is yet to be discovered in this important science of earthquake prediction. Ultimately it will be possible to minimize the disastrous effects of earthquakes – but first the tools of prediction must be perfected. One area of major research for earthquake forecasting has been in the use of groundwater composition variance. This research centers on changes in: isotope ratios, trace elements, ions, gases, temperature, pH, conductivity, water level, etc.

With regard to gases in water, helium is an outstanding element to monitor because it is present everywhere in the earth where measurements can be carried out. Earth movements will cause immediate gas displacement to occur and helium will migrate along fault/fracture systems. This movement of helium is not confined to a local area, but in fact may be observed tens or even hundreds of kilometers from the epicenter.

HELIUM SURVEY APPLICATIONS

Scientists engaged in local or regional monitoring of precursory effects must maintain observation stations or collection sites during time periods adequate to bracket a seismic event. This implies the use of continuous monitoring instrumentation or measurements taken at regular intervals. In the specific case of helium monitoring, remote-unit/telemetered-data type installations are not too practical due to frequent calibration requirements. However, it is relatively simple to establish a standardized system of water collection from wells and springs throughout a regional area. A gaseous sample is extracted from the water sample and this gas is then analyzed for helium content. It is essential to utilize considerable data from broad regions and over prolonged periods of time; this is a procedure that cannot be accelerated.

The monitoring of seismic event precursors is not generally regarded as a "commercial" activity, as is the case of energy and mineral resource exploration. Earthquake prediction projects have been functions of universities and governments, whereas the private sector has not been involved on a funding basis. However, there is an increasing awareness by private companies of the need to conduct adequate investigations for siting studies for power plants, multi-story residential and commercial buildings, mines, underground storage facilities, etc. For those geoscientists who have responsibilities in the area of siting studies, helium monitoring will provide a high-technology tool to use in conjunction with geology and geophysics. For government and academic research into earthquake prediction, helium surveys provide a cost-effective and valuable addition to other geochemical, geophysical, geological and biological investigations.

WESTERN SYSTEMS INCORPORATED

As can be seen in the list of selected references, helium geochemistry has taken a significant place in the field of earthquake forecasting. Western Systems has the equipment and precise analytic capability to conduct helium studies for this type of research. Western Systems is available to discuss your particular project and to set up a sampling program to fit your requirements.

HELIUM – A PREMONITOR OF SEISMIC (EARTHQUAKE) ACTIVITY SELECTED REFERENCES

(Some of these articles appear also in the publication Chemical Abstracts [CA]
and are so noted with volume and item number)

- Barsukov, V. L. et al, 1979, Geochemical Methods of Predicting Earthquakes: *Geochemistry International*, v. 16, no. 2, pp. 1-13. (CA 90-190175.)
- Borodzich, E. V. et al, 1979, Preliminary Results of Helium-Pattern Variations in Seismically Active Zones: *Geochemistry International*, v. 16, no. 2, pp. 37-41. (CA 90-172022.)
- Chalov, P. I. et al, 1977, Short Term Variations in the Radioisotopic Parameters of the Water in Faults in the Earth's Crust and Their Relationship to Earthquake Forecasting: *Physics of the Solid Earth*, v. 13, no. 8, pp. 567-574. (CA 88-77046 and 88-77047.)
- Chalov, P. I. et al, 1978, Fluctuations of Helium and Radon Anomalies in Some Springs Located Along Faults of the North Tien-Shan Seismic Zone During the Period Preceding the Kochker Earthquake of 1974: *AGI Doklady*, v. 231, pp. 26-28. (CA 86-143390.)
- Chalov, P. I. et al, 1978, Time Dependent Variations in Helium Content of Ground Water: *AGI Doklady*, v. 233, pp. 184-186. (CA 87-58265.)
- Chemical & Engineering News, 1979, Earthquakes, Volcanoes Give Chemical Signals, v. 57, no. 16, pp. 20-22.
- Craig, H. et al, 1975, Investigation of Radon and Helium as Possible Fluid-Phase Precursors to Earthquakes: *Scripps Institution of Oceanography, Technical Reports*, no. 1, SIO Ref. no. 75-15, 27p. and Technical Report no. 2, SIO Ref. no. 75-23, 19p.
- Craig, H. et al, 1980, Investigation of Radon and Helium as Possible Fluid-Phase Precursors to Earthquakes: in *Summaries of Technical Reports, Volume X, National Earthquake Hazards Reduction Program, U.S. Geological Survey, Open-File Report 80-842*, pp. 346-350.
- Craig, H., 1981, Investigation of Radon and Helium as Possible Fluid-Phase Precursors to Earthquakes: in *Project Summaries – 1979-1980, U.S. Geological Survey, Open-File Report 81-41*, pp. 79-80.
- Doering, W. P. and Friedman, I., 1980, Survey of Helium in Natural Water Wells and Springs in Southwest Montana and Vicinity: *U.S. Geological Survey, Open-File Report, 80-181*, 42p.
- Friedman, I. et al, 1980, Geochemical Precursors in Well Waters for Earthquake Prediction – Helium: in *Summaries of Technical Reports, Volume X, National Earthquake Hazards Reduction Program, U.S. Geological Survey, Open-File Report 80-842*, p. 359.
- Gold, T., 1979, Terrestrial Sources of Carbon and Earthquake Outgassing: *Journal of Petroleum Geology*, v. 1, no. 3, pp. 3-19.
- Gold, T. and Soter, S., 1980, The Deep-Earth-Gas Hypothesis: *Scientific American*, v. 242, no. 6, pp. 154-161.
- Gorbushina, L. V. et al, 1973, Significance of Radiohydrogeological Anomalies in a Seismically Active Area for Predicting Earthquakes: *International Geology Review*, v. 15, no. 4, pp. 380-383. (CA 76-89862.)
- Hyashida, B. S. et al, 1981, 1980 Annual Index of Current Earthquake Literature: *U.S. Geological Survey, Open-File Report 81-454*.
- Kerr, R. A., 1978, Earthquakes – Prediction Proving Elusive: *Science*, v. 200, pp. 419-421.
- King, C. Y., 1980, Fault-Zone Water and Gas Monitoring: in *Summaries of Technical Reports, Volume X, National Earthquake Hazards Reduction Program, U.S. Geological Survey, Open-File Report 80-842*, pp. 388-389.
- Kissin, I. G., 1979, Current Hydrogeochemical and Geochemical Research in Earthquake Forecasting: *Geochemistry International*, v. 16, no. 2, pp. 14-18. (CA 90-172019.)
- Kravtsov, A. I. and Fridman, A. V., 1974, Geology and Geochemistry of Gases in Zones of Depth Fractures and Forecasting of Earthquakes: *Russian Text* (CA 85-81354.)
- Mamyrin, I. N. et al, 1979, $^3\text{He}/^4\text{He}$ Ratios in Earthquake Forecasting: *Geochemistry International*, v. 16, no. 2, pp. 42-43. (CA 90-190110.)

- Naughton, J. J. et al, 1973, Helium Flux from the Earth's Mantle as Estimated from Hawaiian Fumarolic Degassing: *Science*, v. 180, pp. 55-57.
- Oelsner, C. et al, 1973, Complex Detection of Tectonic Disturbances by Geochemical and Geophysical Methods: *German Text – Neue Bergbautech*, v. 3, no. 7, pp. 482-489. (CA 80-72828.)
- Osika, D. G. et al, 1978, Hydrogeochemical Anomalies Preceding Earthquakes and Reflecting Development of Focal Zones: *AGI Doklady*, v. 233, pp. 8-10. (CA 87-138779.)
- Osika, D. G., 1979, Geochemical and Hydrogeological Methods of Forecasting Location, Magnitude and Time of Shallow Earthquakes: *Geochemistry International*, v. 16, no. 2, pp. 27-36. (CA 90-172020.)
- Press, F., 1975, Earthquake Prediction: *Scientific American*, v. 232, no. 5, pp. 14-23.
- Reimer, G. M., 1979, The Use of Soil-Gas Helium Concentrations for Earthquake Prediction – Studies of Factors Causing Diurnal Variations: U.S. Geological Survey, Open-File Report 79-1623, 67p.
- Reimer, G. M., 1980, Use of Soil-Gas Helium Concentrations for Earthquake Prediction – Limitations Imposed by Diurnal Variation: *Journal of Geophysical Research*, v. 85, no. B-6, pp. 3107-3114.
- Reimer, G. M., 1980, Helium Monitoring for Earthquake Prediction: in *Summaries of Technical Reports, Volume X, National Earthquake Hazards Reduction Program*, U.S. Geological Survey, Open-File Report 80-842, p. 433.
- Rikitake, T., 1976, *Earthquake Prediction: Developments in Solid Earth Geophysics*, Elsevier Publishing Company, Amsterdam, 357p.
- Simpson, D. W., 1979, Soviet Prediction of a Major Earthquake: *Earthquake Information Bulletin*, U.S. Geological Survey, v. 11, no. 6, pp. 234-235.
- Sugisaki, R., 1978, Changing Helium/Argon and Nitrogen/Argon Ratios of Fault Air May Be Earthquake Precursors: *Nature (London)*, v. 275, no. 5677, pp. 209-211. (CA 90-124892.)
- Thomas, D. M. and Naughton, J. J., 1979, Helium/Carbon Dioxide Ratios as Premonitors of Volcanic Activity: *Science*, v. 204, pp. 1195-1196.
- Valyayev, B. M. et al, 1979, Short-Period Variations in Helium Flow, Produced by the Aftershocks of the July 28-29 (1976) Earthquake at Groznyy: *AGI Doklady*, v. 235, pp. 195-197.
- Voytov, G. I. et al, 1973, Some Geologic and Geochemical Consequences of the Dagestan Earthquake of May 14, 1970: *AGI Doklady*, v. 202, pp. 6-9. (CA 76-102211.)
- Wakita, H., 1978, Helium Spots Caused by a Diapiric Magma from the Upper Mantle: *Science*, v. 200, pp. 430-431.
- Wakita, H., 1978, *Geochemistry as a Tool for Earthquake Prediction*: Published by Center for Academic Publications, Japan Scientific Societies Press, Tokyo, pp. 175-183.
- Wakita, H. et al, 1980, Radon Anomaly – A Possible Precursor of the 1978 Izu-Oshima-kinkai Earthquake: *Science*, v. 207, pp. 882-883.
- Ward, P. L., 1977, Earthquake Prediction – A Perspective for a National Program: *Earthquake Information Bulletin*, U.S. Geological Survey, v. 9, no. 6, pp. 10-13.

Pages 79-81

Re: Helium geochemistry
in earthquake prediction

EARTHQUAKE HAZARDS REDUCTION PROGRAM

PROJECT SUMMARIES — 1979-80

Marilyn P. MacCabe, Editor

U.S. Geological Survey
345 Middlefield Road
Menlo Park, California 94025

1981

Open-File Report 81-41

LIGHT STABLE ISOTOPES, L. Friedman, U.S. Geological Survey, Branch of Isotope Geology, Box 25046, Denver Federal Center, Denver, Colorado 80225, (303) 234-3876.

Goal: To explore the possibility of using helium and hydrogen in earthquake prediction.

Investigations: Helium appears to be the most likely element to pursue in the prediction of earthquakes. Eight atoms of helium are formed for every decay of U-238 and six atoms for every decay of Th-232. Unlike radon, which decays away with a half-life of 3.8 days, helium is stable. We are currently monitoring helium in wells and in soil and natural gases. Daily samples are collected from two networks. One well sampling network extends along the Brawley-Salton Sea area and another is located in Montana adjacent (100 km radius) of Hebgen Lake. An automated helium sniffer has operated continuously near Gardiner, Montana, for over 1-1/2 years. This instrument makes hourly analysis of a nearby water well that is highly enriched in helium. The data is recorded on the spot and also telemetered via GOES satellite.

INVESTIGATION OF RADON AND HELIUM AS POSSIBLE FLUID-PHASE PRECURSORS TO EARTHQUAKES, H. Craig, University of California, San Diego, Geological Research Division, Scripps Institute of Oceanography, La Jolla, California 92093, (714) 452-3260.

Goals: To measure radon, helium, dissolved gas, and stable isotope relationships in thermal waters and their correlations with seismic activity.

Investigations: We are measuring dissolved radon, helium, nitrogen, argon, and methane in 16 thermal wells and springs along the Elsinore, San Jacinto, and San Andreas faults (fig. 16). Helium-3/helium-4 and stable isotope ratios in water are also measured, as well as lead-210 and radium-226. Based on linear arrays of dissolved gas concentrations, we developed a two-component model for the origin of these gases. Pre-seismic event fluctuations in radon and helium are being studied in terms of variations in these gaseous components. We are also installing and collecting film strips at sites on the Imperial Fault and at our radon monitoring sites for soil radon studies being carried out at Menlo Park.

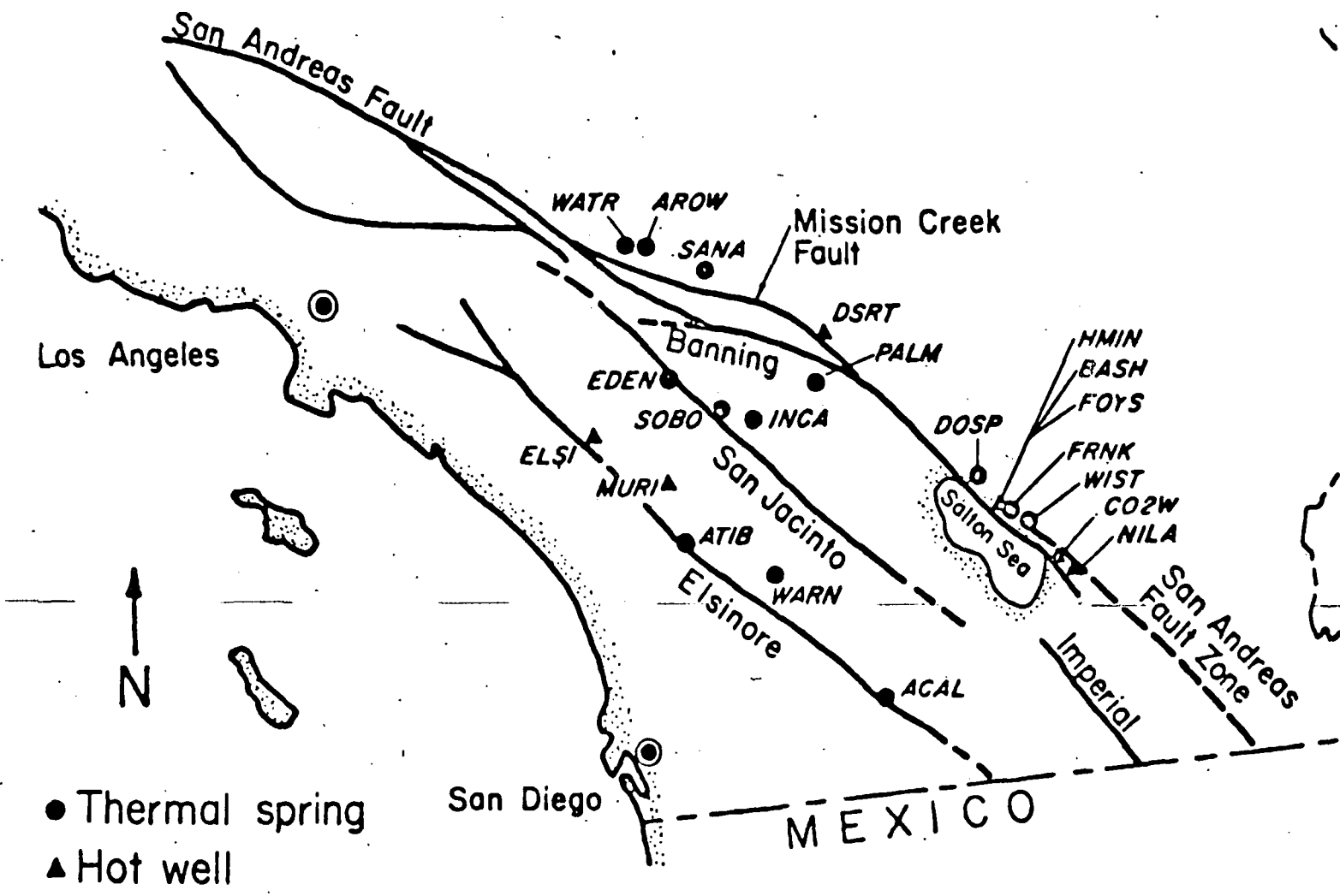


FIGURE 16.—Radon and helium monitoring sites in southern California.

current
contents

J.H.

Physics of the Earth and Planetary Interiors, 10 (1975) 167-176
© Elsevier Scientific Publishing Company, Amsterdam - Printed in The Netherlands

UNIVERSITY OF UTAH
RESEARCH INSTITUTE
THE ANACONDA COMPANY LIBRARY
EARTH SCIENCE LAB.

SUBJ
GCHM
HPP

HIGH-PRESSURE PHASE TRANSFORMATIONS AND COMPRESSIONS OF ILMENITE AND RUTILE, I. EXPERIMENTAL RESULTS

LIN-GUN LIU

Research School of Earth Sciences, Australian National University, Canberra, A.C.T. (Australia)

(Received January 2, 1975; revised and accepted March 11, 1975)

Natural ilmenite (Fe,Mg)TiO₃ has been found to transform to the perovskite structure and then to disproportionate into its component oxides, (Fe,Mg)O plus a cubic phase of TiO₂, at loading pressures of 140 and 250 kbar respectively, and at temperatures of 1,400 to 1,800°C. Samples were compressed in a diamond-anvil press and heated by irradiation with a YAG laser. The lattice parameters of the perovskite phase of (Fe,Mg)TiO₃ at room temperature and 1 bar are $a_0 = 4.471 \pm 0.004$, $b_0 = 5.753 \pm 0.005$, and $c_0 = 7.429 \pm 0.006$ Å with 4 molecules per cell. The zero-pressure volume change is 8.0% for the ilmenite-perovskite transition, 13.3% for the perovskite-mixed-oxides transition, and 20.2% for the ilmenite-mixed-oxides transition. The cubic phase of TiO₂ can be indexed on the basis of space group Fm3m with $Z = 4$ and $a_0 = 4.455 \pm 0.008$ Å at room temperature and 1 bar, which corresponds to a decrease in zero-pressure volume of 29.2% for the rutile-cubic-phase transition. An isentropic bulk modulus at zero pressure of 5.75 ± 0.30 Mbar and a pressure derivative greater than 8 were calculated for the high-pressure cubic phase. The calculated bulk modulus for the mixture of (Fe,Mg)O and cubic TiO₂ is 2.48 ± 0.25 Mbar. All the phase transformations, the calculated lattice parameters, and the bulk moduli observed in this study are in good agreement with published shock-Hugoniot data for ilmenite and rutile.

1. Introduction

The ilmenite structure has been suggested as a successor to pyroxene (e.g., Birch, 1952; Ringwood and Seabrook, 1962) and garnet (e.g., Ringwood, 1962; Clark Jr. et al., 1962; Boyd, 1964; Ringwood and Major, 1967) in the earth's transition zone. Pyroxene-ilmenite transformation was strongly indicated by studies of the MgGeO₃-MgSiO₃ solid solution by Ringwood and Major (1968). The high-pressure hexagonal-form of MgSiO₃ reported by Kawai et al. (1974) is probably of the ilmenite structure. The garnet-ilmenite transformation was supported from studies of Mg₃Al₂(Ge,Si)₃O₁₂ garnets in the range from pure germanate to 50 mole% of silicate by Ringwood and Major (1967). Subsequently, it has been claimed to have been observed in recovery shock experimental studies of iron-silicate garnets by Ahrens and Graham (1972), although their limited X-ray data cannot yield an unambiguous determination of the crystal structure of the high-pressure phase.

Studies of further phase transformations of ilmenite may therefore contribute to the understanding of the earth's interior.

2. Samples and experimental

The ilmenite sample employed in this study is the same material used by the author in his early study of its compressional behaviour (Liu et al., 1974). It was separated from a kimberlite pipe in Elliott County, Kentucky, and was provided by Prof. J.F. Lovering of the University of Melbourne. Microprobe analyses of the sample (by N. Ware, Australian National University) indicate that the chemical composition varies from grain to grain but is fairly homogeneous for a single grain. The average composition from six analyses is listed in Table I, along with that provided by Lovering (personal communication, 1967). The FeO and Fe₂O₃ concentrations were also analysed using the spectrophotometric method (by E. Kiss, Australian National

University). These results have also been shown in Table I. It is noted that the FeO and Fe₂O₃ concentrations are quite uncertain, but the specimen does contain a high concentration of MgO. All the evidence suggests that the sample is a solid solution of three major end-members, FeTiO₃-MgTiO₃-Fe₂O₃, with lattice parameters $a_0 = 5.075 \pm 0.002$ and $c_0 = 13.972 \pm 0.005$ Å (Liu et al., 1974).

Details of the experimental procedure have been described earlier (Liu, 1975a). A diamond-anvil press with a lever-and-spring type assembly was employed for the experimental studies. A sample in fine polycrystalline form was compressed between two flat anvil faces and heated by a continuous YAG laser. The loading pressures at the central portion of the sample were estimated from the length of the spring, which was calibrated according to the NaCl pressure scale at room temperature. Pressures thus estimated are probably accurate to $\pm 10\%$. The real pressure

TABLE I

Chemical composition of the ilmenite specimen from Elliott Co., Kentucky

	Microprobe analyses (wt.%)		Spectrophotometry (wt.%)
	Loving	Ware (6 analyses)	
TiO ₂	48.41	52.94	
FeO		35.38*	25.67
Fe ₂ O ₃	39.90*		10.37
MgO	11.47	10.69	
Al ₂ O ₃	0.42	0.51	
Cr ₂ O ₃		0.21	
MnO		0.26	
CaO	<0.1	<0.1	
Total	100.30	100.09	
	Mole%		
FeTiO ₃	45.9	54.8	
MgTiO ₃	40.7	36.9	
MnTiO ₃		0.5	
Fe ₂ O ₃	12.8	6.9	
Al ₂ O ₃	0.6	0.7	
Cr ₂ O ₃		0.2	
Total	100.0	100.0	

* Total Fe is expressed as FeO and Fe₂O₃, respectively.

attained by the samples is probably 50 kbar higher at a nominal load pressure of about 140 kbar, due to transient increase of pressure during the local and rapid laser heating process (Liu, 1975a). The sample temperature could be estimated using an optical pyrometer, but the uncertainties would be rather large. The temperatures are probably between 1,400 and 1,800°C.

3. Ilmenite-perovskite phase transformation

Ilmenite displays two steps of phase transformations in the loading pressure range 120–250 kbar. The first high-pressure phase is a perovskite-like structure. Listed in Table II are the X-ray diffraction data for a sample quenched from a loading pressure of about 140 kbar and a temperature of about 1,400–1,800°C (see also Fig. 1). The observed d -spacings can be indexed as a two-phase mixture of ilmenite and an orthorhombic cell with the perovskite-like structure. The perovskite cell dimensions are $a_0 = 4.471 \pm 0.004$, $b_0 = 5.753 \pm 0.005$ and $c_0 = 7.429 \pm 0.006$ Å with 4 molecules per cell. This corresponds to an idealized cubic perovskite sub-cell with $a_0 = 3.628 \pm 0.003$ Å. It is noted in Table II that there are three reflections, 3.303, 2.712, and 2.155 Å, which are not observed in ilmenite and cannot be indexed on the usual orthorhombic cell configuration. However, all of these reflections can be indexed on a cell with the a - and b -axes doubled. In an earlier study of the perovskite phase of MgSiO₃, the author (Liu, 1974) has pointed out that a doubling of a - or b -axis indicates that the symmetry of the structure, while still orthorhombic, is lower than that of the usual orthorhombic perovskites, Pbnm, for example ScAlO₃ (Reid and Ringwood, 1975) and MnVO₃ (Syono et al., 1971). The lowered symmetry can be ascribed to a distortion of the ideal cubic perovskite structure, Pm3m, which is even greater than that shown by the usual orthorhombic perovskite structure. The degree of distortion in (Fe,Mg)TiO₃ is probably even greater than that in (Mg,Fe)SiO₃ which is further from the usual orthorhombic perovskite. The large distortion may be associated with the tolerance factor $t = (r_A + r_O)/\sqrt{2}(r_B + r_O)$ derived by Goldschmidt (1926), where r_A , r_B , and r_O are the ionic radii for atoms in the formula ABO₃. The ideal value

TABLE II

Room temperature and 1 bar pressure X-ray diffraction data for ilmenite quenched from a loading pressure of about 140 kbar and temperature of 1,400–1,800°C (Co-K α)

Observed		Ilmenite ²			Perovskite ³	
I/I_{100}	d (Å)	I/I_{100}	d (Å)	hkl	d (Å)	hkl
60	3.716	60	3.718	102	3.715	002
30	3.525				3.530	110
25b	3.303				3.287	(112)
30	2.877				2.877	020
100	2.738	100	2.736	104	2.738	(140)
20	2.712				2.710	(231)
90	2.547	80	2.539	110	2.558	112
5	2.476				2.476	003
90	2.230	70	2.228	113	2.236	200
5	2.155				2.155	(322)
70	1.859	70	1.860	204	1.857	004
5	1.717	80	1.715	116	1.715	131
50	1.701				1.704	032
10	1.662				1.659	203
5	1.619	40	1.622	108	1.621	(530)
					1.611	(502)
5	1.594				1.594	213
					1.592	132
30	1.503	50	1.500	214		
30	1.469	50	1.463	300	1.466	(105)
5	1.306				1.303	321
5	1.266	15	1.269	220		
10	1.149	50	1.151	314	1.151	(355)
					1.143	(505)
10	1.112	40	1.113	226	1.118	400

¹ Estimated visually; the letter b denotes broad line.

² Measured from standard power method (Fe-K α).

³ Calculated from $a_0 = 4.471$, $b_0 = 5.753$, and $c_0 = 7.429$ Å; indexes in parentheses correspond to reflections for cell with a - and b -axes doubled.

of t is unity, but the observed values range from 0.77 to 0.97 (Reid and Ringwood, 1975). For FeTiO₃ and MgTiO₃, t equals 0.77 and 0.75 respectively, using the values of effective ionic radii reported by Shannon and Prewitt (1969).

The zero-pressure volume for the high-pressure perovskite phase is 28.77 ± 0.08 cm³/mole, which is 8.0% smaller than that of the starting material, ilmenite. This volume change is comparable to those found in the similar ilmenite-perovskite transformation in MnVO₃ (6.6%) by Syono et al. (1971) and in CdTiO₃ (6.9%) and CdSnO₃ (5.4%) by Liebertz and Rooymans (1955). If the hexagonal MgSiO₃ reported by Kawai

et al. (1974) is of the ilmenite structure, the perovskite phase of MgSiO₃ found by Liu (1974) indicates a volume change of 7.4% for the ilmenite-perovskite transition in MgSiO₃.

A shock Hugoniot for ilmenite in the range 100–550 kbar has been reported by King (1973), who found that the data indicate the onset of a phase transformation at about 300 kbar which accompanies an increase in zero-pressure density of about 10–15%, corresponding to a decrease in volume of 9–13%. The lower-bound is very close to that found in the present study. Shock-Hugoniot data for ilmenite to about 1,100 kbar have been obtained by McQueen

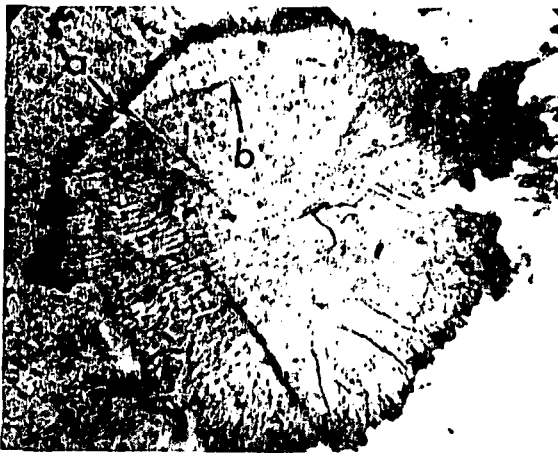


Fig. 1. The photograph shows the sample of ilmenite after it has been quenched from a loading pressure of about 140 kbar and laser heated to about 1,400–1,800°C; *a* indicates the edge of the sample which was compressed in the diamond-anvil, and *b* denotes the phase boundary between ilmenite and perovskite due to different reflectivity (under reflected light).

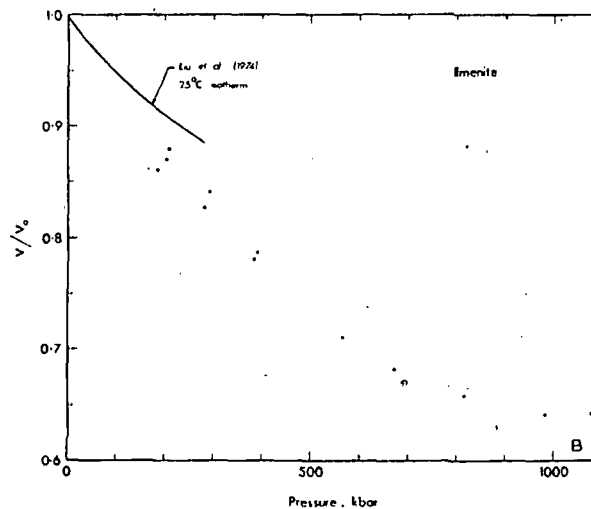
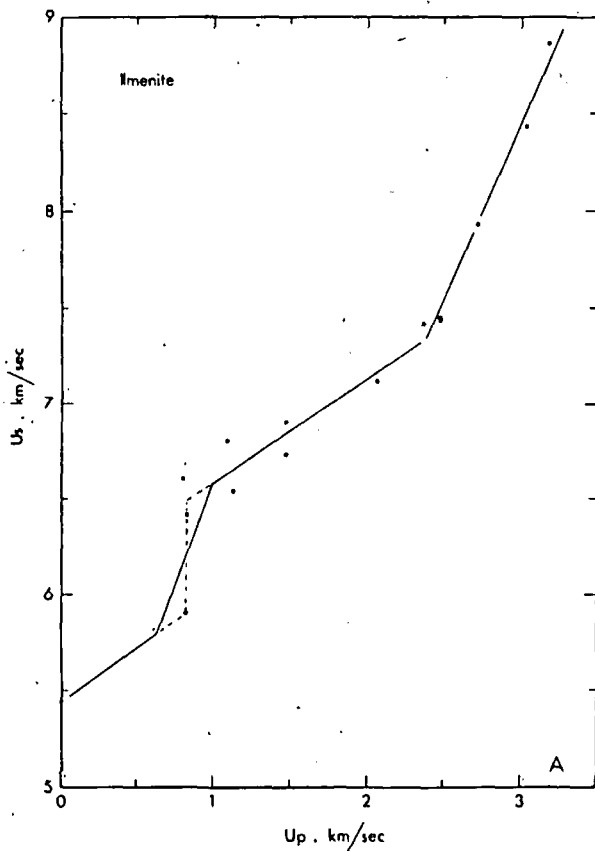


Fig. 2A. Shock velocity (U_s) vs. particle velocity (U_p) for ilmenite from McQueen and Marsh (unpublished, 1965). The straight lines are arbitrary. B. The same data of Fig. 2A plotted in the pressure–volume plane together with the 25°C-isothermal compression curve of ilmenite reported by Liu et al. (1974); the discontinuity between the isotherm and the shock data is apparent; temperature corrections for the shock data would enhance the discrepancy; this figure indicates a first-order phase transformation of ilmenite at a pressure near 200 kbar.

and Marsh (unpublished, 1965). Values of the shock velocity, U_s , vs. particle velocity, U_p , reproduced in Fig. 2A show that the data for U_s less than 7.2 km/sec are quite scattered. However, the same data in a pressure–volume plot (Fig. 2B), which are compared with the isothermal compression curve reported by Liu et al. (1974), indicate an apparent first-order phase transformation in the vicinity of 200 kbar. Temperature corrections for the shock data would strengthen the foregoing conclusion. The chemical composition for the shock sample, which is not known, may differ from that of the present study, but it is believed that any minor discrepancy resulting from composition will not significantly affect our conclusion.

4. Further phase transformation in the perovskite phase

From Figs. 2A, B, it is apparent that the perovskite phase of $(\text{Fe,Mg})\text{TiO}_3$ further transforms to a still

TABLE III

Room temperature and 1 bar pressure X-ray diffraction data for ilmenite quenched from a loading pressure of about 250 kbar and temperature of 1,400–1,800°C

Observed		Ilmenite ¹			Mixed oxides ²	
I/I_{100} ¹	d (Å)	I/I_{100}	d (Å)	hkl	d (Å)	hkl
$(C_{\alpha}-K_{\alpha})$:						
25	2.733	100	2.736	104		
30	2.604				2.572	C(111)
30	2.464				2.460	R(111)
80	2.223	70	2.228	113	2.228	C(200)
100	2.129				2.130	R(200)
50	1.508	50	1.500	214	1.506	R(220)
$(M_{\alpha}-K_{\alpha})$:						
20	2.73	100	2.736	104		
30	2.58				2.572	C(111)
30	2.46				2.460	R(111)
100	2.221	70	2.228	113	2.228	C(200)
70	2.129				2.130	R(200)
50	1.568				1.575	C(220)
40	1.505	50	1.500	214	1.506	R(220)
80	1.284				1.286	C(222)
5	1.235				1.284	R(311)
20	1.1106	40	1.1133	226	1.230	R(222)
20	0.9954				1.1138	C(400)
5	0.9549				0.9962	C(420)
					0.9526	R(420)

¹ Refer to Table II.

² Calculated from $a_0 = 4.260$ Å for the rocksalt structure and $a_0 = 4.455$ Å for the cubic phase.

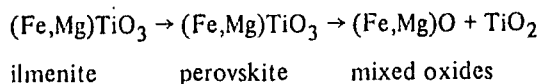
denser phase or phase assemblage at U_s greater than 7.4 km/sec or at pressures greater than 650 kbar. This second phase transformation in $(Fe,Mg)TiO_3$ has been confirmed in the present study.

The X-ray diffraction data for the starting material, ilmenite, which was laser heated at about 250 kbar, are shown in Table III. The $Co-K_{\alpha}$ radiation gives better information for the low-angle reflections and the $Mo-K_{\alpha}$ radiation provides the high-angle reflections. It is seen that the relative intensities depend on the X-ray source. The products are mainly a mixture of rocksalt structure, $(Fe,Mg)O$, and another cubic form together with some ilmenite. The cubic form (TiO_2) can be indexed on the same space group as that of the fluorite structure, $Fm\bar{3}m$, but its relative intensities do not show a strong resemblance to the usual fluorite crystals, for example CaF_2 and UO_2 . The intensities for (111) and (200) reflections are reversed

and reflection (311) is missing but reflection (200) was interfered by a reflection line of ilmenite. No detailed intensity calculations for the fluorite TiO_2 have been made.

The lattice parameter for the rocksalt structure is $a_0 = 4.260 \pm 0.005$ Å. Assuming that the lattice parameters for a solid solution of $MgO-FeO$ are a linear function of mole fraction, the lattice parameter obtained above indicates a composition of $(Fe_{0.48}Mg_{0.49})O$ and $(Fe_{0.43}Mg_{0.57})O$, corresponding to a lattice parameter of 4.306 Å for a nonstoichiometric $Fe_{0.95}O$ and to 4.323 Å for a stoichiometric FeO (Katsura et al., 1967). These Fe/Mg ratios are in fairly good agreement with that of the starting ilmenite, especially when account is taken of other constituents of the specimen. The lattice parameter for the possible fluorite structure is $a_0 = 4.455 \pm 0.008$ Å. If, as appears to be quite definite, the idealized phase transformations of ilmenite at increasingly high pres-

tures can be represented as follows:



the values of the lattice parameter found for the rock-salt and the cubic phase indicate a decrease of 13.3% in the zero-pressure volume from the perovskite to the mixture. This corresponds to a 20.2% volume decrease from ilmenite to the mixture. These are in excellent agreement with the apparent change of volume in the shock-Hugoniot data shown in Fig. 2B.

5. High-pressure phase transformations of TiO_2

There are three naturally occurring polymorphs of titanium dioxide. Rutile is the one that will be of interest in this study. Rutile has been reported to transform to an orthorhombic $\alpha\text{-PbO}_2$ structure at a static pressure range from 40 to 120 kbar by Bendeliani et al. (1966) and in a diamond-anvil press at approximately 133 kbar by Liu (1975b), and also in a shock-recovery experiment by McQueen et al. (1967). However, it was pointed out by Liu (1975b) that the major phase transformation in the shock-Hugoniot data up to 1.25 Mbar reported by McQueen et al. (1967) does not correspond to the rutile-orthorhombic transition. From fig. 3 of the work of McQueen et al. (1967), the metastable Hugoniot implies a decrease of about 26% in the zero-pressure volume for the high-pressure phase. This finding has also been confirmed in a recent shock experiment study of rutile up to 3 Mbar by Al'tshuler et al. (1973). From fig. 2 of the work of Al'tshuler et al. (1973), the apparent zero-pressure volume for the high-pressure phase is approximately 70–72% of that for rutile. There have been some suggestions for that the shock-induced phase in rutile is probably a fluorite-like phase (McQueen et al., 1967; Ahrens et al., 1969; Al'tshuler et al., 1973).

If $Z = 4$ is assumed, the lattice parameter for the cubic phase of TiO_2 reported in the previous section gives a molar volume of $13.31 \pm 0.07 \text{ cm}^3/\text{mole}$, which corresponds to a decrease in volume of 29.2%. This is, in turn, almost what was found by Al'tshuler et al. (1973) in their shock-experimental study. Hence, the shock-induced high-pressure phase in TiO_2 may well have the same structure.

The lattice parameter of 4.455 \AA for the cubic phase of TiO_2 would imply a Ti–O distance of 1.929 \AA in eight-fold coordination if the structure is of the fluorite type. This is less than the normal octahedral Ti–O distance of 1.985 \AA (Shannon and Prewitt, 1969) and 1.952 \AA (Brown and Shannon, 1973), and compares with an average Ti–O distance of 2.0676 \AA for eight-coordinated Ti in $\text{Ti}(\text{NO}_3)_4$ observed by Garner and Wallwork (1966). The last value gives $a_0 = 4.775 \text{ \AA}$ and the molar volume of $16.39 \text{ cm}^3/\text{mole}$ for the fluorite structure of TiO_2 . Hence, the calculated zero-pressure volume change for TiO_2 from the rutile to the fluorite structure would be 12.8%, which is less than 50% of the shock observed volume change in TiO_2 and fails to account for the observed volume changes in the shock data for both TiO_2 and ilmenite.

This discrepancy between the measured lattice parameter for the "fluorite" phase of TiO_2 and that predicted from ionic radius considerations cannot be resolved at the present time. It may be that the observed cubic form of TiO_2 is a distorted fluorite structure or a distinctly different structure such as $\alpha\text{-PbCl}_2$, which is commonly observed for MF_2 fluorides at high pressures (e.g., Dandekar and Jamieson, 1969). This ambiguity can only be clarified in a future study of pure TiO_2 .

6. Compression of the cubic phase of TiO_2

If the shock-Hugoniot data for TiO_2 reported by McQueen et al. (1967) and by Al'tshuler et al. (1973) in the pressure regime between 1 and 3 Mbar represent a single homogeneous phase of the cubic phase of TiO_2 found in this study, it is possible to derive the bulk modulus and its first pressure derivative from these data. On the basis of the bulk modulus and its pressure derivative, using an appropriate equation of state, the isentrope and the isotherms of the cubic phase of TiO_2 can be calculated.

This has been done by reducing the experimental pressure–volume Hugoniot data for the high-pressure phase to a metastable Hugoniot, which represents the shock-wave data centered on the zero-pressure volume of the high-pressure phase (McQueen et al., 1963). The metastable pressure–volume Hugoniot data thus obtained were then converted to its corresponding shock-velocity–particle-velocity (U_s-U_p) data using:

P
t
L
w
st
o
H
L
L
ar
to
K
th
K
an
K
wh
su
pr
to
tio
doi

pm

wh
fic
scri
Hug

TAB
Calc
TiO
—
Case
1
2
3

$$U_s = V_0 [P^m / M(V_0^m - V^m)]^{1/2}$$

$$U_p = [P^m (V_0^m - V^m) / M]^{1/2}$$

where P^m and V^m are the metastable Hugoniot pressure and volume, respectively, V_0^m the initial volume of the high-pressure phase, and M the molecular weight. It has been shown by Ruoff (1967) that if data in the U_s-U_p plane can be represented by:

$$U_s = C_0 + sU_p + s'U_p^2 + \dots$$

and if an equation of state is assumed to have the following form:

$$K^s = K_0^s + K_0^{s'}P + \frac{1}{2}K_0^{s''}P^2$$

then:

$$K_0^s = \rho_0 C_0^2$$

and

$$K_0^{s'} = 4s - 1$$

where K_0^s is the isentropic bulk modulus at zero-pressure, $K_0^{s'}$ is its first pressure derivative evaluated at zero-pressure, and ρ_0 is the initial density.

The method of converting the experimental Hugoniot to a new Hugoniot centered at a different initial condition was demonstrated by McQueen et al. (1963). In doing so, they obtained:

$$P^m = \frac{P^e \left[1 - \frac{\gamma}{2} \left(\frac{V_0^e}{V^e} - 1 \right) \right] - \frac{\gamma}{V^e} (E_0^e - E_0^m)}{1 - \frac{\gamma}{2} \left(\frac{V_0^m}{V^e} - 1 \right)}$$

where P , V , E , and γ are the pressure, volume, specific internal energy, and the Grüneisen parameter, superscripts e and m denote the experimental and metastable Hugoniots, and subscript zero represents the initial con-

dition. Two quantities have to be evaluated before calculations from the foregoing equation can be performed. First is the change of the specific internal energy between the starting material and the high-pressure phase at zero pressure:

$$\Delta E_{tr} = E_0^e - E_0^m = P[(V^m - V^e) + (V_0^m - V_0^e)]/2$$

assuming that the temperature effect is negligible. Using a value of $P = 0.33$ Mbar for the phase change in TiO_2 , as indicated in fig. 3 of McQueen et al. (1967), rough estimates of V^m and V^e from their figure yield $\Delta E_{tr} = -1.48$ Mbar \cdot cm³ \cdot mole⁻¹. Second is the dependence of the Grüneisen parameter on volume. An accurate relation for computing the volume dependence of the quasi-harmonic Grüneisen parameter of solids has been reported by Pastine and Forbes (1968). However, the use of their relation for computing the volume-dependent Grüneisen parameter of the cubic phase of TiO_2 requires evaluation of all parameters of specific heat at constant pressure, C_p , thermal expansivity, α ; initial Grüneisen parameter, γ_0 , and the Anderson-Grüneisen parameter, δ . Even though it has been shown that the calculated bulk moduli are insensitive to the choices of these parameters for the "high-pressure phase" of garnet by Graham and Ahrens (1973), it is rather difficult to estimate values of the specific heat and the thermal expansivity within $\pm 50\%$ for the cubic phase of TiO_2 . A simple scheme was adopted for computing the volume-dependent Grüneisen parameter as:

$$\gamma = \gamma_0 (V/V_0)^A$$

where A is a constant normally between 0.5 and 1.5 for many solids (Bassett et al., 1968). γ_0 was chosen to be between 1 and 2. From Table IV it is seen that the calculated isentropic bulk moduli are not sensitive to the values of γ_0 and A , but values of $(\partial K^s / \partial P)_{s|p=0}$

TABLE IV

Calculated isentropic bulk moduli and their first pressure derivatives by using various assumed values of γ_0 and A for the cubic TiO_2 .

Case	V_0 (cm ³ /mole)	γ_0	A	K_0^s (Mbar)	$(\partial K^s / \partial P)_{s p=0}$
1	13.31	1.5	1	5.75	10.1
2	13.31	2.0	1	5.93	8.2
3	13.31	1.5	1.5	5.67	10.5

are sensitive to γ_0 . The metastable U_s-U_p data calculated from $\gamma_0 = 1.5$ and $A = 1$ (case 1 of Table IV) are displayed in Fig. 3. The scatter of the data is similar to that of stishovite presented by Graham (1973). The linearity has been assumed in Fig. 3. In conclusion, Table IV shows $K_0^s = 5.75 \pm 0.30$ Mbar and $(\partial K^s / \partial P)_{s, P=0} > 8$ for the cubic phase of TiO_2 . It was noted that the latter value is anomalously large, but it is anomalously large for the rutile (TiO_2) as well (Manghnani, 1969).

The calculated metastable pressure-volume Hugoniot data of TiO_2 from case 1 of Table IV have been normalized to an initial volume of the cubic phase of $13.31 \text{ cm}^3/\text{mole}$, and are shown in Fig. 4. Since all the values of bulk modulus and the first pressure derivative listed in Table IV are calculated from the relations which were used to derive the Murnaghan equation of state (Murnaghan, 1944), it would be consistent to employ the Murnaghan equation for computing the pressure-volume relationship for the cubic phase of TiO_2 . Isentropic pressure-volume relationships thus calculated on the three sets of data listed in Table IV are displayed in Fig. 4, which indicates that at $V/V_0 = 0.86$ the calculated pressures of case 1 and case 3 differ by 2%, whereas between case 1 and

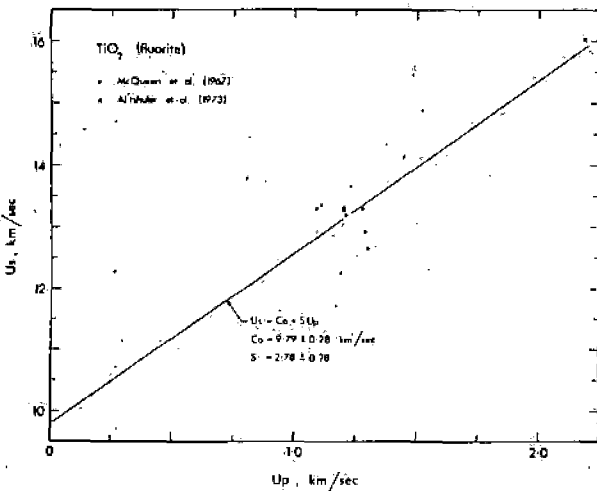


Fig. 3. The metastable U_s-U_p plot for the data of TiO_2 at pressures in excess of 1 Mbar reported by McQueen et al. (1967) and Al'tshuler et al. (1973). The calculated metastable Hugoniot was centered at an initial condition of $V_0 = 13.31 \text{ cm}^3/\text{mole}$, $\gamma_0 = 1.5$ and $A = 1$, where V is the volume, γ is the Grüneisen parameter, and A a constant. For details refer to the text.

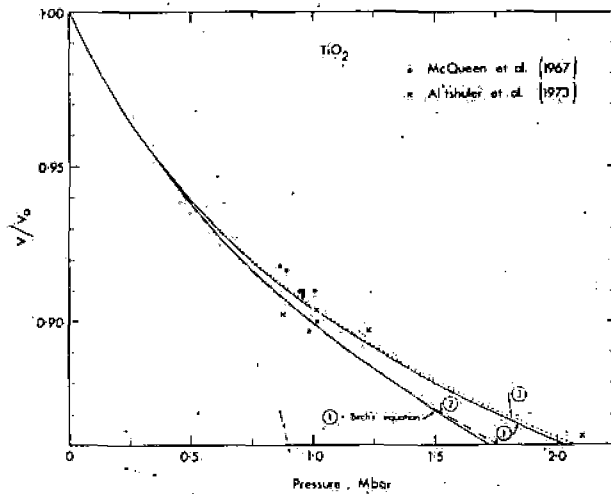


Fig. 4. Comparison between the metastable pressure-volume Hugoniot data of Fig. 3 with the isentropes calculated from three sets of values of bulk modulus and pressure derivative of Table IV by the Murnaghan equation of state. For comparison, the data of case 1 of Table IV were also used to compute the isentrope by means of the Birch equation.

case 2 the difference is about 13%. For comparison, case 1 has also been calculated by means of the Birch (1952) equation of state and is shown in Fig. 4.

7. Compression of the high-pressure phases of ilmenite

It has previously been shown that ilmenite first transforms to the perovskite structure and then disproportionates into a mixture of oxides. The bulk modulus of the mixture can be calculated by using equations proposed by Liu (1973). Taking $K_0 = 5.75$ Mbar for the cubic TiO_2 calculated in the previous section and $K_0 = 1.50$ Mbar for the rocksalt phase, the calculated K_0 value for the mixture is 2.48 ± 0.25 Mbar. Here the small difference between the isentrope and the isotherm has been neglected. The pressure-volume relationship for the mixture calculated by means of the Birch (1952) equation of state is shown in Fig. 5. (Little difference is obtained by using other forms of equation of state at pressures less than 1 Mbar.) Two curves are shown; each corresponds to different values of $K_0' = 4$ and 5. Taking the scattering of the data and the temperature correction into account, it is concluded that the calculated curves

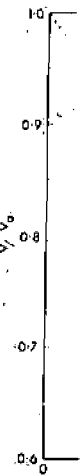


Fig. 5. Comparison between the metastable pressure-volume Hugoniot data of Fig. 3 with the isentropes calculated from three sets of values of bulk modulus and pressure derivative of Table IV by the Murnaghan equation of state. For comparison, the data of case 1 of Table IV were also used to compute the isentrope by means of the Birch equation.

are in excellent agreement with the experimental data. No additional behavior is observed on the basis of the present data. The transition to the perovskite phase is predicted to occur at pressures above 140 kbar and the mixture of oxides is predicted to occur at pressures above 300 kbar.

8. Conclusion

(1) Nature of the high-pressure phase of ilmenite from a kinetic point of view. The transition to the perovskite phase is predicted to occur at about 140 kbar and the mixture of oxides is predicted to occur at about 300 kbar. The further observation of the high-pressure phase of ilmenite at higher temperatures is necessary. The author's knowledge of the high-pressure phase of ilmenite is limited. It is the first time that the

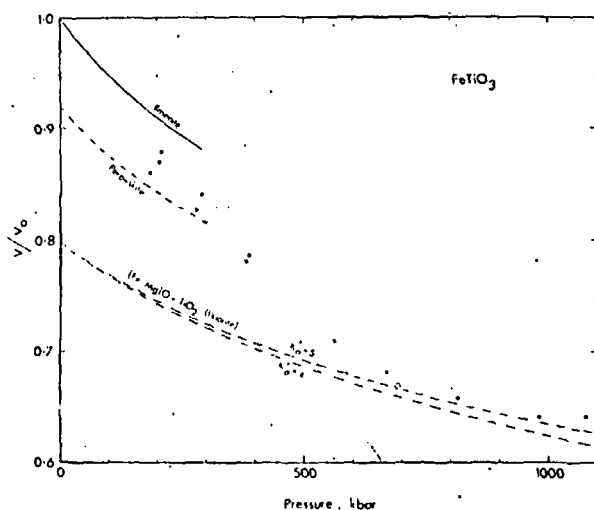


Fig. 5. Comparison of the experimental shock data of ilmenite reported by McQueen and Marsh (unpublished, 1965) with the measured or calculated compression curves for ilmenite, perovskite, and the mixture of $(\text{Fe,Mg})\text{O}$ plus TiO_2 (fluorite).

are in excellent agreement with the experimental data in the pressure range 600 to 1,100 kbar.

No attempts were made to evaluate the compressional behaviour of the perovskite phase on theoretical basis. However, a simple construction, on the assumption that the compression curve of the perovskite phase is proportional to curves of both the ilmenite and the mixture, is shown in Fig. 5. This rough approach suggests that the Hugoniot data between 200 and 300 kbar may correspond to the perovskite phase.

8. Conclusions

(1) Natural ilmenite with composition of $(\text{Fe,Mg})\text{TiO}_3$ from a kimberlite pipe was found to transform to the perovskite structure at a loading pressure of about 140 kbar and temperatures between 1,400 and 1,800°C. The perovskite phase of $(\text{Fe,Mg})\text{TiO}_3$ was further observed to disproportionate into a mixture of oxides at a loading pressure of about 250 kbar and temperatures between 1,400 and 1,800°C. To the author's knowledge, the breakdown of the perovskite phase of $(\text{Fe,Mg})\text{TiO}_3$ observed in the present study is the first reported example of phase transformation

of the crystal group of perovskite at high pressures.

(2) One of the products (perhaps of the fluorite structure) of the high-pressure phase of the perovskite $(\text{Fe,Mg})\text{TiO}_3$ is a new polymorph of TiO_2 . It has long been expected that rutile (TiO_2) would eventually transform to the fluorite phase at ultra-high pressures (McQueen et al., 1967; Al'tshuler et al., 1973). Although the density change observed in the shock-experimental studies of rutile at pressures greater than 1 Mbar is strongly indicative of formation of the cubic phase (McQueen et al., 1967; Ahrens et al., 1969; Al'tshuler et al., 1973), the shock-recovery experiment (McQueen et al., 1967) at pressures in excess of 0.75 Mbar (the exact pressure was not reported) showed that the high-pressure phase has the orthorhombic structure, and the density change for this transformation is not consistent with that indicated by the data. The observed lattice parameter of the cubic phase of TiO_2 in this study is $a_0 = 4.455 \pm 0.008 \text{ \AA}$, which corresponds to a decrease of volume from rutile of 29.2%. This value is in close agreement with those found in the shock experimental studies by McQueen et al. (1967) and Al'tshuler et al. (1973).

(3) On the basis of the shock data of TiO_2 at pressures greater than 1 Mbar by McQueen et al. (1967) and Al'tshuler et al. (1973) and the initial volume of the cubic phase of TiO_2 found in this study, an isentropic zero-pressure bulk modulus of $5.75 \pm 0.30 \text{ Mbar}$ and a first pressure derivative of greater than 8 were found for the cubic phase.

(4) From the equations proposed by Liu (1973) for a mixture, the zero-pressure bulk modulus for the high-pressure mixture of $(\text{Fe,Mg})\text{O}$ plus TiO_2 , with the rocksalt and the cubic phases respectively, was calculated to be $2.48 \pm 0.25 \text{ Mbar}$. The pressure-volume relations calculated from the Birch equation of state, on the assumption that the first pressure derivative of bulk modulus is in the range 4–5, compare well with the shock data of ilmenite in the pressure regime of 600 to 1,100 kbar obtained by McQueen and Marsh (unpublished, 1965).

Acknowledgement

The author thanks A.E. Ringwood and J.R. Cleary for reading and commenting on the manuscript. He is also grateful to J.C. Jamieson and the anonymous re-

viewer of this paper for their comments on the discussion of the high-pressure phase of TiO_2 . The support by NSF (U.S.) Grant GA-38056X for the laser work while he was at the Department of Geological Sciences, University of Rochester, Rochester, N.Y., U.S.A., is also gratefully acknowledged.

References

- Ahrens, T.J., Anderson, D.L. and Ringwood, A.E., 1969. *Rev. Geophys.*, 7: 667.
- Ahrens, T.J. and Graham, E.K., 1972. *Earth Planet. Sci. Lett.*, 14: 87.
- Al'tshuler, L.V., Podurets, M.A., Simakov, G.V. and Trunin, R.F., 1973. *Sov. Phys. Solid State*, 15: 969.
- Bassett, W.A., Takahashi, T., Mao, H. and Weaver, J.S., 1968. *J. Appl. Phys.*, 39: 349.
- Bendeliani, N.A., Popova, S.V. and Vereshchagin, L.F., 1966. *Geokhimiya*, 5: 499.
- Birch, F., 1952. *J. Geophys. Res.*, 57: 227.
- Brown, I.D. and Shannon, R.D., 1973. *Acta Cryst.*, A29: 266.
- Boyd, F., 1964. *Science*, 145: 13.
- Clark Jr., S.P., Schairer, J.F. and De Neufville, J., 1962. *Carnegie Inst. Washington, Yearb.*, 61: 59.
- Dandekar, D.P. and Jamieson, J.C., 1969. *Trans. Am. Crystallogr. Assoc.*, 5: 19.
- Garnier, C.D. and Wallwork, S.C., 1966. *J. Chem. Soc.*, A: 1496.
- Goldschmidt, V.M., 1926. *Naturwissenschaften*, 14: 477.
- Graham, E.K. and Ahrens, T.J., 1973. *J. Geophys. Res.*, 78: 375.
- Graham, E.K., 1973. *Geophys. J.*, 32: 15.
- Katsura, T., Iwasaki, B., Kimura, S. and Akimoto, S., 1967. *J. Chem. Phys.*, 47: 4559.
- Kawai, N., Tachimori, M. and Ito, E., 1974. *Proc. Jpn. Acad.*, 50: 378.
- King, D.A., 1973. *Eos (Trans. Am. Geophys. Union)*, Fall Program 54: 35 (abstract).
- Liebertz, J. and Rooymans, C.J.M., 1965. *Z. Phys. Chem. Neue Folge*, 44: 242.
- Liu, L., 1973. *J. Geophys. Res.*, 78: 3501.
- Liu, L., 1974. *Geophys. Res. Lett.*, 1: 277.
- Liu, L., Bassett, W.A. and Takahashi, T., 1974. *J. Geophys. Res.*, 79: 1171.
- Liu, L., 1975a. *Earth Planet. Sci. Lett.*, 24: 357.
- Liu, L., 1975b. *Phys. Earth Planet. Inter.*, 9: 338.
- McQueen, R.G., Fritz, J.N. and Marsh, S.P., 1963. *J. Geophys. Res.*, 68: 2319.
- McQueen, R.G., Jamieson, J.C. and Marsh, S.P., 1967. *Science*, 155: 1401.
- Manghnani, M.H., 1969. *J. Geophys. Res.*, 74: 4317.
- Murnaghan, F.D., 1944. *Proc. Nat. Acad. Sci. U.S.A.*, 30: 244.
- Pastine, D.J. and Forbes, J.W., 1968. *Phys. Rev. Lett.*, 21: 1582.
- Reid, A.F. and Ringwood, A.E., 1975. *J. Geophys. Res.*, 80 (in press).
- Ringwood, A.E., 1962. *J. Geophys. Res.*, 67: 4005.
- Ringwood, A.E. and Seabrook, M.J., 1962. *J. Geophys. Res.*, 67: 1690.
- Ringwood, A.E. and Major, A., 1967. *Earth Planet. Sci. Lett.*, 2: 331.
- Ringwood, A.E. and Major, A., 1968. *Earth Planet. Sci. Lett.*, 5: 76.
- Ruoff, A.L., 1967. *J. Appl. Phys.*, 38: 4976.
- Shannon, R.D. and Prewitt, C.T., 1969. *Acta Crystallogr.*, Sec. B, 25: 925.
- Syono, Y., Akimoto, S. and Endoh, Y., 1971. *J. Phys. Chem. Solids*, 32: 243.

SUBJ
GCHM
HTA

High-Temperature Activity-Composition Relations of Equilibrium Spinel, Olivines, and Pyroxenes in the System Mg-Fe-O-SiO₂

RALPH H. NAFZIGER

908 South Ferry Street, Albany, Oregon 97321

Abstract

Sufficient high-temperature data delineating the equilibrium compositions of coexisting phases in the Mg-Fe-O-SiO₂ system have become available to permit calculation of activity-composition relations of the important spinels, olivines, and pyroxenes. Three methods of calculation involving (1) the thermodynamic properties of equilibrium magnesiowüstites, (2) spinel-hematite equilibria, and (3) magnesiowüstite defect data are employed. Within estimated uncertainties, the spinels generally exhibit negative deviations from ideality at 850°C and 1300°C, whereas the activity-composition relations at 1160°C are less well defined due to greater uncertainties in phase composition data. Spinel data calculated by methods 1 and 3, and 2 and 3, agree within the uncertainties inherent in the calculations at 1300°C. These uncertainties in the calculated data preclude meaningful correlations with temperature. At 1160°C, olivines and pyroxenes in equilibrium with spinels exhibit positive deviations from ideality, with olivines showing a more significantly pronounced deviation and pyroxenes showing near-ideality. This is similar to previous determinations at 1200–1250°C at lower oxygen fugacities where the silicate phases are in equilibrium with metallic iron. At 1300°C, olivines and pyroxenes in equilibrium with spinels show nearly ideal or slightly negative deviations from ideality in their activity-composition relations. Internal consistency of the data calculated from different equilibrium phase assemblages is demonstrated for the olivines.

Introduction

The spinel phase in the system Mg-Fe-O is recognized as an important constituent in many basic igneous rock-forming systems (see, for example, Muan and Osborn, 1956; Osborn, 1959, 1962). It is also the major stable phase in the Fe-O system at oxygen fugacities associated with such rocks (Nafziger, 1970). Osborn (1956) has pointed out the effect of this phase in the steel industry with respect to refractory brick. In addition, ferrites are finding increased applications in electronics, computer technology, and communication systems. However, little attention has been directed toward the thermodynamic properties to aid in understanding the behavior of this important phase. On the basis of thermal balance experiments in a controlled atmosphere, Schmahl *et al* (1961) concluded that the spinel phase is nearly ideal at 800–1000°C. Using emf methods, Gordeev and Tretyakov (1963) observed small positive deviations from ideality for the spinel solid solution at 900–1200°C. However, no activity values were presented. Additional experimental equilibrium phase composition data have become available in the past few years to permit

calculations of component activities in the spinel phase at high temperatures in the Mg-Fe-O system.

Methods for Calculation of Spinel Activities

Inasmuch as there is a considerable area of spinel solid solution in the system Mg-Fe-O at temperatures above approximately 850°C (see, for example, Katsura and Kimura, 1965; Speidel, 1967), and because wüstite exhibits a cation-deficient structure (Darken and Gurry, 1945), relatively simple thermodynamic calculations cannot be applied. Figure 1 shows a schematic subsolidus isothermal section of a portion of this system derived from data presented by the aforementioned authors. At temperatures in the range 850°–1300°C, complete solid solution exists along the spinel join (Phillips and Muan, 1962; Alcock and Iyengar, 1967; Katsura and Kimura, 1965; Speidel, 1967). Three different methods were used to calculate activity-composition relations of these spinels.

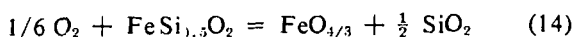
Calculation from magnesiowüstite thermodynamic properties (method 1)

High-temperature activity-composition relations of magnesiowüstites in equilibrium with metallic iron

data presented by Williams (1971). The free energies of formation for FeSiO_3 used in the present study were interpolated and extrapolated from data presented by Schwerdtfeger and Muan (1966) and Nafziger and Muan (1967). These values were -1.26 kcal at 1160°C and -0.7 kcal at 1300°C . Compositions of the coexisting pyroxene and spinel phases were obtained from Speidel and Osborn (1967). Calculated activity values for FeSiO_3 and MgSiO_3 in pyroxenes at 1160° and 1300°C are shown in Figure 6. At 1160°C , a slight positive deviation from ideality is indicated, whereas at 1300°C , a slight negative deviation is shown. However, the uncertainties derived from the data and calculations, as represented in the figure, show that the activity-composition relations for the FeSiO_3 - MgSiO_3 pyroxenes in equilibrium with spinels may be considered nearly ideal. This is essentially the same result obtained by Nafziger and Muan (1967) at 1200 - 1250°C for pyroxenes in equilibrium with metallic iron at lower oxygen fugacities.

Olivine activity-composition relations from olivine-silica-spinel equilibrium data

For the olivine-silica-spinel equilibria in the Mg-Fe-O-SiO_2 system, the reaction



applies. Hence,

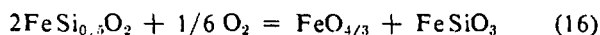
$$\begin{aligned} \log a_{\text{FeSi}_{1.5}\text{O}_2} \\ = \frac{\Delta G^\circ_{(14)}}{2.303RT} + \log a_{\text{FeO}_{4/3}} - 1/6 \log f_{\text{O}_2} \quad (15) \end{aligned}$$

Spinel activity, oxygen fugacity, and condensed phase equilibrium compositional data were obtained from previously cited sources. The value for $\Delta G^\circ_{(14)}$ (see Table 1) were derived from calculations using data presented by Stull *et al.* (1971) for the free energies of formation of $\text{FeO}_{4/3}$ and $\text{FeSi}_{1.5}\text{O}_2$. Data for the latter compound were also obtained from the work of Schwerdtfeger and Muan (1966), and interpolated from Kelley (1962). Comparisons of resulting $\Delta G^\circ_{(14)}$ values with those calculated from Williams' (1971) data are shown in Table 1. The calculated olivine activity-composition relations are shown in Figure 6 for 1160°C and 1300°C . The relations with respect to the two temperatures are similar to those obtained for the pyroxenes, although greater deviations from ideality at 1160°C are indicated. This also conforms with the results obtained

for lower oxygen fugacities at 1200°C (Nafziger and Muan, 1967). Uncertainties preclude precise comparisons between olivines and pyroxenes, however. Correlations of activity data with temperature are also not possible, although a closer approach to ideality with increasing temperature seems plausible.

Activity-composition calculations from olivine-pyroxene-spinel equilibrium data

As a check for internal consistency with the previous calculations, additional literature data for the olivine-pyroxene-spinel equilibrium in the Mg-Fe-O-SiO_2 system may be used (Speidel and Osborn, 1967). In this region, the reaction



is of interest. Either pyroxene or olivine activities may in principle be calculated using previously cited data and the activity-composition relations shown in Figure 6 of the equilibrium olivines or pyroxenes, respectively, together with olivine-pyroxene-spinel equilibrium composition data. Olivine results are plotted in Figure 6 and agree well with values derived from the olivine-silica-spinel calculations. However, not enough data are available to permit this type of calculation for the pyroxenes.

Acknowledgments

I thank Professors E. F. Heald, D. H. Lindsley, and D. F. Weill for reviewing the manuscript and suggesting improvements.

References

- ALCOCK, C. B., AND G. N. K. IYENGAR (1967) A study of the oxidation-reduction equilibria of dilute magnesio-wüstites. *Proc. Brit. Ceram. Soc.* **8**, 219-229.
- BENNER, R. L., AND H. KENWORTHY (1966) The thermodynamic properties of the $\text{ZnO-Fe}_2\text{O}_3\text{-Fe}_3\text{O}_4$ system at elevated temperatures. 1. The thermodynamic properties as related to the spinel structure. *U.S. Bur. Mines Rep. Invest.* **6754**, 44 pp.
- DARKEN, L. S., AND R. W. GURRY (1945) The system iron-oxygen. I. The wüstite field and related equilibria. *J. Amer. Chem. Soc.* **67**, 1398-1412.
- GORDEEV, I. V., AND YU. D. TRET'YAKOV (1963) Thermodynamics of solid solutions of magnesium ferrite with magnetite. *Zh. Neorgan. Khim.* **8**, 1814-1819 [*Russ. J. Inorg. Chem.* **8**, 943-947].
- HAHN, W. C., JR., AND A. MUAN (1962) Activity measurements in oxide solid solutions: The system "FeO"-MgO in the temperature interval 1100° to 1300°C . *Trans. AIME*, **224**, 416-420.

- KATSURA, T., AND S. KIMURA (1965) Equilibria in the system FeO-Fe₂O₃-MgO at 1160°C. *Bull. Chem. Soc. Japan*, **38**, 1664-1670.
- KELLEY, K. K. (1962) Heats and free energies of formation of anhydrous silicates. *U.S. Bur. Mines Rep. Invest.* **5901**, 32 pp.
- LARIMER, J. W. (1968) Experimental studies on the system Fe-MgO-SiO₂-O₂ and their bearing on the petrology of chondritic meteorites. *Geochim. Cosmochim. Acta*, **32**, 1187-1209.
- MUAN, A., AND E. F. OSBORN (1956) Phase equilibria at liquidus temperatures in the system MgO-FeO-Fe₂O₃-SiO₂. *J. Amer. Ceram. Soc.* **39**, 121-140.
- NAFZIGER, R. H. (1970) The join diopside-iron oxide-silica and its relation to the join diopside-forsterite-iron oxide-silica. *Amer. Mineral.* **55**, 2042-2052.
- , AND A. MUAN (1967) Equilibrium phase compositions and thermodynamic properties of olivines and pyroxenes in the system MgO-FeO-SiO₂. *Amer. Mineral.* **52**, 1364-1385.
- OLEINIKOV, N. N., R. YU. DOBROVINSKII, V. F. BALAKIREV, A. N. MEN', YU. D. TRETYAKOV, AND G. I. CHUFAGOV (1968) Determination of component activities in a Fe₂O₃-FeCr₂O₄ solid solution. *Izv. Akad. Nauk SSSR, Neorg. Mater.* **4**, 1362-1384. [*Inorg. Mater.* **4**, 1216-1218].
- OSBORN, E. F. (1956) Importance of the spinel phase in the steel industry. *Regional Tech. Pap., Amer. Iron Steel Inst.*, 1-16.
- (1959) Role of oxygen pressure in the crystallization and differentiation of basaltic magma. *Amer. J. Sci.* **257**, 609-647.
- (1962) Reaction series for subalkaline igneous rocks based on different oxygen pressure conditions. *Amer. Mineral.* **47**, 211-226.
- PHILLIPS, B., AND A. MUAN (1962) Phase equilibria in the system MgO-FeO-Fe₂O₃ in temperature range 1400° to 1800°C. *J. Amer. Ceram. Soc.* **45**, 588-591.
- SCHUHMAN, R., JR. (1955) Application of Gibbs-Duhem equations to ternary systems. *Acta Met.* **3**, 219-226.
- SCHMAHL, N. G., B. FRISCH, AND G. STOCK (1961) Gleichgewichtsuntersuchungen an magnesiowüstiten und magnesioferriten. *Arch. Eisenhüttenw.* **32**, 297-302.
- SCHWERDTFEGGER, K., AND A. MUAN (1966) Activities in olivine and pyroxenoid solid solutions of the system Fe-Mn-Si-O at 1150°C; with appendices by L. S. Darken and K. Schwerdtfeger. *Trans. AIME*, **236**, 201-211.
- , AND ——— (1967) Phase equilibria in the system Fe-Mn-O involving "(Fe,Mn)O" and (Fe,Mn)₂O₃ solid solutions. *Trans. AIME*, **239**, 1114-1119.
- SPEIDEL, D. H. (1967) Phase equilibria in the system MgO-FeO-Fe₂O₃: The 1300°C isothermal section and extrapolations to other temperatures. *J. Amer. Ceram. Soc.* **50**, 243-248.
- , AND E. F. OSBORN (1967) Element distribution among coexisting phases in the system MgO-FeO-Fe₂O₃-SiO₂ as a function of temperature and oxygen fugacity. *Amer. Mineral.* **52**, 1139-1152.
- STULL, D. R., et al. (1971) *JANAF thermochemical tables*, Second Ed. The Thermal Research Laboratory, Dow Chemical Co., Midland, Michigan. **NSRDS-NBS-37**.
- WILLIAMS, R. J. (1971) Reaction constants in the system Fe-MgO-SiO₂-O₂ at 1 atm between 900° and 1300°C: Experimental results. *Amer. J. Sci.* **270**, 334-360.
- WONES, D. R., AND M. C. GILBERT (1969) The fayalite-magnetite-quartz assemblage between 600°C and 800°C. *Amer. J. Sci.* **267-A**, 480-488.

Manuscript received, August 28, 1972; accepted for publication, December 13, 1972.



IAEA-SM-228/19

ISOTOPE HYDROLOGY OF THE VAL CORSAGLIA, MARITIME ALPS, PIEDMONT, ITALY

G.C. BORTOLAMI, B. RICCI, G.F. SUSELLA,
G.M. ZUPPI*
Istituto di Geologia e Paleontologia,
Turin, Italy

Abstract

ISOTOPE HYDROLOGY OF THE VAL CORSAGLIA, MARITIME ALPS, PIEDMONT, ITALY.

Environmental isotopes and geochemistry were used in a hydrogeological study of the Val Corsaglia (northern Italy). The small catchment area (110 km²) is located on the northern side of the Maritime Alps and formed by a variety of different rock types. The air masses entering the basin originate in the Mediterranean Sea as well as the Atlantic Ocean. Therefore, the chemical load and isotopic composition of the respective precipitations change with the season as a consequence of different wind patterns. Fifty-two sampling sites were established throughout the basin and sampling was carried out during the two "extreme" periods – April, 1976 and October, 1974. The problems considered in this investigation are: (1) Altitude effect in isotopic compositions of rain-waters for oxygen and deuterium, which were found to be close to 0.3‰/100 m for ¹⁸O and 2.5‰/100 m for deuterium; (2) the relation between δ²H and δ¹⁸O as a function of geographic locations and climatic conditions: the deuterium excess varies between $d = 12.08 \pm 1.29$ and 13.43 ± 2.57 ; (3) the altitude of recharge as determined from isotope data. Both the altitude effect and the deuterium excess can be used as labels which characterize different water masses and permit the identification of specific recharge areas; (4) water flow in reservoir rocks and fluctuations of chemical and isotopic contents. Two principle flow systems can be recognized: the first, deep, isotopically and chemically homogeneous, representing the base flow; the second, shallow and faster, with sensitive isotopic variation and a low content of dissolved salts.

INTRODUCTION

The alpine basins in the Piedmontese mountains flanking the Po Valley are largely impermeable and surface runoff is dominant. Where infiltration occurs in different types of rock subsurface circulations can be established. Groundwater flows can occur through faults and fractures in crystalline rocks or through karstified carbonates and other sedimentary rocks. Since aquifers underlying the Po Valley carry "alpine water", it is interesting to study the surface and subsurface circulation originating in these alpine basins.

This study deals with groundwater movements in karst terrain in a small basin (110 km²) located on the northern side of the Maritime Alps, Val Corsaglia (Fig.1). Its location is rather particular, since it borders on France and is

* At present with the International Atomic Energy Agency, Vienna.

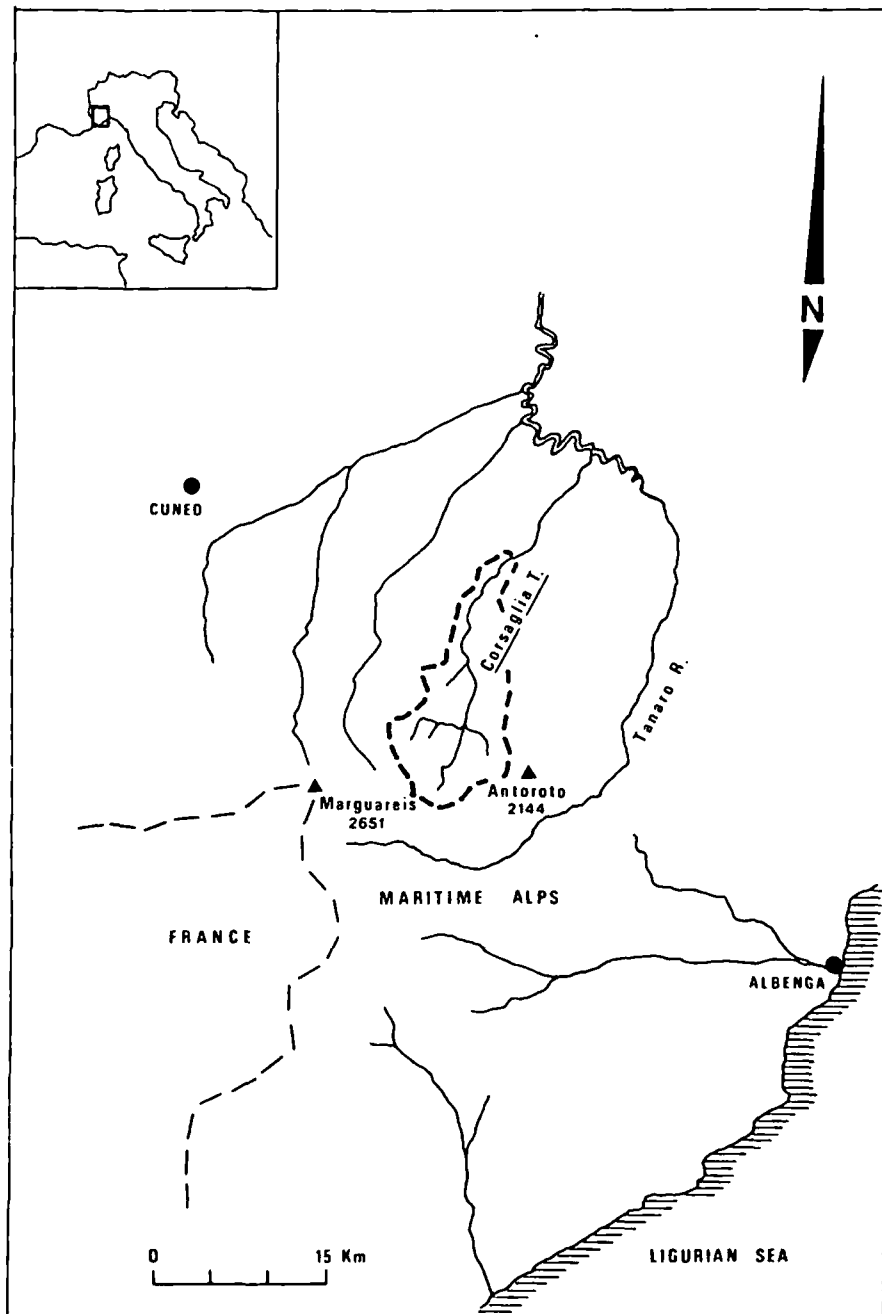


FIG.1. Location of study area.

characterized by "mix during the summer mo basin. Because of the isotopic composition investigations.

1. HYDROGEOLOGY

The basin of the characterized by dissim and groundwater flow

- (1) The highest side stones and dolomite degree.
- (2) Crystalline rocks of Permian meta deriving from rhy which include ser One of these hos
- (3) An area in the ne of Mesozoic calc-

The hydrogeology thus possible to find z impermeable rocks in. Because of the comple and are located in diff

2. METHODOLOGY

The chemical and seasonal variation and to recharge areas, dire

Fifty-two sites w isotopic study during These two sampling p runoff during snow m In this study, the 18 s geological setting are

characterized by "mixed weather conditions". It receives Atlantic precipitation during the summer months and winter precipitation originates in the Mediterranean basin. Because of their dissimilar origin, they have a different chemical load and isotopic composition which can be used as a natural tracer in hydrogeological investigations.

1. HYDROGEOLOGICAL SETTING

The basin of the Val Corsaglia can be divided into three different zones characterized by dissimilar geo-lithologic formations with various infiltration and groundwater flow patterns (Fig.2):

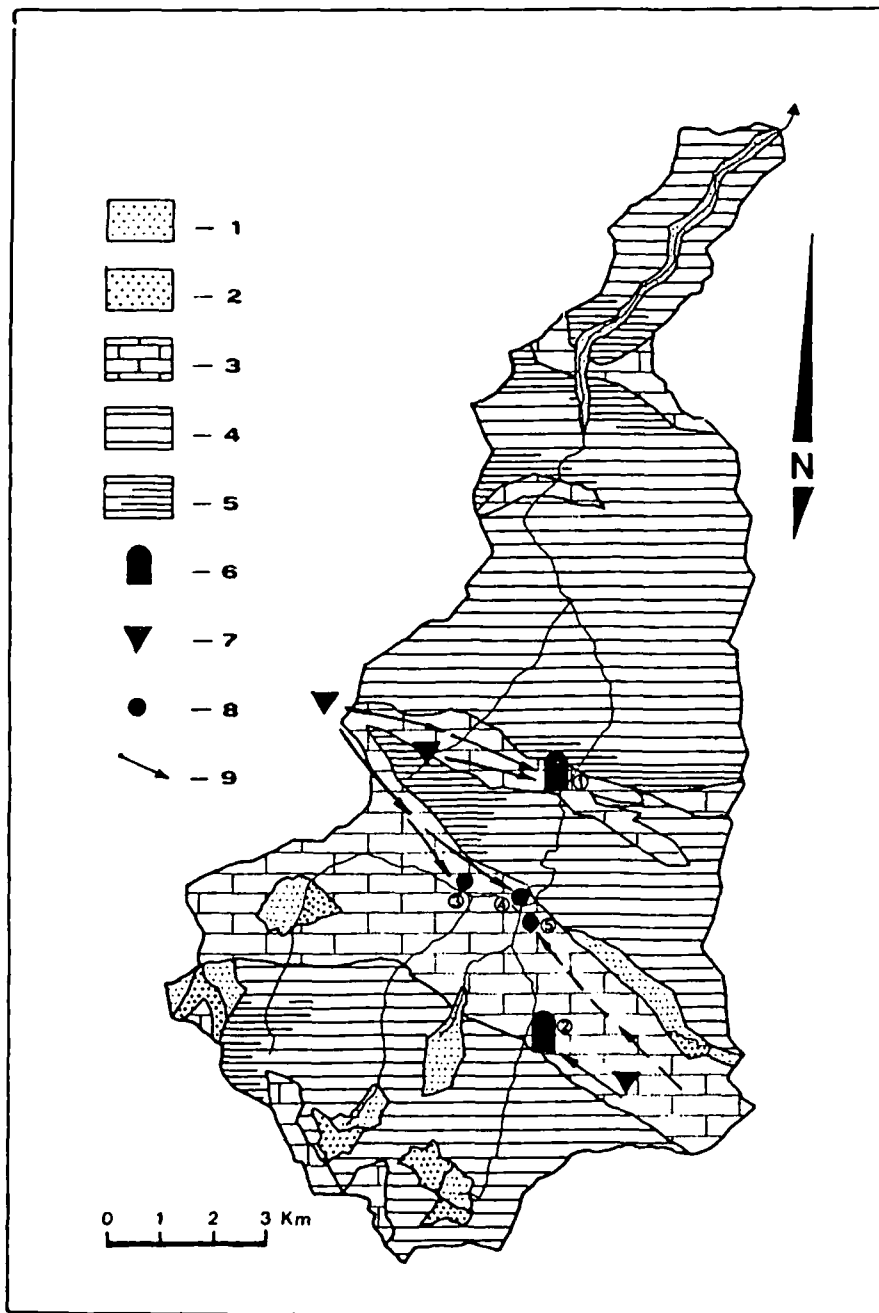
- (1) The highest side of the valley consists of Mesozoic carbonate rocks (limestones and dolomitic limestones) which are karstified to a considerable degree.
- (2) Crystalline rocks dominate in a small area at mean altitude and are composed of Permian metaporphyrries ("Porfiroidi", i.e. low green-schists facies rocks deriving from rhyodacitic volcanic deposits) and of Eotriassic quartzites which include several large tectonic slices of Mesozoic carbonate rocks. One of these hosts the karst system of Bossea.
- (3) An area in the northern part of the basin at low altitude consisting essentially of Mesozoic calc-schists ("Formazione dei Calcescisti", i.e. Schistes lustrés).

The hydrogeological setting depends obviously on the geolithology. It is thus possible to find zones with important karst systems adjacent to very impermeable rocks in which local groundwater flow occurs along fractures. Because of the complex geology, all karst systems are independent of one another and are located in different catchment areas.

2. METHODOLOGY

The chemical and isotopic composition of rain-waters show a regular seasonal variation and provide us with an important tool to solve problems related to recharge areas, direction and velocity of the groundwater flow.

Fifty-two sites were sampled in the Val Corsaglia for the chemistry and isotopic study during two different months – October 1974 and April 1976 [1]. These two sampling periods were chosen because they coincide with the maximum runoff during snow melt and minimum discharge during late summer and autumn. In this study, the 18 springs most characteristic for a hydrological regime and geological setting are presented. During the same periods precipitation was sampled



monthly at seven pluviometers at altitudes of 400 to 2000 m. To reduce errors, rain was added to the pluviometer.

The isotopic analyses were carried out at Zuppi at the Laboratorio di Geochimica in the usual units, i.e. ‰. The errors are of 0.3‰ and 0.07‰.

Chemical analyses were carried out at the Laboratory attached to the Institute of Geology. The results show a statistical correlation between the emission of CO₂ and all chemical data have been published by the US Geol. Survey [4].

The data in this study are given in Table 1. The precipitation samples were collected close to the molar carbonate.

The following parameters were determined for the springs:

- (a) Altitude effect in the isotopic composition
- (b) Relation of $\delta D/\delta^{18}O$ and $\delta^{13}C/\delta^{12}C$
- (c) "Isotopic altitude"
- (d) Hydrogeochemical characteristics and content in spring

This isotope study is part of a larger chemical investigation of the seasonal variations in the

FIG. 2. Geological sketch map showing: 1. Tills and fluvial deposits; 2. Scree deposits: high in the mountains; 3. Mesozoic limestones; 4. Mesozoic calc-schists and 5. Mesozoic calc-schists and 6. Most important karst features; 7. Shallow hole (doline); 8. Springs with an average flow rate: (c) Stalla Buorch; (d) Po; 9. Underground flow direction.

monthly at seven pluviometric stations located at different elevations from 400 to 2000 m. To reduce the evaporation effect during the month, liquid paraffin was added to the pluviometer.

The isotopic analyses (deuterium and ^{18}O) were performed by Susella and Zuppi at the Laboratoire de Géologie Dynamique, Paris: the results are given in the usual units, i.e. $\delta\text{D}\text{‰}$, $\delta^{18}\text{O}\text{‰}$ (both versus SMOW, with a standard deviation of 0.3‰ and 0.07‰, respectively) [2].

Chemical analyses were routinely performed by the Hydrogeochemistry Laboratory attached to the Istituto di Geologia dell'Università di Torino. The results show a statistical error ranging from 3% in sodium and potassium determination by the emission method to 6% for sulphates done by colorimetry [3]; all chemical data have been treated by the computer program WATEQ of the US Geol. Survey [4]. For this reason, some of the results of groundwaters obtained in this study are given as ion activities; the same expression has been used for the precipitation samples, but it is obvious that, in this case, the ion activity is very close to the molar concentration [5].

The following problems have been studied through chemical analyses and determination of the abundances of environmental isotopes in precipitation and springs:

- (a) Altitude effect in isotopic composition of rain-water
- (b) Relation of $\delta\text{D}/\delta^{18}\text{O}$ as a function of geographic and climatic conditions
- (c) "Isotopic altitude" of recharge
- (d) Hydrogeochemical evolution in reservoir rocks and variation of isotopic content in spring waters.

This isotope study is a part of a complete hydrogeological and hydrogeochemical investigation in which the major and minor elements are related to the seasonal variations in precipitation and the local change of lithology and tectonics.

◀ FIG.2. Geological sketch and locations of sampling sites in the Corsaglia Valley.

1. Tills and fluvial deposits: high to medium intergranular permeability.
2. Scree deposits: high intergranular permeability
3. Mesozoic limestones: very high karst permeability
4. Mesozoic calc-schists and Permian metaporphyries: generally impermeable
5. Mesozoic calc-schists and Permian metaporphyries: low fracture permeability
6. Most important karst caves
7. Shallow hole (doline)
8. Springs with an average flow greater than 50 l/s: (a) Bossea Cave; (b) Mottera Cave; (c) Stalla Buorch; (d) Ponte Murao; (e) Captazione Borello
9. Underground flow directions discovered by colorimetric method

TABLE I. ISOTOPIC AND SELECTED CHEMICAL DATA IN VAL CORSAGLIA PRECIPITATION WATERS

Pluviometer	Elevation above sea level (m)	Conduct. ($\mu\text{S}\cdot\text{cm}^{-1}$)	pH	a Cl ⁻ $\times 10^{-5}$	$\delta\text{D}\text{‰}$ SMOW	$\delta^{18}\text{O}\text{‰}$ SMOW	d ‰
October 1974							
Mondovi	400	28	5.6	2.4	-60.0	-9.00	+12.0
Corsagliola	620	23	5.7	2.8	-66.3	-9.81	+12.2
Prea	830	21	5.8	0.7	-72.5	-10.49	+11.4
Distretti	1080	18	6.0	3.0	-79.9	-11.52	+12.3
Case Momo	1380	19	5.8	3.8	-84.9	-12.20	+12.7
M.Malanotte	1780	17	5.5	3.1	-95.7	-13.50	+12.3
R. Garelli	2000	16	5.8	0.6	-101.2	-14.08	+11.4
April 1976							
Mondovi	400	56	5.4	6.7	-60.1	-9.36	+14.8
Corsagliola	620	46	5.7	5.2	-67.2	-10.10	+13.6
Prea	830	47	5.8	5.1	-71.8	-10.66	+13.5
Distretti	1080	35	6.0	8.0	-79.1	-11.88	+15.9
M.Malanotte	1780	18	6.1	6.1	-96.2	-13.81	+14.3
R. Garelli	2000	17	6.2	6.3	-99.3	-14.23	+14.5

Note: a Cl⁻ = activity of chloride ion.

3. RESULTS AND DISCUSSION

3.1. Altitude effect in isotopic composition of rain-water

An average isotopic gradient with altitude ($d\delta^{18}\text{O}/dh$) can be determined directly by collecting samples in an integrating pluviometer located in various stations at different altitudes. Indirect determination can be made if the variation in isotopic contents of rain-waters as a function of temperature ($\delta^{18}\text{O}/dt$) is known for one or more stations, and by subsequent transformation with temperature/temperature/altitude gradients (dt/dh [6]).

Only the direct measurement method has been used here and the monthly mean isotopic composition is well correlated with altitudes (Table I). The

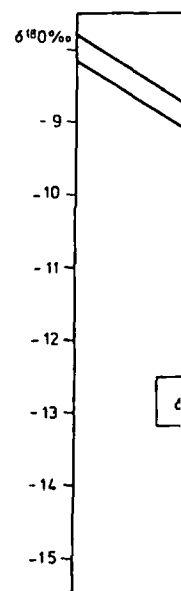


FIG. 3. $^{18}\text{O}/\text{altitude}$ gradient April 1976 are 0.98 and 0.15 (April).

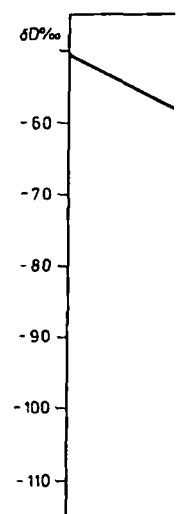


FIG. 4. Deuterium/altitude gradient is 0.98, whereas the es

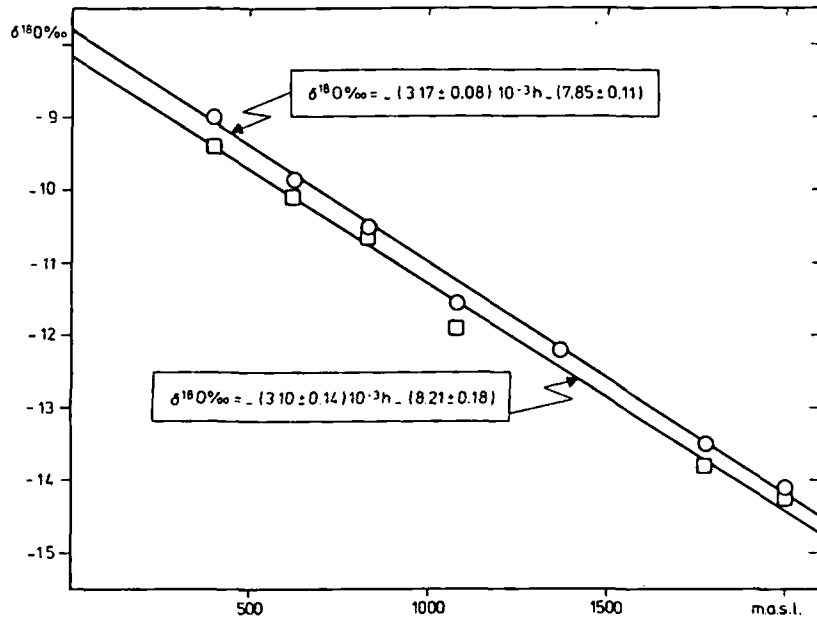


FIG.3. ^{18}O /altitude gradient. The determination coefficients (r^2) for October 1974 and April 1976 are 0.98 and 0.99, respectively, whereas the standard errors are 0.13 (October) and 0.15 (April).

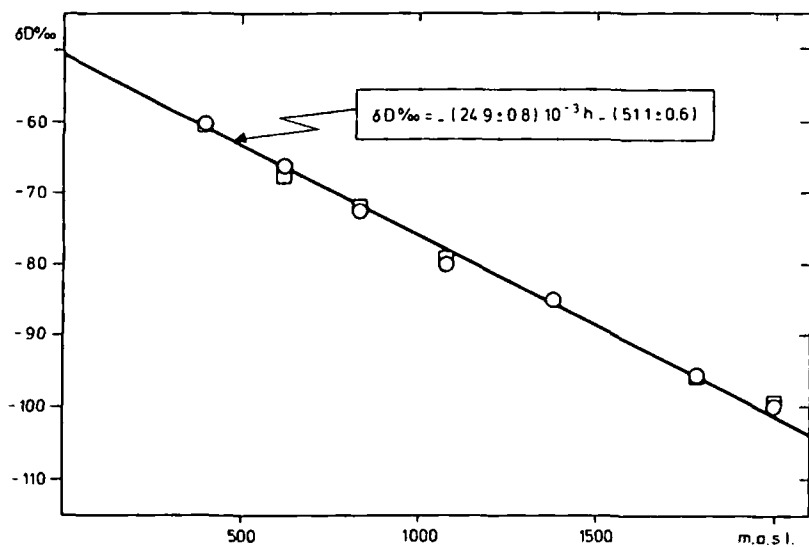


FIG.4. Deuterium/altitude gradient. The determination coefficient (r^2) for both months is 0.98, whereas the estimated standard error is 0.6.

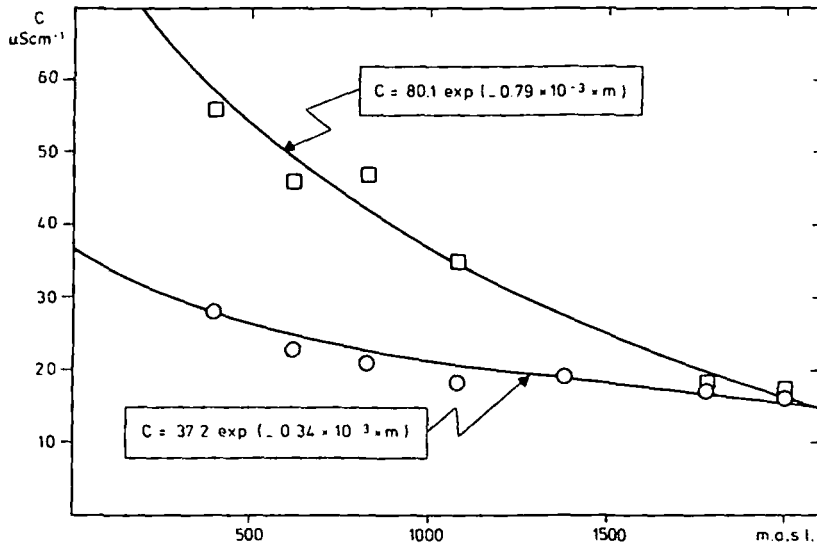


FIG.5. Conductivity/altitude gradient. The coefficients of determination (r^2) are 0.99 and 0.98, respectively, for October 1974 and April 1976. The estimated standard errors are 0.32 (October) and 0.28 (April).

relation ($d\delta^{18}O/dh$) changes somewhat between April and October, both in the slope, i.e. the gradient, and in the intercept (Fig.3) and one finds for April:

$$\delta^{18}O\text{‰} = -(3.10 \pm 0.14)10^{-3}h - (8.24 \pm 0.18) \quad (1a)$$

and for October:

$$\delta^{18}O\text{‰} = -(3.17 \pm 0.08)10^{-3}h - (7.85 \pm 0.14) \quad (1b)$$

where h (the altitude) is expressed in m. By using the same isotopic composition in the two equations, a calculated difference of 100 m would result.

Generally, the mean temperatures for April and October are quite near the annual mean temperature. Therefore, the combination of these two equations closely describes the average annual isotopic gradient as a function of the altitude:

$$\delta^{18}O\text{‰} = -(3.12 \pm 0.10)10^{-3}h - (8.03 \pm 0.13) \quad (1c)$$

An altitude gradient has also been obtained for δD (Fig.4). In this case, all the data for both months are distributed along the following correlation line:

$$\delta D\text{‰} = -(24.9 \pm 0.8)10^{-3}h - (51.1 \pm 0.6) \quad (2)$$

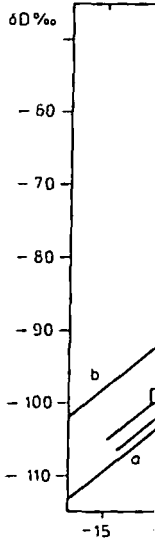


FIG.6. Deuterium and ^{18}O October 1974 (line 2) is characteristic of Mediterranean character. October and April meteoric errors are 0.51 and 0.99, respectively.

A similar relation is observed on the French side (northern to 4.0‰ \pm 1‰ per 1000 m) which we believe to be a weighted average.

An interesting observation is related to altitude at Atlantic rains which are at 1200 metres and an exponential

conductivity = 3

is observed; h is the altitude

In April, on the west Mediterranean Sea following relationship

conductivity = 8

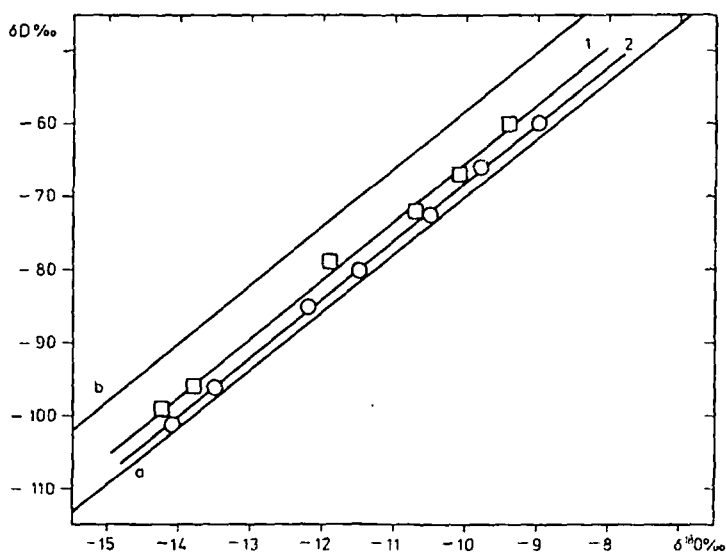


FIG. 6. Deuterium and ^{18}O variation in precipitation. The local meteoric water line in October 1974 (line 2) is close to the world meteoric line (a) [8], whereas in April 1976 (line 1) Mediterranean characteristics appear (b) [9]. The coefficients of determination (r^2) for October and April meteoric waters are 0.99 and 0.98, respectively. The estimated standard errors are 0.51 and 0.99, respectively, for October and April.

A similar relationship has been determined on samples of fresh snow on the French side (northern side) of Mont Blanc [7], where a deuterium gradient equal to $4.0\text{‰} \pm 1\text{‰}$ per 100 m was found. This is somewhat larger than our values, which we believe to be more representative since they are based on monthly weighted averages.

An interesting observation is also that the chemical load of precipitation is related to altitude and origin of vapour masses. Figure 5 shows that for Atlantic rains which arrive in October, the conductivity decreases fast up to 1200 metres and an exponential relationship of the form

$$\text{conductivity} = 37.2 \exp(-0.34 \times 10^{-3} h) \quad (3a)$$

is observed; h is the altitude and is expressed in metres.

In April, on the other hand, the vapour masses originate primarily from the west Mediterranean Sea and up to an altitude of 1800 metres one observes the following relationship:

$$\text{conductivity} = 80.1 \exp(-0.79 \times 10^{-3} h) \quad (3b)$$

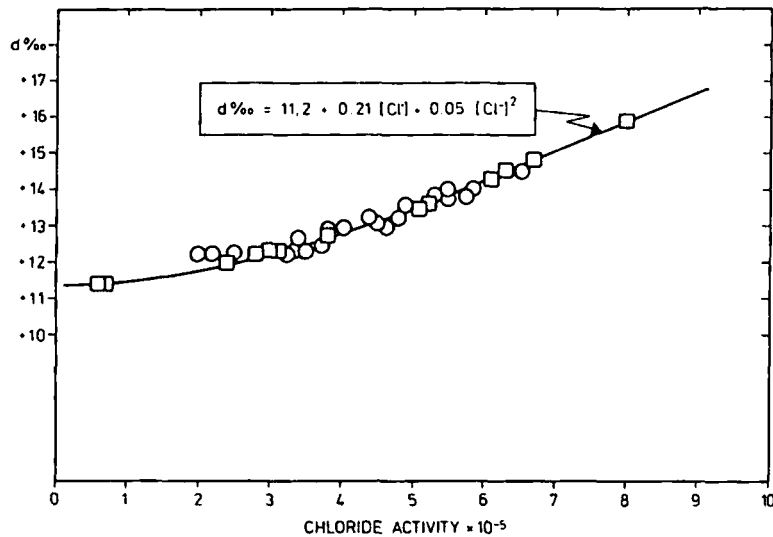


FIG. 7. Deuterium excess plotted versus chloride activity. Circles indicate the spring samples, squares the precipitation samples. The coefficient of determination (r^2) for this correlation is 0.98 and the estimated standard error is 0.03.

3.2. Deuterium and ^{18}O relationships depending on geographic and climatic conditions (Fig. 6)

In precipitation, the ^{18}O and D contents show a good correlation with temperature of condensation. Therefore, it is normal that the heavy isotope contents of precipitations are interdependent, and on a world-wide basis precipitations which did not undergo evaporation obey the relation:

$$\delta D = 8 \delta^{18}\text{O} + d \quad [8] \quad (4)$$

It is believed that the constancy of slope ~ 8 during most meteoric events is due to the fact that the condensation is always a phenomenon of equilibrium because it takes place during conditions of saturation [6]. The "d" quantity designated as "deuterium excess" is usually close to +10‰, especially at oceanic stations [8]. However, if a significant part of the vapour mass has originated in a closed basin, the "d" parameter changes. For example, in the eastern Mediterranean basin, the isotopic composition of precipitation obeys the relation:

$$\delta D = 8 \delta^{18}\text{O} + 22 \quad [9] \quad (5)$$

In this context, the variations in the area studied are defined as "mixed" variations (Table 1). From the coast towards the interior (Fig. 7), the best correlation is given by a second-order polynomial (Eq. 5).

April δD :

October δD :

This intermediate situation can be defined as "mixed" variations (Table 1). From the coast towards the interior (Fig. 7), the best correlation is given by a second-order polynomial (Eq. 5). In general, low chloride activity (Fig. 7), the best correlation is given by a second-order polynomial (Eq. 5). In general, low chloride activity (Fig. 7), the best correlation is given by a second-order polynomial (Eq. 5). In general, low chloride activity (Fig. 7), the best correlation is given by a second-order polynomial (Eq. 5).

3.3. "Isotopic altitude"

The isotopic composition of precipitation in altitude recharge areas [11-12] waters infiltrate into the ground or subsequent modification is considered quite valid. The isotopic composition of rain-water is allowed to vary.

On the basis of a study of the isotopic composition with variations in isotopic composition, we introduce the concept of "isotopic altitude" or "reappearance" at the surface. In the underground system, isotopic composition has taken place. In this context, the isotopic composition coinciding with the meteoric water in April 1976.

In this context, the two correlation lines obtained from $\delta^{18}\text{O}$ and δD values in the area studied are placed between the line of Craig (Eq.(4)), and that of Nir (Eq.(5))

$$\text{April} \quad \delta\text{D} = (8.00 \pm 0.11)\delta^{18}\text{O} + (12.08 \pm 1.29) \quad (6a)$$

$$\text{October} \quad \delta\text{D} = (7.91 \pm 0.22)\delta^{18}\text{O} + (13.43 \pm 2.57) \quad (6b)$$

This intermediate position is due to the meteoric contributions which can be defined as "mixed". Also chloride contents in rain-waters show seasonal variations (Table I). Plotting the deuterium excess "d" versus chloride activity (Fig.7), the best correlation between these two parameters is obtained by a second-order polynomial function, i.e. an asymptotic line. The points representing summer and autumn are closely grouped at the lower end of the line, whereas the points of winter and spring show a larger spread at the upper part of the line. In general, low chloride activity corresponds to a constant value of deuterium excess: +11.2‰. It is known that the chloride contents at a certain distance from the coast become rather low and constant [10]; in our case the constant deuterium excess characterizes the maximum oceanic component in the rainfall in a region with mixed precipitations. The increasing chloride activity in rain-waters is paralleled by increases in deuterium excess. This substantiated the observations that air masses from the western Mediterranean arrive during winter.

3.3. "Isotopic altitude" of recharge

The isotopic composition of spring samples was compared with that of precipitation in altitude in order to determine the average altitudes of the recharge areas [11-12]. This assumes that in the recharge area the meteoric waters infiltrate into the subsurface without having been subject to the evaporation or subsequent modification of their isotopic ratios. This assumption can be considered quite valid here since, particularly in karst regions, a rapid infiltration of rain-water is allowed.

On the basis of a comparison of the isotopic data of the different springs with variations in isotopic content of precipitation at different altitudes, one can introduce the concept of "phase displacements" between a meteoric event and its "reappearance" at the point of discharge which depends on the residence time in the underground system, provided no mixing with base flow from the reservoir has taken place. In this case, samples were taken during two different periods coinciding with the monthly sampling of meteoric waters - October 1974 and April 1976.

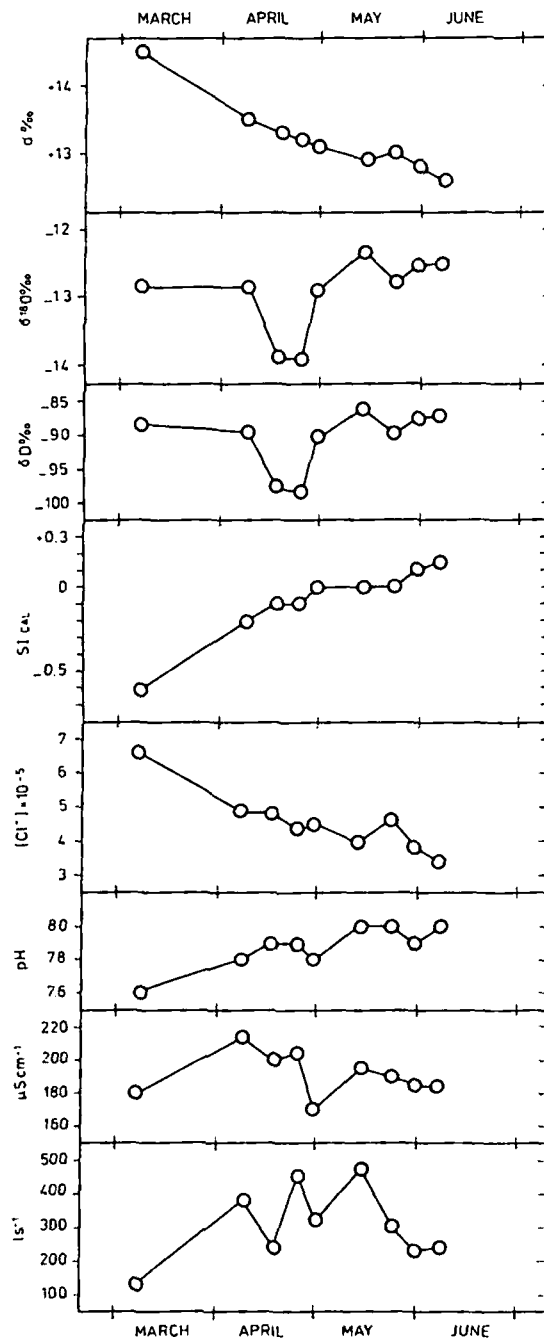


FIG. 8. Seasonal evolution of discharge, conductivity, pH, chloride activity, calcite saturation index, deuterium, ¹⁸O and deuterium excess in Bossea Cave during spring 1976. Of all the caves and springs of this basin only Bossea has a discharge gauge.

The regression equation is slightly different for

April $h = -1$

$h = -1$

October $h = -1$

$h = -1$

However, there are differences from these equations

- (1) The calculated recharge elevation (Gias 1 Ponte Murao, S)
- (2) The calculated recharge catchment area

Therefore, only spring isotopic composition preceding the sampling is enriched in heavy isotopes must be referred to a second case, the isotopic water results from

Rain-water composition the average recharge in Navonera, which have precipitation and sugar similar to a subterranean computed from composition from isotope gradient errors on the average the ¹⁸O and deuterium

3.4. Hydrogeochemistry

If no geochemical input "signal" may

The regression equations of the altitude versus the isotopic content are only slightly different for April and October:

$$\text{April} \quad h = -(320 \pm 15)\delta^{18}\text{O} - (2616 \pm 173) \quad (7a)$$

$$h = -(40.5 \pm 1.4)\delta\text{D} - (2075 \pm 108) \quad (8a)$$

$$\text{October} \quad h = -(315 \pm 9)\delta^{18}\text{O} - (2474 \pm 105) \quad (7b)$$

$$h = -(39.4 \pm 1.1)\delta\text{D} - (1977 \pm 89) \quad (8b)$$

However, there are two cases for which the altitudes of recharge calculated from these equations do not agree with the topography:

- (1) The calculated recharge altitude is lower or close to the spring topographic elevation (Gias Brona, Bossea, 13 October, Captazione Borello, Mottera, Ponte Murao, Stalla Buorch);
- (2) The calculated recharge altitude is higher than the highest altitude of the catchment area watershed (Ante Murao, Bossea, 18 and 25 April).

Therefore, only one altitude/ $\delta\%$ relationship is valid: in the first case, the spring isotopic composition must be referred to a gradient of the meteoric event preceding the sampling, in which the isotopic content of rain-waters was more enriched in heavy isotopes than the monthly mean rainfall (Gias Brona); or they must be referred to a summer gradient because the underground systems discharge waters related to the precipitation from the months preceding October. In the second case, the isotopic content must be referred to a winter gradient because the water results from the melting of snow stored throughout the winter.

Rain-water conductivity gradients (Fig.5) similarly permit the calculation of the average recharge altitudes for springs such as Case Bertoni, Case Torno and Navonera, which have a very low salinity. Their conductivity is close to that of precipitation and suggests that the subterranean flow paths are very short and similar to a subterranean runoff of snow melt. The elevations of recharge areas computed from conductivity gradients are very close to the elevation computed from isotope gradients and agree with hydrogeological observations. The statistical errors on the average altitude of recharge are about 70 and 40 m respectively for the ^{18}O and deuterium gradients, and 30 m for the conductivity gradients.

3.4. Hydrogeochemical evolution and isotopic composition of springs

If no geochemical processes affect the waters during underground passage, an input "signal" may occur with some delay at the spring.

TABLE II. ISOTOPIC AND SELECTED CHEMICAL DATA IN VAL CORSAGLIA KARST SPRINGS

Spring	Elevation above sea level (m)	Flow (litres·s ⁻¹)	Conductivity ($\mu\text{S}\cdot\text{cm}^{-1}$)	pH	a Cl ⁻ X 10 ⁻⁵	IS Calcite	$\delta\text{D}\text{‰}$ SMOW	$\delta^{18}\text{O}\text{‰}$ SMOW	d ‰	h_{δ} h_c above sea level (m)
Bossea	810									
13-10-74		72	137	8.3	3.2	+0.30	-81.4	-11.70	+12.2	1210
07-03-76		132	180	7.6	6.6	-0.60	-88.4	-12.86	+14.5	1500
09-04-76		368	212	7.8	4.9	-0.20	-89.4	-12.86	+13.5	1530
18-04-76		238	200	7.9	4.8	-0.10	-97.3	-13.83	+13.3	1840
25-04-76		446	204	7.9	4.4	-0.10	-97.6	-13.85	+13.2	1850
01-05-76		316	170	7.8	4.5	0.00	-90.2	-12.91	+13.1	1550
14-05-76		464	195	8.0	4.0	0.00	-85.8	-12.34	+12.9	1570
23-05-76		291	190	8.0	4.6	0.00	-89.6	-12.83	+13.0	1530
30-05-76		225	185	7.9	3.8	+0.10	-87.6	-12.54	+12.8	1440
06-06-76		243	185	8.0	3.4	+0.15	-87.5	-12.51	+12.6	1440
Captazione Borello	945									
08-10-74		≅300	124	7.9	2.0	+0.25	-74.7	-10.87	+12.3	950
09-04-76			184	7.5	5.8	-0.40	-86.0	-12.50	+14.0	1400
Case Bertoni	1108									
14-05-76		<1	27	6.8	4.7			-12.08		1250 1210
Case Lardini	645									
10-10-74		<1	420	7.7	2.9	+0.20		-11.33		1200
18-04-76		<1	360	7.8	5.4	-0.10		-12.15		1270
Case Torno	1060									
15-10-74		<1	17.5	6.8	3.0			-11.63		1240
14-05-76		<1	20.0	6.5	5.5		-84.0	-12.22	+13.8	1290 1280

340

BORTOLAMI et al.

Spring	Elevation above sea level (m)	Flow (litres·s ⁻¹)	Conductivity ($\mu\text{S}\cdot\text{cm}^{-1}$)	pH	a Cl ⁻ X 10 ⁻⁵	IS Calcite	$\delta\text{D}\text{‰}$ SMOW	$\delta^{18}\text{O}\text{‰}$ SMOW	d ‰	h_{δ} h_c above sea level (m)
Costa Lumenda 10-10-74	730	<1	279	7.9	3.7	+0.20	-79.4	-11.48	+12.5	1240

15-10-74	<1	17.5	6.8	3.0		-11.03	1240
14-05-76	<1	20.0	6.5	5.5		-12.22	1290 1280

Spring	Elevation above sea level (m)	Flow (litres·s ⁻¹)	Conductivity ($\mu\text{S}\cdot\text{cm}^{-1}$)	pH	a Cl ⁻ X 10 ⁻⁵	IS Calcite	$\delta\text{D}\%$ SMOW	$\delta^{18}\text{O}\%$ SMOW	d‰	h_g h_c above sea level (m)
Costa Lumenda	730									
10-10-74		<1	279	7.9	3.7	+0.20	-79.4	-11.48	+12.5	1240
18-04-76		<1	320	7.3	5.8	-0.30	-84.0	-12.21	+13.8	1310
Gias Brana	1270									
01-05-76			44	7.6	4.9		-82.6	-11.98	+13.3	1250
Molline	495									
27-10-74		1	375	7.9	3.5	+0.50	-78.9	-11.40	+12.30	1120
Mottera	1350									
01-05-76		≈ 300	165	8.4	2.5	+0.40	-90.3	-12.82	+12.3	1535
Murao (Ante)	960									
08-10-74		2	215	8.1	4.8	-0.10	-98.5	-13.97	+13.3	1890
Murao (Ponte)	966									
12-11-74		≈ 80	160	8.0	2.4	+0.55	-74.4	-10.95	+12.3	980
09-04-76		≈ 90	100	7.7	5.1	-0.20	-85.8	-12.41	+13.5	1380
Navonera	1145									
15-05-76		4	19.0	6.0	5.5		-85.0	-12.37	+14.0	1360 1320
Piano	500									
25-04-76		1	160	7.7	5.3	-0.30	-83.0	-12.10	+13.8	1270
Presa Mondini	910									
17-11-74		≈ 100	92	8.3	4.0	+0.15		-12.20		1370

IAEA-SM-228/19

TABLE II. (cont.)

Spring	Elevation above sea level (m)	Flow (litres · s ⁻¹)	Conductivity (μS · cm ⁻¹)	pH	a Cl ⁻ × 10 ⁻⁵	IS Calcite	δD‰ SMOW	δ ¹⁸ O‰ SMOW	d‰	h _δ h _c above sea level (m)
Presa Mondini (Ante) 14-05-76	910	≈ 10	126	7.6	5.3	-0.15	-83.9	-12.17	+13.5	1310
Stalla Buorch 20-10-74	1056	≈ 50	180	7.6	3.7	+0.20	-78.6	-11.39	+12.5	1110
02-05-76		≈ 100	204	8.1	4.5	-0.05	-92.1	-13.16	+13.2	1630
Stalla Rossa 01-05-76	1050	1	213	7.9	5.1	-0.20	-86.2	-12.46	+13.5	1500
Valloni 27-10-74	580	1	290	7.8	3.2	+0.20		-11.61		1200

Note: a Cl⁻ = activity of chloride ions.

IS calcite = Sat. index for calcite; IS = log IAP · log K_s with IAP = a Ca²⁺ · a CO₃²⁻ and K_s = sol. product.

d = deuterium excess d = δD - 8δ¹⁸O

h_δ = "isot. alt." of recharge (average of calculated altitude values according to Eqs (7) and (8))

h_c = "cond. alt." of recharge (Eq.(3)).

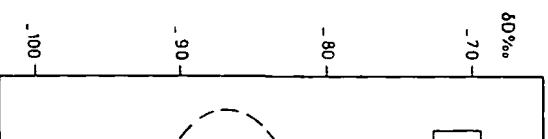


FIG. 9. Deuterium content Bossa Cave, squares sample arrival in spring of waters for or less. They represent the points close to the corrected standard error is (filled square corresponds to spring has still a composition

Chemical and isotope which can best be used to and deuterium excess re differentiation between in spring); deuterium are seasonal variations; con the water/rock interaction Variations in time (Fig.8) since this is the are made. Figure 8 parallel variation between tends to constant values index, chloride activity,

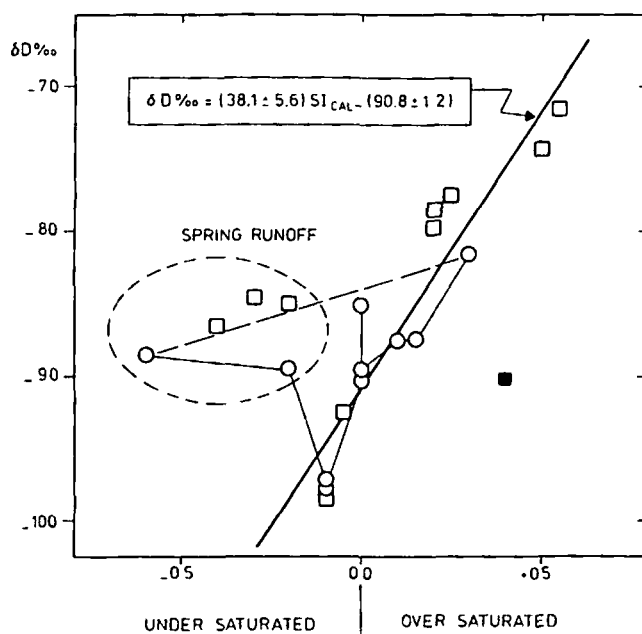


FIG.9. Deuterium content versus calcite saturation index. Circles indicate samples from the Bossea Cave, squares samples from other springs. The points within the circle show the arrival in spring of waters from snow melt occurring at an average altitude of 1500 metres or less. They represent the non-homogenous and non-dispersive underground circulation. The points close to the correlation line (the coefficient of determination is 0.90 and the estimated standard error is 0.8) represent a homogeneous and dispersive circulation. The filled square corresponds to a sample from Mottera Cave in which the water at the end of spring has still a composition characteristic of base flow.

Chemical and isotopic characteristics important for these karst circuits which can best be used to describe origin and underground history are: chloride and deuterium excess reflecting seasonal variations of meteoric waters (i.e. differentiation between direct contributions as rainfall and indirect as snow melt in spring); deuterium and ^{18}O as indicators for mean altitude of recharge and seasonal variations; conductivity and calcite saturation indexes which describe the water/rock interactions (i.e. indirect length of the circuit).

Variations in time for all these parameters are reported for Bossea Spring (Fig.8) since this is the only spring for which continuous discharge measurements are made. Figure 8 permits two important hydrological observations: first, a parallel variation between discharge, conductivity and isotopic composition which tends to constant values thereafter; second, variation of pH, calcite saturation index, chloride activity, deuterium excess, which are independent of discharge

but which tend to change in an exponential manner approaching constant values during the summer. However, these differences in behaviour are caused by the existence of both dispersive and non-dispersive flow in these karst systems.

- (1) For non-dispersive and non-homogeneous circulation the following are observed: the precipitation "signal" is not masked and the chemical composition of the water indicates low rock/water interaction: pH and calcite saturation indexes are far from the water carbonate equilibrium; the input variations are maintained and non-homogenized water appears at the beginning of the spring season (March and April). During this time conductivity, deuterium and ^{18}O follow the discharge variations in time – chloride activity and deuterium excess show the values close to the precipitations fallen (snow melt) or falling during that time in the catchment area. The meteoric signal is also preserved.
- (2) During the later part of the spring season and the summer the subsurface flows become homogeneous and dispersive and meteoric input variations are not recognized. The conductivity, deuterium and ^{18}O become rather constant and independent of discharge variations; chloride activity and D excess move away from spring values and during October reach values corresponding to a weighted annual mean (minimum discharge occurs at this time); pH and SI_{cal} indicate that the equilibrium with carbonate rocks is reached.

Thus, in the annual cycle of the geochemical evolution of these karst waters, one observes a transition from non-dispersive (piston) flow with maximum discharge to a dispersive low flow condition. The latter homogenizes input variations and permits prolonged contact between water and aquifer rocks. Similar behaviour is noted in other karst systems of Val Corsaglia, if the deuterium content is plotted versus the calcite saturation index (Table II).

One notes that the snow meltwaters (left side of Fig.9) are different from those coming from base flow (right side of the same Figure). In the first case waters do not reach the equilibrium with carbonate rocks and deuterium changes according to the increasing altitude at which snow melt occurs. Therefore, it is clear that precipitations during the spring season can infiltrate only in those areas in which snow melt has already occurred.

After spring runoff, saturation with respect to calcite is gradually approached in the different karst systems. This is due to an increasing contribution of isotopically and geochemically homogeneous base flow to the springs. These base-flow dominated waters fall close to a line described by:

$$\delta\text{D}\text{‰} = 38.1 \text{SI}_{\text{cal}} - 90.8 \quad (9)$$

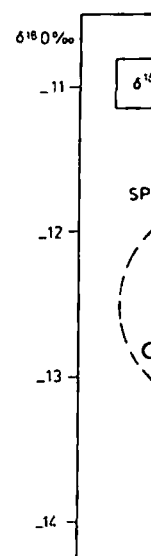


FIG.10. ^{18}O versus calcite saturation index. Squares other springs with the same ^{18}O and calcite saturation index. The error is 0.14.

A sample from the left side of the plot shows a considerable oversaturation with respect to calcite and a higher deuterium content than the other springs, similar to that of spring runoff waters because it is located at a high altitude.

Similarly, the plot of $\delta^{18}\text{O}$ versus SI_{cal} shows the same hydrological regime as the previous one, following spring runoff by isotopically and chemically homogeneous base flow. The following relationship is observed:

$$\delta^{18}\text{O}\text{‰} = 4.89 \text{SI}_{\text{cal}} - 10.8$$

The mixing, or at least the base flow component, is thus identified by its isotopic and chemical composition.

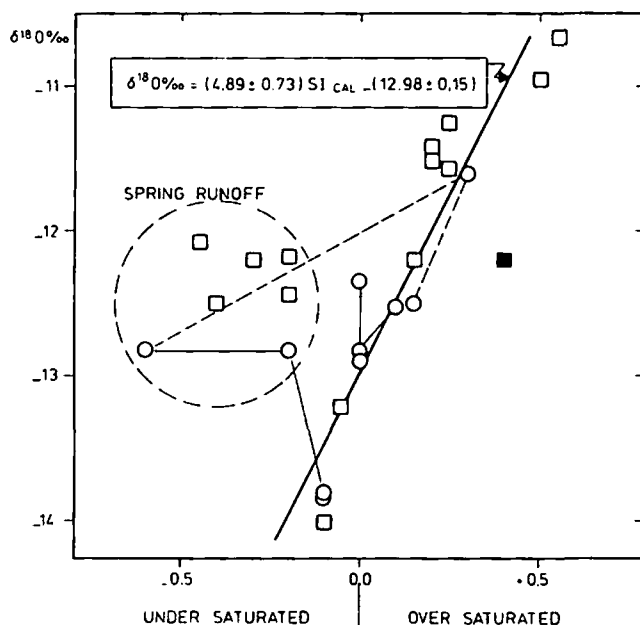


FIG.10. $\delta^{18}\text{O}$ versus calcite saturation index. Circles indicate Bossea Cave samples, the open squares other springs with the exception of Mottera Cave (filled square). The correlation between $\delta^{18}\text{O}$ and calcite has a coefficient of determination of 0.91 and the estimated standard error is 0.14.

A sample from the karst system of Mottera collected during the spring shows considerable oversaturation with respect to calcite (Fig.9, filled square) and a higher deuterium content. This is explained as a "phase displacement" if compared with the other springs, since at the moment of sampling the conditions were such that spring runoff waters had not yet arrived. The catchment area was still frozen because it is located at a higher altitude.

Similarly, the plot of $\delta^{18}\text{O}$ versus calcite saturation index (Fig.10) describes the same hydrological regime: a shallow, fast and non-dispersive groundwater circulation following spring runoff and later, deeper subsurface flow dominated by isotopically and chemically homogeneous base flow. For base-flow conditions the following relationship exists:

$$\delta^{18}\text{O}\text{‰} = 4.89 \text{ SI}_{\text{cal.}} - 12.98 \quad (10)$$

The mixing, or at least the contribution of spring runoff with a base-flow component, is thus identifiable by the parallel, seasonal variation of the isotopic and chemical composition of waters. This is shown in Fig.11, where the deuterium

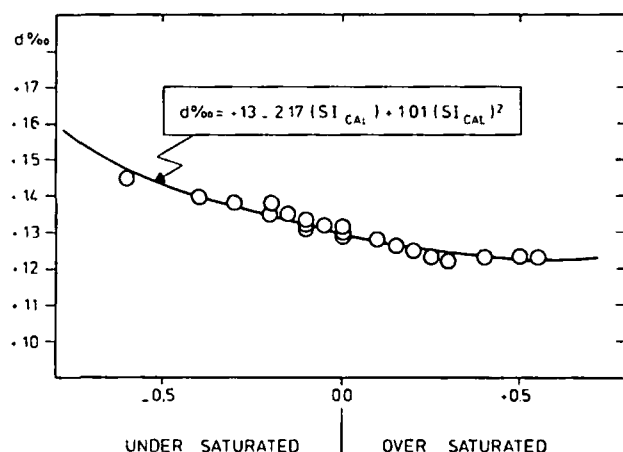


FIG. 11. Deuterium excess "d" in per mille versus calcite saturation index. The constant values $d = +12.2\text{‰}$ represent the weighted annual mean of deuterium excess in the springs of Corsaglia Valley. The coefficient of determination is 0.98 and the estimated standard error is 0.25.

excess is plotted versus calcite saturation index for water samples of springs collected at different times. The following equation

$$d\text{‰} = +13 - 2.17 (SI_{\text{cal.}}) + 1.01 (SI_{\text{cal.}})^2 \quad (11)$$

shows that, with increasing deuterium excess, the dilution of waters increases. On the other hand, more oversaturated waters are those in which a smaller "d" occurs. The deuterium excess tends to a constant value which coincides with one characteristic for base flow. This "d" value is equal or very close to the weighted mean value of deuterium excess during the year: $+12.2\text{‰}$, indicating that it has components of all precipitations falling on the basin. The base flow is further characterized by a very high saturation index.

Similar conclusions are reached if deuterium excess is plotted versus chloride activity where then two different meteoric "signals" are compared. The behaviour of these two parameters during the season proves that during summer and autumn the circuits are the most dispersive and a complete homogenization of the different components is reached; during spring, deuterium excess and chloride activity indicate that the underground flow is essentially non-dispersive.

Unfortunately, the data do not yet suffice to separate quantitatively the spring discharge into snow melt and base-flow component. However, there is a strong indication that the snow melt dominates the systems during the spring

runoff, in agreement with where base flow was in the spring runoff. This in the same manner.

An important observation used in this area to differentiate has been possible because of where the calculated saturation index compared with $4-5\text{‰}$ a

4. CONCLUSIONS

The examples quoted environmental isotope a basin.

The information that such as altitude of recharge with geochemical parameters

Generally the groundwater winter the snow melt occurs isotopic composition of which in this season is a two different types of ground

- (1) A deep one, isotopic base flow;
- (2) A shallow and fast altitude at which snow

The mixing, or at least identifiable by the parallel composition of water.

We gratefully acknowledge the contribution of the manuscript discussions.

runoff, in agreement with the observations in the Baget karst system (Pyrenees) [6], where base flow was an insignificant component of the spring discharge following the spring runoff. This does not signify that all karst systems respond in the same manner.

An important observation in the study is that the deuterium excess can be used in this area to differentiate between different karst circulations. This has been possible because of the increased precision of deuterium and ^{18}O analyses where the calculated standard deviation of deuterium excess at 1σ is $\pm 0.64\text{‰}$, compared with 4–5‰ annual variation.

4. CONCLUSIONS

The examples quoted here demonstrate the complementary nature of environmental isotope and geochemical analyses in hydrological studies of a karst basin.

The information that stable isotopes can provide about the origin of water – such as altitude of recharge and seasonal variation of the input – can be combined with geochemical parameters to help interpret the history of karst groundwaters.

Generally the groundwater flow patterns are short and fast. At the end of winter the snow melt occurs at progressively increasing altitude. Therefore, the isotopic composition of water in springs changes parallel to that of snow melt, which in this season is a major component of spring discharge. There are, in fact, two different types of groundwater circulation:

- (1) A deep one, isotopically and chemically homogeneous, representing the base flow;
- (2) A shallow and faster one, isotopically variable according to the increasing altitude at which snow melt occurs and with a low content of dissolved salts.

The mixing, or at least the contribution of the superficial circulation, is thus identifiable by the parallel, seasonal variation of the isotopic and chemical composition of water.

ACKNOWLEDGEMENTS

We gratefully acknowledge the help of P. Fritz, who assisted in the translation of the manuscript from Italian into English and participated in many discussions.

The manuscript was also critically read by J.Ch. Fontes from the Laboratoire de Géologie Dynamique, Paris; and M. Dray, R. Gonfiantini, B.R. Payne and L. Quijano from the Section of Isotope Hydrology, International Atomic Energy Agency.

REFERENCES

- [1] SUSELLA, G.F., Studio idrogeologico della Val Corsaglia, Thèse Università di Torino (1976).
- [2] CLARKE, M., DUPLESSY, J.C., LEGER, P., LETOLLE, R., VILA, R., ZUPPI, G.M., Adaptation d'un spectromètre de masse à l'analyse isotopique en ligne de l'hydrogène de l'eau et du gaz carbonique des carbonates, *Spectra* 2000, 3 12 (Dec. 1974) 75-79.
- [3] ANON., Standard methods for the examination of water and waste water, American Public Health Association Inc., New York (1967).
- [4] TRUESDELL, A.H., JONES, B.F., WATEQ, a computer programme for calculating chemical equilibria of natural waters, *US Geol. Survey* (May, 1973) 220-464.
- [5] GARRELS, R.M., CHRIST, C.H., *Solutions, Minerals and Equilibria*, Harper and Row, New York (1965).
- [6] FONTES, J.C., *Isotopes du milieu et cycles des eaux naturelles: quelques aspects*, Thèse de doctorat d'État, Paris (1976).
- [7] MOSER, H., STICHLER, W., "Deuterium measurements on snow samples from the Alps" *Isotope Hydrology 1970* (Proc. Symp. Vienna, 1970), IAEA, Vienna (1970) 43.
- [8] CRAIG, H., Isotopic variations in meteoric waters, *Science* 133 (1961) 1833-34.
- [9] NIR, A., Development of isotope methods applied to groundwater hydrology, *Am. Geophys. Union, Monograph* 11 (1967) 109-16.
- [10] JUNGE, C.E., *Airchemistry and Radioactivity*, Academic Press, New York (1963).
- [11] PAYNE, B.R., YURTSEVER, Y., "Environmental isotopes as a hydrogeological tool in Nicaragua", *Isotope Techniques in Groundwater Hydrology 1974* (Proc. Symp. Vienna 1974) I, IAEA, Vienna (1974) 193.
- [12] ZUPPI, G.M., FONTES, J.C., LETOLLE, R., *Isotopes du milieu et circulations d'eaux sulfurées dans le Latium*, *Ibid.*, p.341.

DISCUSSION

E. ERIKSSON (*Chairman*): This paper is of great value in demonstrating the comprehensive use of hydrochemical and environmental isotope applications for difficult problems of karst hydrology.

J.P. MOLINARI: The Bossea spring has a discharge gauge (see caption to Fig.8). Can you say something about the type and extent of variations in flow observed and about how you took these variations into account in collecting representative weekly samples?

G.M. ZUPPI: As shown in Table II, the Bossea spring's discharge shows a constant variation with time during the spring. If one considers the monthly

averages of data from 197 (a characteristic minimal discharge average) and a maximum discharge average), a low summer discharge during the autumn. Discharge more regular as the catchment. So I think that the weekly

J.P. MOLINARI: I would like to know which are generally found in karst which are generally found in karst melting in high Alpine karst

G.M. ZUPPI: Karst discharge during snow melt only if the subject is pronounced climate. In the Bossea karst basin, where you have in mind occurs in karst which is the largest spring with an average discharge of 100 l/s. The hydraulic régime of Bossea (see Ref.[1]). I believe a new study in the future by my colleagues at

H. ZOJER: Your paper shows a relation in precipitation of karst in the southern Alps in an area where no longer the mean residence time is a disadvantage of having mixed karst is overridden, and so in such karst the mean altitude of the recharge is

G.M. ZUPPI: I agree. The study is very useful for studying karst. The mean residence time is long in karst. The large base-flow component is the contribution of superficial karst. The seasonal variation in deuterium in the Apennines the range of δD is from -11.1‰ in winter (G.M. Zuppi) and +11.1‰ in winter (G.M. Zuppi). The same effect in the Venice karst (J. Ch. Fontes, G.M. Zuppi, 1974) in summer and +10.2‰ during winter.

J. MARTINÉC: Have you observed a difference between snow and rain?

averages of data from 1974 onwards, when the limnigraph was started, one notes a characteristic minimal discharge during the winter months (100 litres/s on average) and a maximum discharge at the end of the spring (700 litres/s on average), a low summer discharge can also be detected, as can a certain increase during the autumn. During the spring, the increase in flow becomes more and more regular as the catchment area affected by snow melt becomes smaller. So I think that the weekly samples are in fact highly representative.

J.P. MOLINARI: I was referring to the large and rapid fluctuations in flow which are generally found to occur within a day or a few days when snow is melting in high Alpine karst regions.

G.M. ZUPPI: Karst systems show large and rapid fluctuations in flow during snow melt only if the feeding basin is irregularly oriented and if it is subject to pronounced climatic or microclimatic variations. This is not true of the Bossea karst basin, which has an area of only some 15 km². However, what you have in mind occurs in the Maritime Alps, especially at the Beinette spring, which is the largest spring of the whole Marguaréiz-Mongioie-Mondolé massif, with an average discharge of about 2 m³/s. I have no data at present about the hydraulic régime of Bossea, but such data have been published, at least in part (see Ref. [1]). I believe a more complete description is to be published in the near future by my colleagues at the University of Turin.

H. ZOJER: Your paper shows how important it is to investigate the D/¹⁸O relation in precipitation of different origins. Similar results were obtained by us in the southern Alps in an area on the border between Austria and Italy. The longer the mean residence time of the spring water, the greater becomes the disadvantage of having mixed water of different origins, as the altitude effect is overridden, and so in such cases it is very difficult or even impossible to fix the mean altitude of the recharge area.

G.M. ZUPPI: I agree with you. The seasonal change in deuterium excess is very useful for studying small karst systems. In large karst systems where the mean residence time is longer the meteoric "signal" is completely masked by the large base-flow component, and in fact the nature of the mixing — or at least the contribution of superficial circulation — is not identifiable. Concerning the seasonal variation in deuterium excess (d), I have found that in the Latium Apennines the range of d values in precipitation is between +15.9‰ in summer and +11.1‰ in winter (G.M. Zuppi, unpublished data). I have observed the same effect in the Venice region and in the Dolomites, too (G.C. Bortolami, J. Ch. Fontes, G.M. Zuppi, unpublished data), where the range is +14‰ during summer and +10.2‰ during winter.

J. MARTINEC: Have you found any difference in the isotopic altitude effect between snow and rain?

G.M. ZUPPI: No, we have not. Unfortunately, we sampled the precipitation over two months during which even at the highest altitude all meteoric events were in liquid phase. Since January 1977 my colleagues in Turin have been sampling the precipitation at different elevations, but at present no stable isotope data are available.

ISOTOPE KARST

U. SCHOTT
U. SIEGEN
H. OESCHG

*Physics Inst
University of

**Geological I
University of
Berne, Swit

Abstract

ISOTOPE STUDY IN THE

An isotope study in 1978 the discharge, ^3H , δ springs, which are influenced and autumn, and in the winter in precipitation during recharge time of winter base flow (difference in $\delta^{18}\text{O}$ between recharge areas to be estimated).

GEOLOGY, EXPERIMENTAL

The study area is in the Alps at 1200 to 3250 m and is part of the Helvetic SSE to the main range folds under the Ultrahelvetics (cf. Fig. 2).

About 20% of the rocks are and boulders and 20% are of approximate mean elevation.

A multiple tracer study allowed us to link several karst systems (cf. Fig. 1). Karst was formed secondarily by the faulting.

SUBJ
GCHM
IMA

Contributions to
Mineralogy and
Petrology
© by Springer-Verlag 1977

Contrib. Mineral. Petrol. 59, 227-235 (1977)

JY

ation of C. W. Correns
trophie". Continued
and from Vol. 12 (1966)
beiträge zur Mineralogie

f. A.)

trology and mineralogy
significance of
eir isotopes in the rocks.

efs
stitut der Universität
1, D-3400 Göttingen
f Germany

sted to submit
licate to any editor
cover page 4).

mation
issues each) will appear
her reserves the right
l volumes during the
ormation about obtaining
microform editions
quest.

ept North America).
DM 740,— plus postage
lers can either be placed
aler or sent directly to:
Heidelberger Platz 3,

scription rate: \$315.00.
and handling. Subscrip-
with prepayment only.
addressed to: Springer-
Inc., 175 Fifth Avenue,
010.

h paper are provided
ditional copies may be
rdred.

vertisements:

237, D-1000 Berlin 15,
11, Telex 01-85 411

y by
rei H. Stürtz AG, Würzburg
lag Berlin Heidelberg 1977

Interpretation of Metamorphic Assemblages Containing Fibrolitic Sillimanite

R.H. Vernon and R.H. Flood

School of Earth Sciences, Macquarie University, North Ryde (Sydney), N.S.W. 2113, Australia

Abstract. Microstructural criteria distinguish two types of fibrolitic sillimanite-bearing aggregates, namely: (1) those with fibrolitic sillimanite in clear microstructural equilibrium with the other minerals, and (2) those with fibrolitic sillimanite that appears to have grown without evident modification of pre-existing grain boundaries of the other minerals. However, microstructural criteria rarely permit unambiguous inferences of the relative "timing" of metamorphic reactions producing fibrolitic sillimanite.

Introduction

Fibrolitic sillimanite in many metapelitic rocks has been inferred to have grown after the other, coarser-grained minerals, which has led to interpretations involving relatively late prograde sillimanite-forming reactions and even multiple metamorphic episodes. On the other hand, fibrolitic sillimanite in certain other rocks has been shown to have grown in metamorphic compatibility with the other minerals [1, 2].

In this paper, microstructural relationships between fibrolitic sillimanite and adjacent or enclosing minerals are examined in detail first, applying the principle that grain boundaries tend towards low-energy arrangements [1-3], and then the metamorphic implications are discussed. Microstructural relationships can indicate whether fibrolitic sillimanite grew before or after the final positioning of boundaries between the other mineral grains, although care must be taken in using such inferences to propose metamorphic reactions.

The term "harmonious" is used where the boundaries of other minerals appear to have adjusted to the fibrolitic sillimanite, and the term "disharmonious" is used where no such adjustment is evident. Photomicrographs of "harmonious" relationships have been published elsewhere [2], so that photographic evidence in this paper concentrates on "disharmonious" relationships.

Criteria for "Harmonious" Fibrolitic Sillimanite

The following microstructural relationships favour an interpretation that fibrolitic sillimanite grains were in position before the final positioning of boundaries between the other minerals of the aggregate:

(1) Grain boundaries of minerals without strongly anisotropic atomic structures (e.g., framework silicates) meet prismatic faces of fibrolitic sillimanite at approximately 90° , or are attached to the corners of the elongate sillimanite grains [1, 2].

(2) Low-energy shapes of inclusions [1, 3] (e.g. quartz in feldspar) are modified where their boundaries intersect grains or aggregates of fibrolitic sillimanite [2].

(3) Grain boundaries of coarser-grained minerals are deflected by grains or aggregates of fibrolitic sillimanite. This can cause irregular grain shapes where fibrolitic sillimanite is present, compared with simple polygonal grain shapes where fibrolitic sillimanite is absent, even in the same thin section [2]. The fibrolitic sillimanite can also prevent an increase in the grain size of associated minerals, owing to restriction of grain growth by small fibrous or tabular grains [4].

(4) Twin boundaries, and possibly growth zones, are deflected where they intersect fibrolitic sillimanite. In particular, growth twins [5, 6] might be expected to change thickness at intersections with the sillimanite, and deformation twins [5, 6] might be expected to taper into pre-existing barriers [6], such as sillimanite aggregates. If the twins are of growth origin, the fibrolitic sillimanite grew before the *growth* of the enclosing mineral, but if the twins are of deformation origin, the fibrolitic sillimanite grew only before the *deformation* of the enclosing mineral, and so may still post-date its growth.

(5) Fibrolitic sillimanite occurs as trails of inclusions in larger grains of other minerals, especially where (i) the orientations of the trails are unrelated to the crystallographic orientation of the host mineral (e.g. [7], p. 315; [8], p. 316); (ii) the trails have curved or intricately folded shapes, whereas the host mineral shows no optical evidence of deformation; (iii) the trails pass continuously from one mineral grain to another of different orientation, without deflection of the trails; and (iv) the trails can be traced across many adjacent or separated, diversely oriented grains of the same or different minerals.

Criteria for "Disharmonious" Fibrolitic Sillimanite

The following microstructural relationships favour an interpretation that fibrolitic sillimanite grew after the final positioning of boundaries between the other minerals of the aggregate:

(1) Grain boundaries of other minerals meet prismatic faces of fibrolitic sillimanite at random angles and orientations.

(2) Low-energy shapes of inclusions are unaffected by the presence of fibrolitic sillimanite (Fig. 1a).

(3) Grain boundaries of other minerals are not deflected by fibrolitic sillima-

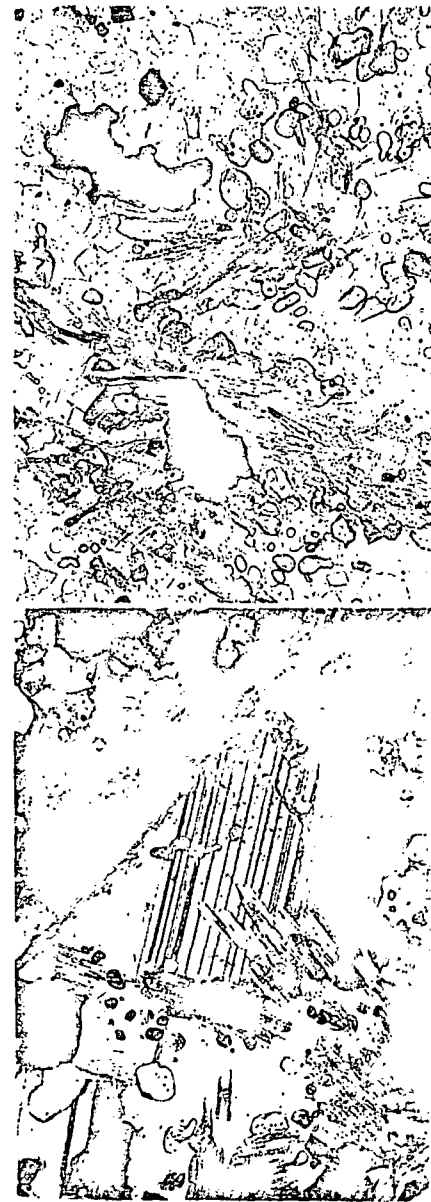


Fig. 1. a Aggregates of fibrolitic sillimanite of andalusite (high relief) and quartz. Quartz N.S.W. Plane-polarized light; base of photo the shapes of which are unaffected by radiation damage as in Figure 1a. Incompletely crossed polars of fibrolitic sillimanite transecting parallel-sided lamellar twins. The boundaries of the twins occur where they intersect the sillimanite. Crossed polars; base of photo 0.8 mm. b The boundaries of polygonal grains of quartz. Plane-polarized light; base of photo 0.8 mm.

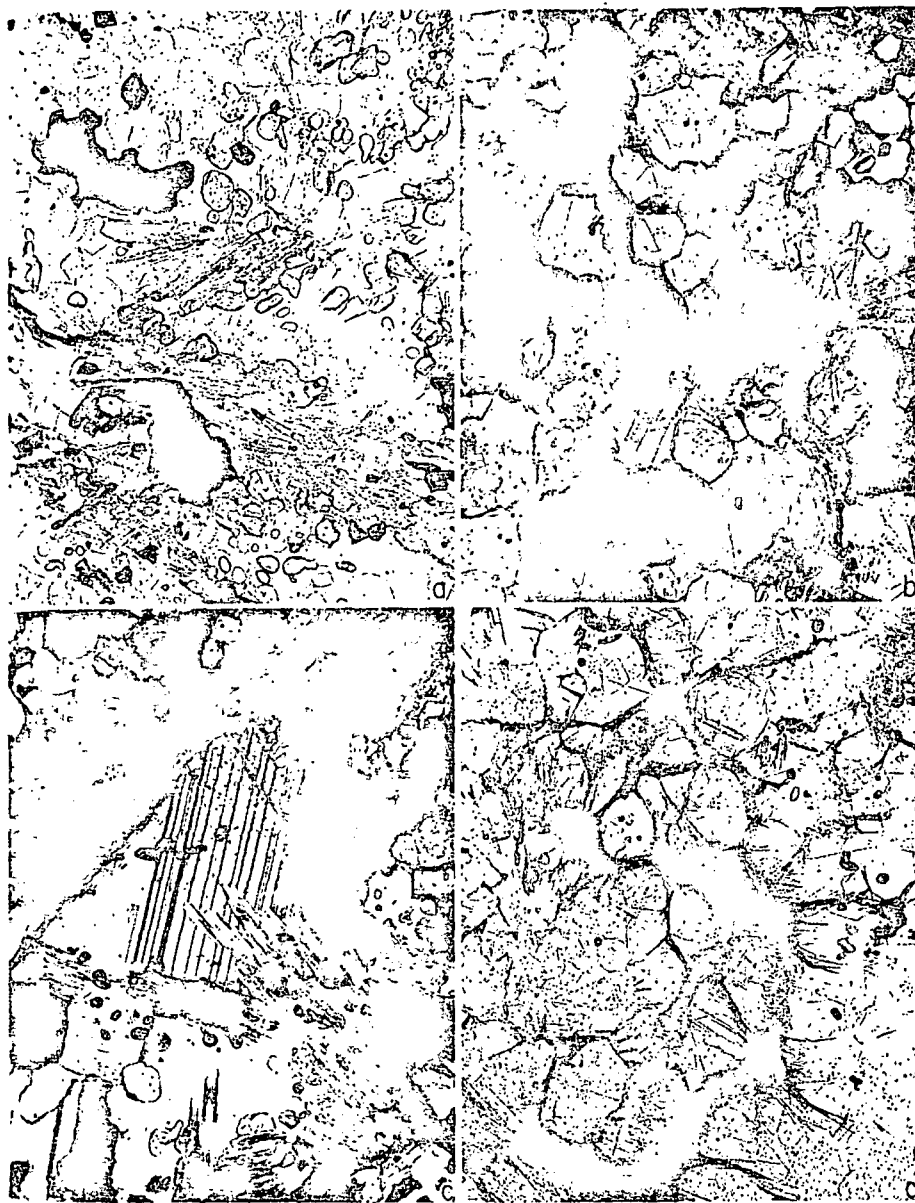


Fig. 1. a Aggregates of fibrolitic sillimanite causing no change of shape of rounded inclusions of andalusite (high relief) and quartz. Quartz-plagioclase-andalusite-sillimanite hornfels, Kentucky, U.S.W. Plane-polarized light; base of photo 0.8 mm. b Polygonal grains of quartz and feldspar, the shapes of which are unaffected by radiating aggregates of fibrolitic sillimanite. Same rock as in Figure 1a. Incompletely crossed polars; base of photo 0.3 mm. c Aggregate of fibrolitic sillimanite transecting parallel-sided lamellar twins in plagioclase. No deflection or change in thickness of the twins occurs where they intersect the fibrolitic sillimanite. Same rock as in Figure 1a. Crossed polars; base of photo 0.8 mm. d Preferential concentration of fibrolitic sillimanite in the boundaries of polygonal grains of quartz and plagioclase. Same rock as in Figure 1a. Plane-polarized-light; base of photo 0.8 mm.

an interpretation that fibrolitic
positioning of boundaries

ngly anisotropic atomic struc-
faces of fibrolitic sillimanite
ers of the elongate sillimanite

quartz in feldspar) are mod-
regates of fibrolitic sillimanite

erals are deflected by grains
cause irregular grain shapes
with simple polygonal grain
in the same thin section [2]
ise in the grain size of associat-
h by small fibrous or tabular

ones, are deflected where they
twins [5, 6] might be expected
anite, and deformations twins
barriers [6], such as sillimanite
the fibrolitic sillimanite grew
f the twins are of deformation
he *deformation* of the enclosing

inclusions in larger grains of
ons of the trails are unrelated
mineral (e.g. [7], p. 315; [8]).
ly folded shapes, whereas the
formation; (iii) the trails pass
of different orientation, without
e traced across many adjacent
ne or different minerals.

ite

ur an interpretation that fibrolitic
f boundaries between the other

set prismatic faces of fibrolitic

deflected by the presence of fibrolitic

ot deflected by fibrolitic sillima-

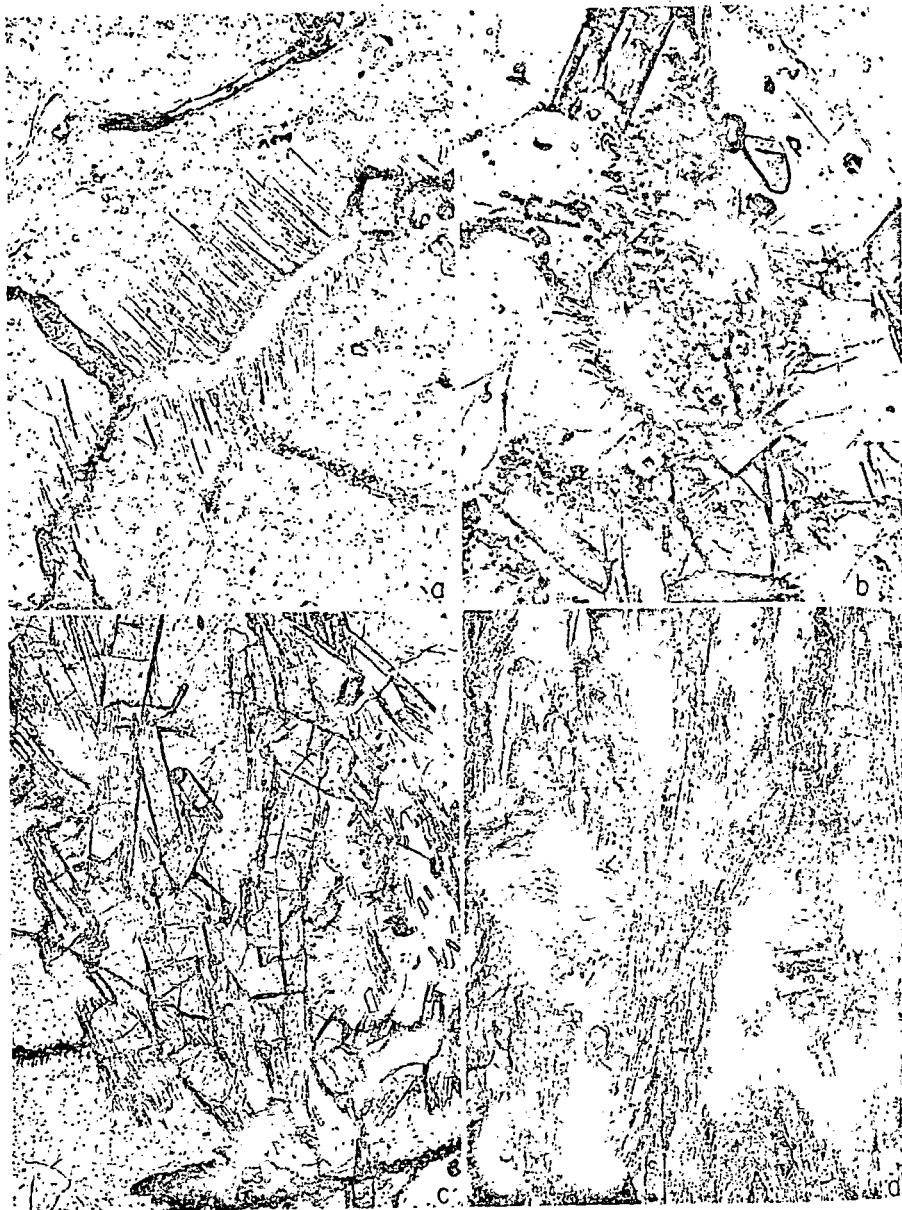


Fig. 2. a Aggregates of parallel and sub-parallel fibres of fibrolitic sillimanite projecting into grain boundaries from a cordierite/cordierite grain boundary. Sillimanite-cordierite-biotite-quartz gneiss, Reynolds Range, central Australia. Plane-polarized light; base of photo 0.3 mm. b Radiating aggregates of fibrolitic sillimanite that nucleated on pre-existing planar garnet/quartz and garnet/feldspar interfaces. Hornfels, Fongen area, Norway. Plane-polarized light; base of photo 0.3 mm. c Relatively large, prismatic grains of sillimanite with terminal fringes of fibrolitic sillimanite. Same rock as in Figure 2b. Plane-polarized light; base of photo 0.8 mm. d Fibrolitic sillimanite occurring in aggregates that are mainly parallel to {001} of larger biotite grains, some being parallel to the rock's foliation (vertical in the photograph) and others lying oblique to the foliation, depending on the orientation of the host biotite. Biotite-sillimanite schist, Pyrenees. Plane-polarized light; base of photo 0.8 mm

Interpretation of Assemblages Containing

nite (Fig. 1b), so that original low-angle foliation (Fig. 1b) even where fibrolitic sillimanite is present. The size of these polygonal grains is often even larger than that in sillimanite.

(4) Twin boundaries are not developed in sillimanite (Fig. 1c), suggesting that the twins (in the mineral itself) pre-date the sillimanite growth or deformation origin.

(5) Fibrolitic sillimanite is commonly associated with other minerals (Fig. 1d), commonly pyroxene. The boundaries (Fig. 2a), radiating aggregates (Fig. 2b), commonly, in parallel orientation to the foliation. For example, Watson ([9], pp. 153-154, p. 818-820) described fibrolitic sillimanite with feldspar boundaries, with some sillimanite fringing biotite ([9], p. 153), Tozer ([7], p. 312), sillimanite fringing biotite. Chinn [10] described sillimanite fringing garnet, as in Figure 2c, where the original grain shapes (in the sillimanite crystal) configurations [1, 3], because of adjacent grains, which would be expected to be parallel to the foliation in the grain boundaries.

(6) Fibrolitic sillimanite occurs in various orientations by pre-existing grain boundaries. (6) Fibrolitic sillimanite occurs in various orientations (p. 290) occurring (i) cutting across grain boundaries, random nucleation and/or growth of sillimanite, (ii) nucleation and/or growth of sillimanite consisting of predominantly parallel aggregates cross a number of different orientations, without deflection.

(7) Fibrolitic sillimanite occurs in various orientations with low-energy grain boundaries. (7) Fibrolitic sillimanite occurs in various orientations with low-energy grain boundaries described aggregates of biotite and sillimanite with prismatic shapes of the garnet crystals.

(8) Fibrolitic sillimanite is commonly associated with other minerals in a way that the two minerals are commonly associated of prograde metamorphic reactions (p. 251-253).

(9) Fibrolitic sillimanite is commonly associated with other minerals for example in kink bands and in various orientations or crossing several grains ([11], p. 111, "strain shadow zones" ([11], p. 111).

Ambiguous Criteria

The following microstructural criteria are used about the relative timing of fi-

ite (Fig. 1b), so that original low-energy, polygonal grain shapes are preserved (Fig. 1b) even where fibrolitic sillimanite is relatively abundant. Furthermore, the size of these polygonal grains in sillimanite-rich areas is the same as or even larger than that in sillimanite-free areas.

(4) Twin boundaries are not deflected where they intersect fibrolitic sillimanite (Fig. 1c), suggesting that the twins (and hence the growth of the twinned mineral itself) pre-date the sillimanite, regardless of whether the twins are of growth or deformation origin.

(5) Fibrolitic sillimanite is concentrated at grain boundaries of enclosing minerals (Fig. 1d), commonly projecting into the grains at a high angle to the boundaries (Fig. 2a), radiating from the boundaries (Fig. 2b), or, less commonly, in parallel orientation to another aluminium silicate mineral (Fig. 2c). For example, Watson ([9], pp. 156, 158), Pitcher ([10], p. 421) and Sturt ([11], p. 818-820) described fibrolitic sillimanite tending to concentrate in quartz or feldspar boundaries, with some projecting into the grains themselves. Watson ([9], p. 153), Tozer ([7], p. 312), and Pitcher ([10], p. 422) described fibrolitic sillimanite fringing biotite. Chinner ([8], p. 314) and Sturt ([11], p. 820) described sillimanite fringing garnet, as in Figure 2b. This is an especially strong criterion where the original grain shapes are of low-energy (e.g. polygonal or rational crystal) configurations [1, 3], because such shapes develop by mutual adjustment of adjacent grains, which would not occur in the presence of fine-grained impurities in the grain boundaries. So, the occurrence of sillimanite is controlled by pre-existing grain boundaries, not *vice versa*.

(6) Fibrolitic sillimanite occurs in markedly radiating aggregates (e.g., [12], p. 290) occurring (i) cutting across the schistosity in foliated rocks (indicating random nucleation and/or growth of sillimanite, in contrast to strongly directional nucleation and/or growth of the other minerals), or (ii) in massive rocks consisting of predominantly polygonal or other low-energy grain shapes. The radiating aggregates cross a number of grains of different minerals and/or different orientations, without deflection.

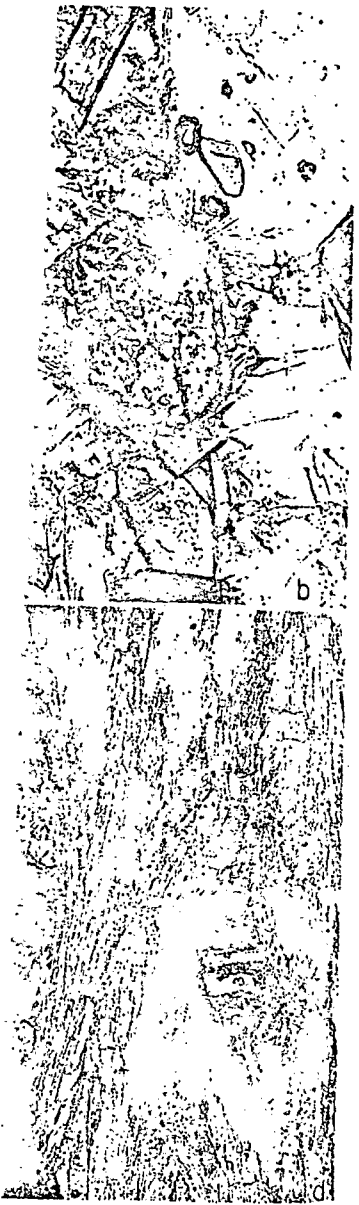
(7) Fibrolitic sillimanite occurs in aggregates demonstrably pseudomorphing minerals with low-energy grain shapes. For example, Guidotti ([13], p. 476) described aggregates of biotite and sillimanite that preserve original dodecahedral shapes of the garnet crystals they replaced.

(8) Fibrolitic sillimanite is intergrown with muscovite or quartz in such a way that the two minerals appear to have grown simultaneously as a result of prograde metamorphic reactions of the type discussed by Carmichael ([14], p. 251-253).

(9) Fibrolitic sillimanite is concentrated in zones of relatively high strain, for example in kink bands in other minerals, in fractures within one grain or crossing several grains ([11], p. 822), and at "boundaries between marked strain shadow zones" ([11], p. 822).

Ambiguous Criteria

The following microstructural relationships have been used to make inferences about the relative timing of fibrolitic sillimanite and the other minerals present,



a. Fibrolitic sillimanite projecting into grains of cordierite-biotite-quartz gneiss. Reynolds photo 0.3 mm. b. Radiating aggregates of sillimanite at garnet/quartz and garnet/feldspar interfaces; base of photo 0.3 mm. c. Relatively parallel fibrolitic sillimanite. Same rock as a. d. Fibrolitic sillimanite occurring in various orientations within grains, some being parallel to the foliation, some being oblique to the foliation, depending on strain shadow zones. Pyrenees. Plane-polarized light.

but they are more ambiguous than the foregoing criteria, and so are considered separately:

(1) Fibrolitic sillimanite occurs as thin veinlets and knots ("faserkiesel"). This is generally interpreted as implying growth of sillimanite after the other minerals, provided that (i) the veinlets transgress the foliation of the rock, with or without side-branches projecting from the transgressive veinlets along the folia ([9], p. 152, 154; [8], p. 313; [10], p. 421); (ii) radiating "sprays" extend out from the veinlets into adjacent minerals; (iii) the foliation ends abruptly against the fibrolitic knots and is not deflected around them ([9], p. 152; [10], p. 422); and (iv) the veinlets cut across individual grains of other minerals, so that parts of grains on each side of the veinlet have matching orientations. In the absence of these specific criteria, it may be impossible to distinguish late-formed veinlets from sillimanite folia or lenses developed in the axial plane of folds.

(2) Fibrolitic sillimanite occurs in bundles of parallel needles, the orientation of which is controlled by the crystallographic orientation of the enclosing mineral. Generally this relationship is taken to imply growth of fibrolitic sillimanite after the enclosing mineral, but simultaneous growth is a possibility. Specific examples are:

(i) Fibrolitic sillimanite is aligned in {001} planes of biotite, regardless of the orientation of the biotite in the rock. For example, Figure 2d shows fibrolitic sillimanite parallel to {001} of biotite grains lying both parallel and perpendicular to the rock's schistosity.

(ii) Fibrolitic sillimanite needles are arranged at angles of 60° or 120° to one another in the cleavage planes of biotite (e.g. [8], p. 313; [15], p. 72), although the arrangement is commonly also irregular to random in the same grain or thin section. The regular arrangement is generally interpreted as resulting from epitaxial nucleation of the sillimanite in the biotite [8], although an interpretation involving simultaneous growth of the two minerals has also been suggested ([14], p. 254). Many writers have interpreted "colour-bleached" biotite as having resulted from advanced stages of replacement of biotite by fibrolitic sillimanite ([7], p. 313; [9], p. 153; [12], p. 267, 268; [16], p. 359, 367; [17], p. 106). However, this appearance of reduced colour absorption may be due merely to a large ratio of sillimanite to biotite, and hence thinner flakes of biotite, rather than to a chemical "bleaching" reaction.

(iii) Watson ([9], p. 156-159) described fibrolitic sillimanite needles arranged at angles of 60° or 90° to one another in feldspar, and also as parallel groups of needles in vein quartz and feldspar, the orientation of the groups being controlled partly by the orientation of the enclosing grains and partly by the local attitude of the wall of the vein.

(iv) Sturt ([11], p. 821) described sillimanite needles arranged parallel to (010), (110) and (001) of enclosing plagioclase.

(3) Fibrolitic sillimanite occurs in "pressure-shadows" or "tails" about augen or porphyroblasts (e.g. [12], p. 288), most interpretations favouring a later growth of the minerals of the "shadows" relative to the porphyroblast, although synchronous growth appears possible, at least in some instances.

(4) Isolated aggregates of fibrolitic sillimanite are intricately folded, whereas

adjacent or enclosing grains show that the sillimanite grew before the final mineral was formed later than the surrounding minerals in the rock escaped deformation to an unknown growth phenomenon. The interpretation is ambiguous, although the latter are intuitively less likely than that

Metamorphic Implications

The relatively unambiguous criterion for fibrolitic sillimanite grew before other mineral grains. Even in low-energy grain shapes, where the orientation of pre-existing grain boundaries is preserved.

Low-energy grain shapes imply that the fibrolitic sillimanite grew before the final adjustment of boundaries. Possible metamorphic explanations are possible.

(1) The fibrolitic sillimanite grew during an earlier metamorphic assemblage.

(2) The fibrolitic sillimanite grew as products of the same reaction as the other minerals, but the boundaries of the fibrolitic sillimanite are the result of adjustment of the more mobile, i.e. the other minerals.

(3) The fibrolitic sillimanite grew after the other minerals underwent recrystallization and the sillimanite. These minerals could be reactants that were stable or metastable in the sillimanite-forming reaction, or (ii) reactants present in the sillimanite-forming reaction, conceivably could have been present at the same time as growth of the fibrolitic sillimanite, (ii) the reaction that released water or

Even where the fibrolitic sillimanite is in such a way that criterion (5) for the sillimanite could have been satisfied by the enclosing mineral, it may well have grown simultaneously with the other minerals.

ria, and so are considered
 and knots ("faserkiesel").
 sillimanite after the other
 the foliation of the rock.
 anagressive veinlets along
 radiating "sprays" extend
 the foliation ends abruptly
 and them ([9], p. 152; [10].
 grains of other minerals.
 ive matching orientations.
 impossible to distinguish
 developed in the axial plane

lled needles, the orientation
 ion of the enclosing miner-
 with of fibrolitic sillimanite
 th is a possibility. Specific

es of biotite, regardless of
 Figure 2d shows fibrolitic
 a parallel and perpendicular

t angles of 60° or 120° to
 o. 313; [15], p. 72), although
 dom in the same grain or
 interpreted as resulting from
], although an interpretation
 ls has also been suggested
 -bleached" biotite as having
 otite by fibrolitic sillimanite
 367; [17], p. 106). However,
 y be due merely to a large
 takes of biotite, rather than

sillimanite needles arranged
 and also as parallel groups
 lation of the groups being
 ng grains and partly by the

eedles arranged parallel to
 hadows" or "tails" about
 interpretations favouring a
 ative to the porphyroblast.
 east in some instances.
 intricately folded, whereas

adjacent or enclosing grains show no optical evidence of deformation, suggesting the sillimanite grew before the final growth of the other minerals. If the sillimanite was formed later than the surrounding or enclosing minerals, the implications are that (i) sillimanite underwent apparent intense folding while the other minerals in the rock escaped deformation ([12], p. 288), (ii) the folding is due to an unknown growth phenomenon ([15], p. 72, 73), (iii) the fibrolitic sillimanite metasomatically replaced previously folded folia of biotite. Therefore, this criterion is ambiguous, although the interpretations involving late-formed sillimanite are intuitively less likely than that involving pre-existing sillimanite.

Metamorphic Implications

The relatively unambiguous criteria discussed above can indicate only whether fibrolitic sillimanite grew before or after the *final positioning of boundaries* between the other mineral grains. Evidently some fibrolite-forming reactions result in low-energy grain shapes, whereas others do not involve significant modification of pre-existing grain boundaries.

Low-energy grain shapes imply that the fibrolitic sillimanite must have existed *before* the final adjustment of boundaries of the other minerals. However, several metamorphic explanations are possible, namely:

(1) The fibrolitic sillimanite grains were stable or metastable relics of an earlier metamorphic assemblage.

(2) The fibrolitic sillimanite and the other minerals grew simultaneously as products of the same reaction. The relatively stable, rational (low-energy) boundaries of the fibrolitic sillimanite grains [2] did not move during the final adjustment of the more mobile, irrational (high-energy) boundaries of the other minerals.

(3) The fibrolitic sillimanite grew after the other minerals, which nevertheless underwent recrystallization and consequent adjustment of their boundaries with the sillimanite. These minerals could have been (i) pre-existing unreactive minerals that were stable or metastable under the conditions of growth of the sillimanite, or (ii) reactants present in excess of the amounts required to participate in the sillimanite-forming reaction. The boundary adjustment of these minerals conceivably could have been promoted by (i) deformation occurring at the same time as growth of the fibrolitic sillimanite and causing recrystallization of the other minerals, (ii) the formation of the sillimanite in a dehydration reaction that released water or hydroxyl to assist grain boundary movement.

Even where the fibrolitic sillimanite occurs as inclusions in other minerals, in such a way that criterion (5) for "harmonious" fibrolitic sillimanite is satisfied, the sillimanite could have belonged to the same assemblage of chemically compatible minerals as the enclosing minerals. Although it may have finished growing before the enclosing minerals completed the adjustment of their boundaries, it may well have grown mimetically in former folded micaceous folia at the same time as the other minerals were growing, eventually to be enclosed by them.

On the other hand, where the microstructures indicate that fibrolitic sillimanite grew after the final positioning of grain boundaries between the other minerals, the metamorphic implication is that the other minerals were not produced in the sillimanite-forming reaction. However, the other minerals were not necessarily unstable with respect to sillimanite. They could have been stable or metastable relics of an earlier metamorphic assemblage, there being insufficient time for them to adjust their boundaries to the fibrolitic sillimanite under the prevailing metamorphic conditions.

Conclusion

Though careful interpretation of microstructural relationships can indicate the time of growth of fibrolitic sillimanite relative to the final adjustment of boundaries of other minerals present, several alternative metamorphic explanations are generally possible. Therefore, caution should be used, first, in making microstructural interpretations (concentrating on relatively unambiguous relationships) and, second, in inferring metamorphic reactions on the basis of microstructural interpretations.

Unless all "harmonious" fibrolitic sillimanite represents pre-existing stable or metastable material, we can say that some fibrolitic sillimanite-forming reactions result in microstructurally well-adjusted aggregates that obliterate pre-existing microstructures, whereas other fibrolitic sillimanite reactions do not involve significant microstructural modification of pre-existing aggregates. The full explanation of this dichotomy of microstructures involving fibrolitic sillimanite is not yet available, but we suggest that microstructurally well-adjusted ("harmonious") aggregates are favoured by one or more of the following conditions, whereas microstructurally non-adjusted ("disharmonious") aggregates are favoured by the absence of one or more of these conditions:

(1) The fibrolitic sillimanite is formed in any reaction other than a polymorphic change from andalusite or kyanite to sillimanite, since other reactions involve other minerals in the rock, and so would promote motion of grain boundaries of these minerals. Even a local metasomatic introduction of aluminium to form sillimanite would involve removal of part of another mineral, although the volume of rock involved might be so small and the replacement so local that most of the grain boundaries between other minerals might not be involved.

(2) The fibrolitic sillimanite is formed in a dehydration reaction, releasing water to assist movement of grain boundaries between other minerals.

(3) Deformation accompanies the growth of the fibrolitic sillimanite, promoting recrystallization of the other minerals.

We hope that our distinction between different types of aggregates involving fibrolitic sillimanite may promote further detailed description and lead to a clearer understanding of the metamorphic significance of the dichotomy of microstructures discussed herein.

Acknowledgements. We thank Dr. D.W. Durney for critically reading the typescript.

References

1. Vernon, R.H.: Microstructures of high-grade granulites. *J. Petrol.* 9, 1-22 (1968)
2. Vernon, R.H.: Microstructural interpretation of granulites. *Mineral. Mag.* 40, 303-306 (1975)
3. Kretz, R.: Interpretation of the shape of fibrolitic sillimanite. *J. Petrol.* 68-94 (1966)
4. Voll, G.: New work on petrofabrics. *Lithol. J.* 1, 1-10 (1966)
5. Vance, J.A.: Polysynthetic twinning in granulites. *Mineral. Mag.* 35, 488-507 (1965)
6. Vernon, R.H.: Plagioclase twins in some granulites. *Mineral. Mag.* 35, 488-507 (1965)
7. Tozer, C.F.: The mode of occurrence of fibrolitic sillimanite. *J. Petrol.* 92, 310-320 (1955)
8. Chinner, G.A.: The origin of sillimanite. *J. Geol.* 56, 1-10 (1948)
9. Watson, J.: Late sillimanite in the migmatites of the granulite facies. *J. Geol.* 56, 1-10 (1948)
10. Pitcher, W.S.: The migmatitic older granulites of the Donegal region. *Philos. Mag. Ser. 7*, 108, 413-441 (1953)
11. Sturt, B.A.: Exsolution during metamorphism. *Mineral. Mag.* 37, 815-832 (1970)
12. Pitcher, W.S., Read, H.H.: Contact metamorphism of the granulites of Donegal, Ireland. *J. Geol.* 60, 1-10 (1952)
13. Guidotti, C.V.: Transition from staurolite to kyanite in pelitic rocks. *Contrib. Mineral. Petrol.* 20, 1-10 (1967)
14. Carmichael, D.M.: On the mechanism of contact metamorphism of pelitic rocks. *Contrib. Mineral. Petrol.* 20, 1-10 (1967)
15. Harte, B., Johnson, M.R.W.: Metamorphism of the granulites of Lethnot, Angus, Scotland. *Scott. J. Geol.* 11, 87-115 (1971)
16. Woodland, B.G.: A petrographic study of the granulites of the northeastern Vermont area. *Am. J. Sci.* 267, 1-10 (1969)
17. Piasecki, M.A.J.: Tectonic and metamorphic evolution of the granulites of Scotland. *Scott. J. Geol.* 11, 87-115 (1971)

Received May 20, 1976 | Accepted September 1976

References

1. Vernon, R.H.: Microstructures of high-grade metamorphic rocks at Broken Hill, Australia. *J. Petrol.* 9, 1-22 (1968)
2. Vernon, R.H.: Microstructural interpretation of some fibrolitic sillimanite aggregates. *Mineral. Mag.* 40, 303-306 (1975)
3. Kretz, R.: Interpretation of the shape of mineral grains in metamorphic rocks. *J. Petrol.* 7, 68-94 (1966)
4. Voll, G.: New work on petrofabrics. *Liverpool & Manchester Geol. J.* 2, 503-567 (1960)
5. Vance, J.A.: Polysynthetic twinning in plagioclase. *Am. Mineralogist* 46, 1097-1119 (1961)
6. Vernon, R.H.: Plagioclase twins in some mafic gneisses from Broken Hill, Australia. *Mineral. Mag.* 35, 488-507 (1965)
7. Tozer, C.F.: The mode of occurrence of sillimanite in the Glen district, Co. Donegal. *Geol. Mag.* 92, 310-320 (1955)
8. Chinner, G.A.: The origin of sillimanite in Glen Clova, Angus. *J. Petrol.* 2, 312-323 (1961)
9. Watson, J.: Late sillimanite in the migmatites of Kildonan, Sutherland. *Geol. Mag.* 85, 149-162 (1948)
10. Pitcher, W.S.: The migmatic older granodiorite of Thorr district, Co. Donegal. *Quart. J. Geol. Soc. Lond.* 108, 413-441 (1953)
11. Sturt, B.A.: Exsolution during metamorphism with particular reference to feldspar solid solutions. *Mineral. Mag.* 37, 815-832 (1970)
12. Pitcher, W.S., Read, H.H.: Contact metamorphism in relation to manner of emplacement of the granites of Donegal, Ireland. *J. Geol.* 71, 261-296 (1963)
13. Guidotti, C.V.: Transition from staurolite to sillimanite zone, Rangeley Quadrangle, Maine. *Geol. Soc. Am. Bull.* 85, 475-490 (1974)
14. Carmichael, D.M.: On the mechanism of prograde metamorphic reactions in quartz-bearing pelitic rocks. *Contrib. Mineral. Petrol.* 20, 244-267 (1969)
15. Harte, B., Johnson, M.R.W.: Metamorphic history of Dalradian rocks in Glens Clova, Esk and Lethnot, Angus, Scotland. *Scott. J. Geol.* 5, 54-80 (1969)
16. Woodland, B.G.: A petrographic study of thermally metamorphosed pelitic rocks in the Burke area, northeastern Vermont. *Am. J. Sci.* 261, 354-375 (1963)
17. Piasecki, M.A.J.: Tectonic and metamorphic history of the Upper Findhorn, Inverness-shire, Scotland. *Scott. J. Geol.* 11, 87-115 (1975)

Received May 20, 1976 | Accepted September 10, 1976

indicate that fibrolitic sillimanite boundaries between the other minerals were not over, the other minerals were They could have been stable assemblage, there being insufficient fibrolitic sillimanite under

relationships can indicate the final adjustment of boundary metamorphic explanations used, first, in making microscopically unambiguous relationships on the basis of microstructural

represents pre-existing stable fibrolitic sillimanite-forming reactions that obliterate pre-existing sillimanite reactions do not of pre-existing aggregates. The reactions involving fibrolitic sillimanite microstructurally well-adjusted or more of the following conditions: "disharmonious") aggregates are conditions:

reaction other than a polymerization, since other reactions would promote motion of granitic somatic introduction of aluminum of part of another mineral. so small and the replacement between other minerals might not

dehydration reaction, releasing between other minerals. fibrolitic sillimanite, promote

types of aggregates involving led description and lead to a significance of the dichotomy of

reading the typescript.

VI.5. LIQUID FRACTIONATION

L. N. Kogarko, I. D. Ryabchikov and H. Sørensen

VI.5.1. Introduction

In a number of igneous provinces differentiation processes, such as fractional crystallization, filter pressing or assimilation, fail to explain the observed serial relationships. Instead the investigators refer to processes involving enrichment in fugitive components, such as gaseous transfer, pneumatolytic, filtrational or diffusional differentiation and thermodiffusion (the Soret effect), or to liquid immiscibility.

Hamilton (1965) has coined the term 'liquid fractionation' in order to describe the processes by which a magma is differentiated into parts of graded or contrasted compositions without involving crystallization of anhydrous minerals. This migration and separation of the components take place in the liquid state by diffusion of mobile components in response to temperature-pressure gradients, by gaseous transfer of volatile material, or by liquid immiscibility (liquation).

These processes may be described under two main headings, pneumatolytic differentiation, resulting in upward migration of volatile constituents towards the apical parts of magma reservoirs, and liquid immiscibility, resulting in a splitting up of the magma during or prior to crystallization.

In cases it may be difficult to distinguish a build-up of volatiles in residual melts due to crystallization of anhydrous minerals from concentration of volatiles brought about by migration of material in the liquid magma.

VI.5.2. Examples of the Application of the Pneumatolytic Differentiation Hypothesis

VI.5.2.1. Volcanic Provinces

In Chapter II.5 pneumatolytic differentiation is invoked to explain the petrology of the

Fitzroy Basin, Western Australia, the Nyiragongo volcanic field, Kivu; and the Roman volcanic province. In Chapter IV.4 this process is considered in order to explain the relations at Mont Dore, and in Cantal, Eifel and Bohemia.

In the Roman volcanic region the first emitted portion of a magma, the most superficial part, is richest in pneumatolytic elements (Locardi and Mitterpergher, 1969, p. 10). This is demonstrated very clearly in the distribution of U and Th and it appears that this effect is best developed in volcanoes fed by magma reservoirs of great vertical extension, as for instance the Vico volcano, while magma chambers of slight vertical extension do not display this phenomenon.

In the Vico complex there is a progressive enrichment in potassium but when pneumatolytic differentiation dominates in the apical part of the magma there is a sharp decrease in potassium which is not balanced by an increase in sodium (Locardi and Mitterpergher, 1967, p. 330). This may be due to a loss of K from the pyromagma and is displayed in low K/Rb ratios and high U/K and Th/K ratios indicating that there is no simultaneous enrichment in K, Rb, U and Th.

Upton (1969, p. 5) has pointed out that in the Midland Valley of Scotland the uprising magma bodies have experienced some form of differentiation such that their upper portions were enriched in silica and alkalis. This process was minimal in the fast rising magmas, which formed the plateau lavas, but more important in slower rising or stagnant magma columns.

VI.5.2.2. Differentiated Sills and Other Intrusions

In differentiated sills and laccoliths there often is a silicified (in tholeiitic intrusions, cf. Hamilton, 1965) or a zeolitized (in alkali basaltic intrusions, cf. Wilshire, 1967) zone

immediately beneath the upper chilled zone. This volatile enrichment is partly caused by a build-up of volatiles in the residual melt, but also by liquid fractionation (Hamilton, 1965; Wilshire, 1967). A famous example is the Shonkin Sag laccolith (Hurlbut and Griggs, 1939; Nash and Wilkinson, 1970) in which the upward increase in the content of volatiles is seen in increasing grain size and zeolite content, and in the change of mafic minerals from olivine-augite to sodic pyroxenes and amphiboles.

In the Gardar province (IV.3)* syenitic and gabbroic rocks are commonly associated within the same dyke fissure. In the giant dykes gabbro is intruded by syenite, in thin dykes the opposite relation is seen. Fractional crystallization cannot alone account for this evolution, but it is suggested that the parent alkali gabbroic magma was split into an upper syenitic and a lower gabbroic part (Bridgwater and Harry, 1968) by means of diffusion of alkalis etc. in the liquid. This differentiation may have taken place during a slow ascend of the magma in the dyke fissure.

The order of succession of the phases of the composite Kûngnât intrusion, the Gardar province (IV.3) suggests an emplacement of magma from an underlying graded magma reservoir consisting of a syenitic top and gabbroic bottom. Each body of syenite in this intrusion displays enrichment in alkalis and volatiles in its upper parts.

This enrichment of volatiles in the uppermost parts of magma bodies has a pronounced influence on the mineralogy and petrochemistry of the intrusions, and also on their internal structures. The density gradients established in this way create stagnant conditions and promote crystallization in the lower parts of the magma body, while crystallization is retarded in the upper parts.

VI.5.3. Mechanism of Pneumatolytic Differentiation

In Chapters I.2.7. and VI.4.1. reference is made to some of the more important papers

* Readers are referred to the relevant Chapters of this book where similarly cited.

discussing the rôle of pneumatolytic differentiation.

As discussed in Chapter VI.4.1, the different authors have reached no unanimous opinion concerning the aggregate state of the volatile components migrating towards the apical parts of magma chambers.

Saether (1948) and Kennedy (1955) emphasized the rôle of diffusion along pressure and temperature gradients resulting in a concentration of gases in the upper parts of magma chambers, characterized by the lower temperatures and pressures, in order to maintain the physico-chemical equilibrium in the magma. Alkalis accompany the volatiles towards the apical parts. The Soret effect is thus not the only cause of differentiation but pressure gradients also provoke diffusion (cf. Wilshire, 1967, p. 153).

The importance of diffusion of volatiles in granitic and granite pegmatitic magmas has been contested by Burnham (1967) and Jahns and Burnham (1969) who point out that the equilibrium water pressure gradients are much smaller than considered by Kennedy (1955) and that this driving force for diffusion of water to establish osmotic equilibrium is thus fairly small.

They favour transportation of volatiles in vapour bubbles rising through the magma. The importance of transportation of material in such high-temperature fluid phases has been demonstrated experimentally, for instance by Orville (1963) and Burnham (1967).

However, Kogarko (Chapter VI.4.2) has pointed out that water is more soluble in syenitic than in granitic magmas and that most volatiles are easily soluble in alkaline or per-alkaline melts. Also granitic melts may dissolve larger quantities of water when they, as demonstrated by Tuttle and Bowen (1958) and Luth and Tuttle (1969), are enriched in sodium or potassium. In these cases crystallization of a granitic melt may take place without separation of a water-rich phase and there may be a continuous passage from granitic melts into water-rich low-temperature liquids.

The authors therefore maintain that liquid fractionation by diffusion of volatile components

in very fluid alkaline and peralkaline melts is an important process in the genesis of alkaline rocks and that a water-rich vapour phase mainly separates from alkaline melts by boiling at near-surface conditions (cf. McCall, 1964 and Locardi and Mittempergher, 1967), or by filter pressing, cf. the Ilimaussaq lujavrites (Sørensen, 1962).

VI.5.4. Examples of the Application of the Liquefaction Hypothesis

Liquid immiscibility has by a number of geologists (e.g. Loewinson-Lessing, 1884, 1935; Fenner, 1948; Holgate, 1954) been recognized as a possible mechanism in the origin of diverse magma types. These investigators suggested that an initially homogeneous silicate melt at a certain stage prior to crystallization splits into two immiscible melts: one approaching rhyolites in composition and the other close to basalts. A number of workers (Afanasiev, ed., 1963) considered some structural features of acid lavas as the results of immiscibility in the liquid state.

Marshall (1914) explained the sequential extrusion of basic, acid and alkaline lavas (including trachytes, phonolites and basanites) within the Cenozoic petrographic provinces of New Zealand by liquation in the essexitic magma of the source reservoir.

The splitting up of alkali basaltic magma into two melts, one of which markedly enriched in water, has been proposed to account for the origin of rounded bodies of analcime trachybasalt in phonolite (Tomkeieff, 1952), for natrolite bearing globules in a picritic sheet at Igdlorssuit, West Greenland (Drever, 1960), and for analcime syenitic ocelli in lamprophyres from the Monteregian alkaline province, Canada (Philpotts and Hodgson, 1968). The relations in the last named example correspond to the common association of nepheline syenite and essexite in this province.

Liquid immiscibility may therefore have played an important petrogenetic rôle in this province (IV.6).

Vugs of primary calcite, analcime and zeolite

in ngurumanite (melteigite with iron-rich mesostasis) may be products of liquid immiscibility (Saggerson and Williams, 1964).

The separation of aqueous-saline liquid solutions immiscible with silicate melts may also take place at the latest stages of crystallization of alkali granites (Roedder and Coombs, 1967).

The formation of immiscible silicate and chloride melts is likely to take place when silicate magma intrudes strata of evaporites (Pavlov and Ryabchikov, 1968). The formation of 'anatectic' salt melts immiscible with alkaline magma at the time of intrusion may be expected at such contacts (cf. Jones and Madsen, 1959).

Analcime-rich spheroids in lujavrites, and 'dense' analcime rocks in naujaite from the Ilimaussaq massif may have originated by separation of two immiscible liquids, one of which extremely rich in water (Sørensen, 1962). An aqueous-saline liquid immiscible with the silicate magma could be separated during the crystallization of agpaitic nepheline syenites. This second liquid phase, depending on the relative enrichment in fluorine, chlorine, or water, could form segregations of respectively villiaumite, sodalite or analcime rocks. Villiaumite is distributed rather irregularly in the Lovozero foyaites forming separate patches, occasionally its content rises to 2-3%. Studies of thin sections suggest that this mineral could crystallize from separate liquids enriched in fluorine, chlorine and water. This is corroborated by the close paragenesis of villiaumite with sodalite and analcime (Fig. 1).

Another possible example of liquid immiscibility in alkaline magma is the formation of carbonatites, which may be correlated with two-liquid equilibria in alkali carbonate-silicate systems. This problem is discussed in detail elsewhere (VI.3; Koster van Groos and Wyllie, 1963, 1966; Wyllie, 1966).

The origin of magnetite (titanomagnetite)-apatite deposits associated with alkali gabbro intrusions is often ascribed to the process of separation of an immiscible liquid. The ore body of magnetite-apatite at Kiruna, Sweden (Geijer, 1931; Asklund, 1949) is made up of magnetite with an admixture of apatite and negligible

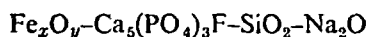
am
po:
cor
ph:

cor
mis
ore
(19
of
ap:
tw:
7
VII
alk
liqu
196
boc
nep
by:
con
urti
al.,



Fig. 1 Villiaumite dark and sodalite (network around villiaumite grains showing 'relief') aggregates in the mesostasis of foyaite from the Lovozero Massif. $\times 30$, 1 nicol

amounts of hornblende. The wall-rocks are porphyries of syenitic and quartz-syenitic composition. Fischer (1950), analyzing the phase-diagram of the system



concluded that experimentally obtained immiscible melts correspond respectively to the ores and wall-rocks (cf. VI.5.5.3). Bogatikov (1966) also demonstrated that the compositions of gabbro-syenites from the Sayans containing apatite-titanomagnetite ores correspond to the two-liquid field.

The Khibina apatite deposits (see IV.2 and VII) may be products of immiscibility in an alkaline magma with the formation of two liquids: silicate and phosphate melts (Ivanova, 1968). The rich apatite deposits form sheet-like bodies along the hanging wall of an apatite-nepheline intrusion. These bodies are underlain by massive urtites. The majority of investigators consider the apatite ores and the underlying urtites to be syngenetic formations (Dudkin *et al.*, 1964; Minakov *et al.*, 1957).

VI.5.5. Experimental Data on Liquid Immiscibility

Liquid immiscibility in silicate-oxide systems (i.e. containing O^{2-} as the only simple anion) was demonstrated experimentally in the classical work of Greig (1927). However, Greig has shown that two liquids may be in equilibrium in these systems only in a rather narrow compositional range, characterized by extremely high concentrations of silica and low amounts of alkalis and alumina. According to Greig (1927) even the most acid of the natural igneous rocks are located outside the immiscibility gap. The compositions of alkaline rocks rich in alkalis and alumina are situated still farther from the two-liquid region.

The addition of volatile components (F, Cl, S, P, etc.) leads to the expansion of the two-liquid regions in silicate systems (Kogarko and Ryabchikov, 1969). This is related to the fact that the dissolution of fugitive constituents in silicate melts results in the replacement of O^{2-} anions by salt-forming anions such as F^- , Cl^- ,

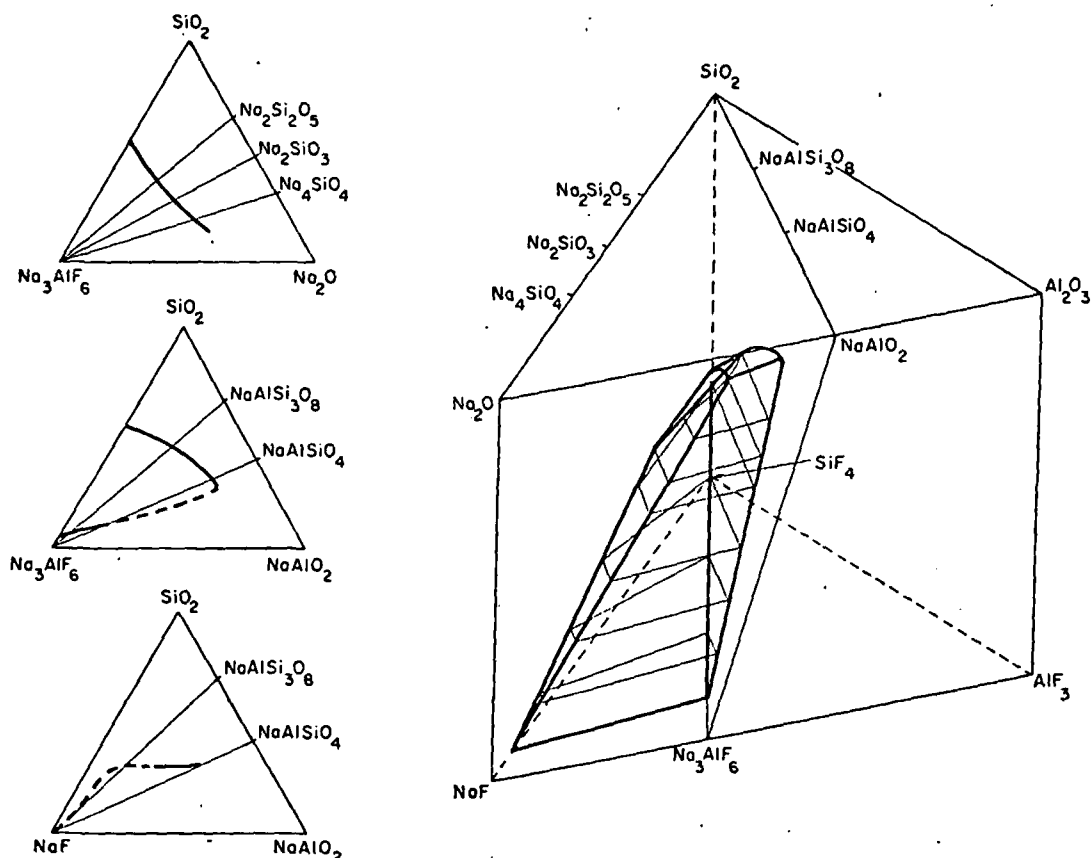
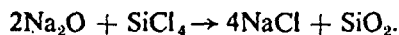


Fig. 2 Tentative diagram of the two liquid region in the system Na, Al, Si|O, F after Kogarko (1967) and Kogarko and Ryabchikov (1969)

S^{2-} , and SO_4^{2-} , which in turn leads to the appearance of exchange equilibria of the type



These equilibria are shifted in such a way that salt-forming anions are bound with basic cations—Na, K, Ca, Mg, etc., while silicon is surrounded by the polarizable oxygen. This leads to a microheterogeneity of the silicate melt, and in the case of strong displacement of equilibria (when ΔG of these reactions is large, see Blander and Topol, 1966) it causes a heterogeneity in a megascopic scale—i.e. two separate melts are formed—one rich in salt components (ionic) and the other rich in silicates (polymerized).

VI.5.5.1. Systems Containing Fluorine

Ol'shansky (1957); Ershova (1957, 1962); Ershova and Ol'shansky (1958) have demonstrated significant increases in the dimensions of the immiscibility gaps in the systems $\text{CaO}-\text{CaF}_2-\text{SiO}_2$, $\text{MgO}-\text{MgF}_2-\text{SiO}_2$, $\text{CaO}-\text{CaF}_2-\text{Al}_2\text{O}_3-\text{AlF}_3-\text{SiO}_2$, etc., as a result of the substitution of oxygen by fluorine. Later it was shown (Kogarko, 1967; Kogarko and Ryabchikov, 1969) that immiscibility exists in the system Na-Al-Si|O-F (Fig. 2). This field of liquid immiscibility includes the petrologically important joins $\text{NaAlSiO}_4-\text{NaF}$, $\text{Na}_3\text{AlF}_6-\text{NaAlSiO}_4$, $\text{Na}_3\text{AlF}_6-\text{NaAlSi}_3\text{O}_8$, $\text{Na}_3\text{AlF}_6-\text{SiO}_2$. The join $\text{NaAlSi}_3\text{O}_8-\text{NaF}$ is probably not far from the critical point of the immiscibility field.

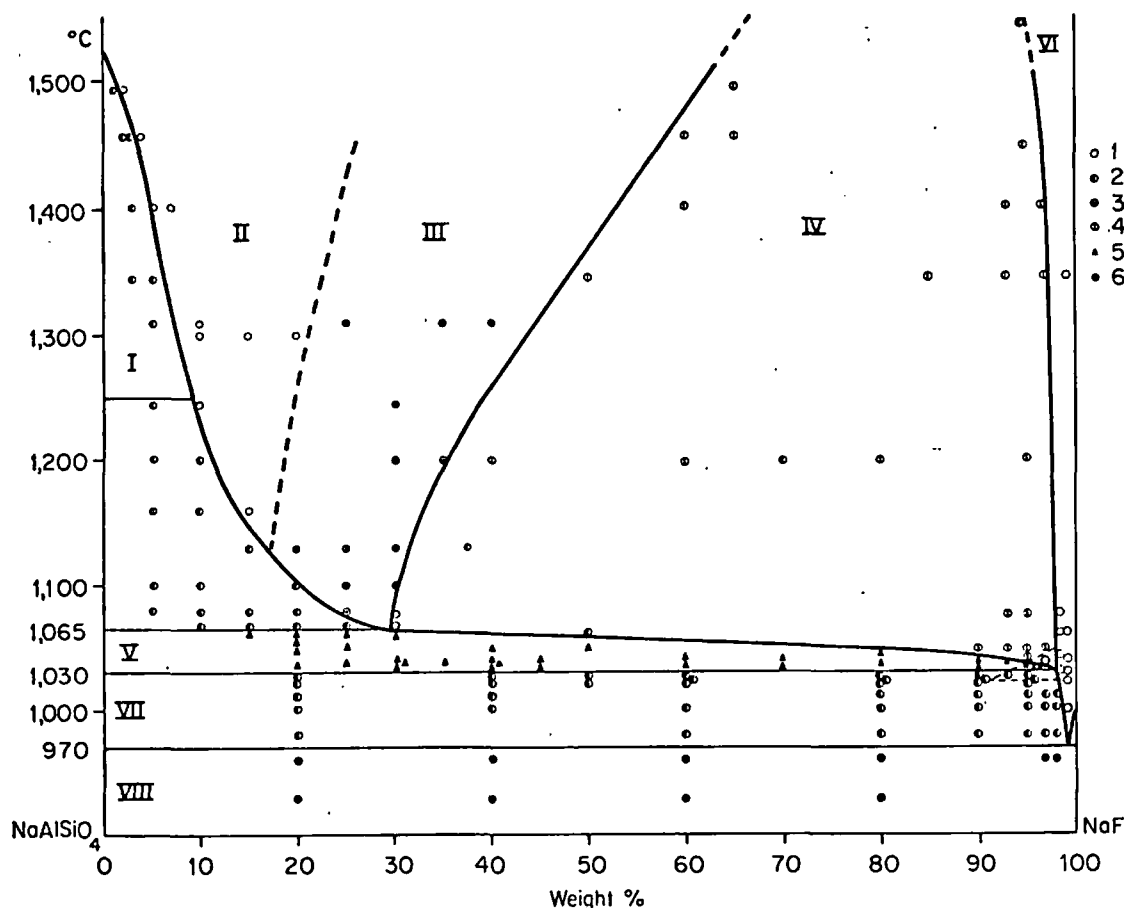


Fig. 3 Phase diagram for the join nepheline-NaF (Kogarko and Krigman, 1970)

- I. nepheline or carnegite and silicate melt;
- II. silicate melt;
- III. liquid immiscibility in microscopic scale;
- IV. two liquids;
- V. two liquids and nepheline;
- VI. fluoride-rich liquid;
- VII. nepheline and fluoride-rich liquid;
- VIII. nepheline and villiaumite;
- △ field of unknown crystalline phase.

(1) homogeneous melt; (2) one crystalline phase + liquid; (3) microliquation; (4) macroliquation; (5) one crystalline phase + two immiscible liquids; (6) below solidus.

In the system $\text{NaAlSi}_3\text{O}_4\text{-NaF}$ (Fig. 3) there is, besides the field of stability of two liquid phases, a field in which nepheline coexists with the two immiscible liquids. This indicates a slightly non-binary behaviour of the join nepheline-NaF.

VI.5.5.2. Systems Containing NaCl

Kotlova *et al.* (1960) established an almost

complete immiscibility of liquids in the system $\text{SiO}_2\text{-NaCl}$. The immiscibility gap in the molten state was shown to extend from this boundary join into the region of considerably more alkalic compositions in the system $\text{NaCl-Na}_2\text{O-Al}_2\text{O}_3\text{-SiO}_2$ (Ryabchikov, 1963). With increasing alkalinity the mutual miscibility of silicate and chloride melts rises, but the addition of even

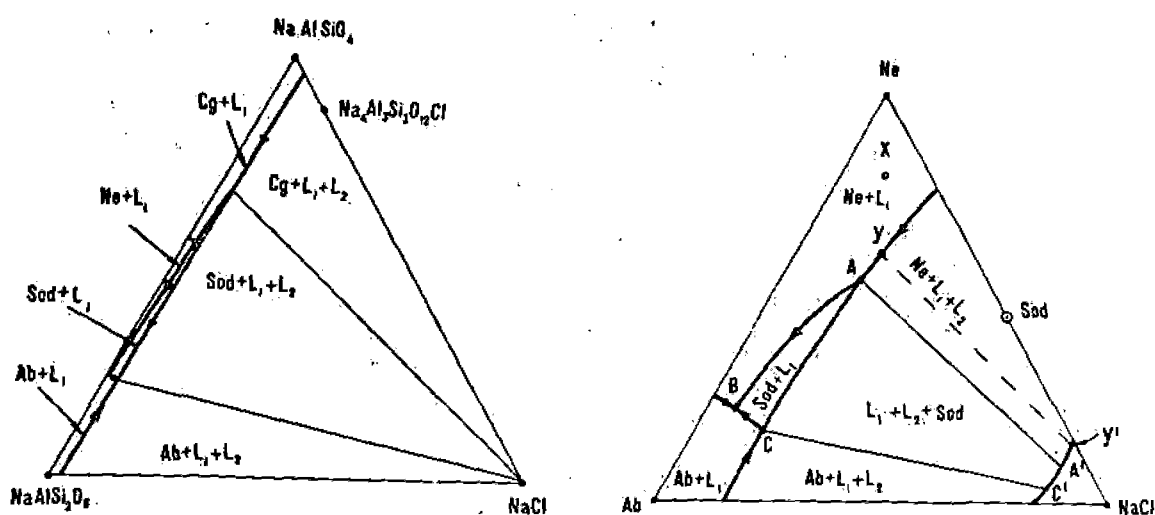


Fig. 4 Tentative phase diagram for the system NaAlSiO_4 - $\text{NaAlSi}_3\text{O}_8$ - NaCl . (a) Semi-quantitative diagram drawn in scale (the composition of the chloride-rich melt coincides with the NaCl corner); (b) Qualitative diagram for the convenience of discussion. The transition nepheline \rightleftharpoons carnegieite is not shown

Legend: Cg = carnegieite; Ne = nepheline; Sod = sodalite; Ab = albite; L_1 = silicate-rich melt; L_2 = chloride-rich melt.

small amounts of NaCl to silicate melts which are close in composition to alkaline magmas leads to the appearance of two immiscible melts. In particular, in the presence of as little as 1% chlorine by weight a melt of natural lujavrite (from the Lovozero massif) splits into two liquids (Pavlov and Ryabchikov, 1968).

The solubility of NaCl in silicate melts in equilibrium with sodium chloride melts in the joins albite- NaCl and the albite + nepheline eutectic- NaCl is within 2-3 wt. % at various temperatures (Ryabchikov, 1963; Koster van Groos and Wyllie, 1969). Even at 1550°C the solubility of NaCl in nepheline melts saturated with respect to sodium chloride melt is only 2.2 wt. % (Kogarko and Ryabchikov, 1969).

VI.5.5.3. Systems Containing Phosphorus, Sulphur or CO_2

Wide fields of immiscibility between melts of almost pure SiO_2 and silicate-phosphate liquids in the system $\text{CaO}-\text{P}_2\text{O}_5-\text{SiO}_2$ were demonstrated by the experiments of Trömel (1943). The immiscibility of fused calcium phosphate and

ferrous oxide in the system $\text{CaO}-\text{FeO}-\text{P}_2\text{O}_5$ was reported by Olsen and Metz (1945-46). Fischer (1950) continued the investigation of iron oxide-phosphate systems. He found an extensive two-liquid field in the system $\text{Fe}_2\text{O}_3-\text{Ca}_3(\text{PO}_4)_2-\text{F}$, which is closer to natural compositions.

In the system $\text{Na}_2\text{O}-\text{SiO}_2-\text{Ca}_3(\text{PO}_4)_2-\text{Al}_2\text{O}_3$ investigated by Melentiev and Ol'shansky (1952) the liquid immiscibility field includes the petrologically important joins: $\text{Ca}_3(\text{PO}_4)_2$ -albite, the albite + silica eutectic- $\text{Ca}_3(\text{PO}_4)_2$, and nepheline + albite eutectic- $\text{Ca}_3(\text{PO}_4)_2$. With increase in the contents of alumina and sodium oxide the immiscibility gap contracts (Fig. 5).

Numerous silicate-sulphide mixtures give two liquids after melting. These systems are reviewed by Ol'shansky (1950), Smith (1961) and MacLean (1969).

The equilibrium of two liquid phases (silicate and carbonate) was also observed at elevated pressures and temperatures in the system $\text{Na}_2\text{O}-\text{CaO}-\text{Al}_2\text{O}_3-\text{SiO}_2-\text{CO}_2-\text{H}_2\text{O}$ (VI.3; Koster van Groos and Wyllie, 1963, 1965, 1966; Koster van Groos, 1966).

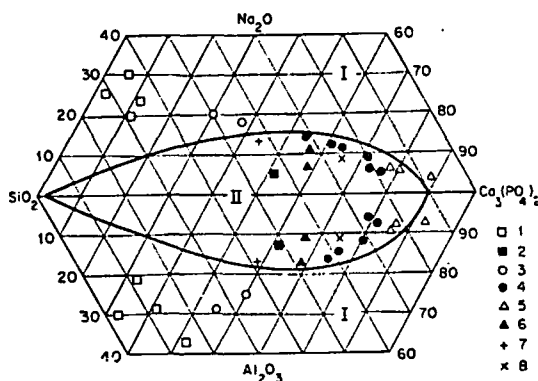


Fig. 5 The two-liquid field in the system $\text{Na}_2\text{O}-\text{Al}_2\text{O}_3-\text{SiO}_2-\text{Ca}_3(\text{PO}_4)_2$ (after Melentiev and Ol'shansky, 1952) with the plotted compositions of various rocks from the Khibina apatite deposit after Dudkin *et al.*, 1964)

I—one liquid; II—two melts; (1) ijolite-urtite; (2) apatite ijolite; (3) reticular apatite-nepheline rocks; (4) lense-like and banded apatite-nepheline rocks; (5) spotted nepheline-apatite rocks; (6) lense-like and banded apatite-titanite-nepheline rocks; (7) spotted apatite-nepheline rock from the Poach-Vumchorr deposit; (8) banded rock from the same deposit.

VI.5.5.4. Systems Containing Aqueous Salt Solutions

Tuttle and Friedman (1948) and Friedman (1951) described equilibria of two immiscible liquids (silicate-rich and water-rich) and vapour in the systems $\text{Na}_2\text{O}-\text{SiO}_2-\text{H}_2\text{O}$ and $\text{Na}_2\text{O}-\text{Al}_2\text{O}_3-\text{SiO}_2-\text{H}_2\text{O}$. The appearance of such equilibria in these systems is due to the considerable decrease of silicate liquidus temperatures caused by the addition of water. Above certain critical temperatures (*c.* 390 °C in the experiments of Tuttle and Friedman) aqueous liquid and gas phases become identical.

An analogous situation arises in systems containing silicates, salts and water at much higher temperatures and pressures, because in the presence of salts the region of coexistence of gaseous and liquid aqueous phases extends to higher parameters than for pure water (*i.e.* addition of salt results in the rise of critical temperatures and pressures, Sourirajan and Kennedy, 1962; Ravich, 1966). With decreasing water content the equilibrium silicate

melt + aqueous saline solution may gradually merge into equilibria of silicate melt + salt melt in boundary systems of silicates-salts.

Due to the immiscibility between silicate melts and concentrated aqueous saline solutions the systems silicate-salt-water must below certain pressures be characterized by the presence of univariant phase assemblages including crystalline silicates, silicate melt, aqueous saline liquid, and gas. This problem is discussed in detail elsewhere (Koster van Groos and Wyllie, 1969; Ryabchikov, 1967).

VI.5.6. Discussion of the Petrological Importance of Liquid Immiscibility

From the brief survey of experimental data for silicate systems displaying immiscibility in the molten state one may conclude that the substitution of the O^{2-} of the silicate melt by such acid anions as F^- , Cl^- , PO_4^{3-} , CO_3^{2-} , SO_4^{2-} , etc. may lead to the formation of immiscible liquids. As has been pointed out in Chapter VI.4, alkaline rocks are characterized by maximum abundances of F, Cl, S and other volatiles. However, the concentrations of volatiles are not sufficient for the separation of liquid phases prior to crystallization. During the crystallization of alkaline magmas the concentrations of volatile components are continuously increasing and the conditions of the separation of immiscible liquid may be realized.

VI.5.6.1. Sodalite Rocks

Among silicate-salt systems the most extensive two-liquid fields are characteristic for the silicate-chloride systems.

The maximum abundance of chlorine is reached in certain varieties of peralkaline nepheline syenites: tawites and poikilitic sodalite syenites from the Lovozero massif, Kola Peninsula (IV.2; Gerasimovsky *et al.*, 1966), naujaites from the Ilimaussaq massif, Greenland (IV.3; Gerasimovsky, 1969). They contain in average about 2.3% of chlorine and sometimes up to 5%. These compositions fall into the two-liquid regions of the experimentally examined systems.

Polyakov and Kostetskaya (1965) suggested on the basis of geological data that the sodalite-rich rocks and the lujavrites of the Lovozero massif were products of two immiscible liquids (cf. IV.2). We shall consider this hypothesis in the light of physico-chemical and geochemical evidence.

For this purpose we constructed the semi-quantitative melting diagram (Fig. 4) for the system $\text{NaAlSi}_3\text{O}_8$ - $\text{NaAlSi}_3\text{O}_8$ - NaCl based upon the experimental data of Koster van Groos (1966), Wellman (1968) and Kogarko and Ryabchikov (1969). The topology of the more complicated phase diagram $(\text{Na}, \text{K})\text{AlSi}_3\text{O}_8$ - $(\text{K}, \text{Na})\text{AlSi}_3\text{O}_8$ - $(\text{Na}, \text{K})\text{Cl}$, more closely corresponding to natural magmas, must be similar. According to this diagram crystallization of certain compositions situated in the field of primary carnegieite (or nepheline under hydrous conditions) will result in the separation of the second chloride-rich liquid phase before any sodalite crystals appear. This liquid is in equilibrium with silicate melt and nepheline crystals. The chloride-rich liquid will either be disseminated in the mixture of silicate melt and crystals or ascend and accumulate in structurally favourable parts of the magma chamber. With further cooling the primary nepheline will react with the chloride-rich liquid under the formation of sodalite. This results in the consumption of the chloride-rich liquid in the major part of the intrusion, while near the places where the chloride-rich liquid is accumulated the crystals of nepheline will disappear. The crystallization of this system is discussed in more detail elsewhere (Kogarko and Ryabchikov, 1969). The residual chloride-rich liquid (if it is preserved) has an extremely low viscosity, it may migrate to places where nepheline is present and be responsible for the metasomatic sodalitization of the latter.

This scheme based upon a tentative phase diagram fits many features of the natural systems: the presence of both primary and metasomatic sodalite and the occurrence of irregularly shaped bodies of sodalite-rich rocks surrounded by lujavrites with lesser amounts of sodalite in the Lovozero massif. These sodalite-rich bodies

may be products of the interaction of NaCl-rich liquid with nepheline and silicate melt near spots of accumulation of the chloride-rich liquid (Kogarko and Ryabchikov, 1969). The data on the distribution of Cl and Br among the poikilitic sodalite-syenite and the surrounding lujavrite of the Lovozero massif corroborates the hypothesis on the leading rôle of liquid immiscibility in the origin of the sodalite-rich bodies (Kogarko and Gulyaeva, 1965).

The poikilitic sodalite syenites of the Ilmaussaq intrusion (naujaites, cf. II.2.2.5) are nearly identical to those of Lovozero. It should, however, be pointed out that all investigators of the Ilmaussaq intrusion favour the view that the naujaites, which form a zone several hundred metres thick in the upper part of this intrusion, are flotation cumulates formed by flotation of sodalite crystals in a very fluid gas-rich magma. This interpretation is in agreement with field, as well as experimental evidence (Sørensen, 1969). It may for instance be pointed out that the naujaite upwards grades into sodalite fôyaite having interstitial sodalite and that it is intruded by the clearly younger lujavrite. Sørensen (1970) has therefore pointed at the possibility that the Lovozero naujaites similarly may, originally, have formed a continuous upper zone which is now partly engulfed by lujavrites.

Sulphide deposits, whose genesis is ascribed to the formation of immiscible sulphide melts, are not related to alkaline magmas: they occur with basic-ultrabasic complexes. However, the presence of S^{2-} alongside with Cl^- in agpaitic nepheline syenites may contribute to the formation of a second immiscible liquid in the case of sodalite-rich rocks which contain significant concentrations of S^{2-} (0.16 wt. %) as contrasted with the surrounding lujavrites (0.08 wt. %) (Gerasimovsky *et al.*, 1966).

VI.5.6.2. Fluorine-Rich Nepheline Syenites

Experimental factual knowledge shows that fluorine expands the two-liquid fields in silicate systems, though to a lesser degree than chlorine. Agpaitic nepheline syenites (Lovozero, Ilmaussaq, Islands of Los) contain exceptional

high c
tinuous
Accord
(taken
and' fel
% of N
When
the syst
ticular
may de
positio
immisci
knowle
ditions

VI.5.6.3

Duck
positio
Khibina
on the
 SiO_2 -A
compos
phosph
region
rich ore
the lin
immisci
cluded,
of ores
second
melting
are alm
hypothe
Our
 H_2O (K
ligible l

Afanasic
liquati
Ac. Sc
Asklund
tion. C
Blander,
of ph
system

high concentrations of fluorine, which continuously rise to the end of crystallization. According to our estimates the residual melt (taken as mesostasis among euhedral nepheline and feldspar) may have contained above 30 wt. % of NaF.

When comparing this value with the data from the system $\text{Na}_2\text{O}-\text{Al}_2\text{O}_3-\text{SiO}_2-\text{NaF}$ and in particular the join nepheline-NaF (cf. VI.5.5.1), one may deduce that under dry conditions the composition of the residual melt is close to the immiscibility gap. (Unfortunately, a detailed knowledge of this system under hydrous conditions is still absent.)

VI.5.6.3. The Apatite-Nepheline Ores of Khibina

Dudkin *et al.* (1964) have plotted the compositions of the apatite-nepheline ores of Khibina (cf. VI.5.4) and the underlying urtites on the melting diagram of the system $\text{Na}_2\text{O}-\text{SiO}_2-\text{Al}_2\text{O}_3-\text{Ca}_3(\text{PO}_4)_2$ (cf. VI.5.5.3). The bulk compositions of numerous ores (silicate + phosphate components) fall into the two-liquid region (Fig. 5). The compositions of the very rich ores and the underlying urtites fall beyond the limits of the experimentally determined immiscibility gap. Hence Dudkin *et al.*, concluded, that the major process in the formation of ores was the separation of an immiscible second liquid. However, the extraordinary high melting points of F-apatite—1650 °C (rich ores are almost monomineralic apatite)—makes this hypothesis less plausible.

Our data on the system apatite-nepheline- H_2O (Kogarko and Lebedev, 1968) show negligible lowering of the apatite liquidus by the

addition of nepheline and by increase in water vapour pressure. There is no basis for assuming that the melting temperatures of the apatite-nepheline rocks were significantly suppressed by the presence of sodium chloride or sodium fluoride, because villiaumite and sodalite are scarce in these rocks. Due to the very extensive field of crystallization of primary apatite (Kogarko and Lebedev, 1968; Kogarko, 1971) only rather high concentrations of NaF and NaCl may noticeably lower the liquidus temperature of apatite.

VI.5.6.4. Conclusions

The students of alkaline igneous provinces often have to invoke pneumatolytic differentiation in order to explain the geological relations observed in the field, and the geochemical trends observed in the laboratory. As most volatiles, including water, are easily soluble in alkaline and peralkaline melts, processes involving migration of volatiles along pressure and temperature gradients in alkaline magmas are likely to be of petrological importance.

The separation by liquation is, however, not likely to be an important factor in the genesis of alkaline magmas. However, at the late stages of crystallization of alkaline magmas the separation of a second immiscible liquid is possible, which consists predominantly of salts and volatile components. This liquid phase differs profoundly in its chemistry from silicate melts, and its crystallization or metasomatic action on the earlier solidified minerals will consequently lead to the appearance of exotic rocks, such as carbonatites, apatite-magnetite ores, sodalite and analcime rocks, and agpaite nepheline syenites strongly enriched in villiaumite.

VI.5. REFERENCES

- Afanasiev, G. D., ed., 1963. Petrographic criteria of liquation in acid lavas (in Russian). *Trudy IGEM Ac. Sci. USSR*, 90, 1-99.
- Asklund, B., 1949. Apatitjärnmalmernas differentiation. *Geol. För. Stockh. Förh.*, 71, 127-76.
- Blander, M., and Topol, L. E., 1966. The topology of phase diagrams of reciprocal molten salt systems. *Inorg. Chem.*, 5, 1641-5.
- Bogatikov, O. A., 1966. *Petrology and Metallogeny of Gabbro-Syenite Complexes from the Altai-Sayan Region* (in Russian). Izd. Nauka, Moscow, 240 pp.
- Bridgwater, D., and Harry, W. T., 1968. Anorthosite xenoliths and plagioclase megacrysts in Precambrian intrusions of South Greenland. *Meddr. Gronland*, 185, 2, 1-66.

- Burnham, C. W., 1967. 'Hydrothermal fluids at the magmatic stage', in Barnes, H. Ed. *Geochemistry of Hydrothermal Ore Deposits*, 36-76. Holt, Reinhart and Winston, Inc.
- Drever, H. I., 1960. Immiscibility in the picritic intrusion at Igdlorssuit, West Greenland. *Rep. 21st Int. Geol. Congr. Norden*, 13, 47-58.
- Dudkin, O. B., Kozyreva, L. V., and Pomerantseva, N. G., 1964. *The Mineralogy of the Apatite Deposits from the Khibina Tundras* (in Russian). Nauka, Moscow and Leningrad, 235 pp.
- Ershova, Z. P., 1957. The equilibrium of two immiscible liquids in systems of the type $\text{MeF}_2\text{-Al}_2\text{O}_3\text{-SiO}_2$ (in Russian, English summary). *Geokhimiya*, 296-303.
- Ershova, Z. P., 1962. Some regularities of immiscibility in fluor-silicate melts (in Russian). *Trudy VI Soveshchaniya po Experimental'noy Tekhnicheskoy Mineralogii i Petrographii*, Moscow, 176-8.
- Ershova, Z. P., and Ol'shansky, Ya. I., 1957. Equilibrium of two liquids in systems of the type $\text{MeF}_2\text{-MeO-SiO}_2$ (in Russian, English summary). *Geokhimiya*, 214-21.
- Ershova, Z. P., and Ol'shansky, Ya. I., 1958. Equilibrium of two liquid phases in fluor-silicate systems, containing alkaline metals (in Russian, English summary). *Geokhimiya*, 144-54.
- Eugster, H. P., and Prostka, H. J., 1960. Synthetic scapolites (Abs.). *Bull. geol. Soc. Am.*, 51, 1859.
- Fenner, C. N., 1948. Immiscibility of igneous magmas. *Am. J. Sci.*, 246, 465-502.
- Fischer, R., 1950. Entmischungen in Schmelzen aus Schwermetalloxyden, Silikaten und Phosphaten, Ihre geochemische und Lagerstättenkundliche Bedeutung. *Neues Jb. Miner.*, 81, 315-64.
- Friedman, I. I., 1951. Some aspects of the system $\text{H}_2\text{O-Na}_2\text{O-SiO}_2\text{-Al}_2\text{O}_3$. *J. Geol.*, 59, 19-31.
- Geijer, P., 1931. The iron ores of the Kiruna type, geographical distribution, geological characters and origin. *Sver. Geol. Unders.*, 367.
- Gerasimovsky, V. I., 1969. *Geochemistry of the Ilmaussaq Massif*. Izd. 'Nauka', Moscow, 174 pp. (in Russian).
- Gerasimovsky, V. I., Volkov, V. P., Kogarko, L. N., Polyakov, A. I., Saprykina, T. V., and Balashov, Yu. A., 1966. *The Geochemistry of Lovozero Alkaline Massif* (in Russian). Izd. Nauka, Moscow, 393 pp.
- Greig, J. W., 1927. Immiscibility in silicate melts. *Am. J. Sci.*, ser. 5, 13, 1-44, 133-54.
- Hamilton, W., 1955. Diabase sheets of the Taylor Glacier region Victoria Land, Antarctica. *Prof. Pap. U.S. geol. Surv.*, 456-B, 1-71.
- Holgate, N., 1954. The role of igneous immiscibility in igneous petrogenesis. *J. Geol.*, 62, 439-80.
- Hurlbut, C. S., jr., and Griggs, D., 1939. Igneous rocks of the Highwood Mountains, Montana. Part I. The laccoliths. *Bull. geol. Soc. Am.*, 50, 1043-112.
- Ivanova, T. N., 1968. The results of long-term investigation of apatite ores and the tasks for further studies, in *Geological Structure, Development, and Ore-Resources of Kola Peninsula* (in Russian). Kol. Filial AN SSSR, Apatity, 86-96.
- Jahns, R. H., and Burnham, C. W., 1969. Experimental studies of pegmatite genesis: I. A model for the derivation and crystallization of granitic pegmatites. *Econ. Geol.*, 64, 843-63.
- Jones, C. L., and Madsen, B. M., 1959. Observations on igneous intrusions in late Permian evaporites, south eastern New Mexico. *Bull. geol. Soc. Am.*, 70, 1625-6.
- Kennedy, G. C., 1955. 'Some aspects of the role of water in rock melts', in Poldervaart, A., Ed., *Crust of the Earth—a Symposium. Spec. Pap. geol. Soc. Am.*, 62, 489-503.
- Kogarko, L. N., 1967. The field of immiscibility in the system Na, Al, Si/O, F (in Russian). *Dokl. AN SSSR*, 176, 918-20.
- Kogarko, L. N., 1971. Phase equilibria in the system nepheline-fluor-apatite (in Russian, English summary). *Geokhimiya*, 160-8.
- Kogarko, L. N., and Gulyaeva, L. A., 1965. Geochemistry of halogens in alkaline rocks on the example of Lovozero Massif (Kola Peninsula) (in Russian, English summary). *Geokhimiya*, 1011-23.
- Kogarko, L. N., and Krigman, L. D., 1970. Phase equilibria in the system nepheline-sodium fluoride (in Russian, English summary). *Geokhimiya*, 162-7.
- Kogarko, L. N., and Lebedev, E. B., 1968. Equilibria in the system nepheline-apatite-water (in Russian). *Geokhimiya*, 375-7.
- Kogarko, L. N., and Ryabchikov, I. D., 1969. Peculiarities of differentiation of alkaline magmas rich in volatiles (in Russian, English summary). *Geokhimiya*, 1439-50.
- Koster van Groos, A. F., 1966. *The effect of NaF, NaCl, and Na₂CO₃ on the phase relationships in selected joins of the system Na₂O-CaO-Al₂O₃-SiO₂-H₂O at elevated temperatures and pressures*. Ph.D. Thesis, Leiden.
- Koster van Groos, A. F., and Wyllie, P. J., 1963. Experimental data bearing on the role of liquid immiscibility in the genesis of carbonatites. *Nature*, 4895, 801-2.
- Koster van Groos, A. F., and Wyllie, P. J., 1965. The system $\text{NaAlSi}_3\text{O}_8\text{-NaCl-H}_2\text{O}$ at 1 kb pressure (Abstract): *Trans. Am. Geophys. Un.*, 46, 179-80.
- Koster van Groos, A. F., and Wyllie, P. J., 1966. Liquid immiscibility in the system $\text{Na}_2\text{O-Al}_2\text{O}_3\text{-SiO}_2\text{-CO}_2$ at pressures to 1 kilobar. *Am. J. Sci.*, 264, 234-55.
- Koster van Melting NaCl-H₂O logical Kotlova, A. I., 1. bility in Russian Locardi, E ship bel process Locardi, meaning recent 33, 1-1. Loewinson Jalguba Mitt., 6 Loewinson of diffi Yalgub Trav. I. Luth, W. vapour granite vaart N 115, 51 McCall, C Rundsc. MacLean the F applica Marshall, Head, Melentiev Equilib Na₂O- AN SS Minakov, M. M. evoluti Khibin. summa Nash, W. Sag lac estimat and sil 241-69 Olsen, W des TI 19, 111 Ol'shanski investit Russian 36, 12- Ol'shanski liquid (in Rus

- Koster van Groos, A. F., and Wyllie, P. J., 1969. Melting relationships in the system $\text{NaAlSi}_3\text{O}_8$ - NaCl - H_2O at one kilobar pressure with petrological applications, *J. Geol.*, **77**, 581-605.
- Kotlova, A. G., Ol'shansky, Ya. I., and Tsvetkov, A. I., 1960. Some regularities of liquid immiscibility in binary silicate and borate systems (in Russian). *Trudy IGEM*, **42**, 3-20.
- Locardi, E., and Mittempergher, M., 1967. Relationship between some trace elements and magmatic processes. *Geol. Rundschau*, **57**, 313-34.
- Locardi, E., and Mittempergher, M., 1969. The meaning of magmatic differentiation in some recent volcanoes of Central Italy. *Bull. volcan.*, **33**, 1-12.
- Loewinson-Lessing, F., 1884. Die Variolite von Jalguba im Gouvernement Olonez. *Tsch. Min. Pet. Mitt.*, **6**, 281-300.
- Loewinson-Lessing, F. J., 1935. On a peculiar type of differentiation represented by variolites of Yalguba, Karelia (in Russian, English summary). *Trav. Instn. Petr. Ac. Sci. USSR*, **5**, 21-7.
- Luth, W. C., and Tuttle, O. F., 1969. 'The hydrous vapour phase in equilibrium with granite and granite magmas', in Larsen, L. H., Ed., Poldervaart Memorial volume, *Geol. Soc. Amer. Mem.*, **115**, 513-48.
- McCall, G. J. H., 1964. Froth flows in Kenya. *Geol. Rundschau*, **54**, 1148-95.
- MacLean, W. H., 1969. Liquidus phase relations in the FeS - FeO - Fe_3O_4 - SiO_2 system and their application to geology. *Econ. Geol.*, **64**, 865-84.
- Marshall, P., 1914. The sequence of lavas at North Head, Otago. *Q. J. Geol. Soc.*, **70**, 382-406.
- Melentiev, B. N., and Ol'shansky, Ya. I., 1952. Equilibrium of immiscible liquids in the system Na_2O - Al_2O_3 - SiO_2 - $\text{Ca}_3(\text{PO}_4)_2$ (in Russian). *Dokl. AN SSSR*, **86**, 1125-8.
- Minakov, F. V., Kamenev, E. A., and Kalinkin, M. M., 1967. On the original composition and evolution of the ijolite-urtite magma from the Khibina Alkaline Massif (in Russian, English summary). *Geokhimia*, 901-15.
- Nash, W. P., and Wilkinson, J. F. G., 1970. Shonkin, Sag laccolith, Montana. I. Mafic minerals and estimates of temperature, pressure, oxygen fugacity and silica activity. *Contr. miner. petrology*, **25**, 241-69.
- Olsen, W., and Metz, H., 1945-6. Zur Metallurgie des Thomasverfahrens. *Archiv. Eisenhüttenw.*, **19**, 111-17.
- Ol'shansky, Ya. I., 1950. The results of experimental investigation of sulphide-silicate systems (in Russian). *Trudy Inst. Geol. Nauk*, **121**, ser. petr., 36, 12-38.
- Ol'shansky, Ya. I., 1957. The equilibrium of two liquid phases in the simplest fluor-silicate systems (in Russian). *Dokl. AN SSSR*, **114**, 1246-9.
- Orville, P. M., 1963. Alkali ion exchange between vapor and feldspar phases. *Am. J. Sci.*, **261**, 201-37.
- Pavlov, D. I., and Ryabchikov, I. D., 1968. On the dolerites solidified in salts (in Russian). *Izv. AN SSSR, ser. geol.*, **2**, 52-63.
- Philpotts, A. R., and Hodgson, C. J., 1968. Role of liquid immiscibility in alkaline rock genesis. *Rep. 23rd Intern. geol. Congr. Czechoslovakia*, **2**, 175-88.
- Polyakov, A. I., and Kostetskaya, E. V., 1965. Poikilitic sodalite syenites of the Lovozero Massif (some problems of petrology and geochemistry) (in Russian). *Izv. AN SSSR, ser. geol.*, **6**, 16-25.
- Ravich, M. I., 1966. Phase equilibria in supercritical regions of some water-salt systems of the type P-Q. (in Russian). *Geokhimia*, 1275-85.
- Roedder, E., and Coombs, D. S., 1967. Immiscibility in granitic melts, indicated by fluid inclusions in ejected granitic blocks from Ascension Island. *J. Petrology*, **8**, 417-51.
- Ryabchikov, I. D., 1963. Experimental investigation of the distribution of alkalis between immiscible silicate and chloride melts (in Russian). *Dokl. AN SSSR*, **142**, 1174-7.
- Ryabchikov, I. D., 1967. Possible rôle of concentrated saline solutions for the mobilization of ore components from magma (Abstract). *Appl. Earth Sci.*, **76**, 14.
- Saether, E., 1948. On the genesis of peralkaline rock provinces. *Rep. 18th Intern. geol. Congr. Great Britain*, **2**, 123-30.
- Smith, F. G., 1961. Metallic sulphide melts as igneous differentiates. *Can. Miner.*, **6**, 663-9.
- Sourirajan, S., and Kennedy, G. C., 1962. The system H_2O - NaCl at elevated temperatures and pressures. *Am. J. Sci.*, **260**, 115-41.
- Sørensen, H., 1962. On the occurrence of steenstrupine in the Ilmaussaq Massif, Southwest Greenland. *Meddr. Gronland*, **167**, 1, 251 pp.
- Sørensen, H., 1969. Rhythmic igneous layering in peralkaline intrusions. *Lithos*, **2**, 261-83.
- Sørensen, H., 1970. Internal structures and geological setting of the three appaitic intrusions—Khibina and Lovozero of the Kola Peninsula and Ilmaussaq, South Greenland. *Can. Miner.*, **10**, 299-334.
- Tomkeicff, S. I., 1952. Analcite-trachybasalt inclusions in the phonolite of Traprain Law. *Trans. geol. Soc. Edinb.*, **15**, 360-73.
- Trömel, G., 1943. Untersuchungen im Dreistoffsystem CaO - P_2O_5 - SiO_2 und ihre Bedeutung für die Erzeugung der Thomasschlacke. *Stahl und Eisen*, **63**, 21-30.
- Tuttle, O. F., and Bowen, N. L., 1958. Origin of granite in the light of experimental studies in the system $\text{NaAlSi}_3\text{O}_8$ - KAlSi_3O_8 - SiO_2 - H_2O . *Mem. Geol. Soc. Am.*, **74**, 153 pp.

Tuttle, O. F., and Friedman, I. I., 1948. Liquid immiscibility in the system $H_2O-Na_2O-SiO_2$. *Am. Chem. Soc. J.*, 70, 919-26.

Upton, B. G. J., 1969. Field excursion guide to the carboniferous volcanic rocks of the Midland Valley of Scotland. *Int. symp. volcan. Oxford*, 1-46.

Wellman, T., 1968. Stability of sodalite in the system $NaAlSi_3O_8-NaCl-H_2O$. *Am. Geoph. Un. Trans.*, 49, 342-3.

Wilshire, H. G., 1967. The Prospect alkaline diabase-picrite intrusion, New South Wales, Australia. *J. Petrology*, 8, 97-162.

Wyllie, P. J., 1966. 'Experimental studies of carbonatite problems: the origin and differentiation of carbonatite magmas', in Tuttle, O. F., and Gittins, J., Eds. *Carbonatites*. Interscience, New York, London and Sydney, 311-52.

VI.6. RESORPTION OF SILICATE MINERALS

W. C. Luth

VI.6.1. Basic Principles

When attempting to evaluate the rôle of resorption of silicate minerals by a magma the overall mass, energy and volume relations in the system must be considered. A key factor is related to the thermal energy, or heat, balance in the resorption process. As Bowen (1928) pointed out, in general the heat of mixing in the liquid term will be small in comparison with the heat of melting. This feature, in combination with the increase of solubility of silicates with temperature, led him to conclude that the solution of a (crystalline) silicate results in absorption of heat, an endothermic process. However, if as a consequence of the solution of a crystalline silicate in a saturated magma, crystallization ensues then some heat (of crystallization) will be liberated, an exothermic reaction.

In the analysis of resorption processes we will be concerned with the interdependence of several thermodynamic variables. Rather than treat the relationships in terms of energy we shall examine these phenomena in terms of the more familiar, and at least potentially measurable, parameters pressure (P , units of bars, = 10^6 dynes/cm²), temperature (T , units of °C, or °K), Volume (V , units of cm³), and mass (units of grammes). In this sense P and T are intensive parameters. V and mass are extensive parameters. It is often useful to represent mass reduced parameters derived from the extensive parameters such as

specific volume ($\bar{V} = 1/\rho$) and mass fraction (or wt. %) in order to evaluate the behaviour of the system in terms of intensive parameters.

A pertinent question relating to an analysis of resorption could be formulated as follows. What are the consequences of adding X g of crystalline material, or mineral, to Y g of a liquid, or silicate melt? Intuitively we would believe this to be dependent on the condition of the crystalline material, as well as on the value of X relative to Y , and whether or not the silicate melt is saturated with respect to the same, or a different, crystalline phase as the one which is being added. Thus we see that the relatively simple question, as stated above, is not capable of a straightforward simple answer, other than to say that changes will, in general, be the result. In order to express the question in an answerable form it must be modified. It is, I think, obvious that the nature and mass of both crystalline material and liquid must be stated.

A modified question would then be: What are the effects on P , T , V , \bar{V} , mass, relative proportions and composition of the phases if 10 g of diopside are added to 100 g of a liquid of the composition 60% $Ca_2MgSi_2O_7$, 40% $CaMgSi_2O_6$ at 1405 °C and 1 bar which is just saturated (at the liquidus) with akermanite? (Fig. 1a). A portion of the question can be answered directly in that the total mass of the system is now 110 g and the bulk composition is composed of 50 g $CaMgSi_2O_6$ and

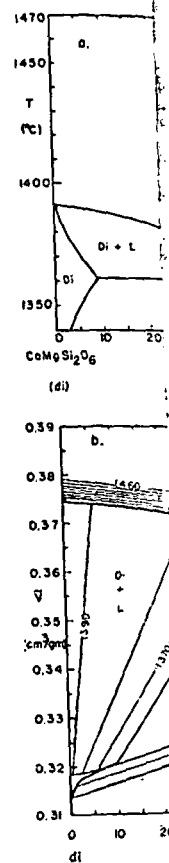


Fig. 1 The syst

(a) Temper
Kushiro and
(b) Specific
Constructed
(1966). Isothe
10 °C interval

60 g of $Ca_2MgSi_2O_7$
 $CaMgSi_2O_6$:
However there
the question d
composition :
phases when c
consider the
stant pressure
terms of a ser
then concerne
composition a
phases. From

SUBJ
GCHM
LRF

[AMERICAN JOURNAL OF SCIENCE, VOL. 276, MARCH, 1976, p. 330-346]

THE LEVER RULE WITH FRACTIONAL CRYSTALLIZATION AND FUSION

S. A. MORSE

Department of Geology and Geography, University of Massachusetts,
Amherst, Massachusetts 01002

ABSTRACT. The lever rule can be used in fractional crystallization and fusion problems with phase diagrams to evaluate the relative proportions of liquids and solids at any stage. The problem in crystallization is to find the total solid composition (TSC), which is a trivial exercise with eutectic systems, but one requiring either a numerical (Rayleigh) solution or a graphical one when solid solutions occur. In either approach to the problem, the ratio of some component in the crystals to that component in the liquid must be estimated. In the numerical case the crystals have the instantaneous solid composition (ISC), and the ratio is the Nernst distribution coefficient. In the graphical case, the crystals have the total solid composition, and the ratio is assumed to vary linearly between known initial and final states. When the total solid composition is known, the fraction of liquid is found by a lever connecting the liquid and the solid compositions, using the bulk composition as a fulcrum. An analogous procedure is used with fractional fusion, except in this case it is the total liquid composition (TLC) that must be found, either numerically or graphically. A few systems pertinent to common basic rocks serve to illustrate the method.

INTRODUCTION

Phase diagrams are quantitative models of natural geologic systems. We tend to take the quantitative aspect more or less seriously, depending on the complexity of the natural system compared to the synthetic one. However, there are times when one would like to explore the quantitative implications of a phase diagram to the hilt, either for their predictive value or for testing the relevance of a synthetic model to a particular well-known natural system. For example, how much rhyolite, in the limit, can be produced by the fractional crystallization of basaltic magmas. Although K_2O is the component that usually provides the limiting answer, it would be nice to know the restrictions implied by, say, the plagioclase system alone.

The lever rule is the graphical device that yields the crystallization ratio when the compositions of the crystals, the liquid, and the system (that is the bulk composition) are known. This rule can be used in fractional crystallization provided the composition taken for the crystals is that of *all* the crystals so far produced by the liquid; this composition may be called the *total solid composition*, or TSC. By contrast the *instantaneous solid composition* is the solidus composition, which always sweeps ahead of the total solid composition in fractional crystallization but which is identical with the total solid composition in equilibrium crystallization. Please refer to figure 1. The total solid composition follows a continuous path (TSC path) in compositional space throughout the fractional crystallization process, and this path always terminates at the bulk composition (BC).¹ The total solid composition also always moves toward the instantaneous solid composition (ISC), which lies on the

¹ Bulk composition is used here as the composition of the system chosen for a particular exercise. It does not vary during the exercise, contrary to the unfortunate practice of some authors.

S. A. M

tangent to the liquid path. Therefore, lies on the leading tangent composition always lies on the extension of the bulk composition and the liquid.

The purpose of this note is to extend the total solid composition lever rule may be applied. The TSC path in some circumstances and may be closely approximated.

The lever rule may be used equally well when the total solid composition is known. If a (TLC) is found, using the same procedure as in fractional crystallization.

The lever rule may be supplanted when dealing with a variable exponent. The value of the exponent estimated from phase diagrams, a procedure

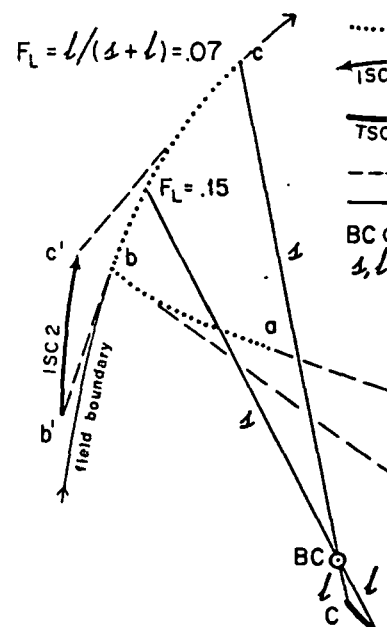


Fig. 1. Portions of fractional crystal and liquid paths. The early stages of crystallization are represented by tangents to the liquid paths \overline{ab} and \overline{bc} yielding the instantaneous solid compositions (ISC 1 and ISC 2). The total solid composition (TSC) moves along path \overline{AB} . When the liquid changes from \overline{ab} to \overline{bc} , the TSC path changes from \overline{AB} to \overline{BC} . The bulk composition (BC) is the same throughout the process.

**LEVER WITH FRACTIONAL
CRYSTALLIZATION AND FUSION**

S. A. MORSE

Department of Geography, University of Massachusetts,
Amherst, Massachusetts 01002

is used in fractional crystallization and fusion to determine the relative proportions of liquids and solids. The method is to find the total solid composition (TSC) in a system, but one requiring either a numerical value when solid solutions occur. In either application, the component in the crystals to that component in the liquid is the Nernst distribution coefficient. In the case of fractional crystallization, the ratio is the Nernst distribution coefficient, the initial total solid composition, and the ratio is assumed constant in the initial and final states. When the total solid composition is known, the total liquid composition is found by a lever connecting the liquid and solid compositions as a fulcrum. An analogous procedure is used in the case of fractional fusion. In this case it is the total liquid composition that is known, and the total solid composition is found numerically or graphically. A few systems permit the use of this method.

INTRODUCTION

Quantitative models of natural geologic systems are of great importance. One aspect more or less seriously, dependent on the system compared to the synthetic system, is the quantitative aspect. One would like to explore the quantitative aspect of a synthetic model to a particular system, for example, how much rhyolite, in the process of fractional crystallization of basaltic magma, is produced that usually provides the limiting factor in the system. The restrictions implied by, say, the phase diagram are not always obvious.

A graphical device that yields the crystallization path of the crystals, the liquid, and the system (TSC) are known. This rule can be used in the process of fractional crystallization to find the composition taken for the crystals produced by the liquid; this composition is the instantaneous solid composition (ISC), or TSC. By contrast the solidus composition, which also yields the total solid composition in equilibrium with the liquid (TSC), is shown in figure 1. The total solid composition (TSC) path (in compositional space through the system) is shown, and this path always terminates at the bulk composition (BC). The total solid composition also always moves toward the bulk composition (ISC), which lies on the tie line.

The composition of the system chosen for any particular exercise, contrary to the unfortunate

is tangent to the liquid path. The instantaneous solid composition, therefore, lies on the leading tangent to the TSC path. The total solid composition always lies on the extension of a line (a lever) connecting the bulk composition and the liquid.

The purpose of this note is to call attention to various means of finding the total solid composition corresponding to any liquid, so that the lever rule may be applied. The TSC may be found rigorously in many circumstances and may be closely approximated in others.

The lever rule may be used equally well in fractional fusion. In this case the total solid composition is known, and the total liquid composition (TLC) is found, using the same principles as for finding the TSC in fractional crystallization.

The lever rule may be supplanted by a Rayleigh distillation equation with a variable exponent. The variation of this exponent can be estimated from phase diagrams, a procedure closely related to the linear

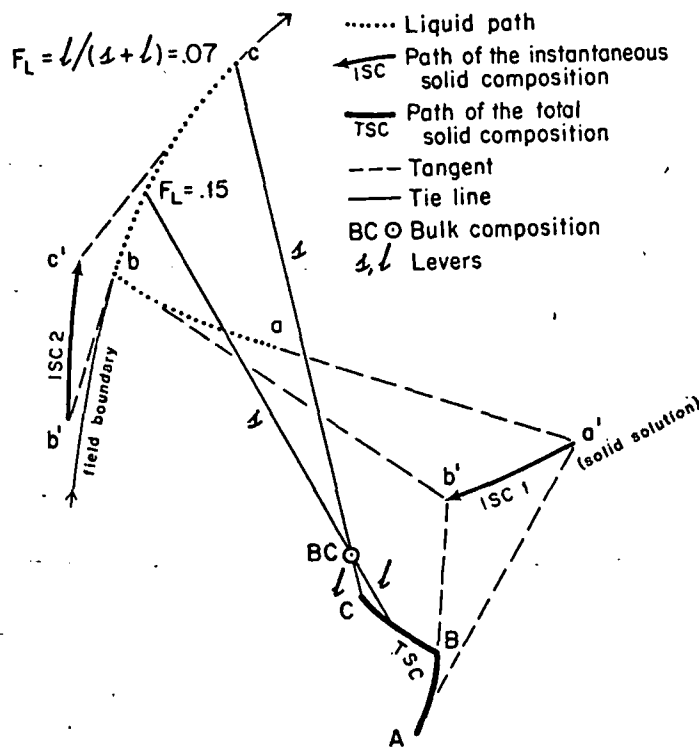


Fig. 1. Portions of fractional crystal and liquid paths in an imaginary X-X phase diagram. The early stages of crystallization are not shown; neither are the final stages. Tangents to the liquid paths \overline{ab} and \overline{bc} yield the instantaneous solid composition (ISC 1 and ISC 2). The total solid composition (TSC) continually moves toward the bulk composition (BC) along path \overline{AB} . When the liquid changes its course abruptly to \overline{bc} , a new ISC results (ISC 2), and the TSC path changes accordingly to \overline{BC} . Two sample levers through the bulk composition yield the fractions of liquid remaining (F_L) 0.15 and 0.07.

approximation used in the graphical method for finding the total composition or total liquid composition.

The principles for fractional crystallization and fusion will be illustrated with three familiar systems: anorthite-albite, diopside-anorthite-albite, and forsterite-diopside-silica, all at atmospheric pressure. An example concerning fractional fusion will be given for forsterite-diopside-silica-H₂O at 20 kb.

NOTATION

- Ab^L, Ab^{TSC}, Ab^{XI} The weight fraction of albite in, respectively, liquid, the total solid composition, and the instantaneously-formed crystals.
- BC Bulk composition, always the composition of the system.
- F_L Fraction of system present as liquid.
- ILC Instantaneous liquid composition (melting).
- ISC Instantaneous solid composition (crystallization).
- K Nernst distribution coefficient; ratio of the weight fraction of a component in the ISC to that in liquid.
- L Liquid.
- R Ratio of the weight fraction of a component in the TSC to that in liquid.
- R' Ratio of the weight fraction of a component in the TLC to that in the TSC.
- TLC Total liquid composition (fractional fusion).
- TSC Total solid composition.

ANORTHITE-ALBITE

Crystallization.—A few qualitative considerations may serve to illustrate the problem. For a liquid with bulk composition (BC) An₆₀ in the plagioclase system (fig. 2), the first crystals produced on cooling have composition An_{85.5}. A continuum of crystal compositions (ISC's) from here down to An₀ is produced on fractional crystallization. The initial and final *total solid compositions* (TSC's) are obviously An_{85.5} and An₀ (= BC) respectively; the proportions and compositions of crystals in this continuum produced over all crystallization history must sum to the bulk composition. Applying the lever rule, the fraction of liquid F_L is 1 when the total solid composition equals An_{85.5} and is zero when the total solid composition equals An₀. The problem is to find the path of total solid composition between the initial and final states. This may be done by a graphical approximation.

For simplicity in the following discussion, let

$$Ab \equiv X_{Ab} \text{ (the wt fraction).}$$

Let the ratio of Ab in the total solid composition to Ab in the liquid be

$$R = Ab^{TSC}/Ab^L \text{ (= } K = Ab^{XI}/Ab^L \text{ for } F_L = 1).$$

An independent solution for R will give the total solid composition associated with any liquid.

The lever rule with fractional crystallization

For the initial and final states, assuming the system has

	Ab ^{TSC}
Initial	0.145
Final	0.40

is assumed constant at its mean value, the TSC path is obtained; errors reach 1% with some other bulk compositions, but only with Ab^L, however, as plotted in

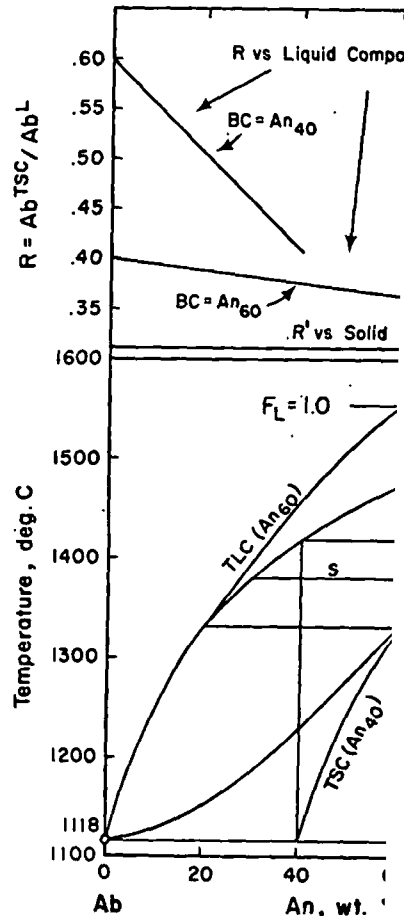


Fig. 2. Phase diagram of the plagioclase feldspar system. The liquidus and solidus lines are shown for the fractional crystallization paths and TSC (total solid composition) paths. The tie lines are shown for these initial tie lines. The TSC path is shown in the upper graph. A single lever is shown corresponding to the fourth line of table 1. The TSC path corresponding to the fourth line of table 1 is 0.31. Fractional fusion of BC An₆₀ is shown in the lower graph. This path is plotted from experimental data are given in table 2.

1. Morse

ical method for finding the total composition.

crystallization and fusion will be as: anorthite-albite, diopside-anorthite, all at atmospheric pressure. A fusion will be given for forsterite.

NOTATION

fraction of albite in, respectively, total solid composition, and the initial and final crystals.

tion, always the composition of the system present as liquid.

s liquid composition (melting).
s solid composition (crystallization).
distribution coefficient; ratio of the weight fraction of a component in the ISC to that in liquid.

weight fraction of a component in the liquid.
weight fraction of a component in the TSC.

l composition (fractional fusion).
composition.

ORTHITE-ALBITE

qualitative considerations may serve to deal with bulk composition (BC) An_{60} in the first crystals produced on cooling have a sum of crystal compositions (ISC's) equal to the bulk composition. The initial compositions (TSC's) are obviously $An_{55.5}$ and An_{40} and compositions of crystals in the final crystallization history must sum to the bulk composition. The lever rule, the fraction of liquid F_L is equal to $An_{55.5}$ and is zero when the composition is An_{40} . The problem is to find the path of the initial and final states. This may be done by the following discussion, let x_{ab} (the wt fraction) be the solid composition to Ab in the liquid $K = Ab^x / Ab^L$ for $F_L = 1$. This will give the total solid composition.

The lever rule with fractional crystallization and fusion 333

For the initial and final states, assuming a bulk composition of An_{60} , we have

	Ab^{TSC}	Ab^L	R
Initial	0.145	0.40	0.363
Final	0.40	1.00	0.400

is assumed constant at its mean value, 0.382, a crude approximation of the TSC path is obtained; errors reach 2 percent An (they get much worse with some other bulk compositions). If R is assumed to vary only with Ab^L , however, as plotted in figure 2, a very close approximation is obtained.

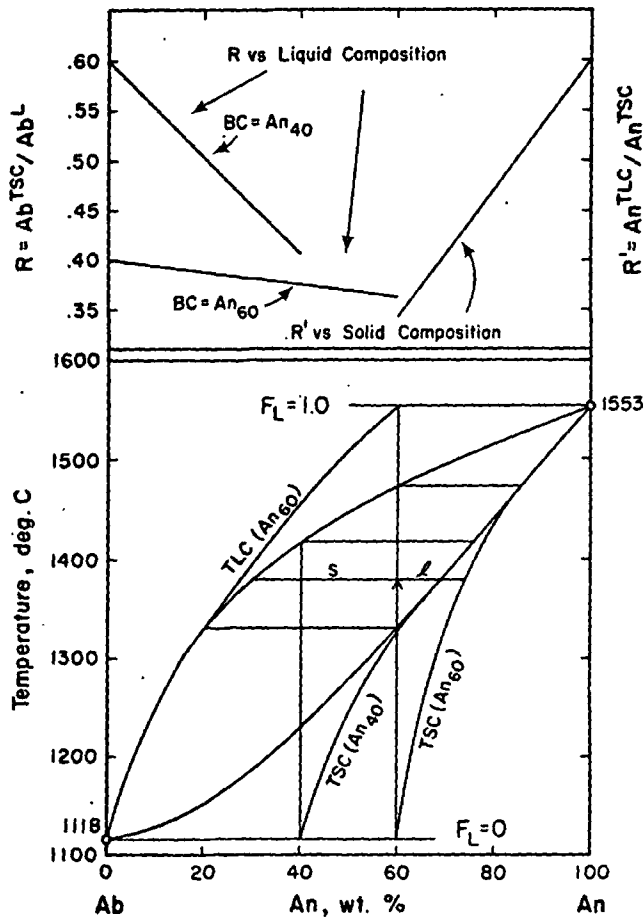


Fig. 2. Phase diagram of the plagioclase feldspars, modified after Bowen (1913). The tie lines are shown for the fractional crystallization of bulk compositions An_{60} , An_{40} , and TSC (total solid composition) paths are shown originating at the solidus compositions for these initial tie lines. The TSC paths are plotted from the values of R in the upper graph. A single lever is shown for the bulk composition An_{60} at 1553°C, corresponding to the fourth line of table 1; this lever yields the fraction of liquid $F_L = 0.31$. Fractional fusion of BC An_{60} is shown by a TLC path originating at the solidus, An_{40} . This path is plotted from the curve for R' in the upper graph. The data are given in table 2.

mation of the TSC path is obtained, using a Rayleigh calculation (below) as the criterion. Table 1 illustrates the results of this procedure for arbitrarily chosen values of Ab^L . The values of the fraction of liquid F_L are calculated from the relation

$$F_L = l/s+l = Ab^{BC} - Ab^{TSC} / Ab^L - Ab^{TSC}$$

The total solid composition path, plotted from the third column of table 1, is shown in figure 2. It is of interest to note from table 1 that one seeks the amount of "rhyolitic" ($An \leq 10$) liquid to be derived from fractional crystallization of a bulk composition An_{60} , the answer is 8 percent of the initial mass.

A similar treatment for the bulk composition An_{40} yields the total solid composition path shown in figure 2. In this case, the yield of "rhyolitic" liquid is 24 percent. One further test of the validity of assuming linear R is provided by this bulk composition: the first few points (not plotted in fig. 2) fall slightly within the loop. This is a forbidden region for TSC's, since the total solid composition cannot advance more rapidly than the instantaneous solid composition that lies on the solidus. The points in question lie up to 0.6 percent An inside the solidus, whereas they should lie very slightly outside of it. The slight amount of the deviation suggests that the assumption of linear R is close enough to the kind of modelling we seek to do with phase diagrams.

A formal calculation of the relation between the total solid composition and the fraction of liquid may be made via the Rayleigh (1896) distillation equation, which may be written for present purposes

$$Ab^{TSC} = Ab_0^L (1 - F_L^K) / (1 - F_L)$$

where Ab_0^L is the initial weight fraction of Ab in the liquid, and the exponent K is the Nernst distribution coefficient Ab^{X1}/Ab^L ; see for example Neuman, Mead, and Vitaliano (1954) and Gast (1968). The distribution coefficient K , however, is not constant but variable (in the plagioclase system and undoubtedly in natural systems as well), and its variation may be plotted and expressed analytically from the phase diagram in the following way.

TABLE 1
Values of R , Ab^{TSC} , and F_L for selected values of Ab^L , fractional crystallization of bulk composition An_{60}

	Ab^L	R	Ab^{TSC}	F_L
Initial	0.4	0.363	0.145	1.0
	0.5	0.369	0.185	0.68
	0.6	0.375	0.225	0.47
	0.7	0.381	0.267	0.31
	0.8	0.388	0.310	0.18
	0.9	0.394	0.355	0.08
	Final	1.0	0.400	0.400

The lever rule with fractional crystallization

The initial values of K and R are equal to the total solid composition. In any plagioclase system, the final value of K is 1, and the final composition is nearly linear. In order to have general utility, it is necessary to express K as a function of the fraction of liquid F_L . Since K spans the range 1 to R_0 , and $F_L = 1 - (F_L(1 - R_0))$. Using this relationship, K may be calculated for chosen values of F_L , or vice versa. The Rayleigh equation for variable K has been discussed for its variation have not been completely worked out. Because K must be evaluated before the lever rule is used, the graphical method is quicker.

Fusion.—Fraction fusion (Presnall, 1969) is calculated in a similar manner to crystallization. The total solid composition (TLC) that is sought moves along the solidus, and its path is determined by calculating $R' = An^{TLC}/An^{TSC}$ for the values of F_L and applying the linearly derived intercept values of the solidus composition (An^{TSC}). The results of such a calculation for the fractional fusion of An_{60} are posted in table 2, and the TSC path is shown above the liquidus in figure 2.

It is interesting to compare the volumes of liquid produced by fractional crystallization and fusion in An-Ab; this is done in figure 3. All the liquid is not produced at all by the fusion process. Fractional crystallization process yields a larger amount of liquid, but at a temperature 20° higher for the same amount of liquid. The temperatures of the fusion process constitute the solidus. For most of the intermediate and high An fields are similar, and if the batch production is considered, there would be little basis for differences in the results of crustal fusion or crystallization.]

TABLE 2
Values of R' , An^{TLC} , and F_L for selected values of F_L , fractional melting of bulk composition An_{60}

	An^{TSC}	R
Initial	0.600	0.342
	0.650	0.374
	0.700	0.407
	0.750	0.439
	0.800	0.471
	0.850	0.503
	0.900	0.536
Final	0.950	0.568
	1.0	0.600

ed, using a Rayleigh calculation. It illustrates the results of this process. The values of the fraction of

$$-Ab^{TSC}/Ab^L - Ab^{TSC}$$

th, plotted from the third column. It is of interest to note from table 1 that for $An \leq 10$ liquid to be derived from a bulk composition An_{60} , the answer is

bulk composition An_{40} yields the result shown in figure 2. In this case, the further test of the validity of the bulk composition: the first few points fall slightly within the loop. This is a total solid composition cannot achieve a solid composition that lies on the liquidus up to 0.6 percent An inside the solidus. The slight assumption of linear R is close enough to work with phase diagrams.

ation between the total solid composition can be made via the Rayleigh (1892) equation written for present purposes

$$(1 - F_L^R)/(1 - F_L)$$

action of Ab in the liquid, and the coefficient Ab^{X1}/Ab^L ; see for example (1954) and Gast (1968). The distribution is constant but variable (in the plagioclase systems as well), and its variation follows from the phase diagram in the

TABLE 1
For selected values of Ab^L , fractional crystallization of bulk composition An_{60}

R	Ab^{TSC}	F_L
0.363	0.145	1.0
0.369	0.185	0.68
0.375	0.225	0.47
0.381	0.267	0.31
0.388	0.310	0.18
0.394	0.355	0.08
0.400	0.400	0

The initial values of K and R are equal, because the first crystals constitute the total solid composition. In any complete loop such as the plagioclase system, the final value of K is 1, and the variation of K with liquid composition is nearly linear. In order to make the equation above of general utility, it is necessary to express K as a function of the fraction of liquid F_L . Since K spans the range 1 to R_0 and F_L spans the range 1 to 0 ($1 - (F_L(1 - R_0))$). Using this relationship, the total solid composition can be calculated for chosen values of F_L or vice versa. Greenland (1970) has discussed the Rayleigh equation for variable K , but analytic expressions for its variation have not been compiled for systems of geologic interest. Because K must be evaluated before the Rayleigh equation can be used, the graphical method is quicker.

Fusion.—Fraction fusion (Presnall, 1969) in An - Ab may be treated analogously in a similar manner to crystallization. In this case, it is the liquid composition (TLC) that is sought; the total solid composition moves along the solidus, and its path is therefore known. The TLC can be found by calculating $R' = An^{TLC}/An^{TSC}$ for the known initial and final values and applying the linearly derived intermediate values of R' to the known values of the solidus composition (An^{TSC}) to find An^{TLC} . The results of such a calculation for the fractional melting of the bulk composition An_{60} are posted in table 2, and the TLC path for this process is shown above the liquidus in figure 2.

It is interesting to compare the volumes and compositions of liquids produced by fractional crystallization and fusion of the same bulk composition in An - Ab ; this is done in figure 3. Albite-rich liquids ($An \leq 20$) are not produced at all by the fusion process, and consequently the crystallization process yields a larger amount of albite-rich liquid and smaller amounts of basic liquid. Identical amounts of An_{33} liquid are produced but at a temperature 20° higher for the fusion process. The higher temperatures of the fusion process constitute the main difference between the two processes. For most of the intermediate and basic liquid compositions, the yields are similar, and if the batch products of the liquids were seen in context, there would be little basis for deciding whether they were products of crustal fusion or crystallization. It is to be noted that the

TABLE 2
Values of R' , An^{TLC} , and F_L for selected values of An^{TSC} , fractional melting of bulk composition An_{60}

	An^{TSC}	R	An^{TLC}	F_L
Initial	0.600	0.342	0.205	0
	0.650	0.374	0.243	0.12
	0.700	0.407	0.285	0.24
	0.750	0.439	0.329	0.36
	0.800	0.471	0.377	0.47
	0.850	0.503	0.428	0.59
	0.900	0.536	0.482	0.72
	0.950	0.568	0.540	0.85
Final	1.0	0.600	0.600	1.0

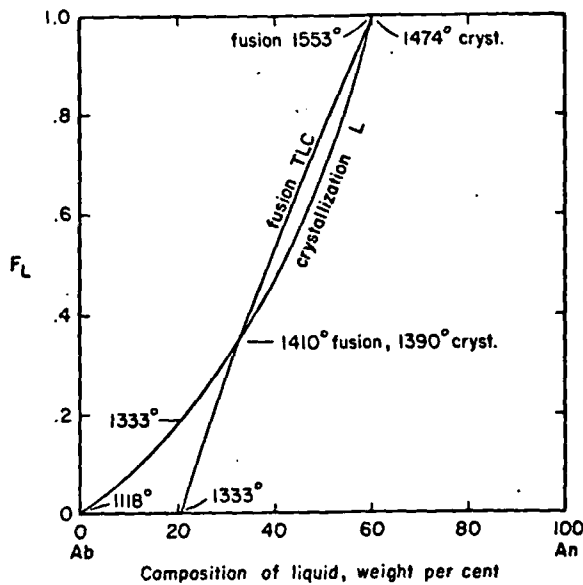


Fig. 3. Comparison of liquid volumes and compositions produced from fractional crystallization and fusion of $BC = An_{60}$ in the plagioclase system. The crystallization curve is also reproduced in figure 6 for comparison with Di-An-Ab. Abbreviations: TLC, total liquid composition; L, liquid.

total liquid composition path is a cumulative curve, and as Bowen often wrote, it would require "selective fusion oft-repeated" to produce the continuum of crystalline products achieved in fractional crystallization.

DIOPSIDE-ANORTHITE-ALBITE

Crystallization.—A portion of the system is shown in figure 4. A bulk composition BC composed of (An_{60}) 85 percent, Di 15 percent, lies in the plagioclase + liquid field. It is assumed for convenience that the system is ternary. A segment of a liquidus fractionation line² BC-F is shown dotted. While the liquid moves from the bulk composition BC to F, the instantaneous solid composition spans the range An_{84} to An_{65} . As long as the total solid composition remains on the plagioclase sideline, there is no problem in rigorously determining F_L ; for example when the liquid has just reached F in the figure, a line from the liquid through the total solid composition to the plagioclase sideline defines the total solid composition, and the lever rule yields $F_L = 0.49$.

Now the trouble starts. As diopside (Di) crystallizes, the total solid composition must rise into the triangle along some such path as shown in figure 4. As in the plagioclase system, we have the initial and final states corresponding to $F_L = 0.49$ and $F_L = 0$ (we ignore all tie-lines).

² Fractionation curve of Bowen; the term "liquidus fractionation line" suggested by Presnall (1969).

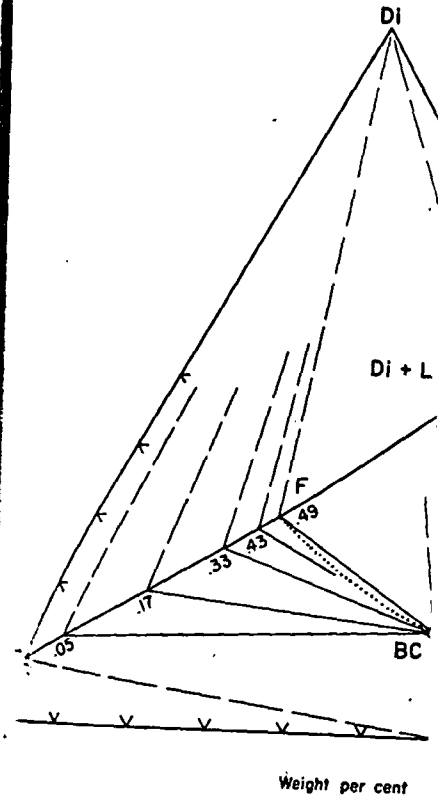
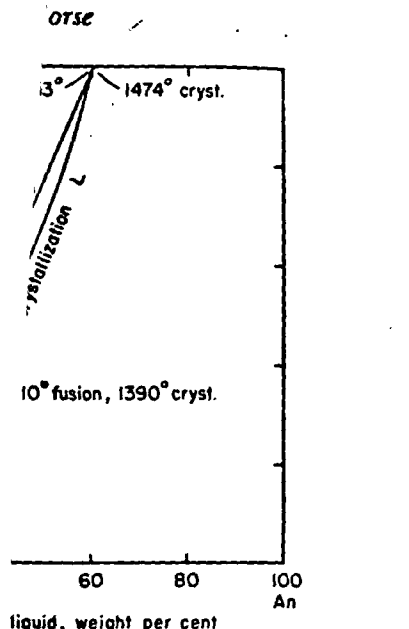


Fig. 4. Portion of the phase diagram Di-Plag-Alb based on data of Osborn (1942) and partitioned into fields as in Morse (1973). The system is treated as ternary. Bulk composition BC is (An_{60}) 85 percent, Di 15 percent. The solid composition of the plagioclase, not the liquid composition, is shown dotted. The remaining solid composition is shown dashed. The positions of the liquid composition are shown with the dashed line. The Ab^{TSC} values for the Di-Plag legs are shown. The Ab^{TSC} values for the Di-Plag legs are shown. The positions of the liquid composition are shown with the dashed line. The TSC path connects the derived instantaneous solid composition for the liquid and the liquid path and the $(Di-An_{60})$ leg.

effects). The corresponding values for F_L are shown as well as flattens the projection of linear R between the initial Ab^{TSC} and F_L in table 3. For each Ab^{TSC} is used to plot the Di-plagioclase lever that defines the position of the liquid. F_L is then found by connecting the values of Ab^L , Ab^{TSC} , and R are taken and they are projected from diopside.



...s and compositions produced on fractionation in the plagioclase system. The crystallization curves are compared with Di-An-Ab. Abbreviations...

...cumulative curve, and as Bowen (1915) described "effective fusion oft-repeated" to produce the products achieved in fractional crystallization...

NORTHITE-ALBITE
 The phase diagram of the system is shown in figure 4. The bulk composition of (An₈₅) 85 percent, Di 15 percent is assumed for convenience that the liquidus fractionation line² BC-F is drawn from the bulk composition BC to F on the plagioclase sideline, through the range An₈₄ to An₆₅. As long as the liquid remains on the plagioclase sideline, the fraction of liquid remaining is F_L ; for example when the liquid composition is at F, the line from the liquid through the bulk composition defines the total solid composition $F_L = 0.49$.

As diopside (Di) crystallizes, the total solid composition moves along some such path as shown in the ternary system, we have the initial and final compositions and $F_L = 0$ (we ignore all the other components). The term "liquidus fractionation line" was...

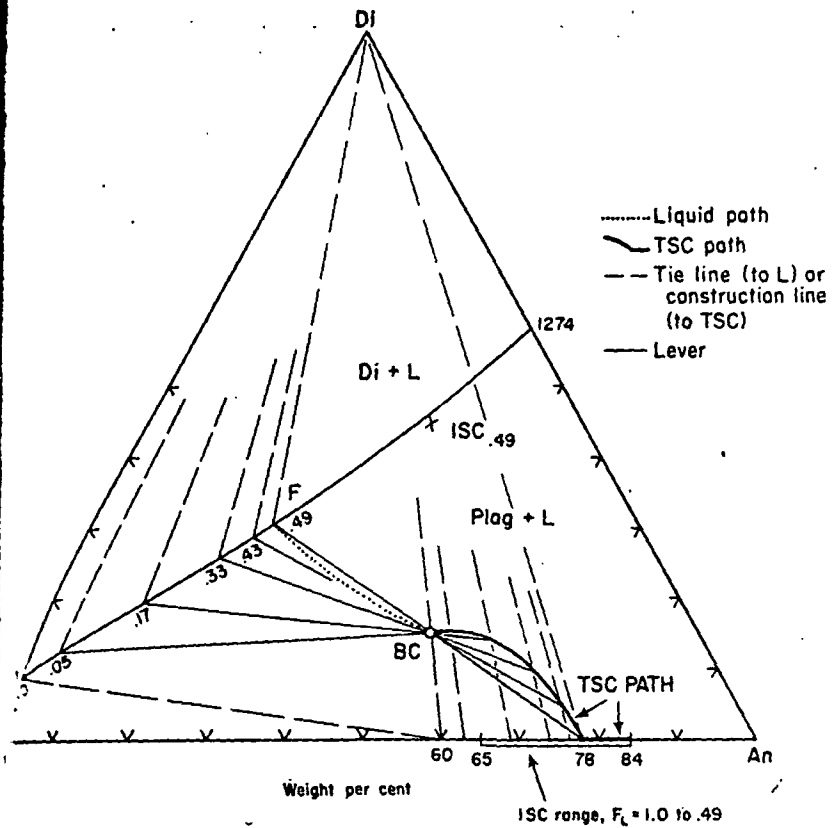


Fig. 4. Portion of the phase diagram Di-An-Ab, modified after Bowen (1915) and particularly Schairer and Yoder (1960), as used in Morse (1973). The system is treated as ternary here, although it is not. The bulk composition BC is (An₈₅) 85 percent, Di 15 percent. Truncated lines radial from the Di apex are like the legs of three-phase triangles, but the Di-Plag legs meet the total solid composition of the plagioclase, not the solidus composition. The L (Plag + Di) fractionation path is shown dotted. The remaining L (Plag, Di) path follows the field boundary. The Ab^{TSC} values for the Di-Plag legs are found from a graph (not shown) of Ab^{TSC} versus liquid composition. The positions of TSC's on these legs are found from the lever rule, passing through BC from the liquids. These levers yield the fractions of liquid remaining, F_L . The TSC path connects the derived TSC points. The point labelled ISC is the invariant solid composition for the liquid at $F_L = 0.49$; it is located by the intersection of the liquid path and the (Di-An₆₅) leg of a three-phase triangle.

...ary effects). The corresponding values³ for R are 0.328 and 0.400, which are significantly smaller than in the plagioclase system, since the component plagioclase is being out as well as flattens the projected plagioclase loop (Wyllie, 1963). The assumption of linear R between the initial and final states yields the values of Ab^{TSC} and F_L in table 3. For each value of Ab^L, the calculated value of Ab^{TSC} is used to plot the Di-plag^{TSC} leg of a construction triangle. A lever that defines the position of the total solid composition on the Di-plag^{TSC} leg is then found by connecting the composition of the liquid with the TSC point. The values of Ab^L, Ab^{TSC}, and R are taken relative only to plagioclase component, and they are projected from diopside.

the bulk composition. The lever rule may be applied to each such lever to yield F_L . These levers are not tie lines in the usual sense. The array of total solid composition points found in this way may be connected to form the TSC path, as shown in figure 4. The Di + Plag instantaneous solid composition path is not shown in figure 4, but it lies just below the cotectic curve, being in turn produced by tangents to that curve. A vertical line, the instantaneous solid composition produced when $F_L = 0$, is also plotted in the figure. A cruder solution for the total solid composition path in this system may be found in Morse (1973), where the ISC path is also discussed.

Fusion.—Fractional fusion of the same bulk composition, illustrated in figure 5, begins with the generation of liquid at 1213°C on the Di boundary. Extraction of this and succeeding liquids (instantaneous liquid compositions, ILC's) drives the total solid composition away from the bulk composition along the TSC path (crystal path of Presnall, 1961), as shown in the figure. The first instantaneous liquid composition is confined to the cotectic. The melting process is arrested at 1229°C, at the loss of all Di from the total solids. Up to and including this moment the total liquid composition is given simply by the intersection of the cotectic with a line through the bulk composition from any chosen point on the TSC path. Henceforward, after a large rise in temperature (1229°C), the total liquid composition accrues plagioclase components only, following the dotted path in the figure. The value of $R' = An^{TLC}/An^{TSC}$ varies from 0.493 to 0.600 during this melting of residual plagioclase, and the variation of R' is assumed in order to estimate intermediate values of An^{TLC} for chosen values of An^{TSC} . The TLC path is then plotted, using An^{TLC} lines radial from diopside, intersected by TSC-BC lines which are also levers from which F_L may be determined. Two levers are shown in figure 5, at $F_L = 0.52$ and 0.59 .

About half the mass of this bulk composition can be extracted to the limit, as haplodioritic liquid before diopside is used up. The increase needed to produce further melting of plagioclase is just adequate insurance against such an event in nature.

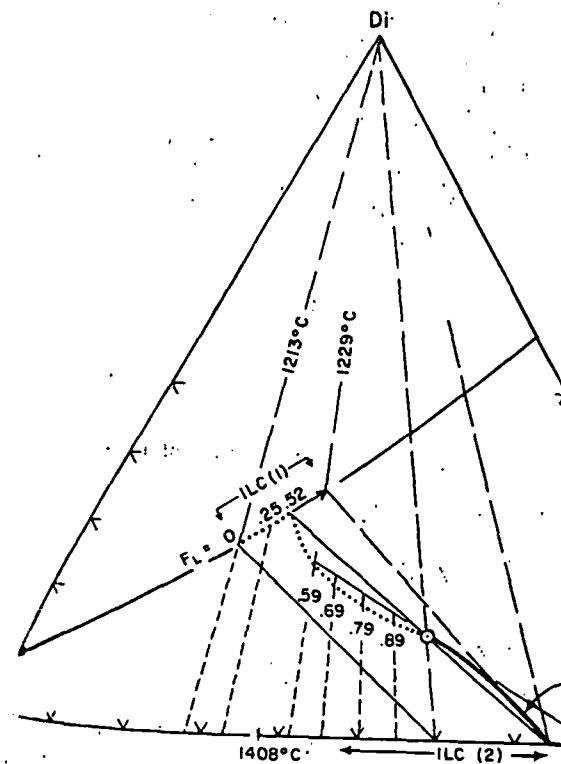
TABLE 3
Values of R , Ab^{TSC} , and F_L for selected values of Ab^L , bulk composition (An_{60}) 85 percent, Di 15 percent

	Ab^L	R	Ab^{TSC}	F_L
Initial	0.4	0.400	0.160	1.0
	0.5	0.350	0.175	0.74
	0.67	0.328	0.220	0.49
	0.70	0.334	0.234	0.43
	0.75	0.346	0.260	0.33
	0.85	0.366	0.310	0.17
	0.95	0.389	0.370	0.05
Final	1.0	0.400	0.400	0

The lever rule with fractional crystallization

It is of interest to compare the volumes and compositions produced by fractional crystallization and fusion in the Di-An-Ab system. The two solid curves in figure 6. As with the Di-An system, there are large differences in the amounts of albite produced, and small differences in the amounts of more basic plagioclase. It is noted, there is a large thermal impediment to the fusion of orthosilicic liquids required in fractional fusion, whereas the liquids produced by fractional crystallization of plagioclase have much lower temperatures.

Also shown in figure 6 is the albite enrichment curve produced by fractional crystallization in the An-Ab system, and a similar trend in Di-An-Ab. Albite enrichment in the ternary system, and an inflection occurs when the albite assemblage.



Fractional fusion in Di-An-Ab, using the same bulk composition as in figure 5. The dotted line is the total liquid composition (TLC) path, and the solid line is the total solid composition (TSC) path. The TSC is driven away from BC by tangents to the cotectic curve, constructed from the ratio R' , which yields An^{TLC} , and the TLC path is constructed through the bulk composition from the total solid composition at $F_L = 0.52$ and 0.59 .

ule may be applied to each such tie line in the usual sense. The area bounded in this way may be connected in figure 4. The Di + Plag instantane- ous liquid composition is shown in figure 4, but it lies just below the curve produced by tangents to that curve. A composition produced when $F_L = 0.52$ is the total liquid composition (TLC) in Morse (1973), where ISC path

of the same bulk composition, illustrating the fractionation of liquid at 1213°C on the Di-Plag system. The succeeding liquids (instantaneous liquid composition) are shown in figure 4, but it lies just below the curve produced by tangents to that curve. A composition produced when $F_L = 0.52$ is the total liquid composition (TLC) in Morse (1973), where ISC path

bulk composition can be extracted before diopside is used up. The further melting of plagioclase is probably an event in nature.

TABLE 3
 F_L for selected values of Ab^{TSC} , Ab^{TLC} 85 percent, Di 15 percent

R	Ab^{TSC}	F_L
0.400	0.160	1.0
0.350	0.175	0.74
0.328	0.220	0.49
0.334	0.234	0.43
0.346	0.260	0.33
0.366	0.310	0.17
0.389	0.370	0.05
0.400	0.400	0

It is of interest to compare the volumes and compositions of liquids produced by fractional crystallization and fusion in Di-An-Ab, as done in figure 6. As with the plagioclase system, there are large differences in the amounts of albite-rich liquids produced and small differences in the amounts of more basic liquids. However, as noted, there is a large thermal impediment to the generation of the anorthositic liquids required in fractional fusion, whereas the ternary liquids produced by fractional crystallization of plagioclase in this system have much lower temperatures.

Also shown in figure 6 is the albite enrichment trend of the liquid produced by fractional crystallization in the An-Ab system, for comparison with the similar trend in Di-An-Ab. Albite enrichment proceeds more rapidly in the ternary system, and an inflection occurs when Di joins the crystallization assemblage.

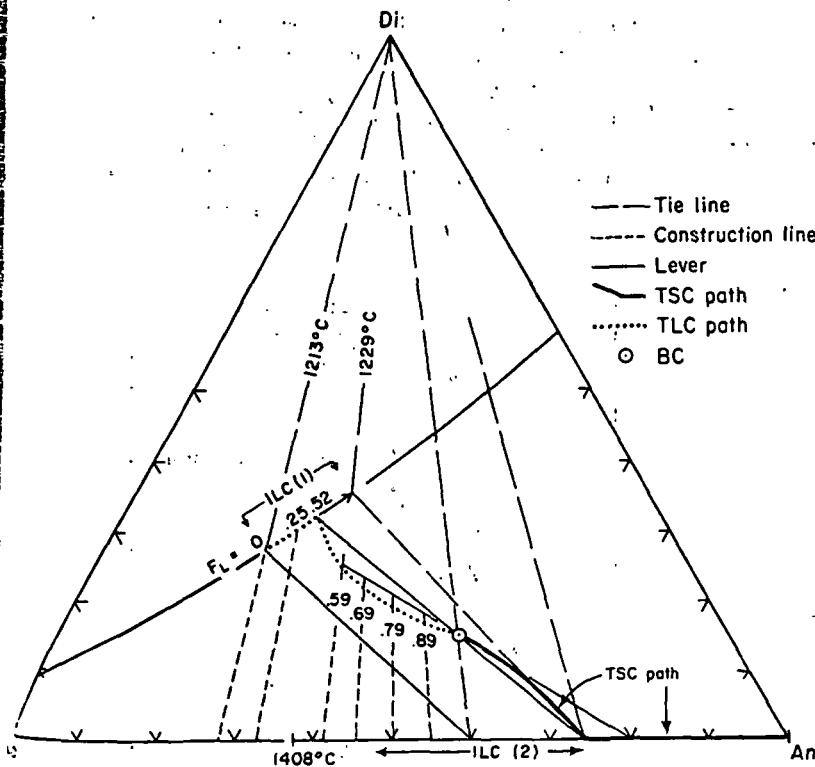


Fig. 5. Fractional fusion in Di-An-Ab, using the same bulk composition as in figure 4. The dotted line is the total liquid composition (TLC) path. Two instantaneous liquid composition (ILC) paths are shown, one on the field boundary and one on the plagioclase sideline. The TSC is driven away from BC by tangents to ILC's. The TLC path is constructed from the ratio R' , which yields An^{TLC} , and from intersections with tie lines through the bulk composition from the total solid composition. Sample levers are shown at $F_L = 0.52$ and 0.59.

FORSTERITE-DIOPSIDE-SILICA

Crystallization.—The fractional crystallization of a bulk composition $Fo_{0.5}Di_{1.5}(SiO_2)_{2.0}$ is illustrated in figure 7. The phase diagram is redrawn from Kushiro, 1972. Relations along the Di_{ss} -Tr boundary are uncertain, but the liquid is assumed to leave the system. The liquid path is shown as a dotted line. The phases and assemblages produced are, in order, $Pig + L$ (assumed invariant for graphical convenience), Pr_{ss} , $Pr_{ss} + Tr$, $Pig + L$ and $Di_{ss} + Tr$. The liquid path L (Fo_{ss}) is treated as though straight; path L (Pr_{ss}) is very slightly curved, and the remaining liquid paths are confined to field boundaries, which are nearly straight. The instantaneous equilibrium for liquid G is L (Pig, Di_{ss}, Tr), and the reaction is odd, that is, $Pig + L = Di_{ss} + Tr$ under continuous equilibrium conditions. The liquid will not stop here in fractional crystallization.

The discontinuous instantaneous solid composition (ISC) paths are as follows. The first ISC is Fo_{ss} , assumed invariant for convenience. The second is Pr_{ss} , varying slightly toward Di; it is difficult to show this correctly at the scale of the drawing, but it must start at a composition along the Fo-SiO₂ sideline and end at a slightly more Di-rich composition. The third is $Pr_{ss} + Tr$, on the extended tangent to the path of the liquid toward S. The fourth is $Pig + Tr$, on the extended tangent to the liquid path from S to G. The fifth is $Di_{ss} + Tr$, again difficult to draw without introducing unwanted confusion; however, the ISC has a fleeting existence on the tie line X-SiO₂ and thereafter follows closely behind:

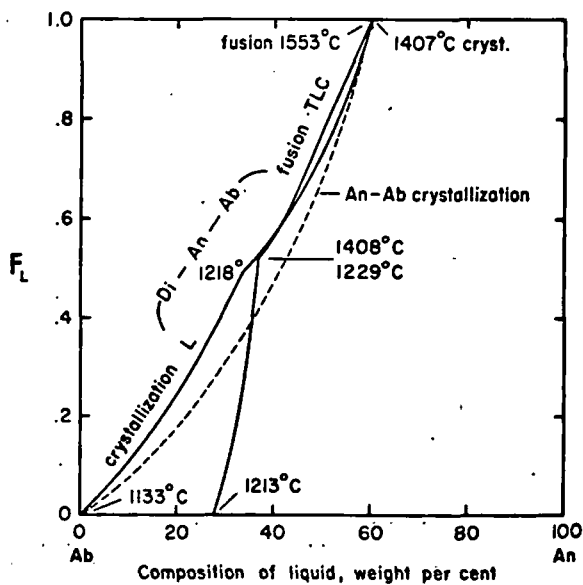


Fig. 6. Comparison of liquid volumes and compositions produced on fractional crystallization and fusion of bulk composition (An_{85}) 85 percent, Di 15 percent. The curve for crystallization in An-Ab is reproduced from figure 3 for comparison with the ternary curve.

The lever rule with fractional c

liquid through G to places unknown. The path is shown in figure 7, because it overlies the liquid path.

The total solid composition moves away from the bulk composition, then toward $Pr_{ss} + Tr$, then toward $Pig + Tr$, then toward the corner, then toward G and the corner, then toward $Di_{ss} + Tr$. The ranges of solid solutions are so small that they are not warranted. Instead, the TSC path is shown as a dotted line, and the lengths of TSC path segments are shown as percentages of the bulk composition from the bulk composition. This is shown in figure 5 as a medium-term application of the lever rule at $F_L = 0.40$ for a mass of dunite and a mass of enstatite. The solid-solid lever with fulcrum at the bulk composition lies at Fo_{ss} and Pr_{ss} .

In this analysis it is assumed that the Di - SiO_2 triangle is trivial, and that

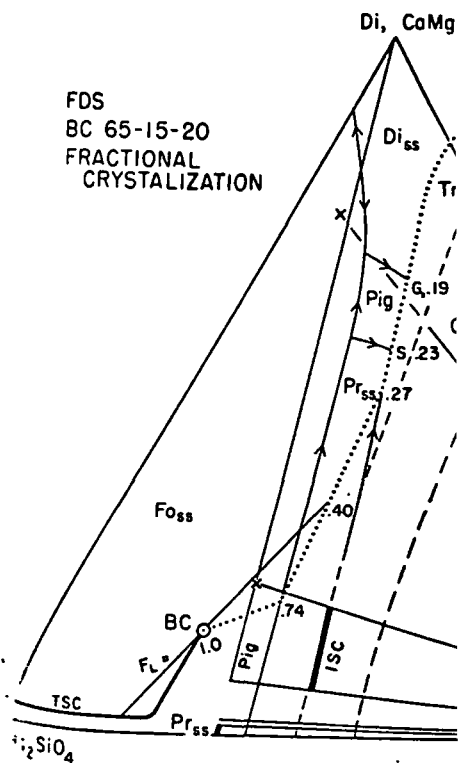
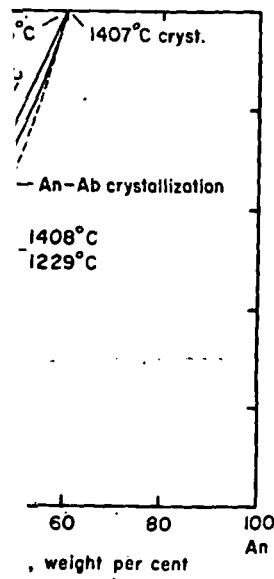


Fig. 7. The system forsterite (Fo)-diopside (Di)-silica (SiO₄) is shown for fractional crystallization, and a sample lever is shown for $F_L = 0.40$. Pig, pigeonite; Cr, cristobalite; Tr, tridymite.

OPSIDE-SILICA

crystallization of a bulk composition...
 re 7. The phase diagram is re...
 the Di_{ss} -Tr boundary are uncer...
 e system. The liquid path is sh...
 mblages produced are, in order...
 (convenience), Pr_{ss} , $Pr_{ss} + Tr$, Pig ...
 (Di_{ss}) is treated as though straight...
 and the remaining liquid path...
 re nearly straight. The instantan...
 (Pr_{ss} , Tr), and the reaction is odd...
 inuous equilibrium conditions. I...
 crystallization.

s solid composition (ISC) path...
 ned invariant for convenience. I...
 l Di; it is difficult to show this...
 it must start at a composition ab...
 htly more Di-rich composition. I...
 tangent to the path of the liq...
 the extended tangent to the liq...
 Tr, again difficult to draw with...
 iver, the ISC has a fleeting ex...
 eafter follows closely behind:



compositions produced on fract...
 An_{60} : 85 percent, Di 15 percent...
 is reproduced from figure 3 for...

... through G to places unknown. The final ISC path is not shown in...
 e 7, because it overlies the liquid path until the latter becomes...
 ed.

The total solid composition moves, after $F_L = 0.74$, from Fo_{ss} toward...
 then toward $Pr_{ss} + Tr$, then toward $Pig + Tr$, where the TSC path...
 the corner, then toward G and the field boundary passing through...
 the ranges of solid solutions are so small that calculations of R are...
 warranted. Instead, the TSC path is constructed by tangents to ISC...
 and the lengths of TSC path segments are determined by lines...
 through the bulk composition from the appropriate liquids. The TSC...
 is shown in figure 5 as a medium-weight line, and a sample lever...
 L through the bulk composition to the TSC path illustrates the...
 lication of the lever rule at $F_L = 0.40$. At this stage, the solids consist...
 a mass of dunite and a mass of enstatite rock in the ratio 43:57, given...
 a solid-solid lever with fulcrum at the end of the tie line and ends...
 lie at Fo_{ss} and Pr_{ss} .

In this analysis it is assumed that the amount of liquid leaving the...
 Di-SiO₂ triangle is trivial, and that the liquid path terminates as

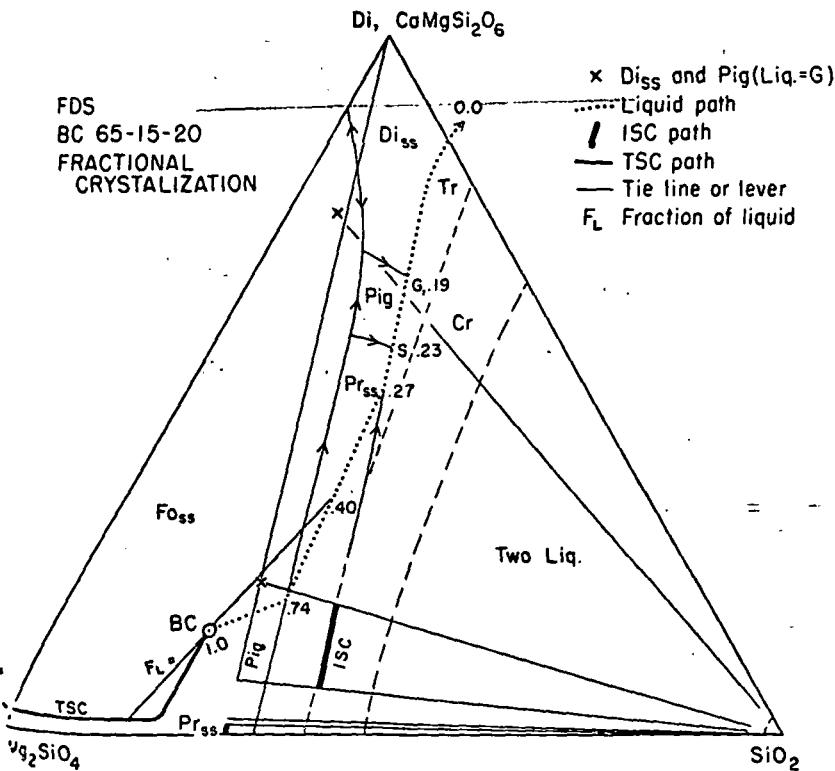


Fig. 7. The system forsterite(Fo)-diopside(Di)-silica, after Kushiro, 1972. The liquid...
 is dotted, and a sample lever is shown for $F_L = 0.40$. Abbreviations: Pr, proto...
 stite; Pig, pigeonite; Cr, cristobalite; Tr, tridymite.

shown in figure 7. The TSC path for the time after the liquid has left is in reality an S curve, but this is not readily shown at the scale of the drawing. Under the simplifying assumptions, the haplo rocks produced by the process are:

dunite	26 percent	(F_L 1.0 - 0.74)
enstatite rock	47 percent	(F_L 0.74 - 0.27)
tridymite-enstatite rock	4 percent	(F_L 0.27 - 0.23)
tridymite-pigeonite rock	4 percent	(F_L 0.23 - 0.19)
tridymite-diopside rock	~19 percent	(F_L 0.19 - 0)

Fo-Di-SiO₂-H₂O AT 20 KB

Fusion.—As a final illustration, consider the fractional fusion processes described by Yoder (1973), based on the 20 kb vapor-saturated system studied by Kushiro (1969), and shown in figure 8. The liquid

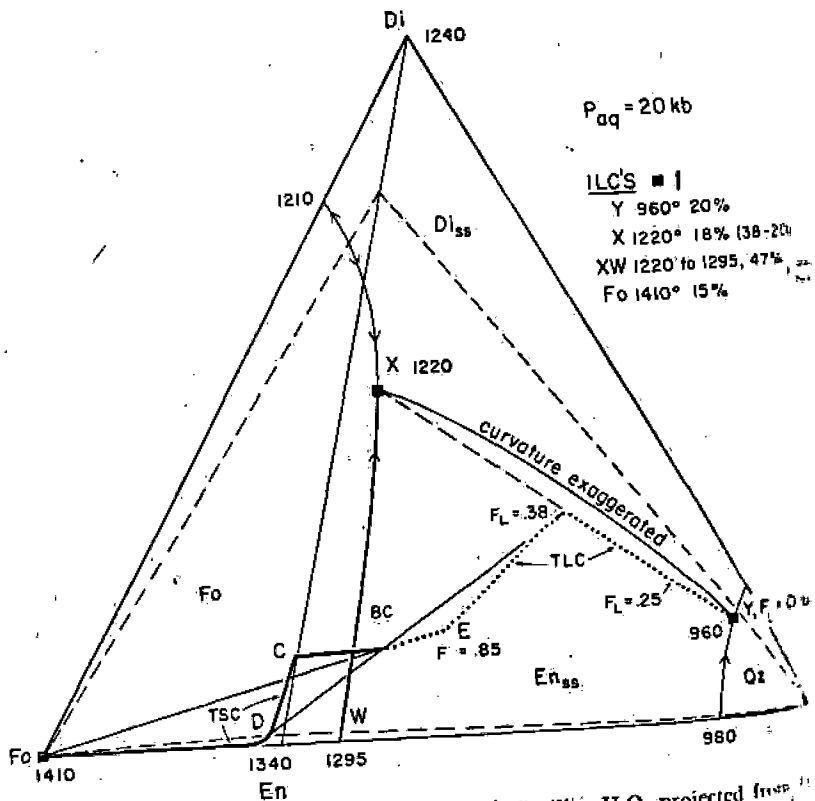


Fig. 8. The system forsterite (Fo)-diopside (Di)-silica-H₂O, projected from 20 kb pressure, after Kushiro (1969). The construction shows total liquid (TLC) paths in fractional fusion, with sample levers at $F_L = 0.38$ and exaggerated curvature of the cotectic line. XY is exaggerated for illustrative purposes and without experimental significance. The TLC moves in two straight-line segments and a curved segment. Dashed lines show the assumed limits of pyroxene solid solution after Yoder (1973).

The lever rule with fractional crystal

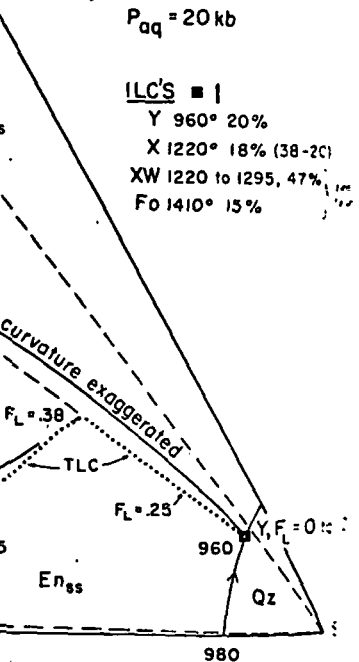
duced have the compositions Y, X, \overline{XW} , path of the total liquid composition, the percent summed composition of all liquids follows at first a straight mixing line, the line cotectic curve XY in the figure is given; that the TLC path has nothing to do with. The extraction of the invariant liquids of composition first from the bulk composition. When the total solid composition has reached the liquids move along XW, the peritectic composition moves toward this collection of liquid by the end of the boundary line. Point D is so close to the Fo-SiO₂ solid solution is difficult. A close approximation can be drawn at D and the curve XW onto the Fo-SiO₂ the problem in the "binary" system. This position (\overline{XW}) 76 percent, crystals of diopside realized to the mass of the entire system, position D, these figures become 47 and 26 percent to the ternary diagram with this composition remaining, a lever can be drawn from D to the position and terminated at E so as to give the position of the last TLC before fusion. The TLC path from $F_L = 0.38$ to 0.85 is a constraint that it must lie everywhere between the two points, which is the leading tangent to point D. The TLC vector toward X is initially short, and that the liquids swept up in the TSC path, which quickly approaches point X. Liquids Y and X correspond to model rocks respectively, in the example used by Yoder (1973) 20 percent (Y) and 18 percent (X) of the system. The correct yield of liquid X is found by subtracting the amount of Y from the total liquid. The array \overline{DCX} is not the desired composition of liquid X generated from solid composition. The amount of liquid X is 18 percent of the system after extraction of liquid Y. The array \overline{DCX} by 0.8 gives the correct result for X.

It may be useful, in such an exercise to find a composition that will yield a specified amount of liquid Y and X on fractional fusion. A problem is now offered. Lines of constant composition are drawn parallel to the En-Di join as can be seen in the figure. Such a line for a yield of 20 percent liquid and marked 0.20Y. The desired bu

... time after the liquid has ... readily shown at the scale ... tions, the haplo rocks prod...

- percent (F_L 1.0 - 0.74)
- percent (F_L 0.74 - 0.27)
- percent (F_L 0.27 - 0.23)
- percent (F_L 0.23 - 0.19)
- percent (F_L 0.19 - 0)

AT 20 KB
 Consider the fractional fusion ... on the 20 kb vapor-saturated ... shown in figure 8. The liqu...



(Di)-silica-H₂O, projected from H₂O construction shows total liquid (TLC) ... levers at $F_L = 0.38$ and 0.85 ... for illustrative purposes and is ... in two straight-line segments join ... med limits of pyroxene solid sol...

... have the compositions Y, X, \overline{XW} , and Fo. Of interest here is ... path of the total liquid composition, the TLC path, marking the ... summed composition of all liquids produced. The TLC path ... at first a straight mixing line, the line \overline{YX} , dashed in the figure. ... cotectic curve XY in the figure is given an exaggerated curvature to ... that the TLC path has nothing to do with the cotectic.

The extraction of the invariant liquids Y and X moves the total composition first from the bulk composition to C, then from C to W. When the total solid composition has reached D, diopside is used up, the liquids move along XW, the peritectic boundary. The total liquid composition moves toward this collection of liquids, but its direction is ... by the end of the boundary line near W as will be seen ... Point D is so close to the Fo-SiO₂ sideline that a ternary treat ... is difficult. A close approximation can be achieved by projecting ... at D and the curve XW onto the Fo-SiO₂ sideline from D and solv ... the problem in the "binary" system. This procedure yields liquid of ... composition (\overline{XW}) 76 percent, crystals of forsterite 24 percent. When ... alized to the mass of the entire system, which has 62 percent solid ... position D, these figures become 47 and 15 percent respectively. Re ... to the ternary diagram with this result of 15 percent solid ... erite remaining, a lever can be drawn from Fo through the bulk ... position and terminated at E so as to give $F_L = 0.85$, $F_{S(=Fo)} = 0.15$, ... which is the position of the last TLC before pure forsterite begins to ... The TLC path from $F_L = 0.38$ to 0.85 may now be constructed with ... constraint that it must lie everywhere below the extension of the line ... E, which is the leading tangent to point E. It quickly becomes ap ... ent that the TLC vector toward X and related liquids is micro ... gically short, and that the liquids sweep rapidly toward W. This is ... lected in the TSC path, which quickly approaches the sideline Fo-En.

Liquids Y and X correspond to model rhyolite and basaltic andesite, respectively, in the example used by Yoder (1973). They amount to 20 percent (Y) and 18 percent (X) of the system. It is of importance to note that the correct yield of liquid X is found only by a stepwise analysis ... as by subtracting the amount of Y from the total yield of liquids ... - Y. The array \overline{DCX} is not the desired lever; instead, it gives the amount of liquid X generated from solid composition C which amounts ... percent of the system after extraction of liquid Y. Multiplication of ... lever \overline{DCX} by 0.8 gives the correct result, 18 percent, for the yield of ... id X.

It may be useful, in such an exercise as Yoder's, to find explicitly a ... k composition that will yield a specified ratio (such as equal amounts) ... liquids Y and X on fractional fusion. A simple graphical solution of ... a problem is now offered. Lines of constant yield of liquid Y are ... ously parallel to the En-Di join as can easily be shown by similar ... angles. Such a line for a yield of 20 percent liquid Y is plotted in ... te 9 and marked 0.20Y. The desired bulk composition, supposing an

METAL ACCUMULATION RATES IN THE SOUTHEAST PACIFIC AND THE ORIGIN OF METALLIFEROUS SEDIMENTS

JACK DYMOND

School of Oceanography, Oregon State University, Corvallis, Ore. (USA)

and

H.H. VEEH

*School of Earth Sciences, The Flinders University of South Australia,
Bedford Park, S.A. (Australia)*

Received November 14, 1975

Revised version received August 7, 1975

Metal accumulation rates over the East Pacific Rise and Bauer Deep rule out normal authigenic precipitation of iron and manganese as the major mechanism of enrichment to the metalliferous sediments. A hydrothermal source located along the East Pacific Rise is compatible with the transition metal and aluminum accumulation rates. For the Bauer Deep the accumulation rate data suggest either that metal-bearing phases are being transported from the rise to the protected basins of the deep or that a second hydrothermal source exists within the Bauer Deep. A major portion of the minor elements being deposited in the Bauer Deep could result from authigenic precipitation, thus accounting for their distinctive chemical composition.

1. Introduction

The enrichment of transition and other metals at the crests of mid-ocean ridges has been well documented [1-6]. The unusual chemical composition [5], distinctive isotopic composition [3,6,7], and close association with submarine volcanism has led to the conclusion that these sediments form by precipitation from submarine hydrothermal solutions resulting from the reaction of seawater with cooling basalt lava [8].

Although these types of deposits are typically associated with active spreading centers, at least one deposit has been described which is adjacent to but not on the ridge crest - the Bauer Deep [7,9,10]. The Bauer Deep [10], which lies between the Galapagos Rise, an extinct spreading center to the east, and the East Pacific Rise (EPR) to the west (Fig. 1), is one of the major basins within the Nazca Plate. The 4000-m contour roughly outlines the basin which appears to

consist of several deep, more-or-less parallel valleys. The deepest valleys are in the western portion of the deep, in a region of great local relief that marks the contact between the older crust generated at the Galapagos Rise and the crust formed by spreading at the EPR [11]. The Y71-7-36 MG2 core used in this study (Table 1) was recovered from one of these valleys.

In this paper we compare metal accumulation rate data for the Bauer Deep, the EPR and the flanks of the EPR, in order to evaluate the origin of these unusual deposits.

2. Data and procedures

Three sediment cores representing the EPR crest, the EPR flank, and the Bauer Deep were selected for dating by the ^{230}Th method (Fig. 1). Uranium and thorium concentrations and isotope activities (Table 1) were measured by alpha spectrometry using procedures

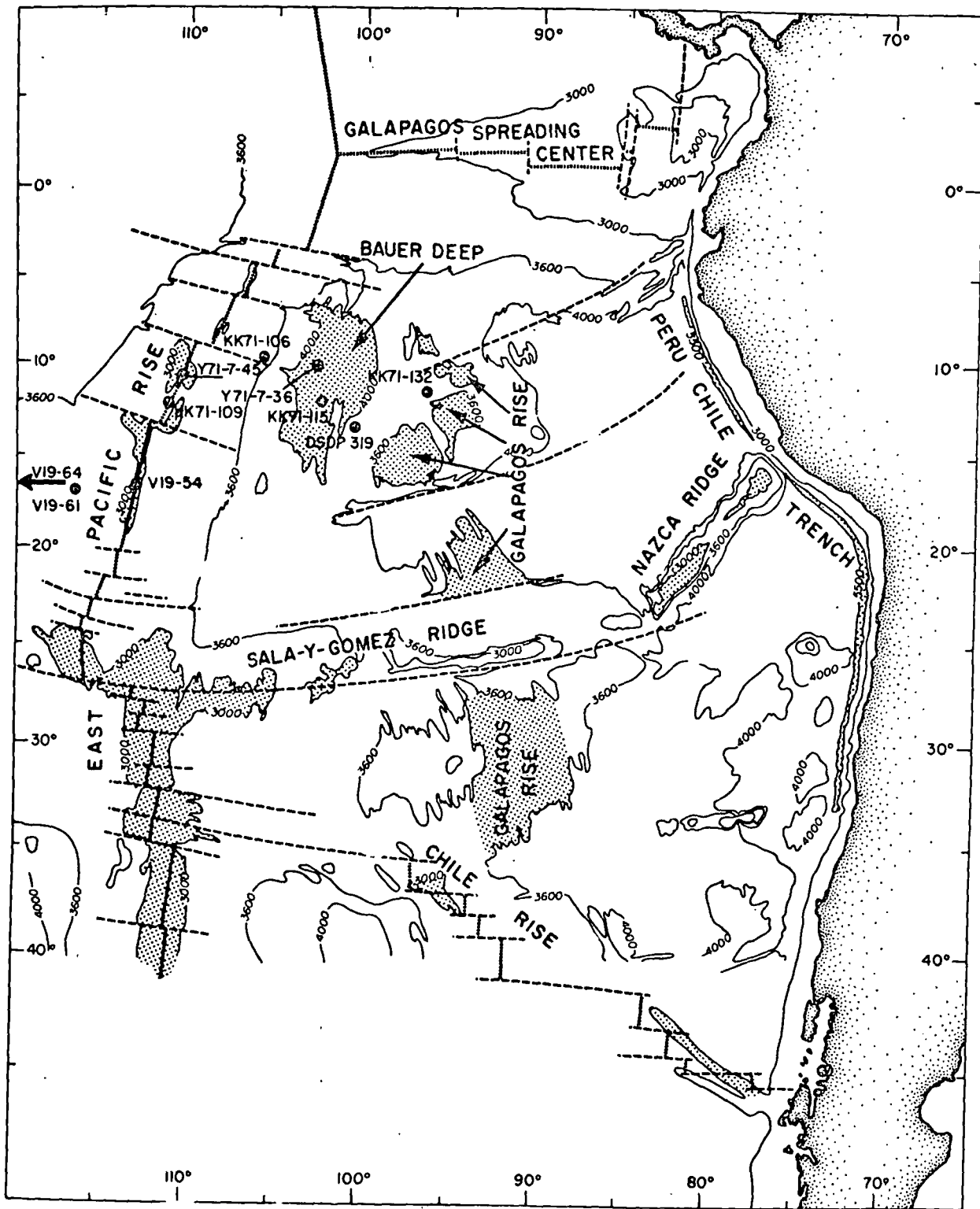


Fig. 1. Physiography of region studied and location of samples used for metal accumulation rates.

TABLE 1
Uranium and thorium

Depth (cm)	
<i>Y71-7-45 P</i>	
10-15	87
50-55	89
92-97	91
142-147	86
192-197	91
260-265	90
300-305	89
343-348	85
<i>KK71-106 GC10</i>	
10-15	91
42-47	86
72-77	90
112-116	91
<i>Y71-7-36 MG2</i>	
0-5	1
15-20	1
35-40	1
50-55	1

All values on total weight
 ^{230}Th , ^{234}U , ^{238}U in dis
 $\text{U}(\sim 3\%); \text{Th}(5-10\%); ^{230}\text{Th}_{\text{ex}}$
 $* ^{230}\text{Th}_{\text{ex}} = ^{230}\text{Th} - ^{234}\text{U}$

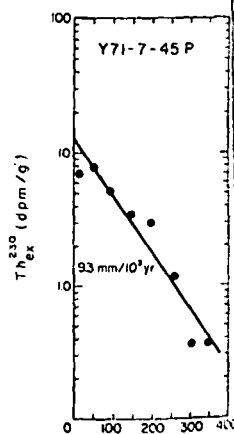


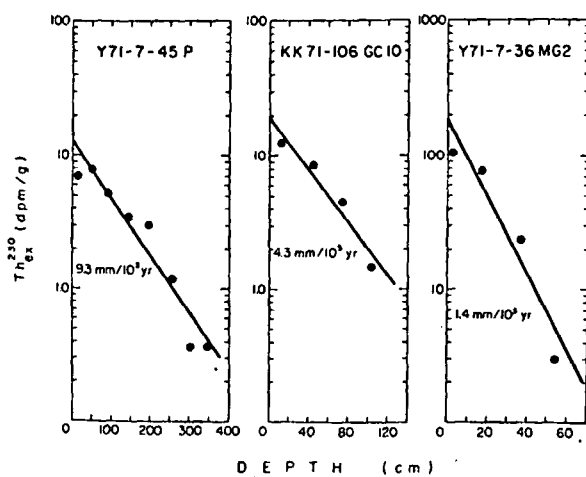
Fig. 2. Sedimentation rate ^{230}Th dating in this study in Table 1.

TABLE 1

Uranium and thorium isotopic data for sediments from the East Pacific Rise and Bauer Deep

Depth (cm)	CaCO ₃	U (ppm)	Th (ppm)	²³⁴ U/ ²³⁸ U	²³⁰ Th (d/m/g)	²³⁰ Th _{ex} (d/m/g)
<i>Y71-7-45 P</i>						
10-15	87	0.29	0.14	1.10 ± 0.03	7.18	6.97
50-55	89	0.32	0.25	1.06 ± 0.03	8.02	7.75
92-97	91	0.49	0.12	1.09 ± 0.03	5.50	5.11
142-147	86	0.39	0.20	1.09 ± 0.03	3.75	3.33
192-197	91	0.35	0.53	1.09 ± 0.03	3.38	3.08
260-265	90	0.69	0.20	1.16 ± 0.03	1.75	1.16
300-305	89	0.71	0.28	1.13 ± 0.03	0.94	0.35
343-348	85	0.66	0.11	1.08 ± 0.03	0.89	0.36
<i>KK71-106 GC10</i>						
10-15	91	0.18	0.25	1.10 ± 0.04	12.5	12.4
42-47	86	0.17	0.25	1.03 ± 0.03	8.57	8.44
72-77	90	0.19	0.38	0.94 ± 0.04	4.59	4.46
112-116	91	0.15	0.31	1.00 ± 0.04	1.57	1.46
<i>Y71-7-36 MG2</i>						
0-5	1.2	1.48	1.48	1.04 ± 0.02	102	101
15-20		1.53	4.57	1.04 ± 0.02	78.2	76.9
35-40	1.6	1.45	3.57	1.02 ± 0.02	24.3	23.2
50-55	1.3	2.14	2.95	1.00 ± 0.02	4.38	2.80

All values on total weight basis.

²³⁰Th, ²³⁴U, ²³⁸U in disintegrations min⁻¹ g⁻¹ (d/m/g). Errors quoted are based on counting statistics (±1σ). Other errors are:U (~3%); Th (5-10%); ²³⁰Th (~3%).* ²³⁰Th_{ex} = ²³⁰Th - ²³⁴U.Fig. 2. Sedimentation rates for each of the cores analyzed for ²³⁰Th dating in this study. ²³⁰Th is taken from the last column in Table 1.

previously discussed [12]. Sedimentation rates were derived from the exponential decrease of excess ²³⁰Th (uranium unsupported ²³⁰Th) with depth in the sediment (Fig. 3) by dividing the half-life of ²³⁰Th (75,200 years) into the depth interval over which ²³⁰Th_{ex} decreases to one-half of its value (Fig. 2).

In addition, following a procedure suggested by Sackett [13], the inventory of ²³⁰Th on the western Nazca Plate was determined by comparing the measured accumulation rate of ²³⁰Th_{ex} in the sediments (²³⁰Th_A) with the expected production rate of ²³⁰Th from uranium in the seawater column directly above each core location (²³⁰Th_P), using an uranium concentration of 3.3 μg/l in seawater and a ²³⁴U/²³⁸U activity ratio of 1.15 [14,15].

In order to apply the sedimentation rate data to the problem of metalliferous sediment origin, we have calculated metal accumulation rates (Table 3) using chem-

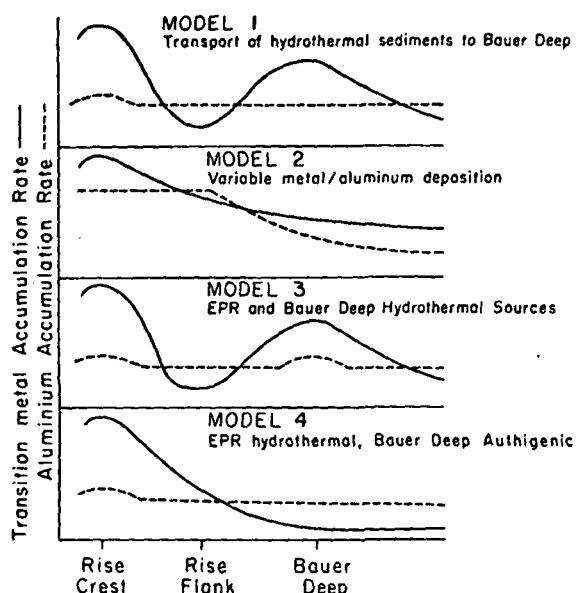


Fig. 3. Four models accounting for the origin of the high transition metal to aluminum ratios observed on the East Pacific Rise and the Bauer Deep [20].

ical analyses determined by atomic absorption spectroscopy (Table 2). See Dymond et al. [3] for analytical details. Metal accumulation rate data for the three cores analyzed in this study and data from seven other cores

analyzed by Bender et al. [6], McMurtry and Burnett [16], and Dymond et al. [17] are listed in Table 3. These ten cores were recovered between 10°S and 17°S and can be considered a traverse from 800 km west of the rise to 1300 km east of the rise. We have recalculated the metal accumulation rates reported by Bender et al. [6] and McMurtry and Burnett [16], by using values of bulk sediment density and water content estimated from the relationship of these variables to the carbonate content, as developed by Lyle and Dymond [19]. This procedure appears accurate to within 25%, whereas the constant dry bulk density used previously can produce errors of >300% in the metal accumulation rates. For example, our estimate for the Fe accumulation rate of sample KK71-84-FFC 115 is 3.3 times lower than the previously published value [16] which assumed a dry bulk density of 0.75. For the higher carbonate samples, the density correction is relatively minor, but has been used for consistency. Also we have not used the accumulation rate data for one of McMurtry and Burnett's [16] rise crest cores (core 109) because it displays an anomalous composition. The Fe/Al value for this core is 0.18. This compares to an average Fe/Al for 30 rise crest cores from between 10°S and 17°S that we have analyzed of 52.4 (Fe/Al range in these 30 cores between 5.3 and 165).

TABLE 2

Bulk sediment compositions

Sample	Fe (%)	Mn (%)	Si (%)	Al (%)	Cu (ppm)	Ni (ppm)	Zn (ppm)
<i>Y71-745 P</i>							
5-10 cm	1.26	1.97	0.56	0.0780	67	146	31
97-102 cm	1.66	0.55	0.90	0.1020	89	26	31
205-210 cm*	1.53	0.39	-	0.1170	-	-	29
305-310 cm*	2.07	0.67	-	0.1800	-	-	38
<i>KK71-106 GC10</i>							
5-10 cm	0.42	0.14	0.71	0.0890	45	13	12
<i>Y71-736 MG2</i>							
5-10 cm	14.1	3.04	16.1	2.18	781	498	308
28-35 cm	12.9	2.99	15.9	2.07	749	430	286
53-60 cm	15.2	3.59	15.0	1.87	857	587	433

* Analyses from Kendrick [18].

Murtry and Burnett listed in Table 3. Between 10°S and 20°S, the distance from 800 km to the rise. We have calculated the metal accumulation rates reported by Murtry and Burnett [16], by using the variability and water content of these variables developed by Lyle and others. It appears accurate to use a dry bulk density of 1.5 g cm⁻³ and a porosity of >300% in the example, our estimate of metal accumulation rate for sample KK71-84-FFC is 1.5 times the previously published value of 0.75. The density correction used for calculating the metal accumulation rate in Murtry's [16] rise crest sediments displays an anomalous pattern. The average for 30 rise crest cores is 0.18, and that we have analyzed 30 cores between

3. Discussion

From a consideration of the metal/aluminum patterns observed over the Nazca Plate, Heath et al. [20] suggest four possible origins for the high metal/aluminum values observed in sediments from the Bauer Deep and EPR: (1) the sediments with high metal/aluminum values originate along the EPR by hydrothermal processes, with some fraction subsequently transported across the flank of the rise to the Bauer Deep, (2) metalliferous sediments are deposited at a rate that decreases away from the rise crest, whereas aluminum-bearing volcanic debris is deposited more or less uniformly over the crest and upper flanks of the rise, (3) the metalliferous sediments from the two regions could be formed by separate hydrothermal systems operating in the two regions, and (4) the rise crest sediments could be hydrothermal, whereas the Bauer Deep deposits could largely be authigenic, hydrothermal phases accumulating in an area of very slow sediment accumulation.

Fig. 3 is a diagrammatic representation of how transition metals and aluminum would accumulate according to the four models. The pattern of aluminum accumulation in these models is quite uncertain since its geochemical behavior in the marine aqueous environments is poorly understood. In models involving hydrothermal activity, either at the rise crest or the Bauer Deep, we expect enhanced Al contribution since it seems likely that Al would be released in hydrothermal reactions involving albitization of plagioclases. Also, particulate volcanic debris should be common in those areas of relatively recent volcanism.

The observed transition metal and aluminum accumulation rates (Fig. 4) appear to rule out model 2, variable metal/aluminum deposition rates, as means of producing the high transition metal/aluminum values observed on the EPR and in the Bauer Deep [1,4,20]. Aluminum accumulation rates drop off rapidly away from rise and Fe, Mn, and Al all exhibit a slight maximum in accumulation rate in the Bauer Deep. This pattern contrasts sharply with that predicted by model 2 (Fig. 3).

Since the deposition rate of Fe and Mn is clearly greatest over the EPR and appears to be enhanced in the Bauer Deep relative to the flanks of the EPR, authigenic metal accumulation (model 4) cannot be the dominant process of metal deposition. Based upon

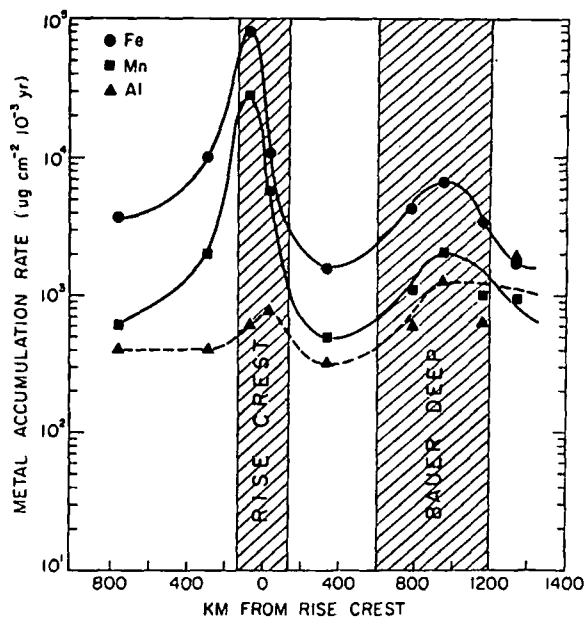


Fig. 4. Metal accumulation rates taken from Table 3 vs. distance from the crest of EPR.

the manganese accumulation rates measured in nodules and sediments over all parts of the sea floor, a uniform and slow precipitation of manganese over the ocean is not an unreasonable assumption. Rates of manganese accumulation in 13 nodules range from 0.2 to 1.0 $\text{mg cm}^{-2} 10^{-3} \text{ yr}^{-1}$ with most nodules having rates less than 0.6 $\text{mg cm}^{-2} 10^{-3} \text{ yr}^{-1}$ [21]. Manganese accumulation rates measured in 38 sediment cores have a median value of 0.8 $\text{mg cm}^{-2} 10^{-3} \text{ yr}^{-1}$ [21], not greatly different from the nodules. For purposes of discussion, we will assume the authigenic Mn accumulation rate in our region is 0.6 $\text{mg cm}^{-2} 10^{-3} \text{ yr}^{-1}$. Some variability in this rate is probable, due to transport to the bottom by biological vectors and sorption onto clays, but this variability is undoubtedly minor compared to the variability exhibited in Fig. 4. Thus, as discussed previously [6], the rate of manganese accumulation on the rise crest is 10–50 times greater than values found in nodules or sediments from non-volcanic regions of the sea floor. This same line of reasoning suggests that for the Bauer Deep the manganese accumulation rate is 2–3 times our assumed authigenic value.

Moreover, since Mn/Fe equals approximately 3 in nodules from the Nazca Plate [22], the authigenic Fe accumulation rate in the region can be assumed to be approximately 0.2 $\text{mg cm}^{-2} 10^{-3} \text{ yr}^{-1}$. Thus, the rate

Zn
(ppm)

31
31
29
38

12

308
286
433

TABLE 3

Metal accumulation rates and ^{230}Th inventory

Sample name and location	Water depth (m)	Sedimentation rate (cm/10 ³ yr)	Bulk density (g/cm ³)	Water content (%)
Y71-7-45 P 11°05'S, 110°06'W	3096	0.93	1.40	50
KK71-106 GC10 9°59'S, 106°02'W	3447	0.43	1.57	45
Y71-7-36 MG2 10°08'S, 102°51'W	4541	0.14	1.11	80
KK71-82-FFC109 ⁴ 12°05'S, 11°37'W	3069	1.08	1.48 ¹	51 ²
KK71-84-FFC115 ⁴ 11°58'S, 103°23'W	4548	0.19	1.15 ¹	80 ²
KK71-87-FFC132 ⁴ 11°33'S, 97°27'W	3996	0.20	1.40 ¹	56 ²
V19-54 ⁵ 17°02'S, 113°54'W	2830	1.50	1.34 ¹	61 ²
V19-61 ⁵ 16°57'S, 116°18'W	3407	0.70	1.48 ¹	51 ²
V19-64 ⁵ 16°56'S, 121°12'W	3540	0.45	1.47 ¹	51 ²
DSDP site 319 ⁶ 0-8 m 13°01'S, 101°31'W	4290	0.11	1.16	79 ²

¹ Bulk density calculated from the expression: $\rho = 0.88 - 0.20X_c - 0.03X_c^2$.

² Water content calculated from the expression: $W = 0.83 - 0.36X_c$.

³ Accumulation rate calculated from the expression: $A = C \cdot S \cdot \rho(100 - w)$, where C = concentration of element, S = sedimentation rate, ρ = bulk density, and w = water.

⁴ Sedimentation rates and element concentration data used to calculate metal accumulation rates from McMurtry and Burnett [16].

⁵ Sedimentation rates, Fe, Mn, Ni, U and Th concentrations used to calculate accumulation rates from Bender et al. [16]. Al accumulation rate determined from concentration data of Dymond (unpublished data, 1975).

⁶ Sedimentation rate from microfaunal determinations (DSDP Leg 34, Hole Summaries), element concentration data used to calculate metal accumulation rates from Dymond et al. [17].

⁷ $^{230}\text{Th}_A$ = accumulation rate of $^{230}\text{Th}_{EX}$. Calculated like metal accumulation rates, except that extrapolated surface values of $^{230}\text{Th}_{EX}$ (dpm/g) from sedimentation rate plots are used in lieu of average metal concentration data.

⁸ $^{230}\text{Th}_p$ = production rate of ^{230}Th in ocean water column at core location. Calculated from water depths shown, and the average seawater values of $3.3 \mu\text{g U/l}$ and $^{234}\text{U}/^{238}\text{U} = 1.15$.

of iron accumulation is more than 500 times greater on the East Pacific Rise and 20–30 times greater within the Bauer Deep (Table 3, Fig. 4) than this value. Some of the iron accumulation in these sediments could be

detrital iron from land-derived clays and volcanic, silicate debris. The low Al content (Table 2) and lack of X-ray identifiable minerals in metalliferous sediments [3], however, limit detrital iron to very low percentage

Accumulation rates ($\mu\text{g cm}^{-2} 10^{-3} \text{ yr}^{-1}$) ³						^{230}Th inventory ($\text{dpm cm}^{-2} 10^{-3} \text{ yr}^{-1}$)		
Fe	Mn	Al	Ni	U	Th	$^{230}\text{Th}_A$ ⁷	$^{230}\text{Th}_P$ ⁸	$^{230}\text{Th}_A/^{230}\text{Th}_P$
11,000	5800	780	56	0.31	0.1	8.3	8.0	1.0
1600	500	330	5	0.06	0.1	7.0	8.9	0.79
4400	1100	620	16	0.05	0.07	5.6	11.8	0.47
710	860	4000	70	-	-	8.6	8.0	1.1
5900	2100	1300	46	-	-	2.0	11.6	0.17
1700	950	1900	46	-	-	6.1	10.6	0.58
82,000	28,000	610	160	4.0	<0.2	11.8	7.4	1.6
10,000	2030	410	27	0.27	<0.1	10.8	8.9	1.2
3800	620	410	17	0.11	0.08	7.8	9.2	0.85
3500	1000	640	19	-	-	-	-	-

Clearly, authigenic precipitation (model 4) cannot explain the pattern of Fe deposition in this region and other processes must be examined.

For other elements, however, authigenic precipitation in the Bauer Deep is not negligible. As calculated above, the Mn accumulation rate in the Bauer Deep is 2-3 times our assumed average ocean value; thus, 30-50% of the manganese in the Bauer Deep could be deposited by authigenic processes. Similarly, assuming an authigenic Mn/Ni value of 30 which is typical for Nazca Plate nodules [22], the observed Ni accumulation rate in the Bauer Deep (Table 3) is approximately equal to the authigenic rate. In fact, Heath et al. [23] have measured a Ni accumulation rate in equatorial

Pacific sediments approximately four times our determination in the Bauer Deep. Consequently, most of the minor transition metals deposited in the Bauer Deep could precipitate from normal seawater rather than hydrothermal sources.

Although the metal accumulation rate pattern for the region differs markedly from that predicted by models 2 and 4 (Fig. 3), the aluminum and iron rates exhibited by Fig. 4 resemble model 1 (mechanical bypassing of EPR flanks and model 3 - Bauer Deep and EPR hydrothermal sources). The distinction between these two models (Fig. 3) is that enhanced Al accumulation in the Bauer Deep due to particulate volcanic debris and hydrothermal Al in the Bauer Deep

ment, S = sedimentation rate (m/yr) (after Murray and Burnett [16], after Healy et al. [16]. Al accumulation data used to calculate surface values of elements shown, and the average values of elements shown are based on 100% siliceous and volcanic, siliceous (model 2) and lack of siliceous sediments (model 1) with very low percentages of

region would be expected if model 3 is correct. Mechanical bypassing of aluminous phases from the EPR and ponding in the Bauer Deep, however, could produce the same effect. Thus, it may not be possible to distinguish model 1 from model 3 on the basis of the Fe and Al accumulation rate data.

If a portion of metalliferous components is wafted away from the rise and reaches a final depositional site in the deeper regions away from the crest, a maximum in metal deposition rate might be expected to the west of the EPR as well as in the Bauer Deep. A maximum in metal accumulation rates west of the EPR is not indicated by the single measurement in this region (Fig. 4). Could bottom currents transport preferentially metalliferous phases to the Bauer Deep and not to the west? We lack deep-current measurements which would directly bear on this question; however, Lonsdale [24], on the basis of hydrographic data suggests that water enters the Bauer Deep by channeled flow through transform faults on the EPR. He further speculates that this bottom water movement can be a means for transporting fine-grained precipitates away from the EPR. On the other hand, the maximum Fe and Mn accumulation appears to be slightly west of the rise crest, and the accumulation rates of these metals drops off less rapidly toward the west than towards the east (Fig. 4). Whether this apparent pattern reflects merely the scatters in metal accumulation rates over the length of the EPR represented by Fig. 4 or the true deep current patterns cannot be determined from the available data.

The general geophysical setting of the Bauer Deep would argue against an off-rise hydrothermal source. Core Y71-7-36 MG2 is from a part of the Nazca Plate generated by the Galapagos spreading center [25] and should be approximately 20 m.y. in age. Persistent hydrothermal activity to the present seems improbable. Anderson and Halunen [26], however, have shown that heat flow measurements in the Bauer Deep exhibit a bimodal distribution, which they suggest results from hydrothermal processes. They conclude that the major reorientation of the spreading region which occurred when spreading jumped from the Galapagos Rise to the EPR approximately 6.5 m.y. ago [27] could have initiated mid-plate volcanism and hydrothermal activity. The bimodal heat-flow distribution they point to, however, is open to question, since it is indicated only by the presence of two or three heat-flow measurements in the Bauer Deep with values between 3 and 5 HFU. In

addition, the basalt recovered from the Bauer Deep by the Deep Sea Drilling Project (site 319), which Anderson and Halunen [26] suggested represented recent mid-plate volcanism because of the fresh nature of the sample, has been dated at 16 m.y. and appears to be crust emplaced at the Galapagos Rise [28].

Neither models 1 or 3 alone can explain some of the chemical distinctions between the Bauer Deep and EPR sediments [29]. A relatively greater proportion of hydrogenous phases in the very slowly accumulating Bauer Deep sediments could account for the higher Ni/Fe and Th/U values observed. Other distinctions such as the relatively high Si and Al concentrations in the Bauer Deep are more difficult to explain. Moreover, the Th and U data suggest that the mechanisms of deposition of these species differ in the Bauer Deep and the rise crest. The U accumulation rates are significantly higher along the crest of the EPR, than on the flanks of the rise, or in the Bauer Deep. Inasmuch as $^{234}\text{U}/^{238}\text{U}$ ratios of continental detritus in deep-sea sediments are equal to or less than unity [30], the $^{234}\text{U}/^{238}\text{U}$ ratios at all core locations considered here reveal some input of uranium with excess ^{234}U to the sediments in this area. A likely source for this additional uranium is seawater, where the $^{234}\text{U}/^{238}\text{U}$ ratio has a constant value of 1.15. The proportion of uranium derived from this source appears to be higher in sediments on the ridge crest than in the Bauer Deep, which is consistent with the higher U accumulation rates there.

Since ^{230}Th is a known seawater-derived nuclide, its inventory in our cores (Table 3) may indicate the origin and pathways of other metals as well. If all of the ^{230}Th observed in the sediments is formed by decay of ^{234}U in the overlying water, the ^{230}Th production ($^{230}\text{Th}_p$) should equal the ^{230}Th accumulation (Th_A). From Table 3 it is apparent that cores from the crest of the EPR have $^{230}\text{Th}_p > ^{230}\text{Th}_A$ while $^{230}\text{Th}_A < ^{230}\text{Th}_p$ for cores from the Bauer Deep and other off-rise areas. It has been demonstrated elsewhere [31] that sediment transport and redeposition on the deep-ocean floor can significantly alter the Th_p/Th_A values in an area such that $^{230}\text{Th}_A < ^{230}\text{Th}_p$ on topographic highs, and $^{230}\text{Th}_A > ^{230}\text{Th}_p$ in basins which may act as sediment traps. Thus, following this reasoning for model 1 (transport of rise-formed precipitates to the Bauer Deep) we would expect the pattern of $^{230}\text{Th}_p/^{230}\text{Th}_A$ exactly opposite that observed. The observed pattern could be explained by transport of Bauer Deep sediments to

om the Bauer Deep by
e 319), which Anders
esented recent mid-
esh nature of the sam-
d appears to be crust
28].

in explain some of
the Bauer Deep and
greater proportion of
slowly accumulating
unt for the higher
Other distinctions
Al concentrations in
to explain. More-
at the mechanisms of
in the Bauer Deep and
rates are significantly
than on the flanks
Inasmuch as $^{234}\text{U}/$
s in deep-sea sedi-
ity [30], the $^{234}\text{U}/$
s considered here reveal
s ^{234}U to the sedi-
for this additional
 $^{234}\text{U}/^{238}\text{U}$ ratio has a
rtion of uranium
o be higher in sedi-
ie Bauer Deep, which
umulation rates there.
er-derived nuclide, its
ay indicate the origin
ell. If all of the ^{230}Th
d by decay of ^{234}U in
duction ($^{230}\text{Th}_p$)
ion (Th_A). From
om the crest of the
 $^{230}\text{Th}_A < ^{230}\text{Th}_p$
l other off-rise areas.
e [31] that sediment
deep-ocean floor can
ues in an area such
phic highs, and
may act as sediment
ig for model 1 (trans-
the Bauer Deep) we
 $^{230}\text{Th}_A$ exactly
ed pattern could be
ep sediments to

the rise crest. Upslope transport of sediment, however, seems sufficiently unlikely that an alternative explanation for the pattern of $^{230}\text{Th}_{\text{ex}}$ accumulation in the region must be sought. It seems probable that Sackett's model of ^{230}Th production and removal in the overlying water column [13] is too simplistic for this region and that some accounting for bottom-water movement and iron hydroxide scavenging must be made. Even with the slow movement of bottom water, hydrothermal precipitates forming on the rise crest would be effectively bathed by hundreds to thousands of times more water than that in the overlying water column. It is possible that the removal of ^{230}Th from moving bottom water by Fe and Mn hydroxyoxides formed from hydrothermal solutions is the explanation for the surplus $^{230}\text{Th}_{\text{ex}}$ deposition observed in the rise crest. Such an explanation necessarily requires that some areas "downstream" of the bottom flow have $^{230}\text{Th}_A < ^{230}\text{Th}_p$. Thus, both the higher $^{234}\text{U}/^{238}\text{U}$ and $^{230}\text{Th}_A/^{230}\text{Th}_p$ for rise crest sediments compared to Bauer Deep sediments indicate different removal processes for these nuclides in the two areas. Neither models 1 or 3 offer clear explanations for these differences.

4. Summary

Metal accumulation rate data for the Nazca Plate indicate that authigenic precipitation of metals (model 4) and variable aluminum deposition (model 2) cannot account for the anomalous metal/aluminum ratios observed on the EPR and the Bauer Deep. Authigenic deposition of ferromanganese phases, however, appears to be important in determining some of the distinctive compositional differences between metalliferous sediments deposited on the Bauer Deep and the rise crest. With the existing data we cannot unequivocally distinguish between either transport of hydrothermally produced precipitates from the rise crest (model 1) or the presence of hydrothermal sources of metals at both the EPR and the Bauer Deep (model 3). The distinction is perhaps important only in that with the transport model, the area of sedimentological influence of a mid-ocean ridge hydrothermal system would be of considerable areal extent. In any case we have demonstrated that the accumulation of metalliferous components in the Bauer Deep is approximately an order of magnitude lower than on the crest of the EPR.

Acknowledgements

This research was supported by the National Science Foundation as a contribution of the International Decade of Ocean Exploration (Nazca Plate Project) under contract with Oregon State University and the Hawaii Institute of Geophysics. We thank G.M. McMurtry and Ron Stillenger for carbonate analyses and atomic adsorption, respectively, and E.J. Dasch, Mitch Lyle, D.Z. Piper, C.C. von der Borch for helpful comments on the manuscript.

References

- 1 K. Boström, The origin and fate of ferromanganese active ridge sediments. *Acta Universitatis Stockholmiensis, Stockholm Contrib. Geol.* 27 (1973) 149.
- 2 D.S. Cronan, The Mid-Atlantic Ridge near 45°N, XVII. Al, As, Hg, and Mn in ferruginous sediments from the median valley. *Can. J. Earth Sci.* 9 (1972) 319.
- 3 J. Dymond, J.B. Corliss, G.R. Heath, C.W. Field, E.J. Dasch and H.H. Veeh, Origin of metalliferous sediments from the Pacific Ocean, *Geol. Soc. Am. Bull.* 84 (1973) 3355.
- 4 D.Z. Piper, Origin of metalliferous sediments of the East Pacific Rise, *Earth Planet. Sci. Lett.* 19 (1973) 75.
- 5 K. Boström and M.N.A. Peterson, The origin of aluminum-poor ferromanganean sediments in areas of high heat flow on the East Pacific Rise, *Mar. Geol.* 7 (1969) 427.
- 6 M. Bender, W. Broecker, V. Gornitz, U. Middel, R. Kay, S.S. Sun, and P. Biscaye, Geochemistry of three cores from the East Pacific Rise, *Earth Planet. Sci. Lett.* 12 (1971) 425.
- 7 E.J. Dasch, J. Dymond, and G.R. Heath, Isotopic analysis of metalliferous sediments from the East Pacific Rise, *Earth Planet. Sci. Lett.* 13 (1971) 175.
- 8 J.B. Corliss, The origin of metal-bearing hydrothermal solutions, *J. Geophys. Res.* 76 (1971) 8128.
- 9 J. Bischoff and F. Sayles, Pore fluid and mineralogical studies of recent marine sediments, Bauer Depression region of the East Pacific Rise, *J. Sediment. Petrol.* 42 (1972) 711.
- 10 R. Revelle, Marine bottom samples collected in the Pacific Ocean by the Carnegie on its seventh cruise, *Carnegie Inst. Washington Publ.* 556, part 1 (1944) 180 pp.
- 11 D. Rea, An analysis of a fast spreading rise crest: the East Pacific Rise, 9° to 12° south, *Geol. Soc. Am. Bull.* (1975) in press.
- 12 H.H. Veeh and K. Boström, Anomalous $^{234}\text{U}/^{238}\text{U}$ on the East Pacific Rise, *Earth Planet. Sci. Lett.* 10 (1971) 372.
- 13 W.M. Sackett, Measured deposition rates of marine sediments and implications for accumulation rates of extra-terrestrial dust, *Ann. N.Y. Acad. Sci.* 119 (1964) 339.
- 14 K.K. Turekian and L.H. Chan, The marine geochemistry of the uranium isotopes, Th-230 and Pa-331. In: *Activa-*

- tion Analysis in Geochemistry and Cosmochemistry, A.O. Brunlett and E. Steinnnes, eds. (Universitetsforlaget, 1971) 311.
- 15 D.L. Thurber, Anomalous $^{234}\text{U}/^{238}\text{U}$ in nature, *J. Geophys. Res.* 67 (1962) 4518.
 - 16 G.M. McMurtry and W.C. Burnett, Hydrothermal metallogenesis in the Bauer Deep of the southeastern Pacific, *Nature* 254 (1975) 42.
 - 17 J. Dymond, J.B. Corliss and R. Stillenger, Chemical composition and metal accumulation rates of metalliferous sediments from sites 319, 320B and 321, In: Hart, S.R., R.S. Yeats et al., Initial Reports of the Deep Sea Drilling Project, Vol. 34 (1975) in press.
 - 18 J.W. Kendrick, Trace element studies of metalliferous sediments in cores from the East Pacific Rise and Bauer Deep, 10°S, M.S. Thesis, Corvallis, Oregon State University (1974).
 - 19 M. Lyle and J. Dymond, Metal accumulation rates in the southeast Pacific - errors introduced from assumed bulk densities (1975) submitted to *Earth Planet. Sci. Lett.*
 - 20 G.R. Heath, J. Dymond and H.H. Veeh, Metalliferous sediments from the Southeast Pacific, in: The IDOE Nazca Plate, Sediments of the Southeast Pacific, A.P. Lizitin ed. (U.S.S.R. Acad. of Sciences) in press.
 - 21 M.L. Bender, T.L. Ku and W.S. Broecker, Accumulation rates of manganese in pelagic sediments and nodules, *Earth Planet. Sci. Lett.* 8 (1970) 143.
 - 22 M. Lyle, oral communication (1975).
 - 23 G.R. Heath, T.C. Moore, Jr., B.L.K. Somayajulu and D.S. Cronan, Sediment budget in a deep-sea core from the central equatorial Pacific, *J. Mar. Res.* 28 (1970) 225.
 - 24 P. Lonsdale, Abyssal circulation of the Southeast Pacific and some geological implications, personal communication (1975).
 - 25 E.M. Herron, Sea-floor spreading and the Cenozoic history of the east-central Pacific, *Geol. Soc. Am. Bull.* 83 (1972) 1671.
 - 26 R.N. Anderson and A.J. Halunen, Jr., The implications of heat flow for metallogenesis in the Bauer Deep, *Nature* 251 (1974) 473.
 - 27 R.N. Anderson and J.G. Sclater, Topography and evolution of the East Pacific Rise between 5°S and 20°S, *Earth Planet. Sci. Lett.* 14 (1972) 433.
 - 28 L. Hogan and J. Dymond, K-Ar and $^{40}\text{Ar}-^{39}\text{Ar}$ dating of site 319 and 321 basalts, In: Hart, S.R., R.S. Yeats et al., Initial Reports of the Deep Sea Drilling Project, Vol. 34 (1975) in press.
 - 29 J.B. Corliss and J. Dymond, Nazca Plate metalliferous sediments, I. Elemental distribution patterns in surface samples, *EOS Trans. Am. Geophys. Union* 56 (1975) 445.
 - 30 T.L. Ku, An evaluation of the $^{234}\text{U}/^{238}\text{U}$ method as a tool for dating pelagic sediments, *J. Geophys. Res.* 70 (1965) 3451.
 - 31 J.K. Cochran and J.K. Osmond, Sedimentation patterns and accumulation rates in the Tasman Basin, personal communication (1975).

Magnesium correction to the Na-K-Ca chemical geothermometer

R. O. FOURNIER and R. W. POTTIER II

Branch of Experimental Geochemistry and Mineralogy, U.S. Geological Survey,
345 Middlefield Road, Menlo Park, CA 94025, U.S.A.

UNIVERSITY OF UTAH
RESEARCH INSTITUTE
EARTH SCIENCE LAB.

(Received 4 January 1979; accepted in revised form 15 May 1979)

Abstract--Equations and graphs have been devised to correct for the adverse effects of magnesium upon the Na-K-Ca chemical geothermometer. Either the equations or graphs can be used to determine appropriate temperature corrections for given waters with calculated Na-K-Ca temperatures $> 70^\circ\text{C}$ and $R < 50$, where $R = \frac{[\text{Mg}]}{[\text{Mg} + \text{Ca} + \text{K}]} \times 100$ with cation concentrations expressed in equivalents. Waters with $R > 50$ are probably derived from relatively cool aquifers with temperatures approximately equal to the measured spring temperature, irrespective of much higher calculated Na-K-Ca temperatures.

INTRODUCTION

ALL WELL-documented high-temperature ($> 175^\circ\text{C}$) waters encountered in wells drilled into active hydrothermal systems have low concentrations of Mg^{2+} relative to the other dissolved cations. At the Reykjanes Peninsula, Iceland, where ocean water reacts with basalt at about $270\text{--}285^\circ\text{C}$, the dissolved magnesium decreases from 1272 to 1.0 mg/kg (ARNÓRSSON, 1978). In the highly saline, CaCl_2 -rich brine from the Salton Sea, Calif., drill hole 11D2 (WHITE, 1968), 54 mg/kg Mg^{2+} accounts for less than 0.1 equivalent % of the total cations. In laboratory experiments in which chlorite, calcite, and quartz were equilibrated with water under CO_2 pressures of 5 and 65 atm. ELLIS (1971) found Mg^{2+} concentrations ranging from ~ 0.5 to 1 mg/kg at 200°C , and from 0.02 to 0.05 mg/kg at 300°C . The above observations and the fact that many apparently low temperature, Mg-rich waters yield estimated Na-K-Ca temperatures (FOURNIER and TRUESDELL, 1973) well above 150°C cast considerable doubt on the usefulness of the Na-K-Ca geothermometer for Mg-rich waters. One example is ocean water ($\sim 4^\circ\text{C}$), with an Na-K-Ca estimated temperature of 173°C .

SELECTION OF DATA

A search of the literature was made to find chemical analyses of well waters that issued from a single aquifer at known temperature and which contained more than 1 mg/kg Mg^{2+} . Only a few well waters from geothermal energy producing systems were found that satisfied these criteria. Most of the Mg-rich thermal waters from known temperature environments are connate brines found in petroleum exploration. The connate brines chosen for inclusion in this study were selected to show a wide range in reservoir temperatures, salinities, and Na-K-Ca-Mg proportions.

Fifty well waters with Mg^{2+} concentrations ranging from 1 to 3920 mg/kg and with aquifer temperatures ranging from 3 to 340°C were used to test the temperature dependence of various cation ratios involving Mg^{2+} . Only one water was selected from those localities where all the wells appear to produce from the same aquifer at about the same temperature. No well waters were added to or subtracted from the list (Table 1) once the correlation process was started.

CATION RATIOS INVOLVING MAGNESIUM

Using molal concentration units, a plot of $\log(\text{Ca}/\text{Mg})$ vs the reciprocal of absolute temperature is shown in Fig. 1. The data on the Ca/Mg ratio are too scattered to be used as a reliable cation geothermometer. Plots of the reciprocal of absolute temperature vs $\log(\sqrt{\text{Mg}/\text{Na}})$ (Fig. 2) and vs $\log(\sqrt{\text{Mg}/\text{K}})$ (Fig. 3) show less scatter than the $\log(\text{Ca}/\text{Mg})$ plot, but still have more scatter than is desirable for use as a cation geothermometer. Correlation coefficients and equations for least squares-fitted straight lines through the points shown in Figs 1, 2, and 3 are given in Table 2.

The logarithmic expressions for the cation ratios Na/K, $\sqrt{\text{Ca}/\text{Na}}$, $\sqrt{\text{Ca}/\text{K}}$, $\sqrt{\text{Mg}/\text{Na}}$, $\sqrt{\text{Mg}/\text{K}}$, and Ca/Mg were plotted in various combinations and proportions (25 plots), as was done in the derivation of the Na-K-Ca chemical geothermometer, without significantly reducing the scatter below that shown in Fig. 3. Scatter would probably be greatly diminished if the plotted points could be restricted to data from systems in which the same solid phases were involved in the reactions. However, at this time there is insufficient data to test this idea.

EMPIRICAL MAGNESIUM CORRECTION

A method of applying a magnesium correction to the Na-K-Ca estimated temperatures was discovered

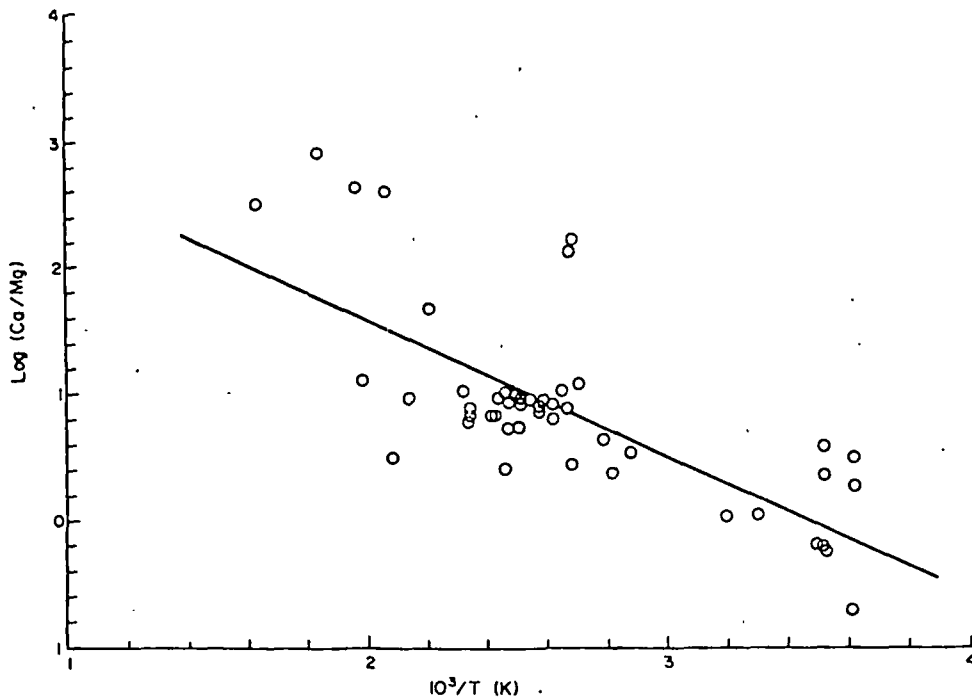


Fig. 1. Log (Ca/Mg), using molal units, vs reciprocal of absolute temperature for well waters from known temperature environments and with Mg^{2+} concentration > 1 mg/kg.

when the data were plotted as shown in Fig. 4. For any given water the magnitude of this correction depends on both the Na-K-Ca estimated temperature and the Mg^{2+} concentration relative to the sum of dissolved Mg^{2+} , K^+ , and Ca^{2+} , with concen-

trations expressed in equivalents. In Fig. 4 the Δt temperature contours (dashed lines) were graphically interpolated. They can be used to obtain a temperature correction that must be subtracted from the Na-K-Ca estimated temperature to arrive at the actual

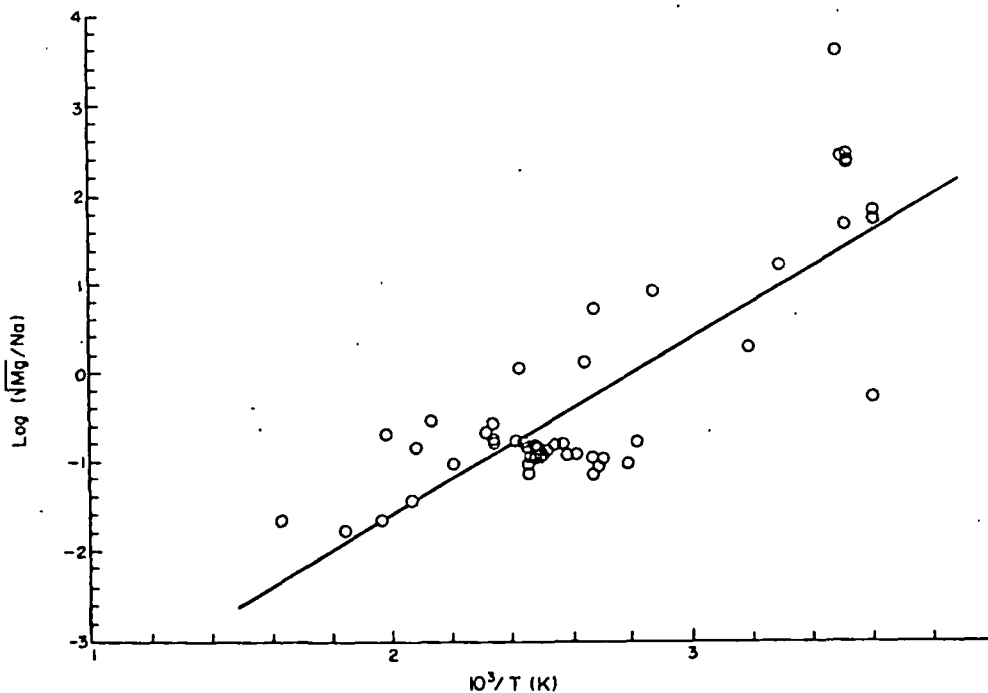


Fig. 2. Log (\sqrt{Mg}/Na), using molal units, vs reciprocal of absolute temperature for well waters from known temperature environments and with Mg^{2+} concentration > 1 mg/kg.

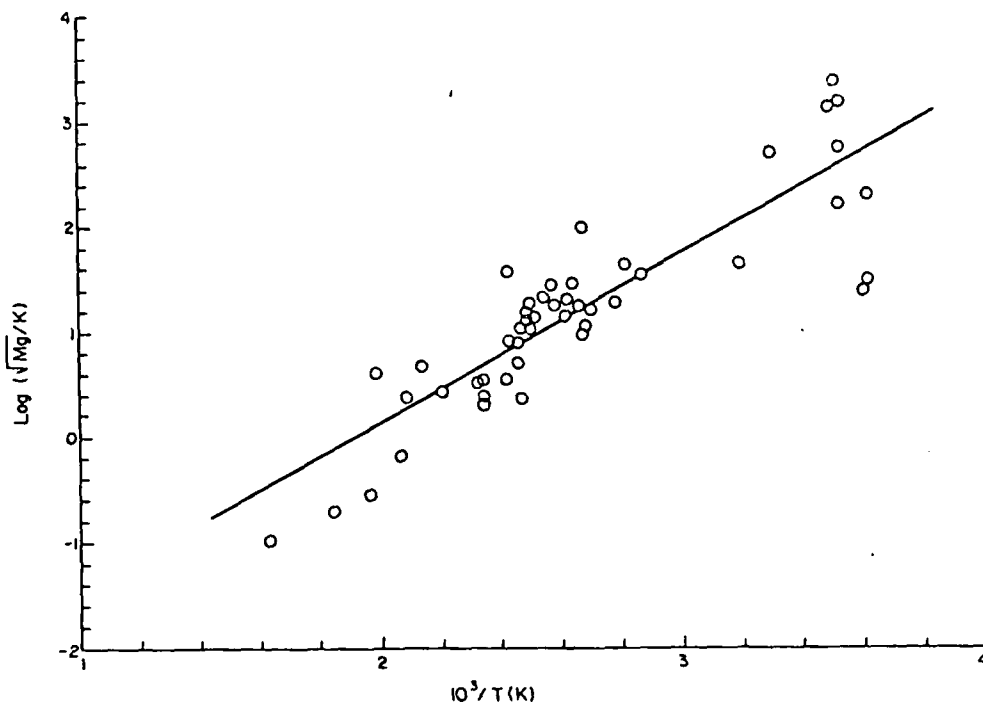


Fig. 3. $\text{Log } (\sqrt{\text{Mg/K}})$, using molal units, vs reciprocal of absolute temperature for well waters from known temperature environments and with Mg^{2+} concentration $> 1 \text{ mg/kg}$.

Table 1. Chemical data for waters with magnesium concentrations greater than 1 mg/kg from known temperature environments. Concentrations are in mg/kg or in mg/L depending upon the units given in the listed references

	Ref.	Well. Temp. °C	Na-K-Ca temp. °C	Na	K	Ca	Mg	%Mg*
Czechoslovakia								
Marklin 1	1	3.2	31	5.5	2.5	18.0	3.6	23.5
Loket 2	1	3.2	28	10.5	4.0	62.5	20.7	32.0
Chili								
El Tatio 1	2	211	205	4480	420	740	1.1	0.2
El Tatio 6	2	180	181	1900	111	99	1.3	1.4
Hungary								
Budapest- Varosliget	3	100	74.6	170	16	160	35.5	25.8
Iceland								
Krisuvik 3	4	105		136	10.8	24.6	1.4	7.1
Krisuvik 7	4	30	36	30.6	1.7	18.4	10.4	47.1
Krisuvik 7	4	139	148	160	8.2	15.3	1.4	10.6
Lysuholl 1	5	40	174	414	31.1	46.0	26.6	41.5
Reykjanes 8	4	270	241	9854	1391	1531	1.15	0.1
Svartsengi 3	6	236	245	6322	1012	906	1.27	0.1
New Zealand								
Ngawha 1	7	230	201	900	78	29	1.4	3.2
Turkey								
Kizildere 15	8	207	232	1173	117	6.0	1.19	2.9
United States								
Cen. Miss. 1	9	132	222	79,000	7080	34,000	3920	14.7
Cen. Miss. 6	9	102	113	52,400	551	16,800	1360	11.6
Cen. Miss. 9	9	141	207	53,800	4430	39,200	3610	12.6
Cen. Miss. 10	9	109	109	52,100	519	22,200	1660	10.9
Cen. Miss. 15	9	129	124	54,200	863	41,200	2550	9.2
Cen. Miss. 16	9	137	158	58,300	2030	55,600	3740	9.8
Cen. Miss. 20	9	116	120	49,900	461	29,500	2290	11.3
Cen. Miss. 21	9	116	105	50,100	474	30,700	2510	11.8
Cen. Miss. 22	9	120	115	48,800	625	37,200	2550	10.1
Cen. Miss. 23	9	131	140	59,700	1340	45,000	3230	10.4
Cen. Miss. 25	9	86	109	40,100	333	4140	582	18.2
Cen. Miss. 26	9	109	125	53,700	750	16,800	1640	13.6

—continued

Table 1 continued

	Ref.	Well Temp. C	Na-K-Ca temp. C	Na	K	Ca	Mg	%,Mg*
Can. Miss. 29	9	125	128	53,900	888	28,900	2150	10.8
Can. Miss. 30	9	127	118	53,600	649	19,300	2200	15.6
Can. Miss. 31	9	154	244	46,500	6800	30,600	2970	12.6
Can. Miss. 32	9	154	227	52,400	5980	37,400	3010	10.9
Can. Miss. 33	9	154	266	29,200	3830	25,700	2480	12.9
Can. Miss. 34	9	154	229	52,000	6080	37,700	3410	12.1
Can. Miss. 38	9	127	133	54,000	979	26,500	1630	9.1
Can. Miss. 39	9	129	123	61,100	854	28,800	1830	9.4
Can. Miss. 42	9	158	214	29,000	3030	25,000	1470	8.4
Can. Miss. 43	9	114	115	53,200	635	27,300	1880	10.1
Can. Penn. 10	10	10.5	2	2.5	1.8	55	15	30.7
Can. Penn. 91	10	11.2	35	13	6.3	92	15	20.6
Can. Penn. 257	10	11.5	-9.8	4.3	0.8	54	54	62.1
Can. Penn. 285	10	13	-16	0.3	1.4	56	55	61.5
Can. Penn. 1040	10	10.6	0.25	5.3	1.3	56	59	63.2
Kettleman Hills								
323-21J	11	134	139	3090	59.4	53.8	3.31	6.1
47-28J	12	101	107	6240	79.4	1780	8.0	0.7
321-20J	11	134	165	3080	75.1	8.6	2.05	6.7
31-18Q	12	82	98	13,200	88.4	797	206	28.7
66-7Q	12	97	112	13,800	149	1700	88	7.6
61-33J	12	99	102	7780	97	5030	18.4	0.6
Salton Sea								
11D1	13	340	317	50,400	17,500	28,000	54	0.2
Yellowstone Park								
Y-10	14	70	100	161	69	455	80	21.2
USSR								
Pauzhetka 4	15	195	209	986	105	52	3.5	5.2
OCEAN WATER	16	4	173	10,560	380	400	1270	77.9

References

1. PACES (1972).
2. CUSICAUQUI *et al.* (1976).
3. BOLDIZAR and KORIM (1976).
4. ARNÖRSSON *et al.* (1976).
5. ARNÖRSSON (1975).
6. LINDAL (1976).
7. MAHON (1970).
8. KURTMAN (1977).
9. CARPENTER *et al.* (1974).
10. LANGMUIR (1971).
11. KHARAKA and BERRY (1976).
12. KHARAKA and BERRY (1974).
13. WHITE (1965).
14. R. O. FOURNIER and R. D. BARNES (unpublished data).
15. VAKIN *et al.* (1970).
16. WHITE (1965).

* Equivalent percent Mg/(Mg + Ca + K).

temperature of the system. For example, point A, with a Na-K-Ca temperature of 200°C and $R = 25.0$, requires a correction of ~125°C that must be subtracted from the 200° Na-K-Ca temperature, where $R = \{Mg/(K + Ca + Mg)\} \times 100$, with cation concentrations expressed in equivalents.

In Fig. 4 the placement and curvatures of the 0, 25, and 100°C temperature correction curves are well constrained below $R = 30$. The upward projections of these curves and the positions of the 150, 200, and 250°C correction curves are controlled by the ocean-water data point and the requirement that the temperature correction, Δt_{Mg} , be always less than the Na-K-Ca estimated temperature. As more and better data become available, the curvatures and positions

of these temperature correction curves will require revision.

The following equation describes most of the relations shown in Fig. 4:

$$\Delta t_{Mg} = 10.66 - 4.7415R + 325.87(\log R)^2 - 1.032 \times 10^5(\log R)^2/T - 1.968 \times 10^7(\log R)^2/T^2 + 1.605 \times 10^7(\log R)^3/T^2, \quad (1)$$

where Δt_{Mg} is the temperature in °C to be subtracted from the calculated Na-K-Ca temperature, and, where

$$T = \text{the calculated Na-K-Ca temperature (K)}, \\ R = \{Mg/(K + Ca + Mg)\} \times 100,$$

with concentrations expressed in equivalents.

Table 2. Equations for the least squares best fit straight lines regressed through the data shown in Figs. 1, 2, and 3. Molar concentrations of Ca, Mg, Na, and K are used; T is absolute temperature; and r^2 is the correlation coefficient

$\log(\text{Ca/Mg}) = \frac{1708}{T} + 3.740$	$r^2 = 0.525$
$\log(\sqrt{\text{Mg/Na}}) = \frac{1982}{T} - 5.583$	$r^2 = 0.671$
$\log(\sqrt{\text{Mg/K}}) = \frac{1598}{T} - 3.061$	$r^2 = 0.733$

Do not apply a Mg^{2+} correction to the Na-K-Ca geothermometer if Δt_{Mg} is negative.

We recommend that eqn (1) be used only when Na-K-Ca estimated temperatures are $> 70^\circ\text{C}$ and when R is in the range 5-50. Although eqn (1) appears to work well for some waters with $R > 50$, the Mg-

corrected temperatures of most spring waters were found to be 10-20°C below the measured temperatures. We have corrected for this difficulty by using a more complicated equation with nine terms, but these complications do not seem warranted because any water with $R > 50$ probably either has equilibrated with rock at about the measured temperature (irrespective of a much higher calculated Na-K-Ca temperature) or represents a nonequilibrium condition.

In the region where $R < 5$ and $\Delta t_{\text{Mg}} < 10$, the values for Δt_{Mg} calculated from eqn (1) diverge from our best guess for Δt_{Mg} (see Fig. 5). Our best guess values for Δt_{Mg} at small R were obtained by projecting constant Na-K-Ca-temperature data onto a plot of R vs Δt_{Mg} . Eqn (2) can be used to calculate Δt_{Mg} for waters with $0.5 < R < 5$:

$$\Delta t_{\text{Mg}} = -1.03 + 59.971 \log R + 145.05(\log R)^2 - 36711(\log R)^2/T - 1.67 \times 10^7 \log R/T^2. \quad (2)$$

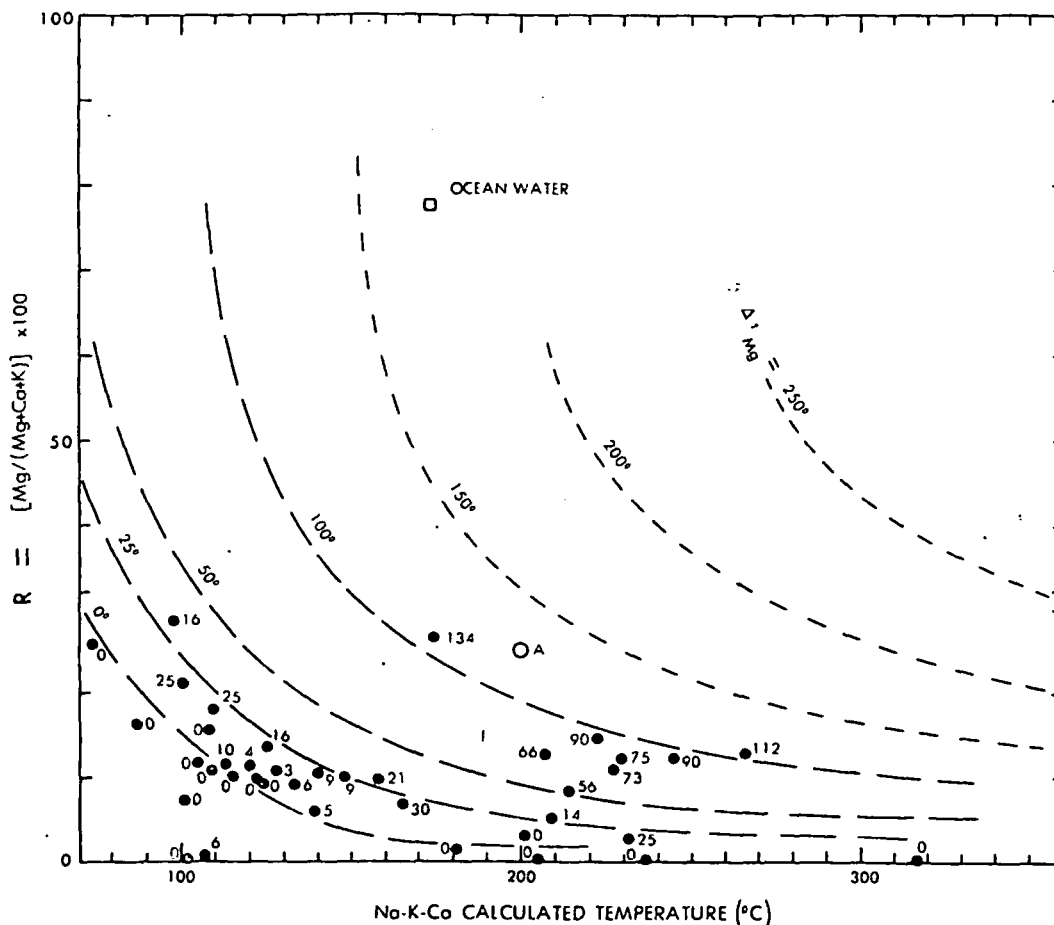


Fig. 4. Plot of $R = [\text{Mg}/(\text{Mg} + \text{Ca} + \text{K})] \times 100$, with concentrations expressed in equivalent units, vs Na-K-Ca calculated temperature. Dashed curves show temperature correction, Δt_{Mg} , to be subtracted from calculated Na-K-Ca temperature to correct for dissolved magnesium. Dots are data from well waters listed in Table 1. Numbers near data points show difference ($^\circ\text{C}$) between Na-K-Ca calculated and probable aquifer temperatures.

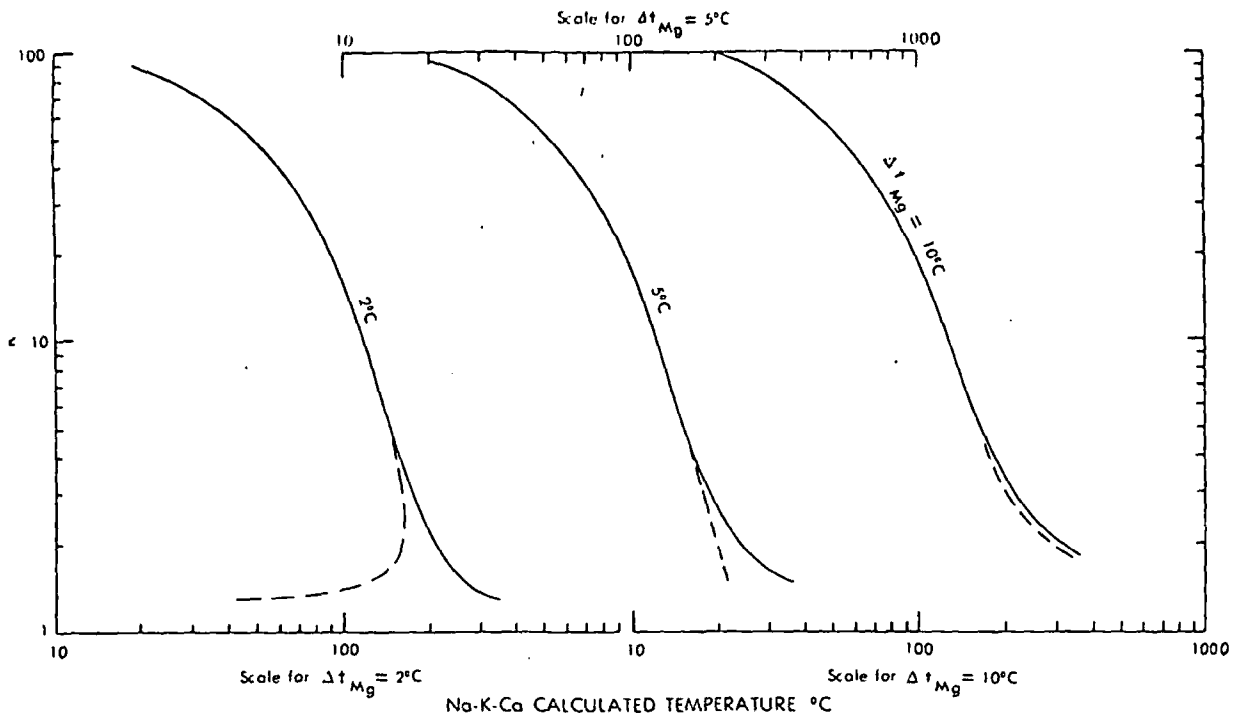


Fig. 5. Logarithmic plot of R vs Na-K-Ca calculated temperature, showing best guess positions of 2, 5, and 10°C temperature correction curves (solid lines). Dashed lines show curves calculated from eqn (1). Dashed and solid curves coincide for values of $R > 5$ and for $\Delta t > 10$ C.

Again, do not apply a Mg^{2+} correction to the Na-K-Ca geothermometer if Δt_{Mg} is negative, or if $R < 0.5$.

Figures 6 and 7, show lines of constant R superimposed on plots of Δt_{Mg} vs Na-K-Ca temperature and present an alternative graphical method of calculating Δt_{Mg} . Figure 6 is for $R = 5$ to 50, and Fig. 7 for $R = 0-5$.

When using Figs 4, 6, and 7 to correct Na-K-Ca calculated temperatures, it should be kept in mind that our method is entirely empirical and may not work equally well for all waters. Problems in calibrating the method are: (i) solid reactants are not specified or structurally characterized; (ii) complexing of dissolved species is not considered (when temperature is the unknown, activity coefficients must be calculated assuming successive approximations of that temperature; a tedious process that isn't warranted given the precision of the result and practical purpose); (iii) individual well waters may not have equilibrated at the maximum measured or estimated temperature (water may be entering a well from a higher or lower temperature aquifer); and (iv) some well waters may be mixtures of two or more waters entering at various depths and not equilibrating after mixing.

This paper provides an additional tool to distinguish waters in equilibrium with rock at high temperatures underground from waters that result from low-temperature (<70°C) water-rock reactions. As with all chemical geothermometers, our Mg-corrected

Na-K-Ca geothermometer is sensitive to near-surface water-rock reactions that occur in response to lowering temperatures or changing mineralogy of wall-rocks. If a rising water acquires magnesium, application of a magnesium correction to the Na-K-Ca geothermometer will probably lead to a calculated aquifer temperature that is too low. However, high Mg^{2+} concentrations indicate that water-rock reactions have occurred at relatively low temperatures. During these low-temperature reactions the concentrations of other dissolved constituents will also likely change. Therefore, in general, chemical geothermometer results should be used with great caution when applied to Mg-rich waters.

SUGGESTED CORRECTION PROCEDURE

1. Calculate the Na-K-Ca temperature as described by FOURNIER and TRUESDELL (1973). Do not apply a magnesium correction if this calculated temperature is below 70°C.

2. Calculate $R = \{Mg/(Mg + Ca + K)\} \times 100$, using equivalent units of concentration.

3. If $R > 50$, assume that the water comes from a relatively cool underground environment at a temperature approximately equal to the measured water temperature, irrespective of high calculated Na-K-Ca temperature.

4. If the calculated Na-K-Ca temperature is greater than 70°C and $R < 50$, use Figs 4, 6, or 7 to calculate

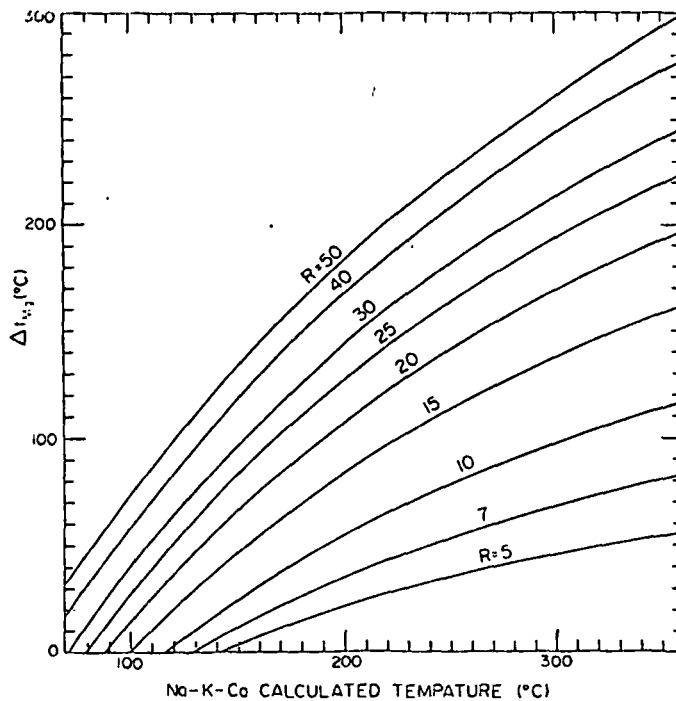


Fig. 6. Graph for estimating magnesium temperature correction, ΔT_{Mg} , using Na-K-Ca calculated temperature and $R = 5-50$. Curves were drawn from eqn (1). Move directly up from the calculated Na-K-Ca temperature to the intersection (or interpolated value) of the line having the calculated R value; move horizontally from the R -value intersection, and read the value of ΔT_{Mg} on the ordinate.

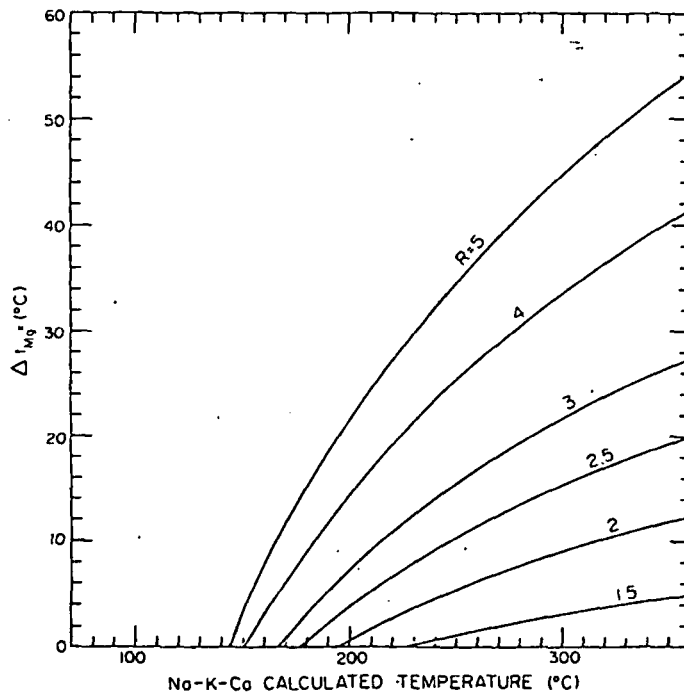


Fig. 7. Graph for estimating magnesium temperature correction, ΔT_{Mg} , using Na-K-Ca calculated temperature and $R = 1.5-5$. Curves were drawn from eqn (2). Move directly up from the calculated Na-K-Ca temperature to the intersection (or interpolated value) of the line having the calculated R value; move horizontally from the R -value intersection, and read the value of ΔT_{Mg} on the ordinate.

surface
lower-
of wall-
a, appli-
a-K-Ca
calculated
er, high
ck reac-
eratures.
concen-
also likely
geother-
caution

URE

e as de-
) Do not
ated tem-

($\times 100$,

comes from
at a tem-
red water
Na-K-Ca

e is greater
o calculate

Δt_{Mg} , which is the temperature correction (in °C) to be subtracted from the Na-K-Ca calculated temperature.

5. When using a computer to calculate Δt_{Mg} the following tests should be included in the program:

(a) Check if the Na-K-Ca calculated temperature is < 70°C. If yes, do not proceed further with a magnesium correction.

(b) Check if $R > 50$. If yes, assume that the water in the aquifer is relatively cold and do not proceed further with a magnesium correction.

(c) If $R = 5-50$, use eqn (1) to calculate Δt_{Mg} . Do not apply a magnesium correction if Δt_{Mg} is negative.

(d) If $0.5 < R < 5$, use eqn (2) to calculate Δt_{Mg} . Do not apply a magnesium correction if Δt_{Mg} is negative, or if $R < 0.5$.

(e) Subtract Δt_{Mg} from the calculated Na-K-Ca temperature.

REFERENCES

- ARNÓRSSON S. (1975) Application of the silica geothermometer in low temperature hydrothermal areas in Iceland: *Am. J. Sci.* 275, 763-784.
- ARNÓRSSON S. (1978) Major element chemistry of the geothermal sea-water at Reykjanes and Svartsengi, Iceland: *Mineral. Mag.* 42, 209-220.
- ARNÓRSSON S., BJÖRNSSON A., GÍSLASON G. and GUDMUNDSSON G. (1976) Systematic exploration of the Krísuvík high-temperature area, Reykjanes Peninsula, Iceland. In *United Nations Symposium on the Development and Use of Geothermal Resources*, 2nd, Proceedings, San Francisco, CA, 1975, Vol. 2, pp. 853-864. U.S. Government Printing Office.
- BOLDIZAR T. and KORIM K. (1976) Hydrogeology of the Pannonian geothermal basin [Hungary]. In *United Nations Symposium on the Development and Use of Geothermal Resources*, 2nd, Proceedings, San Francisco, CA, 1975, Vol. 1, pp. 297-303. U.S. Government Printing Office.
- CARPENTER A. B., TROUT M. L. and PICKETT E. E. (1974) Preliminary report on the origin and chemical evolution of lead- and zinc-rich oil field brines of central Mississippi: *Econ. Geol.* 69, 1191-1206.
- CUSICANQUI H., MAHON W. A. J. and ELLIS A. J. (1976) The geochemistry of the El Tatio geothermal field, northern Chile. In *Second United Nations Symposium on the Development and Use of Geothermal Resources*, 2nd, Proceedings, San Francisco, CA, 1975, Vol. 1, pp. 703-711. U.S. Government Printing Office.
- ELLIS A. J. (1971) Magnesium ion concentrations in the presence of magnesium chloride, calcite, carbon dioxide, quartz: *Am. J. Sci.* 271, 481-489.
- FOURNIER R. O. and TRUESDELL A. H. (1973) An empirical Na-K-Ca geothermometer for natural waters: *Geochim. Cosmochim. Acta* 37, 1255-1275.
- KIARAKA Y. K. and BERRY F. A. F. (1974) The influence of geological membranes on the geochemistry of subsurface waters from Miocene sediments at Kettleman North Dome in California: *Water Resour. Res.* 10, 313-327.
- KIARAKA Y. K. and BERRY F. A. F. (1976) The influence of geological membranes on the geochemistry of subsurface waters from Eocene sediments at Kettleman North Dome, California—an example of effluent-type waters. In *International Symposium on Water-Rock Interaction*, 1st, Proceedings, Prague, Czechoslovakia, 1974, pp. 268-277.
- KURTMAN F. (1977) Geothermal energy investigations in Turkey: Unpublished report presented at the CENTO Workshop on Geothermal Energy, Ankara, Turkey, 1977.
- LANGMUIR D. (1971) The geochemistry of some carbonate ground waters in central Pennsylvania: *Geochim. Cosmochim. Acta* 35, 1023-1043.
- LINDAL B. (1976) Development of industry based on geothermal energy, geothermal brine, and sea water in the Reykjanes Peninsula, Iceland. In *United Nations Symposium on the Development and Use of Geothermal Resources*, 2nd, Proceedings, San Francisco, CA, 1975, Vol. 3, pp. 2223-2228. U.S. Government Printing Office.
- MAHON W. A. J. (1970) Chemistry in the exploration and exploitation of hydrothermal systems. In *United Nations Symposium on the Development and Utilization of Geothermal Resources*, Pisa, Italy, 1970, Proceedings: *Geothermics* Special Issue 2, pt. 2, 1310-1322.
- PÁČES T. (1972) Chemical characteristics and equilibration in natural water-felsic rock-CO₂ system: *Geochim. Cosmochim. Acta* 36, 217-240.
- VAKIN E. A., POLAK B. G., SUGROBOV V. M., ERLIKH E. N., BELOUSOV V. I. and PILIPENKO G. F. (1970) Recent hydrothermal systems of Kamchatka [U.S.S.R.]. In *United Nations Symposium on the Development and Utilization of Geothermal Resources*, Pisa, Italy, 1970: *Geothermics* Special Issue 2, pt. 2, 1116-1133.
- WHITE D. E. (1965) Saline waters of sedimentary rocks. In *Fluids in Subsurface Environments—a Symposium*, American Association of Petroleum Geologists Memoir No. 4, pp. 342-366.
- WHITE D. E. (1968) Environments of generation of some base-metal ore deposits: *Econ. Geol.* 63, 301-335.

SUBJ
GCHM
MCM

A method for computing multicomponent chemical equilibria based on equilibrium constants

DAVID A. CREER

Department of Geological and Geophysical Sciences, Princeton University,
Princeton, N.J. 08540, U.S.A.

(Received 21 November 1974; accepted in revised form 10 March 1975)

Abstract—The equilibrium activities and concentrations of N chemical species in a multicomponent system may be calculated given M independent equilibrium constants relating these species and $N-M$ mass balances. These N equations are solved by Newton-Raphson iteration. Where initial concentration estimates are poor or the number of species large, an additional curve crawler technique introduces components by stepwise infinitesimal increments.

INTRODUCTION

MANY AVAILABLE techniques for the computation of chemical equilibria in complex systems have been reviewed by VAN ZEGGEREN and STOREY (1970), who recognized two main methods: (1) the solution of a generalized set of simultaneous non-linear equations which usually incorporate equilibrium constants (e.g. FELDMAN *et al.*, 1969), and (2) optimization techniques, which normally minimize the total Gibbs free energy function (e.g. REESE, 1973; KARPOV and KAZ'MIN, 1972). Such techniques are typically generalized and apply to arbitrary systems for which suitable thermodynamic data are available.

Two additional methods often used within the geosciences, could be added to this list. Method (3), developed by HELGESON (1968, 1970), determines compositional changes, mass transfers, and the order of appearance of stable and metastable phases in tracing irreversible reaction paths from an initial set of non-equilibrium conditions to a final state of equilibrium. The fourth method entails specific, as opposed to generalized, calculations. Here, a set of equations describing a given system is reduced to one or more equations amenable to simple numerical solution. Typical procedures are described by BUTLER (1964), BLACKBURN (1969), and FREISER and FERNANDO (1966). Various geochemical examples are given by HELGESON (1964, p. 56), who calculates galena solubility in the system NaCl-HCl-H₂O, and by CREER and ANDERSON (1971), who calculate quartz solubility in the systems H₂O-NaOH and H₂O-NaOH-NaHS. On a larger scale, TRUESDELL and JONES (1974) have now developed the program WATEQ, which computes the equilibrium distribution of inorganic species

in natural waters, given total element concentrations, pH, and Eh.

This paper introduces a method of the first type for computing generalized chemical equilibria. Equilibrium concentrations or activities are derived from simple mass and charge balances and arbitrary independent equilibrium constants. Non-ideality corrections may be included in the computation. The resultant non-linear equations are solved by combining Newton-Raphson iteration and supportive curve crawler techniques. Because it uses arbitrary equilibrium constants, the method can be particularly appropriate to geochemical systems lacking complete free energy data.

GLOSSARY OF SYMBOLS

a_{ij}	number of atoms of the l th element in 1 molecule of the j th component.
b_{ei}	number of atoms of element e in 1 molecule of species i .
B_e	total molal concentration of the e th element in the system.
C	total number of independent chemical components in the system.
C_{ah}^i	molarity of the i th species corrected for association and hydration.
f_e^i	mole-fractional specific ion activity coefficient correcting for electrostatic interaction.
$\Delta G_{f,i}^0$	Gibbs free energy of formation of the i th species.
h_i	average moles of solvent hydrating 1 mole of solute species i .
I	true ionic strength.
K_i	i th equilibrium constant.
m_i	molal concentration of the i th species.
m_a^i	molarity of the i th species corrected for association.

m_{ah}^i	molality of the i th species corrected for association and hydration.
M	total number of independent equilibrium constants.
n	total number of moles of all components in the system.
N	total number of chemical species in the system.
q_j	total number of moles of the j th component in the system.
Q_i	total number of moles of the i th element in the system.
R	total number of components in the system.
S	total number of constituent species formed from 2 or more components.
x_j	mole-fraction of the j th component in the system.
X_j	j th component species.
y_i	mole-fraction of the i th constituent in the system.
Y_i	i th constituent species formed from 2 or more components.
Z_i	signed valence of the i th species.
γ_i	true molal activity coefficient of the i th species.
γ_e^i	molal activity coefficient of the i th species correcting for electrostatic interaction.
γ_h^i	molal activity coefficient of the i th species correcting for hydration.
γ_{eh}^i	molal activity coefficient of the i th species correcting for electrostatic interaction and hydration.
v_{ij}	number of moles of the j th component in 1 mole of the i th constituent species.
v_{ki}	signed stoichiometric coefficient representing the number of formulae of the i th species written in the k th reaction; sign is negative for reactants and positive for products.
ρ	solution density (g/ml).
ψ_i	i th mass balance, charge balance, or equilibrium constant equation.

STATEMENT OF THE PROBLEM

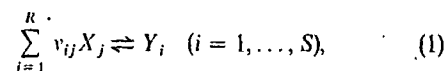
Most simpler geochemical applications are satisfied by the fourth, or specific, type of equilibrium calculation cited above. In other words, a system-defining set of specific charge and mass balances and mass action expressions is solved by algebraic manipulation. However, as the number of components or species increases, the defining equations more frequently reduce to difficult non-linear expressions. With the simpler systems, the alternative generalized routines can be time-saving; for more complex problems, they may often provide the only practical solution.

As a case in point, generalized routines have now been applied to geochemical systems so complex that they could not be solved by simple algebraic manipulation. For example, HOLLOWAY and REESE (1974) have used free-energy minimization programs to solve for the equilibrium fugacities of over 40 species in

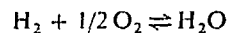
the system C—O—H—N at elevated temperatures. Similarly, KARPOV and KAZ'MIN (1972) have determined the equilibrium activities of 21 species in seawater using an alternative minimization algorithm. Where Gibbs free energies of all chemical species are available, optimization methods are convenient and reliable.

Unfortunately, free-energy data are often frustratingly incomplete for systems of practical interest. This is particularly true, for example, with the high temperature mineral-water systems crucial to the current demand for alternative geothermal power (BARNES, *in press*). Note, however, that equilibrium constants may be available for such systems even when free-energy data are not—see, for example, SILLÉN and MARTELL (1964), BARNES *et al.* (1966), HELGESON (1969), and TRUESDELL and JONES (1974). Although any equilibrium constants can be calculated given formation free-energies of all reacting species, the converse is not necessarily true. Accordingly, there is a growing demand for computational methods based exclusively on equilibrium constants, which represent a minimal set of free-energy information.

Using one such method, FELDMAN *et al.* (1969) have now computed equilibrium compositions of high temperature coal combustion mixtures containing up to 65 species including gases, liquids, free electrons, and ions. Their basic method was originally described by BRINKLEY (1947) and KANDINER and BRINKLEY (1950) (see also VAN ZEGGEREN and STOREY, 1970, Chap. 4). Typically, all N chemical species of a given system are divided into R components, and S constituents, defined by the following set of formation reactions:



where each v_{ij} is a stoichiometric coefficient representing formation of the i th constituent, Y_i , from the j th component, X_j . For example, choosing H_2O as a constituent formed from the components H_2 and O_2 , then reaction (1) would be written:



and the stoichiometric coefficients v_{H_2} and v_{O_2} would be 1 and 1/2, respectively. Reactions (1) can be described by S mass action expressions:

$$y_i = K_i \prod_{j=1}^R x_j^{v_{ij}} \quad (i = 1, \dots, S), \quad (2)$$

where y_i and x_j represent mole-fractional compositions of constituents Y_i and components X_j , respectively, and each K_i is a conventional equilibrium constant.

Assur
of each
the num
ments (i
ponent ;

where q_i
system. ;
number
with the
carbon.
Const
in terms
ponent. ;
stituent ;

where n ;
in the sys

Finally
expressed

The ab
equilibri
methods :
or k th se
(ii) Using
correspon
(iii) With
equations
one of the
ponent cc
is given by
(iv) Return
time settir
The rev
al. (1969)
omitted h
become n
the total r
The mass
Raphson i
bra.

The Brit
ling multi
siderable 0

Assume now that the total number of moles, Q_l , of each element in the system is known, and that the number of components equals the number of elements ($l = 1, \dots, R$). Then mass balances on each component give

$$Q_l = \sum_{j=1}^R a_{lj} q_j \quad (l = 1, \dots, R), \quad (3)$$

where q_j is the total moles of j th component in the system, and each a_{lj} represents the stoichiometry, or number of atoms of element l in component j . Thus, with the component CO_2 , a_{lj} is 1 for the element carbon, 2 for oxygen, and 0 for any other element.

Constituent mass balances now may be expressed in terms of the concentrations of each pure component, and of those components tied up in each constituent species of the system:

$$q_j = x_j n + \sum_{i=1}^S v_{ij} y_i n \quad (j = 1, \dots, R), \quad (4)$$

where n represents the total moles of all components in the system

$$\left(n = \sum_{j=1}^R q_j \right).$$

Finally, the mole fraction identity condition may be expressed by the single equation

$$1 = \sum_{j=1}^R x_j + \sum_{i=1}^S y_i. \quad (5)$$

The above equations (1)–(5) may be solved for the equilibrium concentrations x_j and y_i by numerical methods such as the following: (i) estimate an initial or k th set of all R component concentrations $x_j^{(k)}$. (ii) Using these $x_j^{(k)}$ and equations (2), calculate the corresponding S constituent concentrations $y_i^{(k)}$. (iii) With these $y_i^{(k)}$ estimates, solve the R mass balance equations (4) [possibly substituting expression (5) for one of these] for new estimates, $x_j^{(k+1)}$, of all R component compositions. The q_j term in equations (4) is given by expression (3), and is constant throughout. (iv) Return to step (1) and repeat to convergence, each time setting $x_j^{(k+1)} = x_j^{(k)}$.

The revised Brinkley method used by FELDMAN *et al.* (1969) includes terms for multiple phases. While omitted here for clarity, the mass balances (4) then become non-linear in x_j , y_i , and $n^{(\phi)}$, where $n^{(\phi)}$ is the total moles of all components in the ϕ th phase. The mass balances must then be solved by Newton-Raphson iteration, rather than by simple matrix algebra.

The Brinkley method has proven effective in handling multicomponent, multiphase problems of considerable complexity. However, the use of mass action

expressions (1) and (2) requires that equilibrium constants be known for the formation of all S constituents from all R components. These specific constants may not be available unless free energies are known for all N species. For example, the equilibrium constants K_i would usually be obtained from the relationship

$$\ln K_i = \frac{1}{RT} \left[-\Delta G_{f,i}^0 + \sum_{j=1}^R v_{ij} \Delta G_{f,j}^0 \right], \quad (6)$$

where $\Delta G_{f,i}^0$ and $\Delta G_{f,j}^0$ are the standard Gibbs free energies of formation from the elements of the i th constituent and j th component, respectively. Because the method typically requires prior knowledge of formation free-energies for all $R + S = N$ species within the system, free energy minimization techniques apply equally well in such cases; thus, the goal of a generalized method using arbitrary equilibrium constants is no closer at hand. Therefore, in order to permit the use of arbitrary equilibrium constants relating any two or more species of the system, the method outlined below does not distinguish so-called component species from constituents.

COMPUTING ROUTINE

Consider an arbitrary system of C components containing N chemical species. Assume that equilibrium constants are known for M independent reactions relating some or all of these species.

If the system is ionic, a charge balance may be written:

$$\Psi_1 = 0 = \sum_{i=1}^N Z_i m_i, \quad (7)$$

for which

$$\frac{\partial \Psi_1}{\partial m_i} = Z_i \quad (i = 1, \dots, N). \quad (8)$$

Z_i is the signed valence of the i th species, and m_i is its concentration (here arbitrarily considered as molality).

Assume next that the total molal concentrations B_e of $N-M-1$ elements or atomic species are specified for the system. Simple mass balances on these elements give,

$$\Psi_j = 0 = -B_e + \sum_{i=1}^N b_{ei} m_i \quad (j = 2, 3, \dots, N-M, \text{ as } e = j - 1) \quad (9)$$

and

$$\frac{\partial \Psi_j}{\partial m_i} = b_{ei} \quad (i = 1, \dots, N) \quad (j = 2, 3, \dots, N-M). \quad (10)$$

Here B_e is the total molal concentration of the e th element in the system, and b_{ei} describes the elemental composition of the i th species according to the formula vector $\beta_i = [b_{i1}, \dots, b_{i,N-M-1}]^T$. For example, if the elements H, C, O, and N are assigned the row positions 1, 2, 3,

and 4 in β_i , respectively, then the formula vector for the species H_2CO_3 is $[2\ 1\ 3\ 0]^T$. If the total number of elements in the system is E , then the scalar quantities b_{ei} define an $E \times N$ system composition matrix of rank C (see VAN ZEGGEREN and STOREY, 1970, p. 16).

Finally, the M mass action expressions may be written in the form:

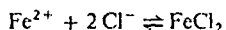
$$\Psi_k = 0 = \frac{-K_k}{N} + \prod_{i=1}^N m_i^{v_{ki}} \quad (k = N - M + 1, \dots, N) \quad (11)$$

and

$$\frac{\partial \Psi_k}{\partial m_i} = v_{ki} m_i^{v_{ki}-1} \prod_{i \neq l} m_l^{v_{li}} \quad (l = 1, \dots, N) \quad (12)$$

$$= v_{ki} m_i^{-1} \prod_{i=1}^N m_i^{v_{li}} \quad (k = N - M + 1, \dots, N).$$

Here, K_k is the k th equilibrium constant. Each v_{ki} is a signed stoichiometric coefficient representing the number of formulae of the i th species involved in the k th reaction; it is negative for reactants, and positive for products. Thus, for the reaction



v_{ki} is -1 , -2 , and 1 for the species Fe^{2+} , Cl^- , and $FeCl_2$, respectively, and is 0 for any other species. γ_i is an activity coefficient correcting the i th species concentration for non-ideality.

Equations (7), (9), and (11) constitute a system of N non-linear equations in N unknowns (m_i , or $\gamma_i m_i$). Note that the charge balance (7) does not apply to nonionic systems where the number of mass balance or mass action expressions must be increased by one. The above system of equations may be solved by combining the Newton-Raphson method with so-called curve crawler techniques.

For a complete description of the Newton-Raphson method, the reader is referred to CARNAHAN and WILKES (1973, p. 368), ACTON (1970, p. 367) or HILDEBRANDT (1956, p. 447). First, equations (7), (9), and (11) are approximated by the linear system:

$$\begin{bmatrix} Z_1 & \dots & Z_N \\ b_{1,1} & \dots & b_{1,N} \\ \dots & \dots & \dots \\ b_{N-M-1,1} & \dots & b_{N-M-1,N} \\ v_{11} m_1^{-1} \prod_{i=1}^N m_i^{v_{1i}} & \dots & v_{1N} m_N^{-1} \prod_{i=1}^N m_i^{v_{1i}} \\ \dots & \dots & \dots \\ v_{M1} m_1^{-1} \prod_{i=1}^N m_i^{v_{Mi}} & \dots & v_{MN} m_N^{-1} \prod_{i=1}^N m_i^{v_{Mi}} \end{bmatrix}$$

Equation (13) can be expressed more succinctly by,

$$\bar{\Psi}_m \cdot \bar{\Delta} = -\bar{\Psi}, \quad (14)$$

where $\bar{\Psi}_m$ is the Jacobian coefficient matrix given by equa-

tions (8), (10), and (12):

$$\bar{\Psi}_m = \frac{\partial(\Psi_1, \dots, \Psi_N)}{\partial(m_1, \dots, m_N)}$$

$\bar{\Psi}$ is the right-hand side vector in (13),

$$\bar{\Psi} = [\Psi_1, \dots, \Psi_N]^T$$

and $\bar{\Delta}$ is the solution vector,

$$\bar{\Delta} = [\delta m_1, \dots, \delta m_N]^T.$$

Note that all Ψ_i scalars are concentration-dependent; thus, if $\bar{m} = [m_1, \dots, m_N]^T$, then $\bar{\Psi} = \bar{\Psi}(\bar{m})$ and $\bar{\Psi}_m = \bar{\Psi}_m(\bar{m})$.

In practice, the linear system of equations (13) is solved for the vector $\bar{\Delta}$ using an initial, or k th, estimate of the concentrations $m_i^{(k)}$. At this stage, activity coefficients, γ_i , are set equal to unity. An improved estimate of the concentrations is given by

$$\bar{m}^{(k+1)} = \bar{m}^{(k)} + \bar{\Delta}$$

or

$$m_i^{(k+1)} = m_i^{(k)} + \delta m_i \quad (i = 1, \dots, N). \quad (15)$$

With $\bar{m}^{(k+1)}$ as a new initial guess, the process is repeated to satisfactory convergence in all m_i .

Note that system (13) will not possess a unique solution when the Jacobian determinant

$$J \equiv \frac{\partial(\Psi_1[m_i^{(k)}], \dots, \Psi_N[m_i^{(k)}])}{\partial(m_1, \dots, m_N)}$$

of the coefficient matrix $\bar{\Psi}_m$ approaches zero. For this reason, it is advisable to write all mass action expressions (11) with the least concentrated species as reactants. Because $v_{ki} < 0$ for reactants, the partials (12) are thereby maximized (see the following example). A test on the magnitude of J is recommended at each iteration.

As a rule of thumb, when initial guesses are accurate to a rough order of magnitude, successful convergence may usually be expected for $N < 10$. For systems containing 10 or more species, the following

$$\begin{bmatrix} \delta m_1 \\ \delta m_2 \\ \dots \\ \delta m_{N-M} \\ \delta m_{N-M+1} \\ \dots \\ \delta m_N \end{bmatrix} = \begin{bmatrix} -\Psi_1 \\ -\Psi_2 \\ \dots \\ -\Psi_{N-M} \\ -\Psi_{N-M+1} \\ \dots \\ -\Psi_N \end{bmatrix} \quad (13)$$

curve crawler technique is recommended (see ACTON, 1970, pp. 379-386):

(i) Choose a subset of the total chemical system con-

tain
chei
cent
Rap;
(ii) C
so si
not
cent
incre
(iii) V
solve
meth
(iv) F
of th
centr;
(v) Re
poner
specif
Up
cients
may i
functio

Variou
dercd.
(1969).
JONES
rationl.
the a_j
cients z

For i
ital $\gamma_i^{(k)}$
 $m_i^{(k)}$. Sy
iteration
improv
then pr
repeats
practice
to the n
In such
fraction

$$\gamma_i^{(k)} =$$

where f_i
While
cussion, t
centratio
units are
stituted f
mass acti

While
tive curv
the foregc

taining fewer than C components and fewer than 10 chemical species. Solve for the equilibrium concentrations of these species using the Newton-Raphson method.

(ii) Consider an increment of one omitted component so small that concentrations of the above species are not significantly changed. Compute the concentrations of any new species appearing with this increment of new component.

(iii) With these new concentrations as initial guesses, solve the expanded system by the Newton-Raphson method.

(iv) Repeat step (iii), each time adding an increment of the new component, up to the desired concentration of this component.

(v) Repeat steps (ii)-(iv), each time adding a new component, until all C components are present at their specified concentrations.

Up to this point in the calculation, all activity coefficients have been set equal to unity. If required, these may now be computed from empirical or *a priori* functions relating each γ_i to species concentrations:

$$\gamma_i = f_i(m_1, \dots, m_N) \quad (i = 1, \dots, N) \quad (16)$$

Various approaches to this problem have been considered, for example, by THOMPSON (1967), HELGESON (1969), HELGESON and JAMES (1968), TRUESDELL and JONES (1969), and CRERAR and BARNES (in preparation). Important uncertainties currently inherent in the *a priori* estimation of single ion activity coefficients are discussed in the latter two papers.

For the present purposes, functions (16) predict initial $\gamma_i^{(k)}$ estimates, given a first set of concentrations $m_i^{(k)}$. System (13) is then solved by Newton-Raphson iteration [using these initial $\gamma_i^{(k)}$, $m_i^{(k)}$ values] for an improved set of concentrations $m_i^{(k+1)}$. Functions (16) then predict corresponding $\gamma_i^{(k+1)}$, and the process is repeated to satisfactory convergence in all γ_i , m_i . In practice, the change in various γ_i from one iteration to the next may be so large that the process diverges. In such cases, successive γ_i are changed by some small fraction δ , of this step by step difference:

$$\gamma_i^{(k)} = \gamma_i^{(k-1)} + \{f_i[m_1^{(k)}, \dots, m_N^{(k)}] - \gamma_i^{(k-1)}\} \delta, \quad (17)$$

where f_i is the function (16).

While molal units have been used in the above discussion, the method applies equally well to other concentration scales. Note that when mole-fractional units are used, the identity condition (5) may be substituted for any of the charge and mass balances, or mass action expressions (7), (9), and (11).

While the Newton-Raphson method with supportive curve crawlers has been applied exclusively in the foregoing, it should be mentioned that the original

equations (7), (9), and (11) may also be solved by standard false position, secant, and interval halving procedures (e.g. CARNAHAN and WILKES, 1973, Chap. 5; ACTON, 1970, Chap. 2, 14). Additional numerical methods specific to the Brinkley approach are cited in VAN ZEGGEREN and STOREY (1970, Chap. 4). The simple method of successive substitution is not recommended here for general use because of its overly restrictive convergence criteria (CARNAHAN and WILKES, 1973, p. 368).

Of all applicable root-solvers, the Newton-Raphson approach offers fastest (quadratic) convergence. The false position, interval halving, and secant methods can be somewhat unwieldy for the present purposes, and converge at a slower (first order) rate. All four procedures require initial estimates, and all four can hang up on undesired multiple roots. In addition, the false position and interval halving procedures require a second set of input points straddling the desired root.

Because the Newton-Raphson method projects derivatives in its search for roots, there is always a danger that it might be led astray along functional slopes and extrema; under such circumstances, it will typically diverge or oscillate indefinitely. For this reason, initial estimates can be crucial with this method, and should always lie as close as possible to the true roots. Fortunately, the simple Newton-Raphson procedure can be enhanced considerably by the addition of so-called fine tuners or curve crawlers of the type introduced above. These have the general effect of improving initial estimates to any desired degree of precision.

Should the Newton-Raphson method fail to converge, even with the addition of supportive curve crawlers, several options remain. As a first approach, initial estimates can be adjusted and the method tried again. Alternatively, the curve crawler step interval may be decreased. Should the method still fail, then a less sensitive algorithm such as interval halving or false position can be invoked. Under some circumstances, the modified, more rapidly converging Newton's methods derived by BROWN (1969) or BOGGS (1971) may improve both computation time and the prospects of convergence. Brown's method is now available in FORTRAN IV through the IMSL Library, Houston, Texas.

NUMERICAL EXAMPLE

As an example, consider a problem requiring equilibrium activities or concentrations of all significant species in the system 0.25 m NH_4Cl -0.25 m NaCl -0.25 m KCl -0.25 m NaHSO_4 - H_2O at 300°C and at vapor saturated pressure. The aqueous species NH_4^+ , NH_4OH , H^+ , HCl ,

NH₄Cl, Cl⁻, Na⁺, NaCl, K⁺, KCl, HSO₄⁻, KSO₄⁻, NaSO₄⁻, NH₄SO₄⁻, KHSO₄, NaHSO₄, and NH₄HSO₄ are considered. Relative activities of the species H₂SO₄, SO₄²⁻, OH⁻, NaOH, and KOH are assumed to be negligible.

The complete system is described by the following equations, analogous to (7), (9), and (11) above:

$$[\text{NH}_4^+] + [\text{H}^+] + [\text{Na}^+] + [\text{K}^+] = [\text{Cl}^-] + [\text{HSO}_4^-] + [\text{KSO}_4^-] + [\text{NaSO}_4^-] + [\text{NH}_4\text{SO}_4^-] \quad (18)$$

$$\sum \text{NH}_3 = 0.25 = [\text{NH}_4^+] + [\text{NH}_4\text{OH}] + [\text{NH}_4\text{Cl}] + [\text{NH}_4\text{SO}_4^-] + [\text{NH}_4\text{HSO}_4] \quad (19)$$

$$\sum \text{Cl} = 0.75 = [\text{HCl}] + [\text{NH}_4\text{Cl}] + [\text{Cl}^-] + [\text{NaCl}] + [\text{KCl}] \quad (20)$$

$$\sum \text{Na} = 0.50 = [\text{Na}^+] + [\text{NaCl}] + [\text{NaSO}_4^-] + [\text{NaHSO}_4] \quad (21)$$

$$\sum \text{K} = 0.25 = [\text{K}^+] + [\text{KCl}] + [\text{KSO}_4^-] + [\text{KHSO}_4] \quad (22)$$

$$\sum \text{S} = 0.25 = [\text{HSO}_4^-] + [\text{KSO}_4^-] + [\text{NaSO}_4^-] + [\text{NH}_4\text{SO}_4^-] + [\text{KHSO}_4] + [\text{NaHSO}_4] + [\text{NH}_4\text{HSO}_4] \quad (23)$$

$$\frac{K_{\text{NH}_4\text{OH}}}{K_{\text{H}_2\text{O}}} = \frac{(\text{NH}_4^+)}{(\text{NH}_4\text{OH})(\text{H}^+)} = 10^{4.57} \quad (24)$$

$$K_{\text{NH}_4\text{Cl}} = \frac{(\text{NH}_4^+)(\text{Cl}^-)}{(\text{NH}_4\text{Cl})} = 10^{-0.82} \quad (25)$$

$$K_{\text{NaCl}} = \frac{(\text{Na}^+)(\text{Cl}^-)}{(\text{NaCl})} = 10^{-0.82} \quad (26)$$

$$K_{\text{HCl}}^{-1} = \frac{(\text{HCl})}{(\text{H}^+)(\text{Cl}^-)} = 10^{1.24} \quad (27)$$

$$K_{\text{KCl}} = \frac{(\text{K}^+)(\text{Cl}^-)}{(\text{KCl})} = 10^{-0.6} \quad (28)$$

$$\frac{K_{\text{KSO}_4^-}}{K_{\text{HSO}_4^-}} = \frac{(\text{K}^+)(\text{HSO}_4^-)}{(\text{KSO}_4^-)(\text{H}^+)} = 10^{4.06} \quad (29)$$

$$\frac{K_{\text{NaSO}_4^-}}{K_{\text{HSO}_4^-}} = \frac{(\text{Na}^+)(\text{HSO}_4^-)}{(\text{NaSO}_4^-)(\text{H}^+)} = 10^{4.06} \quad (30)$$

$$\frac{K_{\text{NH}_4\text{SO}_4^-}}{K_{\text{HSO}_4^-}} = \frac{(\text{NH}_4^+)(\text{HSO}_4^-)}{(\text{NH}_4\text{SO}_4^-)(\text{H}^+)} = 10^{4.06} \quad (31)$$

$$K_{\text{KHSO}_4} = \frac{(\text{K}^+)(\text{HSO}_4^-)}{(\text{KHSO}_4)} = 10^{-0.3} \quad (32)$$

$$K_{\text{NaHSO}_4} = \frac{(\text{Na}^+)(\text{HSO}_4^-)}{(\text{NaHSO}_4)} = 10^{-0.3} \quad (33)$$

$$K_{\text{NH}_4\text{HSO}_4} = \frac{(\text{NH}_4^+)(\text{HSO}_4^-)}{(\text{NH}_4\text{HSO}_4)} = 10^{-0.3} \quad (34)$$

In equations (18)-(34), square brackets denote molal concentrations (*m_i*) and parentheses denote activities (*γ_im_i*). Note that all mass action equations (24)-(34) are written with smallest expected activities in the denominator, as previously discussed.

Table 1 lists appropriate values of the constants *Z_i*, *b_{ei}*, *B_e*, *v_{ei}*, and *K_i* used in matrix equations (13). In this table, the rows labeled *ψ₁*-*ψ₁₇* represent equations (18)-(34), arranged in the same order as in the text. Numerical values of the equilibrium constants *K_{H₂O}*, *K_{NH₄OH}*, and *K_{KSO₄⁻}* were obtained from SWEETON *et al.* (1974). FISHER and BARNES (1972), and OHMOTO (1972), respectively; *K_{NaCl}}*, *K_{HCl}}*, *K_{KCl}}*, *K_{HSO₄⁻}*, and *K_{KHSO₄}* were taken from HELGESON (1969). For present purposes, *K_{NH₄Cl}* was approximated by

Table 1. Data for the system 0.25 m NH₄Cl-0.25 m NaCl-0.25 m KCl-0.25 m NaHSO₄-H₂O at 300°C

		1	2	3	4	5	6	7	8	9	10	11	12	13	14	15	16	17	
		NH ₄ ⁺	NH ₄ OH	H ⁺	HCl	NH ₄ Cl	Cl ⁻	Na ⁺	NaCl	K ⁺	KCl	HSO ₄ ⁻	KSO ₄ ⁻	NaSO ₄ ⁻	NH ₄ SO ₄ ⁻	KHSO ₄	NaHSO ₄	NH ₄ HSO ₄	
<i>ψ₁</i>	<i>Z₁</i>	1	0	1	0	0	-1	1	0	1	0	-1	-1	-1	-1	0	0	0	
<i>ψ₂</i>	<i>b_{NH₃,1}</i>	1	1	0	0	1	0	0	0	0	0	0	0	0	1	0	0	1	<i>B_{NH₃}</i> =0.25
<i>ψ₃</i>	<i>b_{Cl⁻,1}</i>	0	0	0	1	1	1	0	1	0	1	0	0	0	0	0	0	0	<i>B_{Cl⁻}</i> =0.75
<i>ψ₄</i>	<i>b_{Na⁺,1}</i>	0	0	0	0	0	0	1	1	0	0	0	0	1	0	0	1	0	<i>B_{Na⁺}</i> =0.50
<i>ψ₅</i>	<i>b_{K⁺,1}</i>	0	0	0	0	0	0	0	0	1	1	0	1	0	0	1	0	0	<i>B_{K⁺}</i> =0.25
<i>ψ₆</i>	<i>b_{S,1}</i>	0	0	0	0	0	0	0	0	0	0	1	1	1	1	1	1	1	<i>B_S</i> =0.25
<i>ψ₇</i>	<i>v_{1,1}</i>	1	-1	-1	0	0	0	0	0	0	0	0	0	0	0	0	0	0	<i>K₁</i> =10 ^{4.57}
<i>ψ₈</i>	<i>v_{2,1}</i>	1	0	0	0	-1	1	0	0	0	0	0	0	0	0	0	0	0	<i>K₂</i> =10 ^{-0.82}
<i>ψ₉</i>	<i>v_{3,1}</i>	0	0	0	0	0	1	1	-1	0	0	0	0	0	0	0	0	0	<i>K₃</i> =10 ^{-0.82}
<i>ψ₁₀</i>	<i>v_{4,1}</i>	0	0	-1	1	0	-1	0	0	0	0	0	0	0	0	0	0	0	<i>K₄</i> =10 ^{1.24}
<i>ψ₁₁</i>	<i>v_{5,1}</i>	0	0	0	0	0	1	0	0	1	-1	0	0	0	0	0	0	0	<i>K₅</i> =10 ^{-0.6}
<i>ψ₁₂</i>	<i>v_{6,1}</i>	0	0	-1	0	0	0	0	0	1	0	1	-1	0	0	0	0	0	<i>K₆</i> =10 ^{4.06}
<i>ψ₁₃</i>	<i>v_{7,1}</i>	0	0	-1	0	0	0	1	0	0	1	0	-1	0	0	0	0	0	<i>K₇</i> =10 ^{4.06}
<i>ψ₁₄</i>	<i>v_{8,1}</i>	1	0	-1	0	0	0	0	0	0	1	0	0	0	-1	0	0	0	<i>K₈</i> =10 ^{4.06}
<i>ψ₁₅</i>	<i>v_{9,1}</i>	0	0	0	0	0	0	0	0	1	0	1	0	0	0	-1	0	0	<i>K₉</i> =10 ^{-0.3}
<i>ψ₁₆</i>	<i>v_{10,1}</i>	0	0	0	0	0	1	0	0	0	1	0	0	0	0	0	-1	0	<i>K₁₀</i> =10 ^{-0.3}
<i>ψ₁₇</i>	<i>v_{11,1}</i>	1	0	0	0	0	0	0	0	0	1	0	0	0	0	0	0	-1	<i>K₁₁</i> =10 ^{-0.3}

K_{NaCl}}
K_{NaOH}}
It is
centra
ple N
insten
KCl-1
sulfur
that 1
0.25 m
Newt
Initial
are list
vergen
calcul
unity.
The
for all
concen
NH₄Cl
are est.

Table 2. Computed equilibria in the system NH₄Cl-NaCl-KCl-NaHSO₄-H₂O at 300°C

	A	B	C	D	E	F
NH ₄ ⁺	0.105	8.48x10 ⁻²	---	8.75x10 ⁻²	1.83x10 ⁻¹	0.326
NH ₄ OH	1.61x10 ⁻³	3.70x10 ⁻³	---	2.01x10 ⁻³	1.29x10 ⁻³	1.21
H ⁺	1.76x10 ⁻³	6.17x10 ⁻⁴	---	1.17x10 ⁻³	3.18x10 ⁻³	0.326
HCl	6.40x10 ⁻³	3.09x10 ⁻³	---	4.76x10 ⁻³	2.60x10 ⁻³	1.21
NH ₄ Cl	0.145	1.61x10 ⁻¹	---	1.35x10 ⁻¹	5.72x10 ⁻²	1.21
Cl ⁻	0.210	2.88x10 ⁻¹	---	2.33x10 ⁻¹	5.37x10 ⁻¹	0.326
Na ⁺	0.105	8.61x10 ⁻²	---	1.76x10 ⁻¹	3.69x10 ⁻¹	0.326
NaCl	0.146	1.64x10 ⁻¹	---	2.72x10 ⁻¹	1.15x10 ⁻¹	1.21
K ⁺	0.105	1.16x10 ⁻¹	---	1.13x10 ⁻¹	2.03x10 ⁻¹	0.326
KCl	0.146	1.33x10 ⁻¹	---	1.05x10 ⁻¹	3.81x10 ⁻²	1.21
HSO ₄ ⁻	---	---	6.20x10 ⁻⁴	1.40x10 ⁻¹	2.17x10 ⁻¹	0.326
KSO ₄ ⁻	---	---	1.02x10 ⁻⁵	1.17x10 ⁻³	1.21x10 ⁻³	0.326
NaSO ₄ ⁻	---	---	7.54x10 ⁻⁶	1.84x10 ⁻³	2.19x10 ⁻³	0.326
(NH ₄) ₂ SO ₄ ⁻	---	---	7.42x10 ⁻⁶	9.13x10 ⁻⁴	1.09x10 ⁻³	0.326
KHSO ₄	---	---	1.44x10 ⁻⁴	3.16x10 ⁻²	7.71x10 ⁻³	1.21
NaHSO ₄	---	---	1.06x10 ⁻⁴	4.95x10 ⁻²	1.40x10 ⁻²	1.21
(NH ₄)HSO ₄	---	---	1.05x10 ⁻⁴	2.45x10 ⁻²	6.97x10 ⁻³	1.21

A and B: Initial estimates and equilibrium molalities respectively, in the system 0.25 m NH₄Cl-0.25 m NaCl-0.25 m KCl-H₂O at 300°C, assuming all γ_i = 1.0.

C: Equilibrium molalities of sulfur species in the system 0.25 m NH₄Cl-0.25 m NaCl-0.25 m KCl-0.001 m NaHSO₄-H₂O at 300°C assuming all γ_i = 1.0.

D: Equilibrium molalities in the system 0.25 m NH₄Cl-0.25 m NaCl-0.25 m KCl-0.25 m NaHSO₄-H₂O at 300°C, assuming all γ_i = 1.0.

E and F: Equilibrium molalities and molal activity coefficients, respectively, in the system 0.25 m NH₄Cl-0.25 m NaCl-0.25 m KCl-0.25 m NaHSO₄-H₂O at 300°C.

K_{NaCl}; K_{NaSO₄} and K_{NH₄SO₄} by K_{KSO₄}; and K_{NaHSO₄} and K_{NH₄HSO₄} by K_{KHSO₄}.

It is unlikely that initial estimates of all 17 species concentrations would be sufficiently accurate to permit a simple Newton-Raphson solution to this problem. Selecting instead the subsystem 0.25 m NH₄Cl-0.25 m NaCl-0.25 m KCl-H₂O eliminates equations (23), (29)-(34), and all sulfur-bearing terms from the remaining 10 equations. Note that the mass balance on total sodium falls to B_{Na} = 0.25 m. The resultant 10 equations can now be solved by Newton-Raphson iteration and a reasonable initial guess. Initial guesses and calculated equilibrium concentrations are listed in Table 2, columns A and B, respectively. Convergence to 0.1% precision required 6 iterations. For this calculation, all activity coefficients, γ_i, were set equal to unity.

The next step uses the curve crawler technique to solve for all concentrations in the full 5-component system. First, concentrations of all sulfur species in the system 0.25 m NH₄Cl-0.25 m NaCl-0.25 m KCl-0.001 m NaHSO₄-H₂O are estimated from equilibrium molalities in the reduced

4-component system (Table 2, column B):

$$(KSO_4^-) = \frac{(K^+)(HSO_4^-)}{10^{4.06}(H^+)} \tag{35}$$

$$(NaSO_4^-) = \frac{(Na^+)(HSO_4^-)}{10^{4.06}(H^+)} \tag{36}$$

$$(NH_4SO_4^-) = \frac{(NH_4^+)(HSO_4^-)}{10^{4.06}(H^+)} \tag{37}$$

$$(KHSO_4) = \frac{(K^+)(HSO_4^-)}{10^{-0.3}} \tag{38}$$

$$(NaHSO_4) = \frac{(Na^+)(HSO_4^-)}{10^{-0.3}} \tag{39}$$

$$(NH_4HSO_4) = \frac{(NH_4^+)(HSO_4^-)}{10^{-0.3}} \tag{40}$$

$$[\text{HSO}_4^-] = 0.001 - [\text{KSO}_4^-] - [\text{NaSO}_4^-] - [\text{NH}_4\text{SO}_4^-] - [\text{KHSO}_4] - [\text{NaHSO}_4] - [\text{NH}_4\text{HSO}_4]. \quad (41)$$

Again, activities are set equal to concentrations. Equations (35)–(41) may be solved by Gauss–Seidel iteration on (HSO_4^-) . Results for the 7 sulfur species considered are listed in Table 2, column C; concentrations of the other original species (Table 2, column B) remain essentially unchanged.

The next step adds successive 0.001 m increments of the NaHSO_4 component to the system. All 17 equations (18)–(34) may now be solved by Newton–Raphson iteration, using calculated molalities at one increment as initial guesses for the next. Thus, concentrations in Table 2, columns B and C, are used to compute a new set of molalities at $[\text{NaHSO}_4] = 0.002$ m. These, in turn, predict new concentrations of all species at $[\text{NaHSO}_4] = 0.003$ m, and so on to $[\text{NaHSO}_4] = 0.25$ m. Activity coefficients are again set equal to unity. Final concentrations are listed in Table 2, column D.

The final step in the calculation imposes an activity coefficient correction on the computed molalities. The subject of *a priori* activity corrections for electrolyte solutions is treated at length in CRERAR and BARNES (in preparation). The model introduced for illustrative purposes here is derived and tested by Crerar and Barnes, and represents one among many possible approaches to the problem. Because of the assumptions required in its present application, it should be considered only a first approximation.

First, the uncorrected molalities in Table 2, column C, are used to estimate specific ion activity coefficients. These molalities may first be corrected for the loss of free solvent molecules to ion hydration spheres:

$$m_{ah}^i = \frac{55.51 m_i^i}{55.51 - \sum_i h_i m_i^i}, \quad (42)$$

where m_i^i is the molality of the *i*th species corrected for ion association as listed in Table 2, column D; m_{ah}^i is the molality of the same species corrected for both hydration and ion association; and h_i represents the average moles of solvent hydrating one mole of solute species *i*. Next, each m_{ah}^i is converted to an association- and hydration-corrected molality, C_{ah}^i :

$$C_{ah}^i = m_{ah}^i \left[\frac{1000 \rho}{1000 + \sum G^* m^*} \right]. \quad (43)$$

Here, ρ is solution density (g/ml), and $\sum G^* m^*$ is the summed products of gram molecular weights and stoichiometric molalities for all solute components.

A mole-fraction specific-ion activity coefficient may now be computed from the complete Debye–Hückel equation:

$$\log f_e^i = \frac{-C(Z_i)^2 \sqrt{I}}{(DT)^{3/2} \left[1 + \frac{Ea\sqrt{I}}{(DT)^{1/2}} \right]}, \quad (44)$$

where Z_i is species valence, D is the dielectric constant of water at temperature (AKERLOF and OSIRY, 1950); a is the empirical Debye–Hückel ‘distance of closest approach’; $E = 50.29158$, and $C = 1.8248 \times 10^6$ (HAMER,

1968). I is the conventional ionic strength,

$$I = \frac{1}{2} \sum_i (Z_i)^2 C_{ah}^i.$$

The mole-fractional activity coefficient f_e^i corrects for long-range electrostatic ion–ion interactions. It is converted to molal units by the relation

$$\log \gamma_e^i = \log f_e^i - \log \left[\frac{1000 + G_{\text{H}_2\text{O}} \sum m_{ah}^i}{1000} \right], \quad (44a)$$

where $G_{\text{H}_2\text{O}}$ is the gram molecular weight of the solvent, water, and γ_e^i is the molal specific ion activity coefficient correcting for electrostatic interaction. It may be converted to a complete molal activity coefficient, γ_{eh}^i , correcting for both hydration and electrostatic interaction by the relation,

$$\gamma_{eh}^i = \frac{\gamma_e^i m_{ah}^i}{m_i^i}. \quad (45)$$

The corresponding coefficient, γ_h^i , correcting the *i*th species for hydration alone is given by

$$\gamma_h^i = \frac{\gamma_{eh}^i}{\gamma_e^i} = \frac{m_{ah}^i}{m_i^i}. \quad (46)$$

With uncharged molecular species, it is assumed that electrostatic interactions are negligible ($\gamma_e^i = 1.0$), and that the complete activity coefficient is given by γ_h^i alone.

For illustrative purposes, the system density ρ and Debye–Hückel a parameter are here approximated by the corresponding values for 1.0 m NaCl at 300°C (0.772 g/ml, HAAS, 1970; and 3.0 Å, LIU and LINDSAY, 1972, respectively). The hydration number, h_i , of neutral molecules is approximated by the value 2.0 for NaCl^0 (QUIST and MARSHALL, 1968), and the hydration number of cations and anions, grouped as pairs, is approximated by 10.0—the total hydration of $\text{Na}^+ + \text{Cl}^-$ at 300°C (YEATTS and MARSHALL, 1972).

The molalities in Table 2, column D, were calculated on the assumption that all $\gamma_i = 1.0$. These concentrations may now be used in equations (42)–(46) for first estimates of γ_{eh}^i and γ_h^i —the activity coefficients of ions and neutral species, respectively. Using these γ_i and m_i as initial estimates, the complete system of equations (18)–(34) may be solved by Newton–Raphson iteration for a new set of concentrations. A corresponding set of new activity coefficients is then calculated from equations (42)–(46) and the process is repeated to satisfactory convergence in all γ_i and m_i . Because successive γ_i change considerably during the first few iterations, and might otherwise diverge, each γ_i is changed by stepwise increments using relationship (17), and setting $\delta = 0.1$; in other words, only 10% of the predicted change in γ_i is used at each step.

Final molalities, m_i , and molal activity coefficients, γ_i , are listed in Table 2, column E, for the full 5-component system. Activities of the less important species H_2SO_4 , SO_4^{2-} , OH^- , NaOH , and KOH may be computed using the above γ_i , m_i values and appropriate equilibrium constants. The inclusion of these additional species has negligible effect on the initial charge and mass balances (18)–(23), justifying the original assumption.

SUMMARY

The equilibrium activities and concentrations of species in multicomponent systems may be calculated

given (1) total concentrations of each component or of selected elements, and (2) the appropriate minimum number of independent equilibrium constants. Because the method does not require complete free-energy data for all species, it may often apply where optimization techniques cannot. Although free-energy data are currently incomplete for many rock-water systems of geochemical interest, equilibrium constants are often either known, or may be estimated for important reactions within many such systems. Indeed, much of modern experimental geochemistry has been concerned, either directly or indirectly, with the compilation and measurement of such equilibrium constants. As interest turns toward multicomponent equilibria of ever increasing complexity, computer-based techniques such as those considered here should find important applications within the geosciences.

Acknowledgements—It is a pleasure to thank N. FRAZER, S. MACRAE, P. MALIN, R. PHINNEY, and R. STRELITZ for their kind assistance. Research supported by the Earth Sciences Section, National Science Foundation, NSF Grant DES75-14929.

REFERENCES

- ACTON F. S. (1970) *Numerical Methods that Work*, 541 pp. Harper & Row.
- AKERLOF G. C. and OSIRY H. I. (1950) The dielectric constant of water at high temperatures and in equilibrium with its vapor. *J. Amer. Chem. Soc.* **72**, 2844-2847.
- BARNES H. L. (in press) Applied hydrothermal geochemistry. In *International Conference on High-Temperature High-Pressure Electrochemistry in Aqueous Solutions*, Vol. 4. Natl. Assoc. Corrosion Engineers, D.S.A.
- BARNES H. L., HELGESON H. C. and ELLIS A. J. (1966) Ionization constants in aqueous solutions. In *Handbook of Physical Constants*, (editor S. P. Clark, Jr.), pp. 401-413. *Geol. Soc. Amer. Mem.* **97**.
- BLACKBURN T. R. (1969) *A Chemistry of Solutions*, 220 pp. Holt, Rinehart & Winston.
- BOGGS P. T. (1971) The solution of nonlinear systems of equations by A-stable integration techniques. *SIAM J. Numer. Anal.* **8**, 767-785.
- BRINKLEY S. R. (1947) Calculation of the equilibrium composition of systems of many constituents. *J. Chem. Phys.* **15**, 107-110.
- BROWN K. M. (1969) A quadratically convergent Newton-like method based upon Gaussian elimination. *SIAM J. Numer. Anal.* **6**, 560-569.
- BUTLER J. N. (1964) *Ionic Equilibrium. A Mathematical Approach*, 547 pp. Addison-Wesley.
- CARNAHAN B. and WILKES J. O. (1973) *Digital Computing and Numerical Methods*, 477 pp. Wiley.
- CRERAR D. A. and ANDERSON G. M. (1971) Solubility and solution reactions of quartz in dilute hydrothermal solutions. *Chem. Geol.* **8**, 107-122.
- CRERAR D. A. and BARNES H. L. (in preparation) *The Estimation of Activity Coefficients of Electrolyte Solutions and Related Thermodynamic Models*. Penn. State Studies Monograph Series, Penn. State Univ. Press.
- FELDMAN H. F., SIMONS W. H. and BIENSTOCK D. (1969) Calculating equilibrium compositions of multicomponent, multiphase, chemical reacting systems. *U.S. Bur. Mines Rep. Invest.* **7257**, 22 pp.
- FISHER J. R. and BARNES H. L. (1972) The ion-product constant of water to 350°. *J. Phys. Chem.* **76**, 90-99.
- FREISER H. and FERNANDO Q. (1966) *Ionic Equilibria in Analytical Chemistry*, 338 pp. Wiley.
- HAAS J. L., JR. (1970) An equation for the density of vapor-saturated NaCl-H₂O solutions from 75° to 325°C. *Amer. J. Sci.* **269**, 489-493.
- HAMER W. J. (1968) Theoretical mean activity coefficients of strong electrolytes in aqueous solutions from 0 to 100°C. *National Standard Reference Data Series—Nat. Bur. Std.* **24**, 271 pp. U.S. Government Printing Office.
- HELGESON H. C. (1964) *Complexing and Hydrothermal Ore Deposition*, pp. 56-64. Macmillan.
- HELGESON H. C. (1968) Evaluation of irreversible reactions in geochemical processes involving minerals and aqueous solutions—I. Thermodynamic relations. *Geochim. Cosmochim. Acta* **32**, 853-877.
- HELGESON H. C. (1969) Thermodynamics of hydrothermal systems at elevated temperatures and pressures. *Amer. J. Sci.* **267**, 729-804.
- HELGESON H. C. (1970) A chemical and thermodynamic model of ore deposition in hydrothermal systems. *Mineral. Soc. Amer. Spec. Paper* **3**, 155-186.
- HELGESON H. C. and JAMES W. R. (1968) Activity coefficients in concentrated electrolyte solutions at elevated temperatures. *Abstracts of Papers, 155th Nat. Meeting, Amer. Chem. Soc.*, April, 1968, San Francisco, California, S-130.
- HILDEBRANDE F. B. (1956) *Introduction to Numerical Methods*, pp. 447-453. McGraw-Hill.
- HOLLOWAY J. R. and REESE R. L. (1974) The generation of N₂-CO₂-H₂O fluids for use in hydrothermal experimentation I. Experimental method and equilibrium calculations in the C-O-H-N system. *Amer. Mineral.* **59**, 587-597.
- KANDINER H. J. and BRINKLEY S. R. (1950) Calculation of complex equilibrium relations. *Ind. Eng. Chem.* **42**, 850-855.
- KARPOV I. K. and KAZ'MIN L. A. (1972) Calculation of geochemical equilibria in heterogeneous multicomponent systems. *Geochem. Int.* **9**, 252-262.
- LIU C. T. and LINDSAY W. T. (1972) Thermodynamics of sodium chloride solutions at high temperatures. *J. Solution Chem.* **1**, 45-69.
- OHMOTO H. (1972) Systematics of sulfur and carbon isotopes in hydrothermal ore deposits. *Econ. Geol.* **67**, 551-578.
- QUIST A. S. and MARSHALL W. L. (1968) Electrical conductances of aqueous sodium chloride solutions from 0 to 800° and at pressures to 4000 bars. *J. Phys. Chem.* **72**, 684-703.
- REESE R. L. (1973) Computed solid-vapor equilibria in multicomponent systems. M.S. Thesis, Arizona State University, Tempe, Arizona.
- SILLÉN L. G. and MARTELL A. E. (1964) *Stability Constants of Metal-Ion Complexes*, 2nd edition, *Chem. Soc. London Spec. Publ.* **17**, 754 pp.
- SWEETON F. H., MESMER R. E. and BAES C. F., JR. (1974) Acidity measurements at elevated temperatures. VII. Dissociation of water. *J. Solution Chem.* **3**, 191-214.
- THOMPSON J. B., JR. (1967) Thermodynamic properties of simple solutions. In *Researches in Geochemistry*, (editor P. ABELSON), Vol. 2, pp. 340-361. Wiley.

- TRUESDELL A. H. and JONES B. F. (1969) Ion association in natural brines. *Chem. Geol.* 4, 51-62.
- TRUESDELL A. H. and JONES B. F. (1974) WATEQ, a computer program for calculating chemical equilibria of natural waters. *J. Res. U.S. Geol. Surv.*, 2, 233-248.
- VAN ZEGGEREN F. and STOREY S. H. (1970) *The Computation of Chemical Equilibria*, 176 pp. Cambridge University Press.
- YEATTS L. B. and MARSHALL W. L. (1972) Electrical conductance and ionization behaviour of sodium chloride in dioxane-water solutions at 300° and pressures to 4000 bars. *J. Phys. Chem.* 76, 1053-1062.

SUBJ
GCHM
PAO

n des
rre

ES DU CANADA

Canadian Journal of Earth Sciences

Journal canadien des sciences de la terre

Published by
THE NATIONAL RESEARCH COUNCIL OF CANADA

Publié par
LE CONSEIL NATIONAL DE RECHERCHES DU CANADA

Volume 13 Number 9 September 1976

Volume 13 numéro 9 septembre 1976

Precambrian atmospheric oxygen: evidence in the sedimentary distributions of carbon, sulfur, uranium, and iron¹

ERICH DIMROTH

Sciences de la Terre, Université du Québec à Chicoutimi, Chicoutimi, Qué., Canada G7H 2B1

AND

MICHAEL M. KIMBERLEY

Erindale College and Department of Geology, University of Toronto, Mississauga, Ont., Canada

Received 9 December 1975

Revision accepted for publication 12 April 1976

The sedimentary distributions of carbon, sulfur, uranium, and ferric and ferrous iron depend greatly upon ambient oxygen pressure and should reflect any major change in proportion of oxygen in the atmosphere or hydrosphere. The similar distributions of these elements in sedimentary rocks of all ages are here interpreted to indicate the existence of a Precambrian atmosphere containing much oxygen.

Organic carbon contents and distributions are similar in Precambrian and Quaternary sedimentary rocks and sediments, although distributions in both would have been sensitive to variations in rates of organic productivity and atmospheric oxygen pressure. Sedimentary pyrite is almost invariably closely associated with organic carbon, suggestive of formation by sulfate reduction, in sedimentary rocks of any age. Archean and Middle Precambrian cherty iron formations and uranium ores resemble Phanerozoic ores and probably formed similarly by diagenetic concentration. In general, we find no evidence in the sedimentary distributions of carbon, sulfur, uranium, or iron, that an oxygen-free atmosphere has existed at any time during the span of geological history recorded in well preserved sedimentary rocks.

La distribution dans les sédiments du carbone, du soufre, de l'uranium, du fer ferreux, et ferrique dépend largement de la pression ambiante de l'oxygène et devrait refléter toute variation majeure dans la proportion d'oxygène de l'atmosphère et de l'hydrosphère. Des distributions semblables de ces éléments dans des roches sédimentaires de tous les âges sont ici interprétées comme indiquant l'existence d'une atmosphère précambrienne contenant beaucoup d'oxygène.

Les teneurs en carbone organique et leur distribution sont semblables dans les roches sédimentaires et les matériaux meubles au Précambrien et au Quaternaire, quoique la distribution dans chaque cas ait pu être sensible aux variations de l'activité organique et de la pression atmosphérique de l'oxygène. La pyrite sédimentaire est presque invariablement associée de près, dans les roches sédimentaires de tout âge, au carbone organique, suggérant une origine par réduction de sulfates. Les formations de fer et de chert de l'Archéen et du Précambrien moyen et les minerais d'uranium ressemblent aux gîtes phanérozoïques et se sont probablement formés de façon semblable par concentration en cours de diagenèse. En général, nous ne trouvons aucune preuve dans la distribution sédimentaire du carbone, du soufre, de l'uranium, et du fer qu'une atmosphère sans oxygène ait existé en aucun moment au cours de l'histoire géologique lorsqu'on considère les roches sédimentaires bien conservées.

[Traduit par le journal]

Can. J. Earth Sci. 13, 1161-1185 (1976)

¹Published with the permission of the Minister of Natural Resources of Quebec.

(Ottawa)
(Ottawa)
Kingston)
Ottawa)
Toronto)
Ottawa (Toronto)

Canada

resser leurs manus-
rtment of Geology,
iland, St. John's,

se rapportant aux
Directeur adminis-
eil national de re-
A 6R6.

vent être achetés au
commande à cet effet
retourné au Printing
ress, 5201 Dufferin
3H 5T8, qui se char-

rimées près de la fin
Sur demande, les
pié du Service de

1976.

aux non livrés
ces de la terre)
Ottawa, (Ont.),

Introduction

Current concepts of atmospheric evolution through the Precambrian are based partly on the model of progressive accumulation of exhaled gases (Rubey 1955) and partly on genetic models of cherty iron formations and uraniferous conglomerates (Cloud 1973). Atmospheric oxygen pressure is popularly presumed to have increased steadily through the Precambrian (Berkner and Marshall 1965). Pyrite and uraninite of Middle Precambrian uranium ores are generally interpreted to be detrital components (Ramdohr 1958) and are considered to be evidence of low atmospheric oxygen pressure. Cherty iron formations are commonly thought to be precipitates onto the sea floor of iron transported in the ferrous state from a continent (Lepp and Goldich 1964) or from a deep oceanic reservoir (Holland 1973c), the precipitation possibly linked to a specific stage of biologic evolution (Cloud 1973).

However, the fundamental differences between Precambrian and Phanerozoic chemical sedimentation implied by these interrelated models are not apparent in the rock record, and differences that do exist between Precambrian and Phanerozoic sedimentary rocks are not readily attributable to a progressive increase in proportion of atmospheric oxygen. Not only do we note fundamental similarities among iron- and uranium-rich sedimentary rocks of all ages but, more significantly, we find similar distributions of organic carbon, sulfide sulfur, and iron in the ordinary sedimentary rocks that constitute the great bulk of the sedimentary rock record, although all three distributions are presently strongly influenced by the ambient partial pressure of oxygen. The similarities in distributions are interpreted to indicate that process-response effects, *i.e.* negative feedback, have been similarly effective throughout recorded geologic history. Differences that do exist between Precambrian and Phanerozoic sedimentary suites, other than those caused by the generally higher degree of metamorphism in Precambrian terrains, are more readily attributable to tectonic and biologic evolution than to major compositional changes in the atmosphere and hydrosphere.

Although we will stress the evidence contained in ordinary sedimentary rocks, we do not exclude sedimentary uranium and iron ores from consideration. The models of diagenetic

ore concentration favored herein require the presence of an oxygen-rich atmosphere. We will not discuss complex details of ore deposit geology or possible modes of origin, because work on these aspects is in progress, and only an outline is required to demonstrate compatibility with the concept of an oxygen-rich Precambrian atmosphere.

Hypotheses concerning the oxidation state of the Precambrian atmosphere have great economic importance because redox reactions can determine the geochemical behavior of many heavy metals. Prospecting for heavy metal deposits in Precambrian terrains has been correspondingly influenced by current concepts of atmospheric evolution. However, the inadequacy of present concepts has become obvious in prospecting for uranium ore in Quebec. The concept that the Middle Precambrian uraninite deposits are placers is too restrictive, as shown by the fact that much of the uraninite in the Witwatersrand deposits occurs not in the form of detrital-looking grains at the base of fining-upward cycles, but at their tops, where it locally replaced and encrusted organic matter (Pretorius 1974). Prospecting for placer uraninite in Middle Precambrian conglomerates of northern Quebec has been a failure because the gravels examined to date apparently experienced oxidative diagenesis, and the localities of possible uranium ores concentrated by groundwater have not been prospected. By contrast, prospecting for Archean Cu-Zn ores has been highly successful because these were interpreted as analogues of Phanerozoic deposits, despite the fact that the geochemistry of both metals depends on redox reactions and that deposits formed in an oxygen-free ocean should be different from those formed in the Phanerozoic.

Sedimentary Carbon Distribution

Introduction

Carbon occurs in two associations in unmetamorphosed and low-grade metamorphic rocks: (1) within the carbonate radical of carbonate minerals, and (2) in a myriad of organic compounds. In the latter association, it is generally called organic carbon, even if the organic molecules are presumed to have been abiologically synthesized from inorganic molecules. Organic carbon compounds, found in virtually all well preserved mudrocks of any age, typically become enriched in carbon with time

and with degree of metamorphism. In the Archean, the Val d'Or area of Quebec is generally considered to be a source of dense bitumen (Degens 1965, p. 20).

The distribution of organic matter in sediments (Riel 1960; Rao 1960; Uchupi 1972) is generally considered to be of biogenic origin; hence, it is generally available for biologic productivity. Inorganic nutrients such as nitrate, phosphate, and silicate are derived from the atmosphere and in areas of high erosion there is no reason to expect the Precambrian organisms depended on enzymes, *e.g.* A

Concentration of

Most marine sediments contain minute, low concentrations of other non-lagrange laterally transported concomitant biotically responsible matter in fine matter is readily presently surviving. Partial degradation of carbon, which is 7×10^{14} kg in (1965), as compared with inorganic diagenetic oxidation and permeability and rates of partial diagenetic oxidation with increasing depth in the sedimentary fine grained during diagenesis.

The resulting

erein require the
osphere. We will
of ore deposit
f origin, because
ogress, and only
emonstrate com-
an oxygen-rich

oxidation state
ere have great
redox reactions
cal behavior of
g for heavy metal
ns has been cor-
rent concepts of
r, the inadequacy
ome obvious in
Quebec. The con-
mbrian uraninite
ictive, as shown
uraninite in the
not in the form
e base of fining-
where it locally
ic matter (Pre-
placer uraninite
erates of north-
cause the gravels
perienced oxida-
ties of possible
y groundwater
ntrast, prospect-
has been highly
interpreted as
sits, despite the
of both metals
id that deposits
ean should be
he Phanerozoic.

tribution

ciations in un-
e metamorphic
radical of car-
erriad of organic
ociation, it is
n, even if the
d to have been
inorganic mol-
unds, found in
cks of any age,
rbon with time

and with degree of metamorphism until the hydrogen/carbon and oxygen/carbon ratios approach zero and the material is termed graphite (Degens 1965, p. 304). However, locally, even in the Archean, as in the well preserved Rouyn - Val d'Or area of Quebec, the organic carbon of mudrocks is generally not pure graphite but is dense bitumen, termed shungite (Easdon 1969, p. 20).

The distribution of carbon in Recent marine sediments (Richards and Redfield 1954; Emery 1960; Rao 1960; Van Andel 1964; Emery and Uchupi 1972) is determined by biologic, sedimentary, and diagenetic processes. All sedimentary organic carbon is presently of biogenic origin; hence, the total mass of organic carbon available for deposition is determined by biologic productivity. Primary biologic productivity is largely controlled by the supply of inorganic nutrients, particularly phosphate and nitrate. Productivity is great in areas of prograding terrigenous coastlines, where nutrients are derived from fine grained terrigenous mud, and in areas of upwelling ocean currents. There is no reason to believe that this was different in the Precambrian, since even the most primitive organisms depend on phosphate-bearing coenzymes, *e.g.* ATP, for their metabolism.

Concentration of Organic Carbon in Mudrocks

Most marine organic sediment originates as minute, low density plankton. Plankton, like other non-lagoonal detritus, is commonly laterally transported before final deposition, and concomitant hydrodynamic separation is partially responsible for the enrichment of organic matter in fine grained sediments. All organic matter is readily oxidizable, and less than 1% presently survives oxidation (Emery 1960). Partial degradation produces dissolved organic carbon, which presently amounts to about 7×10^{14} kg in the world ocean (Wangersky 1965), as contrasted with about 3.5×10^{16} kg of inorganic carbon (Turekian 1968). Partial diagenetic oxidation rates depend upon sediment permeability, which controls diffusivity and rates of pore fluid exchange. For this reason, diagenetic oxidation rates generally increase with increasing grain size of the sediment, and the sedimentary enrichment of organic carbon in fine grained sediments is further enhanced during diagenesis.

The resulting organic carbon distribution in

marine sediments is fairly simple. Organic carbon contents statistically increase with the clay content of the sediment in all large-scale geologic units (Richards and Redfield 1954; Emery 1960; Rao 1960; Van Andel 1964). Differences in average organic carbon content among sediments deposited in different environments are quite large. In particular, lagoonal and estuarine muds are rich in organic carbon because of the exceptionally high productivities in such environments (Emery and Uchupi 1972). A second organic carbon maximum exists at about 800 m depth, because less of the deposited organic detritus is oxidized diagenetically in the zone of minimum concentration of oxygen in the ocean between 200 and 2000 m depth (Richards and Redfield 1954). Virtually all organic carbon in sandstones is diagenetically destroyed, except where the sandstones contain a clayey matrix. However, later introduction of hydrocarbons is locally common. Organic carbon is destroyed in permeable organogenic rocks such as reef rock or stromatolitic limestone, despite the relatively high organic carbon content of living reefs and stromatolites. The organic matter of fresh aragonitic oolite (*ca.* 1%; Milliman 1974, table 12) is also rapidly destroyed during diagenesis. Meadows of sea-grasses growing on sand-banks, and similar accumulations of organic matter on very shallow sands, have an extremely low preservation potential. They are destroyed by oxidation in nearly all cases.

The distribution of organic carbon deposited from life-sustaining seas under an oxygen-deficient atmosphere would differ markedly from the present distribution. Planktonic matter would, of course, accumulate preferentially with the clay fraction of the sediment. However, some planktonic matter does accumulate in sands, and this would largely not be oxidized. Consequently, all marine sandstones deposited from life-sustaining seas under an anoxygenic atmosphere should contain considerable organic carbon. The 1% or more of organic carbon, presumably like that present in Recent calcareous oolite (Milliman 1974, table 12), should have survived diagenesis, as should have stromatolitic organic carbon. Living stromatolites may be composed of over 80% organic matter (Hofmann 1973). Of course, this is mostly water but there are several percent of organic carbon. Stromatolites lithified under

anoxigenic conditions should contain this amount of organic carbon, and algal mats developed on shallow-marine quartzose sand banks should also be preserved.

It may be theoretically possible that the organic compounds found in Archean mudrocks have formed from organic molecules abiologically synthesized in the Early Precambrian by radiative ionization of atmospheric methane or other hydrocarbons and complex reconstitution (Lasaga *et al.* 1971). Organic compounds so synthesized in a primordial ocean would have contained a high proportion of hydrocarbons because these are among the most stable organic substances. These hydrocarbons would have accumulated on the ocean as a 'primordial oil slick' that would have behaved sedimentologically like modern oil slicks. The modern ocean is highly polluted by petroleum and is an excellent laboratory where the aging and sedimentation of hydrocarbons may be studied. Light hydrocarbons form thin films on the surface of the sea. They age rapidly and polymerize to heavy bitumen, which drifts as lumps a centimetre across or larger. These bituminous lumps eventually are deposited on beaches in the intertidal and supratidal zones. Here they are slowly destroyed under present conditions, but would have been better preserved in the absence of atmospheric oxygen. Thus, abiologically synthesized organic carbon compounds would have been concentrated in littoral deposits, mainly sandstones and calcarenites, but also in pelites deposited in the intertidal and supratidal zones. They should have given rise to littoral sandstones and calcarenites containing bituminous grains or a bituminous matrix, and intertidal and supratidal pelites (easily recognized by their sedimentary structures) also should contain bituminous grains or their deformed equivalents.

Presently available analytical data on the organic carbon distribution in Precambrian sedimentary rocks are rather sketchy (Table 1; Fig. 5). However, the distribution observed in the field is not that expected from such anactualistic models but is quite consistently similar to the present distribution. For example, we know of no littoral sediments containing the bituminous grains or deformed equivalents that would have formed from deposition of hydrocarbons. Middle Precambrian littoral sandstones of the Labrador trough are

generally either stained red by fine grained hematite or are gray but devoid of microscopically recognizable organic carbon; littoral calcarenites and stromatolitic dolostones, associated with intraformational flat-pebble conglomerates typical of the intertidal and supratidal zones, are devoid of visible organic carbon as are the sandstones deposited in deltaic environments (Dimroth 1973). Archean sandstones of a coastal sequence south of the Rouyn-Noranda area, Quebec (M. Rocheleau, *in* Dimroth *et al.* 1975) contain no recognizable organic carbon, whereas the pelitic rocks are richly carbonaceous. Precambrian sedimentary rocks studied by others are generally similar (Pettijohn 1943; Roscoe 1969). However, conglomerates and sandstones rich in uranium and/or gold are characteristically also rich in organic carbon, which appears to be at least partly the remains of algal mats, or of mats of other organisms, that grew on the sediments covered by the coarse clastics (Hallbauer and Van Warmelo 1974).

Extensive microscopic and field observations have confirmed a generally negative correlation between organic carbon contents and grain size in Precambrian sedimentary rocks. Where Precambrian pelite and arenite are interbedded, organic carbon is invariably enriched in the pelite (Figs. 1, 2). Where coarse and fine pelite are interlaminated, organic carbon is concentrated in the finer-grained pelitic laminae. Highly carbonaceous rocks invariably are mudrocks. Matrix-free sandstones, cemented oolitic and stromatolitic limestones, dolostones, and oolitic and intraclastic cherts of Archean and Lower Proterozoic age (Figs. 6, 7, 8) are generally free of microscopically identifiable organic carbon, like Phanerozoic rocks of comparable lithologies. Sandstones and other psammites (calcarenites, coarse grained volcanoclastic rocks) containing some organic carbon are rare (Fig. 4), and in these cases organic carbon is nearly always concentrated in a pelitic matrix (Fig. 3) regardless of the age of the rock.

The negative correlation of grain size with organic carbon content is found in nearly all Precambrian mudrocks, regardless of the source of the sediment or the environment of deposition. In terrigenous suites, organic carbon is concentrated in terrigenous pelite; in volcanogenic suites, it occurs in fine grained tuff or tuffaceous sediment; and in carbonate rocks, it is con-

TABLE 1.

Red Lake
Atikokan
Lac des I
Beardmo
Geraldton
Michipic
Oba, Ont
Timmins
Matache
Larder L
Kinojevis
Desmelo
Amos-Ba
Chapais,
Unwei

Correlati

Correlati

(Σ)

Note:
sulfur in
is roughl
Easdon
Easdon's

centrated in
pelitic equiva
mentary rocks,
lapilli tuffs, t
generally are fre
organic carbon
In the Protero
trough (Dimro
ment is found
deltaic, coasta
ments. Relative
mudrocks inde
found in the
Noranda area.
organic carbon
astal, and
M. Rocheleau
However, avera

TABLE 1. Correlation coefficients for organic carbon concentrations and estimates of pyrite contents in Archean mudrocks

Cameron and Jonasson (1972)				Easdon (1969)		
Areas	No. of samples	Mean % C	Mean % S	Township (NW Quebec)	% C	% Fe
Red Lake, Ontario	12	1.73	4.6	Surimau	8.27	9.56
Atikokan, Ontario	27	0.20	0.22	Desboues	15.01	31.61
Lac des Iles, Quebec	48	0.21	0.35	Desboues	10.39	15.17
Beardmore, Ontario	7	0.10	0.10	Desboues	0.53	3.13
Geraldton, Ontario	48	0.10	0.15	Desboues	6.18	5.92
Michipicoten, Ontario	7	1.76	10.3	Desboues	0.61	2.38
Oba, Ontario	5	7.6	10.9	Desboues	16.74	23.38
Timmins, Ontario	141	1.27	1.93	Desboues	0.57	2.09
Matachewan, Ontario	9	0.48	0.74	Desboues	10.01	14.81
Larder Lake, Ontario	47	0.19	0.17	Desboues	0.33	2.68
Kinojevis Riv., Quebec	11	0.16	0.14	Desboues	9.85	7.31
Desmeloizes, Quebec	6	0.12	0.28	Desboues	0.59	1.74
Amos-Barraute, Quebec	9	0.39	0.10	Desboues	9.79	5.16
Chapais, Quebec	29	0.30	0.16	Desboues	4.30	2.44
Unweighted grand means		1.04	2.15	Desboues	3.84	4.67
				Desboues	13.69	7.76
				Desboues	13.22	6.10
				Desboues	3.71	1.73
Correlation coefficient = 0.83				Launay	5.79	4.80
				Languedoc	11.83	6.67
				Berry	4.29	3.57
Correlation coefficient is defined to be				Languedoc	5.45	5.42
				Guyenne	5.35	14.21
				Guyenne	2.70	4.95
				Barraute	0.71	4.22
				Barraute	4.17	6.71
				Pascalis	2.56	6.15
				Fiedmont	17.60	33.76
				La Sarre	3.90	4.95
				Means	6.62	8.38

$$\frac{\sum(X_i - \bar{X})(Y_i - \bar{Y})}{(\sum(X_i - \bar{X})^2 \sum(Y_i - \bar{Y})^2)^{1/2}}$$

Note: Pyrite content is closely represented by percent sulfur in data from Cameron and Jonasson (1972) and is roughly approximated by percent iron in data from Easdon (1969). Each analysis is of one sample only in Easdon's data.

Correlation Coefficient = 0.81

concentrated in micrite. The psammitic and psephitic equivalents of these fine grained sedimentary rocks, e.g. sandstones, conglomerates, lapilli tuffs, tuff breccias, and calcarenites, generally are free of microscopically recognizable organic carbon unless they contain a mud matrix. In the Proterozoic sequence of the Labrador trough (Dimroth 1973), such carbon enrichment is found in pelites deposited in fluvial, deltaic, coastal, and deep marine environments. Relative organic carbon enrichment in mudrocks independent of environment is also found in the Archean suites of the Rouyn-Noranda area, where mudrocks containing organic carbon have been deposited in lacustrine, coastal, and deep marine environments (M. Rocheleau, in Dimroth *et al.* 1974, 1975). However, average carbon contents of mudrocks

deposited in different environments are not the same.

Concentration of Organic Carbon in Shallow-Water Sedimentary Rocks

Organic carbon content is not a simple function of grain size. Just as lagoonal and estuarine mudrocks are much more carbonaceous than other mudrocks in the Phanerozoic, so they also appear to be in Precambrian suites. Recently discovered, excellently preserved, Archean oolitic limestone and iron formation in the upper Back River area, Northwest Territories, Canada, is stratigraphically correlative with highly carbonaceous and pyritic mudrock that is interpreted to be of lagoonal origin (M. M. Kimberley, unpublished data 1975). Similar mudrock is interbedded with a lean, sideritic iron forma-



0 1cm Fig. 6



0 1cm Fig. 7



0 1cm

Fig. 8

FIG. 6. Oolitic dolarenite. The ooids and pisolites (or algal oncolites) are carbon-poor, as is the sandy matrix. Section W 38-7, Alder Formation, Lace Lake area, Labrador trough. Scale = 1 cm.

FIG. 7. Stromatolitic dolostone from the Alder Formation, Lace Lake area, Central Labrador trough. The dolostone is free of microscopically recognizable carbonaceous matter despite the probable high original organic content. Note the fenestral textures. Section P 39-5. Scale = 1 cm.

FIG. 8. Stromatolitic dolostone from the Alder Formation, Lace Lake area, Central Labrador trough. Note fenestral textures. These dolostones are virtually carbon-free despite the high organic content of living stromatolites. Section A 10-6. Scale = 1 cm.

depends upon
able organic
clear that
matter not

Organic Carbon

Oxygen
principally
photosynth
proximate
estimated f
average c
(Holland,
mentation
more epher
Estimates c
sediment r:
 10^{13} kg (K
Garrels and
 10^{13} kg. As
to the ocea
sulfate (G
amounts o
total mari
 2×10^{13} kg

The aver
tion of or
estimated
(Trask and
higher for
Migdisov 1
an interme
organic car
 10^{11} kg. At
presently in
1972). could

The cur
oxygen is
(1973a) has
rock weath
 10^{11} kg and
hydrogen g
these rates
consumed v

The gen
Phanerozoic
the product
and oxygen
Middle to
to have bee
two orders

depends upon the presence of readily metabolizable organic compounds (Berner 1971), it is clear that this organic carbon was in organic matter not long dead.

Organic Carbon and Atmospheric Oxygen Transfer

Oxygen is presently added to the atmosphere principally through the burial of organic carbon photosynthesized from carbon dioxide. The approximate rate of oxygen production may be estimated from the rate of sedimentation and the average carbon content of that sediment (Holland, in preparation). Only marine sedimentation need be considered because of the more ephemeral nature of non-marine sediment. Estimates of the annual marine influx of detrital sediment range from 0.93×10^{13} kg to 3.25×10^{13} kg (Kuenen 1950). The value accepted by Garrels and Mackenzie (1971) and by us is 1.83×10^{13} kg. Assuming that the annual fluvial supply to the oceans of dissolved calcium, silica, and sulfate (Gibbs 1972) results in equivalent amounts of limestone, chert, and gypsum, the total marine sedimentation rate is roughly 2×10^{13} kg/y.

The average Phanerozoic sedimentary proportion of organic carbon has been variously estimated at 0.8 to 1.1% for North America (Trask and Patnode 1942, p. 25) and 0.4% or higher for the Russian Platform (Ronov and Migdisov 1971; Ronov *et al.* 1965). Accepting an intermediate value of 0.75%, the annual organic carbon burial would amount to 1.5×10^{11} kg. At this rate, the 1.2×10^{18} kg of oxygen presently in the atmosphere (Goody and Walker 1972) could be generated within 3×10^6 y.

The current consumption of atmospheric oxygen is also geologically rapid. Holland (1973a) has estimated the annual loss due to rock weathering to be presently about 4×10^{11} kg and the loss due to oxidation of volcanic hydrogen gas to be only $2(\pm 1) \times 10^9$ kg. At these rates, all atmospheric oxygen could be consumed within 3×10^6 y.

The general similarity of Proterozoic to Phanerozoic supracrustal rocks is too close for the production or consumption rates of carbon and oxygen to have differed radically. Even Middle to Late Archean volcanism is unlikely to have been greater than present volcanism by two orders of magnitude, or the weathering rate

less by an order of magnitude, given that Archean mudrocks in northwestern Quebec (Easdon 1969) and in South Africa (Visser 1956) are compositionally distinct from tuffs, the Canadian mudrocks containing very little calcium. There is no evidence that such weathering of Precambrian sediments was caused by carbon dioxide instead of oxygen since biotite, which is susceptible to oxidation, apparently survived no better than in the Phanerozoic and feldspar, susceptible to carbonation, survived as well. The 2250 to 2450 m.y. old Huronian sequence of Ontario is rich in detrital feldspar but contains no reported detrital biotite (Young 1973). Moreover, we know of no evidence to support the proposal by Cloud (1973) that all or a large part of Archean organic carbon is the residue of photoautotrophic bacteria. On the contrary, all evidence presented in this paper appears to be inconsistent with such a proposal.

The concept of a gradual increase in atmospheric oxygen through the Precambrian (Berkner and Marshall 1965) is difficult to reconcile with consumption-production rates even an order of magnitude less than current rates. The negative feedback processes that presently seem to control the amount of atmospheric oxygen could have been just as effective as they are today in any part of the Archean when there were photosynthesizing algae. These processes include oxidation of variable proportions of organic matter depending upon atmospheric oxygen level (Broecker 1970), inhibition of photosynthesis by overly abundant oxygen, oxidation of variable proportions of hydrogen produced by photodissociation of water (Van Valen 1971), and coupling, during periods of increased erosion and weathering, of increased oxygen consumption to increased photosynthetic activity through increased supply of dissolved phosphate (Holland 1973a). Initiation of an oxygenic atmosphere could have occurred a few million years after the initiation of aerobic photosynthesis. The occurrence of blue-green algal remains in the approximately 2600 m.y. old Vaal Reef Carbon Seam of the Witwatersrand Sequence (Nagy 1975) offers a probable minimum age for our oxygenic type of atmosphere. However, the petrographic similarity of the Isua Complex iron formation and associated sedimentary rocks (Bridgwater *et al.* 1973), dated at about 3750 m.y. (Moorbath



Fig. 7

1cm

oor, as is the
ale = 1 cm.
rador trough.
probable high

tral Labrador
high organic

et al. 1973), to younger rocks suggests that this earlier date is a better minimum.

What the proportion of atmospheric oxygen may have been before photosynthesis depends largely upon the Early Archean rates of photodissociation of water and escape of hydrogen from the earth's upper atmosphere. Brinkmann (1969) has estimated that, under current conditions, this process alone could produce one-quarter or more of the present atmospheric level of oxygen. Van Valen's (1971) objection that Brinkmann (1969) should have emphasized oxidation of volcanic gases relative to rock weathering as an oxygen-consumptive process is not substantiated by Holland (1973a), who showed weathering of sulfide-bearing rock to be more important.

Carbon Isotopic Ratios and Atmospheric Oxygen Transfer

Not only is the mass distribution of carbon between organic molecules and carbonate minerals relevant to atmospheric oxygen levels but also isotopic fractionation of carbon between these two reservoirs (Broecker 1970; Holland 1973b). In a hydrosphere-atmosphere system of constant carbon content, supplied with carbon of unchanging isotopic ratio, and with continual high degree of fractionation by organisms, comparable organic and carbonate carbon isotopic ratios in sedimentary rocks of all ages would indicate a constant rate of separation of carbon between the two reservoirs, and hence an unchanging rate of free oxygen production.

Available analyses indeed indicate constancy with time for the isotopic ratios of sedimentary carbonate and organic carbon (Becker and Clayton 1972; Schidlowski *et al.* 1975), provided organic carbon is relatively unmetamorphosed. There is no reason to suspect that the carbon supplied volcanically has varied isotopically, nor is any significant variation in organic fractionation apparent (Oehler *et al.* 1972). However, the mass of carbon in the hydrosphere-atmosphere may have changed. Using Holland's (1973a) assumption for the rate of volcanic degassing and measurement of carbon in volcanic gasses (Eaton and Murata 1960), integration over all of earth history gives an exhaled mass potentially greater than Rubey's (1951) estimate of total carbon in the crust. Although the basis for this calculation is doubtful, it clearly indicates,

as suggested by Becker and Clayton (1972), that volcanic carbon contribution must be considered. The major evidence against their contention, that volcanic contributions may have increased the mass of carbon in the hydrosphere-atmosphere with time, is the high proportion of organic carbon found in Archean mudrocks, including those associated with limestones as in the Michipicoten (Goodwin 1962) and upper Back River (M. M. Kimberley, unpublished data) areas previously mentioned. It is concluded that the constancy of carbon isotopic fractionation in sedimentary rocks is, in fact, an indication of relative constancy of free-oxygen production.

Sedimentary Sulfur Distribution

Introduction

The distribution of sulfur in Recent sediments, like that of organic carbon, is largely a function of primary and diagenetic redox reactions (Berner 1971) and is correspondingly sensitive to variations in atmospheric oxygen pressure. There are two major sources of sulfide sulfur in present-day sediments, *i.e.* seawater sulfate reduced bacterially and organic sulfur released during decay; and two minor sources, *i.e.* volcanically-exhaled sulfur and detrital pyrite.

Detrital Pyrite

Detrital pyrite is present in some fluvial placers (Ramdohr 1960, p. 741) and is common in eskers and in some glaciofluvial sands of Quebec (P. LaSalle and J. Radziminiska-LaSalle, personal communication 1974). However, its preservation potential is low. In a few cases, detrital pyrite may survive diagenesis, provided deposition is rapid and reducing diagenetic conditions are established rapidly after deposition. One may expect to find detrital pyrite locally in braided stream and alluvial fan environments, particularly in cold climates. Preservation of pyrite in deposits of meandering streams and in shallow-marine or beach sediments of the temperate and warm climatic zone is unlikely (Davidson 1964), although some pyrite is known to occur in Recent alluvium in Central Europe (Müller and Negendank 1974).

By contrast, pyrite should have been a consistent and important component of all fluvial and shallow-marine sandstones deposited under a hypothetical oxygen-deficient atmosphere. Pyrite is common in all source rocks and is

relatively resistant, present, pyrite mechanically at crystal edges (LaSalle and J. communication largely by bioc

No detrital thin sections (or shallow-marine trough of Quebec is no more than basal phase of glomerates of Quebec (as described *et al.* 1975). In pyrite pebbles a basal conglomerate some concentration obviously detrital-appearing pyrite Pocatière mer Damase Forn although this is as for the Precambrian most Proterozoic the Labrador t despite the common in the source during transport of the gold- and of the Witwaters Elliot Lake a sections to be filling cracks like a cement, plate IV), and detrital texture

Bacterially-Reduced

Most sulfides formed by the and is closely (Berner 1970) association of equally characteristic sequence in (Dimroth 1977) sedimentary rocks and Quebec (1974), and of rocks, about

Clayton (1972), distribution must be in accordance with their contributions may of carbon in the time, is the high found in Archean associated with limestone (Goodwin 1962). M. Kimberley, obviously mentioned. constancy of carbon in sedimentary rocks is, relative constancy of

Distribution

Recent sediments, largely a function of redox reactions being sensitive to pressure. There is sulfur in present-sulfate reduced released during, i.e. volcanically.

in some fluvial and is common in fluvial sands of Radziminiska (Radziminiska 1974). How is low. In a few survive diagenesis, and reducing established rapidly to find detrital and alluvial fan in cold climates. of meandering or beach sediment climatic zone although some cent alluvium in Goodwin (1974). have been a content of all fluvial deposited under atmosphere. rocks and is

relatively resistant to abrasion (Koen 1958). At present, pyrite does not appear to be rounded mechanically because oxidative corrosion of crystal edges is a more efficient process (P. LaSalle and J. Radziminiska-LaSalle, personal communication 1974) and pyrite is eliminated largely by biochemical oxidation.

No detrital pyrite has been found in any thin sections of the Lower Proterozoic fluvial or shallow-marine sandstones of the Labrador trough of Quebec (Dimroth 1973), and pyrite is no more than a mineralogical rarity in the basal phase of the Archean piedmont fan conglomerates of the Rouyn-Noranda area of Quebec (as described by Rocheleau, *in* Dimroth *et al.* 1975). In the latter case, detrital-appearing pyrite pebbles occur only in several outcrops of a basal conglomerate of local provenance, and some concentrically laminated pyrite nodules, obviously diagenetic, are present with the detrital-appearing pyrite. Similar detrital-appearing pyrite occurs in the Cambrian La Pocatière member (Hubert 1973) of the St. Damase Formation at La Pocatière, Quebec, although this is as unusual for the Phanerozoic as for the Precambrian. Absence of pyrite from most Proterozoic and Archean sandstones in the Labrador trough and Rouyn-Noranda areas, despite the common presence of the mineral in the source rocks, is evidence for oxidation during transport and/or diagenesis. The pyrite of the gold- and uraninite-bearing conglomerates of the Witwatersrand, the Serra de Jacobina, and Elliot Lake areas is found in polished thin sections to be partially replacing quartz grains, filling cracks in clasts, or occurring interstitially like a cement, as illustrated by Du Toit (1953, plate IV), and so is not considered to display detrital textures.

Bacterially-Reduced Sulfate

Most sulfide-sulfur in Recent sediments has formed by the action of sulfate-reducing bacteria and is closely associated with bituminous shales (Berner 1970). As for organic carbon, the association of pyrite with clayey sediment is equally characteristic of the Lower Proterozoic sequence in the Labrador trough, Quebec (Dimroth 1973), of 2700 m.y. old Late Archean sedimentary rocks in the Abitibi belt of Ontario and Quebec (Goodwin 1973; Dimroth *et al.* 1974), and of Middle Archean metasedimentary rocks, about 3750 m.y. old, in Greenland

(D. Bridgwater, personal communication 1975). Some Precambrian pyrite occurs as laminae like some of the Recent diagenetic pyrite (Berner 1971), but much is nodular, more obviously diagenetic. Nodules in the Michipicoten area of Ontario (Goodwin 1962) are delicately concentrically layered. Easdon (1969, p. 30) found a linear increase in pyrite content with increase in organic carbon content in 27 Archean carbonaceous mudrocks of the Rouyn-Val d'Or area of Quebec and adjacent Ontario. A similar relationship can be seen in the carbon and sulfur contents reported by Cameron and Jonasson (1972, p. 991) for several Archean greenstone belts in the Superior Province of the Canadian Shield. This consistency of the sulfide-sulfur-carbonaceous mudrock association, which is so characteristic of Precambrian (Table 1) as well as Phanerozoic rock associations, is evidence for (1) the continually abundant presence of sulfate in the oceans and (2) the continual diagenetic bacterial reduction of that sulfate, at least since deposition of the earliest known Precambrian sediment.

Volcanically-Exhaled Sulfur

Volcanic exhalations generally include hydrogen sulfide. Under present conditions, most of the exhaled hydrogen sulfide is rapidly oxidized and precipitation of exhalative heavy metal sulfides occurs only under exceptional conditions. In the absence of atmospheric oxygen, the products of volcanic exhalation would have differed, particularly if most of the primordial ocean had been saturated with respect to siderite, as is assumed by Cloud (1973), Holland (1973c), and Drever (1974). All hydrogen sulfide exhaled by submarine volcanoes would have precipitated as iron sulfide close to the volcanic vents. Volcanogenic sulfide deposits should be many orders of magnitude more voluminous in Precambrian volcanic sequences than in Phanerozoic volcanic sequences, and they should occur around all Archean submarine volcanic centers. Archean copper and zinc ores would have been more diluted than Phanerozoic ores by the marine ferrous iron presumed to have been abundant and reactive with exhaled chemicals. Proximal pyroclastic rocks would have been cemented by pyrite.

In fact, none of these inferred differences between volcanogenic sulfide deposits of Precambrian and Phanerozoic age are consistently

found. Massive sulfide deposits certainly did not form around every Archean volcanic center. On the contrary, the special conditions for their formation were realized only under peculiar volcanologic and stratigraphic conditions (Sangster 1972; Spence and de Rosen-Spence 1975). Base metal contents, base metal zonation, and geologic setting of the Archean ore deposits of the Rouyn-Noranda area, Quebec, are comparable to Miocene deposits in Japan (Sangster 1972; Simmons *et al.* 1973; Horikoshi and Sato 1970; Sato 1971, 1972). Archean sulfide deposits in the Abitibi belt (Dugas 1967) do not appear to be more voluminous than sulfide deposits in comparable Phanerozoic volcanic belts, e.g. the Paleozoic belt of southern Portugal and Spain (Strauss and Madel 1974) and the Green Tuff belt of Japan (Matsukuma and Horikoshi 1970). Moreover, pyrite cement is absent from even the most proximal pyroclastic rocks of the Rouyn-Noranda area. The distribution of volcanic exhalative sulfide deposits in Archean terrains does not appear to differ substantially from the Phanerozoic distribution, and the hypothesis that the Early Precambrian primordial ocean was saturated with respect to siderite is similarly unsubstantiated.

Precambrian Evaporites

Scarcity of Precambrian evaporites has been cited as evidence against substantial sulfate concentrations in sea water. However, most Archean sedimentary rocks are deep-water turbidites. There are some fluvial deposits (Turner and Walker 1973; Rocheleau, *in* Dimroth *et al.* 1975), but Archean shallow-marine and littoral deposits are virtually unknown except for a few probable eroded-volcanic-island coverings, largely of iron formation. Most Archean sedimentation apparently occurred on tectonically active, steep slopes surrounding volcanic piles. Such a setting is not conducive to evaporite deposition or preservation. On the other hand, there is evidence that evaporites were present in all Lower Proterozoic miogeosynclinal sequences of the Canadian Shield deposited under appropriate climatic and paleogeographic conditions. Evidence for evaporites is provided by gypsum and anhydrite nodules as in the Gordon Lake Formation of the Huronian Supergroup (Wood 1973), gypsum and halite casts in the east arm of Great Slave Lake (Hoffman 1968, 1973) and on the Belcher

Islands (Bell and Jackson 1974), length-slow chalcedony in the Labrador trough (Chauvel and Dimroth 1974), and by probable evaporite-solution-collapse breccias. Survival of the actual evaporite minerals cannot be expected to be common in Precambrian Shields because presently-exposed rocks have been fairly close to the surface since the end of Precambrian time and have experienced prolonged, albeit slow, ground-water flow.

The relationship of sulfur geochemistry to atmospheric oxygen production is much like that of carbon (Holland 1973b). Volcanically-exhaled sulfur dioxide dissolves to form sulfate ions that, upon bacterial reduction and formation of pyrite, release free oxygen. Bacterially-fractionated sulfur varies considerably in isotopic ratio and is generally light. Conversely, highly variable or light isotopic concentrations of sulfur in unmetamorphosed and low metamorphic-grade sedimentary rocks are an indication of bacterial fractionation during sedimentation because inorganic fractionation is probably too slow to be significant at such low temperatures. The discovery by Goodwin *et al.* (1976) of a wide spread of sulfur isotopic values in pyrite of the Archean Michipicoten and Woman River iron formations east of Lake Superior, Ontario, coupled with very isotopically light carbon in associated carbonaceous mudrocks, is interpreted by them to indicate Archean autotrophic organisms and reducing bacteria.

Sedimentary Uranium Distribution

Uranium is generally concentrated in sedimentary rocks relatively rich in carbonaceous matter. Certain extensive carbonaceous mudrocks and lignites contain several tens of times the mean crustal abundance of uranium, which is about 3.4 ppm (Swanson 1960, 1961; Wright 1972). Stratiform ores of uranium, largely sandstones and conglomerates with over 300 times mean crustal abundance, are also generally richer in carbonaceous matter than unmineralized sandstones and conglomerates. This relationship is well documented for the Cenozoic (Rackley 1972) and Mesozoic (Petersen 1960) deposits of the U.S.A., in which reduction of groundwater sulfate and uranyl ions by organic oxidation is generally taken to be the cause of pyrite-uraninite precipitation. The abundance of dense, isotopically light hydrocarbon in the

South Af
ores (Pras
its occurre
Elliot La
suggestive
Middle P
ization (D

There a
common t
rand (Pret
1969) dep
sandstone-
(Kimberle
stratiform
kilometres
Austrian T
centration
bedding p
Wyoming
of quartz
and uranin
of Arizona
of fossil p
concentrati
host ore t
Italian Tyr

Differenc
Phanerozoi
two major
of Middle I
range of s
pyrite (R
Thorium is
can be trar
solvents (C
been more
than in Pha

The Mid
sulfur isoto
than less-st
has a wide
This could
sulfur leach
elastics and
tion.

Direct ev
bility has
organisms v
and Van W
dynamically
have occur
sures (Holl
carbonaceo

1974), length-slow
trough (Chauvet
probable evaporite-
revival of the actual
be expected to be
fields because pres-
sion fairly close to the
Cambrian time and
albeit slow, ground-

r geochemistry to
tion is much like
73b). Volcanically-
ves to form sulfate
duction and forma-
xygen. Bacterially-
siderably in isotopic
Conversely, highly
entrations of sulfur
low metamorphic-
an indication of
ing sedimentation
on is probably too
low temperatures.

al. (1976) of a wide
res in pyrite of the
Yoman River iron
superior, Ontario,
ly light carbon in
udrocks, is inter-
rechean autotropic
ria.

Distribution

concentrated in sedi-
in carbonaceous
arbonaceous mud-
veral tens of times
of uranium, which
260, 1961; Wright
uranium, largely
es with over 300
are also generally
atter than un-
nglomerates. This
3 for the Cenozoic
c (Petersen 1960)
high reduction of
elutions by organic
o be the cause of

The abundance
drocarbon in the

South African Witwatersrand gold-uranium
ores (Prashnowsky and Schidlowski 1967) and
its occurrence in rich portions of the Canadian
Elliot Lake uranium ores (Roscoe 1969) is
suggestive of a similar diagenetic control on
Middle Precambrian pyrite-uraninite mineral-
ization (Derry 1960).

There are a number of other characteristics
common to the Middle Precambrian Witwaters-
rand (Pretorius 1974) and Elliot Lake (Roscoe
1969) deposits, which are found in Phanerozoic
sandstone-conglomerate uraninite deposits
(Kimberley 1974a), including: lateral extent of
stratiform uraninite mineralization of several
kilometres, as in the Permian of the
Austrian Tyrol (Schulz and Lukas 1970); con-
centration of pyrite and uraninite along cross-
bedding planes, as in the Shirley Basin of
Wyoming (Harshman 1972); partial replacement
of quartz by pyrite, and roundness of pyrite
and uraninite, as in the Shinarump conglomerate
of Arizona (Petersen 1960); partial replacement
of fossil plants (Finch 1967); and preferential
concentration of uraninite at the base of the
host ore bed, as in the Permian of the
Italian Tyrol (Ippolito 1958).

Differences between Middle Precambrian and
Phanerozoic uraninite deposits do exist, the
two major ones being the high thorium content
of Middle Precambrian uraninite and the narrow
range of sulfur isotopic values in associated
pyrite (Roscoe 1969; Schidlowski 1968).
Thorium is virtually insoluble in pure water, but
can be transported by certain dissolved organic
solvents (Galkin *et al.* 1963) that could have
been more abundant within Middle Precambrian
than in Phanerozoic sediments.

The Middle Precambrian pyrite, with narrow
sulfur isotopic range, is much coarser grained
than less-stratiform Phanerozoic pyrite, which
has a wide range of isotopic ratios (Finch 1967).
This could be related to precipitation of all
sulfur leached from overlying weathering pyro-
clastics and homogenization upon recrystalliza-
tion.

Direct evidence of diagenetic uranium mo-
bility has been found in uraninite-replaced
organisms within Witwatersrand ores (Hallbauer
and Van Warmelo 1974). Although it is thermo-
dynamically possible that this mobility could
have occurred at exceedingly low oxygen pres-
sures (Holland 1962), it is more likely that the
carbonaceous replacements indicate an oxygenic

groundwater-atmosphere system more like that
at present. However, the concept of an oxygen-
rich Middle Precambrian atmosphere is in-
consistent with the concept of physical sorting,
having produced the bulk of Middle Pre-
cambrian uraninite concentration (Pretorius
1974; Roscoe 1969). M. M. Kimberley (un-
published matter) proposes an alternate genetic
model, in which groundwater leachate of over-
lying weathered volcanic ash is reduced by
oxidation of remains of organisms along dis-
conformities. Among the evidence for this model
is the occurrence of mafic to felsic Huronian
volcanics with weakly uraniferous conglomerates
directly beneath the ore-bearing Matineenda
Formation in the Elliot Lake area (Robertson
1973), the similar abundance of volcanics in the
base (Dominion Reef) of the Witwatersrand
(Pretorius 1974), and the occurrence of vol-
canics through the entire Witwatersrand se-
quence, which has a much greater stratigraphic
range of richly mineralized beds than does the
Huronian sequence.

Sedimentary Iron Distribution

Recent Iron Sedimentation and Ancient Red Beds

Recent sedimentation of ferriferous minerals
at sediment-water interfaces and diagenesis of
these minerals are largely controlled by redox
reactions and, like sulfur and organic carbon
sedimentation, should be sensitive to variations
in atmospheric oxygen pressure. At present,
iron in tropical weathering products is trans-
ported principally in the ferric state in clay-
sized particles (Van Houten 1972). This ferric
iron is readily reducible to aqueous ferrous iron
in the presence of decaying organic matter
within shallowly buried, anoxygenic sediment
(Berner 1970), and dissolved ferrous iron may
be transported in anoxygenic subsurface waters.
Subsequent precipitation as hydroxide, oxide,
silicate, carbonate, or sulfide minerals may occur
under a variety of conditions characterized by
certain ranges of oxygen fugacity and pH.
Recent iron concentration occurs in a number
of forms, including iron-rich encrustations at
the sediment-water interface (James 1969),
iron-rich cements and concretions within detrital
sediment, and ferriferous partial replacements
of calcareous sediment. (Kimberley 1975a).

Present-day formation of presumed red-bed
precursors is dependent upon the currently
high level of atmospheric oxygen, despite the

fact that hematite is stable with respect to any predominantly ferrous minerals at exceedingly low oxygen fugacities (Garrels and Christ 1965). Red-bed formation is believed to require that organic matter readily metabolizable bacterially either not be co-sedimented with the detritus, or that it be oxidized before sediment burial below the zone of substantial groundwater flow. Generally, the latter appears to be the case. No predominantly ferric minerals are thermodynamically stable in the presence of any organic compounds (Stumm and Morgan 1970), but co-existence with relatively unreactive carbonaceous compounds is fairly commonly found. In continental red-beds, igneous and metamorphic ferriferous minerals may be diagenetically oxidized and detrital grains coated by hematite under the influence of a strongly variable water table, especially in arid areas where organic productivity and organic sedimentation are minimal (Walker 1967; Glennie 1970). Some shallow-marine red-beds may form by a similar process during periods of regression and subaerial exposure of the sediment. However, some thick red-bed sequences seem to have been deposited in deep water, like part of the Cambro-Ordovician sequence in the lower St. Lawrence River area of Quebec (Lajoie *et al.* 1974). In this case, oxidation of the sediment is believed to have taken place by diffusion of oxygen into the sediment, aided by low sedimentation rates and bioturbation. Weathered basalts on the present deep-ocean floor, particularly their fragmental (hyaloclastic) varieties, are commonly also heavily oxidized due to reaction between ferrous iron in basaltic glass and oxygen-rich sea water.

Well documented red-beds, more than 1900 m.y. old (Fryer 1972), occur in the Labrador trough of Quebec and lie well beneath one of the largest cherty iron formations in the world

(Dimroth 1968). These red-beds are of two types, fluvial arkose and feldspathic conglomerate, and shallow-marine shale, dolostone, and sandstone. The feldspathic conglomerate contains andesite pebbles bearing oxidized weathering crusts (Fig. 9). These pebbles provide unambiguous evidence for oxidation during weathering in a subaerial environment. Within the weathering crusts, mafic minerals have been replaced by hematite, and grain boundaries and cracks have been coated with hematite (Figs. 10, 11). In the associated arkoses, grain boundaries are coated by fine grained hematite, and hematite-rich clay binds the component grains. The sediment was clearly deposited under oxidizing conditions, and oxidizing conditions were maintained until the final closure of pore space. During metamorphism, the red arkoses and shallow-marine red-beds have been somewhat discolored due to conversion of hematite to magnetite and recrystallization of hematite, coarse grained hematite being generally gray.

The fluvial red-beds are overlain by shales, siltstones, dolostones, and sandstones that were deposited near a coastline in a zone of mixed terrigenous and chemical sedimentation. All the marginal facies of the pelitic units as well as the intercalated thin interbeds of dolostone and dolomitic sandstone are red or variegated red-green (Figs. 12, 13, 14, 15). The thick units of dolostone and dolomitic sandstone generally are not red, with the exception of the du Portage and Dunphy Formations, but any detrital grains are generally hematite-coated (Fig. 12). Reddening of the sediments may have occurred during early diagenesis, but green concretions less compacted than surrounding red pelite provide evidence for subsequent reduction (Fig. 15). It is unknown whether hematite in the marine red-beds formed during brief intervals of subaerial exposure or by submarine dia-

FIG. 9. Red arkosic conglomerate, Chakonipau Formation, Chakonipau Lake area, Central Labrador trough. Pebbles of andesite (a) and gneiss (gn), in an arkosic matrix. Note the red weathering crusts (arrows) of andesite pebbles, indicating oxidizing conditions during deposition. Section A 13-9A. Scale = 1 cm.

FIG. 10. Details of Fig. 9. Biotite (bi) of a gneiss pebble has been oxidized, discolored, and replaced by hematite. Biotite of an andesite pebble (top left) has also been replaced by hematite. Fine grained hematite coats the elastic grains. Scale = 1 mm.

FIG. 11. Detail of Fig. 9. Biotite of an andesite pebble (an) has been replaced by hematite. Clastic grains are hematite-coated. Scale = 1 mm.

FIG. 12. Gray, shallow marine or littoral orthoquartzite. Organic matter is absent. Clastic grains are coated by hematite. Gray color of sample is due to relatively coarse grain size of hematite. Wishart Formation, de la Broche Lake area. Section W 21-6. Scale = 1 mm.

beds are of two
 spathic conglom-
 e, dolostone, and
 conglomerate con-
 oxidized weather-
 bbles provide un-
 ion during weath-
 ment. Within the
 rals have been re-
 n boundaries and
 h hematite (Figs.
 es; grain bound-
 ed hematite, and
 component grains.
 deposited under
 idizing conditions
 al closure of pore
 the red arkoses
 have been some-
 rsion of hematite
 tion of hematite,
 generally gray.
 overlain by shales,
 dstones that were
 a zone of mixed
 dimentation. All
 ic units as well as
 of dolostone and
 or variegated red-
 The thick units of
 tone generally are
 of the du Portage
 but any detrital
 coated (Fig. 12).
 ay have occurred
 green concretions.
 nding red pelite
 at reduction (Fig.
 hematite in the
 g brief intervals
 submarine dia-



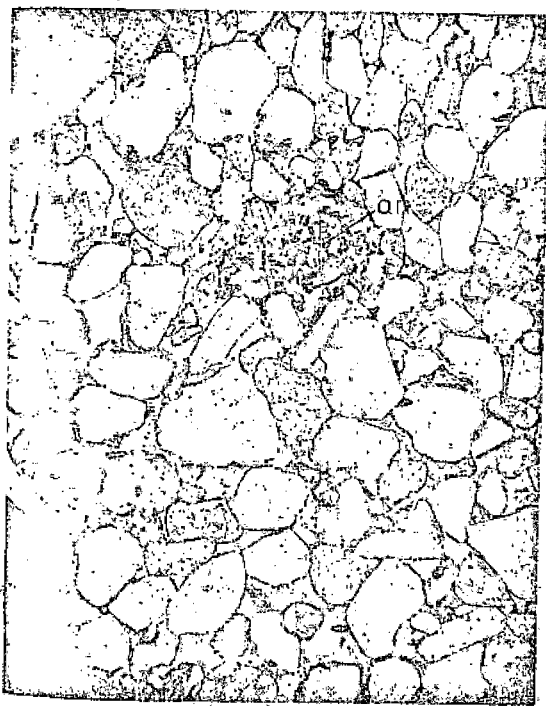
0 1cm

Fig. 9



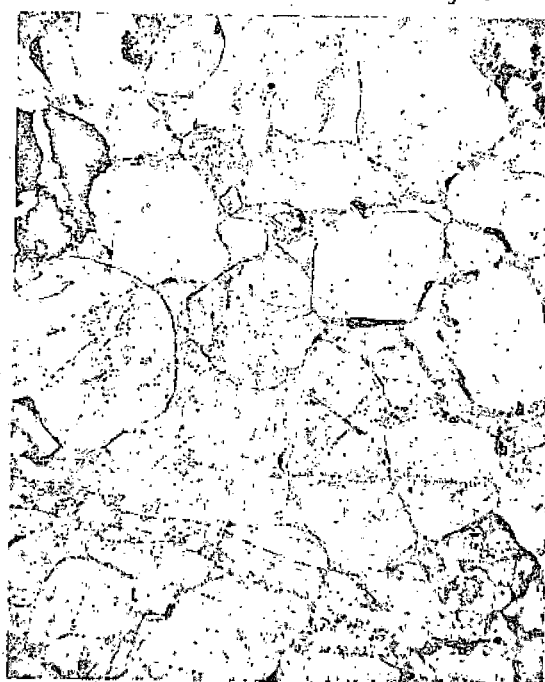
0 1mm

Fig. 10



0 1mm

Fig. 11



0 1mm

Fig. 12

area, Central
 d weathering
 ion A 13-9A.
 and replaced-
 Fine grained
 atite. Clastic
 Clastic grains
 atite, Wishart

genesis, but minor disconformities do suggest repeated emergence of the sequence (Dimroth 1968). The similarities between these Precambrian red beds and their Phanerozoic counterparts are sufficiently obvious that we have no reason to doubt that they have had comparable origins.

Evidence for diagenetic oxidation during submarine weathering of basalts and andesites is widespread in Archean volcanic sequences, like those in the Rouyn-Noranda area of Quebec. In these rocks, iron of the volcanic glass has been partially oxidized to goethite and hematite, just as in Recent submarine weathered glass. Oxidized margins of sideromelané shards and of pillow rims (Figs. 16, 17) are well preserved

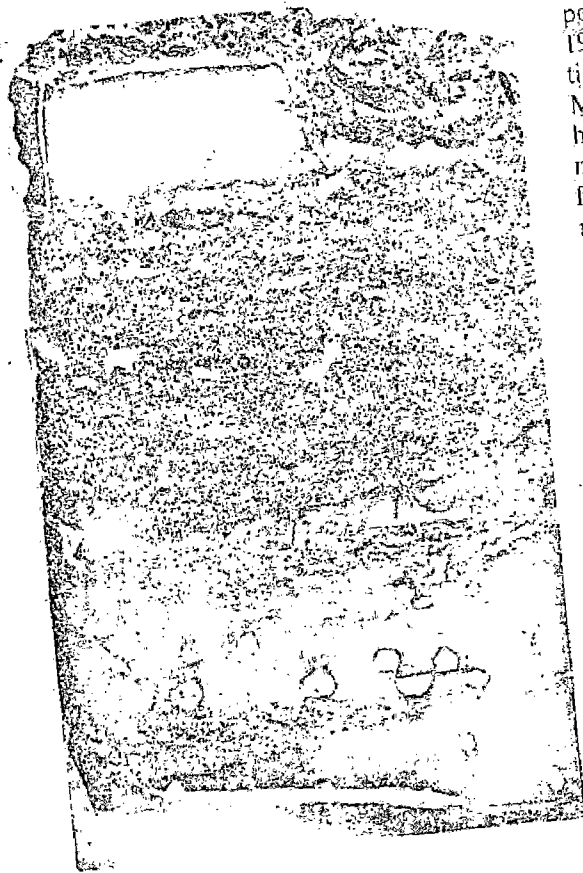


FIG. 13. Stromatolitic and intraclastic red dolostone. Dark areas are intraclasts and stromatolitic crusts stained red by fine, evenly distributed hematite pigment. Light gray areas are sparry cement. Note the fenestral textures due to gas blisters. Section W 3-11, du Portage Formation, Central Labrador trough. Scale = 1 cm.

where rocks are of pumpellyite-prehnite metamorphic grade. However, iron oxides have been reduced and iron incorporated into silicate minerals where greenschist metamorphic conditions have been attained. These observations indicate that oxidation took place before the Kenoran metamorphism, about 2600 m.y. ago. M. Rocheleau (*in* Dimroth *et al.* 1975) has also observed oxidized alteration halos in pebbles of an Archean fluvial conglomerate. These oxidized alteration zones, presently being studied by Rocheleau, were overprinted by a strong, reducing diagenesis and only rare relicts are now preserved.

Red-beds would generally not be expected and have not yet been found among Canadian Archean sedimentary sequences, since these are dominantly turbidites and the few fluvial deposits (Turner and Walker 1973; Dimroth *et al.* 1974, 1975; R. S. Hyde, personal communication 1974) formed on small volcanic islands. Moreover, the vast majority of Archean rocks have experienced at least greenschist-facies metamorphism, at which metamorphic grade, fine grained hematite of Middle Precambrian red-beds in the Labrador trough recrystallized with consequent loss of red-coloration.

Red-beds are by no means absent from other Middle Precambrian sequences, and Archean red-beds have been reported from the Fig Tree Group of South Africa by M. Muir (personal communication 1975). In Canada, red-beds occur in the upper part of the pre-2200 m.y.-old Huronian Supergroup in the Lorrain and Bar River Formations (Roseoe 1969; Young 1973). Middle Precambrian South African red beds have been reported from the Witwatersrand and Transvaal Supergroups (Beukes, 1973).

Origin of Iron Formation Under an Oxygen-Rich Atmosphere

This section is intended neither to be a comprehensive critique of existing genetic hypotheses nor a detailed description of an alternate genetic model. We will only note major problems with the currently popular Precambrian iron formation models, which rely on an anoxic atmosphere for ferrous iron stability, and briefly outline a possible genesis under an oxygenic atmosphere. We define iron formations to be composed of glauconite-poor chemical sedimentary rock of any age that contains over 15% Fe. Iron formations so defined are not necessarily banded.

FIG. the gre LF-3-2

FIG. 15. green (thero ferential co the Le Fer

We-fer formation First, P ferriat formation Precam

te-prehnite meta-oxides have been red into silicate metamorphic con- these observations place before the at 2600 m.y. ago. al. 1975) has also als in pebbles of te. These oxidized being studied by by a strong, re- re relicts are now

t be expected and among Canadian s, since these are e few fluvial de- 3; Dimroth *et al.* onal communica- volcanic islands. of Archean rocks greenschist-facies amorphic grade. dle Precambrian igh recrystallized oration.

bsent from other s, and Archean om the Fig Tree Muir (personal anada, red-beds ore-2200 m.y.-old Lorrain and Bar 9; Young 1973). frican red beds atwatersrand and 1973).

an Oxygen-Rich

ter to be a com- genetic hypo- of an alternate major problems recambrian iron n an anoxygenic ility, and briefly ter an oxygenic ormations to be chemical sedi- ntains over 15% are not neces-

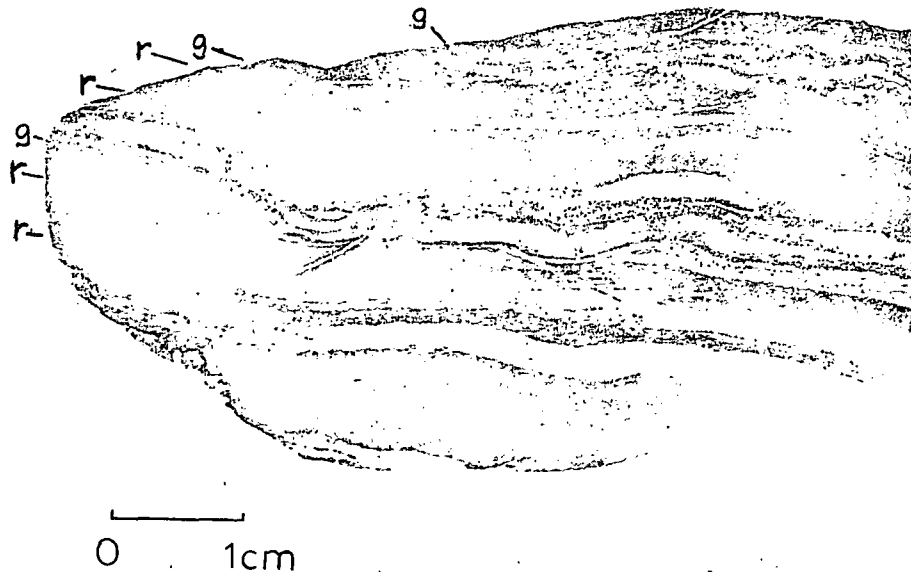


FIG. 14. Red (r) and green (g) shale, Lac le Fer Formation, Central Labrador trough. Note that the green discoloration appears, in part, to proceed from the (light gray) sandstone laminac. Section LF-3-20, Lac le Fer. Scale = 1 cm.

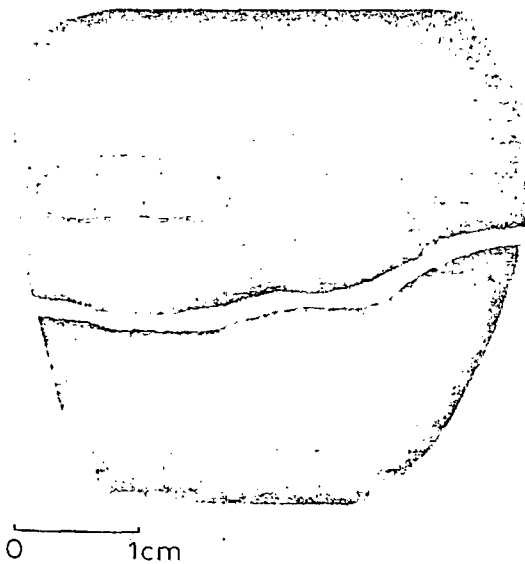


FIG. 15. Red shale, Lac le Fer Formation. Note the green (here light gray) reduced spot in upper left. Differential compaction around the reduced spot indicates an early diagenetic age of coloration. Section 9-1-7, Lac le Fer. Scale = 1 cm.

We feel that most current discussions of iron formation suffer from three major shortcomings. First, Precambrian iron formations are differentiated too sharply from Phanerozoic iron formation (James 1966, 1969), whereas most Precambrian iron formations so closely re-



FIG. 16. Oxidized shards of ultramafic hyaloclastite. Shards are stained brown by finely divided Fe^{3+} and Ti^{4+} oxides. Iron oxides coat shards and cracks. Archean ultramafic flows of Munro township, Ontario. Section Mu-5. Scale = 1 mm.



0 1mm

FIG. 17. Shards of basaltic hyaloclastite with oxidized surface crusts. Centers of shards have been replaced by dark green chlorite (gray) and the outer parts by colorless quartz and chlorite stained dark brown by finely divided Fe^{3+} and Ti^{4+} oxides. Note the Liesegang-like rings at the margins of the hyaloclastic shards. Archean basaltic flows east of Matheson, Ontario. Section ONT-2. Scale = 1 mm.

semble typical Phanerozoic iron formations (Cayeux 1911a,b) that processes of origin must have been closely related. Second, available microscopic textural evidence (e.g. Dimroth and Chauvel 1973) is insufficiently considered relative to bulk chemistry (e.g. Drever 1974). Third, it is commonly assumed *a priori* that other sedimentary rocks, particularly uranium ores, clearly indicate a contemporaneous lack of atmospheric oxygen (Cloud 1973).

Precambrian and Phanerozoic iron formations generally differ in that the former are more cherty, less aluminous, less oolitic, commonly banded, and thicker. These are, however, differences in degree rather than kind. Portions of certain Archean and Proterozoic iron formations closely resemble typical Phanerozoic iron formations. For example, the extensive Lower Proterozoic Clayband bed of the Transvaal, South Africa (Wagner 1928) is largely chamositic

oolite, much like the Upper Pliocene iron formation at Kerch, Sea of Azov, Soviet Union, which is less than 5 m.y. old (Sokolova 1964). The basal portion of Archean iron formation in the upper Back River area of the Northwest Territories of Canada (M. M. Kimberley, unpublished data 1975) is locally ferriferous and calcitic oolite, like the Jurassic Marlstone Rock Bed near Edge Hill, England (Edmonds *et al.* 1965).

Phanerozoic iron formations contain a substantial component of silica precipitated *in situ* (James 1966; Einecke 1950). However, this silica is mostly within authigenic clay minerals and relatively little occurs as chert. The dominant clay mineral is aluminum-rich iron serpentine, chamosite, whereas the dominant clay mineral in little-metamorphosed Precambrian iron formations is aluminum-poor iron serpentine, greenalite (Floran and Papike 1975).

The micros are typically sedimentary many textural oolitic, pisolitic, have been (1973) to be stones. Most to recrystallize compaction a different material generally do that were br than do oolitic limestones formations (Halley

The Upper tion must ha similar to th cipitated iron deposit (Marl very-shallow-formed in a by leaching o lying calcareo A Quaternary has recently Island, Bahar oolite has be weathered to partially ferr (Kimberley 19 been subseq remnants are in sink-holes.

The texture ruginized oolitic tions of nea formations, formations ar and submarin possibly of aragonitic sec erosion of the proposed to b tion origin (k able oxygen a the Gunflint in 1973) are con calcareous replac structures of L iron formatio parable to the

The microscopic textures of iron formations are typically among the best preserved of any sedimentary rocks of comparable ages. The many textural types of iron formation, e.g. oolitic, pisolitic, intraclastic, pelletal, and micritic, have been shown by Dimroth and Chauvel (1973) to be closely similar to those of limestones. Most of the differences can be attributed to recrystallization and to different effects of compaction and dewatering on the physically different materials. However, iron formations generally do have a higher proportion of ooids that were broken and regrew before burial than do oolitic limestones, except where the limestones formed in highly saline environments (Halley 1974).

The Upper Pliocene Kerch-Azov iron formation must have formed under an atmosphere similar to that at present. The mass of precipitated iron and aluminum in this extensive deposit (Markevich 1960) is too great for this very-shallow-water sedimentary rock to have formed in a reasonable length of time except by leaching of soils and replacement of underlying calcareous sediment (Kimberley 1974*a,b*). A Quaternary analogue of this general process has recently been found on northern Andros Island, Bahamas, where aragonitic Pleistocene oolite has been covered by volcanic ash, which, weathered to a soil and soil leachate, has partially ferruginized the underlying oolite (Kimberley 1975*a,b*). Nearly all of this soil has been subsequently eroded off Andros and remnants are only found in depressions, mostly in sink-holes.

The textural similarities among Andros ferruginized oolite, Cenozoic iron formations, portions of nearly all Lower Proterozoic iron formations, and even some Archean iron formations are sufficiently great that subaerial and submarine weathering of volcanic ash, and possibly of some terrigenous mud, above aragonitic sediment, leaching, and subsequent erosion of the leached ash and mud, have been proposed to be the key processes of iron formation origin (Kimberley 1975*b*). Presently available oxygen and hydrogen isotopic analyses of the Gunflint iron formation of Ontario (Knauth 1973) are consistent with a soil leachate-calcareous replacement origin. Some of the internal structures of Lower Proterozoic Labrador trough iron formation (Figs. 18, 19, 20, 21) are comparable to those of silicified limestones.

Composition, thickness, and banding differences between typical Precambrian and Phanerozoic iron formations have been attributed by Kimberley (1975*b*) to biochemically different leaching processes, differences in tectonic setting and carbonate sedimentation, and lack of metazoan burrowing, respectively. The dominant sedimentary environment of iron formations has also changed with time, the change having occurred at the end of the Archean when continental platform sedimentation generally superseded volcanic pile sedimentation (Bridgwater and Fyfe 1974). A large proportion of Archean iron formations occur as beds a few centimetres thick near or at the tops of Bouma sequences. Submarine ferriferous mud leaching and replacement of thin beds of closely underlying aragonite mud is a possible mode of origin for this type of iron formation (Kimberley and Dimroth 1976). Aragonite mud could have been eroded from shallow-marine areas along with accompanying non-chemical sediment or, possibly, could have continually settled from the photic zone of the ocean.

The similarity in mode of iron formation origin through earth history suggested by the carbonate-replacement model would not be expected if there had been major changes in atmospheric oxygen content. Under an anoxygenic atmosphere, all algal communities producing free oxygen locally (Fischer 1965) should have caused local oxidation and precipitation of iron. However, most Archean and Middle Precambrian algal stromatolites are iron-poor limestones and dolostones (Henderson 1975; Hoffman 1973; Hofmann 1974). The suggestion by Cloud (1973), that the thick Middle Precambrian iron formations predate red-bed sedimentation and mark the initiation of an oxygenic atmosphere, is demonstrably incorrect for the Early Proterozoic iron formations of the Labrador trough (Dimroth 1971) and Belcher Islands, Northwest Territories (Bell and Jackson 1974; Dimroth *et al.* 1970), which are stratigraphically well above red-beds; and, of course, for the cherty iron formations of Late Precambrian and Phanerozoic age.

Conclusions

The distributions of carbon, sulfur, uranium, and iron in Precambrian sedimentary rocks are similar to those in Phanerozoic sedimentary rocks. Enrichment of organic carbon in fine

have been
ite stained
margins of
2. Scale =

ne iron forma-
Soviet Union,
okolova 1964).
iron formation
the Northwest
4. Kimberley,
ferriferous and
Earlstone Rock
Edmonds *et al.*

contain a sub-
ipitated *in situ*
However, this
clay minerals

The dominant
on serpentine,
clay mineral in
n iron forma-
serpentine, green-

grained sedimentary rocks, irrespective of the source and the sedimentary environment, suggests that planktonic matter has always been a major sediment contributor. Average organic carbon contents of mudrocks and carbon isotopic ratios have remained remarkably constant through geologic time. Organic matter of fresh oolite and of organogenic sediments has largely been destroyed during diagenesis, and algal mats have rarely been preserved except where silicified shortly after death. These observations indicate considerable continuity in organic productivity and free oxygen production, and the existence of a large reservoir of molecular oxygen in the atmosphere.

Most Precambrian sulfide sulfur in sedimentary rocks occurs as pyrite within carbonaceous mudrocks, just as does most Phanerozoic sulfide sulfur, and seems to have been similarly produced by early diagenetic sulfate reduction. The distribution of volcanogenic sulfide deposits is restricted to specific volcanologic environments and to a few stratigraphic levels much like Phanerozoic volcanogenic sulfide deposits. There is evidence, mostly from crystal casts, for widespread evaporative sulfate sedimentation having occurred in Middle Precambrian platform sequences. The lack of reported Archean sulfates is attributed to the general lack of Archean continental platform sedimentation.

Many Middle Precambrian and some Archean rock sequences contain evidence for diagenetic oxidation. Continental and shallow-marine red beds are known from a number of Proterozoic sequences and at least one suite of shallow-marine red beds has been reported from the

Archean. However, the tectonic environment of Archean sedimentation was not favorable for red-bed formation, and the generally higher grade of metamorphism of Archean rocks has been unfavorable for preservation of red coloration. Evidence for oxidation of volcanic glass shards during sea floor alteration is common in Archean hyaloclastites, where their metamorphic grade has been low enough to permit preservation of the delicate iron oxide stains.

Precambrian and Phanerozoic iron formations are generally similar texturally and lithostratigraphically. Chronological differences in degree of development of certain features are more readily attributable to chronological changes in tectonic setting and organic activity than to compositional changes in the atmosphere or hydrosphere. Iron formations are interpreted on the basis of textures and stratigraphic relationships to be early diagenetic replacements of dominantly aragonitic sediment, much like the local replacement of Quaternary Bahaman aragonite. Stratiform concentrations of uranium within Precambrian sedimentary rocks are similarly attributed to diagenetic processes comparable to Phanerozoic ore-forming processes.

We conclude that uniformitarian models of chemical sedimentation may be applied to the Precambrian, and that there is no evidence of orders-of-magnitude changes in average atmospheric or hydrospheric abundances of chemically reactive inorganic species. However, the proportions of distinct sedimentary environments and the forms and compositions of life have profoundly changed. Archean topography was dominantly controlled by volcanism, where-

FIG. 18. Solution porosity in cherty carbonate iron formation. Note vugs filled with rim-cement of chalcedony and columnar quartz. The thin section reveals about 15% solution porosity. Such solution porosity is characteristic of many carbonate rocks, but would not be expected in primary cherts. Sokoman Formation, de la Concession Lake area, Central Labrador trough. Section C2-11. Scale = 1 mm.

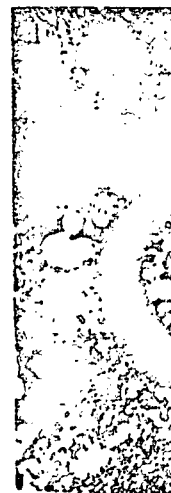
FIG. 19. Half-moon ooid as defined by Carozzi (1960). Sokoman Formation, W of Lac le Fer, Central Labrador trough. Scale = 1 mm.

FIG. 20. Same as Fig. 19, under crossed nicols. Rim cement of quartz with columnar texture filling the intergranular porosity and half-moon-shaped space between core and rim of an ooid. Interpretation of the texture is ambiguous. Either there was shrinkage of the core of the ooid and filling of the resulting pore space by quartz or dissolution of a layer in the ooid and subsequent infilling of the solution porosity. Half-moon ooids are common in limestone-replacement cherts. Scale = 1 mm.

FIG. 21. Interior of a hematitic iron formation ooid either replaced by coarse grained quartz or dissolved and infilled by coarse grained quartz. Filling by quartz of moldic porosity is common in oolitic limestone-replacement cherts. Sokoman Formation, NW of Attikamagen Lake, Central Labrador trough. Section 13-3-9. Scale = 1 mm.



0



0

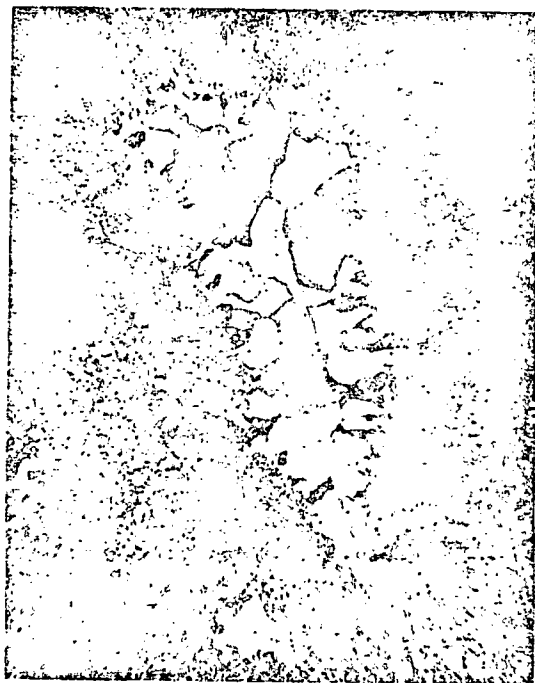
environment of
 favorable for
 generally higher
 mean rocks has
 n of red colora-
 volcanic glass
 is common in
 ir metamorphic
 permit preserva-
 tions.
 iron formations
 ly and litho-
 differences in
 in features are
 chronological
 organic activity
 the atmosphere
 ons are inter-
 and stratigraphic
 ic replacements
 ent, much like
 nary Bahaman
 ons of uranium
 ry rocks are
 processes com-
 ing processes.
 rian models of
 applied to the
 no evidence of
 average atmo-
 spheric chemi-
 stry. However, the
 primary environ-
 ments of life
 can topography
 tectonism, where-

rim-cement
 osity. Such
 in primary
 ion C2-11.

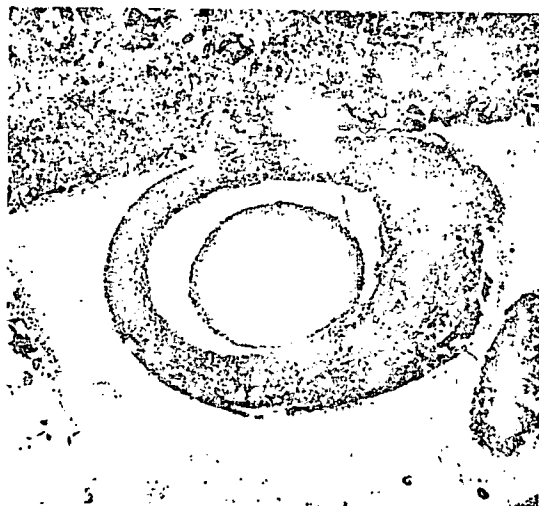
Lac le Fer,

var texture
 f an ooid.
 s ooid and
 subsequent
 ent cherts.

quartz or
 common in
 e, Central



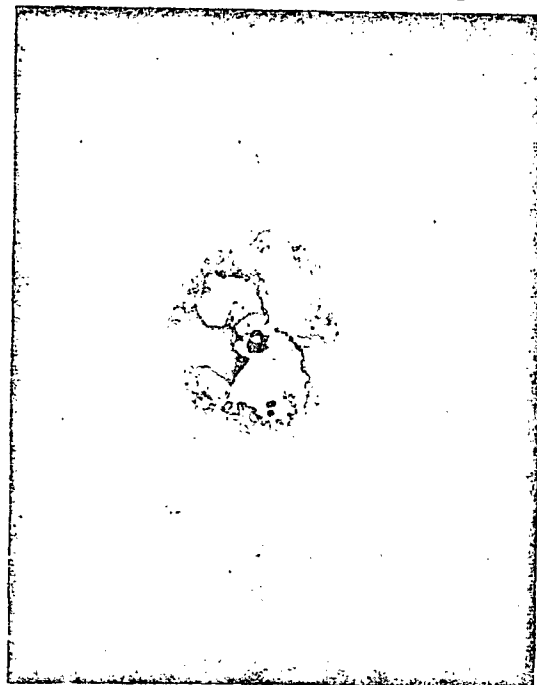
0 1mm Fig. 18



0 1mm Fig. 19



0 1mm Fig. 20



0 1mm Fig. 21

as Middle Precambrian continental shelf sequences are among the most extensive and thickest preserved. The lack of metazoan burrowing through most of the Precambrian permitted better preservation of carbonaceous laminae.

Acknowledgments

Field work that served, in part, as the basis for this paper was performed by E. Dimroth for the Quebec Department of Natural Resources and by M. M. Kimberley in the Northwest Territories of Canada. This work was supported by National Research Council of Canada operating grants A-9145 and A-9019, to E. Dimroth and M. M. Kimberley, and by Geological Survey of Canada research contract 1135-D13-4-71/75 to E. Dimroth. We are grateful to Miss R. C. Bald for the preparation of the drawing and photomicrographs.

- BECKER, R. H. and CLAYTON, R. N. 1972. Carbon isotopic evidence for the origin of a banded iron-formation in Western Australia. *Geochim. Cosmochim. Acta*, 36, pp. 577-595.
- BELL, R. T. and JACKSON, G. D. 1974. Apehbian halite and sulphate indications in the Belcher Group, Northwest Territories. *Can. J. Earth Sci.* 11, pp. 722-728.
- BERKNER, L. V. and MARSHALL, L. C. 1965. On the origin and rise of oxygen concentration in the earth's atmosphere. *J. Atmos. Sci.* 22, pp. 225-261.
- BERNER, R. A. 1970. Sedimentary pyrite formation. *Am. J. Sci.* 268, pp. 1-23.
- 1971. *Chemical sedimentology*. McGraw-Hill Book Co., New York, NY, 240 p.
- BEUKES, N. J. 1973. Precambrian iron-formations of Southern Africa. *Econ. Geol.* 68, pp. 960-1004.
- BRIDGWATER, D., ESCHER, A., JACKSON, G. D., TAYLOR, F. C., and WINDLEY, B. F. 1973. Development of the Precambrian Shield in West Greenland, Labrador and Baffin Island. *In: Geology of the Arctic*. Am. Assoc. Pet. Geol. Mem. 19, pp. 99-116.
- BRIDGWATER, D. and FYFE, W. S. 1974. The pre-3 b.y. crust: fact-fiction-fantasy. *Geosci. Can.* 1(3), pp. 7-11.
- BRINKMANN, R. T. 1969. Dissociation of water vapor and evolution of oxygen in the terrestrial atmosphere. *J. Geophys. Res.* 74(23), pp. 5355-5368.
- BROECKER, W. S. 1970. A boundary condition on the evolution of atmospheric oxygen. *J. Geophys. Res.* 75, pp. 3553-3557.
- CAMERON, E. M. and JONASSON, I. R. 1972. Mercury in Precambrian shales of the Canadian Shield. *Geochim. Cosmochim. Acta*, 36, pp. 985-1005.
- CAROZZI, A. V. 1960. *Microscopic sedimentary petrography*. John Wiley and Sons, Inc., New York, NY, 485 p.
- CAYEUX, L. 1911a. Existence de restes organiques dans les roches ferrugineuses associées aux minerais de fer huroniens des Etats-Unis. *Acad. Sci., Paris, C. R.* 153, pp. 910-912.
- 1911b. Comparaison entre les minerais de fer huroniens des Etats-Unis et les minerais de fer oolithique de France. *Acad. Sci., Paris, C. R.* 153, pp. 1188-1190.
- CHAUVEL, J.-J. and DIMROTH, A. 1974. Facies types and depositional environment of the Sokoman Iron Formation in the central Labrador trough, Quebec, Canada. *J. Sed. Petrol.* 44, pp. 299-327.
- CLOUD, P. E. 1973. Paleogeological significance of the banded iron-formations. *Econ. Geol.* 68, pp. 1135-1143.
- DAVIDSON, C. F. 1964. Uniformitarianism and ore genesis. *Min. Mag., London*, 110, pp. 176-185 and 244-253.
- DEGENS, E. T. 1965. *Geochemistry of sediments, a brief survey*. Prentice-Hall Inc., Englewood Cliffs, NJ, 342 p.
- DERRY, D. R. 1960. Evidence of the origin of the Blind River uranium deposits. *Econ. Geol.* 55, pp. 906-927.
- DIMROTH, E. 1968. The evolution of the central segment of the Labrador geosyncline. Part I: Stratigraphy, facies, and paleogeography. *Neues Jahrb. Geol. Palaeontol. Abh.* 132, pp. 22-54.
- 1973. Geology of the central Labrador trough between lat. 56°30' and the height-of-land. Quebec Dep. Nat. Res., Open File Rep. GM 28619, 300 p.
- DIMROTH, E., BARAGAR, W. R. A., BERGERON, R., and JACKSON, G. D. 1970. The filling of the Circum-Ungava Geosyncline. *In: Symposium on basins and geosynclines of the Canadian Shield*. (A. J. Baer, Ed.) *Geol. Surv. Can. Pap.* 70-40, pp. 45-142.
- DIMROTH, E. and CHAUVEL, J.-J. 1973. Petrography of the Sokoman Iron Formation in part of the central Labrador Trough, Quebec, Canada. *Geol. Soc. Am. Bull.* 84, pp. 111-134.
- DIMROTH, E., CÔTÉ, R., PROVOST, G., ROCHELEAU, M., TASSÉ, N., and TRUDEL, P. 1975. Third progress report on the stratigraphy, volcanology, sedimentology and tectonics of Rouyn-Noranda area. Quebec Dep. Nat. Res. Open File Rep. D.P. 300, 50 p.
- DIMROTH, E., ROCHELEAU, M., BOIVIN, P., LAROCHE, M., and CÔTÉ, R. 1974. Preliminary report on stratigraphic and tectonic work in Rouyn-Noranda area. Quebec Dep. Nat. Resour., Open File Rep. D.P. 240, 40 p.
- DREVER, J. I. 1974. Geochemical model for the origin of Precambrian banded iron formations. *Geol. Soc. Am. Bull.* 85, pp. 1099-1106.
- DUGAS, J. 1967. *Metallic mineralization, regions of Noranda, Mattagami, Val d'Or, Chibougamau*. Quebec Dep. Nat. Res. E. S. No. 2.
- DUTOIT, A. L. 1973. *Geology of South Africa*, 3rd ed. (S. H. Haughton, Ed.) Hafner Publishing Company, Inc., New York, NY, 611 p.
- EASDON, M. M. 1969. A compilation of graphitic occurrences in the Archean of part of northwestern Quebec. Unpubl. MSc Diss., McGill Univ., Montreal, P.Q., 119 p.
- EATON, J. P. and MURATA, K. J. 1960. How volcanoes grow. *Science*, 132, pp. 925-938.
- EDMONDS, E. A., POOLE, E. G., and WILSON, V. 1965. Geology of the country around Banbury and Edge Hill. *Mem. Geol. Surv. G. B.* 137 p.
- EINECKE, G. 1950. *Die Eisenerzvorräte der Welt und der Anteil der Verbraucher- und Lieferländer an deren Verwertung: Text und Atlas*. Verlag Stahl Eisen M. B. H. Düsseldorf, W. Ger., 418 p.
- EMERY, K. O. 1960. Basin plains and aprons off southern California. *J. Geol.* 68, pp. 464-479.
- EMERY, K. O. and UCHUPI, E. 1972. Western North Atlantic ocean: top sediment. *Am. J. Sci.* 270, pp. 1188-1190.
- FINCH, W. I. 1966. in sandstone in Pap. 538, 121 p.
- FISCHER, A. G. 1966. *Geological history*. Proc. 1st Int. Geol. Cong., Prague, 1964, 10, pp. 1-10.
- FLORAN, R. J. 1966. *Low-grade rocks of the Ontario-Minnesota border*. Geol. Surv. Can. Pap. 70-40, 1190.
- FRYER, B. J. 1966. *Ungava geosyncline*. Geol. Surv. Can. Pap. 70-40, 1190.
- GALKIN, N. P. 1963. *The tectonic evolution of the Canadian Shield*. (R. V. Macmillan, New York, 1963), 1190.
- GARRELS, R. M. 1966. *Aluminum and equilibrium*. Geol. Surv. Can. Pap. 70-40, 450 p.
- GARRELS, R. M. 1966. *Sedimentary rocks*. McGraw-Hill, New York, 1190.
- GARRELS, R. M. 1973. *Genesis and development of the Canadian Shield*. Geol. Surv. Can. Pap. 70-40, 1173-1179.
- GEHMAN, H. M. 1972. *Geochim. Cosmochim. Acta*, 36, pp. 577-595.
- GIBBS, R. J. 1972. *Geochim. Cosmochim. Acta*, 36, pp. 577-595.
- GLENNIE, K. W. 1972. *Elsevier, Amsterdam*.
- GOODWIN, A. M. 1973. *Iron formation in Ontario, Canada*. Geol. Surv. Can. Pap. 70-40, 1190.
- 1973. *Archean of the Canadian Shield*. Geol. Surv. Can. Pap. 70-40, 1190.
- GOODWIN, A. M. 1973. *Carbon and sulfur formations and press*. Geol. Surv. Can. Pap. 70-40, 1190.
- GOODY, R. M. 1973. *Prentice-Hall Inc., New York, NY*.
- HALLBAUER, D. K. 1973. *Silicified plants in the Witwatersrand*. Geol. Surv. Can. Pap. 70-40, 1190.
- HALLEY, R. B. 1973. *Unusual salinity*. Geol. Surv. Can. Pap. 70-40, 1190.
- HARSHMAN, E. N. 1973. *Shirley Basin*. Geol. Surv. Can. Pap. 70-40, 1190.
- HENDERSON, J. B. 1973. *Northern Slave*. Geol. Surv. Can. Pap. 70-40, 1190.
- HOLMES, P. 1968. *Geology of the Slave Lake District*. Geol. Surv. Can. Pap. 70-40, 1190.
- 1973. *Evolution of the margin: the Corraleros of the Trans. R. Soc. Lond.*

- minerais de fer hurois de fer oolithique de 1973, pp. 1188-1190.
1974. Facies types and Proterozoic Iron Formations, Quebec, Canada. J. Geol., pp. 185 and 244-253.
- Significance of the Blind River Group. *Can. J. Earth Sci.* 68, pp. 1135-1143. Volcanism and ore genesis. *Can. J. Earth Sci.* 185 and 244-253.
- Of sediments, a brief report. *Geol. Soc. Am. Bull.* 68, pp. 906-927.
- The central segment of the Blind River Group. *Stratigraphy, facies, and geology. Palaeontol.*
- Central Labrador trough. *Quebec Dep. Nat. Res. Rep.* 19, 300 p.
- B. BERGERON, R., and others. *Basins and geosynclines of the central Labrador trough. Geol. Soc. Am. Bull.* 84, pp. 1173-1179.
- G. ROCHÉLEAU, M. Third progress report on the geology, sedimentology and stratigraphy. *Quebec Dep. Nat. Res. Rep.* 19, 300 p.
- IVIN, P., LAROCHE, M. and others. *Geological report on the stratigraphy of the Yukon-Noranda area. File Rep. D.P.* 240.
- Model for the origin of iron formations. *Geol. Soc. Am. Bull.* 73, pp. 561-586.
- Classification, regions of iron formation. *Chibougamau, Quebec, Canada. 3rd ed. (S. J. Richardson, Ed.)* Geol. Soc. Am. Bull. 73, pp. 561-586.
- Origin of graphitic iron formations in the northwestern Quebec. *Geol. Soc. Am. Bull.* 73, pp. 561-586.
1960. How volcanoes affect iron formations. *Geol. Soc. Am. Bull.* 73, pp. 561-586.
- and WILSON, V. 1965. Iron formation and Edge Hill. *Geol. Soc. Am. Bull.* 73, pp. 561-586.
- Rate der Welt und der Erde. *Geol. Soc. Am. Bull.* 73, pp. 561-586.
- d aprons off southern Labrador. *Geol. Soc. Am. Bull.* 73, pp. 561-586.
- Western North Atlantic ocean: topography, rocks, structure, water, life and sediment. *Am. Assoc. Pet. Geol. Mem.* 17, 532 p.
- FINCH, W. I. 1967. Geology of epigenetic uranium deposits in sandstone in the United States. *US Geol. Surv., Prof. Pap.* 538, 121 p.
- FISCHER, A. G. 1965. Fossils, early life, and atmospheric history. *Proc. US Nat. Acad. Sci.* 53 (6), pp. 1205-1215.
- FLORAN, R. J. and PAPIKE, J. J. 1975. Petrology of the low-grade rocks of the Gunflint Iron-formation, Ontario—Minnesota. *Geol. Soc. Am. Bull.* 86, pp. 1169-1190.
- FRYER, B. J. 1972. Age determinations in the Circum-Ungava geosyncline and the evolution of Precambrian iron formations. *Can. J. Earth Sci.* 9, pp. 652-663.
- GALKIN, N. P., MAIOSOV, A. A., and VERYATIN, U. D. 1963. The technology of the treatment of uranium concentrates. (R. W. Clarke and A. E. R. E. Harwell, Eds.) Macmillan, New York, NY, 204 p.
- GARRELS, R. M. and CHRIST, C. L. 1965. Solutions, minerals, and equilibria. Harper and Row, New York, NY, 450 p.
- GARRELS, R. M. and MACKENZIE, F. T. 1971. Evolution of sedimentary rocks. Norton, New York, NY, 397 p.
- GARRELS, R. M., PERRY, E. A., JR., and MACKENZIE, F. T. 1973. Genesis of Precambrian iron-formation and the development of atmospheric oxygen. *Econ. Geol.* 68, pp. 1173-1179.
- GEHMAN, H. M., JR. 1962. Organic matter in limestones. *Geochim. Cosmochim. Acta.* 26, pp. 867-884.
- GIBBS, R. J. 1972. Water chemistry of the Amazon river. *Geochim. Cosmochim. Acta.* 36 (9), pp. 1061-1066.
- GLENNIE, K. W. 1970. Desert sedimentary environments. Elsevier, Amsterdam, Neth., 222 p.
- GOODWIN, A. M. 1962. Structure, stratigraphy and origin of iron formations, Michipicoten area, Algoma District, Ontario, Canada. *Geol. Soc. Am. Bull.* 73, pp. 561-586.
- 1973. Archean iron-formation and tectonic basins of the Canadian Shield. *Econ. Geol.* 68, pp. 915-933.
- GOODWIN, A. M., MONSTER, J., and THODE, J. G. 1976. Carbon and sulfur isotope abundance in Archean iron-formation and Early Precambrian life. *Econ. Geol.* (in press).
- GOODY, R. M. and WALKER, J. C. 1972. Atmospheres. Prentice-Hall Inc., Englewood Cliffs, NJ, 150 p.
- HALLBAUER, D. K. and VAN WARMELO, K. T. 1974. Fossilized plants in thucholite from Precambrian rocks of the Witwatersrand, South Africa. *Precambrian Res.* 1, pp. 199-212.
- HALLEY, R. B. 1974. Broken ooids, radial ooid fabric, and unusual salinity. *Geol. Soc. Am., Abstracts with Programs.* 6 (7), p. 773.
- HARSHMAN, E. N. 1972. Geology and uranium deposits, Shirley Basin area, Wyoming. *US Geol. Surv., Prof. Pap.* 745, 82 p.
- HENDERSON, J. B. 1975. Archean stromatolites in the northern Slave Province, Northwest Territories, Canada. *Can. J. Earth Sci.* 12, pp. 1619-1630.
- HOFFMAN, P. 1968. Stratigraphy of the Lower Proterozoic (Aphelbian), Great Slave Supergroup, East Arm of Great Slave Lake, District of Mackenzie. *Geol. Surv. Can. Pap.* 68-42, 93 p.
- 1973. Evolution of an early Proterozoic continental margin: the Coronation geosyncline and associated calcareous rocks of the northwestern Canadian Shield. *Phil. Trans. R. Soc. Lond. A.* 273, pp. 547-581.
- HOFMANN, H. J. 1973. Stromatolites: characteristics and utility. *Earth Sci. Rev.* 9 (4), pp. 339-373.
- 1974. Mid-Precambrian prokaryotes (?) from the Belcher Islands, Canada. *Nature*, 249 (5452), pp. 87-88.
- HOLLAND, H. D. 1962. Model for the evolution of the earth's atmosphere. *In: Petrologic studies.* Geol. Soc. Am., New York, NY, pp. 447-477.
- 1973a. Ocean water, nutrients and atmospheric oxygen. *In: Proc. Symp. Hydrogeochem. and Biochem.* Vol. 1. The Clarke Company, Washington, DC, pp. 68-81.
- 1973b. Systematics of the isotopic composition of sulfur in the oceans during the Phanerozoic and its implications for atmospheric oxygen. *Geochim. Cosmochim. Acta.* 37, pp. 2605-2616.
- 1973c. The oceans: a possible source of iron in iron-formation. *Econ. Geol.* 68, pp. 1169-1172.
- 1976. The evolution of seawater. *In: The early evolution of the earth.* (B. F. Windley, Ed.) Proc. NATO Adv. Study Inst. (in press).
- (in preparation). The chemistry and chemical evolution of the atmosphere and oceans. Springer-Verlag.
- HORIKOSHI, E. and SATO, T. 1970. Volcanic activity and ore deposition in the Kosaka Mine. *In: Volcanism and ore genesis.* (T. Tatsumi, Ed.) Univ. Tokyo Press, Tokyo, Jpn., pp. 181-195.
- HUBERT, C. 1973. Kamouraska area. *Quebec Dep. Nat. Res. Geol. Rep.* 151.
- IPPOLITO, F. 1958. The uranium-bearing formations of the sediments of the Late Alpine Paleozoic. *Proc. 2nd UN Int. Conf. Peaceful Uses of Atomic Energy, Vol. 2.* Survey of Raw Material Resources, Geneva, Switz., pp. 612-621.
- JAMES, H. L. 1966. Chemistry of the iron-rich sedimentary rocks. Chapter W. *In: Data of geochemistry.* 6th ed. (M. Fleischer, Ed.) US Geol. Surv., Prof. Pap. 440-W, 61 p.
- 1969. Comparison between Red Sea deposits and older ironstone and iron formation. pp. 525-532. *In: Hot brines and recent heavy metal deposits in the Red Sea.* (E. T. Degens and D. A. Ross, Eds.) Springer-Verlag, Berlin, 600 p.
- KIMBERLEY, M. M. 1974a. Origin of iron ore by diagenetic replacement of calcareous oolite. Unpubl. PhD Diss., Princeton Univ., Princeton, NJ. Vol. 1, 345 p.; Vol. 2, 386 p.
- 1974b. Origin of iron ore by diagenetic replacement of calcareous oolite. *Nature.* 250, pp. 319-320.
- 1975a. Alteration and replacement of Pleistocene oolite by soil leachate on Northwestern Andros Island, Bahamas: a modern analogue of ironstone origin. *Geol. Soc. Am., Abstracts with Programs.* 7 (6), pp. 796-797.
- 1975b. Proposal of iron formation origin by cycles of aragonite sedimentation, cover by volcanic ash or terrigenous mud, weathering, organic acid leaching of mud, acid-base aragonite replacement, and mud erosion: a Quaternary analogue. *Geol. Soc. Am., Abstracts with Programs.* 7 (7), pp. 1146-1147.
- KIMBERLEY, M. M. and DIMROTH, E. 1976. Basic similarity of Archean to subsequent atmospheric and hydro-spheric compositions as evidenced in the distributions of sedimentary carbon, sulphur, uranium and iron. *In: The early evolution of the earth.* (B. F. Windley, Ed.) Proc. NATO Adv. Study Inst. (in press).
- KNAUTH, P. 1973. Oxygen and hydrogen isotope ratios in

- cherts and related rocks. Unpubl. PhD Diss., Calif. Inst. Technol., Pasadena, Calif. 369 p.
- KOEN, G. M. 1958. The attrition of uraninite. *Geol. Soc. S. Afr. Trans.* 61, pp. 183-196.
- KUENEN, P. H. 1950. *Marine geology*. John Wiley and Sons Inc., New York, NY.
- LAJOIE, J., HÉROUX, Y., and MATHEY, B. 1974. The Precambrian Shield and the Lower Paleozoic shelf: the unstable provenance of the Lower Paleozoic flysch sandstones and conglomerates of the Appalachians between Beaumont and Bic, Quebec. *Can. J. Earth Sci.* 11 (7), pp. 951-963.
- LASAGA, A. C., HOLLAND, H. D., and DWYER, M. J. 1971. Primordial oil slick. *Science*, 174, pp. 53-55.
- LEPP, H. and GOLDICH, S. S. 1964. Origin of Precambrian iron formations. *Econ. Geol.* 59 (6), pp. 1025-1060.
- MARKEVICH, V. P. 1960. The concept of facies, part I. *Int. Geol. Rev.* 2, pp. 367-379.
- MATSUKUMA, T. and HORIKOSHI, E. 1970. Kuroko deposits in Japan, a review. *In: Volcanism and ore genesis*. (T. Tatsumi, Ed.) Univ. Tokyo Press, Tokyo, Jpn., pp. 153-179.
- MILLIMAN, J. D. 1974. Recent sedimentary carbonates Vol. 1. Marine carbonates. Springer-Verlag, New York, NY.
- MOORBATH, S., O'NIONS, R. K., and PANKHURST, R. J. 1973. An early Archean age for the Isua iron-formation. *Nat. Phys. Sci.* 245, pp. 138-139.
- MÜLLER, M. J. and NEGENDANK, J. F. W. 1974. Untersuchungen von Schwermineralien in Moselsedimenten. *Geol. Rundsch.* 63, pp. 998-1034.
- NAGY, L. A. 1975. Comparative micropaleontology of a Transvaal stromatolite (~2.3 × 10⁹ Y. old) and a Witwatersrand carbon seam (~2.6 × 10⁹ Y. old) (abstr.). *Geol. Soc. Am., Abstracts with Programs*, 7 (7), pp. 1209-1210.
- OEHLER, D. Z., SCHOPF, J. W., and KVENVOLDEN, K. A. 1972. Carbon isotopic studies of organic matter in Precambrian rocks. *Science*, 175 (4027), pp. 1246-1248.
- PETERSEN, R. G. 1960. Detrital-appearing uraninite grains in the Shinarump member of the Chinle formation in northern Arizona. *Econ. Geol.* 55 (1), pp. 138-149.
- PETTJOHN, F. J. 1943. Archean sedimentation. *Geol. Soc. Am. Bull.* 54, pp. 925-972.
- PRASHNOWSKY, A. A. and SCHIDLowski, M. 1967. Investigation of Precambrian thucholite. *Nature* 216 (5115), pp. 560-563.
- PRETORIUS, D. A. 1974. The nature of the Witwatersrand gold-uranium deposits. *Univ. Witwatersrand, Econ. Geol. Res. Unit, Inform. Circ.* 86, 50 p.
- RACKLEY, R. I. 1972. Environment of Wyoming Tertiary uranium deposits. *Am. Assoc. Pet. Geol.* 56 (4), pp. 755-774.
- RAMDOHR, P. 1958. New observations on the ores of the Witwatersrand in South Africa and their genetic significance. *Geol. Soc. S. Afr. Trans., Annexure to vol.* 61, 50 p.
- 1960. *Die Erzminerale und ihre Verwachsungen*. Akademie-Verlag, Berlin, 1089 p.
- RAO, M. S. 1960. Organic matter in marine sediments off the east coast of India. *Am. Assoc. Pet. Geol. Bull.* 44, pp. 1705-1713.
- RICHARDS, F. A. and REDFIELD, A. C. 1954. A correlation between the oxygen content of sea water and the organic content of marine sediments. *Deep-sea Res.* 1, pp. 279-281.
- ROBERTSON, J. A. 1973. A review of recently acquired geological data, Blind River-Elliott Lake area. *In: Geol. Assoc. Can., Spec. Pap.* 12. (G. M. Young, Ed.), pp. 169-198.
- RONOV, A. B., GIRIN, Y. P., KAZAKOV, G. A., and ILYUKHIN, M. N. 1965. Comparative geochemistry of geosynclinal and platform sedimentary rocks. *Geochem. Int.* 2, pp. 692-708.
- RONOV, A. R. and MIGDISOV, A. A. 1971. Geochemical history of the crystalline basement and the sedimentary cover of the Russian and North American Platforms. *Sedimentology*, 16, pp. 137-185.
- ROSCOE, S. M. 1969. *Huronian rocks and uraniferous conglomerates in the Canadian Shield*. *Geol. Surv. Can. Pap.* 68-40, 205 p.
- RUBEY, W. W. 1951. Geologic history of sea water. An attempt to state the problem. *Geol. Soc. Am. Bull.* 62, pp. 1111-1148.
- 1955. Development of the hydrosphere and atmosphere, with special reference to probable composition of the early atmosphere, pp. 631-650 *In: Crust of the earth*. (A. Poldervaart, Ed.) *Geol. Soc. Am. Spec. Pap.* 62, 762 p.
- SANGSTER, D. F. 1972. Precambrian volcanogenic massive sulphide deposits in Canada: a review. *Geol. Surv. Can. Pap.* 72-22.
- SATO, T. 1971. Physicochemical environments of Kuroko mineralization at Uchinotai deposit of Kolaka Mine, Akita Prefecture. *Soc. Min. Geol. Jpn., Spec. Issue* 2, pp. 137-144.
- 1972. Model for ore-forming solutions and ore-forming environments: Kuroko vs. veins in Miocene "Green Tuff" region of Japan. *Geol. Surv. Jpn. Bull.* 23, pp. 457-466.
- SCHIDLowski, M. 1968. Sulfur isotope abundances in pyrite from the Witwatersrand conglomerates. *Econ. Geol.* 63 (8), pp. 975-977.
- SCHIDLowski, M., EICHMANN, A., and JUNGE, C. E. 1975. Precambrian sedimentary carbonates: Carbon and oxygen isotope geochemistry and implications for the terrestrial oxygen budget. *Precambrian Res.* 2, pp. 1-69.
- SCHULZ, O. and LUKAS, W. 1970. Eine Uranerzlagerstätte in permotriadischen Sedimenten Tirols. *Tschermaks Mineral. Petrogr. Mitt.* 10, pp. 213-231.
- SIMMONS, B. D. and MILLENBACH STAFF. 1973. *Geology of the Millenbach massive sulphide deposit, Noranda, Quebec*. *Can. Inst. Min. Metall. Bull.* 66 (739), pp. 67-78.
- SOKOLOVA, E. I. 1964. Physicochemical investigations of sedimentary iron and manganese ores and associated rocks. *Isr. Prog. Sci. Transl., Jerusalem, Isr.*, 220 p.
- SPENCE, C. D. and DE ROSEN-SPENCE, A. F. 1975. The place of sulfide mineralization in the volcanic sequence at Noranda, Quebec. *Econ. Geol.* 70, pp. 90-102.
- STRAUSS, G. K. and MADEJ, J. 1964. *Geology of massive sulphide deposits in the Spanish-Portuguese pyrite belt*. *Geol. Rundsch.* 63, pp. 191-211.
- STUMM, W. and MORGAN, J. J. 1970. *Aquatic chemistry*. Wiley-Interscience, New York, NY, 583 p.
- SWANSON, V. E. 1960. Oil yield and uranium content of black shales: uranium in carbonaceous rocks. *US Geol. Surv. Prof. Pap.* 356-A, 44 p.
- 1961. *Geology and geochemistry of uranium in marine black shales, a review: uranium in carbonaceous rocks*. *US Geol. Surv. Prof. Pap.* 356-C, pp. 67-112.

TRASK, P. D. and
petroleum. *Am.*
TUREKIAN, K.
glewood Cliff.
TURNER, G. C.
stratigraphy a
stone belt near
Sci. 10, pp. 81
VAN ANDEL, T.
Gulf of Calif.
California (T.
Assoc. Pet. G.
VAN HOUTEN, F.
alluvium, non
origin of red
2761-2772.
VAN VALEN, L.
spheric oxyge

- of recently acquired lake area. *In: Geol. J. Young. Ed.*, pp.
- YAKOV, G. A., and five geochemistry of igneous rocks. *Geochem. Int.* 1971. Geochemical and the sedimentary basins of the American Platforms.
- YOUNG, G. M. and uraniumiferous conglomerates. *Geol. Surv. Can. Bull.* 62.
- YOUNG, G. M. and geochemistry of sea water. *Am. Soc. Am. Bull.* 62.
- YOUNG, G. M. and atmosphere and atmospheric composition of the crust of the earth. *Am. Spec. Pap.* 62.
- YOUNG, G. M. and diagenetic massive iron ores. *Geol. Surv. Can. Bull.* 62.
- YOUNG, G. M. and comments of Kuroko type of Kolaka Mine. *Jpn. Spec. Issue* 2.
- YOUNG, G. M. and solutions and ore deposits in Miocene basins. *Geol. Surv. Jpn. Bull.* 23.
- YOUNG, G. M. and abundances in pyrites. *Econ. Geol.* 66.
- YOUNG, G. M. and JUNGE, C. E. and uraniferous ores: Carbon and implications for the uranium resource. *Can. Res.* 2, pp. 1-69.
- YOUNG, G. M. and Uranerzlagerstätte (iron ores). *Tschermaks Mon.* 31.
- YOUNG, G. M. and 1973. Geology of the Barberton area. *Geol. Surv. S. Afr. Spec. Publ.* 15, 242 p.
- YOUNG, G. M. and 1928. The iron deposits of the Union of South Africa. *Geol. Surv. Union S. Afr., Mem. No.* 26, 268 p.
- YOUNG, G. M. and 1967. Formation of red beds in modern and ancient deserts. *Geol. Soc. Am. Bull.* 78, pp. 353-368.
- YOUNG, G. M. and 1965. The organic chemistry of sea water. *Am. Sci.* 53, pp. 358-374.
- YOUNG, G. M. and 1973. Stratigraphy and depositional environments of Upper Huronian rocks of the Rawhide Lake-Flack Lake area. *Ontario. Geol. Assoc. Can. Spec. Pap.* 12, pp. 73-92.
- YOUNG, G. M. and 1972. Uranium: economic deposits. *In: The encyclopedia of geochemistry and environmental sciences* (R. W. Fairbridge, Ed.) Van Nostrand Reinhold Co., New York, NY. 1321 p.
- YOUNG, G. M. (Ed.) 1973. Huronian stratigraphy and sedimentation. *Geol. Assoc. Can. Spec. Pap.* 12.
- TRASK, P. D. and PATNODE, H. W. 1942. Source beds of petroleum. *Am. Assoc. Pet. Geol., Tulsa, Okla.*
- TUREKIAN, K. K. 1968. *Oceans*. Prentice-Hall, Inc., Englewood Cliffs, NJ. 120 p.
- TURNER, G. C. and WALKER, R. G. 1973. Sedimentology, stratigraphy and crustal evolution of the Archean greenstone belt near Sioux Lookout, Ontario. *Can. J. Earth Sci.* 10, pp. 817-845.
- VAN ANDEL, T. H. 1964. Recent marine sediments of the Gulf of California. *In: Marine geology of the Gulf of California* (T. H. Van Andel and G. G. Shor, Eds.). *Am. Assoc. Pet. Geol. Mem.* 3, pp. 216-310.
- VAN HOUTEN, F. B. 1972. Iron and clay in tropical savanna alluvium, northern Columbia: a contribution to the origin of red beds. *Geol. Soc. Am. Bull.* 83, pp. 2761-2772.
- VAN VALEN, L. 1971. The history and stability of atmospheric oxygen. *Science*, 171 (3970), pp. 439-443.
- VISSER, D. J. L. 1956. The geology of the Barberton area. *Geol. Surv. S. Afr., Spec. Publ.* 15, 242 p.
- WAGNER, P. A. 1928. The iron deposits of the Union of South Africa. *Geol. Surv. Union S. Afr., Mem. No.* 26, 268 p.
- WALKER, T. R. 1967. Formation of red beds in modern and ancient deserts. *Geol. Soc. Am. Bull.* 78, pp. 353-368.
- WANGERSKY, P. J. 1965. The organic chemistry of sea water. *Am. Sci.* 53, pp. 358-374.
- WOOD, J. 1973. Stratigraphy and depositional environments of Upper Huronian rocks of the Rawhide Lake-Flack Lake area. *Ontario. Geol. Assoc. Can. Spec. Pap.* 12, pp. 73-92.
- WRIGHT, R. J. 1972. Uranium: economic deposits. *In: The encyclopedia of geochemistry and environmental sciences* (R. W. Fairbridge, Ed.) Van Nostrand Reinhold Co., New York, NY. 1321 p.
- YOUNG, G. M. (Ed.) 1973. Huronian stratigraphy and sedimentation. *Geol. Assoc. Can. Spec. Pap.* 12.

Permeability Changes During the Flow of Water Through Westerly Granite at Temperatures of 100°–400°C

R. SUMMERS, K. WINKLER, AND J. BYERLEE

U.S. Geological Survey, Menlo Park, California 94025

**UNIVERSITY OF UTAH
RESEARCH INSTITUTE
EARTH SCIENCE LAB.**

Changes in permeability have been studied during the flow of water through granite for periods of time up to 17 days at temperatures of 100°, 200°, 300°, and 400°C with a constant confining pressure of 500 bars, differential stresses of 0–3500 bars, inlet pore pressure of 275 bars, and outlet pressure of 1 bar. In all cases the initial permeability at elevated temperatures was found to be higher by 1–2 orders of magnitude than the permeability at room temperature, perhaps because of thermal stress cracking. The high initial permeability did not persist with time and in nearly all cases decreased significantly during the first ½ day of water flow. Dissolution of plagioclase and quartz was concentrated near the inlet, where the pore pressure was highest. Precipitation occurred throughout the samples because of oversaturation as the pore pressure dropped, causing significant reduction in permeability. The final permeability after 10 days was less at 300°C than at lower temperatures, and measurable flow stopped in most of the 400°C samples.

SUBJ
GCHM
PCD

INTRODUCTION

Natural geothermal steam is currently being harnessed for energy in several places throughout the world. Unfortunately, these natural steam sources occur only in limited areas. There are, however, many more places where hot, dry rock is accessible. Current proposals for producing energy from these dry geothermal sources suggest that energy can be extracted by drilling into the hot igneous rocks, injecting water to produce a large hydraulic fracture, and circulating water through the fracture [Smith *et al.*, 1975; Kruger, 1975]. The fracture would provide a large heat transfer area from which steam or hot water could be drawn off through a recovery well.

A viable plan for circulating water through a fracture system in the hot rock is fundamental to carrying out this geothermal energy extraction plan. It is important to know how permeability in large and small fracture systems will change with time. Measurements of the permeability of intact samples of Westerly granite at room temperature have been made by Brace *et al.* [1968], and changes in permeability due to dilatant cracking in Westerly granite have been investigated by Zoback and Byerlee [1975].

M. L. Batzle and G. Simmons (unpublished manuscript, 1975) speculated that in natural hydrothermal systems, fracturing would tend to increase the permeability and deposition of secondary minerals would tend to decrease it, but to date, there are no data in the published literature that would allow us to determine whether the permeability of rock would decrease or increase with time as water circulated through the hot rock.

In this paper we report the results of some experiments designed to study how the permeability of initially intact samples of granite changes with time as water is pumped through the rock at temperatures up to 400°C.

EXPERIMENTAL PROCEDURE

The samples used were Westerly granite cylinders 1.59 cm in diameter and 3.81 cm in length (Figure 1). They were placed under a confining pressure (P_c) of 500 ± 5 bars and subjected to an axial differential stress (σ_D) of $0-3500 \pm 15$ bars. The inlet pore pressure was 275 ± 5 bars, and the outlet pore pressure 1 bar. The nominal values given for the experimental temperatures are correct within 5% for the top and bottom

ends of the samples. Temperatures at the centers of the samples are higher than those at the ends by 5°, 7°, 9°, and 13°C for 100°, 200°, 300°, and 400°C, respectively. All samples except one were solid cylinders. The remaining sample (run at 300°C and 0-bar σ_D) had a saw-cut joint along the length of the cylinder. All samples were enclosed in an inner gold sleeve (1.59-mm wall) and sealed in a copper jacket (0.25-mm wall).

The mass flow rate of water into the sample was measured on the basis of the input pumping rate. The mass flow rate (dm/dt) is proportional to the permeability (k), where

$$k = dm/dt C_1 \quad (1)$$

and

$$C_1 = \frac{1}{A} \nu \left(\frac{dp}{dx} \right)^{-1} \quad (2)$$

Equation (2) was rearranged to the form

$$C_1 = \frac{L}{A} \left(\int_{P_o}^{P_i} \frac{dp}{dx} \right)^{-1} \quad (3)$$

which allows us to deal with the variable viscosity over the length of the sample. The constant C_1 was calculated by using a Fortran computer program. The kinematic viscosity (ν) of water as a function of temperature and pressure was entered in the program in tabular form from steam tables [Keenan *et al.*, 1969]. The integral in (3) was evaluated by the trapezoidal method by using the inlet and outlet pressures as limits.

In an attempt to keep the calculations simple we assumed uniform permeability throughout the sample. Since we know, however, that the permeability was not uniform, this simplifying assumption introduced a significant error into our estimates. In all experiments the effective pressure varied from 224 bars at the top of the sample to 500 bars at the bottom. This effective pressure gradient was sufficient to cause the permeability at the top of the sample to be about twice that at the bottom [Brace *et al.*, 1968]. In addition, temperature gradients in the samples produced small local variations in permeability. Thus the calculation of permeability at the beginning of each experiment has an uncertainty of about 50%. Since the alteration of minerals during each experiment is not uniform throughout the sample, permeability should become less uniform with time. Because of the remarkable decrease in flow rate observed in all experiments this means that the

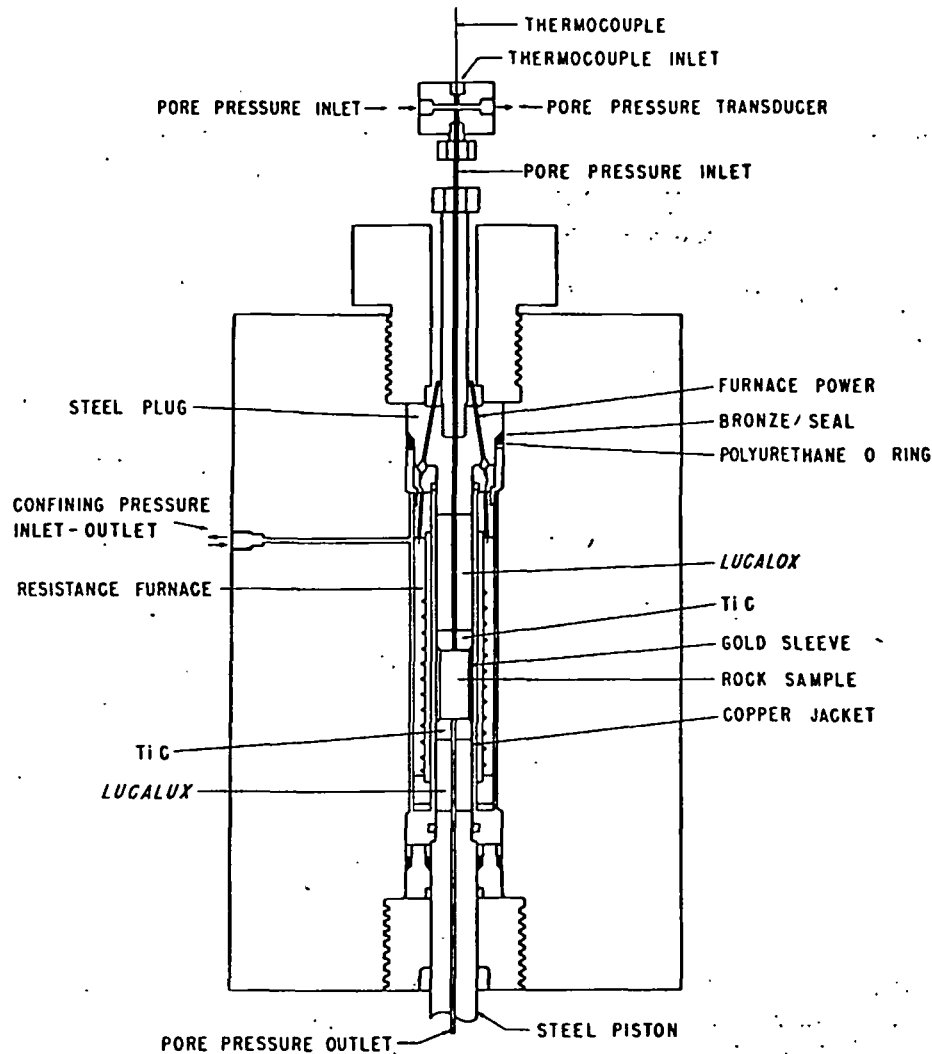


Fig. 1. Sample arrangement used in this study.

permeability that we calculated using (1) is exactly an upper limit for the permeability in the blocked regions of the samples. Because of the limited number of parameters that could be measured in these experiments this is the best estimate that could be made of the true local permeability. The outstanding result is not the precise value of the permeability but is rather the fact that permeabilities decrease significantly with time.

EXPERIMENTAL RESULTS

For the six samples run at 100°C (Figure 2), each curve is marked with the value of the differential stress to which the individual sample was subjected. For this set of tests, there was a wide spread in the mass flow rate. Those samples that were run under higher differential stress tended to have higher flow rates during the first day. However, this tendency is not solidly established, since lines for different stress levels cross, and the sample run at a 500-bar differential stress does not fit the trend for higher differential stress to produce a greater flow rate.

The seven tests run at 200°C (Figure 3) exhibited behavior similar to that of the 100°C tests in terms of having high initial flow rates which decreased rapidly during the first $\frac{1}{2}$ day of testing and more slowly thereafter. The applied differential stress did not have a regular effect on the flow rate at 200°C, although for part of the time the tests under higher differential

stress did exhibit lower flow rates than those under lower stress. Two of the samples, one at 0-bar differential stress and one at 500-bar differential stress, showed temporary increases in flow rate. These increases did not persist, and the final values were near those of the other 200°C samples, in which the flow rate had decreased steadily.

The six tests run at 300°C (Figure 4) had initial flow rates that tended to be lower than those of tests run at 100°C and 200°C. All these tests exhibited a rapid decrease in flow rate during the first $\frac{1}{2}$ day. The changes in flow rate with time observed in these samples were by far the most uniform of any of the groups of tests. The test run at 3500-bar differential stress and 300°C deviated from the uniform behavior of the other samples at 300°C. Its initial flow rate was similar but then decreased more slowly than the others until the point at which it failed in compression and the test was stopped. In this one sample the higher flow rate may result from dilatancy.

The results of the flow rate measurements for the six tests at 400°C (Figure 5) were significantly different from the results for the tests run at 100°-300°C. In addition, the behavior of the different samples within this 400°C group was erratic. In five tests, all measurable flow stopped in less than 2 days. Two of these samples had relatively high flow rates which dropped to zero, no indication being given that this was about to occur.

A single sample continued to have a low flow rate until day 11, when the test was stopped.

In order to investigate further the phenomenon of permeability decrease, one test was conducted by using a sample with a sawcut (Figure 6) at 300°C with a hydrostatic confining pressure of 500 bars. This artificial clean joint plane was made parallel to the long axis of the cylinder. The initial flow rate of about 22 mg/s was similar to the highest flow rates observed with the intact samples. For 2½ days the flow rate varied between 7 and 33 mg/s, large increases occurring abruptly and decreases occurring gradually. After 2½ days the flow rate abruptly decreased from 10 mg/s and did not increase again. The final value at the end of the 6-day test was 0.01 mg/s.

ALTERATION WITHIN SAMPLES

The samples were examined for alteration by the use of the optical microscope, scanning electron microscope (SEM), X ray diffraction, and X ray emission spectroscopy. On the inlet face of many samples, feldspar grains were dissolved at points where the water had best access to the surface. Within the samples, plagioclase, orthoclase, and quartz showed evidence of dissolution. Some of the plagioclase was partially altered to sericite, and albite twin structures were blurred or absent over portions of many plagioclase crystals. Deposits of aluminum silicates (identified by X ray spectroscopy) were observed both

on the faces of the saw-cut sample and within a grain boundary crack in an intact sample. In approximately half of the samples, deposits formed on the outlet end in quantity sufficient (up to 0.2 g) to be collected for X ray diffraction. These deposits contained quartz, orthoclase, plagioclase, sericite, cristobalite, and calcite. Several of the 100°C and 200°C tests yielded amorphous deposits, and the deposit from one test run at 400°C was nearly amorphous (two very small peaks). The cristobalite appeared in deposits from several of the 300°C and 400°C tests. Flow rate decrease did not correlate with the amount of material deposited on the outlet end of the sample.

DISCUSSION

Our study has produced data showing that permeability is clearly time and temperature dependent. There appears to be no comparably traceable flow rate stress dependence.

This lack of clear stress dependence agrees with the conclusion of *Sprunt and Nur* [1976] that the rate of porosity decrease is not related to stress on the rock matrix. The extent of time and temperature dependence was unforeseen.

The high initial flow rate of our samples was in marked contrast to the results of work done with Westerly granite at room temperature [*Brace et al.*, 1968; *Zoback and Byerlee*, 1975]. This initial high permeability at elevated temperatures was probably caused by cracks produced in the samples by

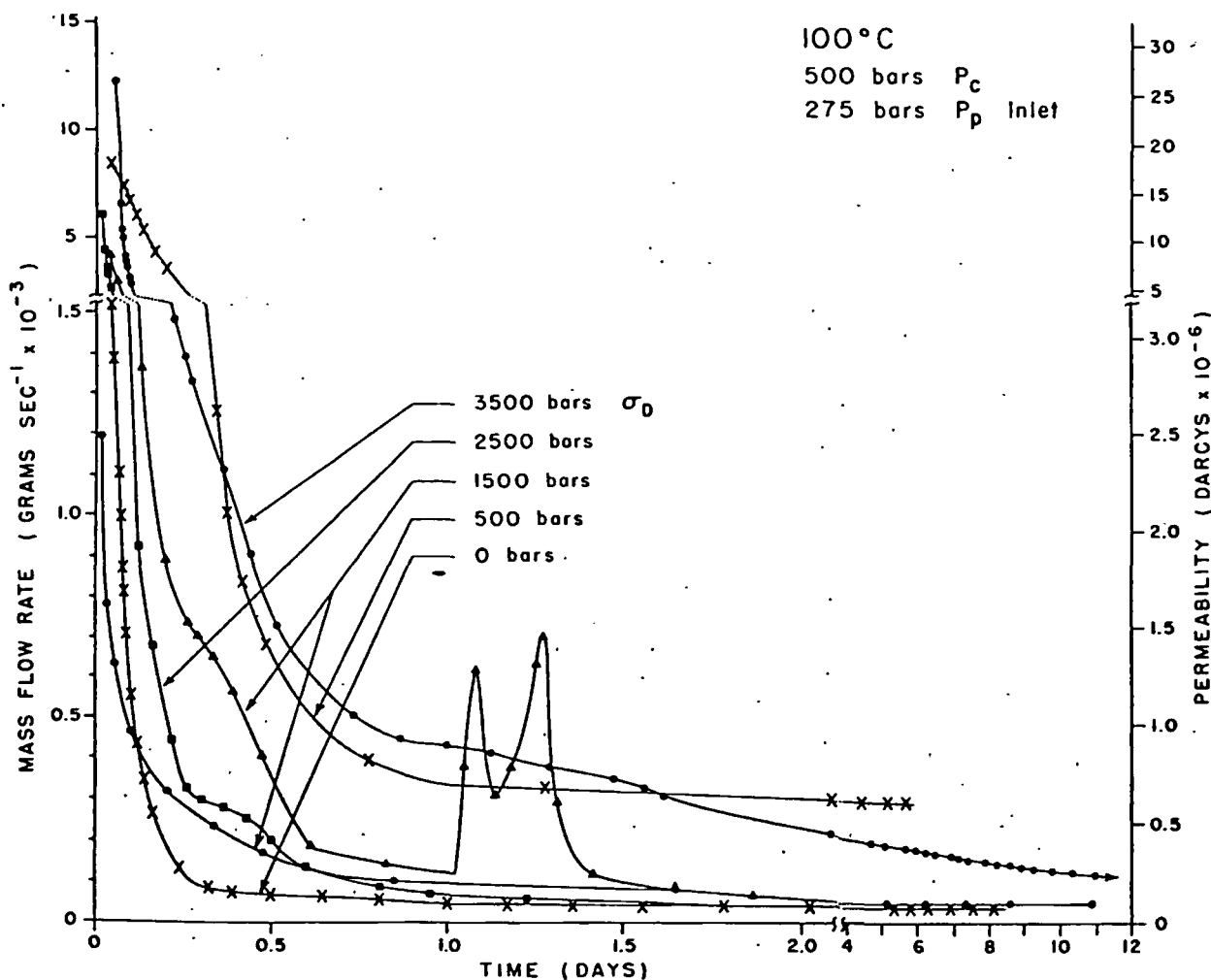


Fig. 2. Flow rates at 100°C plotted as a function of time.

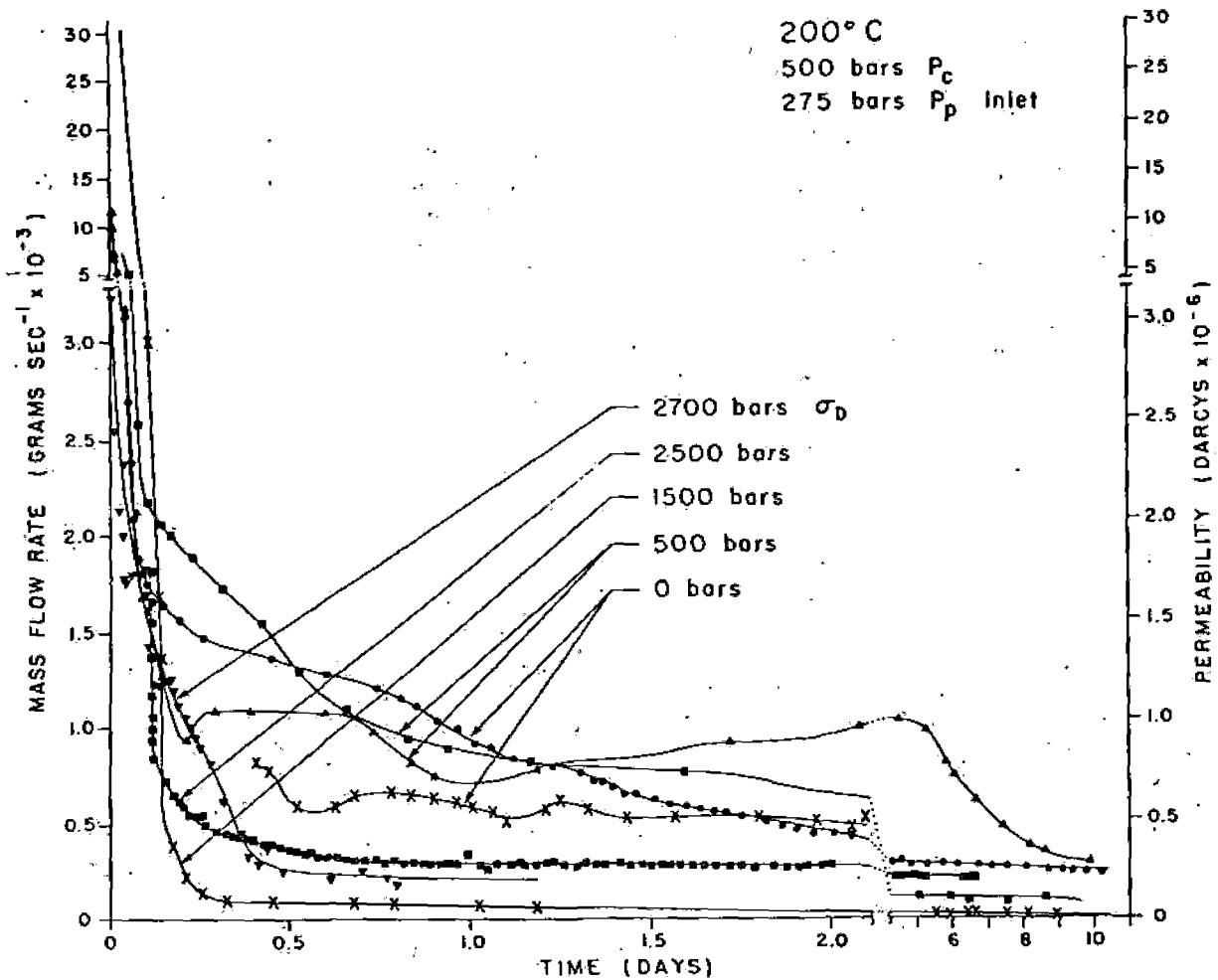


Fig. 3. Flow rates at 200°C plotted as a function of time.

differential thermal expansion of the minerals. This cracking could be detected by monitoring the acoustic emission during heating of the rock samples. A detailed study of this phenomenon was carried out and will be reported on elsewhere.

The dramatic decrease of flow rate with time exhibited by all our tests, without exception, is noteworthy, particularly since the greatest part of the decrease in intact samples occurred quite rapidly.

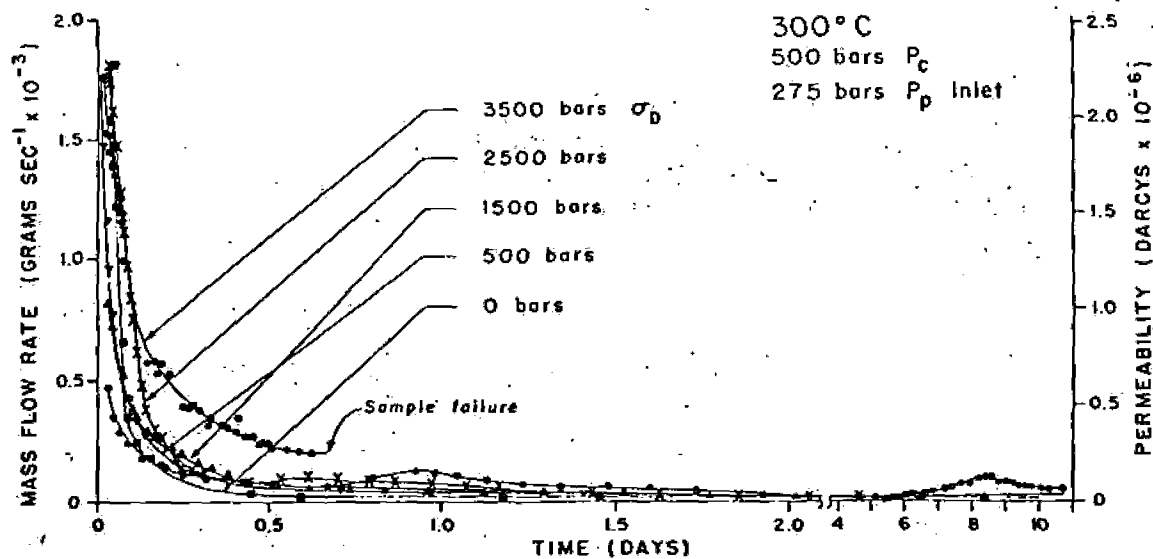


Fig. 4. Flow rates at 300°C plotted as a function of time.

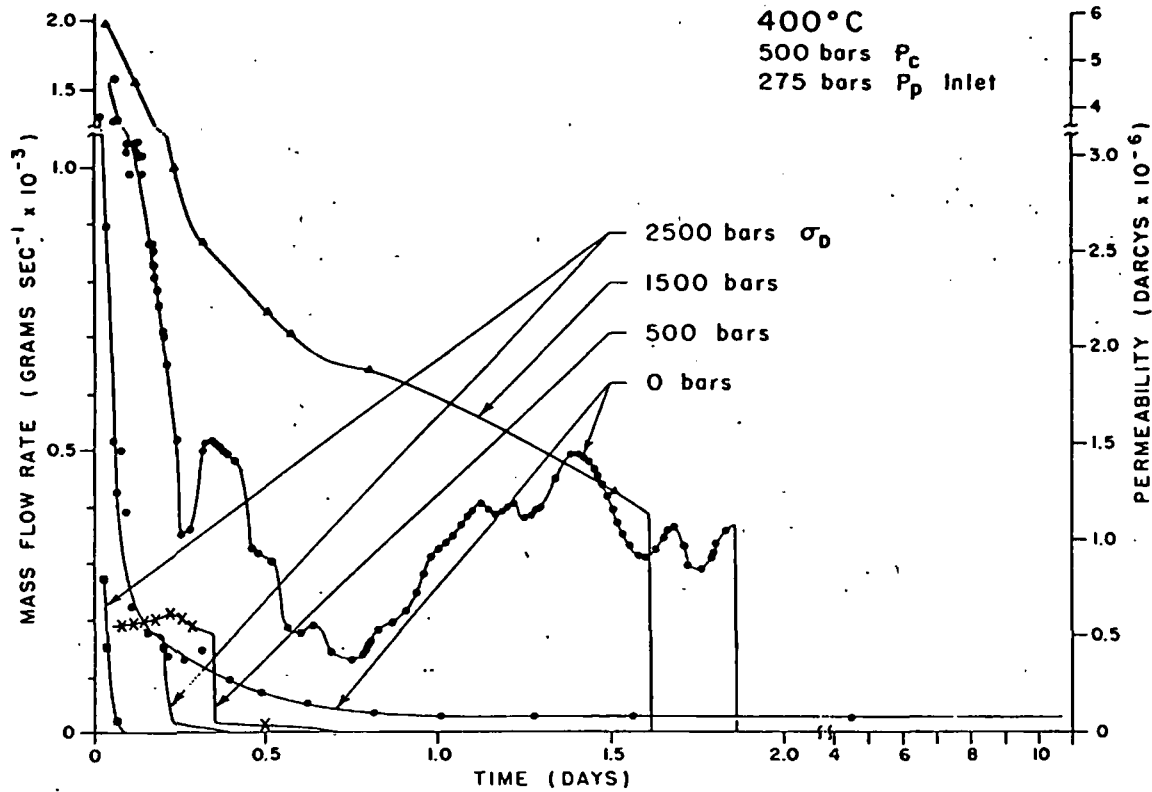


Fig. 5. Flow rates at 400°C plotted as a function of time.

These results may be of particular relevance to the design and operation of artificial geothermal systems. It has been theorized that hydrofracturing and then injecting water into a hot batholith will produce a hydrothermal crack system which will remain open and energy productive for an undetermined but economically profitable length of time. However, the ex-

tent of mineral alteration and deposition within the crack systems of our samples run at high temperatures indicates that geothermal power developers may want to investigate the nature and extent of mineralogical alteration likely to occur at any chosen site and include it as an important consideration at all stages of planning.

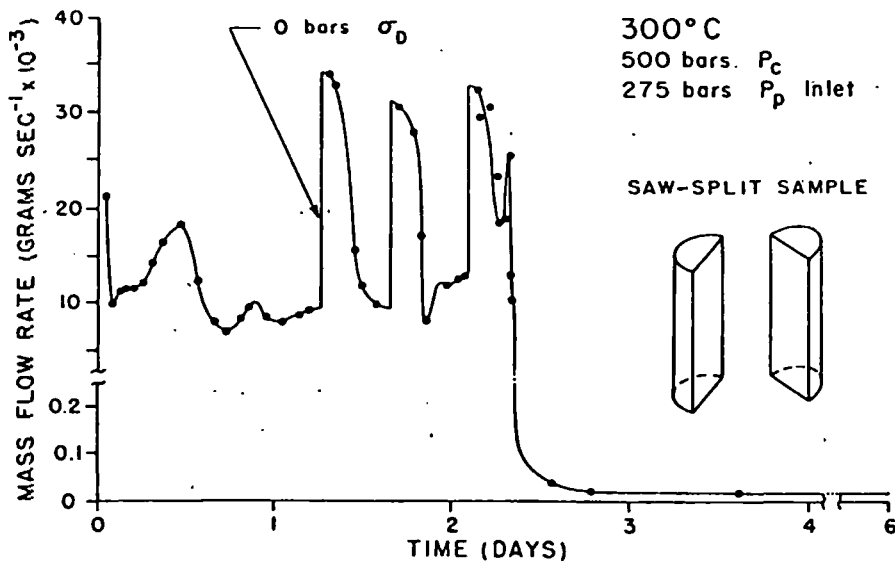


Fig. 6. Flow rate for the saw-cut sample run at 300°C plotted as a function of time.

REFERENCES

- Brace, W. F., J. G. Walsh, and W. T. Frangos, Permeability of granite under high pressure, *J. Geophys. Res.*, **73**(6), 2225-2236, 1968.
- Keenan, J. H., F. G. Keys, P. G. Hill, and J. G. Moore, *Steam Tables—Thermodynamic Properties of Water Including Vapor, Liquid and Solid Phases*, int. ed., p. 114, John Wiley, New York, 1969.
- Kruger, P., Stimulation of geothermal energy resources, *Rep. ERDA-37*, Energy Res. and Develop. Admin., Washington, D. C., 1975.
- Smith, M. C., D. W. Brown, and R. A. Pettitt, Los Alamos dry geothermal source demonstration project, *Mini Rev. 75-1*, Los Alamos Sci. Lab., Los Alamos, N. Mex., 1975.
- Sprunt, E. S., and A. Nur, Reduction of porosity by pressure solution: Experimental verification, *Geology*, **4**, 463-466, 1976.
- Todd, T., Effect of cracks on elastic properties of low porosity rocks, Ph.D. thesis, Mass. Inst. of Technol., Cambridge, 1973.
- Zoback, M. D., and J. D. Byerlee, The effect of microcrack dilatancy on the permeability of Westerly granite, *J. Geophys. Res.*, **80**, 752-755, 1975.

(Received August 16, 1976;

revised July 22, 1977;

accepted August 1, 1977.)